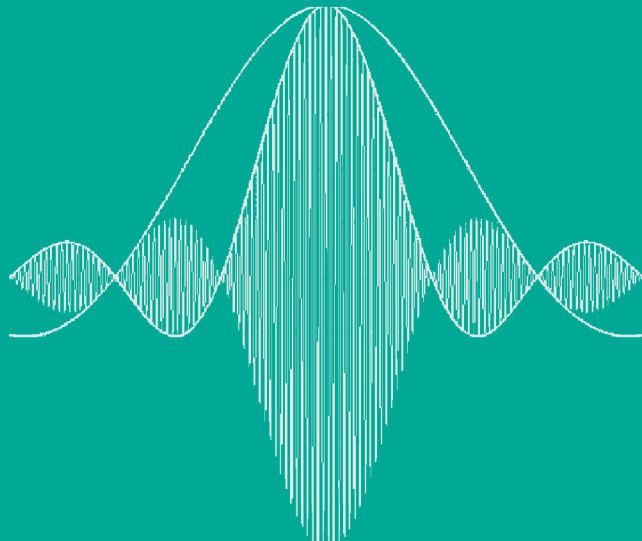


# Precision FMCW Short-Range Radar for Industrial Applications



**Boris A. Atayants**  
**Viacheslav M. Davydochkin**  
**Victor V. Ezerskiy**  
**Valery S. Parshin**  
**Sergey M. Smolskiy**

# **Precision FMCW Short-Range Radar for Industrial Applications**



# **Precision FMCW Short-Range Radar for Industrial Applications**

Boris A. Atayants  
Viacheslav M. Davydochkin  
Victor V. Ezerskiy  
Valery S. Parshin  
Sergey M. Smolskiy



**ARTECH  
HOUSE**

BOSTON | LONDON  
[artechhouse.com](http://artechhouse.com)

**Library of Congress Cataloging-in-Publication Data**

A catalog record for this book is available from the U.S. Library of Congress.

**British Library Cataloguing in Publication Data**

A catalog record for this book is available from the British Library.

ISBN 13: 978-1-60807-738-0

Manuscript created under the supervision of Dr.Sci. Professor Victor V. Ezerskiy and Dr.Sci. Professor Sergey M. Smolskiy

English translation by Sergey M. Smolskiy

© 2014 ARTECH HOUSE

685 Canton Street

Norwood, MA 02062

All rights reserved. Printed and bound in the United States of America. No part of this book may be reproduced or utilized in any form or by any means, electronic or mechanical, including photocopying, recording, or by any information storage and retrieval system, without permission in writing from the publisher.

All terms mentioned in this book that are known to be trademarks or service marks have been appropriately capitalized. Artech House cannot attest to the accuracy of this information. Use of a term in this book should not be regarded as affecting the validity of any trademark or service mark.

10 9 8 7 6 5 4 3 2 1

*To Ryazan State Radio Engineering University, which recently celebrated its 60th anniversary, and JSC Contact-1, which recently celebrated its 20th anniversary*



# Contents

Preface	xv
Introduction	xvii

## CHAPTER 1

Counting Method of Estimation of Difference Frequency	1
1.1 Introduction	1
1.2 Main Calculation Relations	1
1.3 The Traditional Counting Method of Range Measurement	5
1.4 Sources of Range Measurement Errors by the FMCW Range-Finder	7
1.5 Adaptive Control of Frequency Modulation Parameters	8
1.6 Truncation Error of Range Measurement at Adaptive Frequency Modulation	13
1.6.1 The Fixed Measuring Time Interval	13
1.6.2 The Measuring Time Interval Multiple to the Modulation Half-Period	16
1.6.3 Calculation of the Range Result Correction	20
1.7 The Range Determination Error Caused by the Inaccuracy of Modulation Adaptation	23
1.8 Noise Influence on the Accuracy of the Range Determination Using the Additive Counting Method	25
1.9 Conclusions	31
References	31

## CHAPTER 2

Weighting Method for the Difference Frequency Averaging	33
2.1 Introduction	33
2.2 The Truncation Error of the Weighting Method of Difference Frequency Averaging	36
2.3 Truncation Error Minimization at the Weighting Average Method of Difference Frequency by Optimization of Weighting Function Parameters	45
2.4 Truncation Error Minimization of the Weighting Averaging Method of the Difference Frequency by Optimization of the FM Parameters	50
2.4.1 Application of Additional Slow-Frequency Modulation	50
2.4.2 Optimization of the FM Sweep	53

2.4.3	Combined Optimization	55
2.4.4	The Combined Procedure of Error Minimization	56
2.5	Noise Influence on the Error of the Weighting Method of Difference Frequency Averaging	56
2.5.1	The Measurement Error for the Weighting Function in the Form of the Trigonometric Series	58
2.5.2	The Measurement Error for the Kaiser-Bessel Weighting Function	62
2.6	Conclusions	64
	References	64

## CHAPTER 3

Estimation of the Difference Frequency by the Position of the Spectrum Maximum	67	
3.1	Introduction	67
3.2	Algorithms of Difference Frequency Estimation	68
3.3	Estimation of the Difference Frequency on the Basis of the Maximum Position of the Spectral Density of Difference Frequency Signal	71
3.3.1	Analytical Estimation of the Truncation Error of Range Measurement	71
3.3.2	The Truncation Error of the Difference Frequency Estimation at the Weighting Functions of Dolph-Chebyshev and Kaiser-Bessel	74
3.3.3	Minimization of the Measurement Error on the Basis of the FM Parameter Optimization	77
3.3.4	Error Minimization on the Basis of Optimization of Weighting Function Parameters	80
3.3.5	Minimization of the Truncation Error Using Adaptable Weighting Functions	86
3.3.6	Algorithms of Frequency Estimation Using Adaptable Weighting Functions	86
3.4	Average Weighted Estimation of the Difference Frequency	88
3.4.1	The Truncation Error of the Average Weighted Estimation	88
3.5	Systematic Inaccuracy of Frequency Estimation for the Algorithm with Correction Coefficients	91
3.6	Influence of Noise Interference on the Error of Range Measurement	92
3.6.1	Statistical Characteristics of Estimation of the Spectral Density of DFS and Noise Sum	92
3.6.2	Influence of Noise on Accuracy of the Central Frequency Estimation	94
3.7	Conclusions	103
	References	104

**CHAPTER 4**

The Maximal Likelihood Method for Range Estimation According to the Difference Frequency Signal	107
4.1 Introduction	107
4.2 Range Estimation Based on the Difference Frequency Signal	108
4.3 Peculiarities of Delay Time Estimation Using the Maximal Likelihood Method	113
4.4 Main Factors Affecting the Measurement Error of Time Delay	116
4.5 Estimation of the Phase Characteristic of FMCW RF	121
4.6 Simulation of the Range Estimation Algorithm	130
4.6.1 Simulation Results at a Known Phase Characteristic	131
4.6.2 Simulation Results at the Unknown Phase Characteristic: The Approach to Practical Estimation of the Phase Characteristic	131
4.6.3 Reduction of the Noise Influence on the Accuracy of the Phase Characteristic Estimation	134
4.7 Conclusions	135
References	136

**CHAPTER 5**

Effects of FM Nonlinearity	137
5.1 Introduction	137
5.2 The Mathematical Model of the Modulation Characteristic	137
5.3 Effects of FM Nonlinearity for the Counting Method of Frequency Measurement	141
5.3.1 The Quadratic Modulation Characteristic	142
5.3.2 The Oscillating Modulation Characteristic	144
5.3.3 The Quadratic Modulation Characteristics with the Oscillating Component	147
5.4 Effects of FM Nonlinearity for the Weighting Method of Difference Frequency Averaging	147
5.5 Connection of the Correction Coefficient with Nonlinearity Parameters of the MC	151
5.5.1 Quadratic Nonlinearity of Modulation Characteristics	151
5.5.2 Oscillating Nonlinearity of the Modulation Characteristic	151
5.5.3 Quadratic and Oscillating Nonlinearity of the Modulation Characteristic	152
5.6 Estimation of the Correction Coefficient According to the Operating Difference-Frequency Signal	153
5.6.1 The Algorithm Sequence	153
5.6.2 Simulation Conditions	154
5.7 Compensation of Modulation Characteristic Nonlinearity	155

5.8	Consideration of Modulation Characteristic Nonlinearity at Range Calculation	160
5.8.1	Estimation of Extreme Period Parts	161
5.8.2	Approximation of the Time Function of Signal Periods	162
5.9	Conclusions	164
	References	165

## CHAPTER 6

	Analysis of the Range Measurement Error at the Interference Presence	167
6.1	Introduction	167
6.2	The Error Caused by the Single Spurious Signal of the Difference Frequency	170
6.2.1	Error Estimation According to DFS Spectrum Maximum Position	170
6.2.2	Error Estimation at Signal Processing in the Time Domain	172
6.3	The Error Caused by the Influence of Spurious Reflectors in the Antenna-Waveguide Path and in the Operating Zone of the FMCW Range-Finder	174
6.3.1	Influence of the Frequency-Independent Spurious Reflectors in the AWP and in the Operating Zone of the FMCW RF	174
6.3.2	Influence of the Spurious Reflection of the Pulse Character	177
6.4	The Error Caused by the Signal Reflection from the Corner Formed by the Reservoir Vertical Wall and the Liquid Surface	181
6.5	Influence of the Edge Modes Caused by the Restricted Sizes of the Probing Object	184
6.6	Influence of Reflected Waves on the Measurement Error of the FM Range-Finder	187
6.6.1	Influence of Echo Signals on the Operating Mode of the SHF Oscillator	187
6.6.2	Influence of the Wave Reflected from the Useful Reflector on the Range Measurement Error	188
6.6.3	Simultaneous Influence of Waves Reflected from the Useful and Spurious Reflectors on the Range Measurement Error	190
6.7	Influence of Combination Components in the Mixer of the FMCW RF on the Measurement Error	192
6.7.1	Virtual Reflectors	192
6.7.2	Influence of Virtual Clutter on the Range Estimation Error	193
6.8	Conclusions	194
	References	195

## CHAPTER 7

	Reduction of the Measurement Error at Interference Presence Using Adaptable Weighting Functions	197
7.1	Introduction	197
7.2	Estimation of the Interference Situation	198

7.3	Error Minimization of Frequency and Amplitude Estimation of the Weak Signal on the Background of Resolvable Single Interference	204
7.3.1	Introduction	204
7.3.2	Minimization of the Range Measurement Error for Weakly Reflecting Liquids	204
7.3.3	Action Sequence at the Level Measurement of the Weakly Reflecting Material Near an Antenna	206
7.3.4	Range Measurement on the Background of Strong Reflection from the Reservoir Bottom	210
7.4	Error Reduction of Difference Frequency Estimation of the Signal Received on the Background of Nonresolvable Interference	210
7.4.1	The Situations Most Often Met in Practice	210
7.4.2	The Method of Error Decrease	211
7.4.3	The Algorithm of Estimation Error Reduction: The Sequence of Actions to Decrease the Range Estimation Errors	216
7.5	Error Decrease Caused by the Virtual Reflector	217
7.5.1	Action Sequence for the Influence Reduction of the Virtual Reflector	218
7.5.2	Measures Providing a Decrease of the Error Caused by an Echo Signal	220
7.6	Conclusions	221
	References	222

## CHAPTER 8

	Parametrical Methods and Algorithms for Increasing the Measurement Accuracy at the Interference Presence	223
8.1	Introduction	223
8.2	Cancellation of Spurious Reflections	223
8.2.1	Using the Complex Spectral Density for Cancellation	226
8.2.2	Using Spectral Power Density for Cancellation	228
8.3	Reduction of Spurious Reflector Influence on the Accuracy of the Range Estimation by the Maximal Likelihood Method	232
8.3.1	The Tracking Range Measuring System	232
8.3.2	Main Stages of the Tracking Procedure After the Local Extreme	236
8.3.3	Tracking Modes	237
8.3.4	Influence of the Phase Characteristic Estimation Error on the Operation of the Tracking Measurer	239
8.3.5	Determination of the Conditions at which the Tracking Loss Occurs	240
8.3.6	Range Measurement at the Presence of the Spurious Reflectors of Small Intensity	242
8.4	Frequency Measurement Using Methods of the Parametric Spectral Analysis	244
8.4.1	The Algorithm of the Frequency Measurement on the Basis of Eigenvector Analysis in the Noise Subspace	244

8.4.2	The Frequency Measurement Algorithm by the Prony Method of Least Squares	247
8.5	Range Prediction on the Basis of Consideration of the Movement Speed	250
8.5.1	Uniform Velocity of the Useful Reflector Movement	250
8.5.2	The Nonuniform Velocity of the Useful Reflector Movement	253
8.6	Conclusions	255
	References	256

## CHAPTER 9

	Testing of Precision Measuring Systems of FM Short-Range Radar and Areas of Its Practical Application	257
9.1	Introduction	257
9.2	Equipment and Approach for the Experimental Estimation of the FM RF Characteristics	257
9.2.1	Synthesis of Radar Reflectors for Precision Measurements	259
9.2.2	The Test Bench for the Measurement of the FM RF Parameters	264
9.2.3	The Procedure of Carrying Out Measurements	266
9.3	Experimental Reduction of the Error Caused by Virtual Interference	266
9.3.1	The Waveguide-Measuring Test Bench	266
9.3.2	Experimental Research of the Possibility of Reducing Virtual Interference Influence	267
9.3.3	Influence of Radiated Power Level on the Distance Estimation Error Caused by Virtual Interference Influence	269
9.4	Results of the Experimental Reduction of the Distance Measurement Error by the Control of the Adaptable Weighted Function Parameters	269
9.5	Testing Results of the Parametric Algorithms of the Distance Measurement in the Measuring Test Bench	272
9.5.1	Algorithms Based on the Methods of Parametric Spectral Analysis	272
9.5.2	The Algorithm Based on the Maximal Likelihood Method	274
9.5.3	Testing of the Tracking Distance Meter	275
9.5.4	Testing Results of the Algorithm “Prediction”	275
9.6	Areas of Practical Application of the FMCW Radar	277
9.6.1	Radio Altimeters for Small and Medium Attitudes	278
9.6.2	Radio Proximity Fuses	279
9.6.3	Navigation Radar	279
9.6.4	Transport Radar	280
9.6.5	Level-Meters	281
9.6.6	Ice and Snow Blanket Thickness Meters	281
9.6.7	FM Geo-Radar	282
9.6.8	Atmosphere Sensing Radar	283
9.6.9	Range Finders for Geodesic Research	283
9.6.10	Birds’ Observation Radar	283
9.6.11	Small Displacement Meters	284

9.6.12 Guarding Systems	284
9.6.13 Robotic Navigation and Mapping Systems	285
9.7 Conclusions	286
References	286
Conclusion	289
Appendix: Weighting Functions for Harmonic Analysis and Adjacent Problems	291
List of Acronyms	315
About the Authors	317
Index	321



# Preface

The idea for this book came about as the result of years of experience in the investigation, development, and production of one class of radar systems: radar level-meters. Our research began at the Ryazan plant TEPLOPRIBOR (located in the center of Russia) in cooperation with the scientists of the Ryazan Radio Engineering Institute and the Institute of Telemechanics and Automatics of Soviet Academy of Sciences during the 1970s and 1980s. The following contributors have participated in this development: B. V. Lunkin, A. S. Sovlukov, A. I. Kiyashev, A. G. Miasnikov, F. Z. Rosenfeld, B. V. Kagalenko, B. A. Atayants, V. M. Izrailson, M. P. Marfin, and many others. During the past fifteen years, this research has been continued by the authors at the company JSC Contact-1 in the development, modernization, and serial production of the level-meter's family of BARS-3XX. In this engineering field, intensive investigations have been carried out in different countries around the world into creating devices that permit continuous checking and measuring of the filling level of various technological reservoirs automatically and with high accuracy and reliability. Besides this narrow but useful application area of radar technology, there are a whole series of industrial applications of short-range systems with similar requirements in terms of their functionality and cost-effectiveness. All these applications can be successfully implemented using frequency-modulated continuous wave (FMCW) radar. In our opinion, a new direction has been taken in traditional short-range radar technology for different applications (including military): precision FMCW radar technology that is oriented to the development, creation, and production of this new class of promising, short-range systems.

Many worldwide manufacturers of these devices have achieved rather highly desirable results. However, market pressures including speed to market rarely allow developers to disclose in detail the operation principles of new devices and algorithms of signal processing with high accuracy and operation reliability. Therefore, we should note that in many cases classical methods of radio signal generation and processing are built into the operation of these devices, but with some modifications characterizing the peculiarities of these applications. Of course, the application of new approaches to radio signal generation and processing for short-range measuring radar systems brings forth new results, which is why we decided to present our own theoretical and practical results along with the information available in patent and engineering publications with the hope that this book will help further innovation in the field of short-range precision radar technology.

We sincerely appreciate the team at JSC Contact-1 for their understanding, help, perpetual supply of new problems to tackle and the subsequent practical, interesting discussions of the results and their applications in new developments.

It is impossible to mention all our colleagues promoting our research, but we especially note I. V. Baranov, V. A. Bolonin, V. S. Gusev, S. V. Miroshin, D. Y. Nagorny, and V. A. Pronin, whose contributions were most significant.

Discussions of some of our dissertations from seminars at the Radio Control and Communication Department at the Ryazan State Radio Engineering University, which form the basis of this book, were promoted to improve the presentation of materials and results. Significant contributions to these discussions were made by Professor S. N. Kirillov, the head of Radio Engineering Radio Control and Communication Department, Professor V. I. Koshelev, the head of Radio Engineering Systems Department, and Professor Y. N. Parshin, the head of Radio Engineering Devices Department.

We express much gratitude to the head of Radio Engineering Systems of National Research University, Moscow Power Engineering Institute, Professor A. I. Perov, for the time-consuming work of reviewing as well as for providing useful feedback and advice.

We especially appreciate recommendations and very valuable comments made by the anonymous reviewer at Artech House Publishers for his attention and desire to improve our material.

B. Atayants, V. Davydochkin, V. Ezerskiy, and V. Parshin express their admiration, sincere respect, and gratitude to their colleague S. M. Smolskiy, who worked on the translation of the text into English.

We are also grateful to all interested readers for remarks and suggestions regarding this book's contents; comments can be sent to Artech House Publishers or to the Russian company CONTACT-1 (e-mail: market@kontakt-1.ru).

# Introduction

The *frequency range-finder* (FRF) using a continuous wave transmitted signal with *frequency modulation* (FM) (these systems are called FMCW short-range radar) has, for many years, been successfully applied as the altimeter for small attitudes in military and civil airplanes and as the navigation radar in the navy for survey of port water areas, for watercraft arrival to the port under conditions of bad visibility, and for a craft's docking to an embankment wall. Radio proximity fuses (the last mile radar) are typical directions of the FRF application. The intensive development of various branches of industry in the beginning and wide distributions of automatic control systems for industrial and revolutionary processes in the elements' base led to a wide application of short-range radar devices in the industry at the end of the 1960s [1–3]. We can attribute to them the devices for precision measurement of very small ranges (from parts of a meter to several tens of meters):

- Various measuring systems of the filling level of technological reservoirs (level meters);
- Systems for the precision positioning of complicated technological equipment (precision machines up to portal cranes);
- Measuring systems for small displacements and vibrations of particles of different machines and mechanisms;
- Range-finders for geodesic measurements;
- Ice thickness measuring systems;
- Systems for range and velocity determination to warn of collisions and for anti-accident parking;
- Radar for atmosphere sensing;
- Radar for bird observations;
- Various guarding systems.

Despite such wide application areas, all these devices can be unified by a general approach to methods of required characteristics achievement and typical features. Fundamentals for the technically competent development of such systems were established in previous decades within the development of various military applications [3–13]. Therefore, in many cases one must provide continuous noncontact process tracking (tracking for trajectory, range, and often velocity of its variations). A part of these tasks can be successfully solved by radio wave methods [1]. However, the entire spectrum of practical applications can be realized only by radar technology systems. In most cases, the frequency-modulated (FM) range-finder that uses the continuous wave (CW) transmitted signal with FM can successfully solve these tasks. We will be oriented in this direction and will only consider such FMCW radar devices.

The Swedish company SAAB and the Dutch company Enraf-Nonius [2, 14, 15] were pioneers in industrial application of FMCW radars, which used them for measurement of the filling level of different technological reservoirs. In 1975, SAAB placed in operation its first level meter. Up to the mid-1990s, this company produced more than 15,000 level meters. In 1976, the German company Krohne [15] created its first level meter. In the same year in Russia, the Ryazan plant Teplopribor developed level meters for tankers. The first level meters did not have high accuracy of measurements; their errors were units and even tens of centimeters. Only in the early 1990s was the measurement accuracy of 1 cm achieved [2]. The Russian level meter LUCH-2, which was developed and prepared for mass production with the participation of Dr. B. A. Atayants at Teplopribor, had an accuracy of 2 cm. However, the accuracy of 1 to 2 cm is not enough in many cases to solve the problems of industry. To increase the measurement accuracy, the much higher level of SHF engineering development and application of modern equipment and methods of digital signal processing were necessary. Increasing the accuracy from 1 cm to 1 mm took almost 10 more years.

Industry requirements in measuring short-range radar are vast. The large industrial and economic effects occur not only because of the exclusion of the usual manual methods of measurements and data processing, but also owing to high reliability, accuracy, operating speed, and simplicity of implementation of such range-finders into automated control systems for production.

It should be noted that the wide application of the FMCW radar for purely civil purposes, which does not relate to military applications, leads to the necessity of renaming the most popular terms. So, in the traditional radar technology, the object of radar observation is usually referred to as a target. In our case we call this object the *useful reflector* (UR), emphasizing that there are other *spurious reflectors* (SRs), which cause trouble for measuring problems.

At present, the development of devices offered by various companies mainly finds its voice in the patent publications and scientific and engineering literature. We note the most interesting publications [14–52]. Among the published results, the most important ones determining the main stages of FMCW range-finder development for industrial application are [14, 17, 18, 23] based on the weighting method of estimation of the difference frequency (DF); investigations [16, 19] offering the additional slow phase modulation of the FM signal; publications [17, 21, 22, 25, 28, 40] using the delay line as the reference (standard) channel; research [15, 37, 43, 49] using the calibration mode of operation for measurement and of nonlinearity compensation of the modulation characteristics (MC) of the transmitter on the basis of the stepped frequency modulation of the CW signal [the accepted abbreviation of this mode is frequency stepped continuous wave (FSCW)]; the suggestions of [48, 49] using the digital synthesis of the transmitter frequency in the FSCW mode; and publications [33, 35, 43–46] studying features of functioning of the FMCW radar under the conditions of the SR presence on the basis of different variations of the *maximal likelihood method* (MLM) or methods of high resolution (for example, the MUSIC method [43]).

Books on FMCW radar theory were published in the 1960s and 1970s that mainly dealt with military systems. Besides the publications mentioned above, we include [50, 51]. The most important and well known is the book by A. S. Vinitsky [3].

However, unfortunately, in spite of the definite achievements, in these books the modern methods of signal generation and processing taking into consideration the revolutionary changes in the element base for the past several decades are not described. At the end of the 1980s, [52] was published. The theoretical fundamentals and structure principles of radio engineering short-range systems for detection and measurement are considered in this book on a serious level as well as the realized features of systems intended for measurement of transport vehicles' movement parameters and for guarding radio engineering systems. We also note the research in [53, 54].

We also found research dedicated to FMCW radar systems, a Russian school-book for technical universities [55], in which the fundamentals of FMCW are described on a modern level, but very laconically. In the last serious investigation, we consider [56], a book published by Artech House Publishers and then translated into Russian. The theoretical fundamentals of received signal processing and transmitters on the basis of the autodyne operation principle (the autodyne is also called a self-oscillating mixer (SOM)] are described in conformity with short-range radar measuring systems for small ranges. The review of several aspects of the current status of the small range's precision measurement problems in the industry is contained in [57, 58].

Taking into consideration the above-mentioned sources, it is clear that there is a need to understand the latest achievements and to pull together the volumes of uncoordinated information available in worldwide publications and obtained by different authors during practical work on these new devices.

The specific characters of FMCW radar in industrial systems for small-range measurement consist of the following:

- A range of measured ranges are from parts of a meter to 30–50 meters for the required measurement accuracy up to 1 mm and even up to parts of a millimeter.
- In many cases, measurements are performed in complicated interference situations, often in closed volumes in the presence of spurious reflectors (SRs) of various types. A great number of rereflections from these elements is observed. If the material under inspection does not have a large value of dielectric constant and weakly absorbs the radio signal at level measurement, the reflection from the reservoir's bottom is also observed. However, all SRs (their parameters) in the RF operating zone can be revealed and estimated in advance.
- The radio signal reception is provided on the background of noises arising in the first stages of SHF units and due to transmitter phase noises.
- Nonlinearity of the transmitter MC has a strong effect on the measurement result.
- Measurements should be provided under the conditions of a great parameter variation of environment (temperature, moisture, pressure) and for variations of environment parameters in the operating zone, under conditions of the typical increased dust level of radio wave propagation mediums, the presence of steam, and the moisture condensate and dust sediment on the antenna.
- A limited volume of samples of the difference frequency signal (DFS) is available for processing. Therefore, for very small measuring ranges, only

several periods of the signal (three to four periods and less) can be processed for analysis.

- The achievement of high measurement accuracy requires a rather complicated algorithm of signal processing. Nevertheless, a result must be obtained in short order of technological process dynamics or information perception by a person (i.e., on a real-time scale).
- Developing algorithms must be practically realizable on the available element base when measuring the economic efficiency condition of a device's application.

The theoretical analysis of FMCW operation can be traditionally provided on the basis of two methods: a spectral method and the simplified method based on DFS processing in the time domain [3, 13, 53–57], which more often consists of the analysis of positions and a number of points of signal intersection with zero level. We will call this method temporal. It exists in the literature in different variants. In this book we use both methods of DFS processing, taking into consideration the advantages of the modern theory of the digital signal processing (DSP) to reach the best results.

It is known that both methods have a permanent error [3, 10, 13] called the *quantization interval* (QI) [51], caused by the periodicity of the frequency modulation law. In many cases this error is inadmissibly large; therefore, one must take measures for its decrease. We can achieve this goal by different methods consisting of definite additional actions on radiated and received signals [3, 10]. We call these the *methods of QI smoothing* (MQIS). These methods allow the achievement of a high accuracy of range measurement; however, each has particular limitations on the minimally achieved measurement error, and not all methods permit the possibility of digital implementation of processing.

The issue of extremely achieved measurement accuracy, which can be obtained on the basis of optimal processing methods; in particular, the method of maximal likelihood, is very interesting and important. This issue is also considered in this book.

The problems of analysis of range measurement errors are caused by interference influence in the form of noises, interference created by the SR in the RF operating zone, by the *parasitic amplitude modulation* (PAM), and by the nonlinearity of transmitter MC.

In examining all these problems, we take into consideration that much information on application areas of the short-range FMCW radar, on construction principles of structural schemes, and on the general theory of signal generation and processing are already stated in detail in the above-mentioned literature sources. Therefore, we do not address these general questions or give the specific information on themes, which, in our opinion, are the most significant, key themes at implementation of practical measurement systems.

Chapter 1 is devoted to the research of the classical counting method of difference frequency estimation. It is shown that this method still does not exhaust all possibilities. The adaptive method of the FM parameter control is offered, which allows a QI reduction up to the practically accepted values. Two variants of counting method implementation are considered and the algorithm of measurement results

correction is proposed allowing a sharp reduction of the error level. The noise influence is examined on both variants of implementation and advantages of the offered variant is proved.

An investigation of characteristics of the weighting method for difference frequency estimation is described in Chapter 2. The exact expressions for the truncation error of range measurement for two *weighting function* (WF) families are given. The possibility for minimization of the measurement error using the optimization of WF and FM parameters and appropriate algorithms are developed. The noise influence on the offered algorithms is studied.

The analysis of the spectral method for DFS processing is provided in Chapter 3. The approximate analytical expressions are obtained, which allow calculation with high accuracy of the truncation error of measurement at estimation of the difference frequency according to position of *spectral density* (SD) maximum at arbitrary WF. The obtained equations are specified for two promising WFs. The possibility of minimizing measurement error using optimization of WF and FM parameters is shown and the appropriate algorithms are developed. The measurement error minimization algorithms on SD maximum are suggested with the help of AWF and it is shown that they have an essential benefit compared with traditional WFs in truncation error level and in noise component, which is especially manifested at the measurement of small ranges. The possibilities of range determination on the basis of weighting average estimation of the difference frequency and using correction coefficients are considered. The estimation of noise influence on these algorithms is provided and their comparison is performed with the help of numerical modeling.

Chapter 4 is devoted to the analysis of practical application of MLM for estimation of the measured range. Equations for the limiting measurement accuracy are obtained and two-stage estimation procedure is offered, permitting to facilitate the search of the global extremum of the signal function. Factors affecting the range error estimation using MLM are analyzed and procedures are developed, which allow for the achievement of the maximal error reduction.

The influence of MC nonlinearity on the range measurement accuracy using the counting method and the method of weight averaging of the difference frequency are discussed. The MC mathematical model and approach for determination of its parameters according to really measured characteristics are offered. It is shown that the high accuracy of approximation can be achieved. The analysis of MC nonlinearity influence on MEDS is provided based on the DFS processing in the time domain. Three algorithms for reduction of the error caused by MC nonlinearity are offered. This is the correction of the measurement result, compensating nonlinearity at the expense of the predistortion introduction into modulating voltage and taking into consideration the nonlinearity at the range calculation. All these algorithms assume the urgent measurement of nonlinearity parameters according to real operating DFS. The quantitative estimation of the benefit providing by each of these algorithms is performed.

Chapter 6 discusses the analysis of the range measurement error caused by the interference presence. The interference types and its physical sense are considered. For each interference type, the theoretical examination is provided with quantitative estimation of interference level and revelation of the main characteristics effecting on error level.

The methods for error reduction caused by the interference presence are described in Chapter 7, specifically the problem of interference detection and estimation of interference situation in the RF operation zone. Methods and algorithms are suggested, which allow for the reduction of a difference frequency estimation using the adaptable WF. The possibility decreases the error caused by the virtual reflector.

Parametric methods and algorithms of range measurement accuracy growth at presence of interference are discussed in Chapter 8. The possibilities of MC compensation, MLM modification to provide its operation for SR presence, and methods of *parametric spectral analysis* (PSA) are described. The algorithm of measurement error reduction is offered, using the idea of result prediction in those places where the error is too large.

Chapter 9 describes the conditions, equipment, and approach of experimental estimation of FMCW characteristics under the conditions of industrial enterprise. Constructions of standard reflectors providing achievement of required measurement accuracy are offered. The measuring complex is described, which was certified as the measuring instrument allowing provision of range measurement error estimation with required reliability. The results of experimental research of the above-considered methods and algorithms, part of which is implemented in serially produced level meters of the BARS series, are discussed. All experimental results coincide well with results obtained theoretically and using the modeling.

The adaptable WF for the spectrum analysis is considered in the Appendix. Requirements for AWF are formulated, analytical expressions are obtained, and sets of coefficients for some AWF are given that present the most interest. Spectral properties of AWF are considered and optimization methods for its properties are offered.

A brief review of possible practical applications of FMCW radars in industry and scientific researches is also provided.

## References

- [1] Victorov, V. A., B. V. Lunkin, and A. S. Sovlukov, *Radio Wave Measurements of Technological Process Parameters*, Moscow, Russia: Energoizdat Publ., 1989. [In Russian.]
- [2] Johanngeorg, O., "Radar Application in Level Measurement, Distance Measurement and Nondestructive Material Testing," *Proc. of 27th European Microwave Conference*, September 8–12, 1997, pp. 1113–1121.
- [3] Vinitskiy, A. S., *Essay on Radar Fundamentals for Continuous-Wave Radiation*, Moscow, Russia: Sovetskoe Radio Publ., 1961. [In Russian.]
- [4] Rytov, S. N., "Modulated Oscillations and Waves," *Trudy FIAN*, Vol. II, No. 1, 1940. [In Russian.]
- [5] Gonorovskiy, I. S., *Frequency Modulation and Its Application*, Moscow, Russia: Sviazizdat Publ., 1948. [In Russian.]
- [6] Luck, D. G., *Frequency Modulated Radar*, New York: McGraw-Hill, 1949.
- [7] Kharkevich, A. A., *Spectra and Analysis*, 4th ed., Moscow, Russia: Fizmatgiz Publ., 1962. [In Russian.]
- [8] Bogomolov, A. F., *Radar Fundamentals*, Moscow, Russia: Sovetskoe Radio Publ., 1954.
- [9] Calmus, G., J. Kacheris, and G. Dropkin, "The Frequency-Modulated Altimeter with Non-Discrete Reading," *Issues of Radar Technology*, No. 3, 1954. [In Russian.]

- [10] Abd-El Ismail, M., *A Study of the Double Modulated F.M. Radar*, Zurich: Verlag Leemann, 1955.
- [11] Astafiev, G. P., V. S. Shebshaevich, and Y. A. Yurkov, *Radio Navigation Devices and Systems*, Moscow, Russia: Sovetskoe Radio Publ., 1958. [In Russian.]
- [12] Skolnik, M., *Introduction to Radar Systems*, New York: McGraw-Hill, 1962.
- [13] Kogan, I. M., *Short-Range Radar Technology (Theoretical Bases)*, Moscow, Russia: Sovetskoe radio Publ., 1973. [In Russian.]
- [14] Swedish Patent No. 381745, INT.CL. G01S 9/24. “Satt och anerdning for avstandsmatning med frekvens-modulerade kontinuerliga mikrovagor,” K. O. Edvardson, No. 7315649-9. Filed November 20, 1973; published December 15, 1975.
- [15] Brumbi, D., “Measuring Process and Storage Tank Level with Radar Technology,” *Records of the IEEE 1995 Intl. Radar Conference*, Alexandria, VA, 1995, pp. 256–260.
- [16] Schilz, W., R. Jacobson, and B. Schiek, “Mikrowellen Entfernungsmebsystem mit  $\pm 2,5$  mm Genauigkeit,” *Mikrowellen Magazine*, No. 2, 1976, pp. 102–107.
- [17] U.S. Patent 4044355, Int. CI. G01S 9/24, “Measurement of contents of tanks etc. with microwave radiations,” K. O. Edvardsson. Filed February 13, 1976. Date of patent, August 23, 1977.
- [18] Edvardson, K. O., “An FMCW Radar for Accurate Level Measurements,” *9th Eur. Microwave Conference*, Brighton, U.K., September 17–19, 1979, pp. 712–715.
- [19] Imada, H., and Y. Kawata, “New Measuring Method for a Microwave Range Meter,” *Kobe Steel Eng. Repts.*, Vol. 30, No. 4, 1980, pp. 79–82.
- [20] Marfin, V. P., V. I. Kuznetsov, and F. Z. Rosenfeld, “SHF Level-Meter,” *Pribory i sistemy upravleniya*, No. 11, 1979, pp. 28–29. [In Russian.]
- [21] Kagalenro, B. V., V. P. Marfin, and V. P. Meshcheriakov, “Frequency Range Finder of High Accuracy,” *Izmeritel'naya technika*, No. 11, 1981, p. 68. [In Russian.]
- [22] Authors certificate 1123387 (USSR), INT.CL. G01S 13/34, “Radio Range Finder,” B. V. Kagalenko and V. P. Meshcheriakov, Bull. No. 41, published July 10, 1984.
- [23] Authors Application 30-1591 (Japan), INT.CL. G01S 13/34, “Approach to Distance Measurement with the Aid of Frequency-Modulated Signal and the Radar Station with Frequency Modulation,” *Izobretenia stran mira*, No. 15, 1985, p. 29. [In Japanese.]
- [24] Authors Application 60-1592 (Japan), MLI G01S 13/34, “Method for Distance Measurement with the Help of the Radar Station with Double Frequency Modulation,” (*Izobretenia stran mira*, No. 15, 1985, p. 29. [In Japanese.]
- [25] Authors certificate 1141354 (USSR), INT.CL. G01S 13/08. “Frequency-modulated radio range finder,” B. V. Kagalenko and V. P. Meshcheriakov. Bull. No. 7. Filed March 5, 1983; published February 2, 1985.
- [26] Marfin, V. P., et al., “Radio Wave Non-Contact Level-Meter of Higher Accuracy,” *Izmeritel'naya technika*, No. 6, 1986, pp. 46–48. [In Russian.]
- [27] Author certificate 1230423 (USSR), INT.CL. G01S 13/34, 13/08. “Radio Range-Finder with Frequency Modulation,” B. V. Kagalenro and V. P. Meshcheriakov. Bull. No. 17. Filed August 13, 1984; published July 5, 1986.
- [28] U.S. Patent 4737791. Int. CI. G01S 13.08. “Radar Tank Gauge,” B. R. Jean, et al. Filed February 19, 1986; date of patent April 12, 1988.
- [29] Author certificate 1642250 (USSR), INT.CL. G01F 23/28. “Non-Contact Radio Wave Method for Level Measurement of Media Surface,” B. V. Lunkin, D. V. Khablov, and A. I. Kanarev. No. 4678472/10. Bull. No. 14. Filed April 14, 1989; published April 15, 1991.
- [30] Author certificate 1700379 (USSR), INT.CL. G01F 23/28. “Non-Contact Radio Wave Method of Level Measurement and Device for Its Implementation,” D. V. Khablov. No. 4773382/10, 4773381/10. Bull. No. 47. Filed December 24, 1989; published December 23, 1991.

- [31] U.S. Patent 5070730, Int. CI. G01F 23/28. “Device for Level Gauging with Microwave,” K. O. Edvardsson. No. 613574. Filed March 27, 1990; date of patent December 10, 1991.
- [32] U.S. Patent 5136299, Int. CI. G01S 13/08. “Device of Radar Level Gauge,” K. O. Edvardsson. No. 687914. Filed January 11, 1990; date of patent August 4, 1992.
- [33] Woods, G. S., D. L. Maskell, and M. V. Mahoney, “A High Accuracy Microwave Ranging System for Industrial Applications,” *IEEE Transactions on Instrumentation and Measurement*, Vol. 42, No. 4, August 1993.
- [34] U.S. Patent 5321408, Int. CI. G01S 13/08. “Microwave Apparatus and Method for ullage Measurement of Agitated Fluids by Spectral Averaging,” B. R. Jean and G. L. Warren. No. 999680. Filed December 31, 1992; date of patent June 14, 1994.
- [35] Bialkovski, M. E., and S. S. Stuchly, “A Study into a Microwave Liquid Level Gauging System Incorporating a Surface Waveguide as the Transmission Medium,” *Singapore ICCS’94. Conference Proceedings*, Vol. 3, 1994, p. 939.
- [36] Stuchly, S., et al., “Microwave Level Gauging System,” *10th International Microwave Conference MIKON-94*, Vol. 2, Poland, 1994, p. 530.
- [37] Stolle, R., H. Heuermann, and B. Schiek, “Novel Algorithms for FMCW Range Finding with Microwaves,” *Microwave Systems Conference IEEE NTC’95*, 1995, p. 129.
- [38] U.S. Patent 5387918, Int. CI. G01S 13/32. “Method and an Arrangement for Measuring Distances Using the Reflected Beam Principle,” W. Wiesbeck, J. Kehrbeck, and E. Heidrich. No. 956882. Filed April 15, 1992; date of patent February 7, 1995.
- [39] U.S. Patent 5406842, Int. CI. G01F 23/28. “Method and Apparatus for Material Level Measurement Using Stepped Frequency Microwave Signals,” J. W. Locke. No. 132981. Filed October 7, 1993; date of patent April 18, 1995.
- [40] Vossiek, M., et al., “Novel FMCW Radar System Concept with Adaptive Compensation of Phase Errors,” *26th EuMC*, Prague, Czech Republic, 1996, p. 135.
- [41] Stolle, R., and B. Schiek, “Precision Ranging by Phase Processing of Scalar Homodyne FMCW Raw Data,” *26th EuMC*, Prague, Czech Republic, 1996, p. 143.
- [42] Chengge, Z., et al., “A Method for Target Estimation of Level Radar,” *International Conference of Radar Proceedings (ICR’96)*, Beijing, China, 1996, pp. 270–273.
- [43] U.S. Patent 5504490, Int. CI. G01S 13/08. “Radar Method and Device for the Measurement of Distance,” J. -C. Brendle, P. Cornic, and P. Crenn. No. 414594. Filed March 31, 1995; date of patent April 2, 1996.
- [44] U.S. Patent 5546088, Int. CI. G01S 13/18. “High-Precision Radar Range Finder,” G. Trummer and R. Korber. No. 317680. Filed October 5, 1994; date of patent August 13, 1996.
- [45] Weib, M., and R. Knochel, “Novel Methods of Measuring Impurity Levels in Liquid Tanks,” *IEEE MTT-S International Microwave Symposium Digest*, Vol. 3, 1997, pp. 1651–1654.
- [46] Weib, M., and R. Knochel, “A Highly Accurate Multi-Target Microwave Ranging System for Measuring Liquid Levels in Tanks,” *IEEE MTT-S International Microwave Symposium Digest*, Vol. 3, 1997, pp. 1103–1112.
- [47] Kielb, J. A., and M. O. Pulkrabek, “Application of a 25 GHz FMCW Radar for Industrial Control and Process Level Measurement,” *IEEE MTT-S International Microwave Symposium Digest*, Vol. 1, 1999, pp. 281–284.
- [48] Patent 2126145 (Russian Federation), INT.CI. G01F 23/284. “Level-Meter,” S. A. Liberman, et al., No. 97114261/28. Bull. No. 4. Filed August 20, 1997; published October 2, 1999.
- [49] Bruimbi, D., “Low Power FMCW Radar System for Level Gauging,” *2000 IEEE MTT-S International Microwave Symposium Digest*, Vol. 3, 2000, pp. 1559–1562.
- [50] Zhukovskiy, A. P., E. I. Onoprienko, and V. I. Chizhov, *Theoretical Fundamentals of Radio Altimetry*, Moscow, Russia: Sovetskoe Radio Publ., 1979. [In Russian.]

- [51] Finkelstein, M. I., *Fundamentals of Radar*, 2nd ed., Moscow, Russia: Radio i Sviaz Publ., 1983. [In Russian.]
- [52] Sheluhin, O. I., *Short-Range Radio Systems*, Moscow, Russia: Radio i Sviaz Publ., 1989.
- [53] Skolnik, M., *Introduction to Radar Systems*, 3rd ed., New York: McGraw-Hill, 1981.
- [54] Brumbi, D., *Fundamentals of Radar Technology for Level Gauging*, 3rd rev., Duisburg: Krohne Messtechnik, 1999.
- [55] Bakulev, P. A., *Radar Systems*, Moscow, Russia: Radiotekhnika Publ., 2004. [In Russian.]
- [56] Komarov, I. V., and S. M. Smolskiy, *Fundamentals of Short-Range FMCW Radar*, Norwood, MA: Artech House, 2003.
- [57] Atayants, B. A., et al., “Precision Industrial Systems of FMCW Short-Range Radar Technology: Truncation Measurement Error and Its Minimization,” *Uspekhi sovremennoi radioelektroniki*, No. 2, 2008, pp. 3–23. [In Russian.]
- [58] Atayants, B. A., et al., “Noise Problem and Non-Linearity of Transmitter Modulation Characteristic in Precision Industrial Short-Range FMCW Radar Systems,” *Uspekhi sovremennoi radioelektroniki*, No. 3, 2008, pp. 3–29. [In Russian.]



# Counting Method of Estimation of Difference Frequency

## 1.1 Introduction

The measurement of a range with the help of a radar operating with a continuous *frequency modulation* (FM) signal can be implemented in different ways [1–6]. One of the many possible ways is by using a range-finder, allowing the provision of theoretical examination and obtaining the calculations necessary for working with upcoming sections of this book, as shown in Figure 1.1. The generator of the transmitted SHF signal excites a transmitting antenna and simultaneously forms a local oscillator signal for the mixer of a receiving section. The interaction of the transmitted (local oscillator) and reflecting signals happens in the mixer, and at its output a useful signal is formed at which frequency is connected with the measured range. The *difference-frequency signal* (DFS) is amplified and goes to a frequency meter and to a range meter. A modulator serves to provide the FM of the transmitted signal. In the structure of a radar-measuring system, the frequency measurement of the limited sample of the continuous sinusoidal DFS is the main measuring operation in the frequency-modulated continuous wave (FMCW).

The simplicity and physical transparency of all stages of useful signal processing and, at first glance, well-studied methods for the frequency measurement ensure a high reliability of the counting method.

Let us examine carefully the traditional methods used at the signal generation and processing in the FMCW range-finder (RF) and in the analysis of its operation. The aim of this examination is to reveal those factors that are not important for rough (traditional) measurements but take on special significance when we have a need for high accuracy.

## 1.2 Main Calculation Relations

Let us examine DFS processing, drawing attention to only the key aspects that we will use later in the book.

In the circuit of Figure 1.1, some monotonous periodic function  $\omega_{\text{mod}}(t) = 2\pi f_{\text{mod}}(t)$  with the period  $T_{\text{mod}}$ , for instance, sinusoidal or saw-tooth, is usually used for modulation. The radian frequency of an emitted signal varies within  $2\pi f_1 \leq \omega \leq 2\pi f_2$  according to the law:

$$\omega(t) = 2\pi f(t) = \omega_0 + \omega_{\text{mod}}(t) = 2\pi[f_0 + f_{\text{mod}}(t)] \quad (1.1)$$

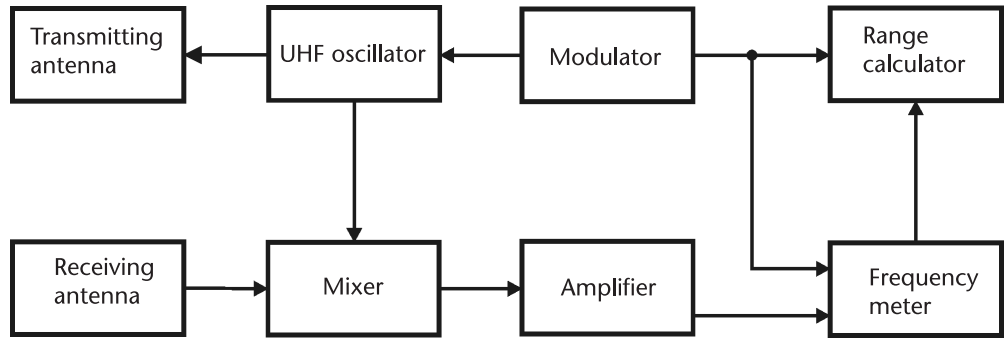


**Figure 1.1** Block diagram of the simplest frequency-modulated range-finder.

where  $\omega_0 = 2\pi f_0$  is the carrying (central) frequency of the transmitted signal and  $f_{\text{mod}}(t)$  is the time function reflecting the law of frequency variation in time. Then the FM sweep of the radian frequency is:

$$\Delta\omega = \omega_2 - \omega_1 = 2\pi(f_2 - f_1) = 2\pi\Delta F \quad (1.2)$$

Here  $\Delta F = f_2 - f_1$  is the difference of extreme frequencies of the FM sweep. As a modulating function, the following functions are most often used [1, 3, 6, 7]:

- Saw-tooth modulation with zero reverse trace:

$$f_{\text{mod}}(t) = \Delta F(t - iT_{\text{mod}})/T_{\text{mod}}, \quad iT_{\text{mod}} \leq t \leq (i+1)T_{\text{mod}}; \quad (1.3)$$

- Symmetric triangular:

$$f_{\text{mod}}(t) = \begin{cases} 2\Delta F(t - iT_{\text{mod}})/T_{\text{mod}} & \text{for } iT_{\text{mod}} \leq t \leq 0.5(2i+1)T_{\text{mod}} \\ 2\Delta F[(i+1)T_{\text{mod}} - t]/T_{\text{mod}} & \text{for } 0.5(2i+1)T_{\text{mod}} \leq t \leq (i+1)T_{\text{mod}} \end{cases} \quad (1.4)$$

- Sinusoidal:

$$f_{\text{mod}}(t) = 0.5\Delta F \sin(2\pi(i+1)/T_{\text{mod}}) \quad (1.5)$$

where  $i = 0, 1, \dots$

After delay time  $t_{\text{del}}$  caused by wave propagation time to the object under investigation and back, the reflected signal passes to the mixer together with the small part of the radiated signal power. The DFS on the mixer output is:

$$u_{\text{dif}}(t) = A_{\text{dif}} \cos \varphi_{\text{dif}}(t) \quad (1.6)$$

where  $A_{\text{dif}}$  and  $\varphi_{\text{dif}}(t)$  are the DFS amplitude and the relative DFS instantaneous phase. The instantaneous phase of the DFS according to (1.1) is equal:

$$\varphi_{\text{dif}}(t) = \int_{t-t_{\text{del}}}^t \omega(t) dt + \varphi_s = \omega_0 t_{\text{del}} + \int_{t-t_{\text{del}}}^t \omega_{\text{mod}}(t) dt + \varphi_s \quad (1.7)$$

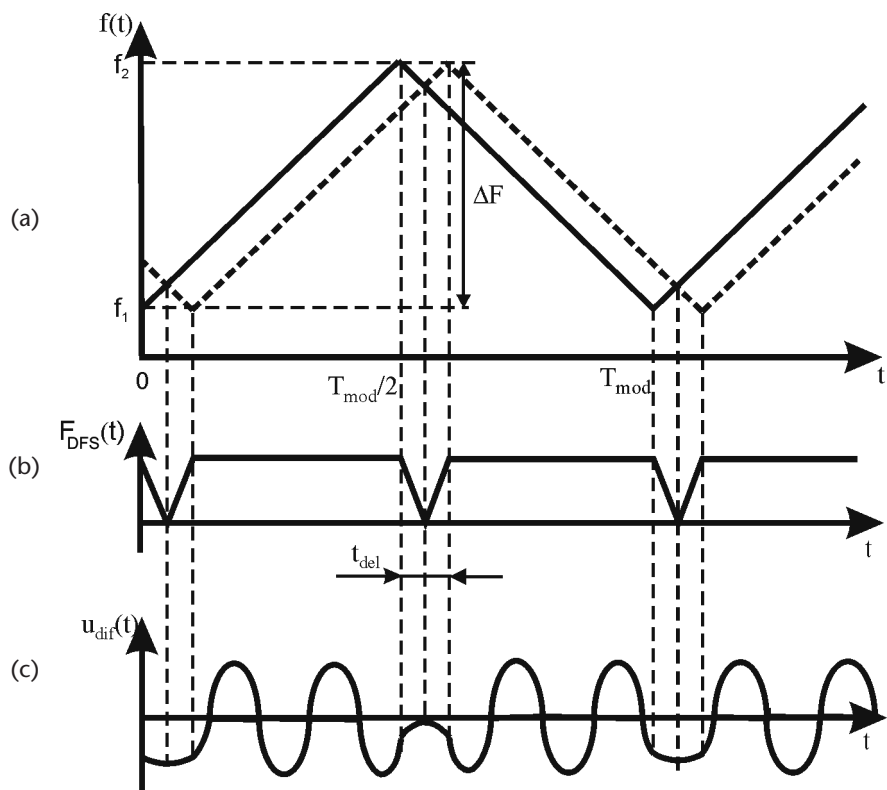
where  $\varphi_s = \varphi_{rf} + \varphi_{pp}$ ,  $\varphi_{rf}$  is some phase of the complex reflection factor from the object, and  $\varphi_{pp}$  is the additional phase shift arising in the circuit of preliminary processing.

Figure 1.2(a) shows diagrams of radiated signal frequency  $f(t)$  variations (solid curve) for symmetric triangle modulation and received delayed signal frequency  $f_{rec}(t)$  (dotted curve) in time. The time function of the difference frequency  $F_{DFS} = |f(t) - f_{rec}(t)|$  is presented in Figure 1.2(b) and the appropriate DFS is presented in Figure 1.2(c). The difference frequency is constant (at the fixed object and the radar) during larger part of the modulation period, and the frequency sharply changes in the short intervals with width  $\pm t_{del}/2$  near intersect points of plots in Figure 1.2, which is repeated every half of the period modulation. These narrow time intervals between signal extremes are called *zones of inversion* [1].

Usually in the short-range radar, the condition  $t_{del} \ll T_{mod}$  is satisfied. In this case, the inversion zone duration in Figure 1.2 becomes negligibly small for analysis. As a result, DFS represents the burst of sine oscillations with duration equal approximately to  $T_{mod}/2$  with a carrier frequency proportional to the measuring range and with phase jumps in the inversion zone [1].

Because the function  $\omega(t)$  in (1.7) changes slowly, the integration result can be approximately written in accordance with the mean value theorem [8] as:

$$\varphi_{dif}(t) = \omega_0 t_{del} + \omega_{mod}(t - 0.5t_{del})t_{del} + \varphi_s \quad (1.8)$$



**Figure 1.2** Graphs of (a) the radiated signal (solid curve), received (dotted curve) signal, (b) DFS, and (c) the output signal of the mixer.

Thus, the law of the DFS phase variation under these assumptions coincides approximately with the law of frequency variation of the transmitted signal, except within the inversion zones. Difference is observed only in inversion zones.

Neglecting in (1.8) by insignificant delay  $t_{\text{del}}/2$ , we examine the plot of the phase  $\varphi_{\text{dif}}(t)$  (1.8) and the appropriate DFS shown in Figure 1.3(a, b) for the case: symmetric linear triangular modulation (1.4), fixed range to the target, and, for distinctness, for  $\varphi_s = 0$ .

The horizontal lines in Figure 1.3(a) correspond to the phase values:

$$\varphi_{\text{dif}} = (n + 0.5)\pi, n = 0, 1, 2 \dots \quad (1.9)$$

The instantaneous DFS value at these phase values becomes zero. Therefore, these points of the graph are called *DFS zeros* [2]. They are concerned to distinctive DFS points. The time moment, where the instantaneous DFS value achieves the extreme values, is another type of typical points. Distinctive points of one type are time-shifted by the DFS half-period.

The DFS from the mixer output passes to the frequency meter. Traditionally, the frequency measurement is provided by means of counting of DFS zero number during some time interval. The value obtained is the basis of range calculation.

The instantaneous value of the difference frequency is [1, 5]:

$$F_{\text{DFS}}(t) = \frac{1}{2\pi} \frac{d\varphi_{\text{dif}}}{dt} = \frac{t_{\text{del}}}{2\pi} \frac{d\omega(t)}{dt} = t_{\text{del}} f'(t) \quad (1.10)$$

where the upper stroke designates, as usual, the first time derivative.

The frequency meter determines its average value  $F_R$ , which is proportional to the  $R$  range, over some time interval. Due to modulation periodicity, the average interval is equal to the half-period of modulation. For this, synchronization pulses

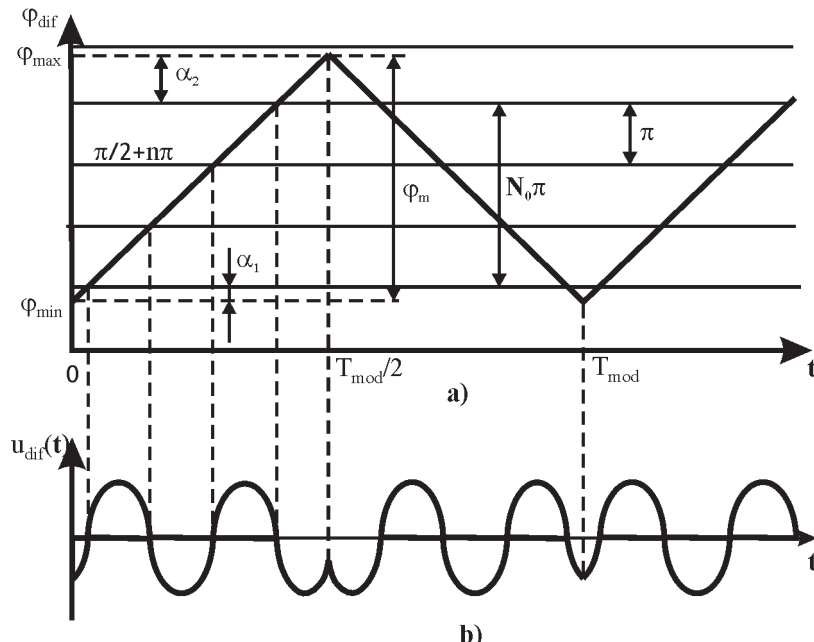


**Figure 1.3** Graphical representation of (a) the phase and (b) DFS.

from a modulator specified margins of the modulation period pass to the frequency meter and a range calculator in Figure 1.1.

In this case, at the symmetric triangular modulation law (1.4) with consideration of (1.10) we can write the value of the average value of difference frequency as:

$$F_R = \frac{2t_{\text{del}}}{T_{\text{mod}}} \int_{t_{\text{min}}}^{t_{\text{min}} + T_{\text{mod}}/2} f'(t) dt = \frac{t_{\text{del}}}{\pi T_{\text{mod}}} (\omega_2 - \omega_1) \quad (1.11)$$

where  $t_{\text{min}}$  is any current moment of the signal frequency equality to the value  $\omega_1$ . This equation remains true at other FM laws as well [1]. Thus, for the chosen measurement method, the average DFS frequency value is connected linearly with  $t_{\text{del}}$  and in the first approximation does not depend upon the modulation law.

Taking into account that  $t_{\text{del}} = 2R/c$ , where  $R$  is the measuring range and  $c$  is the propagation speed of the electromagnetic wave in the medium, we find out the formula for the range:

$$R = \frac{c T_{\text{mod}} F_R}{4 \Delta F} \quad (1.12)$$

Thus, the measuring range is proportional to the modulation period, the light speed, and the difference frequency, and it is inversely proportional to the quadruplicate range of the FM sweep.

### 1.3 The Traditional Counting Method of Range Measurement

The product  $T_{\text{mod}} F_R$  in the numerator of (1.12) factually corresponds to the number of DFS periods, which are stacked in the modulation period. If we use the counting method [1, 4] to measure the difference frequency, then we obtain in the numerator of (1.12) the integer number  $N_{\text{DFS}}$  of the DFS periods:

$$N_{\text{DFS}} = \text{Int}(T_{\text{mod}} F_R) \quad (1.13)$$

where  $\text{Int}(\cdot)$  is the operation of calculation of the integer part of a number and (1.12) takes a form:

$$R = \frac{c N_{\text{DFS}}}{4 \Delta F} \quad (1.14)$$

The calculation result according to (1.14) changes discretely, and the QI  $\delta_R$  is:

$$\delta_R = \frac{c}{4 \Delta F} \quad (1.15)$$

The practical number of zeros  $N_{\text{DFS}}$  falling into the average interval depends not only upon  $F_R$  but upon the product  $\omega_0 t_{\text{del}}$ , which is included in (1.7) and determines a position of the lower point of phase plot in Figure 1.3(a):

$$\varphi_{\text{min}} = \omega_0 t_{\text{del}} + \varphi$$

It is easy to show that the true number of DFS zeros between two adjacent phase extremes is determined by the following equation [9]:

$$\begin{aligned}
 N &= \text{Int}\left(\frac{4R}{\lambda_2} + \frac{\varphi_s}{\pi} - 0.5\right) - \text{Int}\left(\frac{4R}{\lambda_1} + \frac{\varphi_s}{\pi} - 0.5\right) \\
 &= \text{Int}\left(\frac{4R}{\lambda_1} + \frac{R}{\delta_R} + \frac{\varphi_s}{\pi} - 0.5\right) - \text{Int}\left(\frac{4R}{\lambda_1} + \frac{\varphi_s}{\pi} - 0.5\right)
 \end{aligned} \tag{1.16}$$

where  $\lambda_2$  and  $\lambda_1$  are, respectively, a wavelength of the carrier oscillation on the upper and lower frequencies on the FM sweep. Figure 1.4 shows functions of the number of zeros  $N_{DFS}$  (thick curve) and  $N$  (thin curve) versus the normalized range  $R/\delta_R$  for  $f_0 = 10$  GHz and  $\Delta F = 1$  GHz drawn according to (1.13) and (1.16), respectively.

As the distance varies continuously over intervals of ED, the number of zeros jumps from  $N_{DFS}$  to  $N_{DFS} + 1$ . The period of such variation is a quarter-wavelength of the carrier oscillation.

From the formula (1.12), we can obtain one more equivalent equation:

$$R = \frac{c\Delta\Phi}{2\Delta\omega} \tag{1.17}$$

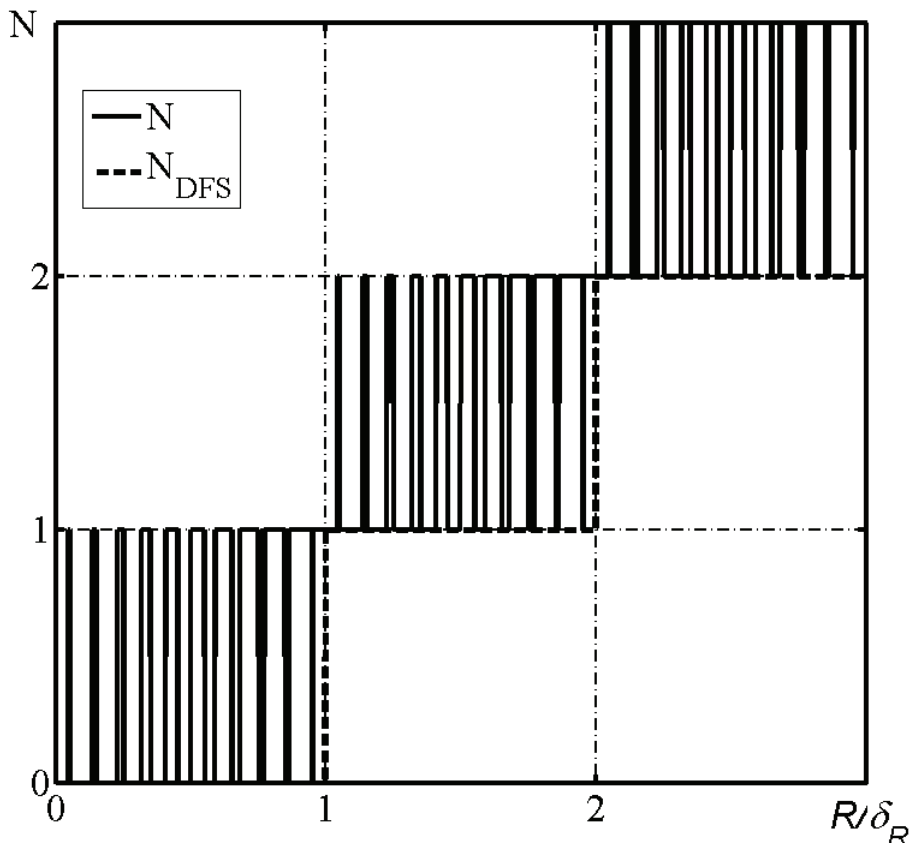


**Figure 1.4** The function of the number of DFS zeros versus the normalized range.

where  $\Delta\Phi = \pi T_{\text{mod}} F_R$  is the DFS phase shift in radians on the appropriate modulation branch. Sometimes, this equation can be useful for an understanding of the processes that occurred.

## 1.4 Sources of Range Measurement Errors by the FMCW Range-Finder

In accordance with formula (1.12) and assuming the independence of included items, the relative variance of the total error of range measurement error  $\bar{\sigma}_R^2$  can be written as [5, 10]:

$$\bar{\sigma}_R^2 = \bar{\sigma}_{\text{sp}}^2 + \bar{\sigma}_{T_{\text{mod}}}^2 + \bar{\sigma}_{\Delta F}^2 + \bar{\sigma}_{F_R}^2 \quad (1.18)$$

where  $\bar{\sigma}_{\text{sp}}^2$ ,  $\bar{\sigma}_{T_{\text{mod}}}^2$ ,  $\bar{\sigma}_{\Delta F}^2$ ,  $\bar{\sigma}_{F_R}^2$  are, accordingly, the relative variances of propagation speed of the electromagnetic wave, of the modulation period, of the FM sweep and of the estimated difference frequency.

Usually, at rough measurements, the propagation speed of the electromagnetic wave in the medium is assumed to be constant and independent upon external conditions. However, when we discuss the high-precision measurements, we must take into consideration its variation at the change of pressure and temperature [11, 12]. These variations have a systematic character, and they can be easily taken into account by introducing compensating corrections at the calculation performance. Therefore, in this book we assume that the propagation speed of the electromagnetic wave in the medium is the constant quantity and then  $\bar{\sigma}_{\text{sp}}^2 = 0$ .

The formation error of the required modulation period  $T_{\text{mod}}$  can be easily made small enough and, therefore, we shall not consider it.

The third component  $\bar{\sigma}_{\Delta F}^2$  is connected with the maintenance of the unchanged value of the FM sweep of the transmitter. This is a rather complicated scientific and engineering problem. The modern FMCW oscillators are based on the principle of the varactor FM sweep [13, 14]. The nonlinearity of the MC is principally peculiar to such oscillators. Therefore, it is difficult to accurately settle the required FM sweep for the analog way of providing modulation. Often, it is not required at all because the device calibration is usually provided. Nevertheless, at the environment temperature variation (or for other external factors), the MC nonlinearity changes that leads to a variation of the FM sweep. These MC variations cannot be considered exactly because they may have the hysteresis character and are individual for each radar's measuring system. Due to this reason, in RF for increase accuracy, it is necessary to examine the influence of the instability of the FM sweep.

In a number of cases, the stabilization problems of the modulation period and the FM sweep of the transmitter happen to be interrelated. For example, it takes place at the range calculation performance according to the equation equivalent to (1.12):

$$R = \frac{cF_R}{2K_f} \quad (1.19)$$

where  $K_f = 2\Delta F/T_{\text{mod}}$  is a slope of transmitter frequency's variation, which is maintained unchanged.

The fourth error component  $\bar{\sigma}_{F_R}^2$ , which is determined by the accuracy of the difference frequency measurement, is the most important for our tasks. To achieve high accuracy, we must use different MQIS.

Frequency measurement time (time of analysis) can be different. The least time of analysis is equal to a half-period of modulation. Therefore, the inversion zone is omitted from consideration and we discuss the frequency measurement of the radio pulse. An increase of analysis time due to any reason leads to the fact that we should measure the average frequency of the phase-shift keyed radio signal. It leads to an increase in additional errors.

The restricted sample volume, according to which the frequency estimate is provided, as we often discuss the range measurement commensurable with the QI value, is the significant peculiarity of these measurements, which hampers obtaining high accuracy. For small ranges, only four to six DFS periods and less can be formed during the one modulation period. Under these conditions, we may achieve high accuracy of frequency measurement only in the case when, during the analysis time interval, the measuring frequency does not change. In the FMCW range-finder, this means that the one of the reasons of the difference frequency measurement error is nonlinearity of the SHF frequency variation of the transmitter. The MC nonlinearity or the influence of the SHF signal reflected from a target upon the FMCW oscillator [15]\* can be a source of this error component.

The noise of the first stages of the receiver, the phase noise of the transmitter, and the interference presence in the received signal are evident and well-known reasons for an increase in measurement error. The SRs located in the operation zone of the FMCW RF are these interference sources.

The PAM of DFS increases because of the nonideality of frequency responses of the SHF oscillator and main units of the SHF path and is one more error source.

Even for ideal conditions of DFS generation and processing, the measurement error occurs peculiar to each MQIS, which is called the *truncation error* [6]. Later we will discuss problems of minimization of this component of the range measurement error.

## 1.5 Adaptive Control of Frequency Modulation Parameters

Periodicity of the modulation law of the transmitted FM signal leads to the fact that the DFS takes a form of the phase-shift keyed oscillation, in which at the boundaries of the modulation half-period, the phase jumps happen (Figure 1.2). The value of this jump depends upon the measuring range and when the last varies, the value periodically changes within the limits from  $0^\circ$  to  $180^\circ$  with a length period equal to a half-wavelength of the carrier oscillation. Such a DFS property forces the limitation of the difference frequency measurement time by the only one half-period of modulation  $T_{\text{meas}} = T_{\text{mod}}/2$ . Moreover, this property does not permit to provide the narrowband DFS filtering, which is necessary to improve the signal/noise ratio (SNR). At large values of the phase jump, the narrowband filtering leads to DFS PAM with a decrease

\* Sometimes this influence can be taken into account in the form of the “autodyne” effect, which is typical for the self-oscillating mixers.

of the DFS amplitude in the inversion zone down to zero (at the phase jump by  $180^\circ$ ), and, as a result, the total SNR decreases in these time intervals.

It is possible to eliminate this phenomenon providing optimization (adaptation) of the FMCW RF signal's generation and processing. Therefore, it is necessary to control the frequency modulation parameters in such a manner to provide the absence of the DFS phase jumps when using the periodic FM. Accordingly, the DFS takes the form of the continuous sine signal. As a result, we can increase the DFS processing interval by reducing the QI of the DFS period counting down to accepted value.

To ensure optimal control by the modulating voltage, it is necessary at first to formulate the optimality criterion. We assume as such a criterion the absence of DFS phase jumps using the periodic FM. In accordance with (1.8), the DFS phase on the receiver output can be written as:

$$\varphi_{\text{dif}}(t) = \omega_0 t_{\text{del}} + \omega_{\text{mod}}(t)_{\text{del}} + \varphi_s \quad (1.20)$$

At the formulation of the condition of the DFS phase jump absence, it is necessary to take into consideration the property of such a signal, which is that its plot is symmetric with respect to a center of the inversion zone (Figure 1.2). The absence of the DFS phase jump corresponds to the equality of the DFS time derivatives calculated in the near vicinity from right and left of the inversion zone:

$$\left. \frac{du_{\text{dif}}(t)}{dt} \right|_{t=n\frac{T_{\text{mod}}}{2}-0} = \left. \frac{du_{\text{dif}}(t)}{dt} \right|_{t=n\frac{T_{\text{mod}}}{2}+0}, \quad n = 0, 1, 2, \dots \quad (1.21)$$

Phase jump absence at changing the sign of the function's  $\omega_{\text{mod}}(t)$  derivative on the boundaries of modulation half-periods corresponds to the DFS extreme presence in these points. Hence, the integer number of the DFS half-periods should be stacked in the modulation half-period. At the variation of the range  $R$ , this can be performed by only changing appropriately the carrier frequency  $\omega_0$  and the frequency deviation  $\Delta\omega$ .

In particular, we can control by the moment of the current modulation half-period's finishing so that this moment would coincide with the one from the DFS extremes [16]. In connection with the fact that many DFS extremes can be on the modulation half-period, it is necessary to put additional limitations, for instance, on the minimal value  $\Delta f_{\min}$  of the transmitter. To limit the FM sweep, we may control boundary frequencies at frequency  $f(t)$  variations of the transmitted signal with the help of standard lower and upper frequencies:  $\omega_{\text{st1}} = 2\pi F_{\text{st1}}$  and  $\omega_{\text{st2}} = 2\pi F_{\text{st2}}$  specified by some simple way. For example, for this we can use *dielectric resonators* (DR) tuned on these frequencies. Then  $\Delta F_{\min} = F_{\text{st2}} - F_{\text{st1}}$ . We can interrupt the modulation half-period only in the moment of DFS extreme appearance after achievement of one of specified values [17] by the frequency of the transmitted signal. The logic function  $V_{\text{con}}(t)$  of modulation voltage control has, in this case, a form:

$$V_{\text{con}}(t) = \begin{cases} 0 & \text{for } t \leq 0.5(2j-1)NT_R \quad \text{and} \quad f(t) \leq F_{\text{st2}} \\ 1 & \text{for } t \leq jNT_R \quad \text{and} \quad f(t) \geq F_{\text{st1}} \end{cases} \quad (1.22)$$

where  $j = 1, 2, 3, \dots$  is a number of the current modulation period,  $T_R = 1/F_R$ . As a result of the above-mentioned procedure performance, phase jumps in the DFS will be eliminated, which takes a form of the continuous sinusoid. This process can be conditionally called the *DFS phase joining*.

The function on DFS phase variations, the DFS plot in the mode of the phase joining, and the logic function  $V_{\text{con}}$  of the modulation control voltage versus time for limitation of the FM sweep of the transmitter are shown in Figure 1.5.

In the mode of the DFS phase joining, the modulation period  $T_{\text{mod}}$  and the FM sweep  $\Delta\omega$  cease to be constants and depend upon the measurement range. These functions are included in the calculation formula (1.9) for the range. The smooth decrease of the range leads to a smooth increase of  $T_{\text{mod}}$  from the minimal range  $2T_{\min}$  to the maximal  $2T_{\min} + T_R$  [17–20]. Accordingly, the FM sweep of the transmitter increases. Then, at the range where the modulation half-period duration achieves the maximal value, the jump returns in the modulation period to its minimum because of transition of the phase joining point to the adjacent DFS extreme located in the time interval  $T_{\min}$ . Exactly in the same manner the FM sweep decreases by a jump. The smooth increase of the range gives birth to the inverse process.

At the nonlinear MC of the transmitter, it is necessary to stabilize the average slope of its frequency variation [21]. For this we need, besides a limitation of the FM sweep by the value  $\Delta F_{\min}$ , to stabilize the operating time interval  $T_{\min}$ , during which the transmitter frequency is inside of this range.

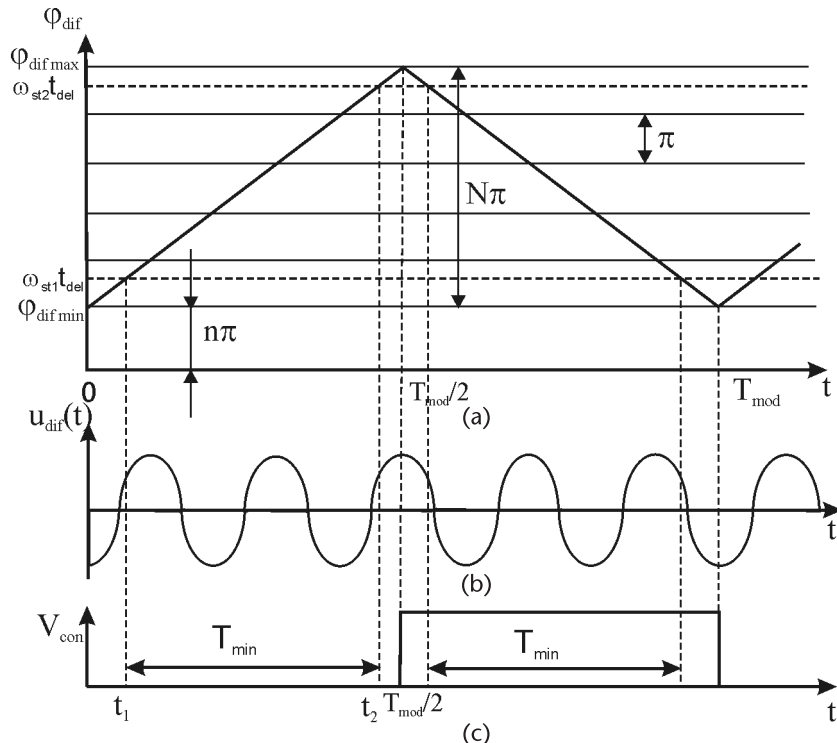


**Figure 1.5** (a) DFS phase, (b) DFS itself, and (c) the control function for limitation of the FM sweep.

We can ensure the stability of the average slope of frequency variations of the transmitted signal in the interval between standard frequencies by the time interval  $T_{\min}$  adjustment between moments  $t_1$  and  $t_2$ , corresponding to equality of the instantaneous phase to DFS values  $\omega_{st1}t_{del}$  and  $\omega_{st2}t_{del}$ . Therefore, discrete regulation is provided. The measurement of the duration  $T_{\min}$  is carried out during one modulation period, and its comparison with the standard meaning  $T_{st}$  and the appropriate variation of modulating voltage is provided at the end of this measuring half-period. The obtained amplitude value remains constant during the entire next period until the new correction performance. It can be written in an analytical form as:

$$U_{mod}^j = U_{mod}^{j-1} \left[ 1 + K_{amp} (T_{\min}^{j-1} - T_{st}) \right] \quad (1.23)$$

where the index  $j$  corresponds to the number of the current period, and  $K_{amp}$  is a coefficient defining the sensitivity of the modulating voltage amplitude to the deviation of operating time interval duration from the specified value. With this adjustment, the value  $T_{st}$  factually gives the lower boundary of  $T_{mod}$ .

Therefore, the range calculation is performed according to the formula:

$$R = \frac{cN_{per}}{2K_{f,st} T_{meas}} = \frac{\delta_{R,st} 2T_{st} N_{per}}{T_{meas}} \quad (1.24)$$

where  $K_{f,st} = \Delta F_{\min}/T_{st}$ ; and  $N_{per}$  is a number of DFS periods calculated during measuring time interval  $T_{meas}$ , requirements of which are given as:

$$\delta_{R,st} = c/(4\Delta F_{\min})$$

We can find the function of the modulation period versus a range caused by the described adaptation. Transferring the time origin in the point corresponding to the equality of the instantaneous phase of the radiated signal and the value  $\omega_{st1}t_{del}$  in Figure 1.5(a), we can obtain the function of the relative modulation period  $\Theta = T_{mod}/(2T_{st})$  versus a range according to the ratio of similar triangle sides with the same name:

$$\Theta = \frac{\delta_R}{R} \left[ 1 + \text{Int}\left(\frac{4R}{\lambda_{st2}}\right) - \text{Int}\left(\frac{4R}{\lambda_{st1}}\right) \right] \quad (1.25)$$

This function has a complex character. It reflects the above-mentioned fact [1] that in the time interval  $T_{mod}$  a number of DFS half-periods  $N_{DFS}$  or  $(N_{DFS} + 1)$  can be stacked. Therefore, the modulation period depends not only upon both the required normalized range and the ratio of the range and wavelengths corresponding to lower and upper standard frequencies. Figure 1.6 shows the function of the normalized modulation period  $\Theta$  versus relative range  $R/\delta_R$  drawn in accordance with (1.25) at  $F_{st1} = 10$  GHz,  $F_{st2} = 10.5$  GHz. These frequencies are used next for all calculations and simulation of signals and for their processing if we do not specially fix the other values.

A modulation period's duration continuously changes at range variation. We can observe fast and slow variations of the plot. Fast variations are caused by the sharp transposition of moments of phase “joining” at range variation by a quarter-wavelength in a point on the range scale corresponding to the DFS half-period

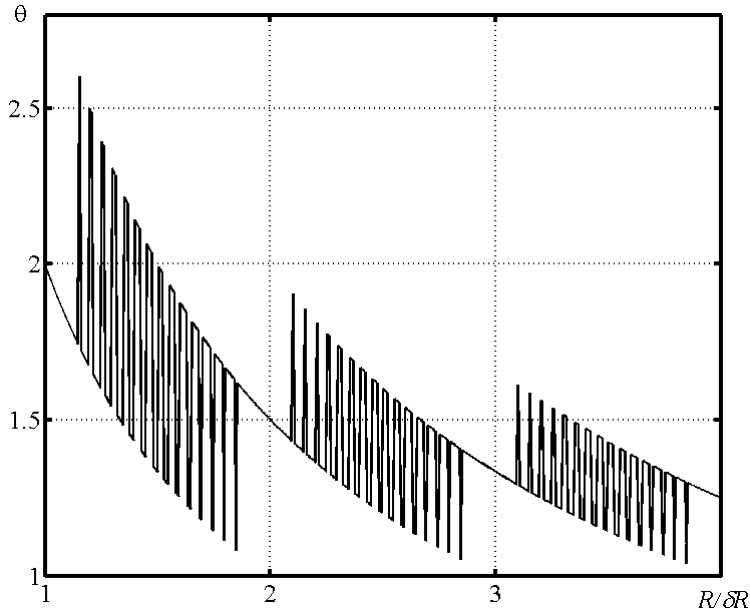


**Figure 1.6** The function of the normalized modulation period versus the relative range.

number variation from  $N_{DFS}$  to  $N_{DFS} + 1$  and vice versa. Slow variations are connected with smooth variation of the difference frequency.

If the modulation is performed so that the linear time-variation of the transmitted signal frequency is provided, the above-mentioned variations of the modulation period and the FM sweep do not adversely affect to calculation results. They are included in (1.9) in the form of ratio representing the slope of FM sweep of the transmitter.

We can manage without automatic regulation of the duration  $T_{\min}$  if performing the simple account of its current value at the range calculation. For this one can use (1.24), where we must substitute the current value of  $K_{f,op}$  instead of the constant value  $K_{f,st}$ :

$$K_{f,op} = \frac{\Delta F_{\min}}{T_{\min}} \quad (1.26)$$

The components from which the range measurement error is formed for the counting method are:

- The truncation error peculiar to the method under ideal conditions;
- Inaccuracy of  $u_{dif}(t)$  phase joining;
- Noise presence;
- MC nonlinearity of the SHF oscillator;
- Accuracy of the position's determination of frequency marks;
- Regulation accuracy of the reference time interval;
- Temperature variations of resonance frequencies of DR.

The influence of the last three reasons is evident and does not present a scientific interest. That is why the analysis of the first three components of the measurement error only will be conducted next.

## 1.6 Truncation Error of Range Measurement at the Adaptive Frequency Modulation

Let us consider a variant of the optimal modulation control in accordance with (1.22) for the stabilization of the time interval duration  $T_{\min}$ . The truncation error in this case is caused by two reasons: the discreteness of DFS period number counting and the pulling of signal  $u_{dif}(t)$  period in each point of phase joining. The result of their influence on the truncation error depends upon the way of the difference frequency measurement [21]. In this case we may use two methods:

- The DFS period number is calculated during the some fixed time interval.
- The DFS period number is calculated during the time interval, which is multiply to the modulation period (in the specific case during the one modulation half-period).

### 1.6.1 The Fixed Measuring Time Interval

Taking into account that the minimal value of the modulation period is  $2T_{st}$ , we designate as  $N_{\text{meas}}$  the ratio of the following time intervals:

$$N_{\text{meas}} = \frac{T_{\text{meas}}}{2T_{st}} \quad (1.27)$$

If phase joining is performed ideally, the DFS period number calculated during time  $T_{\text{meas}}$  is equal to the following value rounded to the integer value  $N_{\text{per}} = \text{Int}[F_R T_{\text{meas}} + 0.5]$ .

The pulling period of the signal  $u_{dif}(t)$  in each phase joining point leads to an increase in the error caused by the fact that after modulation voltage's transition from the forward path to the inverse path (and vice versa), the difference frequency passes through zero and one period by the delay value  $t_{\text{del}}$  of the delayed signal is prolonged [17]. This is shown in a deliberately distorted scale in Figure 1.7.

We can write the modulation period duration at the range variation in the following form taking into consideration pulling in the points of phase joining:

$$T_{\text{mod}} = \frac{2T_{st}\delta_{Rst}}{R} \left[ 1 + \text{Int}\left(\frac{4R}{\lambda_{st2}}\right) - \text{Int}\left(\frac{4R}{\lambda_{st1}}\right) \right] + 2t_{\text{del}} \quad (1.28)$$

As a result of pulling in the interval  $T_{\text{meas}}$ , the number of counted periods  $T_R$  will be less. We can determine the total number of counted periods during one modulation period  $N_{T_{\text{mod}}}$  from Figure 1.7:

$$N_{T_{\text{mod}}} = 2F_R(0,5T_{\text{mod}} - t_{\text{del}}) = 1 + \text{Int}\left(\frac{4R}{\lambda_{st2}}\right) - \text{Int}\left(\frac{4R}{\lambda_{st1}}\right) \quad (1.29)$$

During  $T_{\text{meas}}$ , the number of DFS periods  $N_{T_{\text{mod}}}$  can be calculated by rounding:

$$N_{\text{per}} = N_{T_{\text{meas}}} = \text{Int}\left(\frac{N_{T_{\text{meas}}}T_{\text{meas}}}{T_{\text{mod}}} + 0.5\right) \quad (1.30)$$

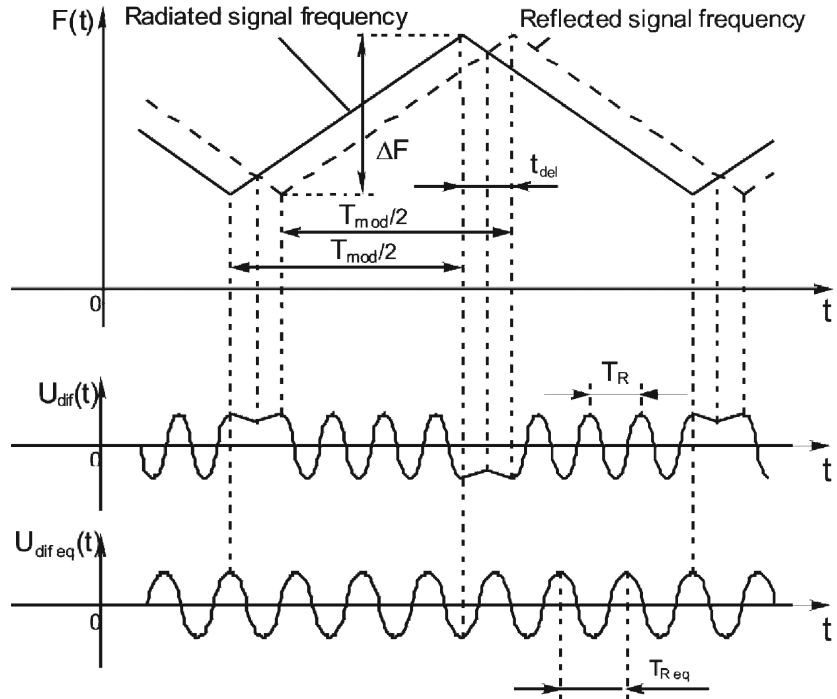


Figure 1.7 Pulling of a DFS period in the points of phase joining.

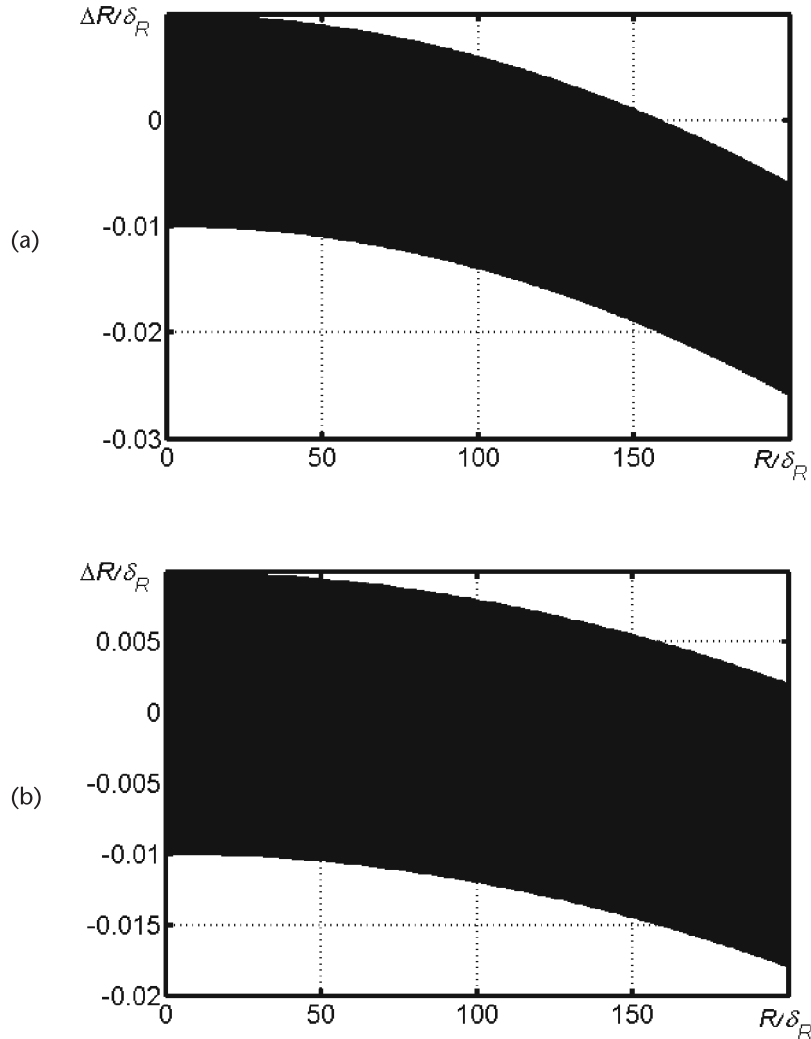
Now we can estimate the difference frequency  $F_R = N_{\text{per}}/T_{\text{meas}}$ , substitute it in (1.13), and, having normalized parameters to QI, obtain the normalized truncation error versus the normalized range:

$$\frac{\Delta R}{\delta_{Rst}} = \frac{\text{Int} \left\{ \frac{N_{\text{meas}}}{1/x + x/(2\Delta F_{\min} T_{\text{st}} N_{T_{\text{mod}}})} + 0.5 \right\} - x}{N_{\text{meas}}} \quad (1.31)$$

where  $x = R/\delta_{Rst}$  is the normalized range.

The general view of this function at  $N_{\text{meas}} = 50$  is shown in Figure 1.8(a) for  $2\Delta F_{\min} T_{\text{st}} = 2,500,000$  and in Figure 1.8(b) for  $2\Delta F_{\min} T_{\text{st}} = 5,000,000$ .

The error in a complicated manner depends upon the number of processed periods  $N_{\text{meas}}$ , the product  $2\Delta F_{\min} T_{\text{st}}$ , and the magnitude of the FM sweep influencing  $N_{T_{\text{mod}}}$  and  $\delta_{Rst}$ . In a used plot scale, fast error variations caused by counting discreteness run into the complete band, in which the width is defined by the value of  $N_{\text{meas}}$ . An increase of the product  $2\Delta F_{\min} T_{\text{st}}$  leads to a reduction of the maximal truncation measurement error at a large range. Nevertheless, it is impossible to increase infinitely  $2\Delta F_{\min} T_{\text{st}}$  because of the physical possibilities of used SHF oscillators and due to restrictions of the measurement interval duration caused by system dynamics. Therefore, it is expedient to fix  $T_{\text{meas}}$  on an acceptable level and to perform such a choice of FM sweep and a number of processed periods  $N_{\text{meas}}$ , which ensures the required measurement error.



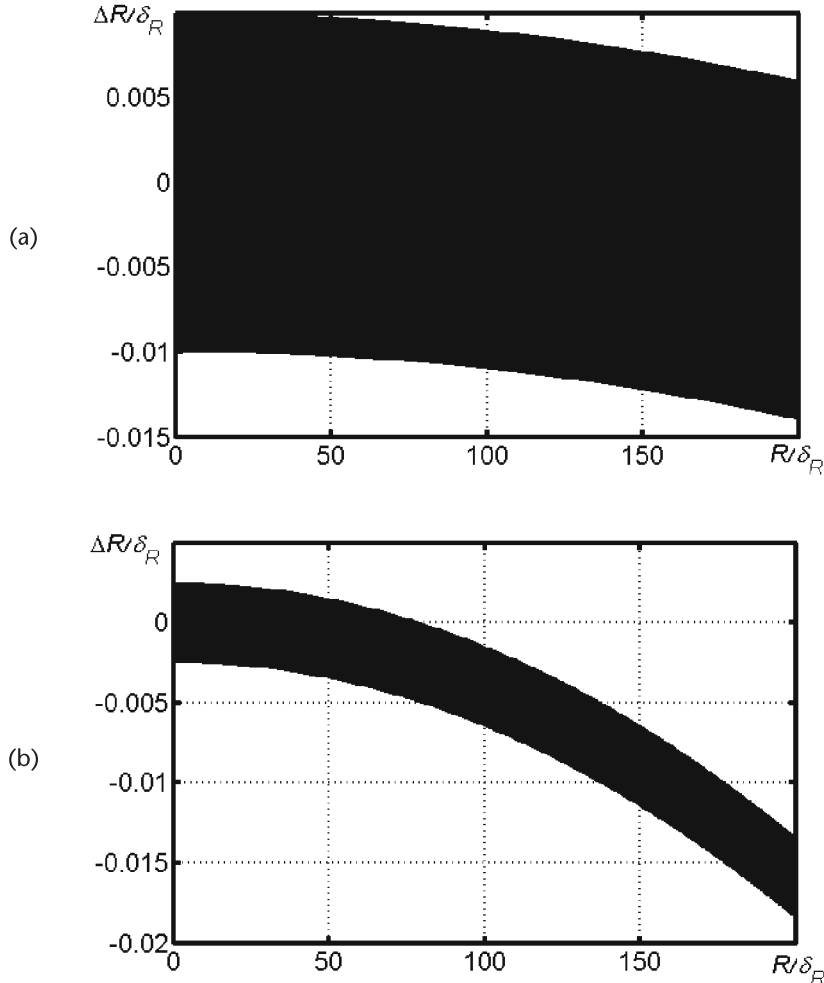
**Figure 1.8** The relative truncation error at  $N_{\text{meas}} = 50$  for (a)  $2\Delta F_{\min} T_{st} = 2,500,000$  and (b)  $2\Delta F_{\min} T_{st} = 5,000,000$ .

Figure 1.9 shows plots of the function of the relative measurement truncation error function versus the normalized range for  $T_{\text{meas}} = 1$  second at  $\Delta F_{\min} = 500$  MHz and for two values of  $N_{\text{meas}} = 50$  [Figure 1.9(a)] and  $N_{\text{meas}} = 200$  [Figure 1.9(b)].

An increase of the FM sweep up to  $\Delta F_{\min} = 1,000$  MHz leads to a decrease of QI modulus  $\delta_{Rst}$  and, hence, to a widening of the variation range of relative range at unchanged of its physical meaning (Figure 1.10). Therefore, the modulus of the measurement error decreases with increasing  $\Delta F_{\min}$ .

With increasing  $N_{\text{meas}}$  the value of the normalized truncation error decreases, but its variation range increases in the actual range.

To reduce the truncation error, it is expedient to increase a number of processed periods up to the maximal frequency deviation and to decrease a number of



**Figure 1.9** The relative truncation error for  $\Delta F_{\min} = 500$  MHz,  $T_{\text{meas}} = 1$  second: (a)  $N_{\text{meas}} = 50$ , and (b)  $N_{\text{meas}} = 200$ .

processed modulation periods owing to reduction of  $N_{\text{meas}}$  and with increasing of duration  $T_{\text{st}}$ . If these measures will be in vain, it is expedient to use the correction of the range calculation results, which is considered next.

### 1.6.2 The Measuring Time Interval Multiple to the Modulation Half-Period

Now we shall consider the DFS phase joining, when the integer number of the difference frequency half-periods is stacked during the modulation half-period between joining moments [21]. To estimate the difference frequency, it is enough to measure the duration of the measuring time interval and to count the number of the DFS zeros in this interval. The number of modulation periods  $N_{\text{mod}}$  is the fixed value. The measuring time interval in this case is variable:

$$T_{\text{meas}} = N_{\text{mod}} T_{\text{mod}} \quad (1.32)$$

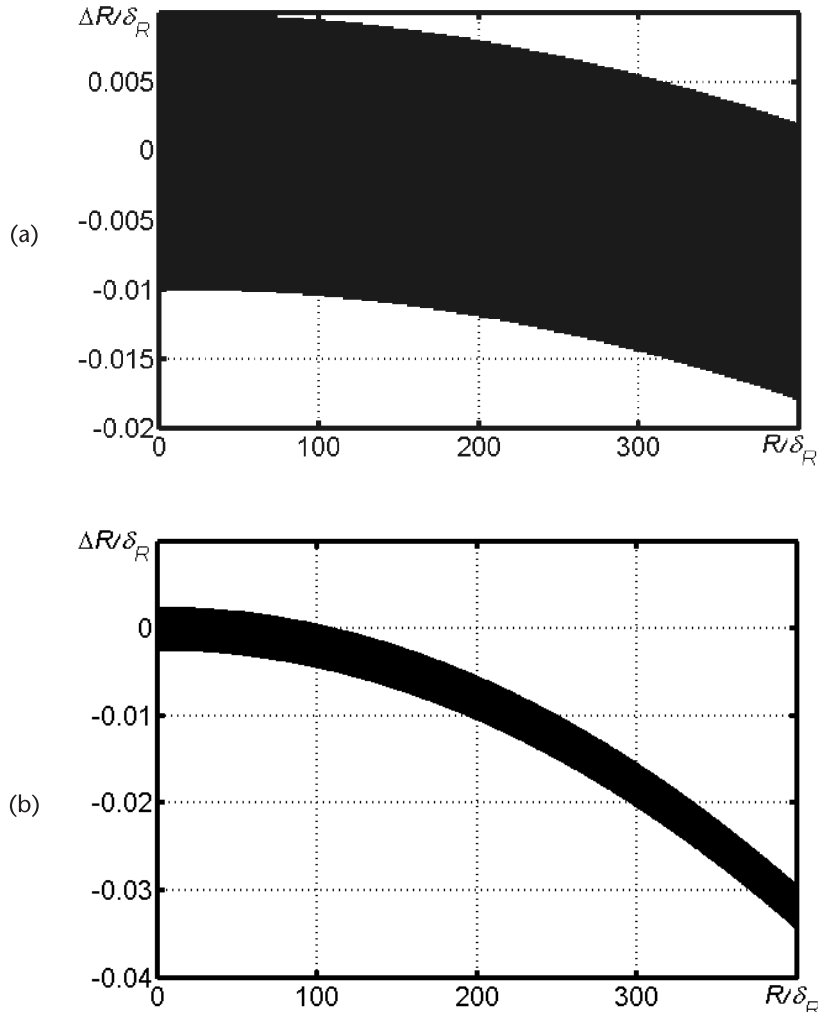


**Figure 1.10** The relative truncation error for  $\Delta f_{\min} = 1,000$  MHz,  $T_{\text{meas}} = 1$  second: (a)  $N_{\text{meas}} = 50$ , and (b)  $N_{\text{meas}} = 200$ .

The minimal duration of the measuring interval can be equal to one modulation half-period. Therefore, in (1.32)  $N_{\text{mod}} = 0.5$ . Evidently, the  $N_{\text{mod}}$  variation step is equal to 0.5.

The measurement of the measuring interval duration can be performed using the count of the pulse number with the standard stabilized frequency (or with the period  $\Delta t$ ). Hence, the counting discreteness error arises, which is determined by the value of the standard frequency. The range estimation result with consideration of the counting discreteness error  $\Delta t$  and the influence of DFS period pulling upon the truncation error can be written taking into account that, at the determination of difference frequency, the integer number of the DFS half-periods is stacked in the interval  $0.5T_{\text{mod}} - t_{\text{del}}$ :

$$\hat{R} = \frac{cF_R N_{\text{mod}}(T_{\text{mod}} - 2t_{\text{del}})}{2K_{\text{fst}}(T_{\text{mod}}N_{\text{mod}} + \Delta t)} \quad (1.33)$$

Assuming as before that  $2t_{\text{del}} \ll T_{\text{mod}}$  and choosing the counting frequency so that  $\Delta t \ll T_{\text{mod}}$  and presenting the fraction in (1.33) as the Taylor series with account of two items, we can write the approximated expression for range estimation neglecting by the item of the second smallness order:

$$\hat{R} \approx \frac{cF_R[1 - 2t/T_{\text{mod}} - \Delta t/(T_{\text{mod}} N_{\text{mod}})]}{2K_{f_{\text{st}}}} \quad (1.34)$$

The counting discreteness error is the quantization noise with the error variance of the time interval measurement [22]:

$$\sigma_T^2 = \frac{(\Delta t)^2}{12} \quad (1.35)$$

From there we obtain the relative variance of truncation error of range measurement caused by the counting discreteness:

$$\frac{\sigma_{R_{\text{count}}}}{\delta_{R_{\text{st}}}} = \frac{x\Delta t}{N_{\text{mod}}T_{\text{mod}}2\sqrt{3}} \quad (1.36)$$

Plots of this function for two values of  $N_{\text{count}} = T_{\text{st}}/\Delta t$  at  $N_{\text{mod}} = 0.5$  are presented in Figure 1.11.

Due to the discrete character of  $T_{\text{mod}}$  variation at the variation of range according to (1.28), plots also have discrete character. However, the value of discrete variations is many times less than the error magnitude and therefore it cannot be distinguishable in Figure 1.11 in this scale. An increase of  $N_{\text{count}}$  leads to variance reduction for range measurement.

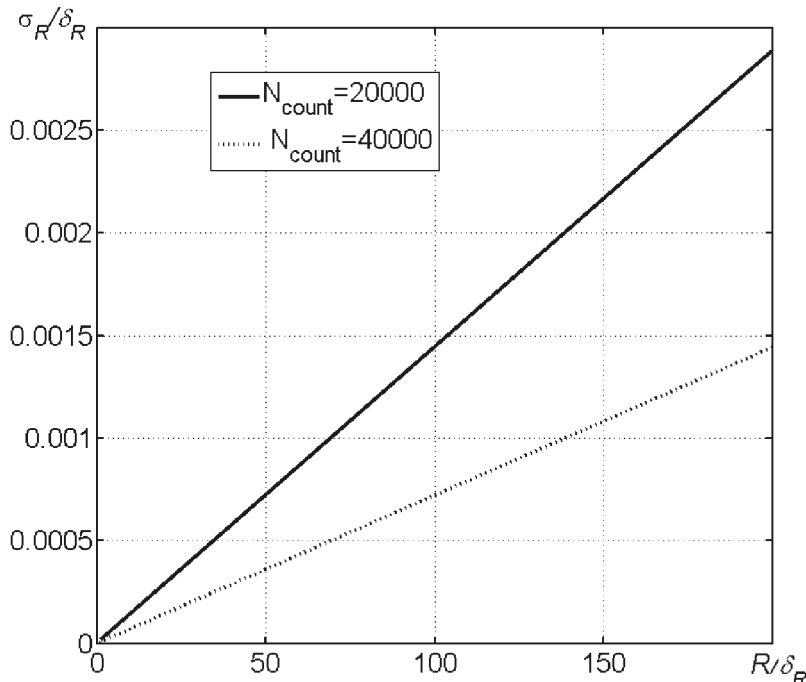


**Figure 1.11** The function of the truncation error variance versus the relative range.

The stable component of the measurement truncation error caused by the DFS period pulling and, being its mathematical expectation, can be transferred to the form after transformations:

$$\frac{\Delta_R}{\delta_{Rst}} = \frac{-x^2}{2\Delta F_{min} T_{mod}} \quad (1.37)$$

This function is shown in Figure 1.12 for the same two values of the product  $2\Delta F_{min} T_{mod}$  as in Figures 1.8 and 1.9.

At the range variation,  $T_{mod}$  periodically changes in accordance with (1.28) and Figure 1.6. This leads to the periodic discrete plot's break; however, these breaks are insignificant compared with the total value of errors and they cannot be seen in Figure 1.12 in the chosen scale. A comparison of plots shown in Figures 1.8 and 1.10 with plots in Figures 1.11 and 1.12 shows that the second variant of the DFS frequency determination in the phase joining method allows an essential reduction of truncation errors and a decrease in the measurement discreteness. It is clearly shown in Figure 1.13.

Here we see the gray plot, which is the best in Figure 1.9(b), and lines are drawn corresponding to the relative mathematical expectation of the error at the same parameter value (solid curve) and a zone of three MSDs (dotted curve) for the method of the DFS frequency estimation according to one modulation half-period. These plots correspond to  $2\Delta F_{min} T_{st} = 5,000,000$  and  $N_{count} = 40,000$ . The widths of the zone of three MSDs can be easily compressed using increasing of  $N_{count}$  and  $N_{mod}$ .

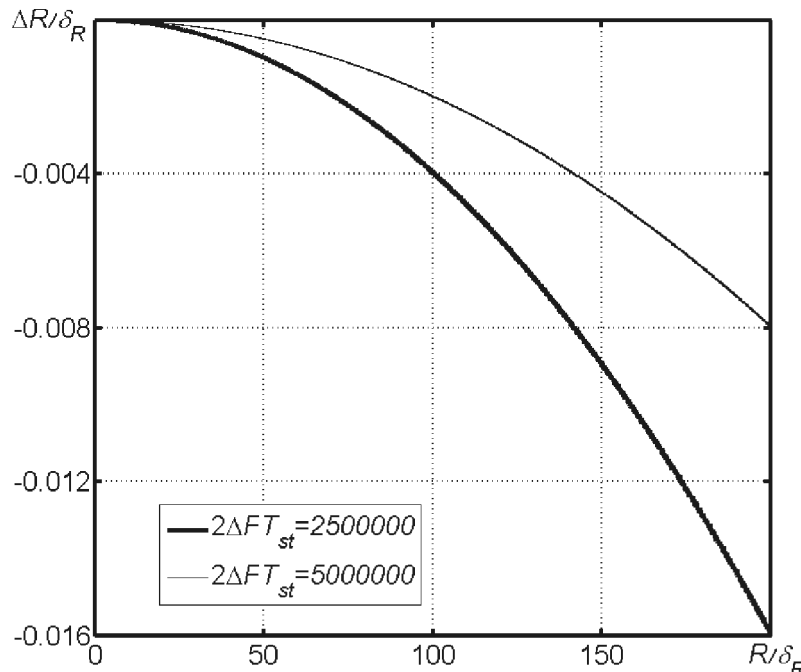
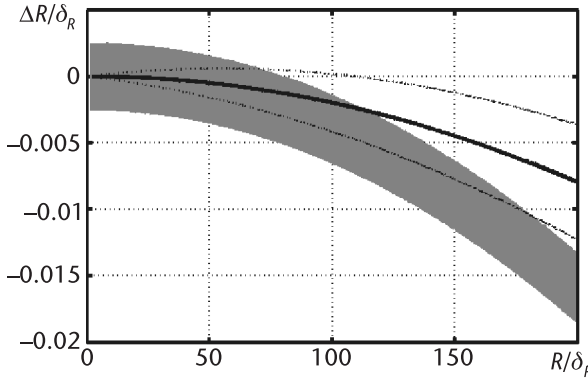


Figure 1.12 Mathematical expectation of the truncation error of the range measurement.



**Figure 1.13** Comparison of truncation errors of range measurement with the help of two ways of the DFS frequency estimation.

### 1.6.3 Calculation of the Range Result Correction

The correction of the range calculation result can be performed on the basis of consideration of error systematic character of measurement caused by the DFS period pulling. For the first method of difference frequency estimation, the correction anticipates the performance of the following stages:

- *Stage 1:* We count the number of the DFS periods  $N_{\text{per}}$  and the number of modulation periods  $K = \text{Int}(T_{\text{meas}}/T_{\text{mod}})$  during the measuring time interval  $T_{\text{meas}}$ .
- *Stage 2:* According to the measurement of the DFS period number during the measurement interval, range calculation is provided on formula (1.24).
- *Stage 3:* The delay time estimation is performed

$$\hat{t}_{\text{del}} = \frac{2\bar{R}}{c} \quad (1.38)$$

- *Stage 4:* The new range value is calculated with consideration of this estimation and the number of modulation periods:

$$\hat{R}' = \frac{cN_{\text{per}}}{2K f_{\text{st}}(T_{\text{meas}} - 2\hat{t}_{\text{del}}K)} \quad (1.39)$$

- *Stage 5:* Stages 3 and 4 are repeated until the required calculation accuracy will be achieved.

A sign for this process stoppage can be the reduction of the difference between the newly calculated result and the previous result, which is less than the specified value. The correction is performed by a calculation way according to one DFS measurement.

The content of the first and third stages is changed for the second approach of the difference frequency estimation. At the first stage, the duration of the measuring interval is measured and the number of the DFS half-periods is determined during the interval. At the third stage, we substitute into (1.39) the measured value of  $T_{\text{meas}}$  and assume that  $K = N_{\text{mod}}$ .

Let us estimate of this process convergence. Using (1.39), we obtain for the first approach of frequency estimation the new value of the measurement error  $\Delta R_{\text{corr}}^{(n)}$ , which has on the  $n$ th step of the result correction with the account that  $T_{\text{st}} \gg \hat{t}_{\text{del}}$ :

$$\Delta R_{\text{corr}}^{(n)} = \hat{R}^{(n)} - R = 2R \frac{\hat{t}_{\text{del}}^{(n-1)} - t_{\text{del}}}{T_{\text{meas}} - 2\hat{t}_{\text{del}}^{(n-1)}} \approx 2R \frac{t_{\text{del}}^{(n-1)} - t_{\text{del}}}{T_{\text{meas}}} \quad (1.40)$$

where  $t_{\text{del}}^{(n-1)}$  is estimation of delay time calculated at the previous correction stage according to formula (1.38). Taking into consideration (1.39) and consequently using (1.40) for recording measurement errors on the previous correction stages, we obtain:

$$\frac{\Delta R_{\text{corr}}^{(n)}}{\delta_{R_{\text{st}}}} = \frac{\Delta R}{\delta_{R_{\text{st}}}} \left( \frac{Kx}{N_{\text{meas}} 2\Delta F_{\min} T_{\text{st}}} \right)^n \quad (1.41)$$

where  $\Delta R/\delta_{R_{\text{st}}}$  is the initial relative error determined by (1.31).

For the second approach of frequency estimation, all relations remain true, but in (1.40) and (1.41) we should substitute  $K = N_{\text{meas}} = N_{\text{mod}}$  and  $T_{\text{meas}} = N_{\text{mod}} T_{\text{mod}}$ . As a result, mathematical expectation of the corrected normalized measurement error will be connected by the following equation with the initial value of this quantity:

$$\frac{\Delta R_{\text{corr}}^{(n)}}{\delta_{R_{\text{st}}}} = \frac{\Delta R}{\delta_{R_{\text{st}}}} \left( \frac{x}{\Delta F_{\min} T_{\text{mod}}} \right)^n \quad (1.42)$$

The expressions in square brackets in (1.41) and (1.42) are much less than 1. Therefore, at increasing  $n$ , the corrected error tends to zero.

Let us estimate the convergence speed of this procedure. We obtain the measurement error achieved on the first stage of such correction procedure. From (1.42) we may express the corrected (on the first stage) relative measurement error  $\Delta R_{\text{corr}}^{(1)}/\delta_{R_{\text{st}}}$  for the first approach of frequency measurement through the initial relative error  $\Delta R/\delta_{R_{\text{st}}}$  determined by (1.31):

$$\frac{\Delta R_{\text{corr}}^{(1)}}{\delta_{R_{\text{st}}}} = \frac{\Delta R}{\delta_{R_{\text{st}}}} \frac{Kx}{2\Delta F_{\min} T_{\text{st}}} \quad (1.43)$$

For the second approach, it is necessary to obtain the mathematical expectation of measurement error and its variance. Taking into consideration that (1.43) represents the linear transformation of the random quantity, we obtain the following formula for the relative mathematical expectation of the corrected measurement error:

$$\frac{\Delta R_{\text{corr}}^{(1)}}{\delta_{R_{\text{st}}}} = \frac{\Delta R}{\delta_{R_{\text{st}}}} \frac{x}{\Delta F_{\min} T_{\text{mod}}} \quad (1.44)$$

where  $\Delta R/\delta_{R_{\text{st}}}$  is determined by (1.31). The relative variance of the corrected truncation error can be obtained by taking into account (1.35) and (1.36):

$$\frac{\sigma_{\Delta R}}{\delta_{Rst}} = \frac{x^2 T_{count}}{\Delta F_{min} N_{mod} T_{mod}^2 2\sqrt{3}} \quad (1.45)$$

The calculations according to (1.44) and (1.45) for  $F_1 = 10$  GHz and  $\Delta F_{min} = 500$  MHz lead to plots shown in Figures 1.14 and 1.15.

Plot discreteness, which is calculated according to (1.44), is essentially less after correction of calculation results. Therefore, the correction for lesser values of  $N_{meas}$  is more effective.

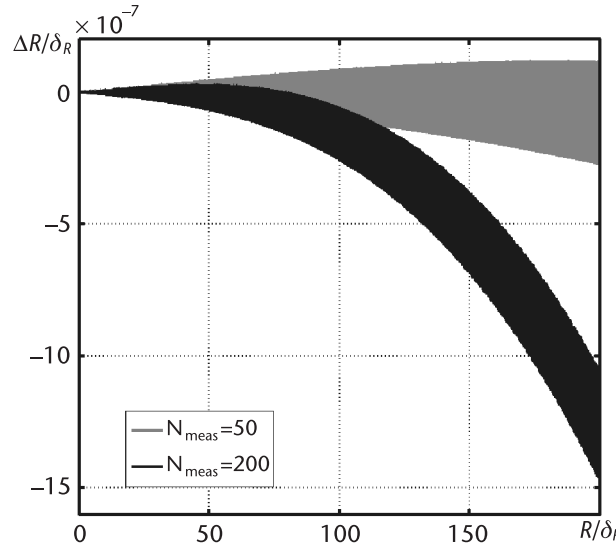


**Figure 1.14** The truncation error of the first approach of frequency measurement after the correction of calculation results.

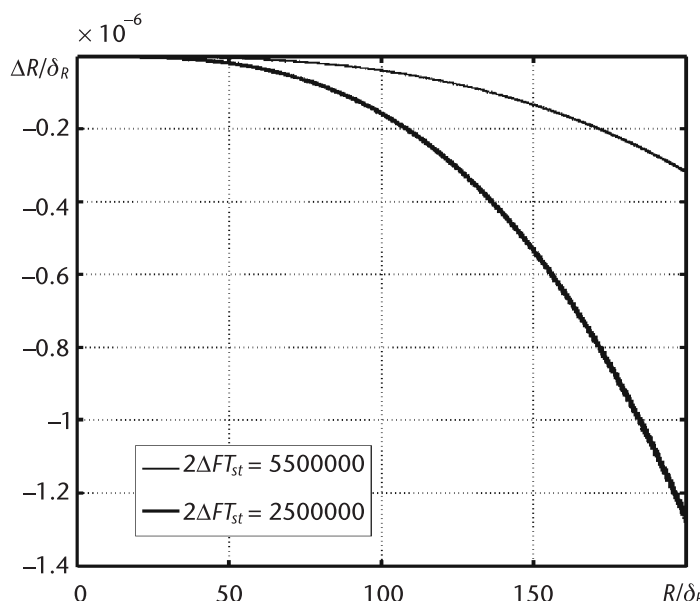


**Figure 1.15** Mathematical expectation of the corrected relative truncation error for the second approach of frequency measurement.

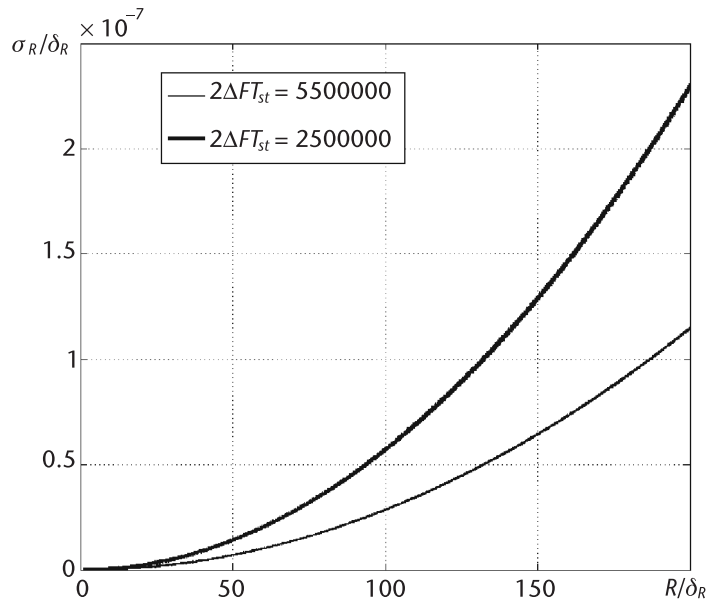


Figure 1.16 Relative MSD for the second approach of the frequency measurement.

Equation (1.45) leads to a smoother variation of the plot at closed magnitudes of the corrected error. A comparison of Figures 1.14, 1.11, and 1.13 shows that correction of calculation results allows a reduction of the measurement error by three orders at the first correction step. Therefore, further repeating the correction procedure is not required.

The calculation result of relative variance according to (1.45) for the second approach of frequency measurement is presented in Figure 1.16 at  $N_{\text{count}} = 20,000$  and  $N_{\text{mod}} = 1$ . A comparison of this figure with Figure 1.10 shows that the calculation result's correction essentially decreases the random component of the measurement error. The increase of  $N_{\text{mod}}$  leads to a proportional decrease of relative variance.

## 1.7 The Range Determination Error Caused by the Inaccuracy of Modulation Adaptation

If the DFS extreme moment is determined with the error  $\Delta t$ , the phase joining inaccuracy increases the signal  $u_{\text{dif}}(t)$  by the appropriate value of  $\Delta\varphi$  (Figure 1.17) [17–20]. Therefore, the delay or advance in phase is possible in the joining point. The joining error increases the device of the DFS extreme determination. The DFS

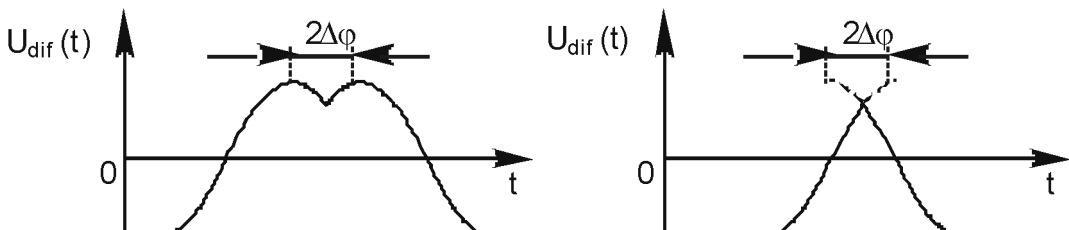


Figure 1.17 DFS phase-joining errors.

phase shifts increasing the process of preliminary processing can be reasons of joining inaccuracies.

Moreover, the circuit itself of extreme determination inserts the above-mentioned inaccuracy due to its own errors and noise presence. Using the evident relation  $\Delta t = \Delta\varphi T_R / (2\pi)$ , we can estimate the measurement error by duration reduction or increasing of one of the DFS periods  $T_R$  in the time interval  $T_{\text{mod}}/2$ :

$$T_{R\text{ eq}} = T_R + \frac{2\Delta t T_R}{0.5T_{\text{mod}} - 2\Delta t} = \frac{T_R T_{\text{mod}}}{T_{\text{mod}} - 4\Delta t} \quad (1.46)$$

Repeating the considerations, similar to the derivation of formula (1.34), we obtain the equation for the relative error of range determination at presence of the phase joining error using the first approach for frequency measurement:

$$\frac{\Delta R}{\delta_{R\text{st}}} = \frac{1}{N_{\text{meas}}} \text{Int} \left\{ \frac{\frac{N_{\text{meas}}}{x}}{\frac{1+2\Delta\varphi/\pi N_{T_{\text{mod}}}}{x} + \frac{x}{2\Delta F_{\min} T_{\text{st}} N_{T_{\text{mod}}}}} + 0.5 \right\} - x \quad (1.47)$$

The phase-joining error in the second approach of measurement affects only the systematic component, which can be obtained in a similar manner as for (1.37):

$$\frac{\Delta R}{\delta_{R\text{st}}} = \frac{-x^2}{\Delta F_{\min} T_{\text{mod}}} - \frac{\Delta\varphi}{\pi} \quad (1.48)$$

From the obtained equation, it follows that owing to the joining error, the DC component arises in the discrete error, in which value is proportional to the phase shift and essentially exceeds the values of the above-mentioned components. Thus, the phase shift value of the tenth parts of a half-period becomes the range measurement error in the tenth parts of the QI, while the relative truncation error is of the hundredth parts. Such a ratio of errors applies the strict requirements on phase-frequency characteristic (PFC) of the passing path of  $u_{\text{dif}}(t)$  and the accuracy of extreme determination.

The phase shift arising in the stage of the preliminary DFS processing can be measured in advance in the form of the phase shift function versus the range  $\Delta\varphi(R)$ . We call this function the *phase characteristic* (PC). A knowledge of PFC allows a discussion of the possibility of range calculation result correction according to the following algorithm.

### **The Algorithm of the Correction of the Range Calculation Results**

The following are the steps of the algorithm of the correction of the range calculation results:

- *Step 1:* At measurement performance, at first, the range estimation  $\hat{R}$  is calculated without taking into account the phase shift.
- *Step 2:* According to (1.38),  $\hat{t}_{\text{del}}$  is calculated.

- *Step 3:* According to the measured phase function versus the frequency (i.e., the range), the determination of the current value of the phase shift  $\varphi_s(\hat{R})$  is performed.
- *Step 4:* The obtained phase value is used for the calculation of the joining moment shift in time:

$$\Delta t = \frac{\varphi_s(\hat{R})T_{\text{st}}}{2\pi\Delta F_{\min}\hat{t}_{\text{del}}} \quad (1.49)$$

- *Step 5:* The result correction is performed:

$$\hat{R}' = \frac{cN_{\text{per}}}{2K_{f_{\text{st}}}(T_{\text{meas}} - 2\hat{t}_{\text{del}}K - 2\Delta tK)} \quad (1.50)$$

When necessary, steps 2 to 5 are repeated until the required calculation accuracy will not be achieved. The convergence of this procedure follows from the convergence of the previous one.

## 1.8 Noise Influence on the Accuracy of the Range Determination Using the Additive Counting Method

We mentioned earlier that the DFS processing obtained after mixing is considered. Therefore, we use the normal white noise  $\xi(t)$  as the noise model on the mixer output, which has zero mathematical expectation and the energy spectrum  $G(\omega) = N_0$ .

Before estimation of noise influence on measurement accuracy, it is necessary to agree with the signal processing procedure, which permits the realization of the above-mentioned algorithm of the modulation control with the DFS phase joining. Usually at the first stage of processing, the filtering (using the narrowband tracking filter) of the additive mixture of the signal  $u(t)$  with the normal white noise is performed:

$$s(t) = u(t) + \xi(t) \quad (1.51)$$

Then, for the DFS zero determination, the amplification with limitation is performed. The moments of the front intersection of the obtained, almost rectangular pulses with a zero level are taken as DFS zero positions.

To determine the DS extreme position, the differentiation of the signal and noise mixture on the output of the narrowband tracking filter and amplification with limitation is performed. The moments of intersection of rectangular pulse fronts with the zero level are taken as DFS extreme positions.

As a result of such processing, the characteristics of input noise will change. Furthermore, we assume that the frequency response of the narrowband tracking filter tuned on the signal frequency  $\omega_R$  approaches to the Gaussian curve [23]:

$$H(\omega) = \exp\left[-\frac{(\omega - \omega_R)^2}{2\beta^2}\right] \quad (1.52)$$

where the parameter  $\beta$  is connected with the filter bandwidth:  $\beta = \beta_f / \sqrt{\pi}$ . After narrowband filtering, the noise remains normal [23] with the correlation function

$$B_\zeta(\tau) = \frac{N_0\beta}{2\sqrt{\pi}} \exp(-0.25\beta^2\tau^2) \cos(\omega_R\tau) \quad (1.53)$$

and with the energy spectrum

$$G(\omega) = \frac{N_0}{2} \left\{ \exp \left[ -\frac{(\omega - \omega_R)^2}{\beta^2} \right] + \exp \left[ -\frac{(\omega + \omega_R)^2}{\beta^2} \right] \right\} \quad (1.54)$$

From (1.53) at  $\tau = 0$ , we may obtain the equation for the noise variance on the output of the narrowband tracking filter:

$$B_\zeta(0) = \frac{N_0\beta}{2\sqrt{\pi}} \quad (1.55)$$

As a result of differentiation of the obtained narrowband process, it remains as before the normal with zero mathematical expectation and the correlation function determined by the equation [23]:

$$B_{\zeta^{(k)}\zeta^{(l)}}(\tau) = (-1)^k B_\zeta^{(k+l)}(\tau) \quad (1.56)$$

From here we have:

$$\begin{aligned} B_{\zeta'}(\tau) &= \frac{N_0\beta}{4\sqrt{\pi}} \sqrt{(\beta^2 + 2\omega_R^2 - 0.5\tau^2\beta^4)^2 + (2\tau\omega_R\beta^2)^2} \\ &\times \exp(-0.25\tau^2\beta^2) \cos \left[ \tau\omega_R + \arctan \left( \frac{4\tau\omega_R\beta^2}{4\omega_R^2 + 2\beta^2 - \tau^2\beta^4} \right) \right] \end{aligned} \quad (1.57)$$

Substituting  $\tau = 0$  into (1.57), we obtain the noise variance on the output of differentiation unit:

$$B_{\zeta'}(0) = B_\zeta(0)(\omega_R^2 + 0.5\beta^2) \quad (1.58)$$

The noise influence on the range measurement error using the method of the DFS phase joining is manifested in the form of two effects. The first one is increasing the DFS period counting error. This effect is studied in the literature in detail, for instance, [24], and the error increasing, which is expressed in variation of the number of counted zeros of the signal and noise mixture, is connected with the SNR and with the duration of the signal processing interval. At a rather large SNR (more than 30 to 40 dB) typical for the case under consideration, this error component becomes negligible compared with the truncation error.

The second effect is concerned with the error in determination the DFS extreme appearance moment, which leads to the error of the DFS phase joining. The influence of the phase-joining error on the measurement error was considered earlier.

Therefore, it is enough to analyze the error characteristics of the joining moment determination.

The displacement  $\Delta t_i$  of the intersect moment of the DFS signal/noise sum derivative of zero level with respect to the intersection moment  $t_i$  of this level with only one DFS derivative is obtained from the following equation:

$$\omega'(t_i)t_{\text{del}}U_m \sin[\omega_0 t_{\text{del}} + \omega(t_i + \Delta t_i)t_{\text{del}}] + \xi' = 0 \quad (1.59)$$

where  $U_m$  is the DFS amplitude and  $t_i$  can be found from the equation  $\sin[\omega_0 t_{\text{del}} + \omega(t_i)t_{\text{del}}] = 0$ . The moments  $t_i$  are repeated with the period of the DFS, but we are interested by not its modulus but its displacement characteristics.

Assuming that the noise level is small compared with  $U_m$ , we can change the function  $\sin x$  by the power Taylor series in each point  $t_i$ , saving in it one item and considering that the FM is provided according to the linear law, which we obtain after the simple transformations:

$$\Delta t_i = \frac{\xi' T_{\text{st}}^2}{U_m x^2 \pi^2} \quad (1.60)$$

From (1.60) it is clear that the distribution law of the probability density for the displacement moment of the DFS phase joining is normal with zero mathematical expectation and with the following correlation function:

$$B_{\Delta t}(\tau) = \frac{B_\xi(0) T_{\text{st}}^4}{2 U_m^2 x^4 \pi^4} \sqrt{(\beta^2 + 2\omega_R^2 - 0.5\tau^2\beta^4)^2 + (2\tau\omega_R\beta^2)^2} \times \exp(-0.25\tau^2\beta^2) \cos \left\{ \tau\omega_R + \arctan \left[ \frac{4\tau\omega_R\beta^2}{4\omega_R^2 + 2\beta^2 - \tau^2\beta^4} \right] \right\} \quad (1.61)$$

From this at  $\tau = 0$ , we obtain the displacement variance of the DFS phase-joining moment:

$$\sigma_{\Delta t}^2 = T_{\text{st}}^2 \frac{1 + 2/(\pi x^2)}{2(q\pi x)^2} \quad (1.62)$$

where  $q^2 = U_m^2 / [2B_\xi(0)]$ . Now we find the variance of the appropriate phase error:

$$\sigma_{1,\Delta\varphi}^2 = \frac{\pi x^2 + 2}{2\pi q^2 x^2} \quad (1.63)$$

We note that the very weak influence of the range variation on the phase shift MSD is observed. That is why the effect of SNR has the most significant sense. Therefore, it is important to know whether the existence area of  $\Delta\varphi$  exceeds the value of  $\pm\pi/2$ . In the case, if this exceeding is observed, the jump of the DFS phase-joining moment occurs to the adjacent extreme (i.e., the zero number changes in the modulation period). Let us obtain from the condition  $3\sigma_{1,\Delta\varphi} \leq \pi/2$  the range

of boundary values of  $q$ , at which this event does not yet arise in the range from  $\delta_{R_{st}}$  to  $\infty$ :

$$q \geq \frac{3\sqrt{2}}{\pi} \sqrt{1 + \frac{2}{\pi x^2}} = 1.727 \dots 1.35 \quad (1.64)$$

Hence, one can state with confidence that if the SNR exceeds 5 dB, the jump of the DFS phase-joining moment is not observed. We are interested with much higher values of  $q$ ; therefore, we do not take into account the phenomenon of the DFS phase-joining jump to the adjacent extreme.

In connection with the fact that in each separate period the additional DFS zeros do not increase, the variation of the total number of zeros occurs only owing to the boundary displacement of the last modulation period with respect to the measurement interval boundary at the displacement of the joining moment under the noise influence. Therefore, the number of zeros fallen into this interval varies and so we cannot use the formula (1.47) directly. Now we must take into account the total phase shift, which changes the DFS number of periods stacked in the remainder of measurement interval.

Starting from this, (1.47) can be rewritten in the form:

$$\frac{\Delta R}{\delta_{R_{st}}} = \frac{1}{N_{\text{meas}}} \text{Int} \left\{ \frac{N_{\text{meas}}}{\frac{1}{x} + \frac{x}{2\Delta F_{\min} T_{\text{st}} N_{T_{\text{mod}}}}} - \frac{\varphi_{\Sigma}}{2\pi} + 0.5 \right\} - x \quad (1.65)$$

where  $\varphi_{\Sigma}$  is the total phase shift of the right boundary of the last modulation period in the measuring interval owing to the phase error on the boundary of each modulation half-period, that is,

$$\varphi_{\Sigma} = \sum_{i=1}^{2K} \Delta\varphi_i \quad (1.66)$$

It is clear from [24] that the distribution law of  $\varphi_{\Sigma}$  remains normal with zero mathematical expectation and with the following variance:

$$\sigma_{\varphi_{\Sigma}}^2 = \sum_{l=1}^{2K} \sum_{k=1}^{2K} \sigma_{\Delta\phi_l} \sigma_{\Delta\phi_k} R_{lk} \quad (1.67)$$

where  $\sigma_{\Delta\phi_l}$  and  $\sigma_{\Delta\phi_k}$  are the MSD of the DFS phase joining error in time moments  $lT_{\text{st}}$  and  $kT_{\text{st}}$ , respectively, and  $R_{lk}$  is the correlation coefficient between the values of the phase-joining error in these time moments.

Now we can write:

$$\sigma_{\varphi_{\Sigma}}^2 = \frac{K(\pi x^2 + 2)}{\pi x^2 q^2} \left[ 1 + \frac{1}{2K} \sum_{k=1}^{2K} \bar{B}_{\xi'}(0.5kT_{\text{mod}}) \right] \quad (1.68)$$

where  $\bar{B}_{\xi'}(\tau) = B_{\xi'}(\tau)/B_{\xi'}(0)$ .

At the determination of the range measurement error variance for the first approach of frequency estimation, it is necessary to take into consideration that, in accordance with (1.65), the nonlinear transformation of the normally distributed random variable  $\varphi_\Sigma$  with the variance determined by the formula (1.68) is provided. Nonlinearity is specified by the function  $\text{Int}(\cdot)$  having the view of the stepwise line at  $\varphi_\Sigma$  increasing. In this case, the variation of measured range as a result of the joining error under noise influence happens only after the sum in (1.65) will exceed the value multiple to  $\pi$ . In the interval between these moments, there are no variations of measurement results. Taking into consideration that the mathematical expectation of the total phase deviation (1.65) is equal to zero, we can determine the relative variance of measurement results  $\sigma_{1\Delta_R}^2/\delta_{R_{st}}$  on the basis of the first approach of the frequency measurement by means of summation of discrete values of calculation deviations according to (1.65) with weights equal to the probability of sum (1.65) falling in the appropriate interval of the phase shift values:

$$\frac{\sigma_{1R}^2}{\delta_{R_{st}}^2} = \frac{1}{N_{\text{meas}}^2} \sum_{L_{\min}}^{L_{\max}} L^2 \{F[(L+1)\pi] - F(L\pi)\} \quad (1.69)$$

where  $L_{\min} = \text{Int}\{\varphi_0 - 3\sigma_{\Delta\varphi}/\pi\} - \text{Int}\{\varphi_0\}$ ;  $\varphi_0 = \frac{N_{\text{meas}}}{x} + 0.5$ ;

$$\frac{x}{x + 2\Delta F_{\min} T_{\text{st}} N_{T_{\text{mod}}}}$$

$L_{\max} = \text{Int}\{\varphi_0 + 3\sigma_{\Delta\varphi}/\pi\} - \text{Int}\{\varphi_0\} + 1$ ;  $F(\cdot)$  is the integral function of the normal distribution law of probabilities and  $\sigma_{\Delta\varphi}^2$  is defined by (1.68).

As we see, in this case, a variance of measurement error depends in the complicated manner upon  $N_{\text{meas}}$ , that is, upon measurement interval duration. Therefore, to estimate the quality of the processing algorithm, the formula (1.69) is unsuitable. For this purpose, we use the result of error averaging over some range interval. The value of averaging interval can be chosen equal to ED because the variation of the DFS zero number happens with the range variation with exactly this step. We write the equation in a discrete form for calculations on the PC, where we consider in an explicit form the function of the error versus the range:

$$\frac{\sigma_{\text{laver}}^2(R_{\text{aver},i})}{\delta R_{\text{rst}}^2} = \frac{1}{N_R \delta_{R_{st}}^2} \sum_{k=0}^{N_R-1} \sigma_{1\Delta_R}^1(R_{ki}) \quad (1.70)$$

where  $R_{\text{aver},i} = 0.5(2i+1)\delta_{R_{st}}$ ,  $i = 1, 2, \dots$ ,  $R_{ki} = (i+k/N_R)\delta_{R_{st}}$ , and  $N_R$  is a number of considered points of range in the segment with the length  $\Delta_{R_{st}}$ .

At the second approach of frequency estimation after carrying out (1.64), additional DFS zeros do not exist in the measuring interval under noise influence. The measurement error is caused by a variation of the processing interval duration happening due to the random variation of the phase-joining moments. In accordance with (1.34), we can write the relative variance  $\sigma_{2\Delta_R}^2/\delta_{R_{st}}^2$  of the range measurement error on the basis of the second approach of frequency measurement as:

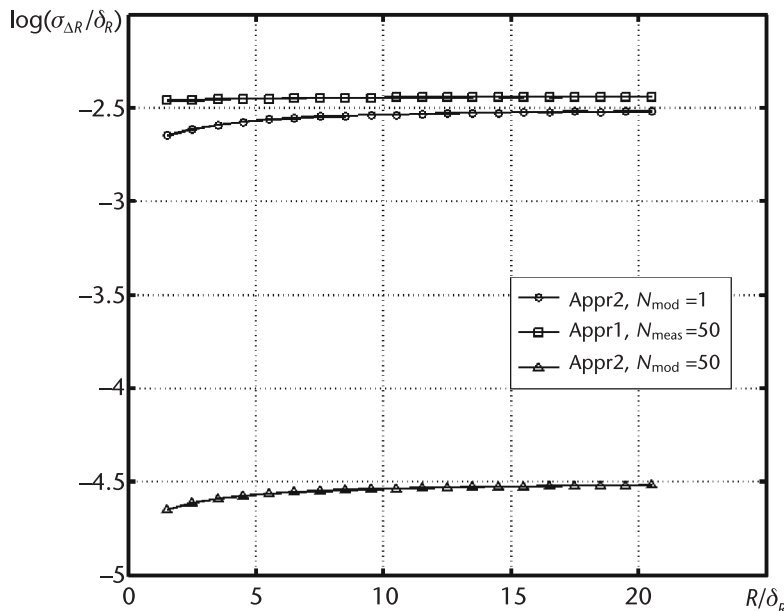


**Figure 1.18** The function of the logarithm of the relative MSD of the measurement error versus the normalized range.

$$\frac{\sigma_{2R}^2}{\delta_{Rst}} = \frac{T_{st}^2 \left[ 1 + 2/(\pi x^2) \right]}{N_{mod}(\pi q T_{mod})} \left[ 1 + \frac{1}{2N_{mod}} \sum_{k=1}^{2N_{mod}} B'_\xi(0.5kT_{mod}) \right] \quad (1.71)$$

where  $T_{mod}$  is defined by (1.28).

The analysis of (1.68) and (1.71) shows that at range variation the measurement error slightly changes. The calculation results on (1.70) for the errors (1.69) and (1.71) are shown in Figure 1.18 in the form of the logarithm of the relative MSD of the measurement error versus the measured range at  $q = 40$  dB. Therefore, for the second approach, two plots are drawn at  $N_{mod} = 0.5$  (estimation for one period) and  $N_{mod} = 50$ . For the first approach of frequency estimation, the plot corresponds to  $N_{mod} = 50$ .

We see that for this approach the error does not practically change at range variation. At the second approach the error variation takes place at range variation, but it is insignificant and we may neglect it. The function of the measurement error versus the noise level is more interesting for us. Therefore, it is expedient to compare two approaches of frequency estimation.

Figure 1.19 shows plots of the logarithm function of the relative MSD of the range measurement versus the SNR drawn according to (1.70), taking into account (1.69) and (1.71) for the above-mentioned processing parameters and  $2\Delta F_{min} T_{st} = 5,000,000$ .

We see that the plot for the first approach of the difference frequency measurement at some SNR intersects the plot corresponding to the second approach for one modulation half-period. Hence, the second approach of the frequency estimation using the mode of the DFS phase-joining is more effective. A prolongation of the measuring interval at the expense of the number increase of the processed modulation half-periods leads to an essential decrease of the measurement error.

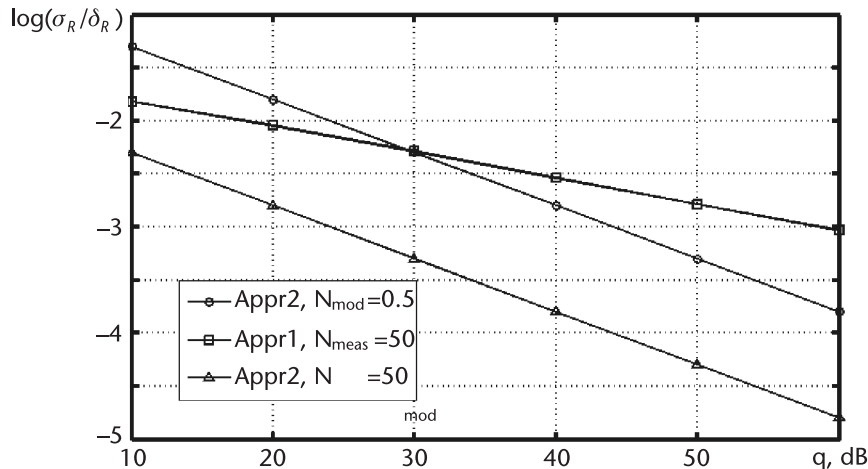


**Figure 1.19** The function of logarithm of the relative MSD of the measurement error versus the SNR.

## 1.9 Conclusions

We investigated the known counting method of the difference frequency estimation for the adaptive control of modulation parameters, which eliminates DFS phase jumps and allows increasing the averaging interval at the estimation of the difference frequency. Conditions were determined that ensure the mode of phase joining, and a control algorithm of modulation parameters was suggested, which will provide stability of the average slope of increasing FM.

An approach for difference frequency estimation was offered, which is possible in the phase-joining mode only, based on counting the DFS period number during a fixed modulation period number and on the duration estimation of the obtained measuring time interval. The truncation error of range measurement was analyzed and it was shown that the approach presented provides an error approximately two times less compared with the known method.

A calculation result correction procedure was offered, allowing at the first correction step a decrease of the measurement error by 1,000 times.

It was shown that the phase-joining error caused by the phase shift in stages of preliminary DFS analog processing leads to an appearance of the constant bias of readings and a correction procedure for the above-mentioned component of the measurement error was offered.

We showed that our approach to difference frequency estimation allows obtaining acceptable values of measurement errors even for an essential noise level due to long accumulation by using the phase-joining mode.

## References

- [1] Vinitkiy, A. S., *Essay on Radar Fundamentals for Continuous-Wave Radiation*, Moscow, Russia: Sovetskoe Radio Publ., 1961. [In Russian.]
- [2] Kogan, I. M., *Short-Range Radar Technology (Theoretical Bases)*, Moscow, Russia: Sovetskoe radio Publ., 1973. [In Russian.]

- [3] Brumbi, D., *Fundamentals of Radar Technology for Level Gauging*, 3rd rev., Duisburg: Krohne Messtechnik, 1999.
- [4] Bakulev, P. A., *Radar Systems*, Moscow, Russia: Radiotekhnika Publ., 2004. [In Russian.]
- [5] Komarov, I. V., and S. M. Smolskiy, *Fundamentals of Short-Range FMCW Radar*, Norwood, MA: Artech House, 2003.
- [6] Atayants, B. A., et al., "Precision Industrial Systems of FMCW Short-Range Radar Technology: Truncation Measurement Error and Its Minimization," *Uspekhi sovremennoi radioelektroniki*, No. 2, 2008, pp. 3–23. [In Russian.]
- [7] Skolnik, M., *Introduction to Radar Systems*, 3rd ed., New York: McGraw-Hill, 1981.
- [8] Korn, G., and T. Korn, *Mathematical Handbook for Scientists and Engineers*, New York: McGraw-Hill, 1961.
- [9] Zhukovskiy, A. P., E. I. Onoprienko, and V. I. Chizhov, *Theoretical Fundamentals of Radio Altimetry*, Moscow, Russia: Sovetskoe Radio Publ., 1979. [In Russian.]
- [10] Sokolinskiy, V. S., and V. G. Sheinkman, *Frequency and Phase Modulators and Manipulators*, Moscow, Russia: Radio i Sviaz Publ., 1983. [In Russian.]
- [11] Imada, H., and Y. Kawata, "New Measuring Method for a Microwave Range Meter," *Kobe Steel Eng. Repts.*, Vol. 30, No. 4, 1980, pp. 79–82.
- [12] U.S. Patent 5070730, Int. Cl. G01F 23/28. "Device for Level Gauging with Microwave," K. O. Edvardsson. No. 613574. Filed March 27, 1990; date of patent December 10, 1991.
- [13] Weib, M., and R. Knochel, "A Highly Accurate Multi-Target Microwave Ranging System for Measuring Liquid Levels in Tanks," *IEEE MTT-S International Microwave Symposium Digest*, Vol. 3, 1997, pp. 1103–1112.
- [14] Patent 2126145 (Russian Federation), INT.CL. G01F 23/284. "Level-Meter," S. A. Liberman, et al., No. 97114261/28. Bull. No. 4. Filed August 20, 1997; published October 2, 1999.
- [15] Atayants, B. A., et al., "Noise Problem and Non-Linearity of Transmitter Modulation Characteristic in Precision Industrial Short-Range FMCW Radar Systems," *Uspekhi sovremennoi radioelektroniki*, No. 3, 2008, p. 3–29. [In Russian.]
- [16] Patent No. 2159923 (Russian Federation). INT. CL. G01F 23/284. "Radar Level-Meter," B. A. Atayants, V. V. Ezerskiy, and A. I. Smutov. No. 99104759/28. Bull. No. 33. Filed March 4, 1999; published November 27, 2000.
- [17] Atayants, B. A., et al., "Adaptive Frequency-Modulated Level-Meter," *Radar Technology, Navigation and Communication: Proceedings of VI Intern. Conf.*, Voronezh, Vol. 3. 2000, pp. 1686–1696. [In Russian.]
- [18] Atayants, B. A., et al., "Non-Contact Radio Wave Distance Sensor of Higher Accuracy and Stability," *Sensors and Information Transducers for Systems of Measurement, Checking and Control: Proceeding of XIII Conf.*, Gurzuf, 2001, pp. 246–247. [In Russian.]
- [19] Ezerskiy, V. V., B. V. Kagalenko, and V. A. Bolonin, "Adaptive Frequency-Modulated Level Meter: An Analysis of Measurement Error Components," *Sensors and Systems*, No. 7, 2002, p. 44. [In Russian.]
- [20] Patent No. 2151408 (Russian Federation). INT. CL. G01S 13/34. "Radar Range Finder," B. F. Atayants, et al. Bull. No. 17. Published June 20, 2000.
- [21] Ezerskiy, V. V., "An Analysis of a Truncation Error of a Range Finder with Adaptive Frequency Modulation for Short-Range Radar," *Vestnik RGRTA*, Ryazan. No. 15, 2004, pp. 40–45. [In Russian.]
- [22] Brillinger, D. R., *Time Series: Data Analysis and Theory*, New York: Holt, Rinehart and Winston, 1975.
- [23] Levin, B. R., *Theoretical Fundamentals of Statistical Radio Engineering*, in three volumes. 2nd ed., Moscow, Russia: Sovetskoe Radio Publ., 1974. [In Russian.]
- [24] Tikhonov, V. I., and V. N. Kharisov, *Statistical Analysis and Synthesis of Radio Engineering Devices and Systems*, Moscow, Russia: Radio i Sviaz Publ., 1991. [In Russian.]

# Weighting Method for the Difference Frequency Averaging

## 2.1 Introduction

The application of the weighting method for the difference frequency averaging for the QI smoothing of the FMCW RF was offered for the first time in [1–3]. In general, the weighted estimation of the DFS is performed in accordance with [3] as:

$$S = \int_0^{T_{\text{an}}} \alpha(t) F_{\text{DFS}}(t) dt \quad (2.1)$$

where  $T_{\text{an}}$  is the interval of frequency analysis and  $\alpha(t) \geq 0$  is the weighting function (WF) satisfying the following normalization condition:

$$\int_0^{T_{\text{an}}} \frac{\alpha(t)}{T_{\text{an}}} dt = 1 \quad (2.2)$$

Taking (1.10) into account, we may rewrite (2.1) as:

$$S = t_{\text{del}} \int_0^{T_{\text{an}}} \alpha(t) f'(t) dt \quad (2.3)$$

For the usual symmetric triangle modulation function (1.4) with the period  $T_{\text{mod}}$ , one chooses  $T_{\text{an}} = T_{\text{mod}}/2$  and WF has a period  $T_{\text{mod}}/2$ . Substituting these parameters in (2.3) and taking into account the normalization condition, we obtain:

$$S = t_{\text{del}} \int_0^{\frac{T_{\text{mod}}}{2}} \alpha(t) f'(t) dt = 2t_{\text{del}} \Delta F K_{\text{WF}} \quad (2.4)$$

where  $K_{\text{WF}} = \frac{1}{2\Delta F T_{\text{mod}}} \int_0^{T_{\text{mod}}/2} \alpha(t) f'(t) dt$  is the constant coefficient depending on the WF shape and the FM function. At the linear FM,  $K_{\text{WF}} = 1$  with an account of the normalization condition (2.2). Therefore, the measuring range is determined by the following equation:

$$R = \delta_R S / K_{\text{WF}} \quad (2.5)$$

At the practical implementation of the weighting method, the estimation of  $\hat{S}$  for (2.5) can be obtained approximately by means of numerical calculation of the integral (2.1) according to the rectangular formula [4]:

$$\hat{S} = \sum_{i=1}^N \alpha(t_i) F_{\text{DFS}}(t_i) \Delta_i \quad (2.6)$$

where  $t_i$  are interpolation nodes,  $N$  is the number of interpolation modes, and  $\Delta_i$  is its step.

If the interpolation step in (2.6) that we assume equals half of the instantaneous value of DFS period  $\Delta_i = 0.5 T_{\text{DFS}_i}(t_i) = 1/[2F_{\text{DFS}}(t_i)]$ , that is, to choose the physically existed DFS zeros as interpolation points, we obtain the calculation equation:

$$\hat{S} = \sum_{i=1}^N \alpha(t_i) \quad (2.7)$$

where  $t_i$  is the position of the  $i$ th zero of the DFS and  $N$  is the number of the DFS zeros in the modulation half-period.

In such a way, at the final counting, the different weight can be attributed to different DFS zeros. To eliminate the discreteness error, the weighting coefficients closed to zero are attributed to zeros, which are located inside the analysis interval in the immediate vicinity to boundaries. As far as zeros will move off from analysis interval boundaries, the increase of the weighting coefficient value occurs. In this case, at the range variation, the zero, which appears again in the analysis interval (or disappears from the analysis interval), does not lead to discrete variation by one of the accumulated results. The smooth zero elimination from the boundaries of the analysis interval leads to a smooth variation of the measurement result.

The mentioned procedure is illustrated in Figure 2.1, where the plots of the DFS phase variations [Figure 2.1(a)], the DFS itself [Figure 2.1(b)], and the WF  $\alpha(t)$  [Figure 2.1(c)] are shown.

The specific position of zeros and their number in accordance with (1.9) is given by the following equation [see Figure 2.1(a)]:

$$\omega_0 t_{\text{del}} + \omega(t_i) t_{\text{del}} + \varphi_s = 0.5\pi + \pi(i + I_1); \quad i = 1, 2, \dots, N \quad (2.8)$$

where  $\omega_0 = 2\pi f_0$ ,  $\omega(t) = 2\pi(f)$ ,  $I_1 = \text{Int}(2f_0 t_{\text{del}} - 0.5)$ , and  $f_0$  is the carrier frequency of the signal.

Equation (2.7) allows a rather simple implementation of the weighting smooth method. Therefore, it is necessary to take into account the following factors:

1. The range calculation according to (2.5) is possible only at the exact knowledge of the FM sweep of the SHF oscillator.
2. It is necessary to carry out good preliminary filtering for the exact determination of the DFS zero position used in (2.7), which is possible at the phase jump absence only.

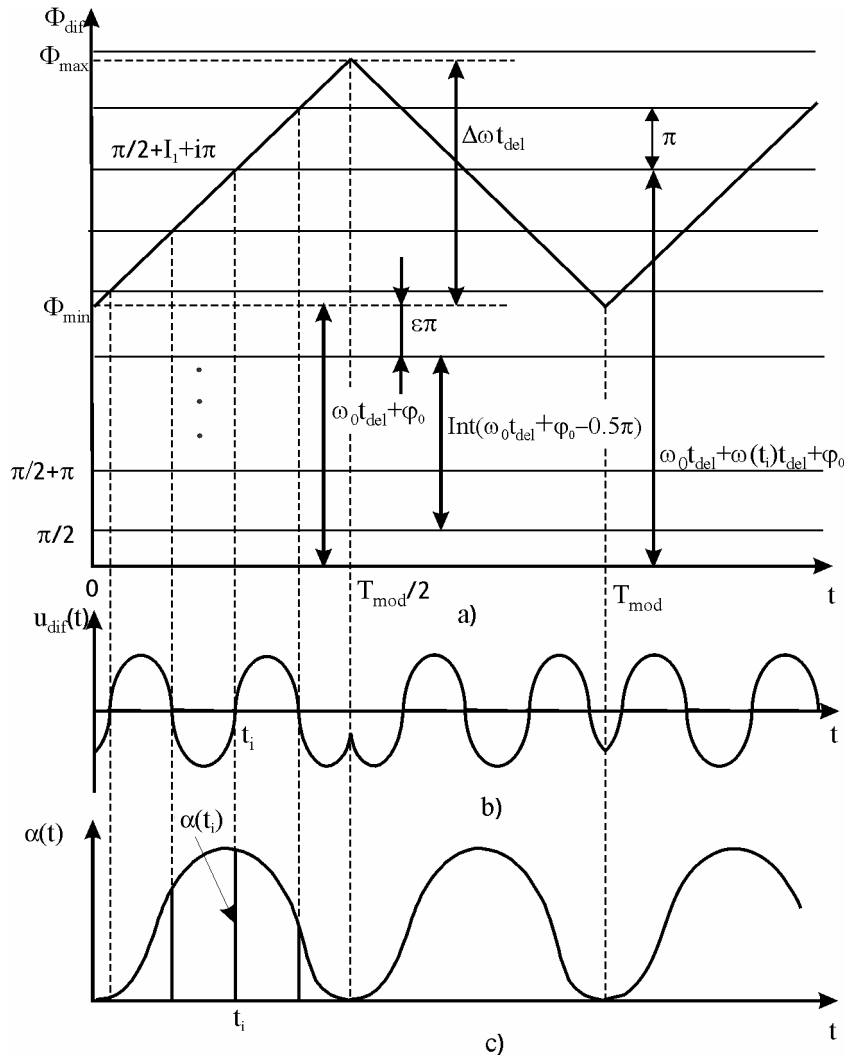


Figure 2.1 Illustration of the weighting averaging method for the difference frequency.

These considerations lead to the necessity of an additional operation performance, which was suggested earlier regarding the monitoring of the boundary frequencies of the analysis interval and the ensuring of the DFS phase continuity (phase joining).

The sources of measurement errors in the method of smooth weighting (besides the instability of the FM sweep that is common for all methods) are:

- The estimation of  $\hat{S}$  according to approximated (2.7), that is, the truncation error;
- The difference of the real frequency modulation law from the specified law owing to the MC nonlinearity;
- The error estimation of moments  $t_i$  of the difference signal transition through zero due to the noise presence;
- The determination error of the WF samples  $\alpha_i(t_i)$ .

## 2.2 The Truncation Error of the Weighting Method of Difference Frequency Averaging

Let us consider the first component, which factually is the error of numerical calculation of the integral (2.1).

The analysis of the truncation error for which we provide the WF class is wide enough. We have mentioned that from heuristic considerations WF should be symmetric with respect to the middle of the analysis interval and reduce its ends practically up to zero. Therefore, we examine the WF family [4], allowing its representation in the form of the trigonometric Fourier series:

$$\alpha(t) = K_W \sum_{m=0}^K A_m \cos(4\pi m t / T_{\text{mod}}) \quad (2.9)$$

where  $A_m = 2 \int_0^{T_{\text{mod}}/2} \alpha(t) \cos(4\pi m t / T_{\text{mod}}) dt / T_{\text{mod}}$ ,  $m = 0, 1, 2, \dots, K$ , and  $K_W$  is a normalizing multiplier, which is  $K_W = 1/A_0$  in accordance with (2.2).

Following the normalization of (2.9), it is necessary to perform the condition of equality to the zero WF value coefficients on boundaries of the analysis interval:

$$\sum_{m=0}^K A_m = 0 \quad (2.10)$$

Now we substitute (2.10) into (2.7):

$$\hat{S} = K_W \sum_{m=0}^K A_m \sum_{i=1}^N \cos(4\pi m t_i / T_{\text{mod}}) \quad (2.11)$$

This equation can be reduced to the more convenient form if the internal series would be represented on the basis of known equation [5]:

$$\sum_{m=1}^N \cos[x + 2(m-1)y] = \cos[x + (n-1)y] \frac{\sin(Ny)}{\sin y} \quad (2.12)$$

With this purpose, we provide the argument transformation of the cosine function in (2.11) to the table from (2.12) using the normalized time [3]:  $t_{\text{norm},i} = 2t_i/T_{\text{mod}}$ . Assuming that the FM is performed in accordance with the linear law (1.4), we can transform (2.8) on the increasing part of the frequency variation as:

$$4f_0 R/c + 8\Delta FR \frac{t_i}{T_{\text{mod}}c} + \frac{\varphi_s}{\pi} = 0.5 + i + I_1 \quad (2.13)$$

From here we obtain the equation for the normalized DFS zeros:

$$t_{\text{norm},i} = (i - \varepsilon - \varphi_s/\pi)\eta \quad (2.14)$$

where  $\varepsilon = \rho - \text{Int}(\rho)$ ;  $\rho = (4f_0R/c - 0.5)$  is reduced by 0.5 the number of quarter-wavelengths of the carrying oscillation with the frequency  $f_0$  stacked in the range to be measured,  $1/\eta = R/\delta_R = x_R = M + \chi$  is the range to be measured normalized to the QI value, and  $M = \text{Int}(R/\delta_R)$  and  $\chi = R/\delta_R - M$  are, respectively, the integer and fraction parts of the number of discreteness error stacked in the range to be measured.

Now we may write, separating the item corresponding to  $m = 0$ :

$$\hat{S} = N + K_W \sum_{m=1}^K A_m \cos \left\{ \pi m \eta \left[ 2 \left( 1 - \varepsilon - \frac{\varphi_s}{\pi} \right) + N - 1 \right] \right\} \frac{\sin(N\pi m \eta)}{\sin(\pi m \eta)} \quad (2.15)$$

Then, having not missed the consideration generality, we assume that  $\varphi_s = 0$ . For further calculation, the relation between variables  $\varepsilon$  and  $\chi$  determining the DFS zero number  $N$  during the half-period of modulation, and, hence, the upper limit of summing in (2.7), (2.9), and (2.15), has the essential significance. It is known [6] that the number of the DFS zeros on the half-period of modulation is  $N = M$  or  $N = M + 1$ . From the definition of the normalized time in (2.14), it follows that in the time interval  $[0, T_{mod}/2]$  the condition  $t_{norm,i} < 1$  is performed. Hence, for the zero with a maximal number  $i = N$ , the equation is true:

$$\frac{N-1+\varepsilon}{M+\chi} \leq 1 \leq \frac{N+\varepsilon}{M+\chi} \quad (2.16)$$

If the inequality  $1 - \varepsilon \geq \chi$  is performed, for carrying out the right part of inequality (2.16) it is enough that  $N = M$ . Otherwise, that is, at the performance of inequality  $1 - \varepsilon < \chi$ , we obtain  $N = M + 1$ . The variation of the relation between variables  $1 - \varepsilon$  and  $\chi$  at the range variation and, accordingly, the variation of  $N$  are shown in Figure 2.2.

Taking into consideration the above-mentioned and the reduction formulas [5], we obtain from (2.15) for both cases under investigation the following relations between variables  $1 - \varepsilon$  and  $\chi$ :

$$\hat{S} = \begin{cases} M - K_W \sum_{m=1}^K A_m G_1[m\eta] & \text{for } 1 - \varepsilon \geq \chi \\ 1 + M + K_W \sum_{m=1}^K A_m G_2[m\eta] & \text{for } 1 - \varepsilon \leq \chi \end{cases} \quad (2.17)$$

where

$$G_1[z] = G_1[z, \chi, \varepsilon] = \cos[\pi z(1 - 2\varepsilon - \chi)] \frac{\sin[\pi z(1 - \chi)]}{\sin(\pi z)}$$

$$G_2[z] = G_2[z, \chi, \varepsilon] = \cos[\pi z(2 - 2\varepsilon - \chi)] \frac{\sin[\pi z(1 - \chi)]}{\sin(\pi z)}$$

In the formula (2.17), the functions  $G_1[*]$  and  $G_2[*]$  are the functions of three arguments. However, in many cases, dependence upon the first argument is determinative. Therefore, to reduce writing, the other two arguments will be taken into account in an explicit form only in cases when it is necessary for the specific situation. From (2.5) and (2.14), it follows that the exact value is  $\hat{S} = x_R = R/\delta_R = M + \chi$ . That

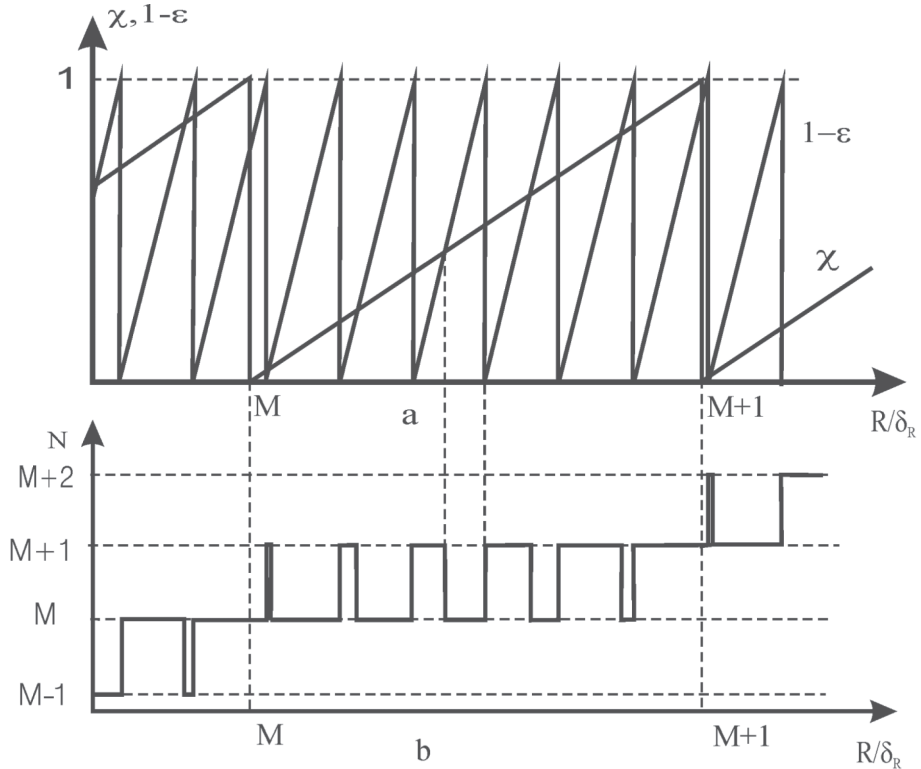


**Figure 2.2** Dependence of the DFS zero number versus the normalized range.

is why, summing and subtracting in each line of (2.17) the quantity  $\chi$ , we obtain the equation for the error  $\Delta_S$ :

$$\Delta_S = \begin{cases} -\chi - K_W \sum_{m=1}^K A_m G_1[m\eta] & \text{for } 1-\varepsilon \geq \chi \\ 1 + \chi + K_W \sum_{m=1}^K A_m G_2[m\eta] & \text{for } 1-\varepsilon < \chi \end{cases} \quad (2.18)$$

The obtained formulas allow a calculation of the truncation error of range measurement using WF of the arbitrary type (2.9).

Many functions are known to satisfy requirements (2.2) and (2.10). For instance, a great number of functions are used at spectral analysis [7–10] for the reduction of the sidelobe levels. We examine in detail the family of functions:

$$\alpha(t) = K_W [1 - \cos(4\pi t/T_{\text{mod}})]^n \quad (2.19)$$

where  $K_W$  is the normalizing multiplier and  $n = 1, 2, \dots$

The plots of these functions for some  $n$  are presented in Figure 2.3. In [3] the similar WF for the case  $n = 1$  is examined, as well as the exact function of the measurement error versus the measuring range. We obtain similar relations for the measurement error estimation at arbitrary  $n$ .

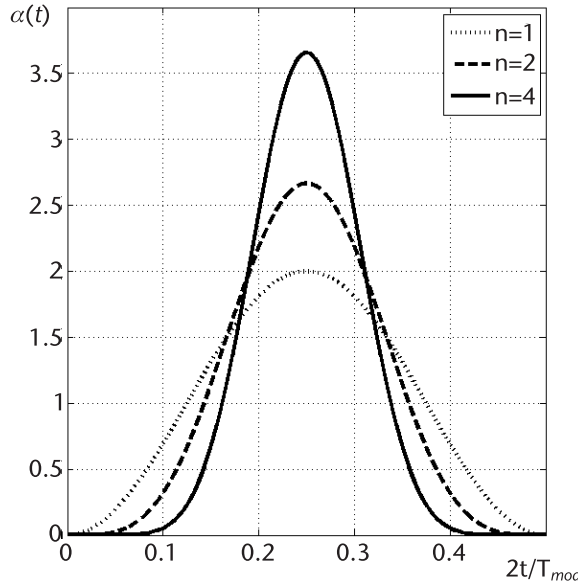


**Figure 2.3** Weighting functions.

Let us determine the value of normalizing coefficient  $K_W$ . Using the known trigonometric relation and the expansion of the sine function of even power into a series [5], we may represent the WF (2.19) as:

$$\alpha(v) = K_W 2^{-n} \left\{ (-1)^n 2 \sum_{j=0}^{n-1} (-1)^j C_{2n}^j \cos[(n-j)v] + C_{2n}^n \right\} \quad (2.20)$$

where  $v = 4\pi t/T_{\text{mod}}$  and  $C_p^q$  is a binomial coefficient [5].

Now we can find from (2.2):

$$K_W = 2^n / C_{2n}^n \quad (2.21)$$

Taking into account (2.21) and (2.15), we can rewrite (2.18) as:

$$\Delta_{S_n} = \begin{cases} -\chi - \frac{2(-1)^n \sum_{j=0}^{n-1} (-1)^j C_{2n}^j G_1[(n-j)\eta]}{C_{2n}^n} & \text{for } 1-\varepsilon \geq \chi \\ 1-\chi + \frac{2(-1)^n \sum_{j=0}^{n-1} (-1)^j C_{2n}^j G_2[(n-j)\eta]}{C_{2n}^n} & \text{for } 1-\varepsilon < \chi \end{cases} \quad (2.22)$$

where the index  $n$  in the error  $\Delta_{S_n}$  designation corresponds to an exponent in (2.19).

Let us perform the quantitative estimation of the above-mentioned errors at various ranges. The character of their variation principally differs from cases of very small ranges (less than  $4\delta_R$ ) and of all others.

The plots of measurement errors  $\Delta_{S1}$ ,  $\Delta_{S2}$ , and  $\Delta_{S4}$  are presented in Figure 2.4.

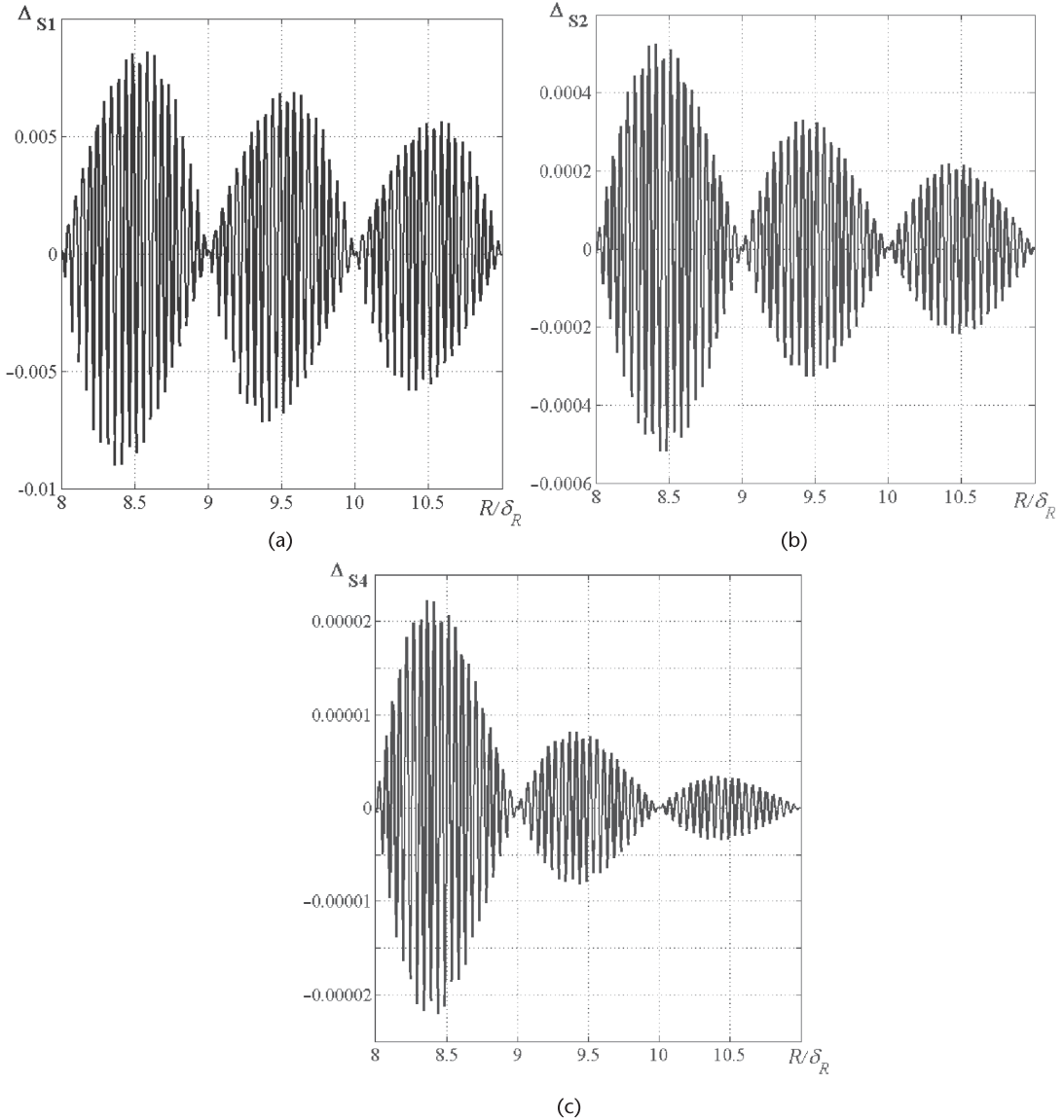


**Figure 2.4** (a–c) Functions of the relative measurement error versus the normalized range.

From the presented plots, we see that for the examined WFs the error is a periodic damping function of the range. As well, at small ranges, the monotonic decrease of the total error level is observed for increasing range. Exactly zero errors are observed on those ranges, when the DFS zeros as the interpolation points are located symmetrically with respect to a center of the analysis interval. In this position, the error of the numerical calculation of the integral (2.1) on the left WF slope is equal in value and opposite in sign to the similar error arising on the right slope and their mutual compensation happens.

In the point at which the envelope is equal to zero, the interpolation point position is symmetrical with respect to the analysis interval center and the end points coincide with the interval boundaries. We call these points the *envelope*

nodes (ENs). At the transfer through each such range point, the DFS zero number increases by one, that is, the increase of interpolation points' number is provided at the numerical calculation of the integral in (2.1). Therefore, there is a reduction of the calculation error. The quantitative values of the error, the speed of its damping with increasing range, and the range point, from which the second periodicity begins to be manifested, depend upon the exponent  $n$ .

The plots of functions of measurement errors versus the range for various WFs in the form presented in Figures 2.4 and 2.5 are inconvenient. It is expedient to use some generalized quantity related to the total error level. For example, it can be the envelope of these plots. However, it is difficult to determine it.

Earlier for this purpose, the integral characteristic (1.70) was introduced equal to the MSD calculated over the range interval. In conformity with the given case, (1.70) can be rewritten as:

$$\sigma_{\Delta}^2 = \overline{\Delta_S^2(M)} = \sum_{k=1}^L \Delta_S^2(R_{M,k})/L \quad (2.23)$$

where  $L = \delta_R/\Delta$ ,  $\Delta$  is a step in range within the limits of the one discrete averaging segment in range  $[M\delta_R, (M + 1)\delta_R]$ ; and  $R_{M,k} = M\delta_R + (k - 1)\Delta$  is the  $k$ th range reading within the limits of the specified  $M$ th segment of averaging.

Figure 2.5 shows error plots calculated according to (2.23) using (2.22).

The general view of plots and quantitative relations between truncation errors corresponding to different WFs strongly depend upon the function type and the range. The smooth decrease of the total error level is observed at the increasing range  $R$ . For a small range, the error values corresponding to WFs with the large value of  $n$  exceed the errors obtained for small values of  $n$ ; however, its speed of reduction is more.

When the range increases, the picture changes. At large ranges, a smaller error and a higher damping speed correspond to higher values of  $n$ , while the truncation error level essentially decreases when the range increases.

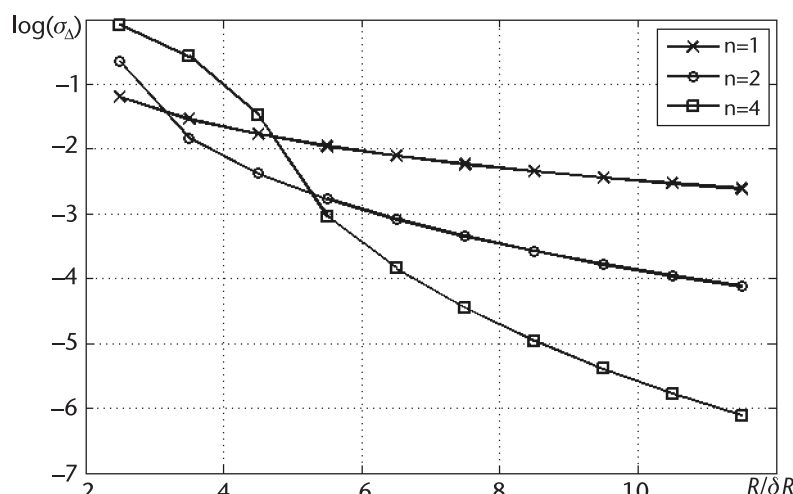


Figure 2.5 The function of normalized MSD versus the relative range.

One more WF is interesting; it has only one shape parameter, allowing the WF shape to change to a great extent. This is the Kaiser-Bessel (KB) WF [8], which has the following analytical record in the closed form:

$$\alpha(t) = \frac{I_0\left[\pi a \sqrt{1 - \left(\frac{2t}{T_{\text{mod}}}\right)^2}\right]}{I_0[\pi a]}, \quad t \in [-T_{\text{mod}}/4, T_{\text{mod}}/4] \quad (2.24)$$

where  $I_0[*]$  is the modified Bessel function of the first kind [5] and  $a$  is a parameter specifying the function shape. In such a view, this function is used during the spectral analysis and it is normalized to 1. In our case, it is necessary that the WF would satisfy the normalization condition (2.2). Using the equation  $I_0(x) = J_0(jx)$ , where  $J_0[*]$  is the Bessel function of the first kind, which is known as the integral [11]:

$$\int_0^y J_0\left(\sqrt{y^2 - x^2}\right) dx = \sin y \quad (2.25)$$

and presenting:

$$\sin y = \frac{e^{-jy} - e^{jy}}{2} \quad (2.26)$$

we can obtain the formula for the WF KB with the required normalization:

$$\alpha(t) = \frac{2\pi a}{e^{\pi a} - e^{-\pi a}} I_0\left[\pi a \sqrt{1 - \left(\frac{2t}{T_{\text{mod}}}\right)^2}\right] \quad (2.27)$$

Taking into account that the real values  $a > 1$  can be written with high accuracy as:

$$\alpha(t) = 2\pi a e^{-\pi a} I_0\left[\pi a \sqrt{1 - \left(\frac{2t}{T_{\text{mod}}}\right)^2}\right], \quad t \in [-T_{\text{mod}}/4, T_{\text{mod}}/4] \quad (2.28)$$

such a WF is suitable by the fact that only one parameter  $a$  changes its shape in wide limits. However, it does not have the second WF property of decreasing to zero on boundaries of the interval  $T_{\text{mod}}$ , although the difference from zero is very small and decreases with the  $a$  parameter increasing.

A change of the WF shape (2.28) at the variation of the  $a$  parameter is shown in Figure 2.6.

Substituting (2.28) into (2.7), we obtain [12]:

$$\hat{S} = 2\pi a e^{-\pi a} \sum_{i=1}^N I_0\left[\pi a \sqrt{1 - \left(\frac{2t_i}{T_{\text{mod}}}\right)^2}\right] \quad (2.29)$$

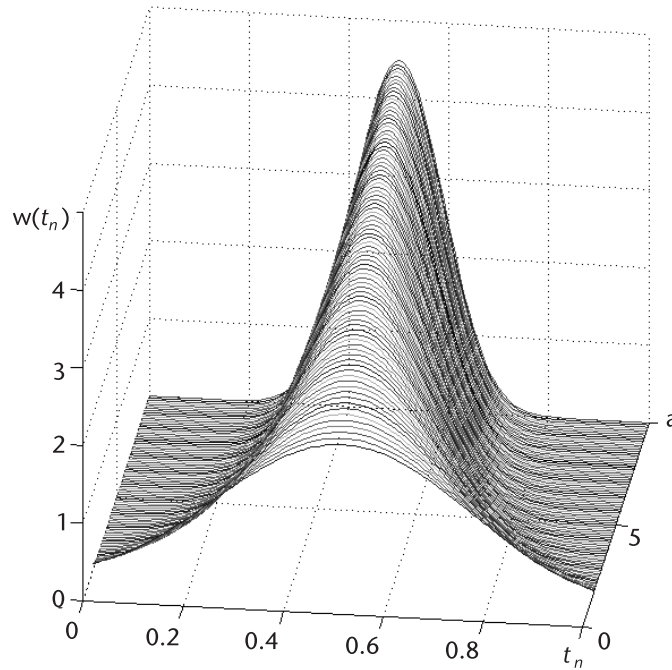


**Figure 2.6** The WF KB profile at variation of the  $a$  parameter.

Using in (2.29) the normalized time (2.14), we obtain:

$$\hat{S} = 2\pi a e^{-\pi a} \sum_{i=1}^N I_0 \left[ \pi a \sqrt{1 - (i-1+\varepsilon)^2 \eta^2} \right] \quad (2.30)$$

Taking into account that  $N = M$  for  $\varepsilon \geq \chi$  or  $N = M + 1$  for  $\varepsilon < \chi$ , we can write:

$$\hat{S} = 2\pi a e^{-\pi a} \begin{cases} \sum_{i=1}^M I_0 \left[ \pi a \sqrt{1 - (i-1+\varepsilon)^2 \eta^2} \right] & \text{for } \varepsilon \geq \chi \\ \sum_{i=1}^{M+1} I_0 \left[ \pi a \sqrt{1 - (i-1+\varepsilon)^2 \eta^2} \right] & \text{for } \varepsilon < \chi \end{cases} \quad (2.31)$$

In a similar manner as in (2.18), we obtain equations for the error  $\Delta_S$  taking into account that the exact value of  $\hat{S} = M + \chi$ :

$$\Delta_S = -M - \chi + 2\pi a e^{-\pi a} \begin{cases} \sum_{i=1}^M I_0 \left[ \pi a \sqrt{1 - (i-1+\varepsilon)^2 \eta^2} \right] & \text{for } \varepsilon \geq \chi \\ \sum_{i=1}^{M+1} I_0 \left[ \pi a \sqrt{1 - (i-1+\varepsilon)^2 \eta^2} \right] & \text{for } \varepsilon < \chi \end{cases} \quad (2.32)$$

The results of the error calculation in accordance with (2.32) for three parameter values  $a = 2, 4, 6$  are presented in Figure 2.7. As we see, similar to Figure 2.4, the error is the periodic damping function of the range. Two types of periodicity are

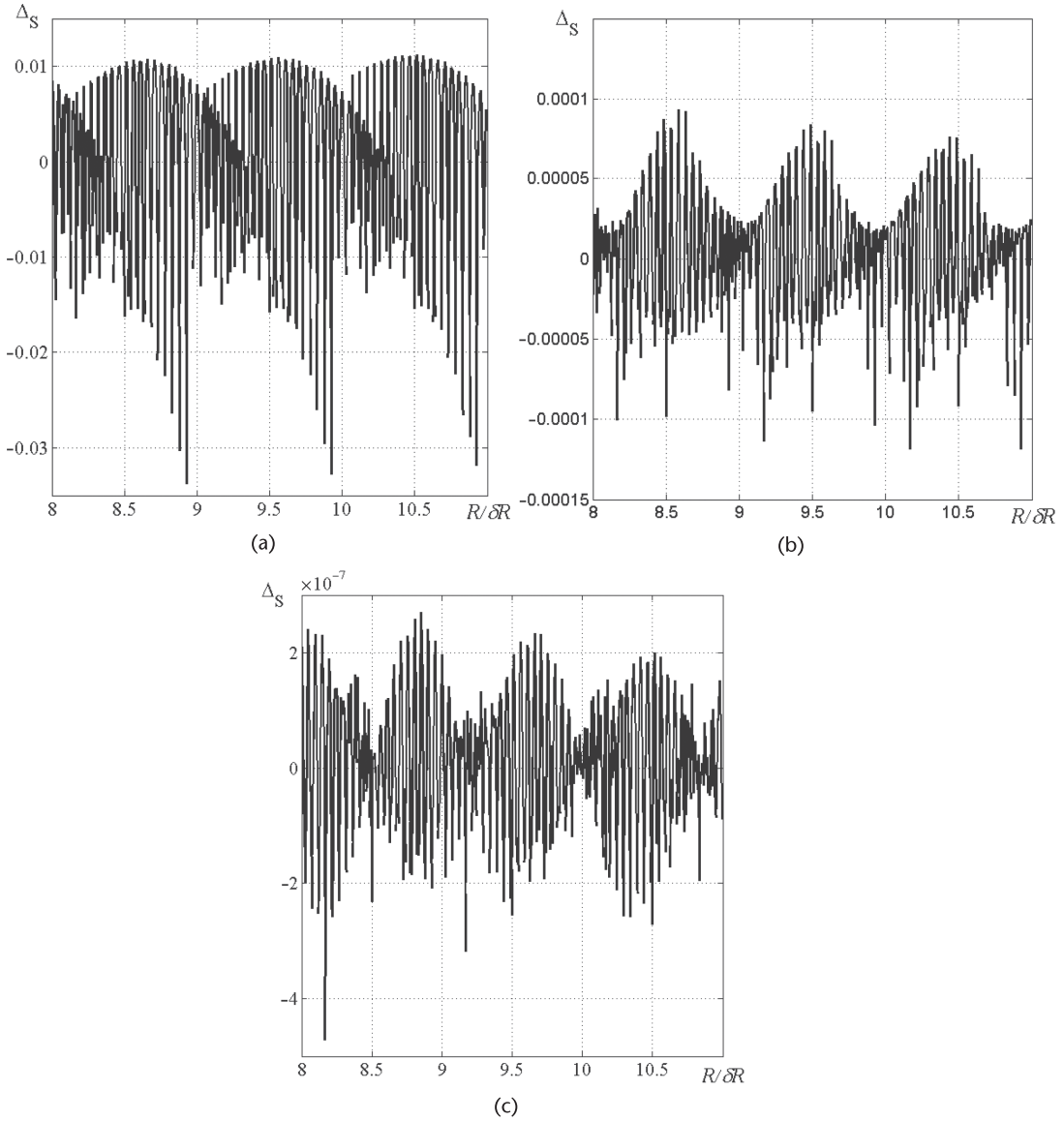


**Figure 2.7** The functions of the instantaneous normalized error versus the normalized range.

observed. The first one has a period equal to a half-wavelength of the carrier oscillation. The second one has the alternating period. The variation of the second period is stronger, manifested with the  $a$  parameter increasing. The error decreases very quickly, with the range increasing except for small ranges when  $M(R) < 3\dots 4$ , and the error may be largely inadmissible. The quantitative values of the error and its damping speed at the increased range depend upon the value of the WF  $a$  parameter. Based on these figures, it is rather difficult to compare WFs with different values of the parameter  $a$ .

Figure 2.8 shows average functions, in accordance with (2.23), of the normalized error versus the normalized range for four values of the parameter  $a = 2, 4, 6$ , and 8.

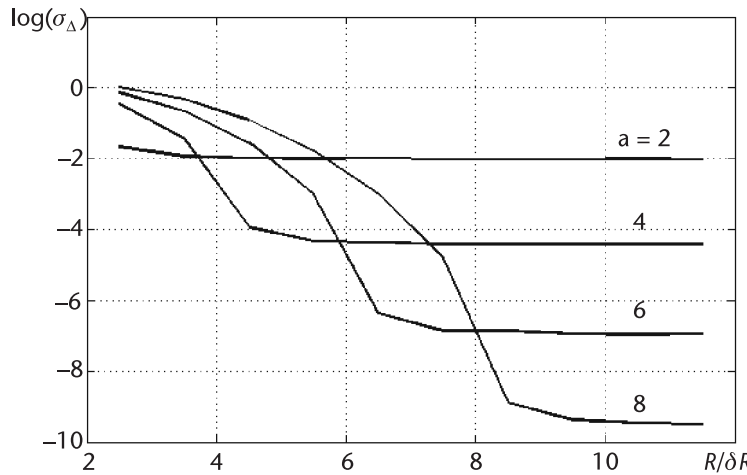


**Figure 2.8** The function of the normalized averaged error versus the normalized range.

From Figure 2.8, we see that in all plots two regions can be distinguished: the initial part in which the error sharply changes and the part in which the averaged error is not practically changed at the range variation. It is clear that at the range variation one can find such a value of the parameter  $a$ , at which the minimum of the average error for a given range is achieved. This is the minimal value of the error that can be designated in Figure 2.8 to draw the tangent to these plots in the points of inflection.

### 2.3 Truncation Error Minimization at the Weighting Average Method of Difference Frequency by Optimization of Weighting Function Parameters

Equation (2.23) permits the formulation of the problem of the parametric optimization of WF  $\alpha(t)$  in (2.9), consisting in the selection of coefficients  $A_m$  with the purpose of minimization of the truncation measurement error [13]. The function of the measurement error's MSD (2.23) versus the range is the complex function, which quickly decreases while the range increases. Therefore, it is expedient to provide the local coefficient optimization trying to minimize the error within the limits of some of the averaging parts in the range.

It was suggested earlier to calculate MSD on the range parts equal to the value of one QI, that is, within the limits

$$M(R)\delta_R < R < [M(R) + 1]\delta_R \quad (2.33)$$

For each such a part, we can determine the set of coefficients corresponding to the minimum of the error's average square. For the optimization of the coefficients  $A_m$ , we can obtain the system of linear equation:

$$\frac{d\overline{\Delta_s^2(M)}}{dA_m} = 0, \quad m = 1, 2, \dots, K \quad (2.34)$$

Substituting (2.18) into (2.34), we reduce the equation system with respect to the unknown values of the coefficients  $A_m$  to the standard form:

$$\sum_{m=1}^K \bar{A}_m d_{i,m}(M) = D_i(M), \quad i = 1, 2, \dots, K \quad (2.35)$$

where  $\bar{A}_m = K_W A_m$  are the normalized values of Fourier series coefficients for WF:

$$d_{i,m}(M) = \frac{1}{\delta_R} \sum_{k=1}^L F_1(i, m, R_{M,k}); \quad D_i(M) = \frac{1}{\delta_R} \sum_{k=1}^L F_2(i, R_{M,k});$$

$$F_1(i, m, R) = \begin{cases} G_1[i\eta(R)]G_1[m\eta(R)] & \text{for } 1 - \varepsilon(R) \geq \chi(R); \\ G_2[i\eta(R)]G_2[m\eta(R)] & \text{for } 1 - \varepsilon(R) < \chi(R); \end{cases};$$

$$F_2(i, R) = \begin{cases} \chi(R)G_1[i\eta(R)] & \text{for } 1 - \varepsilon(R) \geq \chi(R) \\ [1 - \chi(R)]G_2[i\eta(R)] & \text{for } 1 - \varepsilon(R) < \chi(R) \end{cases}$$

Here we note in an explicit form the function of the main parameters versus range  $[\chi(R), \varepsilon(R), \eta(r)]$ . The obtained equation system allows the calculation of the WF optimal parameter sets on each  $M$ th part for the given value of  $K$ , that is, to provide the local WF optimization of the specified view.

The calculation results of optimal coefficients according to (2.35) for several values of  $K$  are shown in Table 2.1.

We should note that at a small range the values of optimal coefficients strongly differ from the initial coefficients for used WFs. With the range increasing, the optimal coefficients tend to these initial values, which can be seen from the plots presented in Figures 2.9, that is, the known WFs give the best results only for the measurement of large ranges.

The variation of the shape of the optimal WFs (2.9) at a variation of measured range is shown in Figure 2.9(a) for  $K = 1$  and in Figure 2.9(b) for  $K = 4$ .

We can note that on small ranges WF has the smoother form. This is caused by the fact that on small ranges the small number of zeros forms during the analysis interval due to the displacement of extreme zeros for the much larger value. Therefore, WF should not sharply change starting from the condition of error minimization.

**Table 2.1** Optimal WF Coefficients

K	A	R/dR						
		2.5	4.5	6.5	8.5	10.5	12.5	14.5
1	$A_1$	-0.88	-0.966	-0.984	-0.991	-0.994	-0.996	-0.997
2	$A_1$	-0.957	-1.257	-1.298	-1.313	-1.32	-1.324	-1.326
	$A_2$	0.0365	0.259	0.298	0.313	0.32	0.324	0.326
4	$A_1$	-0.94	-1.366	-1.514	-1.55	-1.568	-1.577	-1.583
	$A_2$	0.0298	0.402	0.636	0.7	0.736	0.755	0.767
	$A_3$	-0.009	-0.036	-0.132	-0.169	-0.189	-0.2	-0.207
	$A_4$	-0.007	0.00008	0.0096	0.0163	0.0201	0.0225	0.024

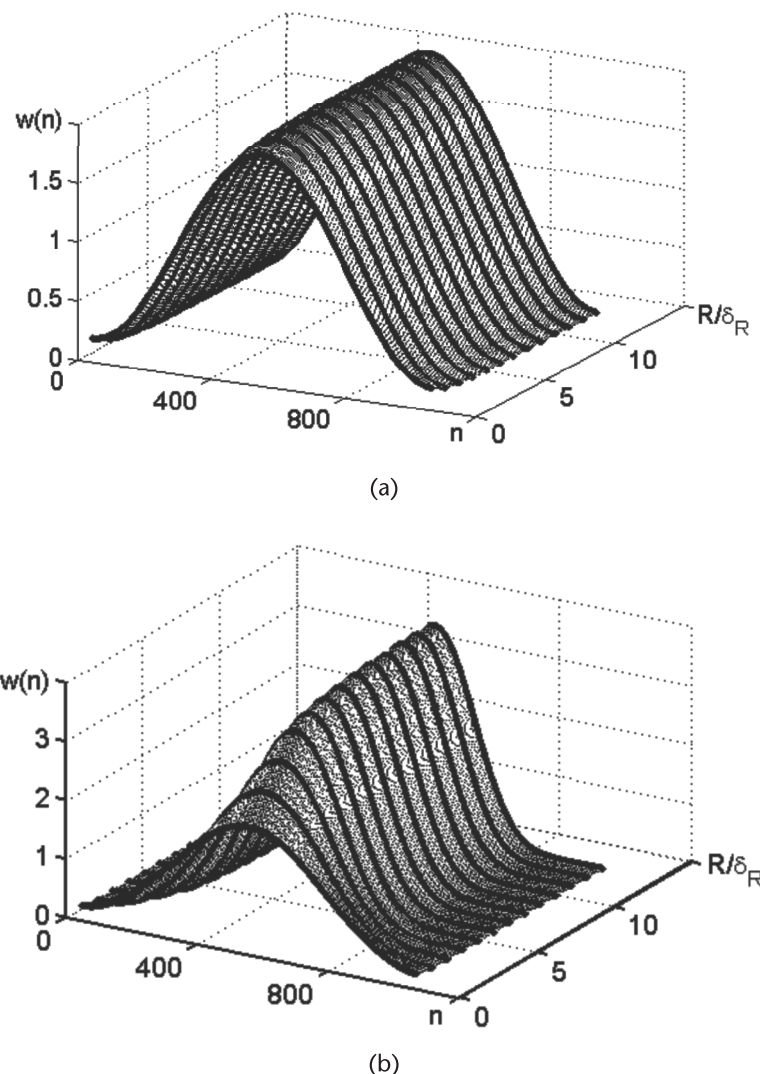


**Figure 2.9** Profiles of optimal WFs: (a)  $K = 1$  and (b)  $K = 4$ .

However, as well, the discreteness error smoothing is less effective and the measurement error on small ranges is increased.

Range increasing leads to a decrease in the maximal deviation of extreme zeros with respect to analysis interval boundaries and, hence, to the assumption of sharper WF variation providing a better suppression of the discreteness error. More complicated WFs have a larger range of shape variation and, therefore, allow for the achievement of the less measurement error.

Figure 2.10 shows functions of normalized MSD of measurement result versus the relative range obtained at the application of WF optimal parameters. The optimization of parameters allows essentially a decrease in the measurement error compared with Figure 2.5. In addition, the effect is larger for more series numbers used for WF representation, that is, for a more complicated WF shape. With increasing range, the error is essentially decreased.

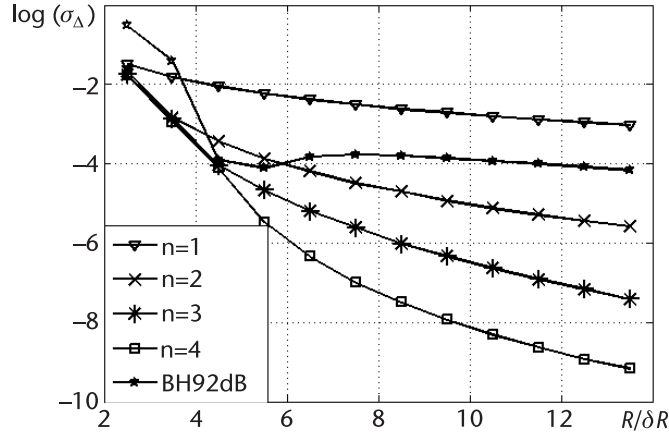


**Figure 2.10** The function of normalized MSD versus relative range for optimal coefficients.

For comparison, Figure 2.10 shows the plot corresponding to the WF of Blackman-Harris (BH 92 dB). We can note that it touches one point of the plot corresponding to  $n = 3$ , that is, this WF is optimal for the one fixed part. At other ranges, the error achieved with the help of the Blackman-Harris WF exceeds the optimal values of parameters. As well, for smaller ranges, the error is sharply increased while for larger ranges it at first smoothly increases and then remains almost unchanged.

Let us examine the problem of the parameter  $a$  optimization of the WF KB (2.28) allowing the provision of the minimum of averaged error determined according to (2.23) using (2.32). For the optimization of the coefficient  $a$ , we can obtain an equation similar to (2.34):

$$\frac{\partial \overline{\Delta_S^2(M)}}{\partial a} = 0 \quad (2.36)$$

Substituting (2.32) into (2.23), we obtain from (2.36):

$$\begin{aligned} & \sum_{k=1}^L \left\{ -M_k - \chi_k + 2\pi a e^{-\pi a} \sum_{i=1}^N I_0 \left[ \pi a \sqrt{1 - (i - 1 + \varepsilon_k)^2 \eta_k^2} \right] \right\} \\ & \times \left\{ (1 - \pi a) \sum_{i=1}^N I_0 \left[ \pi a \sqrt{1 - (i - 1 + \varepsilon_k)^2 \eta_k^2} \right] \right. \\ & \left. + \pi a \sum_{i=1}^N \sqrt{1 - (i - 1 + \varepsilon_k)^2 \eta_k^2} I_1 \left[ \pi a \sqrt{1 - (i - 1 + \varepsilon_k)^2 \eta_k^2} \right] \right\} = 0 \end{aligned} \quad (2.37)$$

where  $N = M_k$  for  $\varepsilon_k \geq \chi_k$  and  $N = M_k + 1$  for  $\varepsilon_k < \chi_k$ .

Equation (2.37) is nonlinear and has no analytical solution. Therefore, optimization was performed in the programming medium MATLAB with the help of the function of the multidimensional “fminseach” for several intervals of ranges. As a result, the function of optimal values of the shape parameter  $a$  of WF KB versus the

average range corresponding to the middle of the averaging interval was obtained. It turns out that this function can be approximated by a straight line having the empirical expression for the optimal value of the WF shape parameter:

$$a_{opt} = 1,067(M + 0.5) - 0.6061 \quad (2.38)$$

The profiles of the optimal WF KB are shown in Figure 2.11.

The function of the normalized averaged truncation error versus the normalized range for WF KB obtained according to (2.23) using optimal values of the parameter  $a_{opt}$  in (2.38) is presented in Figure 2.12 by the solid curve.

We see that it is practically tangent to earlier drawn plots designated by dotted curves and corresponding to specific values of the parameter  $a$  ( $a = 2, 4, 6, 8$ ). The measured range increase leads to an error decrease. If the normalized range is more than 12, the quantization noise begins to proclaim itself caused by the finite accuracy of computer calculations.

Comparing Figures 2.10 and 2.12, we may notice that the WF KB with optimal parameters allows us to obtain the lesser measurement error than the WF in (2.9) at the same ranges. It can be explained by the fact that the range of WF KB shape variation at the changing of the shape parameter  $a$  is much larger than for the WF

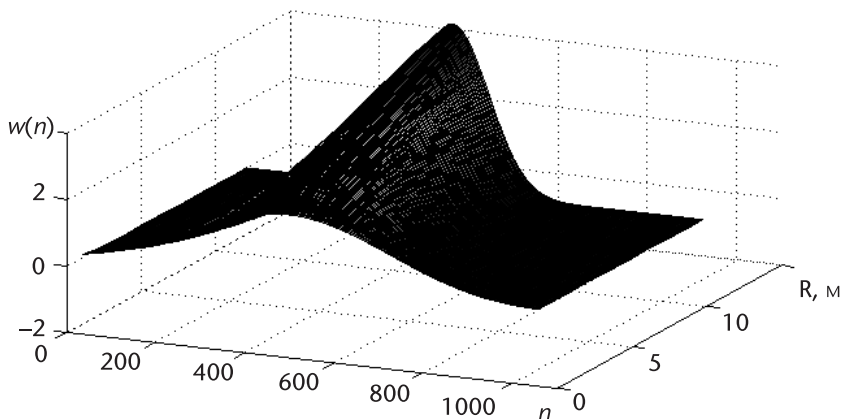


**Figure 2.11** Profiles of the optimal WF KB.

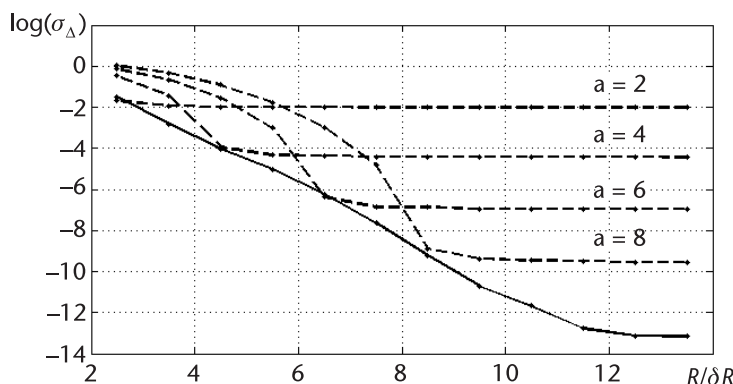


**Figure 2.12** The function of the normalized averaged truncation error versus the normalized range for the WF KB.

in (2.9) for a small number of items. The results of the previous section allow the assumption that at the increase of the WF item number in (2.9), we can approach the average error, ensuring it to the error obtained using WF KB. Nevertheless, the application of the WF KB is much more convenient as it requires optimization of the only one WF shape parameter, and for the WF in (2.9) the number of such parameters sharply increases with the item number increasing.

For a practical application, the sets of optimal coefficients calculated in advance for each part of the range should be saved in the memory of the calculating device of the FMCW RF and be extracted as far as the measured range will change.

At the first measurement after the RF switching on, it is expedient to use sets of coefficients corresponding to the least range, at which the error does not exceed some admissible limit. In this case, the measurement error at all other ranges will be enough to determine the number of the current discrete parts of averaging. According to this result, the value on normalized range is determined and the number of the averaging part  $M = \text{Int}(R/\delta_R)$  can be determined. After that, based on Table 2.1 for the WF in (2.9) or on the formula (2.34) for the WF KB, the optimal values of parameters are determined and new measurement is executed.

In most cases for the WF in (2.9), we are limited by the small set of optimal coefficients for small ranges (up to  $M \leq 7$ ). At other ranges typical for this set, it is necessary to use coefficients corresponding to the largest range from the considered ones. As well, the truncation measurement error for large ranges remains about constant corresponding to the last considered set of optimal coefficients.

## 2.4 Truncation Error Minimization of the Weighting Averaging Method of the Difference Frequency by Optimization of the FM Parameters

The analysis of functions of the instantaneous measurement error versus the normalized range shown in Figures 2.3 and 2.4 for the WF in (2.9) allows the suggestion of algorithms for the FM parameter optimization, which reduces the truncation error [14]. These algorithms consider the periodicity of the truncation error at the range variation and the modulation parameter influence on the EN error position on the axis of normalized range.

The almost periodic character of the function of instantaneous truncation error allows the assumption that by controlling by the carrier frequency similar to the approach offered in [15, 16] and investigated in detail and averaging the measurement results, we can reduce the measurement error almost to a zero level.

The EN presence on the plot of the instantaneous error versus the normalized range allows getting the point corresponding to the specific normalized range in the nearest EN by controlling the FM sweep. Evidently, joining these two approaches, we can combine their positive properties.

### 2.4.1 Application of Additional Slow-Frequency Modulation

The instantaneous truncation error presented in Figure 2.4 shows that the truncation error has a period of fast oscillations in range equal to a half-wavelength of the

carrier signal. The same conclusion follows from the formula (2.8) representing the equation for DFS zero determination. From this equation, we see that the period of error variation in phase is  $\pi$ . Varying the phase  $\Phi$  in the limits  $[0, \pi]$  at a fixed range and averaging the obtained results, we may minimize the average value of the range measurement error. We can vary the DFS phase using additional slow FM of the carrier frequency  $\omega_0$  by the value of  $\Delta\omega_{\text{slow}}$ . From this, it follows that at a fixed range we may obtain one period of error variation by varying the frequency of the carrier signal in such a manner to perform the condition:

$$\Delta\omega_{\text{slow}}t_{\text{del}} = \pi \quad (2.39)$$

or the similar condition:

$$\Delta F_{\text{slow}} = \Delta F\eta \quad (2.40)$$

Let us estimate the extremely possible benefit in the value of the truncation error, when we use the additional slow modulation. For estimation, we use the numerical approach. For this, we calculate the truncation error obtained using algebraic WFs with the assumption that we know the exact measuring range. Of course, this is a practically unrealistic case, but it allows the estimation of the extreme possibilities of the method. To calculate the error, we use the formula (2.22). At each fixed range, using (2.40), we obtain the value of an additional slow FM sweep. After that, we change the carrier frequency in the range from  $f_0$  to  $f_0 + \Delta F_{\text{slow}}$  with the fixed step  $\Delta F_{\text{slow}}/N_{\text{aver}}$  (where  $N_{\text{aver}}$  is the number of the average measurements) and calculate on each frequency the measurement truncation error. Then, after the selection of all frequencies in the specific frequency range, we average the results. The resulting function of such measurements in each fixed range point versus the measuring range is oscillation. The character of these oscillations reminds the oscillating character of the truncation error shown in Figures 2.4. Therefore, we present the calculation results on the basis of the mentioned approach in the form of logarithm of normalized averaged (over the range) within the limits of the one QI in accordance with (2.23) and Figure 2.13. These plots are obtained under condition when in the mentioned frequency range of slow tuning of the carrier frequency, 100 points were used.

We see from these plots that this optimization method allows the determination of the less essential errors than the optimization of the WF shape. With the measuring range increasing, the error decreases. If the number of averaging points increases, the error also decreases. More complicated WFs ensure less error. However, there is a limit of error reduction caused by computer digit capacity, which is seen from the plot corresponding to  $n = 4$ . In this plot the segment is demonstrated beginning from the normalized range  $R/\delta_R = 5.5$ , when the error is almost unchanged. Therefore, there is a limit for the number of averaging points, which depends upon microprocessor digit capacity used for implementation of this method.

In practice, the measuring range is unknown before measurement performance. Therefore, it is expedient to make this optimization algorithm an iterative one with frequent repetition of measurements and specification  $\Delta F_{\text{slow}}$  according to (2.40) at the each iteration.

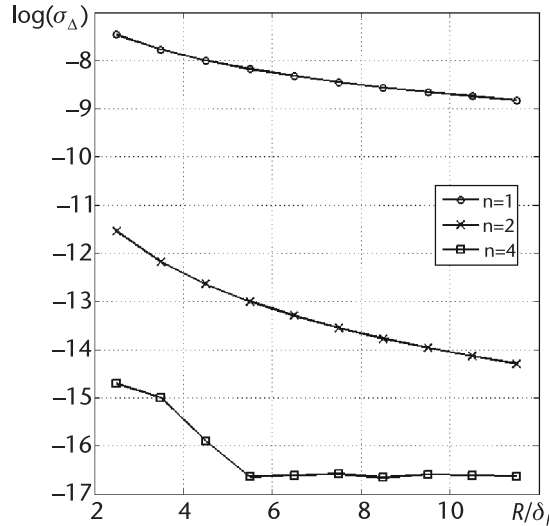


**Figure 2.13** The function of the logarithm of the extreme averaged normalized error versus the normalized range.

- *Step 1:* The first measurement of the range is provided without additional FM for determination of the zero approximation  $\hat{\eta}^{(0)}$  and calculation of  $\Delta F_{\text{slow}}^{(0)}$  according to (2.40).
- *Step 2:* N measurements of the range are provided at discrete variation of the carrier frequency from the one measurement to another in the range from  $f_0$  to  $f_0 + \Delta F_{\text{slow}}^{(n)}$  with the step  $\Delta F_{\text{slow}}^{(t)}/N$  and the following approximation is found:

$$\frac{1}{\hat{\eta}^{(n)}} = \frac{1}{N} \sum_{i=1}^N \frac{1}{\hat{\eta}_i^{(n)}} \quad (2.41)$$

where  $\hat{\eta}_i^{(n)}$  is the estimation of quantity  $\eta$  for the  $i$ th measurement.

- *Step 3:* The calculation of the new value of the slow FM sweep  $\Delta F_{\text{slow}}^{(n+1)}$  is performed according to (2.40).
- *Step 4:* Steps 2 and 3 are repeated until the reduction of the modulus of difference between the new obtained value  $\hat{\eta}^{(n)}$  and its previous value  $\hat{\eta}^{(n-1)}$  will be lesser than that specified in the advance value  $\Delta_\eta$ :

$$|\hat{\eta}^{(n-1)} - \hat{\eta}^{(n)}| \leq \Delta_\eta \quad (2.42)$$

The value of the provided error depends upon the given advance value of  $\Delta_\eta$  and the quantity of averaging points  $N$ . Calculations show that by decreasing  $\Delta_\eta$  and increasing  $N$ , we may achieve the limiting measurement error shown in Figure 2.13.

A number of iterations necessary for achievement of condition (2.42) strongly depend upon the measuring range, the WF shape, the given value  $\Delta_\eta$ , and the number of averaging points  $N$  and varies from 4 to 5 to 50 to 60. In other words, the total number of measurements will vary from  $4N$  to  $60N$ .

The function of the FM sweep value of additional slow FM normalized to the FM sweep value of fast FM versus the normalized measuring range is shown in Fig-

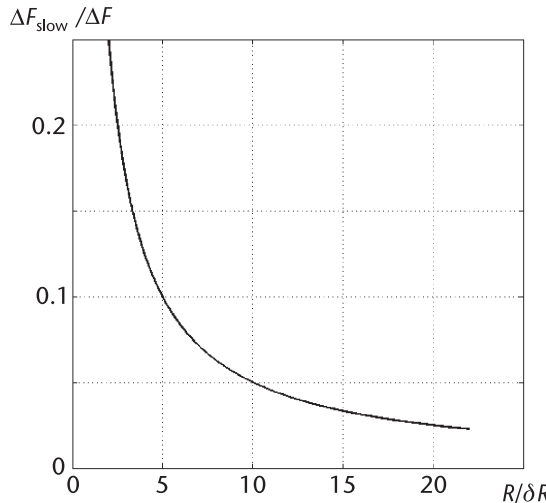


Figure 2.14 The function of the normalized FM sweep of slow FM versus the normalized range.

ure 2.14. The plot view does not depend upon the WF shape. Therefore, for small ranges, the FM sweep value of additional slow FM achieves 50% from the main FM sweep of fast modulation.

The described method for error reduction requires significant additional resources in the FM sweep and the measurement time.

#### 2.4.2 Optimization of the FM Sweep

This method of optimization takes into account invariability of position on the axis of the EN normalized range with the zero measurement error at invariability of WF parameters. At the same time, the position of the point corresponding to the measured range depends upon the value  $\delta_R$ ; that is, upon the value of FM sweep  $\Delta F$ . Therefore, in each point of the normalized range axis, we can displace this point along this axis to the one of the nearest EN (Figures 2.4 and 2.5) by varying  $\Delta F$ . Therefore, we should take into consideration that the position of the first EN on the normalized range axis depends on the parameter  $n$  as follows:

$$\frac{R_{\text{nodes}}}{\delta_R} = n + 1 \quad (2.43)$$

The procedure of optimization of the FM sweep supposes the multiple repeat of measurements with correcting of the FM sweep  $\Delta F$  in accordance with measured range, that is, it is iterative and with the account of (2.43), it consists of the following steps:

- *Step 1:* The measurement of the range  $R_{\text{meas}}^{(0)}$  is performed at some initial value  $\Delta F^{(0)}$  to obtain zero approximation  $\hat{\eta}_R^{(0)} = \delta_R^{(0)}/R_{\text{meas}}^{(0)}$  and to determine on the normalized range axis the exact position of the nearest EN, which is located on the left of the current normalized point

$$\frac{1}{\hat{\eta}_{R\text{exact}}} = \max \left\{ n + 1; \text{Int} \left[ \frac{R_{\text{meas}}^{(0)}}{\delta_R^{(0)}} \right] \right\} \quad (2.44)$$

- Step 2: The value of the FM sweep is corrected

$$\Delta F^{(n)} = \frac{\Delta F^{(n-1)} \hat{\eta}_R^{(n-1)}}{\hat{\eta}_{\text{Reexact}}} \quad (2.45)$$

- Step 3: Using the obtained value  $\Delta F^{(n)}$ , we perform a new range measurement for the calculation of the next approximation  $\hat{\eta}_R^{(n)}$ .
- Step 4: Steps 2 and 3 are repeated until condition (2.42) is performed.

From (2.43) and (2.45), it follows that if the measuring normalized range is less than  $n + 1$ , the nearest EN on the normalized range axis turns out to be on the right of the current point. Therefore, to displace the current point in EN, we need to increase the FM sweep compared with the initial value. Otherwise, the FM sweep should be reduced. The maximal degree of the FM sweep increase corresponds to the minimal measuring range. If we assume that the minimal measuring range is such that there is the only one zero in the beating signal, which corresponds to the normalized range equal to 2, the FM sweep increase will achieve  $(n+1)/\sqrt{2}$  for the minimal range. If normalized range grows from the minimal to  $(n+1)$ , the smooth decrease of required FM sweep occurs to the initial value corresponding to the normalized range  $(n+1)$ . At the further increase of the normalized range, the character of the dependence becomes more complicated, being determined by the second parameter in (2.44).

The calculation results for the range measurement error in accordance with (2.22), which are used in the mentioned algorithm, are shown in Figure 2.15. These results are obtained for the initial FM sweep at 500 MHz. The view of plots strongly depends upon the WF type and the specified limit in the condition (2.38).

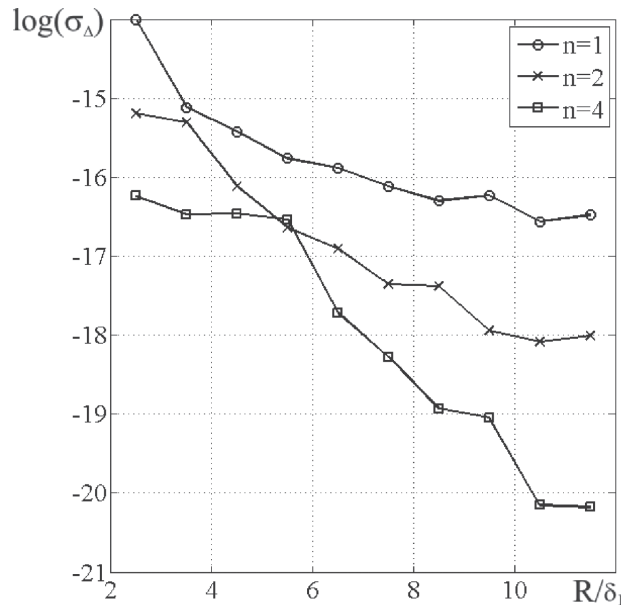


**Figure 2.15** The function of the normalized error logarithm versus the normalized range at optimization of the frequency FM sweep.

The reduction of this value to  $10^{-15}$  leads to the fact that all plots, beginning from some range, are connected to each other. Plots essentially differ only for normalized ranges, which are less than  $n + 1$ . In this case, the smaller error corresponds to the larger  $n$ , but this is achieved by the essential increase of the required FM sweep. In the comparison of Figures 2.15 and 2.16, the function of required FM sweep versus the normalized range is presented for different WFs.

The number of iterations required for achievement of the given error depends upon the value  $\Delta_\eta$ , the measuring range, and the WF shape, and at the variation of these parameters it can be changed from 2 to 3 to 100 to 150. It is clear that restricted frequency resource of the SHF module leads to a limitation of the minimal range for WF with large values of  $n$ . This method of FM sweep optimization does not require application of the complicate WFs. For this algorithm, the required number of measurements to achieve the given condition is equal to number of iterations.

#### 2.4.3 Combined Optimization

Let us examine how we can combine the above-mentioned minimization methods to save their positive properties and to reduce of required iteration number. The method of error averaging with the help of additional slow modulation allows obtaining the smaller error compared with optimization of the FM sweep and we may expect that it is less sensitive to the noise effect. However, this method requires the performance of a greater number of measurements.

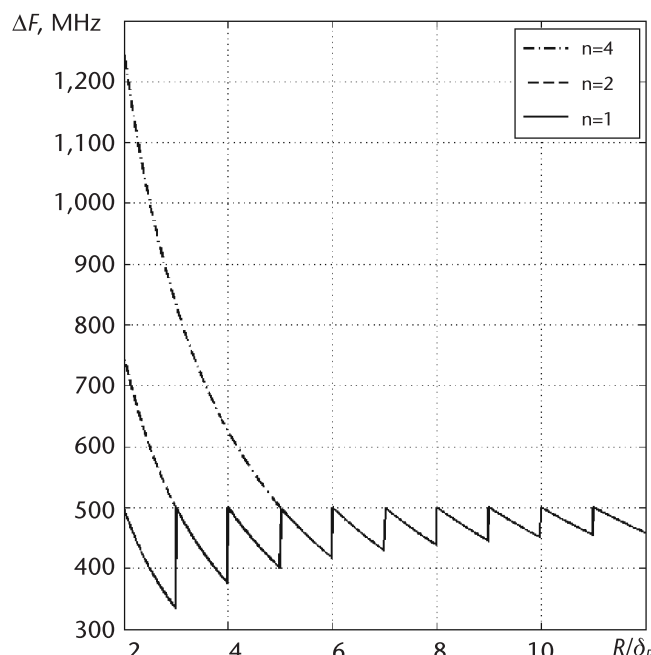


**Figure 2.16** The function of the FM sweep required for minimization of the measurement error versus the normalized range at various WFs.

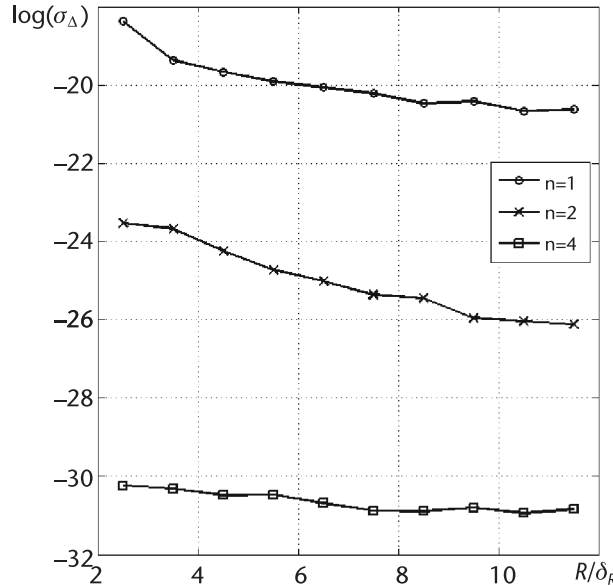


**Figure 2.17** The function of the normalized error logarithm versus the normalized range using the combined optimization.

#### 2.4.4 The Combined Procedure of Error Minimization

The following combined procedure is used to minimize error:

- *Step 1:* The optimization of the FM sweep of fast FM is provided, which ensures the displacement of the current operating point in the point corresponding to the nearest node.
- *Step 2:* Using the obtained value of the FM sweep, the preliminary range measurement is executed.
- *Step 3:* According to the measured range, with the application of (2.40), we determine the required value of the FM sweep of slow FM.
- *Step 4:* Using the obtained values of the FM sweep of fast and slow FM, we provide one cycle of slow tuning of the carrier frequency with the measurement result averaging for a more precise specification of the range measured at the first step.

The results of truncation error calculation according to formula (2.22) obtained with the help of the combined algorithm are shown in Figure 2.17. We see that theoretically such the combined algorithm allows the essential reduction of the truncation error at measurement. In addition, the dependence of achieved level of measurement error upon the WF shape is kept.

### 2.5 Noise Influence on the Error of the Weighting Method of Difference Frequency Averaging

Let us estimate the additive noise effect on results of range measurement with the help of the weighting method of QI smoothing according to formulas (2.5) and

(2.7). Due to the noise affect, time moments  $t_i$  are displaced by the value  $\Delta t_i$  of the true meaning. Then, for the estimation of  $\hat{S}$  assuming that the noise level is small compared with the signal [13], we may write:

$$\hat{S} = \sum_{i=1}^N \alpha(t_i + \Delta t_i) \approx \sum_{i=1}^N [\alpha(t_i) + \alpha'(t_i)\Delta t_i] \quad (2.46)$$

The second item can be presented as the measurement error caused by the noise  $\Delta_{S,\text{noise}}$ :

$$\hat{S} = \sum_{i=1}^N \alpha(t_i) + \sum_{i=1}^N \alpha'(t_i\Delta t_i) = S + \Delta_{S,\text{noise}} \quad (2.47)$$

The moment displacement  $\Delta t_i$  of intersection by the sum of DFS derivative and the noise  $\Delta_U$  of the zero level was found in Chapter 1 in the form of the formula (1.60). Using the similar transformations to the sum of DFS and noise, we obtain:

$$\Delta t_i = \Delta_U T_{\text{mod}} / (2\pi U_m x_R) \quad (2.48)$$

Now the noisy component of the measurement error can be presented as:

$$\Delta_{S,\text{noise}} = T_{\text{mod}} \sum_{i=1}^N \alpha'(t_i) \Delta U_i / (2\pi U_m x_R) \quad (2.49)$$

We assume that noise on the filter output is normally distributed with the zero mean value and the variance  $\sigma_{\text{noise}}^2$ . From (2.48) and (2.49), it follows that the distribution law of the noise component of the measurement error remains normal. Let us find the mathematical expectation  $m_{S,\text{noise}}$  and the variance  $D_{S,\text{noise}} = \sigma_{S,\text{noise}}^2$  of the noise component of the measurement error. It is clear that:

$$m_{S,\text{noise}} = E[\Delta_{S,\text{noise}}] = 0 \quad (2.50)$$

where  $E[*]$  means the calculation of the mathematical expectation. So we can write:

$$\begin{aligned} D_{S,\text{noise}} &= E[\Delta_{S,\text{noise}}^2] = \frac{T_{\text{mod}}\eta^2}{4\pi^2 U_m^2} \left\{ E\left[\sum_{i=1}^N \alpha'(t_i)\right]\right\} \\ &= \frac{T_{\text{mod}}\eta^2}{(2\pi U_m)^2} \left\{ E\left[\sum_{i=1}^N \sum_{j=1}^N \alpha'(t_i)\Delta U_i \alpha'(t_j)\Delta U_j\right]\right\} \\ &= \left(\frac{T_{\text{mod}}\eta}{2\pi U_m}\right)^2 \left\{ \sum_{i=1}^N \sum_{j=1}^N \alpha'(t_i)\alpha'(t_j)B(t_i - t_j)\right\} \end{aligned} \quad (2.51)$$

where  $B(t_i - t_j)$  are samples of the covariance function of the noise [17].

The variance of the noise error component is determined by WF type and the covariance noise function. Let us examine its influence for WF (2.9) and (2.28).

### 2.5.1 The Measurement Error for the Weighting Function in the Form of the Trigonometric Series

The derivative of the weighting function (2.9) is:

$$\alpha'(t) = -K_W \frac{4\pi}{T_{\text{mod}}} \sum_{m=1}^K mA_m \sin\left(\frac{4\pi mt}{T_{\text{mod}}}\right) \quad (2.52)$$

Then, from (2.51), taking into account (2.14) and (2.52), we obtain:

$$D_{S,\text{noise}} = \left( \frac{2\eta K_W}{U_m} \right)^2 \left\{ \sum_{i=1}^N \sum_{j=1}^N B \left[ \frac{\eta T_{\text{mod}}(i-j)}{2} \right] \right. \\ \left. \times \sum_{m=1}^K \sum_{k=1}^K mnA_mA_k \sin[2\pi m\eta(i-j+\varepsilon)] \sin[2\pi k\eta(j-1+\varepsilon)] \right\} \quad (2.53)$$

Let us consider the noise influence on an example of typical frequency responses of filters. In [18] the covariance functions of the process at the output of the single oscillating circuit, the ideal filter and the multistage resonance amplifier at input impact of the white normal noise. Using the above designations, we give here the covariance function of the output process for the multistage amplifier only:

$$B[2\eta T_{\text{mod}}(i-j)] = (-1)^{i-j} \sigma_n^2 e^{-16\pi\eta^2(i-j)^2} \quad (2.54)$$

where  $\sigma_n^2 = N_0\Delta f$  is a noise variance at filter output,  $\Delta f = 2/T_{\text{mod}}$  is the filter pass-band matched with duration of processing signal, and  $i$  and  $j$  are the numbers of the appropriate DFS zeros.

As a result, the variance  $D_{S,\text{noise}}$  can be presented in the form:

$$D_{S,\text{noise}} = \frac{\eta^2}{q_{s/n}} \sum_{i=1}^K \sum_{k=1}^K e^{-2\eta|i-j|} (-1)^{i-j} \\ \times \sum_{m=1}^K \sum_{k=1}^K mkA_mA_k \sin[2\pi m\eta(i-1+\varepsilon)] \sin[2\pi k\eta(j-1+\varepsilon)] \quad (2.55)$$

where  $q_{s/n} = E/N$  is SNR.

Let us analyze the noise effect. Determining in accordance with (2.20) the coefficients  $A_m$  and  $A_k$  in (2.55) for different  $n$ , we draw the plots of MSD of the noise error component versus the relative range.

The calculations show that the MSD  $\sigma_{S,\text{noise}}$  at small ranges has the complicated oscillating character and its total level decreases when the range increases. The oscillating character can be explained by the presence of points in the WF plot, in which the derivative is equal to zero. These are two points on the boundary of the appropriate time interval and one point in the center of the interval. The appropriate item of (2.47) vanishes in these points. At the small range, there are few items in (2.47) and, therefore, their contribution to the total sum is high. So, at a range equal to the one QI, there is the only one item and its number will be periodically 1 to 2 and vice versa (in general case from  $M$  to  $M + 1$ ), with the range increasing up to the value equal to

two QI. Accordingly, when only one DFS zero, moving at a range variation inside the modulation period, falls in the point with zero derivative, the error variance becomes zero. During the range interval equal to one discreteness error, such an event arises several times.

The number of such events is equal to the integer part of a ratio of the discreteness error value and the wavelength of the carrier oscillation. Between these points, the derivative achieves maximum and, accordingly, the variance is also maximal. As far as the range grows, the contribution of these items in the total sum of (2.47) will decrease and, hence, the amplitude of MSD oscillations of the noise error decreases. As a result, at a large range the plot of the MSD versus range is degenerated into the continuous line, which smoothly falls at a range increase individually for different WFs.

The reduction of the total MSD level with range increasing can be explained by the effect of the result accumulation with the signal zero number increasing and, hence, a number of noncorrelated noisy data occur. The more the power of the function (2.19), the more frequently the range will lead to an essential decrease of MSD oscillations and the larger the total error level.

The most intensive variation occurs for more complicate WFs. The variation of the noise level does not change the character of plots and their ratio but changes the modulus of error values.

At small ranges ( $R/\delta_R < 2\dots 6$ ), the noise correlation practically does not manifest itself on the MSD value and on the character of the range dependence. With the measuring range increasing, the zero number in the modulation period increases and the time interval between them decreases. In addition, the noise correlation becomes manifested, which can be expressed in the fact that the noise component of the error decreases. The specific value of range, at which the noise correlation becomes manifested, depends on the WF shape. The more complicated the WF shape, the more frequently will the range lead to this effect manifestation.

For convenience of quantitative comparison of error components corresponding to different WFs, following (2.23), we use the averaged MSD, which with designations of the formula (2.23) takes the form:

$$\bar{D}_{S,\text{noise}}(M) = \sigma_{S,\text{noise}}^2(M) = \frac{1}{L} \sum_{k=1}^L D_{S,\text{noise}}(R_{M,k}) \quad (2.56)$$

Figure 2.18 shows the function  $\bar{\sigma}_{S,\text{noise}}(M) = \sqrt{\bar{D}_{S,\text{noise}}(M)}$  versus the normalized range for initial values of WF parameters at the noise level  $-40$  dB for the noncorrelated noise (solid lines) and for a filter in the form of multistage (dotted lines) for  $n = 1, 2, 4$ .

From Figure 2.18, we can make the conclusion that with an  $n$  increase, that is, the complication of the weighting function shape leads to an increase of the noise component of the error caused by the noncorrelated noise. The application of filtering gives the expected result in the form of reduction of the noise component of the error. The more this reduction, the larger the measuring range because, when the range grows, the number of accumulated values increases. The noise affects very strongly the more complicated WFs. For these functions, the filtering ensures less benefit.

The functions of the logarithm of the average MSD of measuring error's noise component versus the normalized range are shown in Figure 2.19. We see that the more effective filtering is observed for more complicated WFs (for larger  $n$ ).

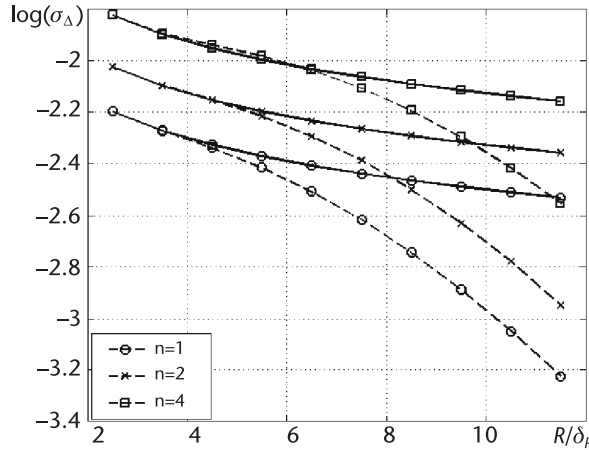


**Figure 2.18** The function of logarithm of the average MSD of the noise component of the measurement error versus the normalized range: the dotted line indicates multistage amplifier and the solid line indicates noncorrelated noise.

A comparison of Figures 2.19 and 2.6 shows that the noise component of the measurement error is commensurable with the truncation error on small ranges and significantly exceeds it on large ranges.

The total error  $\Delta(M)$  is of interest, which can be determined as:

$$\Delta^2(M) = \Delta_S^2(M) + D_{S,\text{noise}}(M) \quad (2.57)$$

The variation character of these quantities at range variation strongly depends upon the noise level and is determined by the fact that the component of the measurement error has more significance.

Figure 2.20 shows plots of the function of the average total error's MSD  $\sigma_\Delta = \sqrt{\Delta^2(M)}$  for the multistage amplifier, where  $\Delta^2(M)$  is calculated according to (2.61) at the noise level  $-40$  dB and  $-80$  dB.

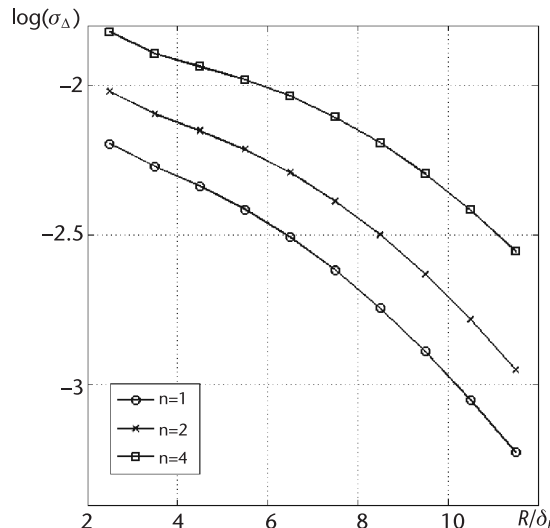


**Figure 2.19** The function of the logarithm of the noise component's averaged MSD of the measurement error for the multistage amplifier.

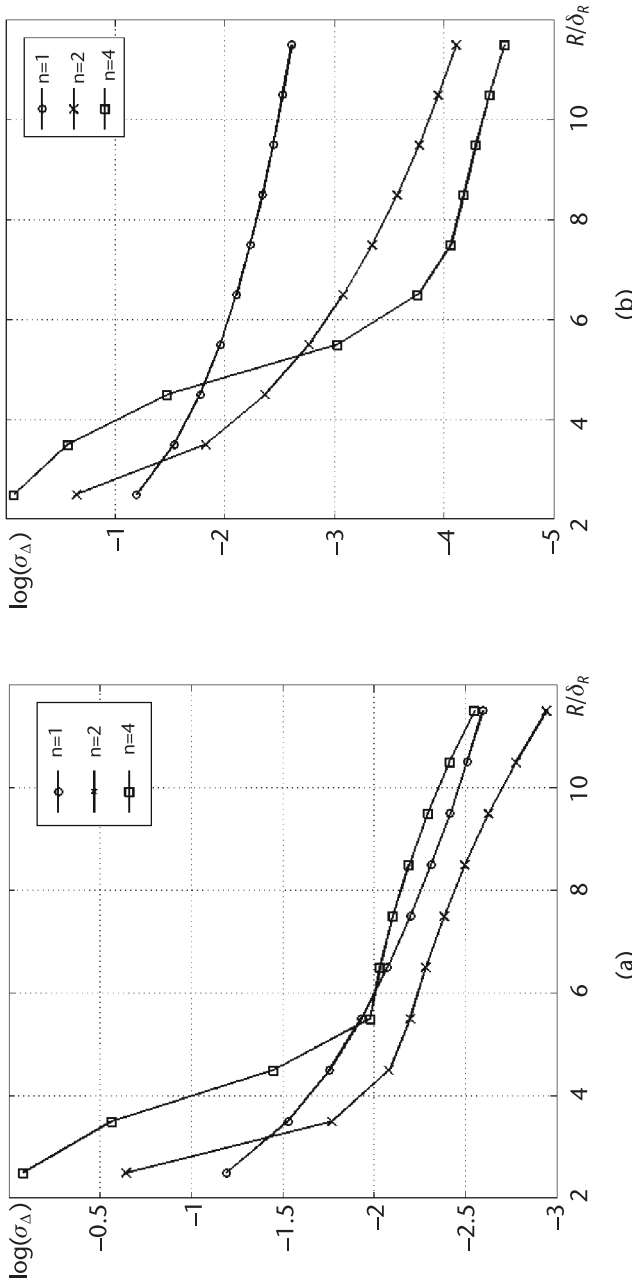


Figure 2.20 The function of the normalized total error's MSD versus the normalized range for the multistage amplifier: (a) the noise  $-40 \text{ dB}$  and (b) the noise  $-80 \text{ dB}$ .

These plots clearly show that the main contribution to the total measurement error on small ranges ( $R/\delta_R < 4$ ) is introduced by the truncation error, while at large ranges it is introduced by the noise component. The more complicated the WF shape, the stronger the noise influence.

### 2.5.2 The Measurement Error for the Kaiser-Bessel Weighting Function

According to [12], the derivative of the Kaiser-Bessel WF in (2.27) is:

$$\alpha'(t) = \frac{-8\pi^2 a^2 e^{-\pi a} t}{T^2 \sqrt{1 - \left(\frac{2t}{T}\right)^2}} I_1\left[\pi a \sqrt{1 - \left(\frac{2t}{T}\right)}\right], \quad t \in [-T/2, T/2] \quad (2.58)$$

Using the previous designations, we obtain:

$$D_{S,\text{noise}} = \frac{\eta^2 4\pi^2 a^4 e^{-2\pi a}}{U_m^2} \sum_{i=1}^N \sum_{j=1}^N \left\{ \frac{(2t_{\text{norm},i} - 1)(2t_{\text{norm},j} - 1)}{\sqrt{(t_{\text{norm},i} - t_{\text{norm},i}^2)(t_{\text{norm},j} - t_{\text{norm},j}^2)}} \right. \\ \left. \times I_1\left[2\pi a \sqrt{t_{\text{norm},i} - t_{\text{norm},i}^2}\right] I_1\left[2\pi a \sqrt{t_{\text{norm},j} - t_{\text{norm},j}^2}\right] B(t_{\text{norm},i} - t_{\text{norm},j}) \right\} \quad (2.59)$$

Now for the mentioned filter in the form of the multistage amplifier, we substitute into (2.59) the corresponding correlation function (2.54) and obtain the variance of the noise error for three above-mentioned filters:

$$D_{S,\text{noise}} = \frac{\pi^2 \eta^2 a^4 e^{-2\pi a}}{q_{s/n}} \sum_{i=1}^N \sum_{j=1}^N \left\{ \frac{(2t_{\text{norm},i} - 1)(2t_{\text{norm},j} - 1)}{\sqrt{(t_{\text{norm},i} - t_{\text{norm},i}^2)(t_{\text{norm},j} - t_{\text{norm},j}^2)}} \right. \\ \left. \times I_1\left[2\pi a \sqrt{t_{\text{norm},i} - t_{\text{norm},i}^2}\right] I_1\left[2\pi a \sqrt{t_{\text{norm},j} - t_{\text{norm},j}^2}\right] e^{-16\pi\eta(i-j)^2} \right\} \quad (2.60)$$

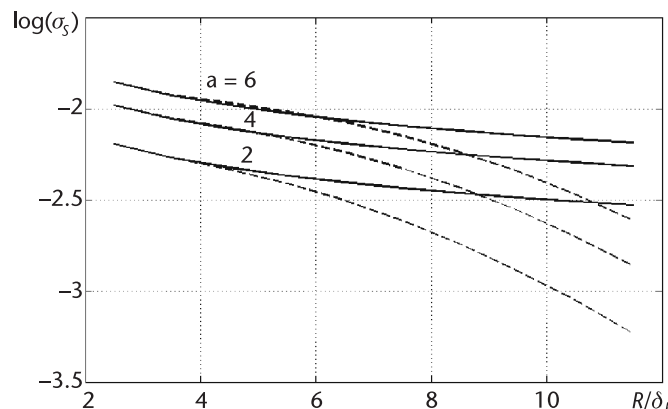


**Figure 2.21** The function of logarithm of the noise component's average MSD of the measurement error versus the normalized range: the dotted line indicates the multistage amplifier and the solid line indicates the noncorrelated noise.

The calculation results performed according to (2.60) for three values of the parameter  $a = 2, 4, 6$  for KB WF (2.28) show that the character of error behavior at the variation of the range and the WF form remains the same, that is, we observe a decrease in error oscillation while the range increases and a delay of the oscillation amplitude process for more complicated forms of WF.

A quantitative comparison of the mentioned error components was performed according to plots of MSD values averaged on the formula (2.56) in the range interval equal to one discrete error. The calculation results are presented in Figure 2.21 by the solid line for the error component caused by the white noise and by the dotted line for the noise error at the filter output.

For the KB WF under consideration as well as for the WF (2.19), we can observe the significant reduction of the noise error component at range increase caused by result accumulation owing to increase of the DFS zero number. Such reduction for more complicated WF has less value.

Figure 2.22 shows the function of normalized MSD of the total error versus the normalized range calculated according to (2.57) for two values of SNR  $q_{s/n} = 40$  dB and  $q_{s/n} = 80$  dB at three values of the WF shape parameters  $a = 2, 4, 6$ . We see that the noise level reduction leads to a sharp decrease of the total error for more

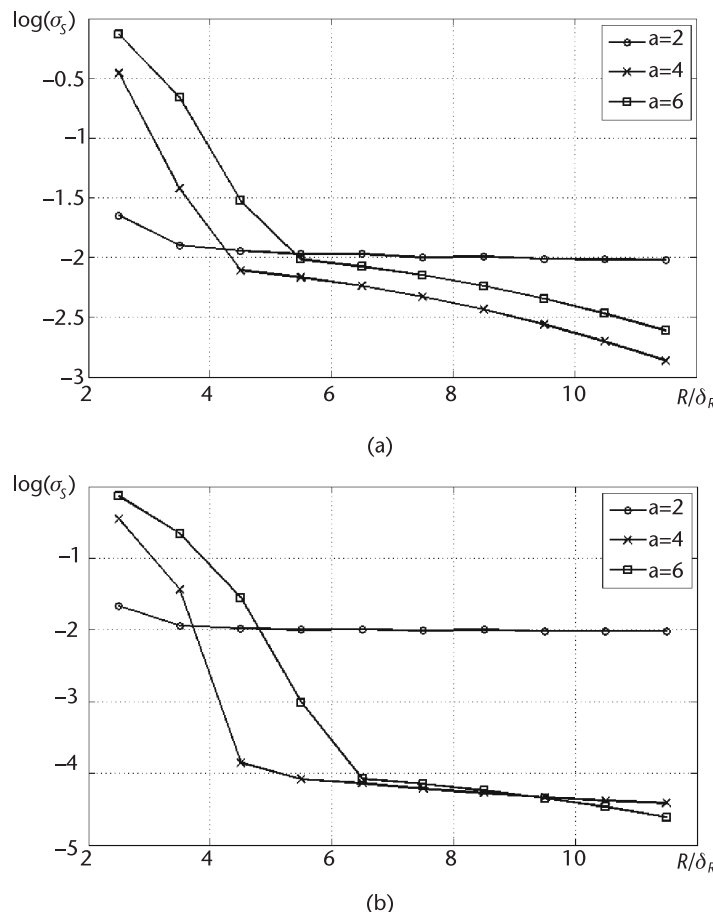


**Figure 2.22** The function of logarithm of the total error normalized MSD versus the normalized range for the multistage amplifier: (a) noise  $-40$  dB and (b) noise  $-80$  dB.

complicated WF shapes. However, this decrease is limited by some value, which is individual for each WF.

## 2.6 Conclusions

The effectiveness of the weighting averaging method depends to a great extent upon the type of WF used. However, at any WF, we observe the measurement error reduction with measuring range increasing. Therefore, one can formulate and solve the problem of optimization of the weighting function shape to achieve the minimum of the truncation error.

The error achieved by the means of optimization of the WF shape decreases while the measuring range increases and it is difficult to achieve a small error on very small ranges.

The oscillating character of the truncation error variation at a range change with two types of periodicity allows the performance of error optimization using a variation of FM parameters separately or in combination.

The degree of truncation error reduction in this case is significantly higher compared with the WF shape variation; therefore, the level of the error achieved weakly depends upon the measuring range. Nevertheless, such an essential benefit can be achieved owing to the significant increase of the frequency resource at FM and the increase of processing time.

An analysis of noise influence on the range measurement error using the weighting MEDS shows that the character of MSD dependence upon the range is also oscillating with two types of periodicity; however, when the range increases, the oscillation amplitude sharply decreases.

The general view of such plots strongly depends upon WF type and the filter type used in stages of preliminary analog DFS processing. In general, we can consider that the level of the measurement noise error component does not exceed values satisfying the practical needs of the industry at the noise level not more than  $-40$  to  $-45$  dB with respect to the DFS level.

## References

- [1] Edvardson, K. O., Satt och anerdning for avstandsmatning med frekvens-modulerade kontinuerliga mikrovagor, Patent No. 381745, Sweden, INT.CL. G01S 9/24, No. 7315649-9, filed November 20, 1973, published December 15, 1975.
- [2] Edvardson, K. O., Measurement of Contents of Tanks etc. with Microwave Radiations, U.S. Patent 4044355, Int. CI, G01S 9/24, filed February 13, 1976, issued August 23, 1977.
- [3] Approach to Distance Measurement with the Aid of Frequency-Modulated Signal and the Radar Station with Frequency Modulation, Authors Application 30-1591, Japan, Int. CI, G01S 13/34, Izobretenia stran mira, No. 15, p. 291985.
- [4] Ezerskiy, V. V., "Measurement Procedure of a Distance Gauge Based on a Frequency-Modulated Range Finder with Weighted Smoothing of the Digitization Error," *Measurement Techniques*, Vol. 46, No. 2003, pp. 841–846.
- [5] Korn, G., and T. Korn, *Mathematical Handbook for Scientists and Engineers*, New York: McGraw Hill Book Company, 1961.

- [6] Vinitskiy, A. S., *Essay on Radar Fundamentals for Continuous-Wave Radiation* (in Russian), Moscow, Sovetskoe Radio Publ., 1961, p. 495.
- [7] Marple, S. L., Jr., *Digital Spectral Analysis with Applications*, Englewood Cliffs, NJ: Prentice-Hall, 1987.
- [8] Harris, F. J., "On the Use of Windows for Harmonic Analysis with the Discrete Fourier Transform," *IEEE Trans. Audio Electroacoust.*, Vol. AU-25, 1978, pp. 51–83.
- [9] Dvorkovich, A. V., "New Calculation Method of Effective Window Functions Used at Harmonic Analysis with the Help of DFT" (in Russian), *Digital Signal Processing*, No. 2, 2001, pp. 49–54.
- [10] Dvorkovich, A. V., "Once More about One Method for Effective Window Function Calculation at Harmonic Analysis with the Help of DFT" (in Russian), *Digital Signal Processing*, No. 3, 2001, pp. 13–18.
- [11] Gradstein, I. S., and I. M. Ryzhik, *Tables of Integrals, Sums, Series and Products*, A. Jeffrey and D. Zwillinger (eds.), New York: Academic Press, 1965.
- [12] Ezerskiy, V. V., and I. V. Baranov, "Analysis of the Truncation Error of the Distance Sensor on the Basis of FMCW Range Finder with Weighting Smoothing of the Discrete Error" (in Russian), *Vestnik RGRTA, Ryazan, RGRTA*, No. 11, 2003, p. 61.
- [13] Ezerskiy, V. V., and I. V. Baranov, "Optimization of Weighting Methods of Smoothing the Discreteness Error of Distance Sensors Based on a Frequency Rangefinder" (in Russian), *Measurement Techniques*, Vol. 47, No. 12, 2004, pp. 1160–1167.
- [14] Baranov, I. V., and V. V. Ezerskiy, "Optimization of Modulation Parameters in Short-Range Radar Technology at Weighting Averaging of Difference Frequency" (in Russian), *Vestnik RGRTU, Ryazan*, No. 2 (28), 2009, pp. 30–37.
- [15] Kagalenko, B. V., and V. P. Meshcheriakov, Frequency-Modulated Radio Range Finder, Authors Certificate 1141354 (USSR), Int. Ci., G01S 13/08, Bull. No. 7, filed May 3, 1983, published February 23, 1985.
- [16] Marfin, V. P., A. I. Kiyashev, F. Z. Rosenfeld, et al., "Radio Wave Non-Contact Level-Meter of Higher Accuracy" (in Russian), *Izmeritel'naya Technika*, No. 6, 1986, pp. 46–48.
- [17] Levin, B. R., *Theoretical Fundamentals of Statistical Radio Engineering*, 2nd Edition (in Russian), Moscow: Sovetskoe Radio Publ., 1974, p. 552.



# Estimation of the Difference Frequency by the Position of the Spectrum Maximum

## 3.1 Introduction

The estimation of the difference frequency in the spectral (frequency) domain assumes obligatory application of methods and devices for digital signal processing (DSP) after preliminary analog processing of the difference frequency signal. Actually, under the conditions of short-range radar technology, this is a problem of frequency estimation of the pure sine signal according to the short sample [1] and further calculation of the range by (1.12). Therefore, going forward, we will conduct the analysis of frequency estimation accuracy and convert it (when necessary) in the range so as not to distract the reader.

The frequency of continuous sinusoid, from which this sample is cut out using some WF [2, 3], is understood as the true value of the DFS sample frequency. DFS processing in the spectral domain is performed on the basis of the Fourier transformation. In the classical variant [2–12], the complex spectrum (CS)  $\dot{S}(n)$  is calculated with the help of the discrete Fourier transformation (DFT):

$$\dot{S}(n) = \sum_{k=0}^{K-1} u_{\text{dif}}(k)w(k)\exp(-j2\pi nk/K), \quad n = 0, 1, \dots, K-1 \quad (3.1)$$

where  $w(k)$  is the WF ensuring a reduction of the sidelobes (SL) of the spectrum.

For calculation speed-up, the fast Fourier transformation (FFT) is usually used [2, 4, 7, 9, 10], which places a limitation on a number of processed samples. The spectrum calculated in such a manner is discrete due to the fact that calculation according to (3.1) supposes the periodic prolongation of the signal. Therefore, the frequency estimation on the basis of this spectrum as well as processing in the time domain leads to QI [11], which, as before, is determined according to (1.15). Hence, the issue about the measuring range error reduction is, as usual, relevant. The various algorithms of the spectrum processing can be used for this purpose. The issue about the limit achievable measurement error, which is determined under ideal conditions by the error only, which is peculiar to the used measurement method (i.e., by the truncation error), is practically important.

The weighted DS samples obtained in the same points of the time axis inside of each repetition period of the FM law on ascending or descending parts with the step  $T_{\text{dis}}$ , determined according to the sampling theorem, are exposed to processing according to (3.1). To implement this method, we do not need the continuous smooth variation of the transmitted signal frequency. It is enough to provide the

transmitted signal radiation at some frequency values fixed in advance. Nevertheless, the requirement of linearity of frequency variation remains. As a result, they come to the method of stepped frequency modulation of the continuous signal (FSCW) [12–19]:

$$\omega_{\text{mod}}(t) = \delta_\omega \sum_{k=1}^K 1(t - kT_{\text{dis}}) \quad (3.2)$$

where  $1(t)$  is a unit step function [20] and  $\delta_\omega$  is the minimal step of the FM sweep.

It is clear that the FM sweep in this case is:

$$\Delta\omega = K\delta_\omega \quad (3.3)$$

Such a mode of the FMCW RF operation agrees well with the peculiarities of digital frequency synthesizers [21, 22], which allow us to obtain the stepped frequency variation with the constant step  $\delta_\omega$ . Therefore, we can ask the question about the optimization of FM parameters to achieve the minimal measurement error. It is clear that in the measurement process we can change the carrier frequency  $F_0$  and the frequency deviation  $\Delta F$  at keeping the linear character of the FM sweep. These methods are known [15, 23, 24].

The application of the WF at the spectrum calculation proposes an answer to the question about its best parameters. In the literature [2, 3, 25], at finding the optimal WFs, the following factors are determinants: the minimum of the SL level, the minimum of the main lobe width, and the minimum of the estimation error of power spectral density. In our case, the range measurement error should be the main factor at some restrictions on the WF characteristics.

The reception of DFS is provided on the background of noise and different types of interference under the influence of destabilizing factors. In this chapter, we are limited by the consideration of the noise influence only. The analysis of other distortion effects will be discussed in later chapters.

To take into account the noise influence on the frequency (range) estimation error in the spectral domain, we need information about the main statistical characteristics of the DFS spectrum received on the background of stationary noise. First, the distribution laws of the spectral components (SC) and the correlation links between them can be attributed to them. The determination of the statistical characteristics of the random process spectra allows us in some cases to obtain analytical equations for noise components of the DFS frequency estimation error in the spectral domain. The statistical characteristics of estimations of the stationary random processes are examined completely enough [26, 27]. The statistical characteristics of the estimation of the power spectral density (PSD) of the sum of the DFS and the white normal noise have obviously not been investigated enough.

## 3.2 Algorithms of Difference Frequency Estimation

Smoothing QI is possible with the help of methods allowing the provision of the spectrum average frequency estimation with the minimal possible error.

The most frequently that one can consider the frequency corresponding to the maximum of the spectral amplitude density (SAD) of the DFS as the frequency estimation is:

$$|\dot{S}(\omega_R)| = \max_{\omega} |\dot{S}(\omega)| \quad (3.4)$$

In [28] it is shown that the algorithm (3.4) is the estimation of maximal likelihood at evaluation of signal frequency with the unknown initial phase. Practically, it is possible to realize the algorithm (3.4) using different procedures.

The variants of this algorithm realization were:

1. An increase of spectrum description detail using zero padding in the processing array [2, 6]. Using  $K_0$  zero padding (in accordance with terminology of [9], from the outside) to the initial array from  $K$  DFS samples, we can provide any required discreteness of the spectrum. Therefore, the expression for the DFS changes as:

$$\dot{S}(n) = \sum_{k=0}^{K-1} u_{\text{dif}}(k) w(k) \exp[-j2\pi nk/(K + K_0)], \quad (3.5)$$

$$n = 0, 1, \dots, (K + K_0) - 1$$

It is unnecessary to physically use zero padding in the array for calculation according to this formula (i.e., we need not to increase the memory capacity of computing device). Only the denominator in the exponent and a number of possible values of the variable  $n$  will change. In the case of the *fast Fourier transformation* (FFT) application, the zero padding in the DFS array is strictly necessary.

Usually these calculations are performed in two stages. At the first stage, the FFT with the initial number  $K$  of DFS samples is calculated and the position of the SAD maximum  $n_{\max}$  is obtained. At the second stage, only in the vicinity of the obtained maximum is the calculation of SAD according to (3.5) performed with the accepted discreteness value, which is specified by the choice of the appropriate value  $K_0$  and the search of the maximum according to (3.1). The range calculation is executed according to (1.14), where instead of  $N_{\text{DFS}}$ , the obtained value  $\hat{n}_{\max}$  is substituted.

2. The application of the discrete-time Fourier transformation [2, 3] and the maximum search of the continuous periodic in the frequency spectrum are performed with the help of one-dimensional optimization methods [29].

At the limit, we can introduce the continuous variable  $x \in [0, 1]$  instead of the ratio  $n/(K + K_0)$  and to transfer to discrete-time [2] or to *integral-discrete* [3] Fourier transformation (IDFT):

$$\dot{S}(x) = \sum_{k=0}^{K-1} u_{\text{dif}}(k) w(k) \exp(-j2\pi x k), \quad 0 \leq x \leq 1 \quad (3.6)$$

Here it is possible, smoothly varying  $x$ , to use any numerical method of the extreme search [29] to determine the maximum of the function

$$\max_{x \in X} S(x) = S(x_{\max}) = |\dot{S}(x_{\max})| \quad (3.7)$$

After that, the value  $\hat{n}_{\max} = xK$  is obtained, which is substituted in (1.14) instead of  $N_{\text{DFS}}$  for the range calculation.

3. The search of spectrum maximum on the basis of spline-interpolation of the DFS spectrum is performed. The algorithm on the basis of spline interpolation of the signal spectrum is used for DFS spectrum calculation using FFT with small number of adding zero samples (it is enough to increase the period length by two to four times). To determine the frequency with the specified truncation error, the spline interpolation of SAD (or PSD) is used within the limits of its main lobe. After interpolation, we obtain additional spectral components following through the interval  $\delta\omega'$ , and then the algorithm (3.4) is used for estimation of signal frequency.
4. The application of correcting coefficients [30, 31] is performed. The algorithm with usage of correction, in which the following quantity [30, 31] is accepted as the DFS frequency estimation, is:

$$\hat{\omega}_R = (n_{\max} - 1 + p) \frac{\Delta\omega}{K + K_0} \quad (3.8)$$

where  $n_{\max}$  is a number of the maximal SC SAD or PSD and  $p$  is a correction considering the difference between the SC intensities calculated on the adjacent frequencies.

If the DFS frequency does not coincide with the central frequency of DFT filter, the SC intensity changes due to the palisade effect [3], which is used for the correction of the frequency estimation. In [30, 31], some different corrections are offered. The most suitable correction is calculated by the formula [30]:

$$p = \frac{z_{a,m}(n_{\max} - 1) - z_{a,m}(n_{\max} + 1)}{z_{a,m}(n_{\max} - 1) + z_{a,m}(n_{\max} + 1)} \Psi_{a,m} \quad (3.9)$$

where  $z_{a,m}(n_{\max} - 1)$  and  $z_{a,m}(n_{\max} + 1)$  are, respectively, intensities of the SC SAD  $A(\omega)$  and the PSD  $G(\omega)$  from the left and from the right from the maximum and  $\Psi$  is a multiplier depending on the number of added zero samples. The initial values of multipliers are accepted as equal:  $\Psi_a = (K + K_0)/K$  and  $\Psi_m = (K + K_0)/(2K)$ . The corrected values of  $\Psi_a$  and  $\Psi_m$  at the calculation are determined by the method of successive approximations when using them as a criterion of range measurement error minimum. A number of adding zero samples are not very large for this algorithm; it is enough to increase the initial number of samples by two to four times. The advantage of this algorithm is its undoubted simplicity.

Besides the described algorithms giving the point frequency estimation, sometimes they use estimations based on the property of the spectrum symmetry. The most interesting one is caused by two algorithms: the application of average-weighted estimation of the carrier frequency [32–34] and the estimation of the spectrum median [35]. Both of these algorithms suppose preliminary calculation of the spectrum using the FFT with an increase of the DFS period by two to four times owing to the zero addition.

The formula for average-weighted frequency estimation can be written as:

$$\hat{n}_R = \frac{\sum_{i=n_{\text{low}}}^{n_{\text{upp}}} i \left| \sum_{l=1}^K u_{\text{dif}}(k) \exp(-j2\pi li/K) \right|^2}{\sum_{i=n_{\text{low}}}^{n_{\text{upp}}} \left| \sum_{l=1}^K u_{\text{dif}}(k) \exp(-j2\pi li/K) \right|^2} \quad (3.10)$$

where  $n_{\text{low}}$  and  $n_{\text{upp}}$  are, respectively, the lower and upper boundaries of numbers of the processed SC, and therefore,  $n_{\text{low}} \leq n_{\text{max}} \leq n_{\text{upp}}$ . After that, the range calculation is provided according to (1.14). The finding of a number  $n_{\text{max}}$  of the maximal SC precedes to the application (3.10) for signal frequency estimation. Then the choice of  $n_{\text{low}}$  and  $n_{\text{upp}}$  is provided, which determine the summation limits and are located symmetrically with respect to SC  $n_{\text{max}}$ . The number of SC (specified by the range of their numbers  $n_{\text{upp}} - n_{\text{low}}$ ) is chosen from the condition of the minimization of the frequency estimation error and it should be not less than a value covered by the main spectrum lobe. As a rule, this quantity in two to four times exceeds the width of the main lobe.

The estimation of the spectrum median  $n_x$  is carried out using the sliding half-gates. This algorithm can be written analytically as [35]:

$$\sum_{n=n_{\text{low}}}^{n_x} |\dot{S}(n)|^2 = \sum_{n=n_x}^{n_{\text{upp}}} |\dot{S}(n)|^2 \quad (3.11)$$

where  $n_{\text{low}}$  and  $n_{\text{upp}}$  are, respectively, the lower and upper boundaries of current numbers of processed SC.

The procedure of frequency estimation by the algorithm (3.11) supposes two half-gates sliding along the frequency axis. The number of SC  $n_x$ , at which the equality (3.11) performance is achieved, is identified with the signal frequency. Reducing the error caused by the discrete character of calculating spectrum and the practical implementation of this algorithm supposes an application of spline interpolation of the signal spectrum within the limits of its main lobe. The width of half-gates should be chosen equally, that is,  $n_x - n_{\text{low}} = n_{\text{upp}} - n_x$ .

Let us consider in detail some of these algorithms. The degree in minuteness will be defined by the level of attention to specific algorithm in known publications, the personal interest of authors, obtained results, and the value of achievable measurement error.

### 3.3 Estimation of the Difference Frequency on the Basis of the Maximum Position of the Spectral Density of the Difference Frequency Signal

#### 3.3.1 Analytical Estimation of the Truncation Error of Range Measurement

The estimation of the difference frequency  $\hat{\omega}_R = 2\hat{\pi}F_R$  on the position of the DFS SAD maximum (3.4) is the most natural. The spurious SC from the area  $\omega < 0$ , SC caused by interference and noise, and frequency-dependent circuits of the device for preliminary analog DFS processing influence the frequency estimation. There is no

analytical solution of this problem, which adequately reflects the frequency estimation error at any amplitude and phase relations between parameters of the signal and interference. Estimations obtained by means of numerical simulation on the PC show that the position of the SAD modulus maximum in general does not coincide with the frequency of the beating signal [1, 36]. If noise, interference, and distortions of the signal are absent, the error is caused by influence of SC from the area  $\omega < 0$ .

In accordance with definition (3.4), it is necessary to solve the following equation for frequency estimation:

$$\frac{d}{dx} |\dot{S}(x)|^2 = \frac{d}{dx} \left| \sum_{i=1}^N \dot{S}_i(x) \right|^2 = 0 \quad (3.12)$$

where  $\dot{S}_i(x) = \int_{-0.5T}^{0.5T} w(t) u_i(t) \exp(-j2\pi xt/T) dt$  is the complex spectral density (CSD) of

the  $i$ th component of the weighted sample of the DFS  $u_i(t)$  obtained over the time interval [-0.5 T to 0.5 T],  $w(t)$  is WF symmetric with respect to the middle of signal sample (from the shift theorem [10], it follows that results obtained for symmetric time interval will be true for the nonsymmetric time interval with an account of the phase variation), and  $x_i = 0.5\omega_i T/\pi$  and  $x = 0.5\omega T/\pi$  are the normalized frequency of the  $i$ th DFS component and the normalized current frequency, respectively.

We assume that  $S_i(x_i)$  corresponds to the signal, which frequency  $x_i$  is required to determine. Now we substitute the detailed record of (3.12) as:

$$\frac{d}{dx} \left| \sum_{i=1}^N e^{j(\Phi_i - \Phi_1)} S_i(x - x_i) + \sum_{i=1}^N e^{-j(\Phi_i + \Phi_1)} S_i(x + x_i) \right|^2 = 0 \quad (3.13)$$

where  $e^{j(\Phi_i - \Phi_1)} S_i(x - x_i)$  and  $e^{-j(\Phi_i + \Phi_1)} S_i(x + x_i)$  are spectrum items from areas  $\omega < 0$  and  $\omega > 0$ :  $(x + x_i)$ ,  $(x - x_i)$ , and  $\Phi_i = \omega_0 t_{\text{del},i} + \varphi_s$ .

The exact solutions of (3.13) can be obtained only for some specific cases. For obtaining the approximated solutions, we use the widely used solution method for transcendent equations by approximation them in the vicinity of the analyzing point  $x_1$  by the Taylor formula. The application of the  $n$ th power of expansion allows us to represent (3.13) approximately by the algebraic equation of the  $n - l$  power.

The quadratic and cubic approximation of the function  $S(x)$  in the vicinity of the point  $x_1$  gives, respectively, the first  $x_{\max 1}$  and the second  $x_{\max 2}$  approximated solutions permitting us to estimate errors  $\Delta_1(x_1)$  and  $\Delta_2(x_1)$ :

$$\Delta_1(x_1) = x_{\max 1} - x_1 \approx - \left\{ \left| \dot{S}(x_1) \right|^2 \right\} \left/ \left\{ \left| \dot{S}(x_1) \right|^2 \right\}'' \right. \quad (3.14)$$

$$\Delta_2(x_1) = x_{\max 2} - x_1 \approx \left\{ \left| \dot{S}(x_1) \right|^2 \right\}''' \left\{ 1 - \sqrt{1 - \frac{2 \left\{ \left| \dot{S}(x_1) \right|^2 \right\}' \left\{ \left| \dot{S}(x_1) \right|^2 \right\}''}{\left[ \left\{ \left| \dot{S}(x_1) \right|^2 \right\}'' \right]^2}} \right\} \quad (3.15)$$

where  $\left\{ |\dot{S}(x_1)|^2 \right\}^{(n)}$  is a value of the  $n$ th derivative of the spectrum modulus square on frequency  $x = x_1$ . In the literature, we can meet the simpler solution of (3.14), which is true at a high signal/interference ratio.

Figure 3.1 shows functions of the estimation error of signal frequency (1.6) determined according to the approximate equation (3.15) (dotted line). This error is caused by the influence of the SL of periodic spectrum prolongation of this signal located in the area  $\omega < 0$ . In addition, the uniform weighting function is used. In the same figure, the frequency estimation error  $\Delta(x_1) = x_{\max} - x_1$  is shown by the solid line, which is obtained from numerical solution of (3.12).

A comparison of the obtained results shows that (3.15) allows determination the difference frequency estimation error caused by the spurious SC with the error accepted for practical application only in the case when in the area of the main lobe the spurious SC is essentially less than the useful item (in the discussed example this is the frequency area of the main lobe interaction with the SL of SC from the area  $\omega < 0$ :  $x_1 \geq 0.7$ ). According to (3.14), the error is determined with the larger mistake (not shown in the figure). However, at a low level of the spurious SC, this simple expression gives the accepted results.

Let us correct the mentioned solutions so that to get the satisfactory result at arbitrary amplitude relation of useful and spurious SC for the equation of not more than the second power. As a result of the comparative analysis of various solutions in different situations, we may translate the approximate estimations of the solution in (2.13) to the form:

$$\Delta_1(x_1) \approx -\frac{\{\text{Re}[\dot{S}(x_1)]\} \cdot \{\text{Re}[\dot{S}(x_1)]'\} + \{\text{Im}[\dot{S}(x_1)]\} \cdot \{\text{Im}[\dot{S}(x_1)]'\}}{\{\text{Re}[\dot{S}(x_1)]\} \cdot \{\text{Re}[\dot{S}(x_1)]\}'' + \{\text{Im}[\dot{S}(x_1)]\} \cdot \{\text{Im}[\dot{S}(x_1)]\}''} \quad (3.16)$$

$$\Delta_2(x_1) \approx \Delta_1(x_1) K_\Delta \quad (3.17)$$

$$\text{where } K_\Delta \approx \frac{pS(x_1)}{(\Delta x_1)^2} \left\{ 1 - \sqrt{1 - \frac{2(\Delta x_1)^2}{pS(x_1)}} \right\}$$

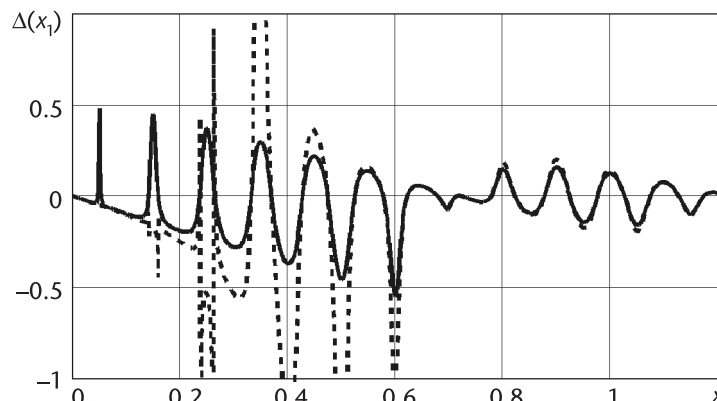


**Figure 3.1** Plots of the frequency estimation error defined by the approximated equation (3.15) (dotted line) and by numerical solution of (2.12) (solid line).

$$pS(x_1) = \frac{\{\text{Re}[\dot{S}(x_1)]\} \cdot \{\text{Re}[\dot{S}(x_1)]'\} + \{\text{Im}[\dot{S}(x_1)]\} \cdot \{\text{Im}[\dot{S}(x_1)]'\}}{\{\text{Re}[\dot{S}(x_1)]\} \cdot \{\text{Re}[\dot{S}(x_1)]\}^{(3)} + \{\text{Im}[\dot{S}(x_1)]\} \cdot \{\text{Im}[\dot{S}(x_1)]\}^{(3)}}$$

At superposition of spectrum lobes of the same amplitude, (3.20) gives the mistake in determination of the estimation error up to 10% at the frequencies  $x_1$  and  $x_2$  difference, which is less than permissible. The reduction of the spurious SC amplitude in the area of the main lobe of estimating spectrum leads to a decrease of errors according to (3.16), (3.17), (3.14), and (3.15). If the ratio of useful SC to the spurious is one more than 10, the values of errors do not exceed 0.4%. In this case, neglecting items of a higher smallness order, we can essentially simplify (3.19). As a result, we obtain:

$$\Delta R/\delta_R = (x_{\max} - x_R) \approx \frac{-2 \cos(2\Phi) S'_{WF}(x_R)}{[S''_{WF}(0) + \cos(2\Phi) S''_{WF}(x_R)]} \quad (3.18)$$

where  $x_{\max}$  is a position of the SD of the DFS maximum and  $S_{WF}(x)$  is the WF spectrum.

We also note that for any WFs and any ranges the sequence of frequencies with zero estimation error is determined by (3.14) to (3.17) without mistakes. In Figure 3.1, these are points of the curves' intersection with the x-axis.

### 3.3.2 The Truncation Error of the Difference Frequency Estimation at the Weighting Functions of Dolph-Chebyshev and Kaiser-Bessel

Let us consider the Dolph-Chebyshev (DC) WF and the Kaiser-Bessel (KB) WF [3] as having the undoubtedly practical and theoretical interest due to properties of their spectra. In our problem, the interest of the mentioned WFs is connected with the fact that their shape and the shape of their SAD (determined by a shape of the main lobe and the level of SLs) can be varied by one parameter, which allows easily enough the connection of the SAD shape variation with the general rules of the truncation error of range measurement. We determine the influence of SAD WF shape upon the frequency estimation error excluding the influence of discretization frequency. Therefore, we use equations for WF and their CSD for the processing of continuous signals, which have a more compact form.

On the basis of results [37], we obtain the normalized expression for CSD of DC in the form of the segment of the sine signal weighted by DC WF:

$$\begin{aligned} \dot{S}_{DC}(x) = & \frac{\exp(j\Phi)}{Q} \left\{ \text{ch} \sqrt{\ln^2(Q + \sqrt{Q^2 - 1}) - (x_\Delta \pi)^2} \right. \\ & \left. + \exp(-j2\Phi) \text{ch} \sqrt{\ln^2(Q + \sqrt{Q^2 - 1}) - (x_\Sigma \pi)^2} \right\} \end{aligned} \quad (3.19)$$

where  $Q^{-1}$  is SL level of SAD items,  $x_\Delta = x - x_1$ ,  $x_\Sigma = x + x_1$ . For DC WF, (3.18) leads to:

$$\frac{\Delta R}{\delta_R} \approx \frac{1}{\pi} \frac{-2 b L Z^2 \cos(2\Phi) \text{sh}Z}{Z^3 \text{sh}L + L \cos(2\Phi) [(b^2 + Z^2) \text{sh}Z - b^2 Z \text{ch}Z]} \quad (3.20)$$

where  $L = \ln(Q + \sqrt{Q^2 - 1})$ ;  $Q^{-1}$  is the SL of the SD;  $Z = \sqrt{L^2 - b^2}$ ;  $b = \pi x_R$ .

Now we write the envelopes of fast-error oscillations (3.20) as:

$$\left( \frac{\Delta R}{\delta_R} \right)_{\max} \approx \frac{1}{\pi} \frac{(-1)^{n+1} 2b L Z^2 \operatorname{sh} Z}{Z^3 \operatorname{sh} L + (-1)^n L [(b^2 + Z^2) \operatorname{sh} Z - b^2 Z \operatorname{ch} Z]} \quad (3.21)$$

From here we have the approximate relation for envelope of slow oscillation:

$$(\Delta R / \delta_R)_{\max, \text{max}} \approx \pm 2bL / [\pi \operatorname{sh} L \sqrt{b^2 - L^2}] \quad (3.22)$$

The functions (3.20) through (3.22) are drawn in Figure 3.2.

We see that the function has a double periodicity. There are fast oscillations with the period equal to a quarter of the carrier oscillation wavelength, and the slow envelope with nodes, in which the range measurement error is equal to zero. Slow oscillations are connected with the presence of SAD SLs. The EN arises under condition that at range variation side lobes of SAD in the area  $\omega > 0$  coincides with the extreme location of the main SAD lobe from the area  $\omega > 0$ . From (3.16), we obtain the equation for ranges corresponding to the ENs:

$$x_{R,ex} = R_{ex}/\delta_R = \sqrt{N^2 + L^2/\pi^2} \quad (3.23)$$

where  $N = 1, 2, 3, \dots$  is EN, index  $ex$  designates the exact value. From (3.24) it follows that the EN position on the axis of normalized range depends upon the SL number  $N$  and the WF parameter  $Q$  and displaces towards increasing at their growth.

Figure 3.3 shows the function of position  $x_{RT}$  on the normalized range axis of first six ENs versus  $Q$ . The numbers at the curves correspond to the EN number.

The CSD of the DFS in the form of the sine signal segment with the KB WF with consideration of introduced designations can be written as [3]:

$$\dot{S}_{KB}(x) = \frac{\pi \alpha \times \exp(j\Phi)}{\operatorname{sh}(\pi \alpha)} \left( \frac{\operatorname{sh} \pi \sqrt{\alpha^2 - x_\Delta^2}}{\pi \sqrt{\alpha^2 - x_\Delta^2}} + \exp(-j2\Phi) \frac{\operatorname{sh} \pi \sqrt{\alpha^2 - x_\Sigma^2}}{\pi \sqrt{\alpha^2 - x_\Sigma^2}} \right) \quad (3.24)$$

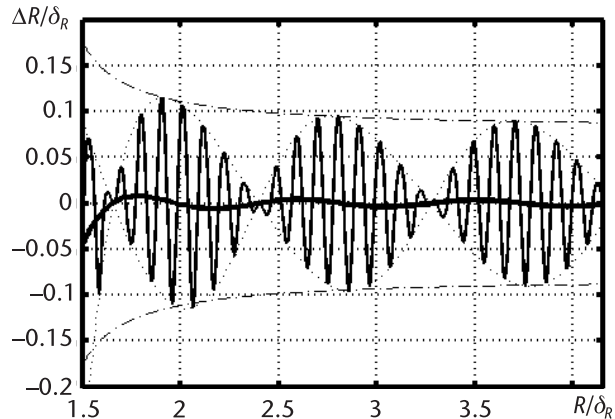


**Figure 3.2** The function of the normalized measurement error versus normalized range for DC WF at  $Q = 30$  dB.

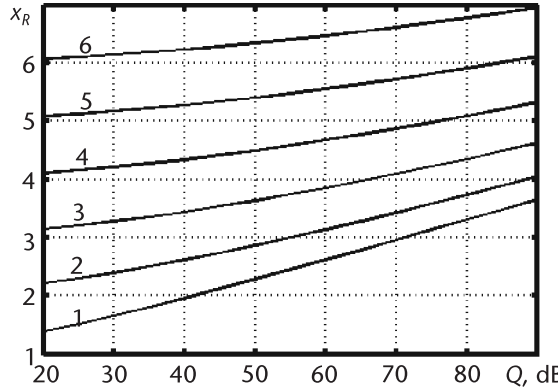


**Figure 3.3** The function of range points positions with zero measurement error versus the root number and  $Q$  for DC WF.

where  $\alpha$  is a parameter determining the main lobe width and the SL level.

We should note that the limit case of KB WF at  $\alpha = 0$  corresponds to the uniform WF, which is widely used in theoretical analysis and practical applications. Thus, KB WF gives possibility to analyze the influence of the sidelobe level (SLL) of the spectrum from the maximal ( $-13.6$  dB) to any low values.

Taking (3.24) into consideration, from (3.18) after transformations, we obtain the following equation for the instantaneous normalized truncation error for range measurement with the KB WF:

$$\frac{\Delta R}{\delta_R} = \frac{1}{\pi} \frac{-2 b \cos(2\Phi) U S^3}{\operatorname{sh} S - S \operatorname{ch} S + S^3 \cos(2\Phi) [U + b^2 V]} \quad (3.25)$$

where  $S = \pi\alpha$ ;  $\alpha$  is a parameter defining the main lobe width and SLL;  $Y = \sqrt{S^2 - b^2}$ ;  $U = (\operatorname{sh} Y - Y \operatorname{ch} Y)/Y^3$ ;  $V = [(Y^2 + 3)\operatorname{sh} Y - 3Y \operatorname{ch} Y]/Y^5$ .

From (3.25), we obtain envelopes of fast error oscillations:

$$\left( \frac{\Delta R}{\delta_R} \right)_{\max} = \frac{1}{\pi} \frac{(-1)^{n+1} 2 b U S^3}{\operatorname{sh} S - S \operatorname{ch} S + (-1)^n S^3 (U + b^2 V)}, \quad n = 1; 2 \quad (3.26)$$

From here we obtain the approximated equation for slow oscillation envelope:

$$(\Delta R / \delta_R)_{\max, \max} \approx \pm 4 b S^3 \exp(-S) / [\pi(S-1)(b^2 - S^2)] \quad (3.27)$$

Functions (3.25) through (3.27) for  $\alpha = 1$  are presented in Figure 3.4. From Figures 3.2 and 3.4, we see that for different WFs the character of functions remains unchanged. The EN position on the range axis in this case is determined by the following equation:

$$\sqrt{b_{ex}^2 - S^2} = \operatorname{tg} \left( \sqrt{b_{ex}^2 - S^2} \right) \quad (3.28)$$

Having designated  $k = \sqrt{b_{ex}^2 - S^2} / \pi$ , we get the first roots of (3.28):

$$\begin{aligned} k_1 &= 1.43029666; & k_2 &= 2.45902403; & k_3 &= 3.47088972; \\ k_4 &= 4.47740858; & k_5 &= 5.48153665; & k_6 &= 6.48438713. \end{aligned} \quad \left. \right\} \quad (3.29)$$

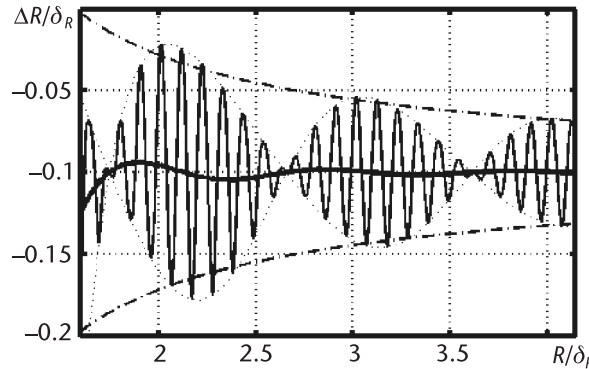


**Figure 3.4** The function of the normalized measurement error versus normalized range for KB WF at  $\alpha = 1$ .

For KB WF the EN position on the normalized range axis depends also upon the root number of equation (3.28) and the WF parameter  $\alpha$ . With a number and the parameter  $\alpha$  increasing, EN displaces toward the large range because at that time the spectrum main lobe increases.

Figure 3.5 shows the function of the first six ENs positions  $x_{Rm}$  on the normalized range axis versus  $\alpha$ . The numbers at each curve correspond to the EN number. Comparing Figures 3.3 and 3.5, we can make a conclusion that both KB WFs have similar characteristics of these functions.

### 3.3.3 Minimization of the Measurement Error on the Basis of the FM Parameter Optimization

#### Application of Additional Slow FM

This method is based on the dependence of the instantaneous measurement error (3.20) and (3.25) upon the DFS phase. Varying the phase  $\Phi_1$  within the limits  $[0, \pi]$  at fixed range and averaging the obtained results, it is possible to minimize the average value of the distant measurement error. We can change the DFS phase at the expense of additional slow FM of the carrier frequency  $\omega_0$  [24]. To provide the required phase shift by  $\pi$ , the range of additional FM sweep should depend upon the measuring range:

$$\Delta F_{\text{slow}} = \Delta F / x_R \quad (3.30)$$

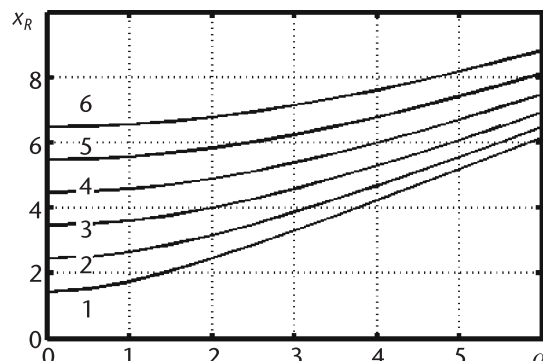


**Figure 3.5** Plots of functions of range point position with zero error versus the point number and  $\alpha$  for KB WF.

Before measurement performance the measuring range is unknown; therefore, this optimization method is in essence the iteration method with a multiple repeat of measurements and further specification of  $\Delta F_{\text{slow}}$  according to (3.30) at each iteration. Therefore, the first measurement is carried out without additional FM to obtain zero approximation  $x_R^{(0)}$  and to calculate  $\Delta F_{\text{slow}}^{(0)}$  according to (3.30). Then the cyclic repeat of the average procedure occurs by means of multiple range measurements with different carrying frequencies, which change discretely in the range from  $\omega_0$  to  $\omega_0 + 2\pi\Delta F_{\text{slow}}$  with the fixed step  $\Delta F_{\text{slow}}/N_{\text{aver}}$  (where  $N_{\text{aver}}$  is a number of averaged measurements), and by means of result average. This procedure repeats up to reduction of modulus of difference between new obtained value  $\hat{x}_R^{(n)}$  and its previous value  $\hat{x}_R^{(n-1)}$  below the value  $\Delta_x$  specified in advance:

$$\left| \hat{x}_R^{(n)} - \hat{x}_R^{(n-1)} \right| \leq \Delta_x \quad (3.31)$$

The described method of error reduction requires significant additional resources in the FM sweep and in measurement time.

The results of such averaging performed with the help of (3.20) and (3.25), are shown, respectively, in Figure 3.2 for  $\alpha = 1$  and in Figure 3.4 for  $Q = 30$  by thick solid curve in the form of the function of the normalized range measurement error  $\Delta R/\delta_R$  versus the relative range. We see that the nonsymmetry of the fast oscillation envelope does not allow the reduction of the measurement error up to zero. For DC and KB WFs, the error decreases by eight to 10 times on small ranges. With the range increasing, the benefit increases.

### Optimization of the FM Sweep

This approach takes into account the invariance of EN position on the axis of normalized range  $x_{R,\text{ex}}$  at invariance of WF parameters. At the same time, position of the point  $x_R$  corresponding the measuring range depends on  $\delta_R$ , that is, on  $\Delta F$ . Therefore, at each range, varying  $\Delta F$ , one can displace  $x_R$  toward to one of the nearest EN  $x_{R,\text{ex}}$  with the zero measurement error.

The following is the procedure of adaptive optimization:

- *Step 1:* The range measurement is carried out at maximal possible value of  $\Delta F^{(0)}$  to obtain zero approximation  $x_R^{(0)}$  and to determine the number of the nearest EN for DC WF:

$$\hat{N} = \text{Int} \sqrt{\left( x_R^{(0)} \right)^2 - L^2/\pi^2} \quad (3.32)$$

and the number of the solution root  $\hat{k}_i$  of (3.28) for KB WF, which is the nearest from below the value

$$k = \sqrt{\left( \hat{x}_R^{(0)} \right)^2 - \alpha^2} \quad (3.33)$$

- *Step 2:* The normalized value of range for EN  $x_{RT}$  according to (3.23) for DC WF and according to the formula  $x_{R,\text{ex}} = \sqrt{\hat{k}_i^2 + \alpha^2}$  for the KB WF.

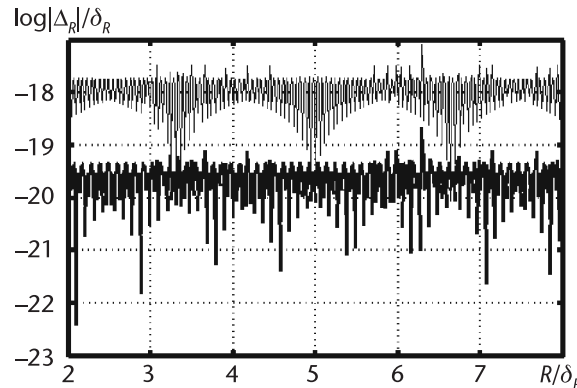


**Figure 3.6** The measurement error at optimal values of the FM sweep for the DC WF.

- *Step 3:* The value of the FM sweep is corrected as

$$\Delta F^{(n)} = \Delta F^{(n-1)} x_{R,ex} / \hat{x}_R^{(n-1)} \quad (3.34)$$

- *Step 4:* Using the obtained value of  $\Delta F^{(n)}$ , we provide measurement of the next approximation for normalized range  $\hat{x}_R^{(n)}$ .
- *Step 5:* Steps 3 and 4 are repeated until the performance of condition (3.31).

For convergence of the iteration process, it is necessary to use EN with a number not less than 2, which is connected with the rather large measurement error level at small  $x_R$ .

The results of optimization are shown in Figure 3.6 for DC WF and in Figure 3.7 for KB WF by thin solid lines. The average level of the achievable error is defined by the value  $\Delta_x$ . In Figures 3.6 and 3.7 we see plots for  $\Delta_x = 10^{-14}$ .

The achieved error level is equal to  $10^{-9}$  for the KB WF with  $\alpha = 1$  and  $10^{-17.5}$  for the DC WF with  $Q = 30$  dB. The fact that the average measurement error level achieved by optimization of the FM sweep does not depend on the range is practically important.

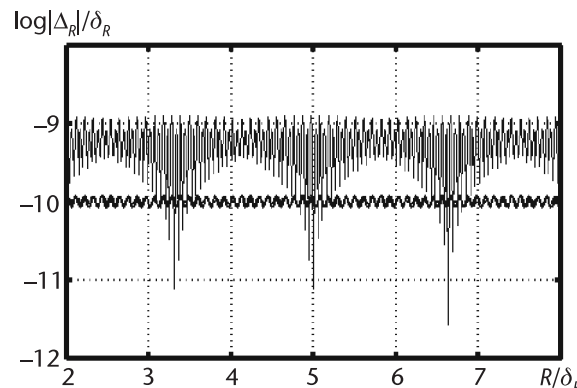


**Figure 3.7** The measurement error at optimal values of the FM sweep for the KB WF.

### The Combined Method of the FM Parameter Optimization

This method combines the above-mentioned approaches. At first, carrying out optimization of the FM sweep obtaining  $\Delta F_{\text{opt}}$  is required. Then for this optimal value, the average results of several measurements are provided for the smooth additional slow variation of  $\omega_0$  by the value defined by (3.30), where the obtained values of  $\Delta F_{\text{opt}}$  and  $\bar{x}_R^{(n)}$  are used. The results obtained at calculations according to this approach are shown in Figures 3.6 and 3.7 by the thick solid line.

We see that the total measurement error level at averaging using the additional slow FM decreases additionally approximately by the order for the KB WF and by two orders for the DC WF.

#### 3.3.4 Error Minimization on the Basis of Optimization of Weighting Function Parameters

This method of optimization is based on the dependence of the SAD WF extreme position upon its parameters.

The possible approaches to optimization and some restrictions are:

1. Parameter variation of the weighting function leads to displacement of SD SL extremes. Figure 3.8 shows the variation of the SAD DC WF shape as an example. In the logarithm scale signal, SAD items with a normalized frequency of three bins and two values of  $Q$  are represented. The SAD item in the positive frequency area with the ratio  $Q = 20 \text{ dB}$  is drawn with a thin solid line. The SA item on the negative frequency area is drawn with a dotted line. It is theoretically possible to see a coincidence of the extremum, at first, of the fifth lobe of the item from the area  $\omega < 0$  with the maximum of the main lobe from the area  $\omega > 0$ . For this, it is necessary that  $Q = 20 \text{ dB}$  (thick solid and dotted lines).

In the general case, thanks to EN displacement along the normalized range axis at variation of WF parameters, its optimization is possible. For considered DC and KB WFs, equations linked parameters of the optimal WF with the mea-

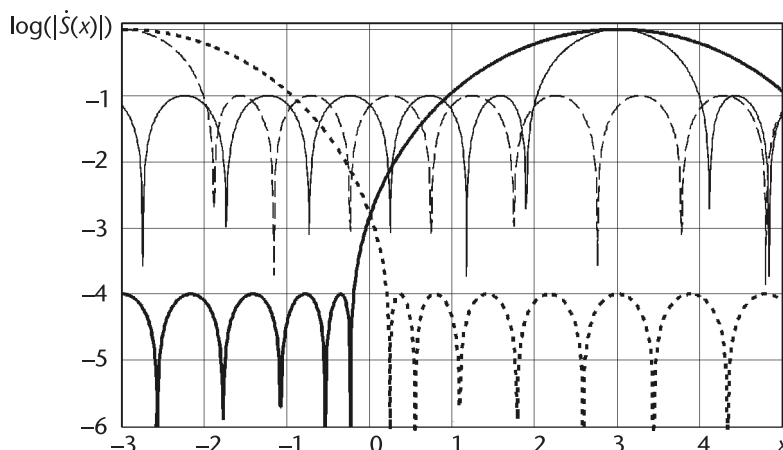


**Figure 3.8** Variation of SD DC WF shape at SLL variation  $Q$ .

suring range are specified by (3.23) and (3.28). The optimization procedure in this case should be iterative. Just after switching on FMCW RF, the measurement should be begun with such WF parameters, at which, on the minimal measuring range, the overlap of the main SAD lobes  $S_{WF}(x_\Delta)$  and  $S_{WF}(x_\Sigma)$  does not happen. These values can be obtained according to formulas:

$$Q_{\min} = \left( B_{\min}^2 + 1 \right) / (2B_{\min}), \quad \alpha_{\min} = \sqrt{(2x_{R\min})^2 - k_1^2}$$

where  $B_{\min} = \exp \left[ \pi \sqrt{(2x_{R\min})^2 - 1} \right]$ ,  $\alpha_{\min} = \sqrt{(2x_{R\min})^2 - k_1^2}$ ;  $k_1$  is the value of the first root in (3.20).

The sequence of actions at the range measurement using the WF parameter optimization is:

- *Step 1:* Samples of measuring DFS are recorded in the computing device memory and according to them for given  $Q_{\min}$  or  $\alpha_{\min}$  the SAD is calculated, the position of the spectrum modulus maximum is obtained, the measuring range and zero approximation for  $x_R^{(0)}$  are calculated.
- *Step 2:* Then, according to (3.23) and (3.28), the number  $\hat{N}$  of SL of  $S_{WF}(x_\Sigma)$  is determined, which overlaps with the main lobe of  $S_{WF}(x_\Delta)$  for DC WF is the value of the root  $\hat{k}_i$  for KB WF.
- *Step 3:* DC WF parameters are specified:

$$\hat{Q}^{(n)} = [(\hat{B}^{(n)})^2 + 1] / [2\hat{B}^{(n)}], \quad n = 1, 2, \dots$$

$$\text{where } \hat{B}^{(n)} = \exp \left[ \pi \sqrt{\left( 2\hat{x}_R^{(n-1)} \right)^2 - \hat{N}^2} \right]$$

or for the KB WF

$$\hat{\alpha}^{(n)} = \sqrt{\left( 2\hat{x}_R^{(n-1)} \right)^2 - \hat{k}_i^2}; \quad n = 1, 2, \dots$$

- *Step 4:* According to the recorded samples (in memory), the  $n$ th approximation  $x_R^{(n)}$  is calculated at specified WF parameter values.
- *Step 5:* Steps 2 to 4 are repeated until the (3.31) performance.

In each iteration cycle, it is necessary to count completely all WF samples, which are used at SAD calculation. For this the computing device must have enough performance.

Calculations performed on the basis of such approach are shown in Figures 3.9 and 3.10 by thin solid lines. We see that in this case the results obtained for the DC WF are better than for the KB WF. The difference achieves approximately six to seven orders. With the range increasing, the error sharply decreases.

It is clear that the considered method for the WF parameter optimization may be added by the results averaging for additional slow FM. Appropriate results are presented in Figures 3.9 and 3.10 by thick solid lines. The benefit achieves approximately two orders.

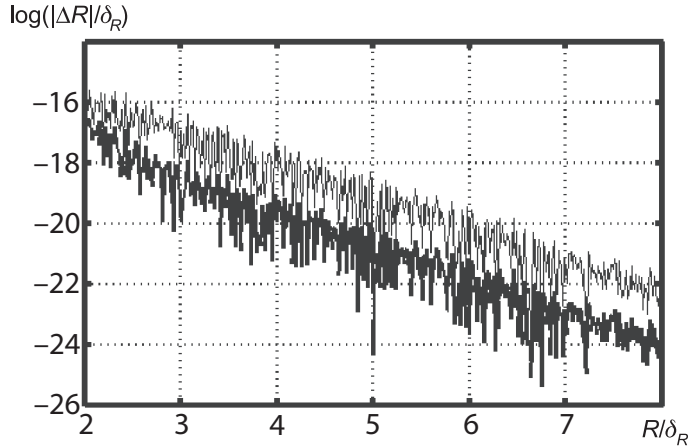


**Figure 3.9** The measurement error at optimal values of the  $\alpha$  parameter for DC WF.

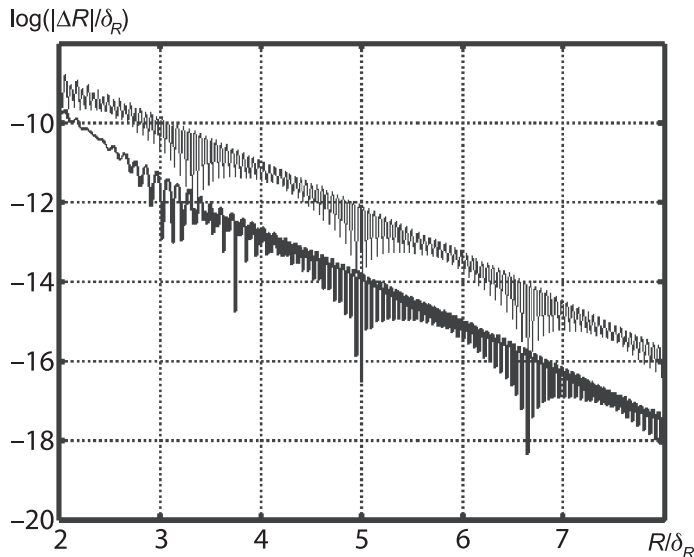


**Figure 3.10** The measurement error at optimal values of the  $\alpha$  parameter for KB WF.

2. There are limitations on practical implementation of measurement error optimization of WF parameters at each measuring range. It is seen from Figure 3.8 that the described coincidence of the fifth SL extremum of the SAD item from the area  $\omega < 0$  with the maximum of the main lobe for the area  $\omega > 0$  led to essential SLL and the main-lobe width variations. The sharp reduction of the nearest SL width and practically unchanged position and widths of far lobes are peculiarities of the signal's SAD processed by both the DC WF and KB WF. This feature is intensified at the discrete signal processing. Therefore, the greater number of signal samples, the more sensitive is the situation to variation of the nearest SL level. Taking into consideration that general regulations are true both for the DC WF and for the KB WF, we describe here the CSD of the discrete signal for DC WF only:

$$\begin{aligned}\dot{S}_{DC}(x, Q, M_0) = & \frac{\exp(j\Phi)}{Q} \left\{ \operatorname{ch} \left[ (M_0 - 1) \cdot \operatorname{ach} \left( \operatorname{ch} \frac{\operatorname{ach} Q}{M_0 - 1} \cdot \cos \frac{x_\Delta \pi}{M_0} \right) \right] \right. \\ & \left. + \exp(-j2\Phi) \operatorname{ch} \left[ (M_0 - 1) \cdot \operatorname{ach} \left( \operatorname{ch} \frac{\operatorname{ach} Q}{M_0 - 1} \cdot \cos \frac{x_\Sigma \pi}{M_0} \right) \right] \right\}\end{aligned}\quad (3.35)$$

The positions of its extrema are:

$$x_{\max}(N, Q, M_0) = \frac{M_0}{\pi} \arccos \left[ \left( \cos \frac{N \cdot \pi}{M_0 - 1} \right) / \left( \operatorname{ch} \frac{\operatorname{ach} Q}{M_0 - 1} \right) \right] \quad (3.36)$$

From here, the required value of  $\hat{Q}$  for error minimization is:

$$\hat{Q}_{(n)} = \operatorname{ch} \left\{ (M_0 - 1) \cdot \operatorname{ach} \left[ \left( \cos \frac{N \cdot \pi}{M_0 - 1} \right) / \cos \left( 2\hat{x}_R \frac{\pi}{M_0} \right) \right] \right\} \quad (3.37)$$

Figure 3.11 shows by the dotted and solid lines, respectively, the positions of extrema of the thirteenth and fourteenth SL of the SAD item in the area of  $\omega < 0$  for these SLs coincident with the main lobe by means of  $Q$  specification. Thick lines correspond to high discretization frequency, at which 1,024 samples are obtained on the signal duration. Therefore, the signal frequency is significantly less than the Nyquist frequency and the redundant discretization frequency is used. Thin lines correspond to the low discretization frequency, at which 32 samples are obtained on the signal duration. Therefore, the signal frequency is commensurable with the Nyquist frequency.

An increase of the relative signal frequency leads to the fact that because of the mentioned features of the signals' SAD with the DC WF and KB WF, the error minimization in the considered form becomes impossible at any high discretization frequency.

We must take into consideration that among popular WFs there are no such WFs, which properties can be easily varied. Therefore, for error minimization by WF parameter variations, we can formulate a task of creation of specific WFs free from this shortcoming.

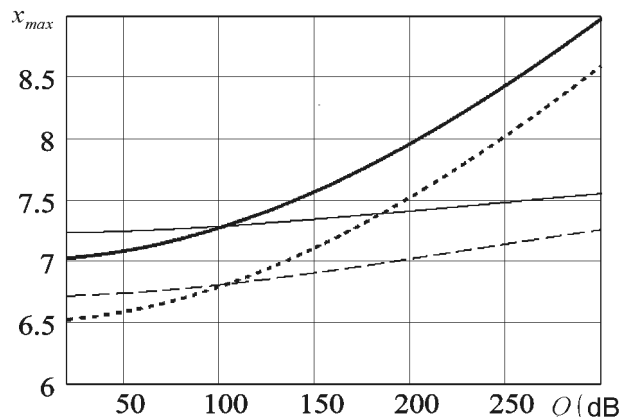


**Figure 3.11** Extremum positions of the thirteenth and fourteenth SL of the SAD item in the negative frequency area at variation  $Q$  for two values of discretization frequencies.

3. We can try to overcome the mentioned limitations by the simplified method of the WF parameter optimization sacrificing by the minimal measurement error and refusing from WF parameter correction in each current point of the range. Let us consider the possibility to use of the method described in Chapter 2 minimizing the average square of the measurement error calculated on range segment equaled to QI by means of WF parameter optimization. The criterion function can be written in the form [38–42]:

$$\sigma_R^2(R_{\text{aver},L}, p) = \sum_{i=1}^{K_R} [\Delta R(R_{Li}, p)]^2 / K_R \Rightarrow \min_p \quad (3.38)$$

where  $K_R = \delta_R / \Delta$  is a number of calculation points on the one range segment;  $\Delta$  is a step in range (in this case  $\Delta \leq \lambda_0 / 4$ );  $R_{Li} = (L - 1)\delta_R + (i - 1)\Delta$  is the  $i$ th current measuring range within the  $L$ th segment;  $p$  is the WF parameter, according to which minimization is provided ( $p = Q$  for the DC WF and  $p = \alpha$  for the KB WF);  $R_{\text{aver},L}$  is the range corresponding to the middle of the  $L$ th segment.

The calculation results according to (3.38), without optimization for the uniform WF, DC WF, and KB WF with parameters, respectively,  $Q = 30$  dB and  $\alpha = 1$ , are presented in Figure 3.12.

The error function character versus range is completely defined by variation of SLL WF SD. It is seen that for the DC WF having the constant SLL of SD, the measurement error remains approximately constant beginning from some range. For uniform WF and KB WF, the monotonic decrease of measurement error occurs for range increasing.

The search of optimal parameter values according to (3.41) from each WF was provided by the numerical method with the help of “fminbnd” program from the MATLAB 6.5 package. After the calculation of optimal parameter values with the

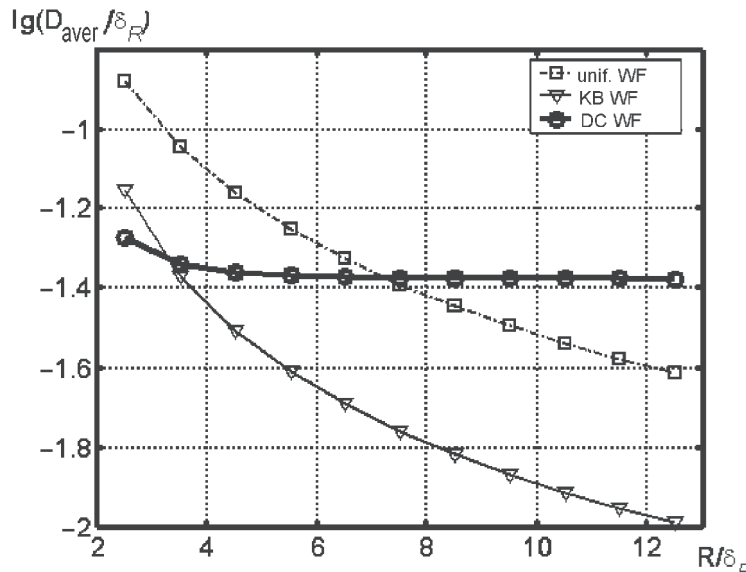


**Figure 3.12** The function of logarithm of the normalized average square of the measurement error versus normalized range for DC WF with  $Q = 30$  dB and KB WF with  $\alpha = 1$ .

help of the method of linear regression [43, 44], the empirical relation was obtained connecting these parameters with the average relative range. For the DC WF and KB WF, respectively, these relations are:

$$Q = 27.392x_{R\text{aver}} - 22.31719 \text{ dB} \quad (3.39)$$

$$\alpha = (1.0073x_{R\text{aver}} - 0.8257)/\pi \quad (3.40)$$

As a result, only two coefficients for each WF should be saved in the memory of the FMCW RF computing device at its manufacture. At first measurement after each activation of FMCW RF, the WF parameters are used corresponding to minimal range. All optimization is provided by calculation manner. For this signal, samples are recorded into online memory and calculation of the initial range estimation is provided according to them. Then, according to this range, measured with an error, the number of the range segment is determined with the unchanged value of WF parameters and the choice of the needed parameter value is performed. Now, basing DFS samples recorded into the online memory, the new range calculation is provided using this parameter value.

Calculation results of the average measurement error according to (3.38) using (3.20) and (3.25) and the optimal parameter values (3.39) and (3.40) remaining unchanged on chosen range segments are presented in Figure 3.13. The measurement error for KB WF is shown by a thin solid line, and the measurement error for DC WF is shown by a thick solid line. For comparison, calculation results without optimization with the uniform WF are shown by a chain line.

At such optimization, it is also required to recount WF samples. However, this should be done much more seldomly, only at the transfer from one range segment to another. As a result, the necessity in the iterative process disappears. Therefore, this method requires minimum time expenses on parameter optimization and provides rather good results.

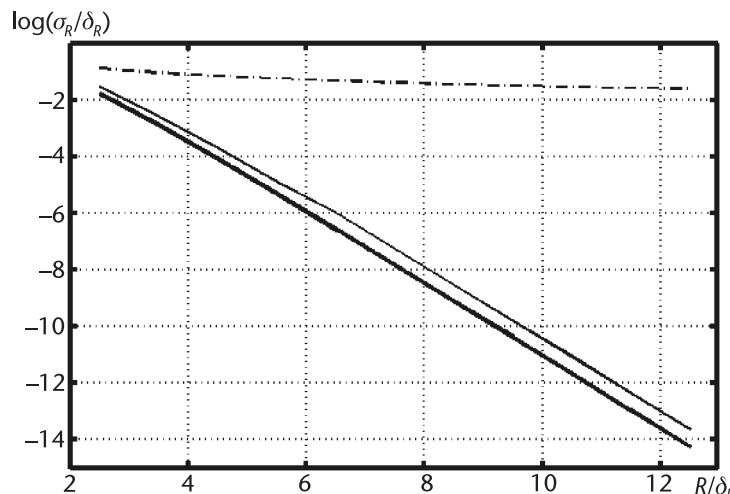


**Figure 3.13** The function of logarithm of normalized averaged square of the measurement error versus normalized range for optimal parameters of DC WF and KB WF.

### 3.3.5 Minimization of the Truncation Error Using Adaptable Weighting Functions

In the Appendix, we show that the problem of elimination of the range measurement error can be solved if there is WF, which shape can be specified by varying parameters in such a manner that at the signal frequency the spurious SAD item would be equal to zero together with the specified number of its derivatives. WFs obtained under these conditions are called adaptable WF (AWF). Important feature of AWF is a possibility of specifying of SAD N zeros at normalized frequencies  $b_1, b_2, \dots, b_N$ .

For effectiveness analysis of the mentioned AWFs in (A.13) and (A.14), we consider the earlier discussed problem of minimization of the DFS frequency estimation error on the background of the spurious SC from the frequency area  $\omega < 0$ .

As earlier, we assume that before the measurement performance, the estimating range is unknown. Due to this, the process of determination of WF necessary parameters is iterative with multiple repeating of calculations and specifying of frequency values of given zeros  $b$  of AWF at each iteration. This procedure is repeated until the performance of the condition (3.31). In each iteration cycle, it is necessary to recalculate completely all AWF samples used at the SD calculation.

For original estimations, one can use different known effective WFs of WFs with optimal parameters, which are presented in the Appendix. Then we use AWFs, whose properties are adapted at range variation.

### 3.3.6 Algorithms of Frequency Estimation Using Adaptable Weighting Functions

The *algorithm 1* is the simplest with constant values of a number varying SAD zeros  $N$  of AWF, and it is the same as analyzed in Section 3.3. However, the procedures of analytical determination of the frequency corresponding to theoretical absence of the truncation error are excluded in it.

The *algorithm 2* realizes possibility of independent control of WF parameters for minimization both the truncation error of frequency estimation and the error. From Figure A.9 we see the opportunity of the ENB limitation increasing both at  $N$  increase and with the increase of estimating frequency  $b_2^{(n)} = b_3^{(n)} = \dots = b_N^{(n)} = 2\hat{x}_1^{(n)}$ , if one from the SD varying zeros, for instance, with number 1, is defined from the condition of the ENB minimum obtaining,  $b_1 = b_{n,\min}$ .

- *Step 1:* Samples of extracted DFS are recorded in the memory of calculation device and according to them, if the optimal WFs of the Appendix are used, for chosen  $N_1$  and  $b_1, b_2, \dots, b_{N_1}$  the estimating frequency and zero approximation for  $\hat{x}_1^{(0)}$  are calculated.
- *Step 2:* The total order of AWF SD varying zeros  $N + 1$ , which is greater by one than the zero order  $N$ , minimizing the spurious SD item and its derivative. The value of  $b_2^{(0)} = b_3^{(0)} = \dots = b_{N+1}^{(0)} = 2\hat{x}_1^{(0)}$  is specified. We accept the value of one of the SD varying zeros  $b_1 = b_{n,\min}$  in accordance with (A.25) or (A.26) using, respectively, AWF  $w_s(m_o, b_1, b_2 \dots b_N)$  or  $w_c(m_o, b_1, b_2 \dots b_N)$ . According to the recorded signal samples, we calculate the next and  $n$ -th approximation at specified WF parameters.
- *Step 3:* Step 2 is repeated until performance of (3.31).

The theoretical error of frequency estimation using AWF at noise absence is equal to zero; therefore, to estimate the achievable error reduction, we consider simulation results of offered process of DFS frequency estimation on the background of the white normal noise.

Numerical simulation was carried out in the MATLAB medium. Taking into consideration that the estimation of the small normalized DFS frequencies (less than 10) has the most interest, the discretization interval in presented examples accepts that DFS contained 32 samples.

The calculation results obtained according to this approach using AWF in (A.12) with three varying zeros  $N + 1 = 3$  are shown in Figure 3.14 by the solid curves:

$$w_s(m) = 1 + \sum_{n=1}^3 (-1)^n C_{sn}(b, b_1) \cos[(2n(m+0.5)M)] \quad (3.41)$$

where  $M = \pi/M_0$

$$\begin{aligned} C_{s1}(b, b_1) &= \frac{2 \sin 3M}{\sin 4M} \frac{\cos(2M) - \cos(2b_1M)}{2 \sin^2(b_1M)} \left[ \frac{\cos(2M) - \cos(2bM)}{2 \sin^2(bM)} \right]^2 \\ C_{s2}(b, b_1) &= \frac{1}{\cos 2M \sin 5M} \frac{\sin 3M}{2 \sin^2(b_1M)} \left[ \frac{\cos(4M) - \cos(2bM)}{2 \sin^2(bM)} \right]^2 \\ C_{s3}(b, b_1) &= \frac{1}{2 \cos 2M \cos 3M} \frac{\sin M}{\sin 5M} \frac{\cos(6M) - \cos(2b_1M)}{2 \sin^2(b_1M)} \\ &\times \left[ \frac{\cos(6M) - \cos(2bM)}{2 \sin^2(bM)} \right]^2 \end{aligned}$$

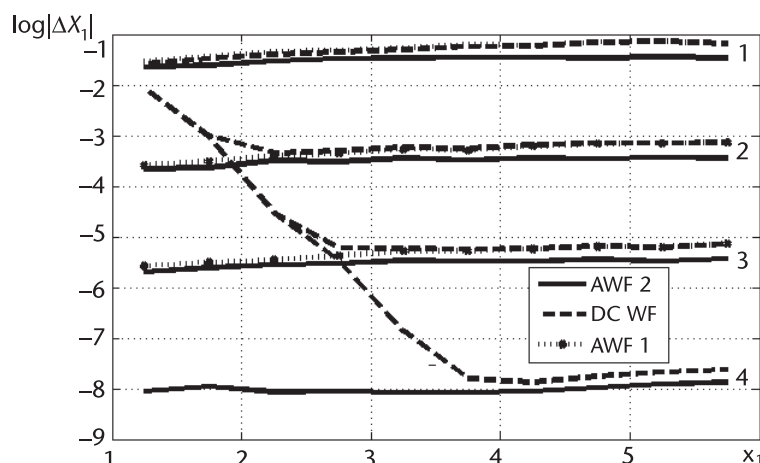


**Figure 3.14** The logarithm of normalized MSD truncation error of frequency estimation of the signal weighted by DC WF and AWF  $w_s = (m_0, b, 3, 32)$  and  $w_s = (m_0, b, 4, 32)$ : 1 indicated  $q = 20$  dB, 2 indicated  $q = 60$  dB, 3 indicated  $q = 100$  dB, and 4 indicated without noise.

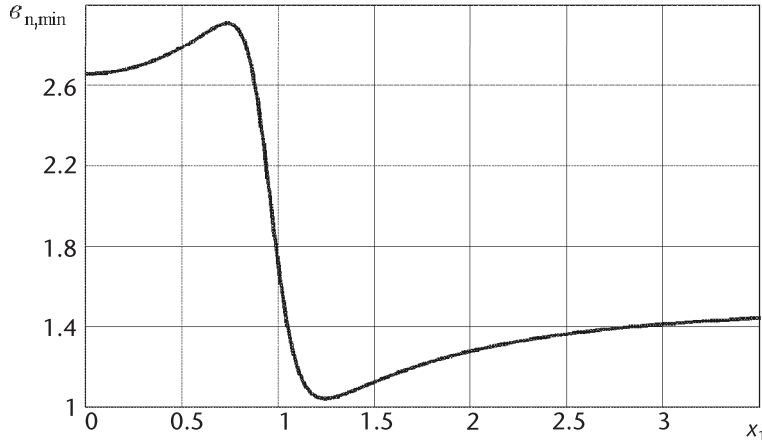


**Figure 3.15** The function of AWF zero frequency ensuring ENB minimization versus signal frequency.

In this example, the frequency of one of the zeros  $b_1 = b_{n,\min}$  is defined by condition of ENB minimization:

$$b_{n,\min}^2 = \frac{25(b_2^2 - 1^2)^4 + 64(b_2^2 - 2^2)^4 + 9(b_2^2 - 3^2)^4}{25(b_2^2 - 1^2)^4 + 16(b_2^2 - 2^2)^4 + 1(b_2^2 - 3^2)^4} \quad (3.42)$$

The frequencies of two other zeros  $b_2 = b_3 = b$  on signal frequency  $x_1 = 0.5b$  minimize of the spurious SC from the area  $\omega < 0$  and its first derivative.

For comparison, the results of frequency estimation using DC WF with optimal values of the shape parameters are presented in Figure 3.14 by the dotted line.

The dependence of zero frequency ensuring the minimum of ENB (3.42) versus signal frequency is shown in Figure 3.15.

The last algorithm provides the minimal error for estimation on the noise background, which confirms obtained theoretical results of the comparative ENB analysis of various AWF (see the Appendix).

Obtained results of numerical experiments show that in contrast to DC WF with the optimal shape parameter, which provides the least truncation error from all traditional WFs and for which at estimations of short signal sample (containing one to two periods of the signal) the main contribution in the error level is introduced by the truncation error, at using of AWF the truncation error component is practically absent, and the component caused by the noise, is 1.15 to 2 times less than at the DC WF application.

## 3.4 Average Weighted Estimation of the Difference Frequency

### 3.4.1 The Truncation Error of the Average Weighted Estimation

In connection with the fact that the estimation (3.10) is based on the analysis of the SD shape, all of these notes concerning the SD shape distortions in areas  $\omega > 0$  and  $\omega < 0$  especially strongly manifested at small ranges.

Having transformed the numerator of (3.10), we obtain the truncation error of frequency measurement [40, 45–47]:

$$\Delta\omega_R = \sum_{n=n_{\text{low}}}^{n_{\text{upp}}} (\omega_n - \omega_R) |\dot{S}(j\omega_n)|^2 \Bigg/ \sum_{n=n_{\text{low}}}^{n_{\text{upp}}} |\dot{S}(j\omega_n)|^2 \quad (3.43)$$

where  $\dot{S}(j\omega_n)$  is a value of the complex DFS spectrum at discrete frequency  $\omega_n$  and  $n_{\text{low}}$  and  $n_{\text{upp}}$  are the lower and upper numbers of processed discrete frequencies.

For future analysis of the measurement error it is necessary to consider the structure of (3.43). We assume that the analysis is performed under conditions listed in designations (3.12). Then the numerator (3.43) can be presented in the form of three items:

$$\begin{aligned} A_1 &= \sum_{n=n_1}^{n_2} \left( \pi \frac{2n - x_R}{K} \right) \left| \dot{S}_{\text{WF}} \left[ \pi \frac{2n - x_R}{K} \right] \right|^2 \\ A_2 &= \sum_{n=n_1}^{n_2} \left( \pi \frac{2n - x_R}{K} \right) \left| \dot{S}_{\text{WF}} \left[ \pi \frac{2n + x_R}{K} \right] \right|^2 \\ A_3 &= 2 \sum_{n=n_1}^{n_2} \left( \pi \frac{2n - x_R}{K} \right) \text{Re} \left\{ \dot{S}_{\text{WF}} \left( \pi \frac{2n + x_R}{K} \right) \dot{S}_{\text{WF}} \left( \pi \frac{2n - x_R}{K} \right) \exp(-j2\Phi) \right\} \end{aligned} \quad (3.44)$$

where  $\text{Re}\{\cdot\}$  designates the calculation of the real part of the complex number.

The denominator  $Den$  in the formula (3.43) has a view:

$$\begin{aligned} Den &= \sum_{n=n_1}^{n_2} \left[ \left| \dot{S}_{\text{WF}} \left( \pi \frac{2n - x_R}{K} \right) \right|^2 + \left| \dot{S}_{\text{WF}} \left( \pi \frac{2n + x_R}{K} \right) \right|^2 \right. \\ &\quad \left. + 2 \text{Re} \left\{ \dot{S}_{\text{WF}} \left( \pi \frac{2n + x_R}{K} \right) \dot{S}_{\text{WF}} \left( \pi \frac{2n - x_R}{K} \right) \exp(-j2\Phi) \right\} \right] \end{aligned} \quad (3.45)$$

Analysis of these formulas allows some conclusions about the function character of the frequency estimation error on spectrum center of gravity versus  $\Omega_R$ , that is, the measuring range. The denominator of (3.43) represents the signal energy concentrated in the processed frequency range  $[\omega_{\text{low}}, \omega_{\text{upp}}]$ . We shall consider ranges, at which there is no overlapping of main lobes of the spectral density. Under these conditions, at correct choice of boundaries of the processed frequency range, the denominator  $Den$  does not practically depend on  $\omega_R$  and the WF shape. The first item  $A_1$  of the numerator (3.43), due to symmetry of the WF spectrum, is equal to zero or very small at calculation according with the formula for the discrete spectrum. The third item  $A_3$  in integrand contains the phase multiplier  $\exp(-j2\Phi)$  and therefore, fast oscillations at a range variation with a period equal to a quarter of a wavelength of the carrying oscillation and with the phase defined by the phase of radio wave reflection coefficient. Moreover, it contains the product of the main lobe of the WF spectrum located on the half-axis  $\omega > 0$  and SL of this spectrum from the half-axis  $\omega < 0$ . At the range variation, these spectra move with respect to each other. Therefore, the result of this multiplication defining the amplitude of fast oscillations varies with periodicity of SL of the WF spectrum and smoothly changes at variation of SL. The second item  $A_2$  is the processing result in the same frequency range of the square

of the SL spectrum located on the half-axis  $\omega < 0$ , therefore, in most of the cases it is significantly less than the third item. Thus, the measurement error is mainly defined by the third item  $A_3$  and strongly depends upon used WF as exactly it depends on the SL level influencing on the oscillation amplitude of the measurement error.

Obtained formulas are true for arbitrary WF. As was shown in [5], all types of WFs can be represented using  $M$  orthogonal basis functions with periods multiple to the interval  $T_{\text{mod}}/2$ . In this case, the discrete spectrum of WF, which is necessary to use in (3.44) and (3.45), has a form [3, 5, 8]:

$$\begin{aligned}\dot{S}_{\text{WF}}(n) = a_0 D\left[2\pi \frac{n}{K}\right] + \frac{1}{2} \sum_{m=1}^M (-1)^m a_m &\left\{ D\left[2\pi \frac{n-m}{K}\right]\right. \\ &\left. + D\left[2\pi \frac{n+m}{K}\right]\right\}\end{aligned}\quad (3.46)$$

where  $D(z) = \exp[j(K-1)z/2]/[\sin(Kz/2)/\sin(z/2)]$  is the normalized Dirichlet core [2, 5] and the coefficients  $a_m$  corresponds to the condition  $\sum_{m=0}^M a_m = 1$ .

Figure 3.16 shows ratios of items  $A_2$  and  $A_3$  from (3.44) to denominator (3.45) for the uniform WF versus the relative range  $R/\delta_R$  for  $F_0 = 10$  GHz and  $\Delta F_0 = 1,000$  MHz. The plots fully confirm the above-mentioned analysis of item properties of the measurement error. We see that  $A_3 >> A_2$  and this inequality becomes more sensible with range increasing. The item  $A_1$  in this figure is not shown even because in a used scale it is not noticeable practically. Thus, the range measurement error with the help of the average-weighted estimation (3.10) is mainly defined by the third item of the numerator in (3.43).

From Figure 3.16, we clearly see that the plot for  $A_3$  oscillates around the zero error value with two typical periodicities. As for SAD maximum, there are two types of points with the zero truncation error. The period of the first sequence is approximately  $\lambda_0/4$ , and the period of the second being the envelope period of the instantaneous error is related to periodicity of SL SAD WF. The measurement error smoothly decreases with range increasing.

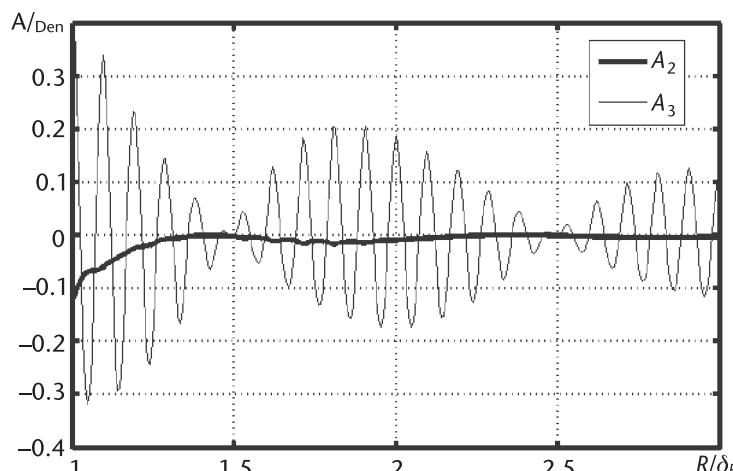


**Figure 3.16** Functions of truncation error components of (3.46) versus the normalized range.

In the range points corresponding to nodes of the envelope  $A_3$  the exact error value is determined by a sum of two items ( $A_2 + A_3$ ). Therefore, from these two points the value  $A_2$  has the determining influence on the value of the minimal possible error. Calculations show that these conclusions are valid as well for other WFs; therefore, the mentioned inequalities become stronger because the SLs of their spectra are much less than for the uniform WF.

The total plots view of instantaneous measurement error versus the relative range reminds us of the same properties of plots obtained earlier for frequency estimation according to spectrum maximum. Therefore, we may expect the applicability of all optimization methods for average weighted estimation. Nevertheless, there is an essential difference consisting in the fact that in points corresponding to zero value of  $A_3$  item envelope; the error is not equal to zero even theoretically, although its value can be very small. In addition, we may note that for optimization of the FM sweep and WF parameters in each point of the range scale it is required knowledge of theoretical dependence of these points' positions with minimal measurement error on the scale of normalized range. These formulas do not allow us to obtain these functions in an explicit form.

Calculations show that above-mentioned methods of measurement error minimization lead to the same results, but the level of the achievable minimal error for average weighted estimation is higher than for estimation according to SD maximum.

### 3.5 Systematic Inaccuracy of Frequency Estimation for the Algorithm with Correction Coefficients

The reason of systematic inaccuracy appearance for the algorithm using correction coefficients is the same as at application the algorithm (3.4), which estimates the DFS frequency based on SAD maximum minus the SL influence of DFS spectrum calculated for  $\omega < 0$ . Figure 3.17 shows the typical dependence of the normalized instantaneous error versus the normalized range obtained with the help of simulation.

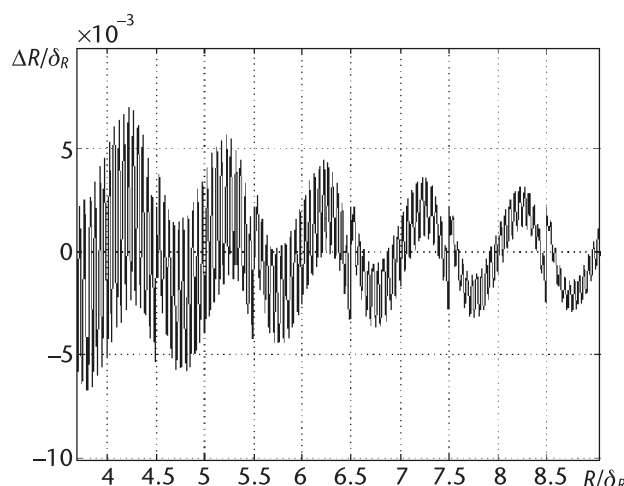


**Figure 3.17** The function of the normalized instantaneous error versus the normalized range for the algorithm using correction coefficients.

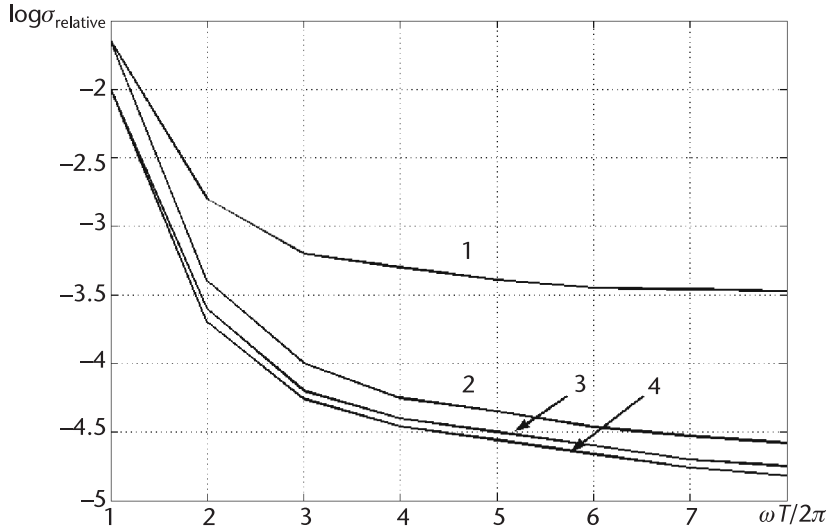


**Figure 3.18** The function of normalizes MSD versus the relative frequency for the algorithm using correction coefficients.

The carrier frequency and the FM sweep at simulation were accordingly 10 GHz and 500 MHz. We see from the plot that the normalized instantaneous error has the double periodicity and oscillates around the zero error. One can observe fast oscillations with a period equal approximately to a quarter of the transmitter wavelength. The period of the envelope of fast oscillations is determined by the frequency diversity of DFT filters. With an increasing in the added zero sample number, the period of the envelope of fast oscillations decreases. The plot in Figure 3.17 is obtained at an increase of two times the DFS realization duration owing to the addition of zero samples.

Functions of normalized systematic inaccuracy  $\sigma_{\text{relative}} = T \sqrt{h_{\text{aver}}} / 2\pi$  versus the relative frequency are presented in Figure 3.18 ( $h_{\text{aver}}$  is the average error square obtained in the interval of signal frequency variation corresponding to the one period of the envelope of fast oscillations). The Blackman WF [3] was used as WF.

Functions 2 to 4 correspond to a range measurement at an artificial increase of the signal period by two, four, or eight times. The function 1 is obtained without addition of zero samples. All functions are found out beginning from the relative frequency equal to 1. It follows from Figure 3.20 that the most expedient process is to increase the signal period by two to four times. A further period increase does not lead to noticeable error reduction. Functions presented in Figure 3.20 are obtained using SAD. Application of SPD leads to the similar results.

## 3.6 Influence of Noise Interference on the Error of Range Measurement

### 3.6.1 Statistical Characteristics of Estimation of the Spectral Density of DFS and Noise Sum

In general, the problem of SC CSD distribution finding for a sum of DFS (or a signal with unknown parameter)  $u_{\text{DFS}}(t)$  and the stationary random signal  $\xi(t)$  (1.51) can be reduced to obtaining of distribution after linear inertial conversion. Obtaining

CPD estimation distribution can be reduced to the same problem with the only difference being that following distribution being obtained after linear inertial conversion, it is necessary to take into account the nonlinear conversion (obtaining the modulus square of the random variable, that is, the estimation of the  $i$ th SPD sample). In general, this problem of obtaining distributions after linear and nonlinear conversions is solved [32].

We assume that the average value and the signal variance are finite. This condition is always satisfied in practice. Then, due to linear inertial Fourier conversion and because of the central limit theorem [32], the SC distribution of the real and imaginary spectrum parts will asymptotically converge to the normal independently upon the distribution of  $\xi(t)$ .

We write for clearness the estimation of the  $n$ th sample of SPD as

$$\hat{F}(\omega_i) = \left\{ \text{Re}^2[\hat{S}(\omega_i)] + \text{Im}^2[\hat{S}(\omega_i)] \right\} / T \quad (3.47)$$

where  $\text{Re}(z)$  and  $\text{Im}(z)$  are real and imaginary parts of the Fourier transform from the sum of DFS and a noise.

It can be noted that a problem of finding the distribution of  $\hat{G}(\omega_i)$  at the normal character of real and imaginary spectrum parts is reduced to a problem of obtaining the distribution of the modulus square of a two-dimensional vector, which projections are normal and, in general, correlated random variables having different mean values and variances.

In some publications (for instance, in [32]) devoted to research of probability models of radio signals, the modulus distribution of the two-dimensional vector with the normal correlated components having the different mean values and variances was received. Working out it in detail for SPD estimation, after not complicated transformations, we can obtain the one-dimensional distribution of the estimation (3.47) for normal distribution of real and imaginary spectrum parts. Complexity of this distribution practically excludes a possibility to work with it in general.

It is advisable to perform an approximation of this distribution by simpler one. For approximation, we calculated positions of image points on the Pirson plane [48]. Calculation results show that image points corresponding to initial distribution lay on the line corresponding to the  $\gamma$  distribution.

In the case when the observation interval is large enough, the distribution of the random variable

$$F(\omega_i) = \frac{1}{T} |\dot{S}_u(j\omega_i) + \dot{S}_\xi(j\omega_i)|^2 \quad (3.48)$$

in assumption that at large enough observation time the real and imaginary spectrum parts are not correlated [27, 49], and their variances are equal, can be presented in the form [50]:

$$W(x) = \frac{1}{G(\omega_i)} \exp \left[ -\frac{x + |\dot{S}_u(j\omega_i)|^2}{G(\omega_i)} \right] I_0 \left[ \frac{2\sqrt{x}|\dot{S}_u(j\omega_i)|}{G(\omega_i)} \right] \quad (3.49)$$

where  $I_0(z)$  is the Bessel function of zero order of imaginary argument and  $G(\omega_i)$  is noise PSD on the  $i$ th frequency.

Mathematical expectation of SPD estimation and its variance can be defined in the form [50]

$$M\{F(\omega_i)\} = |\dot{S}_u(j\omega_i)|^2 + G(\omega_i) \quad (3.50)$$

$$D\{F(\omega_i)\} = G(\omega_i) \left[ 2|\dot{S}_u(j\omega_i)|^2 + G(\omega_i) \right] \quad (3.51)$$

If there is no a signal, that is,  $u_{\text{DFS}}(t) = 0$ , the distribution (3.49) is transferred to exponential with the distribution parameter  $G(\omega_i)$ .

Distribution of SAD probabilities  $|\dot{S}_u(j\omega_i)|$  obeys the Rice distribution [32]

$$W(x) = \frac{2x}{G(\omega_i)} \exp \left[ -\frac{x^2 + |\dot{S}_u(j\omega_i)|^2}{G(\omega_i)} \right] I_0 \left[ \frac{2x|\dot{S}_u(j\omega_i)|}{G(\omega_i)} \right] \quad (3.52)$$

that follows from its definition (in this case, asymptotic independence of real and imaginary spectrum parts and equality of their variances). Moments of distribution (3.52) can be found in [32]. Please remember that at rather a large SNR, the distribution (3.52) can be approximated by the normal distribution [32].

SC of the sum of signal with unknown parameter and the white normal noise, as it was shown in [50], we can consider as statistically independent random variables.

### 3.6.2 Influence of Noise on Accuracy of the Central Frequency Estimation

Let us assume that the additive mixture of DFS and the noisy interference (1.51) applies to the input of a calculating device. The interference  $\xi(t)$  is the stationary random process (SRP) with zero mean and SPD  $G(\omega)$ . After the analog-digital conversion and WF application, we obtain a realization of the process (1.51) presented in the discrete form:

$$s(t_l) = u(t_l)w(t_l) + \xi(t_l)w(t_l), l = \overline{1, K} \quad (3.53)$$

Calculating the spectra of signals in (3.53), we obtain a random function of frequency, SAD  $\hat{A}(\omega)$ , or an estimation of the SPD  $\hat{F}(\omega)$ , which are used for DFS frequency estimation. Calculation of frequency estimation errors caused by the noisy interference leads to essential difficulties caused, in the general case, by non-Gaussian SC distribution and their statistical dependence.

#### Calculation of Frequency Estimation Variance for the Algorithm Using the Addition of Zero Samples

For algorithm (3.5) with addition of zero samples, we determine the estimation variance using their multidimensional distribution of probabilities  $w(z_1, z_2, \dots)$  of random variables  $\hat{A}(\omega_i)$  or  $\hat{F}(\omega_i)$ . The probability  $P_m$  that maximal SC will be at the frequency  $\omega_m$ ,  $m = \overline{m1, m2}$  is determined by the integral [32]:

$$P_m = \int_0^\infty dx_m \int_0^{x_{m1}} \dots \int_0^{x_{m2}} w(x_{m1}, \dots, x_{m2}) dx_{m1} \dots dx_{m2} \quad (3.54)$$

Assuming that the frequency interval, in which the maximal SC is searched, if wide enough, we suppose that

$$\sum_{m=m1}^{m2} P_m = 1 \quad (3.55)$$

At the performance of condition (3.55), as a result of calculation of (3.54), we can obtain some discrete law of probability distribution, where each event  $z_m$  (determination of a number of maximal SC) will correspond its own probability  $P_m$ . In this case, we can calculate the frequency estimation variance as:

$$D(\hat{\omega}_R) = \sum_{m=m1}^{m2} [z_m - M(z_m)]^2 P_m \quad (3.56)$$

Because at the addition of zero samples SC turns out the correlated (correlation coefficient is proportional of DFT filter overlapping), the calculation according to (3.54) can only be executed by numerical methods and only when the multidimensional SC distribution is approximated by the normal law (i.e., at large SNR). Taking into consideration the calculation of labor intensiveness, it is more expedient to use the PC modeling for determination of estimation variance.

### Influence in Noise on Accuracy of DFS Central Frequency Estimation in the Spectral Domain Using Correction Coefficients

The generation of estimation with the help of correction coefficients, according to (3.8), anticipates calculation of the ratio of the sum and difference of random variables, estimations of  $\hat{A}(\omega)$  or  $\hat{F}(\omega)$ . Estimation of signal (1.51) SD is

$$\hat{F}(\omega) = |S_u(j\omega)|^2 + \hat{G}(\omega) + 2 \operatorname{Re} S_u(j\omega) S_\xi(j\omega) \quad (3.57)$$

where  $\hat{G}(\omega)$  is estimation of noise SPD and  $S_u(j\omega)$  and  $S_\xi(j\omega)$ , respectively, were estimations of CSD of a signal and a noise. Therefore, the frequency estimation obtained using the algorithm (3.8) will be shifted. It will be shifted as well when using SAD. The quantitative measure of estimation shift, by definition, is the following quantity [32]

$$\Delta_{sh} = M\{\hat{\omega}_R\} - \omega_R \quad (3.58)$$

where  $\omega_R$  is the true value of estimating quantity and  $M$  is a symbol of mathematical expectation.

To find out the variance and the frequency estimation shift, it is necessary to determine the distribution law of correction (3.9) or its moments. The non-Gaussian character of spectra  $\hat{A}(\omega)$  and  $\hat{F}(\omega)$ , calculating on arbitrarily frequencies  $\omega_i$  and determining according to (3.49) and (3.52), practically eliminates obtaining the exact distribution of correction and exact expression for its moments. Therefore, we use the approximate method.

Let us define spectra of a signal and a noise after WF application. The signal spectrum  $S_s(j\omega)$  in this case can be easily calculated using the following relations [3]:

$$\begin{aligned} S(j\omega) &= \frac{1}{\sqrt{T}} \int_0^T u(t) w(t) e^{-j\omega t} dt \\ &= \frac{1}{\sqrt{T} 2\pi} \int_{-\infty}^{\infty} S_u(j\nu) S_{WF}[j(\omega - \nu)] d\nu \end{aligned} \quad (3.59)$$

where  $w(j\omega)$  is the WF spectrum. The SPD of a noise  $G'(\omega)$  after WF application will be defined by the known relation [3]:

$$G'(\omega) = \int_{-\pi T}^{\pi T} G(\omega) |S_{WF}(j\omega)|^2 d\omega / 2\pi \quad (3.60)$$

that is, a noise has arbitrary SPD.

We assume that the SNR for SC with numbers  $n - 1$  and  $n + 1$  (the maximal SC is in the frequency with a number  $n$ ) is large enough (the value of  $q_{s/n} > 40$  dB). Let us find the shift and a variance of frequency estimation for SAD and SPD. We note that the addition of zero samples leads to the appearance of correlation links between SC estimations. However, at two times the SC period increase, estimations of SPD (and SAD) noise on the left and on the right from the maximal SC remain noncorrelated because the frequency response of DFT filters with numbers  $l$  and  $l + 2$  do not overlap.

Using relations for mathematical expectations and a variance of distribution in (3.52) [32] of DFS SAD, we expand (3.9) into a multidimensional Taylor series with respect to the point in which random parameters take values equal to their mathematical expectations. As a result, after transformations [51, 52], we obtain the following formula for the determination of the shift  $\Delta_{sh,a}$  of the frequency estimation caused by the influence of noisy interference

$$\begin{aligned} \Delta_{sh,a} &= \frac{(C_1 + C_2 - C_3 - C_4)\Psi_a}{C_1 + C_2 + C_3 + C_4} - \frac{(C_1 - C_2)\Psi_a}{(C_1 + C_2)} \\ &+ 4 \left\{ \frac{(C_1 + C_3) \left[ \frac{G'(\omega_{n-1})}{4} - C_3^2 \right] - (C_2 + C_4) \left[ \frac{G'(\omega_{n+1})}{4} - C_4^2 \right]}{(C_1 + C_2 + C_3 + C_4)^3} \right\} \Psi_a \end{aligned} \quad (3.61)$$

$$\text{where } C_1 = |S_u(\omega_{n-1})|, \quad C_2 = |S_u(\omega_{n+1})|, \quad C_3 = \frac{G'(\omega_{n-1})}{4|S_u(\omega_{n-1})|}, \quad C_4 = \frac{G'(\omega_{n+1})}{4|S_u(\omega_{n+1})|}.$$

The equation for frequency estimation variance determination can be presented for the amplitude spectrum as:

$$\begin{aligned} D\{\hat{\omega}_a\} &= D\{p_a\} = \frac{8}{(C_1 + C_2 + C_3 + C_4)^4} \\ &\times \left[ (C_2 + C_4)^2 \left( \frac{G'(\omega_{n+1})}{4} - C_4^2 \right) + (C_1 + C_3)^2 \left( \frac{G'(\omega_{n-1})}{4} - C_3^2 \right) \right] \Psi_a^2 \end{aligned} \quad (3.62)$$

After the determination of first two moments, we can select for the correction  $p_a$  the approximated distribution for it. The interval of the random variable  $p_a$ , as follows from (3.9), is in the limits  $-\Psi_a \leq p_a \leq \Psi_a$ . Therefore, it is expedient to approximate the quantity  $p_a$  by generalized beta-distribution [53]

$$W(x) = \frac{1}{2\Psi_a} \frac{\Gamma(\gamma + \eta)}{\Gamma(\lambda)\Gamma(\eta)} \left( \frac{x + \Psi_a}{2\Psi_a} \right)^{\gamma-1} \left( 1 - \frac{x + \Psi_a}{2\Psi_a} \right)^{\eta-1} \quad (3.63)$$

where  $\Gamma(*)$  is the gamma function [20], and parameters  $\gamma$  and  $\eta$  are determined according to [54, 55] taking into account limits of random quantity variation  $p_a$  using equations:

$$\eta = \frac{[2\Psi_a - M\{p_a\}][M\{p_a\}(2\Psi_a - M\{p_a\})2\Psi_a D\{p_a\}]}{2\Psi_a D\{p_a\}}; \quad (3.64)$$

$$\gamma = \frac{M\{p_a\}}{2\Psi_a - M\{p_a\}}$$

$$\text{where } M\{p_a\} = \Delta_{sh,a} + \frac{C_1 - C_2}{C_1 + C_2} \Psi_a$$

By obtaining the frequency estimation shift and variance using SPD, we expand the function (3.9) in the multidimensional Taylor series with respect to the point, in which random parameters take values equal in its mathematical expectations, using distribution moments (3.49). As a result of transformations, we obtain for estimation shift that (index  $m$  notes the power spectrum)

$$\begin{aligned} \Delta_{sh} &= \frac{(b_1 - b_2 + b_3 - b_4)\Psi_m}{b_1 + b_2 + b_3 + b_4} + \frac{2\Psi_m}{(b_1 + b_2 + b_3 + b_4)^3} \\ &\times [(b_1 + b_3)D\{\bar{G}(\omega_{n-1})\} - (b_2 + b_4)D\{\bar{G}(\omega_{n+1})\}] - \frac{b_1 - b_2}{b_1 + b_2}\Psi_m \end{aligned} \quad (3.65)$$

and its variance

$$\begin{aligned} D(\bar{\omega}_m) &= \frac{4}{(b_1 + b_2 + b_3 + b_4)^4} \\ &\times [(b_1 + b_3)^2 D\{\bar{G}(\omega_{n-1})\} + (b_2 + b_4)^2 D\{\bar{G}(\omega_{n+1})\}] \end{aligned} \quad (3.66)$$

$$\text{where } b_1 = |S_u(\omega_{n-1})|^2; \quad b_2 = |S_u(\omega_{n+1})|^2; \quad b_3 = G'(\omega_{n-1}); \quad b_4 = G'(\omega_{n+1}).$$

The distribution of the random quantity  $p_m$  as a quantity  $p_a$  is expedient to approximate by the generalized beta-distribution with parameters  $\gamma$  and  $\eta$ , which are defined according (3.64) through a variance (3.66) and mathematical expectation of the correction coefficient, which can be presented as:

$$M\{p_m\} = \Delta_{sh} + \frac{(b_1 - b_2)}{(b_1 + b_2)}\Psi_m \quad (3.67)$$

Formulas obtained for determination of the frequency estimation shift and the variance are approximate. First, to obtain the numerical characteristics, we used the expansion in the Taylor series. Second, at the calculations, we did not take into consideration the shift of noise SPD estimation  $G(\omega)$ .

To check the obtained formulas, we conducted the result comparison for the calculation of the frequency estimation shift and estimation variance with results of numerical modeling of the range measurement process using the algorithm (3.8). The calculations and simulation were conducted for relative frequencies  $T\omega_R/2\pi > 3$ . With numerical modeling we used signal SAD and calculations were performed according to (3.61) through (3.65). The period of the signal was increased by two times using the addition of zero samples. Simulation was carried out under the condition that the FM sweep is equal to 500 MHz and the useful signal is received on the background of the white normal noise. The sample volume  $L$  for the performance of modeling was  $L = 10,000$ . The estimations of the mean value of the measuring frequency and MSD were determined according to known formulas and after were reduced to the range. Besides, we calculated estimations of asymmetry  $\beta_1$  and excess  $\beta_2$  coefficients.

Figure 3.19 shows typical functions of the range estimation MSD versus SNR.

Functions are obtained on the relative frequency  $T\omega_R/2\pi = 10$ . The solid line corresponds to modeling results, and the dotted line corresponds to the calculation results according to the above-mentioned formulas. It follows from the calculation results that MSD that is more than one order exceeds the estimation shift. Hence, we can practically neglect the estimation shift caused by a noise. The value of MSD does not practically change with variation of signal frequency. The artificial increase of the signal period more than two times does not change the MSD value. The calculation results for asymmetry and excess coefficients showed that at SNR, which is more than 20 dB, we have:  $\beta_1 \approx 0$ ,  $\beta_2 \approx 3$ , that is, the correction distributions are symmetrical with regard to its mathematical expectations and can be approximated by the normal distribution. The application of the Kolmogorov fitting

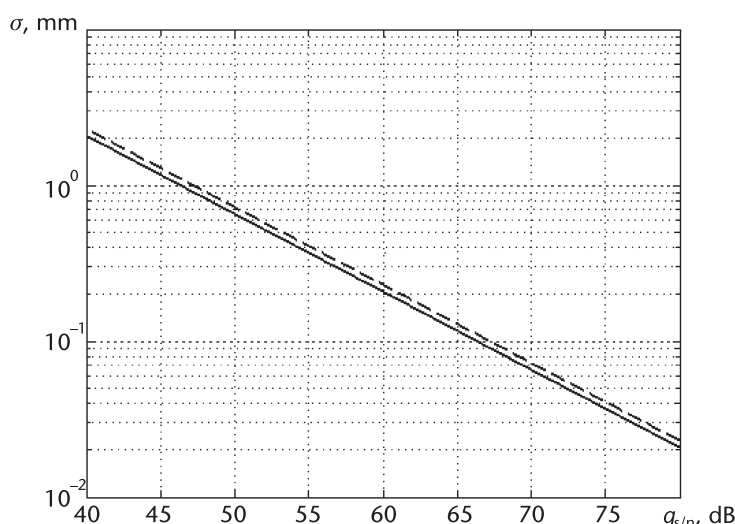


Figure 3.19 The function of range estimation MSD versus SNR.

criterion showed that both the beta distribution and the normal distribution are a good approximation of the correction distribution with the same confidence level. The character of MSD function, asymmetry, and excess coefficients do not practically change when using the power spectrum for frequency estimation.

### Influence of Noise on the Average-Weighted Estimation of DFS Frequency

As in the previous case, we shall make the decision about the frequency of the  $S(t)$  signal filling based on one signal  $y(t)$  realization according to the algorithm (3.10). It is impossible to find out the exact distribution for frequency estimation obtained in accordance with (3.10) or its moments. Nevertheless, the preliminary conclusion about estimation behavior can be made. It follows from (3.10) that the DFS frequency estimation will be shifted due to influence of the noisy interference, because it is the weighted ratio of SPD of the signal and noise sum. Besides, we may expect that noisy interference will affect with the more influence than algorithms using the search of maximal SC. It can be explained by the fact that the denominator of (3.10) is a random variable.

Let us define the approximate distribution of the frequency estimation. Because earlier it was assumed that the noise  $\xi(t)$  is SRP with the normal probability density, the zero mean value, and the spectral density  $N(\omega)$ , the estimations of SC spectrum will be either noncorrelated (for the white noise) or weakly correlated for the colored noise [as  $O(1/K)$ ].

We assume that SCs of DFS are calculated on the multiple frequencies  $\omega_i = 2\pi i/K$ , that is, the additional zero samples are not used for determination of average-weighted estimation. Their application will lead to the appearance of correlation links between SCs, which, in essence, will lead to an impossibility of finding out the distribution law for frequency estimation. We rewrite (3.10) as:

$$\hat{\omega}_R = \sum_{i=n_1}^{n_2} \omega_i |F(j\omega_i)|^2 \Bigg/ \sum_{i=n_1}^{n_2} |F(j\omega_i)|^2 \quad (3.68)$$

where  $F(\omega) = \frac{1}{K} |S_u(j\omega_i) + S_\xi(j\omega_i)|^2$  is an SPD estimation of the signal  $s(t)$  weighted by WF and calculated using discrete or fast Fourier transform on frequencies  $\omega_i = 2\pi i/K$ .

It is rather difficult to use the distribution (3.49) for obtaining the distribution of the random quantity  $\hat{\omega}_R$ , applying approaches based on the functional transformations of random quantities. We approximate (3.49) by the more suitable distribution using the method of moments [48]. Having calculated the asymmetry and excess coefficients, we can be sure that image points corresponding to distribution (3.49) lay in the Pirson plate on the line corresponding to the gamma distribution. Using the mean value and a variance of the distribution (3.49), we determine parameters  $\alpha$  and  $\beta$  gamma distributions:

$$\alpha_n = M^2 \{F(\omega_n)\} / D\{F(\omega_n)\}, \beta_n = D\{F(\omega_n)\} / M\{F(\omega_n)\} \quad (3.69)$$

The index  $n$  indicates that parameters  $\alpha_n$  and  $\beta_n$  are related with the gamma distribution, which was used for distribution of quantity  $F(\omega_n)$  on the  $n$ th frequency.

A quality of the distribution (3.49) approximation  $w_1(x)$  by the gamma distribution  $w_2(x)$  is estimated by the relation

$$d = \max \left| \int_0^Z W_1(x) dx - \int_0^Z W_2(x) dx \right| \quad (3.70)$$

Calculations show that at the variation of the integration limit in all intervals of the  $W_1(x)$  definition, the quantity  $d$  does not exceed the value 0.01 at  $|S_u(j\omega_n)|^2/G'(\omega_n) > 20$  dB and quickly decreases with the ratio  $|S_u(j\omega_n)|^2/G'(\omega_n)$  increasing.

Because the estimation of the frequency  $\hat{\omega}_R$  is a sum of dependent quantities

$$\hat{\omega}_{Rn} = \omega_n |F(j\omega_n)|^2 / \left[ |F(\omega_n)|^2 + \sum_{i \neq n} |F(j\omega_n)|^2 \right], \quad n = \overline{n_1, n_2} \quad (3.71)$$

for the determination of statistical characteristics of estimation  $\hat{\omega}_R$ , it is necessary to find out the joint distribution of quantities  $\hat{\omega}_{Rn}$ . Such distribution was obtained in [56] and it is called a generalized Dirichlet distribution. Nevertheless, relations obtained in [56] are complicated and practically unsuitable for calculations.

To obtain the simpler calculation formulas allowing the discovery of the mean value and a variance of the frequency estimation  $\hat{\omega}_R$ , we must take into consideration the following circumstance. The DFS frequency is measured, as a rule, at a large enough SNR. However, already at the ratio,  $|S_u(j\omega_n)|^2/G'(\omega_n) > 20$  dB  $\beta_n \approx 2G'(\omega_n)$ . In the case when the delta-correlated noise is acting in the system, distribution laws of all quantities included in (3.71) can be approximated by the gamma distribution with the same parameters  $\beta_n$ . Therefore, the joint distribution of  $\hat{\omega}_{Rn}$  ( $n = \overline{n_1, n_2}$ ) will be transformed to the usual Dirichlet distribution [54].

Using the equation for moments of the Dirichlet distribution, we can determine equations for the mean value and the variance of the random quantity  $\hat{\omega}_R$  (index  $l$  notes lower number and  $h$  is high number of processed frequency):

$$M\{\hat{\omega}_R\} = \omega_R \quad (3.72)$$

$$D\{\hat{\omega}_1\} = \sum_{n=n_1}^{n_h} \omega_n^2 \left\{ \frac{\alpha_n(\alpha_{n_1} + \alpha_{n_1+1} + \dots + \alpha_{n_h} - \alpha_l)}{(\alpha_{n_1} + \dots + \alpha_{n_h})^2 (\alpha_{n_1} + \dots + \alpha_{n_h} + 1)} \right. \\ \left. - 2 \sum_{i=n_1}^{n_h} \sum_{n=n_1}^{n_h} \frac{\alpha_i \alpha_n}{(\alpha_{n_1} + \dots + \alpha_{n_h})^2 (\alpha_{n_1} + \dots + \alpha_{n_h} + 1)} \right\} \quad (3.73)$$

To check the obtained formulas, the calculation results comparison is performed according to these formulas of the frequency estimation shift and the estimation variance with results of numerical modeling of the range measurement process with the help of the algorithm (3.8). Calculations and modeling were conducted for different relative frequencies. Modeling was carried out under the condition that the FM sweep is 500 MHz and DFS is received on the background of the white normal noise. The sample volume  $L$  at modeling was  $L = 10,000$ . Estimations of the mean

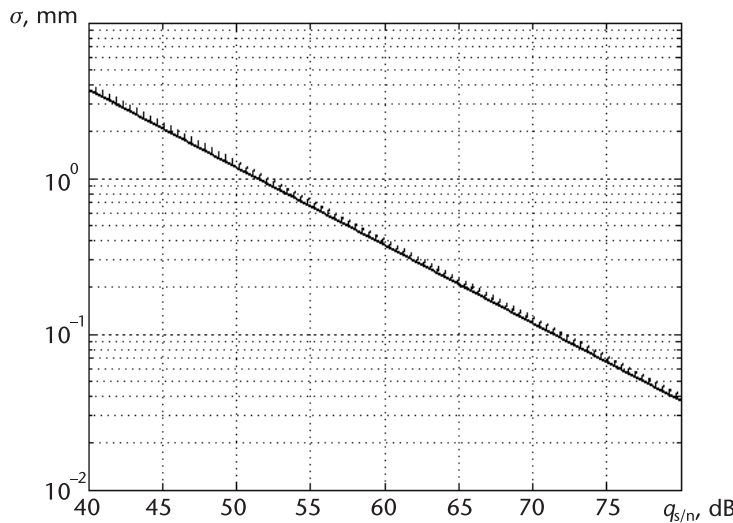


Figure 3.20 The function of normalized MSD versus SNR at  $T\omega_R/2\pi = 10$ .

value of measuring frequency and MSD were determined according to known formulas and then were reduced into the range. Similar results are obtained for different frequency values.

Results are presented in Figure 3.20 for the relative frequency  $T\omega_R/2\pi > 10$ .

Results of modeling are presented by the dotted line and the solid line shows the similar function calculated using (3.73).

The coincidence of modeling results with the theoretical ones can be considered to be good. However, as the Dirichlet distribution, which approximates the true distribution of the frequency MSD, the estimation shift caused by noisy interference cannot be determined with this approach. At the simulation of the estimation shift, we determined that the quantity  $\Delta_{sh}$  is one order greater than MSD calculated according to (3.73).

### Influence of Noise on the DFS Frequency Estimation with the Help of Sliding Half-Strobes

It is impossible to determine a variance of frequency estimation for the algorithm (3.11). It can be proved simply enough that if the signal frequency is estimated, which is received on the background of the white noise, then the estimation will be unbiased. Having rewritten (3.11) in the form:

$$\begin{aligned} & \sum_{i=n_H}^{n_x} \left\{ |S_u(j\omega_i)|^2 + \hat{G}'(\omega_i) + 2 \operatorname{Re} S_u(j\omega_i) S_\xi(\omega_i) \right\} \\ &= \sum_{i=n_x}^{n_B} \left\{ |S_u(j\omega_i)|^2 + \hat{G}'(\omega_i) + 2 \operatorname{Re} S_u(j\omega_i) S_\xi(\omega_i) \right\} \end{aligned} \quad (3.74)$$

and obtaining the mathematical expectation of left and right parts, we find:

$$\sum_{i=n_H}^{n_x} \left\{ |S_u(j\omega_i)|^2 \right\} = \sum_{i=n_x}^{n_B} \left\{ |S_u(j\omega_i)|^2 \right\} \quad (3.75)$$

that is, the estimation will be unbiased. The shift will appear at the estimation of signal frequency, which is received on the background of the colored noise. The last statement is valid for all considered algorithms.

### Simulation of Algorithms of DFS Frequency Estimation

This simulation represents the practical interest for the estimation of noise immunity of all these algorithms of frequency measurement under similar conditions. With this aim, the measurement process simulation was performed at rather large relative frequencies ( $\omega_R T / 2\pi = 10$ ), that is, for the case when the noisy error component is the main one. At calculation of MSD, we used the sample average value, which allows the elimination of the residual spectrum SL influence on the modeling results. At drawn plots presented in Figure 3.21, the DS frequency is recalculated into range.

Results are obtained at an FM sweep of 500 MHz a and carrier frequency of 10 GHz. Function 1 corresponds to application of the algorithm providing the search of the maximal spectral component including based on the spline interpolation and the algorithm performing the median estimation. Function 3 is obtained using the Blackman WF for these algorithms. Function 2 corresponds to application of the algorithm on the basis of correction coefficients without WF usage. Functions 4 and 5 correspond to average-weighted estimation application using the Blackman WF (function 5) and without this application. The analysis of functions shown in Figure 3.21 allows the statement that the algorithm (3.6), which provides the search of maximal SC, the modification of the algorithm (3.6) on the basis of spline interpolation, and the median frequency estimation have practically the same noise immunity. At simulation, the difference in MSD did not exceed 1% to 3% at the sample volume of  $10^4$  realizations. The MSD for the algorithm with correction coefficients is 1.25 times more compared with the mentioned algorithms. The application of the Blackman WF increases the MSD for all algorithms about 1.85 times. The average-weighted estimation has the least noise immunity. It loses to all mentioned algorithms on the MSD about 2.25 times without the Blackman

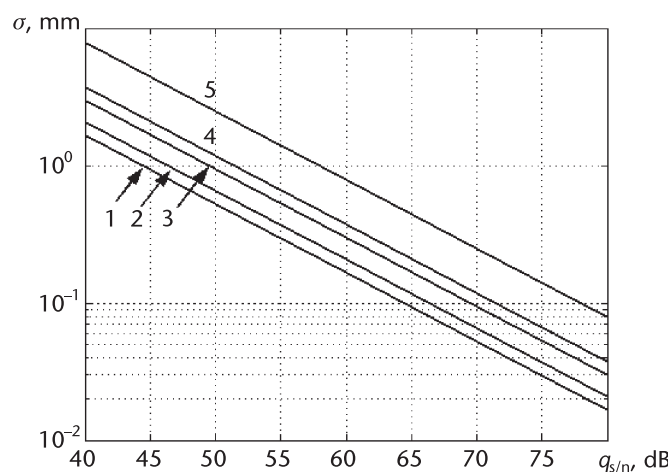


Figure 3.21 Mean-square deviation of range estimation versus SNR.

WF application. The explanation of this fact is rather simple: for the estimation formation, the ratio of two random quantities is used, that is, the noisy interference acts on the nominator and on the denominator of (3.10); therefore, the noise is picked up in the frequency range that is wide enough. Similarly, we can explain the loss in noise immunity for the algorithm using correction coefficients. The application of the Blackman WF increases MSD of the frequency estimation.

### 3.7 Conclusions

Possible algorithms of difference frequency estimation in the spectral domain are considered to be the means of the maximum search of the spectral amplitude density with the help of a two-step procedure of rough estimation on the basis of FFT and specification is considered to be the means of the following algorithms:

1. Addition of zero samples into the initial DFS sample array;
2. Application of IDFT;
3. Spline interpolation of the spectrum;
4. Calculation of correcting coefficients.

In some cases, one uses algorithms for spectrum symmetry estimation on the basis of average-weighting estimation or determination of the spectrum median.

For frequency estimation according to the maximum of spectral amplitude density calculated using the arbitrary WF, the approximated equations are obtained, which allow error estimation of the normalized frequency. The limits of these equation applications are analyzed. These formulas are specified for DC WF and KB WF, which allow us to easily change the shape and the spectrum sidelobe level by means of variation of one parameter.

The detailed analysis of the instantaneous truncation error for normalized frequency measurement versus the range is performed and it is shown that independently on the WF type the measurement error has a periodic oscillating character. There are fast oscillations with the period equal to a quarter-wavelength of the carrying oscillation inscribed into the slow envelope with clearly expressed nodes corresponding to the zero error value. The period of slow oscillations depends on the periodicity of sidelobes of the WF spectrum.

The obtained formulas allow the statement of the problem of range measurement error minimization to be the means of FM parameter optimization (the FM sweep and the carrier frequency) and WF parameters. Optimization algorithms are iterative with gradual specification of parameters until the error will decrease to the accepted level. The limited achievable error at optimization of the carrier frequency and WF parameters has the very minimal measuring ranges. For the range increase, the error gradually decreases. The optimization of the FM sweep allows the approximately the same error level practically at any ranges.

We offer the algorithm of the WF parameter optimization, which allows the elimination of the iteration procedure at some acceptable increase of the achievable error level of range measurement.

The possibility of measurement error minimization is considered by means of adaptable WFs allowing changing the spectrum form in such a manner that spurious items on the useful signal frequency would be equal to zero. Two iterative algorithms for AWF parameters control are offered: the first algorithm, which is simplest but it provides much less values of measurement error compared with the optimization of the DC WF parameters, especially for small measuring frequencies; and the second algorithm, which simultaneously provides minimization of measurement error provides ENB minimization.

The analysis of the measurement error of normalized frequency is performed on the basis of average-weighted estimation. The general form of the instantaneous measurement error coincides with the variant of maximum estimation of the spectral density.

One can also apply the iteration procedures of the FM parameter optimization and the simplified procedure of WF parameter optimization.

The function of the instantaneous measurement error versus range has another character for the algorithm of normalized frequency estimation using correction coefficients. Here there are also two types of periodicity; however, the slow component is not an envelope but has an additive character. With measuring range increasing, we observe the gradual level decrease of the slow and fast oscillating components. This algorithm can be expediently used when adding zero samples to DFS samples to increase the period of the processing signal approximately two to four times.

Using modeling, we conducted an investigation of the noisy interference influence on the range measurement error by different algorithms. It is shown that frequency estimation based on the amplitude spectral density maximum has the less sensitivity compared with the average-weighted estimation providing approximately the 2.25 times less measurement error.

## References

- [1] Marple, S. L., Jr., *Digital Spectral Analysis with Applications*, Englewood Cliffs, NJ: Prentice-Hall, 1987.
- [2] Harris F. J. "On Use of Windows for Harmonic Analysis with the DiscreteFourier Transform." *IEEE Trans. Audio Electroacoust*, Vol. AU-25, 1978, pp. 51–83.
- [3] Dvorkovich, A. V. "New Calculation Method of Effective Window Functions Used at Harmonic Analysis with the Help of DFT," *Digital Signal Processing*, No. 2, 2001, pp. 49–54. [In Russian]
- [4] Dvorkovich, A. V. "Once More About One Method for Effective Window Function Calculation at Harmonic Analysis with the Help of DFT," *Digital Signal Processing*, No. 3, 2001, pp. 13–18. [In Russian]
- [5] Sergienko, A. B., *Digital Signal Processing*. Sankt-Peterburg: Piter Publ., 2003, 604 p. [In Russian]
- [6] Khanyan, G. S. "Analytical Investigation and Estimation of Errors Involved in the Problem of Measuring the Parameters of a Harmonic Signal Using the Fourier Transform Method," *Measurement Techniques*, Vol. 48, No. 8, 2005, pp. 723–735.
- [7] Vinitskiy, A. S. *Essay on Radar Fundamentals for Continuous-Wave Radiation*, Moscow: Sovetskoe Radio Publ., 1961, 495 p. [In Russian]
- [8] Woods, G. S., D. L. Maskell, M. V. Mahoney, "A High Accuracy Microwave Ranging System for Industrial Applications," *IEEE Transactions on Instrumentation and Measurement*. Vol. 42, No. 4, August 1993

- [9] Bialkovski, M. E., S. S. Stuchly, "A Study Into a Microwave Liquid Level Gauging System Incorporating a Surface Waveguide as the Transmission Medium," *Singapore ICCS'94, Conference Proceedings*, Vol. 3, 1994, p. 939.
- [10] Patent 5504490 (USA), INT. CL. G01 S 13/08. "Radar Method and Device for the Measurement of Distance," J. C. Brendle, P. Cornic, P. Crenn. No. 414594. Filed March 31, 1995; date of patent April 2, 1996
- [11] Patent 5546088 (USA), INT. CL. G01 S 13/18. "High-Precision Radar Range Finder," G. Trummer, R. Korber. No. 317680. Filed October 5, 1994; date of patent August 13, 1996.
- [12] Weib, M., Knochel R. "Novel Methods of Measuring Impurity Levels in Liquid Tanks," *IEEE MTT-S International Microwave Symposium Digest*, Vol. 3, 1997, pp. 1651–1654.
- [13] Weib, M., and R. Knochel, "A Highly Accurate Multi-Target Microwave Ranging System for Measuring Liquid Levels in Tanks," *IEEE MTT-S International Microwave Symposium Digest*, Vol. 3, 1997, pp. 1103–1112.
- [14] Patent 2126145 (Russian Federation), INT. CL. G01 F 23/284. "Level-meter," S. A. Liberman, V. L. Kostromin, S. A. Novikov, A. V. Liberman, Yu.G. Nevhepurenko, G. V. Alexin No. 97114261/28. Bull. No. 4. Filed August 20, 1997; published February 10, 1999.
- [15] Zhukovskiy, A. P., E. I. Onoprienko, V. I. Chizhov, *Theoretical Fundamentals of Radio Altimetry*, under ed., of A. P. Zhukovskiy, Moscow: Sovetskoe Radio Publ., 1979, 320 p. [In Russian]
- [16] Korn, G., and T. Korn, *Mathematical Handbook for Scientists and Engineers* New York: Toronto: London: McGraw Hill Book Company, 1961.
- [17] Atayants, B. A., V. M. Davydochkin, V. V. Ezerskiy, D. Ya. Nagorny, "FMCW Radio Range Finder with Adaptive Digital Generation of the Transmitted Signal," *Proceedings of Russian NTORES Named after A.S. Popov. Series: Digital Signal Processing and Its Application. 6th Intern. Conf.* No VI – 2, Moscow, 2004, pp. 26–28. [In Russian]
- [18] Kagalenro, B. V., V. P. Marfin, and V. P. Meshcheriakov, "Frequency Range Finder of High Accuracy," *Izmeritel'naya Technika*, No. 11, 1981, p. 68. [In Russian.]
- [19] Marfin, V. P., A. I. Kiyashev, F. Z. Rosenfeld, V. M. Israilson, B. A. Atayants, B. V. Kagalenko, and V. P. Mashcheriakov, "Radio Wave Non-Contact Level-Meter of Higher Accuracy," *Izmeritel'naya Technika*, No. 6, 1986, pp. 46–48. [In Russian.]
- [20] Kirillov, S. N., M. Yu. Sokolov, and D. N. Stukalov, "Optimal Weighting Processing at Spectral Analysis of Signals," *Radiotekhnika*, No. 6, 1996, pp. 36–38. [In Russian.]
- [21] Brillinger, D. R., *Time Series: Data Analysis and Theory*, New York: Chicago: San Francisco: Atlanta: Dallas: Montreal: Toronto: London: Sydney: Holt, Rinehart and Winston, Inc., 1975.
- [22] Jenkins, G. M., and D. G. Watts, *Spectral Analysis and Its Applications*, San Francisco: Cambridge: London: Amsterdam: Holden-Day, 1969.
- [23] Tikhonov, V. I., *Optimal Reception of Signals*, Moscow: Radio i Sviaz Publ., 1983, 320 pp. [In Russian.]
- [24] Yarkho, T. A., "Determination of Peak Position of the Spectral Component at Fast Fourier Transform," *Radiotekhnika Publ.*, Kharkov, No. 90, 1989, pp. 6–11. [In Russian.]
- [25] Koshelev, V. I., and V. N. Gorkin, "Accuracy Increase of Central Frequency Estimation of the Narrow-Band Process in FFT Processor," *Izvestia VUZov, Radio Electronics*, Vol. 47, No. 1, 2004, pp. 67–73. [In Russian.]
- [26] Levin, B. R., *Theoretical Fundamentals of Statistical Radio Engineering*, In three volumes. 2nd edition. Moscow: Sovetskoe Radio Publ., 1974, 552 pp. [In Russian.]
- [27] Zander, F. V., "Algorithms for the Optimum Estimation of the Parameters of a Radio Signal in a Measurement Time of Less Than a Period and a Nonmultiple of a Period in Which the Result Is Tied to the Beginning of the Measurement Interval," *Measurement Techniques*, Vol. 46, No. 2, 2003, pp. 172–176.
- [28] Stolle, R., H. Heuermann, and B. Schiek, "Novel Algorithms for FMCW Range Finding with Microwaves," *Microwave Systems Conference IEEE NTC'95*, 1995, p. 129.

- [29] Sokolov, I. F., and D. E. Vakman, "Optimal Linear In-Phase Antennas with Continuous Current Distribution," *Radiotekhnika and Elektronika*, No. 1, 1958, pp. 46–55. [In Russian.]
- [30] Ezerskiy, V. V., and I. V. Baranov, "Optimization of Weighting Methods of Smoothing the Discreteness Error of Distance Sensors Based on a Frequency Range Finder," *Measurement Techniques*, Vol. 47, No. 12, 2004, pp. 1160–1167.
- [31] Patent No 2234717 (Russian Federation), INT.CL.. G01 S 13/34. "Method of Distance Measurement," B. A. Atayants, V. M. Davydochkin, V. V. Ezerskiy, and D. Ya. Nagorny. No. 2003105993/09. Bull. No. 23. Filed 04.March 4, 2003; published August 20, 2004.
- [32] Davydochkin, V. M., and V. V. Ezerskiy, "Minimization of Distance Measurement Error at Digital Signal Processing in Short-Range Radar Technology," *Digital Signal Processing*, No. 3, 2005, pp. 22–27. [In Russian.]
- [33] Ezerskiy, V. V., and V. M. Davidochkin, "Optimization of the Spectral Processing of the Signal of a Precision Distance Sensor Based on a Frequency Range Finder," *Measurement Techniques*, Vol. 48, No. 2, 2005, pp. 133–140.
- [34] Ezerskiy, V. V., V. S. Parshin, I. V. Baranov, V. S. Gusev, and A. A. Bagdagiulyan, "Comparative Noise Immunity Analysis of Algorithms for Distance Measurement in FMCW Range Finder in the Spectral Domain," *Vestnik RGRTA*, Ryazan, No. 14, 2004, pp. 43–48. [In Russian.]
- [35] Parshin, V. S., and V. V. Ezerskiy, "Estimation of Average Frequency of Radio Pulse Filling, Which is Received on the Background of the Normal Noise," *Nauchny vestnik MGTUFA, Series Radio Physics and Radio Engineering*, No. 87 (5), 2005.
- [36] Hahn, G. J., and S. S. Shapiro, *Statistical Models in Engineering*, New York: London: Sydney: John Wiley & Sons, Inc., 1967.
- [37] Parshin, V. S. "Estimation of Pulse Interference Influence on Stationary Signal Recognition in the Spectral Domain," *Radio Elektronika*, Vol. 42, No. 3, 1999, pp. 73–79. [In Russian.]
- [38] Parshin, V. S., and V. S. Gusev, "The Effect of Noise on the Accuracy of the Estimate of the Center Frequency of the Spectrum of a Narrow-Band Signal," *Measurement Techniques*, Vol. 48, No. 7, 2005, pp. 711–717.
- [39] Atayants, B. A., V. V. Ezerskiy, and A. F. Karpov, "Research of Generalized Probability Model of the Radio Signal," *Izvestia VUZov of USSR, Radio Elektronika*, Vol. 31, No. 4, 1988, pp. 43–49. [In Russian.]
- [40] Wilkes, S., *Mathematical Statistics*, Moscow: Nauka Publ., 1967, 632 pp. [In Russian.]
- [41] Atayants, B. A., V. V. Ezersky, and A. F. Karpov, "Distribution of Normalized Power of the Signal," *Radiotekhnika i Elektronika*, Vol. 28, No. 9, 1983, pp. 1864–1868. [In Russian.]

# The Maximal Likelihood Method for Range Estimation According to the Difference Frequency Signal

## 4.1 Introduction

The determination of the potential accuracy of range estimation at DFS reception on the noise background and determination of the algorithm structure of optimal processing is undoubtedly of practical interest.

The potential accuracy of delay estimation is provided using for the optimal processing a direct reflected signal without any preliminary transformation. For this, the synthesis of the estimation algorithm for interesting parameters (delay time or the range linear connected with the first) is required on SHF. Nevertheless, processing of the SHF signal is limited by possibilities of practical implementation. Exactly because of this reason, this chapter is devoted to estimation of a potential accuracy of delay time estimation after preliminary transformation, that is, the potential accuracy of delay time estimation in DFS. We assume, as we did earlier, that the one-sided spectral density of the noise after a mixer is equal to  $N_0$ .

From (1.6), it follows that information about range is contained in DFS frequency and in its initial phase. Evidently, the range estimation using the algorithm (3.4) and its modifications does not allow realization in full measure of the FMCW RF possibilities because in this case we do not use information contained in the signal phase. However, the phase approach for range estimation also allows the application of only part of the information contained in the signal.

The modern component base providing the high-stable FMCW RF characteristics (at first, the carrier frequency and the FM sweep stability) allows the realization in practice of the optimal DFS processing algorithms, and the performance of modern processors allows calculation results in the real-time scale.

Many publications are presently devoted to the synthesis of optimal algorithms of radio signal parameter estimation [1–3]. In these and another publications, many general problems are solved, which arise at the estimation of different parameters of the radio signal, including the delay time and the frequency.

We determine the potential accuracy of range measurement (linearly connected with the delay or the beating frequency) in DFS using the results of [1], the boundaries of the maximal likelihood method application, taking into account the DFS phase at range estimation, are determined, and the restrictions on its practical application are defined.

## 4.2 Range Estimation Based on the Difference Frequency Signal

At the estimation of some parameter  $z$  [1–3], the most complete information about its possible values is given by a posteriori probability density, which can be written as:

$$W_{ps}(z) = g W_{pr}(z) \Lambda(z) \quad (4.1)$$

where  $g$  is a normalizing multiplier, which is independent on the parameter  $z$ ,  $W_{pr}(z)$  is a priori density of the parameter  $z$ , and  $\Lambda(z)$  is the likelihood function (LF) at discrete processing of received signal. At continuous processing, the likelihood functional  $F(z)$  [1–3] should be substituted in (4.1) instead of  $\Lambda(z)$ . One can substitute instead of LF or the likelihood functional in (4.1) the functions of likelihood ratio functions (LRF), taking into consideration that the normalizing coefficient  $g$  will be changed at that point. We assume that its value, which corresponds to the maximum of  $W_{ps}(z)$ , is the estimation of parameter  $z$ .

A priori distribution of the estimating parameter  $z$  (in our case, it is the range to the reflected surface) is unknown. It is reasonable to assume that a priori distribution density of the estimating parameter  $z$  obeys the uniform distribution. Then it follows from (4.1) that in this case a posteriori distribution in the vicinity of estimation  $z$  coincides with LF or LRF [1–3]. The estimation according to the maximum of a posteriori probability in this case is transformed to the estimation of maximum likelihood, which is determined for the parameter  $z$  as the position of global maximum of LF or LRF. As MLM estimation does not depend on one-to-one nonlinear signal transformation [5], we shall use the logarithm of likelihood function (LLF) or the logarithm of likelihood ratio likelihood (LLRF) for calculation simplification.

It is known [1–3] that the MLM at the estimation of radio signal parameters has a series of advantages. We may note its unbiasedness as the most essential advantages for unlimited increase of SNR. Moreover, it is proved [1–3] that if there is an effective estimation, then the exact MLM estimation is effective.

Let us consider the estimation of delay time  $t_{\text{del}}$  by the maximal likelihood method using DFS obtained during the only half-period, that is, during the time interval  $(0, T_{\text{mod}}/2)$ . We suppose for simplicity that we provide the continuous processing of DFS.

Taking into account designations of (1.6), LLF  $\ln F(A_{\text{dif}}, t_{\text{del}}, \varphi_s)$  can be presented in the form [1–3]:

$$\ln F[A_{\text{dif}}, t_{\text{del}}, \varphi_s] = -\frac{1}{N_0} \int_0^{T_{\text{mod}}/2} \{y(t) - S_{\text{ref}}(t)\}^2 dt \quad (4.2)$$

where  $S_{\text{ref}}(t) = S[t, A_{\text{dif, ref}}, t_{\text{del, ref}}, \varphi_{s, \text{ref}}]$  is the reference signal,  $A_{\text{dif, ref}}$ ,  $t_{\text{del, ref}}$ ,  $\varphi_{s, \text{ref}}$  are parameters of the reference signal,  $N_0$  is the one-sided spectral density on the white noise,  $y(t)$  is the additive mixture of DFS and the white normal noise, and  $\varphi_s$  is the signal phase.

Let us determine the limited accuracy of delay time  $t_{\text{del}}$  and the DFS phase  $\varphi_s$  estimation when using MLM, that is, the algorithm (4.2) assuming that the DFS

amplitude is known. For the accuracy estimation of the DFS parameter determination [1], we use the signal function (SF) calculated for relative frequencies  $\omega T_{\text{mod}}/2 \gg 1$ .

$$\begin{aligned} q_s(t_{\text{del}}, \varphi_s) &= \frac{2}{N_0} \int_0^{T_{\text{mod}}/2} S(t, A_{\text{dif}}, t_{\text{del}}, \varphi_s) S_{\text{ref}}(t) dt \\ &= \frac{2}{N_0} \int_0^{T_{\text{mod}}/2} A_{\text{dif}} \cos[\omega_0 t_{\text{del}} + \omega_{\text{mod}}(t)t_{\text{del}}] \\ &\quad \times A_{\text{dif}} \cos[\omega_0 t_{\text{del,ref}} + \omega_{\text{mod}}(t)t_{\text{del,ref}} + \varphi_{s,\text{ref}}] dt \end{aligned} \quad (4.3)$$

As MLM is asymptotically effective, it is enough to obtain the lower boundary of the error variance. Let us find these boundaries for the case of delay time estimation assuming that the phase  $\varphi_s$  is known, and then we obtain the lower boundaries for mutual estimations of delay time  $t_{\text{del}}$  and the phase  $\varphi_s$  of the signal.

The lower variance boundary of delay time at known phase  $\varphi_s$  is defined from the known equation [1]

$$D_t = -\frac{1}{\left[ \frac{d^2 q_s(t_{\text{del}})}{dt_{\text{del}}^2} \right]_{t_{\text{del}}=t_{\text{del,ref}}}} \quad (4.4)$$

Having found the variance estimation of delay time  $t_{\text{del}}$  and taking into consideration that  $R = ct_{\text{del}}/2$ , the lower boundary of variance estimation of the  $\hat{R}$  range can be presented as

$$D(\hat{R}) \geq \frac{N_0}{2E} \frac{c^2}{4(\omega_0^2 + \Delta\omega\omega_0 + \Delta\omega^2/3)} \quad (4.5)$$

where  $E$  is the signal energy defined in the time interval  $(0, T_{\text{mod}}/2)$ , that is,  $E = A_{\text{dif}}^2 T_{\text{mod}}/4$ .

For modern FMCW RF the carrier frequency exceeds approximately by the order of its FM sweep. Therefore, the first item in the denominator of (4.5) is more by two to four orders than the second and third items. As a result, the lower boundary of the range variance estimation at a priori known initial phase can be presented as:

$$D(\hat{R}) \geq \frac{N_0}{2E} \frac{c^2}{4\omega_0^2} \quad (4.6)$$

In other words, the lower boundary of the range variance estimation at fully known signal phase decreases proportionally to a square of carrier frequency.

At the unknown signal phase  $\varphi_s$ , the problem of delay time estimation is reduced to the problem of the global functional (4.2) maximum obtaining, that is, to the problem of joint estimation of  $t_{\text{del}}$  and  $\varphi_s$ . Determining derivatives

$$J_{ij} = \left[ \frac{\partial^2 q_s[t_{\text{del}}, \varphi_s]}{\partial t_{\text{del}} \partial \varphi_s} \right]_{(t_{\text{del,ref}}, \varphi_{s,\text{ref}})} \quad (4.7)$$

and forming the correlation matrix of estimations [1], variance  $D(\hat{R})$  and  $D(\hat{\varphi}_s)$  at the mutual estimation of the range  $R$  and the phase  $\varphi_s(t_{\text{del}})$  of the signal (i.e., at mutual estimation of the delay time  $t_{\text{del}}$  and the phase  $\varphi_s(t_{\text{del}})$ ) can be presented in the form:

$$D(\hat{R}) \geq \frac{N_0}{2E} \frac{3c^2}{\Delta\omega^2} \quad (4.8)$$

$$D(\hat{\varphi}_s) \geq \frac{N_0}{2E} \frac{12(\omega_0^2 + \Delta\omega\omega_0 + \Delta\omega^2/3)}{\Delta\omega^2} \approx \frac{N_0}{2E} \frac{12\omega_0^2}{\Delta\omega^2} \quad (4.9)$$

From (4.9), it follows that the variance of phase estimation increases with the carrier frequency increasing.

From a comparison of (4.6) and (4.9), the evident result follows: the lower boundary of the range variance estimation can be essentially decreased using a priori information about the signal phase. Therefore, the benefit  $B$  is

$$B = 12\omega_0^2/\Delta\omega^2 \quad (4.10)$$

As an example, we can indicate that for FMCW RF with carrier frequency  $f_0 = 10^{10}$  Hz and the carrier FM sweep  $5 \times 10^8 \div 1 \times 10^9$  Hz, the reduction of variance estimation is, accordingly,  $4,800 \div 1,200$ . The estimation variance of the range can be decreased for increase of FM sweep of the carrier frequency as it will lead to increase of DFS signal period in the time interval  $(0, T_{\text{mod}}/2)$  that allows accurate DFS frequency measurement in accordance with (4.8). However, the possibilities of decreasing the range variance estimation by increasing the FM sweep are essentially limited by engineering reasons.

A significant decrease of estimation variance of the delay  $t_{\text{del}}$  at using the MLM taking into account the signal phase is explained by peculiarities of DFS SF. Figure 4.1 shows the vertical SF section (line 3) for DFS FMCW RF depending on the relative

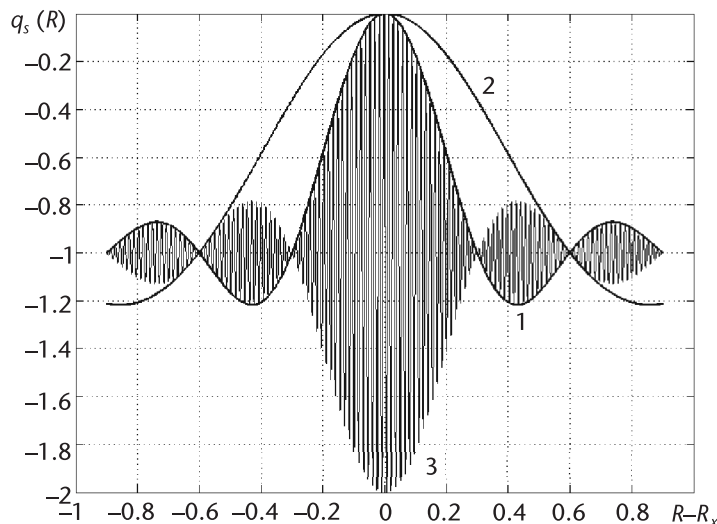


**Figure 4.1** Vertical section of SF depending on the relative range.

range  $R - R_x$ , where  $R$  is the true range,  $R_x$  is the current range (i.e., the delay  $t_{\text{del}}$  is recalculated into the range in accordance with  $t_{\text{del}} = 2R/c$ ). At the creation of the figure, amplitudes and phases of the reference signals are assumed to be equal.

From Figure 4.1 we see that SF is the oscillating function with the period equaled to  $\lambda/2$ , that is, the oscillation period is equal to a half of the carrying oscillation wavelength. We would like to note that such form of SF is typical for linear-frequency modulated signal [1], and the qualitative analysis of this SF is performed in [4]. The presence of narrow SF maxima (4.3) defines the benefit at estimation of time delay taking into account the signal phase, which acts at the FMCW RF output.

For comparison, Figure 4.1 shows SFs for estimation of signal frequency with unknown initial phase with the help of algorithms searching the maximal SC (line 1) and calculated using equations obtained in (line 2) at estimation of frequency  $\omega$  of the narrowband signal, which can be presented as:

$$S(t) = A_{\text{dif}} \cos \left[ \frac{2\Delta\omega t_{\text{del}}}{T_{\text{mod}}} t + \varphi_0 \right] + \xi(t) \quad (4.11)$$

The main maximum width of such SFs exceeds considerably the width of the main SF maximum in (4.2). We must note that for the signals in (4.11) the benefit in variance of the frequency estimation [1] is a value equal to 4 taking into consideration the initial signal phase at signal observing in the time interval  $(0, T)$ .

The normalized correlation coefficient  $r_{\text{cor}}$  between estimations of time delay  $t_{\text{del}}$  and the phase  $\varphi_s$  determined in accordance with [1] is:

$$r_{\text{cor}} = \frac{M(t_{\text{del}}\varphi_s)}{\sqrt{D_{t_{\text{del}}} D_{\varphi_s}}} = - \frac{\omega_0 + \Delta\omega/2}{\left( \omega_0^2 + 2\Delta\omega\omega_0 + \Delta\omega^2/3 \right)^{1/2}} \approx -1 \quad (4.12)$$

Such a value causes the fact that variance decrease of the range estimation at carrier frequency increase of the transmitter accompanies by proportional increase of the DFS phase estimation variance, which follows from (4.5) and (4.9).

From (4.7), accounting for (4.8), (4.9), and (4.12), one can determine the variance of initial DFS phase estimation  $\varphi_{\text{init}}$ , which can be defined as  $\varphi_{\text{init}} = \omega_0 t_{\text{del}} + \varphi_s$ :

$$D(\bar{\varphi}_{\text{init}}) = \frac{N_0}{2E} 4 \quad (4.13)$$

which coincides with the known result [1] for the variance of the initial phase estimation at mutual estimation of frequency and initial phase of the radio pulse.

Lower boundaries of DFS frequency and phase estimation variances are obtained for the case of continuous time. In [1], the lower boundaries of estimation variances are obtained in the case of discrete time and it is shown that at transfer to discrete time we can neglect of accuracy loss at enough discretization frequency.

The obtained formulas for the variance of time delay estimations are checked with the help of computer modeling. Simulation results practically coincided with calculation results for the variances in accordance with (4.5) and (4.8) both for estimation of DFS frequency with the unknown initial phase and using the algorithm realizing the MLM at the a priori known DFS phase.

Because in modern FMCW RFs the DFS frequency estimation is often performed in the spectral domain, the determination of the algorithm structure realizing MLM in the spectral domain causes the practical interest. We assume that we use FFT for spectrum calculation. Frequencies, at which the spectrum is calculated, are determined as  $\omega_i = 2\pi i/(KT_{\text{dis}})$ ,  $i = 0, 1 \dots (K - 1)/2$ . Taking into account that distribution of real and imaginary parts of the Fourier CS is normal [5] and SC calculated at frequencies  $\omega_i$  for the white normal noise are noncorrelated, LLF in the spectral domain can be presented in the following form:

$$\begin{aligned} \ln F_s(A_{\text{dif}}, t_{\text{del}}, \varphi_s) = & -\frac{1}{N_0} \sum_{i=1}^{(K-1)/2} \left\{ [\text{Re}(y(j\omega_i)) - \text{Re}(S_{\text{ref}}(j\omega_i))]^2 \right. \\ & \left. + [\text{Im}(y(j\omega_i)) - \text{Im}(S_{\text{ref}}(j\omega_i))]^2 \right\} \Delta\omega_x \end{aligned} \quad (4.14)$$

where  $S_{\text{ref}}(j\omega) = S(j\omega_i)$ ,  $A_{\text{dif},\text{ref}}$ ,  $t_{\text{del},\text{ref}}$ ,  $\varphi_{s,\text{ref}}(t_{\text{del}})$ ) is the DFT of the reference signal,  $y(j\omega_i)$  is DFT of the sum of DFS and the white normal noise, and  $\Delta\omega_x = 2\pi/(K\Delta_t)$ . The SF shape for (4.14) corresponds to Figure 4.1 (curve 3).

Properties of LLF in the spectral domain are the same with its properties in the time domain at reception of the signal on the background of the white normal noise. This is clear because the CS of the white normal noise obeys the normal distribution. As for the time domain, we can use LLRF for delay estimation, which in the spectral domain has the following form:

$$\begin{aligned} \ln l_s[A_{\text{dif}}, t_{\text{del}}, \varphi_s] = & \frac{2}{N_0} \sum_{i=1}^{(K-1)/2} \left\{ \text{Re}[y(j\omega_i)] \text{Re}[S_{\text{ref}}(j\omega_i)] \right. \\ & \left. + \text{Im}[y(j\omega_i)] \text{Im}[S_{\text{ref}}(j\omega_i)] - \frac{1}{2} G_{\text{ref}}(\omega_i) \right\} \Delta\omega_x \end{aligned} \quad (4.15)$$

where

$$G_{\text{ref}}(\omega_i) = |S(\omega_i, A_{\text{dif},\text{ref}}, t_{\text{del},\text{ref}}, \varphi_{s,\text{ref}})|^2$$

Sometimes, one neglects (4.15) by the item  $G_{\text{ref}}(\omega_i)/2$ . At the DFS frequency measurement for small normalized ranges, such neglect leads to noticeable additional systematic inaccuracy. The application of LLRF in the time domain leads to exactly the same inaccuracy:

$$\ln l(A_{\text{dis}}, t_{\text{del}}, \varphi_c) = \frac{2}{N_0} \sum_{i=1}^K \left[ y(t_i) S_{\text{ref}}(t_i) - \frac{1}{2} S_{\text{ref}}^2(t_i) \right] \quad (4.16)$$

when neglecting by the second item in the square brackets.

Figure 4.2 shows the estimation error of delay time recalculated into the range error versus range obtained for neglect the item  $G_{\text{ref}}(\omega_i)/2$  in (4.15) and  $S_{\text{ref}}^2(t)/2$  in (4.16) defined in the form:

$$\Delta R = |R_x - R| \quad (4.17)$$

where  $R_x$  and  $R$  are, respectively, measured and true ranges.

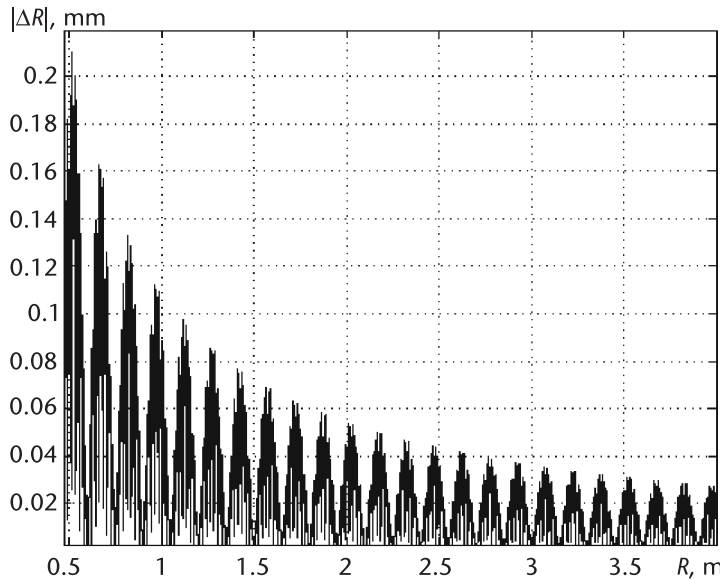


**Figure 4.2** The plot of measuring systematic inaccuracy versus range.

This plot is obtained for no-interference situation with the help of modeling. The FM sweep is 500 MHz, and the carrier frequency is 10 GHz. From the figure we see the presence of a noticeable systematic error, which monotonically decreases (albeit slowly) with the range increasing or (that is the same) with the DFS increasing. For example, we can note that the MSD of the range measurement result caused by the noise  $n(t)$  influence and calculated at  $q_{s/n} = 70$  dB is  $0.75 \times 10^{-3}$  mm. The only advantage of the (4.15) and (4.16) application compared with (4.2) is the independence of the error  $|\Delta R|$  upon the amplitude difference of received and reference signals. In practice, amplitudes of DFS and the reference signal may be significantly different due to the nonideal operation of automatic gain control. Essential reduction of the influence of amplitude difference upon the error of MLN parameter estimation can be implemented by the application of the following invariant transformation:

$$\bar{z}_i = z_i / \sqrt{\sum_{i=1}^K z_i^2} \quad (4.18)$$

where  $z_i$  are samples of DFS and reference signals and  $\bar{z}_i$  are corresponding modified samples.

Simulation results show that the variance of range estimation using transformation (4.18) increases approximately by 2%, 5%, and 10% compared with the variance determined according to (4.5) at the ratios  $q = 70$  dB, 60 dB, and 50 dB, respectively. Such an increase of estimation variance may be accepted as insignificant.

### 4.3 Peculiarities of Delay Time Estimation Using the Maximal Likelihood Method

The fast oscillating character of LLF determines the peculiarities of its application. To find the estimation of the unknown parameter  $t_{\text{del}}$ , it is necessary to determine the global maximum of LLF. From this, two features are noted:

- At the unknown phase  $\varphi_s$ , we should estimate two parameters for evaluating the delay time. At first, using MLM, we estimate  $\varphi_s$  and then this estimation  $\hat{\varphi}_s$  is substituted to the likelihood equation:

$$\left. \frac{\partial \ln F(A_{\text{dif}}, t_{\text{del}}, \hat{\varphi}_c)}{\partial t_{\text{del}}} \right|_{t_{\text{del}}=t_{\text{del,ref}}} = 0 \quad (4.19)$$

The value of the  $t_{\text{del}}$  estimation will be a solution of (4.19). The Rao-Cramer boundaries for the variance of delay time estimation in this case are determined in accordance with (4.8). Taking into consideration that the beating frequency  $\omega_{\text{beat}}$  and the range are connected by the linear function (1.12), it is easy to find out the Rao-Cramer boundary for variance of frequency estimation in the form  $D(\omega_{\text{beat}}) = \frac{12N_0}{2E} \left( \frac{2}{T_{\text{mod}}} \right)^2$ . This formula coincides with the Rao-Cramer boundary for the variance of radio pulse frequency estimation with unknown initial phase [1], when that frequency, on which the maximal SC is, can be accepted as the radio pulse frequency value. We wish to obtain the variance of the range estimation determined by (4.5). Such an estimation variance can be obtained when knowing the signal phase only. Therefore, to obtain the range estimation with less variance than that defined by (4.8), we should take measures for obtaining the estimation  $\hat{\varphi}_s$  with less variance.

- Even for the known phase  $\varphi_s$ , obtaining of the LLF global maximum in the delay range that is large enough leads to anomalous errors. One of these reasons is the iterative process of global irregularity search for the multi-extreme function does not guarantee its obtaining with unitary probability.

The next reason of anomalous error arising is the noise influence, under which the LLF maxima change. As a result, the anomalous errors arise caused by erroneous acceptance of one of the local LLF maximums as the global maximum. The value  $\Delta_{\text{an}}$  of anomalous errors can be determined as:

$$\Delta_{\text{an}} = m\lambda/2, \quad m=1,2,3\dots \quad (4.20)$$

where  $m$  is a number of the local maximum, which was accepted as the global counted with respect to the true global maximum, and  $\lambda$  is the wavelength of the carrying signal.

To find out the probability of anomalous errors caused by noise influence, it is necessary to determine the probability of the event that under the noise  $n(t)$  action, the value of the LLF local maximum  $L_m$  will exceed the value of the global maximum  $L_0$ , that is, to determine the probability of the event  $P_m(L_m > L_0)$ .

Let us present the LLF in (4.2) for the relative frequencies  $(\omega T_m/2) \gg 1$  in the form:

$$\ln l[A_{\text{dif}}, t_{\text{del}}, \varphi_s] = \frac{2}{N_0} \int_0^{T_{\text{mod}}/2} y(t)S(t, t_{\text{del}})dt = q_s(t_{\text{del}}) + q_n(t) \quad (4.21)$$

where  $q_s(t_{\text{del}})$  and  $q_n(t)$  are, respectively, signal and noise functions [1].

Let the phases of received and reference signals be equal. From (4.21), it follows that the value of the global maximum of the function  $q_s(t_{\text{del}})$  is equal to  $q_{s/n} = 2E/N_0$ , the average value and the variance of the noise function  $q_n(t)$  are equal, respectively, to zero and  $2E/N_0$ . The distribution law  $w(x)$  of the function  $q_n(t_{\text{del}})$  is considered to be normal with the mentioned average value and the variance. The probability of the fact that the maximum with a number  $m$  exceeds the global maximum can be determined as  $\Gamma$ . The values  $L_m$  and  $L_0$  will be random variables with the definition domain in the interval  $(-\infty, \infty)$  due to noise influence. Therefore, to define the probability  $P_m(L_m > L_0)$ , it is necessary to average the probability  $P(L_m > L_0)$  over all possible values of  $L_0$ . As a result, the probability  $P_m(L_m > L_0)$ , that is, the probability of the fact that the maximum value with a number  $m$  will exceed the global maximum value, is determined as

$$\begin{aligned} P_m &= \frac{1}{\sqrt{2\pi q_{s/n}}} \int_{-\infty}^{\infty} \exp\left[-(x_1 - L_0)^2/2q_{s/n}\right] \\ &\times \left\{ \frac{1}{\sqrt{2\pi q_{s/n}}} \int_{x_1}^{\infty} \exp\left[-(x - L_m)^2/2q_{s/n}\right] dx \right\} dx_1 \\ &\approx \frac{1}{2} \left\{ 1 - \Phi\left[ \frac{q(1 - L_m/L_0)}{\sqrt{2q_{s/n}}} \right] \right\} \end{aligned} \quad (4.22)$$

where  $L_m$  is the value of LLF maximum with a number  $m$  corresponding to the delay  $t_{\text{del},m}$  and defining through the DFS SF envelope

$$L_m = (2E/N_0) \sin[\Delta\omega(t_{\text{del}} - t_{\text{del},m})/2]/[\Delta\omega(t_{\text{del},0} - t_{\text{del},m})/2] \quad (4.23)$$

where  $t_{\text{del},0}$  is delay time corresponding to the LLF global maximum.

Figure 4.3 shows functions of the probability logarithm of anomalous error arising versus the signal/noise  $q_{s/n}$  for  $L_m = 1$  and  $L_m = 2$ . It follows from Figure 4.3 that real achieved values of  $q_{s/n}$  of the probability of an anomalous error arising are sensible enough due to noise influence. At  $q_{s/n} \approx 60$  dB, the probability  $P_1 \approx 10^{-4}$ , and the error value is  $\lambda/2$ . For accurate range measurement, such a probability of anomalous error arising is inadmissible. The application of iterative algorithms for a global extreme search leads to anomalous error multiple to  $\lambda/2$ .

To eliminate the anomalous errors in [3], the two-stage procedure of range estimation is offered. In conformity with FMCW RF, this procedure ensuring elimination of anomalous errors has been modified as follows:

- *Stage 1:* It is necessary to perform the preliminary estimation of  $t_{\text{del}}$  using the algorithm (3.4) providing estimation falling into the vicinity of the LLF global maximum. The measurement error at the first stage recalculated into range should not exceed  $\lambda/4$ , that is, the following obvious condition should be satisfied

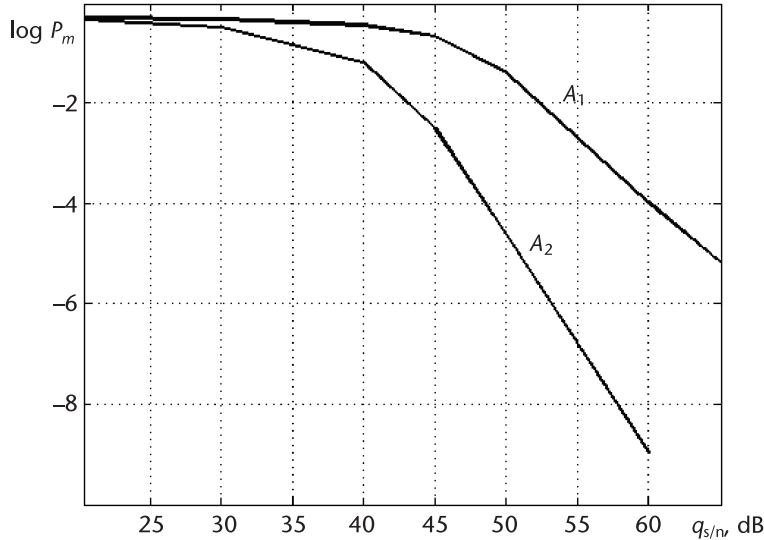


**Figure 4.3** Plots of the probability logarithm of anomalous error arising as function of SNR for the first ( $A_1$ ) and the second ( $A_2$ ) local maxima.

$$-\lambda/4 < \hat{R} - R < \lambda/4 \quad (4.24)$$

where  $\hat{R}$  is the range estimation obtained on the basis of the algorithm (3.4).

- *Stage 2:* The specification of the estimation using MLM is carried out. Therefore, the search is performed in the range interval satisfying the condition (4.24). Naturally, we may ensure the potential accuracy in the case only when phases, carrying frequencies, and FM sweeps of both signals (DFS and the reference signal) are equal. In this case, the LLF global maximum for the SNR  $q_{s/n} \rightarrow \infty$  will coincide with the true range and will be located symmetrically inside the interval (4.24).

The two-stage procedure of range estimation leads to simpler MLM program realization as it allows refusal from methods of multiparameter optimization at the search of the global extremum. The search of the global maximum, which is located inside the interval (4.24), can be performed by methods of single-parameter optimization at preliminarily measured phase of the reference signal.

#### 4.4 Main Factors Affecting the Measurement Error of Time Delay

Obtaining of delay time estimation with the variance defining in accordance with (4.8), that is, for known phase  $\varphi_s$ , is limited by a set of reasons. Let us list the main factors, which lead to additional errors at the application of MLM. We can note first the inaccuracy of DFS signal determination, instabilities of the carrier frequency, the FM sweep, and PAM. We mentioned earlier that the difference in amplitudes of DFS and the reference signal does not lead to noticeable increase of the measurement error at application of invariant transformation (4.18).

Algorithms of frequency estimation using the power spectrum of the signal do not take into account information containing in the DFS phase. However, we see from (1.6) that the unknown parameter, which should be defined, contains both in the frequency and in its phase. It follows from (1.6) that DFS phase is not the random variable. It is unknown variable as the DFS frequency. Successful MLM implementation with the known DFS phase allows not only decrease the estimation variance but decrease the FMCW RF transmitter power, which follows from (4.5) as SNR  $2E/N_0$  is included in this equation.

The DFS phase shift arising in the path of preliminary analog processing depends on frequency and, accordingly, on the delay time of the reflected signal. Therefore, the formula (1.8) should be rewritten in the form:

$$\varphi_{\text{dif}}(t) = \omega_0 t_{\text{del}} + \omega_{\text{mod}}(t - 0.5t_{\text{del}})t_{\text{del}} + \varphi_{\text{rf}} + \varphi_{\text{pp}}(t_{\text{del}}) \quad (4.25)$$

where  $\varphi_{\text{pp}}(t_{\text{del}})$  is a phase characteristics (PC) of the circuit of preliminary processing. We introduce  $\varphi_s = \varphi_{\text{rf}} + \varphi_{\text{pp}}$ .

To estimate the PC definition inaccuracy influence, in accordance with (4.3), we calculate SF. After integration and transformations, neglecting by items with doubled frequency, we determine that SF is:

$$q_s(t_{\text{del}}) = \frac{2E}{N_0} \frac{\sin \Delta\omega(t_{\text{del}} - t_{\text{del,ref}})/2}{\Delta\omega(t_{\text{del}} - t_{\text{del,ref}})/2} \times \cos[(\omega_0 + \Delta\omega)(t_{\text{del}} - t_{\text{del,ref}}) + \varphi_s - \varphi_{s,\text{ref}}] \quad (4.26)$$

where  $t_{\text{del,ref}}$  and  $\varphi_{s,\text{ref}}$  are relatively true values of delay time  $t_{\text{del}}$  and  $\varphi_{s,\text{ref}}$ .

Calculating the derivative  $\left. \frac{\partial q_s(t_{\text{del}})}{\partial t_{\text{del}}} \right|_{t_{\text{del}}=t_{\text{del,ref}}}$  and assuming that the item  $\sin z/z$  influences insignificantly on the SF extrema position, we see that the measuring error  $\Delta R_\varphi$  due to inaccurate determination of DFS phase can be presented as:

$$\Delta R_\varphi = \lambda[\varphi_s - \varphi_{s,\text{ref}}]/[4\pi(1 + \Delta\omega/\omega_0)] \quad (4.27)$$

where  $\varphi_s$  and  $\varphi_{s,\text{ref}}$  are in radians and  $\lambda$  is the wavelength corresponding to the carrier frequency of the SHF oscillator.

It follows from (4.27) that the difference in values of DFS phase  $\varphi_s$  and the reference signal  $\varphi_{s,\text{ref}}$  leads to significant increase of the error. For example, we may note that the value  $\Delta\varphi = \varphi_s - \varphi_{s,\text{ref}}$  equal to  $10^\circ$  leads to the error of 0.406 mm for the transmitter wavelength of 3 cm. The maximal error value for  $\Delta\varphi = 180^\circ$  approached  $\lambda/4$ , which is evidently unacceptable. The maximal error value  $\lambda/4$  in this case is caused by the fact that two-stage procedure of range estimation is used. The delay interval, within which we are searching the specified value of  $t_{\text{del}}$  at the second stage, is located so that two adjacent LLF (4.2) maxima fall to their boundaries due to the phase difference (equal to  $\Delta\varphi = 180^\circ$ ) between DFS and the reference signal. The accurate value of measuring range corresponds in this case to the LLF minimum between these adjacent maxima.

The influence of the frequency deviation  $\delta_{f_0}$  of the master oscillator from the rating value, as it follows from (1.6), leads to variation of initial signal phase and, hence, to variation of  $\varphi_s$  for each value of  $t_{\text{del}}$ . Substituting the phase variation  $\delta_\varphi$  due to frequency deviation  $\delta_{f_0}$  as  $\delta_\varphi = 2\pi f_0 \delta_{f_0} 2R/c$ , calculating the derivative  $\frac{\partial q_s(t_{\text{del}})}{\partial t_{\text{del}}} \Big|_{t_{\text{del}}=t_{\text{del,ref}}}$ , and finding SF (4.26) extremums, we present the range measurement error  $\Delta R_f$  caused by inequality of the transmitter carrier frequency and the frequency of the reference signal, in the following form:

$$\Delta R_f = R \delta_{f_0} / (1 + \Delta f/f_0) \quad (4.28)$$

When obtaining (4.28), as for (4.27), we assumed that the item of  $\sin z/z$  type influences insignificantly of SF extremum offset.

The error  $\Delta R_f$  depends proportionally upon the measuring range. Assuming that the long-term instability  $\delta_{f_0}$  of the carrier frequency of the modern FMCW RF is not worse than  $10^{-6}$  (which follows from technical specifications for modern master crystal oscillators), it follows from (4.28) that for  $f_0 = 10$  GHz  $\Delta R_f$  is approximately 0.03 mm for the range of 30 m from RF.

Figure 4.4 shows functions of measured range errors determined in accordance with (4.28) for the transmitter carrier frequency 10 GHz and the FM sweep 500 MHz versus measuring range.

Curve 1 corresponds to increasing of the measuring range from 1 m to 30 m at the difference of DFS frequency and the frequency of the reference signal by  $-1 \times 10^4$  Hz. Curve 2 corresponds to the situation when at achievement of the range of 30 m the DS frequency increases with respect to the rating frequency by  $2 \times 10^4$  Hz and the decrease of measuring range occurs. Curve 3 corresponds to the case when with an increase of measuring range from 1 m to 30 m, the DFS frequency varies

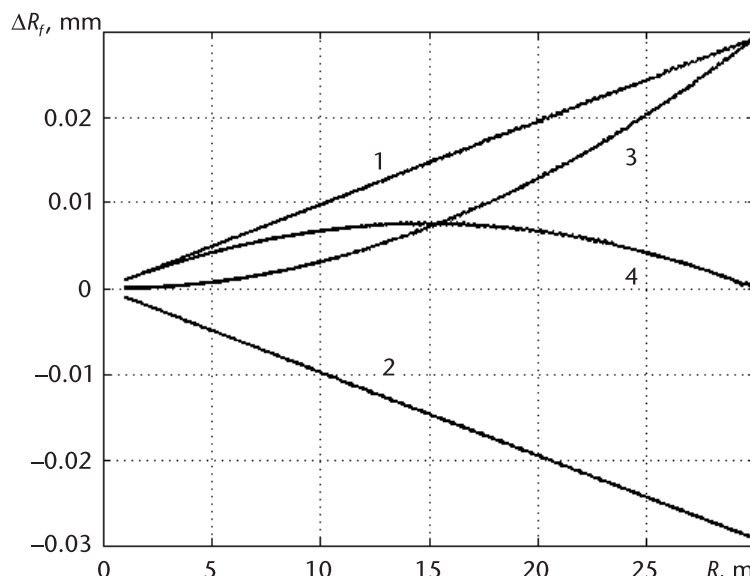


**Figure 4.4** Functions of the range measurement error versus the range for DFS frequency deviation from the carrier frequency of the beating signal.

in accordance with the linear law (from  $f_0$  to  $f_0 + f_0\delta_{f_0}$ ). Curve 4 corresponds to the situation when at a decrease of the measuring range from 30m to 1m, the DFS frequency decreases linearly from  $f_0$  to  $f_0 - f_0\delta_{f_0}$ .

From Figure 4.4 it follows that the error value  $\Delta R_f$  at carrier frequency variations within these limits cannot exceed values restricted by curves 1 and 2. The maximal range measurement error is achieved in the case when  $\delta_{f_0}$  takes the maximal value and does not change during the measurement process.

Functions similar to those presented in Figure 4.4 have a place at the difference of the FM sweep  $\Delta f$  and the FM sweep used at generation of the reference signal, which can be presented as  $\Delta f_{\text{ref}} = \Delta f + \Delta f\delta_{f_0}$ . Having obtained SF extrema for these cases and having performed the necessary transformations, we can present the error  $\Delta R_{\Delta f}$  caused by the difference of  $\Delta f$  and  $\Delta f_{\text{ref}}$  as:

$$\Delta R_{\Delta f} = \Delta f \delta_{f_0} R / (f_0 + \Delta f) \quad (4.29)$$

At these FM parameters and the long-range frequency instability  $\delta_{f_0}$  is equal to  $10^{-6}$ , the error  $\Delta R_{\Delta f}$  does not exceed  $0.15 \times 10^{-3}$  mm at the range of 30 m. The calculation according to (4.29) and the simulation results completely coincide. We can neglect such an error value of  $\Delta R_{\Delta f}$ .

The PAM influence analysis will be carried out on the example of PAM presented in the form  $\varphi_{\text{rf}}$

$$y(t) = \cos(\Omega t) A_{\text{dif}} \cos[\omega_0 t_{\text{del}} + \omega_{\text{mod}}(t)t_{\text{del}} + \varphi_{\text{rf}}] \quad (4.30)$$

where  $0 \leq \Omega \leq \Omega_{\text{max}}$ ,  $\Omega_{\text{max}} \leq \pi/T_{\text{mod}}$ .

In this case, due to the PAM influence, the DFS envelope is the monotonous function. Varying  $\Omega$ , we may change the PAM deepness  $\mu$ , which can be defined as:

$$\mu = (A_{\text{dif,max}} - A_{\text{dif,min}})/A_{\text{dif,max}} \quad (4.31)$$

where  $A_{\text{dif,min}}$ ,  $A_{\text{dif,max}}$  are, respectively, the minimal and maximal values of the DFS envelope with account of PAM, which can be easily determined according to practical DFS.

At  $\Omega = 0$ , DFS is not modulated on the amplitude ( $\mu = 0$ ), and for  $\Omega = \Omega_{\text{max}}$  the PAM deepness is maximal ( $\mu = 1$ ). The choice of PAM in the form (4.30) is explained by the fact that such PAM can be met in practice and, moreover, according to the simulation results, which causes the essential error at the MLM application.

PAM presence reduces the problem of range  $R$  estimation to the problem of estimation of unknown radio signal envelope. PAM influence on the range measurement error depending on the PAM deepness  $\mu$  defined in accordance with (4.31) is presented in Figure 4.5 (curve 1). The plot is obtained with the help of modeling. The carrier frequency and the FM sweep were, respectively, 10 GHz and 500 MHz. We used the rectangular envelope of the reference signal in (4.2) or the rectangular envelope spectrum in (4.14).

We see that influence of PAM on DFS leads to noticeable increase of the total error, which is calculated as:

$$\sigma_{\text{total}} = \sqrt{D + b^2} \quad (4.32)$$

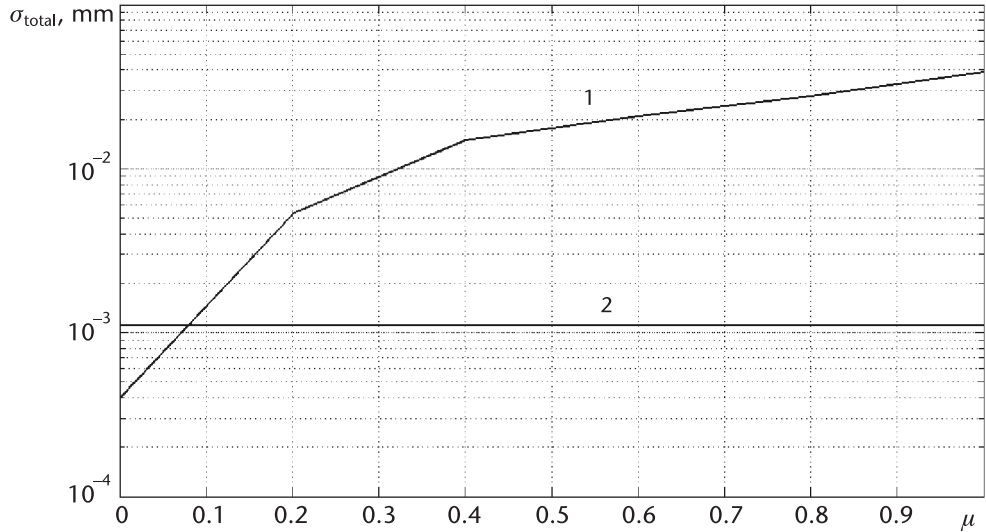


**Figure 4.5** PAM influence on the total error of range estimation.

where  $D$  is the variance of range estimation,  $b^2 = \sum_{n=1}^n (R_{\text{meas}} - R)^2 / n$  is the systematic error caused by PAM, and  $n$  is the number of counted points in the range interval, which is specified within the limits from 0.9 m to 1.8 m (relative frequencies were varied from 3 to 6).

From this figure we see that already at small PAM level the measurement error is mainly defined by not noise interference (at simulation, we assumed that  $q = 70$  dB), but by the systematic error caused by the difference of the reference signal shape and DFS. The range measurement error at  $\mu = 0$  corresponds to potentially possible at the MLM using, which can be defined by (4.5). With the range increasing, the value  $b$  decreases monotonically. For example, we may note that  $b$  becomes equal to the variance  $D$  for relative frequencies on the order of 60 to 70.

One can decrease the PAM influence by two methods.

- *Method 1:* One may use the adaptive procedures allowing the estimation of some coefficients describing the DFS shape, which is a subject to PAM. As a result, we can substitute into LLF the reference signal, for which the envelope is closed to the DFS envelope. The serious computation expenses and difficulties related to the fact that DFS frequency varies within rather wide limits (from hundreds of hertz to tens of kilohertz, depending on the measuring range) is a disadvantage of this method.
- *Method 2:* To minimize the influence of the shape difference of the reference signal and DFS, we use WF  $w(t)$ . We can write LLF as:

$$\ln F(A_{\text{dif}}, t_{\text{del}}, \varphi_s) = \quad (4.33)$$

$$-\frac{1}{N_0} \int_0^{T_m/2} [y(t) w(t) - S(t, A_{\text{dif}}, t_{\text{del}}, \varphi_s) w(t)]^2 dt$$

The multiplication of the reference signal with rectangular envelope and DFS with PAM by the same WF allows the reduction of the envelope shape difference. We use the following relative criterion as a measure of difference of the reference signal and DFS:

$$\sigma_0^2 = \int_0^{T_{\text{mod}}/2} w^2(t) [\Pi(t)S_s(t) - S(t)]^2 dt / \int_0^{T_{\text{mod}}/2} S^2(t) dt \quad (4.34)$$

where  $S_s(t)$  is DFS with rectangular envelope,  $S(t)$  is the reference signal, and  $\Pi(t)$  is a function describing the PAM shape. We can be sure that WF multiplication by DFS with PAM and by the reference signal decreases  $\sigma_0^2$ , that is, decreases the difference degree of DFS with PAM and the reference signal by an order for  $\mu$  values from 0.2 to 1. Such a reduction of the signal difference degree is fully sufficient to reduce the average square of the systematic error of range measurement caused by PAM until the value, which is two orders less than the MSD, is caused by the noise interference. Figure 4.5 (curve 2) shows the behavior of  $\sigma_{\text{full}}$  as a function of PAM deepness obtained for the ratio  $q_{s/n} = 70$  dB and for the application of the Blackman WF. The behavior of curve 2 is defined by the noise interference only. PAM influence is negligible small. The last statement is true for relative frequencies beginning from 3 to 5. Nevertheless, the elimination of PAM influence with the help of WF acting on results of frequency estimation leads to an increase of the noise interference influence. The MSD increase caused by application of the Blackman window is about 1.54.

## 4.5 Estimation of the Phase Characteristic of FMCW RF

The analysis of errors performed above allows the statement that for MLM practical application it is necessary to have information about the PC of FMCW RF. The only way to determine the PC is to calculate it according to DFS. The DFS initial phase can be presented in the following form using (4.25):

$$\begin{aligned} \varphi_{\text{init}} &= \omega_0 t_{\text{del}} + \varphi_{\text{rf}} + \varphi_{\text{pp}}(t_{\text{del}}) \\ &= \omega_0 t_{\text{del}} + \varphi_s(t_{\text{del}}) \end{aligned} \quad (4.35)$$

It follows from (4.35) that for the determination of PC of FMCW RF  $\varphi_s(t_{\text{del}})$ , we should calculate the estimation of the delay time  $t_{\text{del}}$  and the initial phase and execute appropriate calculations.

The estimation of the maximal likelihood of the initial phase of radio pulses with unknown frequency is obtained in [1] in the form:

$$\varphi_{\text{init}} = -\arctan \left[ \frac{\int_0^T y(t) \sin \hat{\omega} t dt}{\int_0^T y(t) \cos \hat{\omega} t dt} \right] \quad (4.36)$$

where  $y(t)$  is a sum of DFS and noise interference.

To estimate the initial phase, it is necessary to estimate the signal frequency and then to execute calculations in accordance with (4.36). In (4.36), sine and cosine Fourier transformations are included and calculated on the frequency  $\hat{\omega}$ , which is an estimation of the radio pulse-filling frequency by the MLM method with the unknown initial phase of the signal. The following relation based on the transformation in (3.6) is the discrete analog of (4.36):

$$\hat{\varphi}_{\text{init}} = -\arctan \left[ \sum_{l=0}^{K-1} y(l) \sin 2\pi xl / \sum_{l=0}^{k-1} y(l) \cos 2\pi xl \right] \quad (4.37)$$

The DFS frequency is designated in (4.36) and (4.37) as an argument of the initial phase. As the DFS frequency is connected linearly with the range and delay time  $t_{\text{del}}$ , we understand below  $t_{\text{del}}$  to be an argument of PC.

We should note that using the program atan 2, which is included into the programming medium MATLAB, the definition domain of the initial phase estimation calculated in accordance with (4.36) and (4.37) is within the limits  $-\pi \div \pi$ . This has essential importance as, in contrast to the signal of type (4.11), which the initial phase does not change at frequency variation, the initial phase of DFS changes with DFS frequency variation, that is, with the range  $R$  variation to the reflected surface.

To estimate the maximal likelihood of the initial phase of the radio pulse with known frequency, we can use also (4.36) and (4.37) with replacement of estimation  $\bar{\omega}$  to the known frequency  $\omega$ .

For a practical determination of PC  $\varphi_s(t_{\text{del}})$ , it is necessary to change the range  $R$  with some step  $\Delta$  in the full range. For each range  $R$  we shall determine the initial DFS phase and to measure the delay time  $t_{\text{del}}$ . Because PC is defined as  $\varphi_s(\hat{t}_{\text{del}}) = \hat{\varphi}_{\text{init}}(\hat{t}_{\text{del}}) - \omega_0 \hat{t}_{\text{del}}$ , we present  $\omega_0 t_{\text{del}}$  as  $2\pi 2R/\lambda$  and shall determine the integer number  $m$  of wavelengths corresponding to the range  $2R$ . Let us introduce the designation  $\varphi_m(\hat{t}_{\text{del}}) = \omega_0 \hat{t}_{\text{del}} - 2\pi m$ . The index  $m$  designates that the phase  $\omega_0 \hat{t}_{\text{del}}$  is within the limits  $0 \div 2\pi$ , that is, it is the main phase value taking into account the fact that for its determination at range  $R$ , the integer number of wavelengths is eliminated. If we omit the integer part of  $\omega_0 \hat{t}_{\text{del}} - 2\pi m$ , the definition domain of  $\varphi_m(\hat{t}_{\text{del}})$  will be within the limits of  $0 \div 2\pi$ . At the calculation of  $\varphi_m(\hat{t}_{\text{del}})$ , we shall leave it unchanged if the  $\varphi_m(\hat{t}_{\text{del}})$  value is defined within the limits  $0 \div \pi$ . If  $\varphi_m(\hat{t}_{\text{del}}) > \pi$ , then  $\varphi_m(\hat{t}_{\text{del}})$  will be defined as  $\varphi_m(\hat{t}_{\text{del}}) = \hat{\varphi}_{1m}(t_{\text{del}}) - 2\pi$ , where  $\hat{\varphi}_{1m}(t_{\text{del}})$  has the definition domain  $\pi \div 2\pi$ . As a result, PC  $\varphi_s(\hat{t}_{\text{del}})$  can be calculated as:

$$\varphi_s(\hat{t}_{\text{del}}) = \varphi_{\text{init}}(\hat{t}_{\text{del}}) - \varphi_m(\hat{t}_{\text{del}}) \quad (4.38)$$

where the functions  $\varphi'_{\text{init}}(\hat{t}_{\text{del}})$  and  $\varphi_m(\hat{t}_{\text{del}})$  have definition domains  $-\pi \div \pi$ .

At the PC calculation in accordance with (4.38), the ambiguity arises at PC estimation (caused by outburst appearance with value about  $360^\circ$ ). The reasons of outburst appearance are the following.

In the case of the value of the estimated PC  $\varphi_s(t_{\text{del}}) = 0$ , the reason of outburst appearance is the influence of DFS spectrum's SLs on frequencies  $\omega < 0$  upon the DFS phase. This influence leads to the fact that the saw-toothed function  $\varphi_{\text{init}}(t_{\text{del}})$  of delay time (i.e., of the range) will be modulated on amplitude, that is, adjacent maximal and minimal values of the function  $\varphi_s(t_{\text{del}})$  will have different values. The phase shift  $\varphi_m(t_{\text{del}})$  will have another modulation law as  $\varphi_{\text{init}}(t_{\text{del}})$  and  $\varphi_m(t_{\text{del}})$  are calculated according to different formulas [ $\varphi_{\text{init}}(t_{\text{del}})$  in accordance with (4.36) or (4.37) and  $\varphi_m(t_{\text{del}})$  through the measured delay time  $t_{\text{del}}$  using the algorithm (3.4)]. As a result, at the initial phase  $\varphi_{\text{init}}(t_{\text{del}}) \approx 180^\circ$ , the phase  $\varphi_m(t_{\text{del}})$  can be equal to  $\varphi_m(t_{\text{del}}) \approx -180^\circ$ . The outburst value is equal to  $360^\circ$ . To eliminate outbursts, it is necessary to compare two adjacent values of calculated PC. If their difference is equal, about  $360^\circ$ , it is necessary to eliminate outbursts according to equation

$\Delta\varphi = \Delta\varphi' + 360^\circ$ , where  $\Delta\varphi'$  is the outburst value. If the PC estimation begins from the outburst appearance, instead of the value  $\varphi_s(t_{\text{del}})$  equal to  $0^\circ$  we will obtain the value  $\varphi_s(t_{\text{del}})$  equal to  $360^\circ$ . It has no significance in order to generate the reference signal since trigonometric functions are periodic functions with the period  $360^\circ$ . With relative frequency increasing greater than 4 to 5, outbursts caused by DFS sidelobes, which are generated on the negative frequencies, will disappear. In the case when  $\varphi_s(t_{\text{del}}) \neq 0$  PC outbursts are caused by the function  $\varphi_m(t_{\text{del}})$ , on the contrary to the function  $\varphi_{\text{init}}(t_{\text{del}})$  does not depend upon the DFS initial phase. Outburst appearances can be easily explained by plots presented in Figure 4.6.

Plots correspond to the case when we estimate  $\varphi_s(\hat{t}_{\text{del}}) = 90^\circ$ . At the drawing of the plots, the delay time is recounted into the range. Functions  $\varphi_{\text{init}}(t_{\text{del}})$  and  $\varphi_m(t_{\text{del}})$  are designated in Figure 4.6 by the numbers 1 and 2. Because  $\varphi_s(t_{\text{del}}) \neq 0$ , plots 1 and 2 are displaced with respect to each other. The resulting PC  $\varphi_s(t_{\text{del}})$  calculated according to (4.38) is designated by the number 3. We see from this figure that due to displacement of functions  $\varphi_{\text{init}}(t_{\text{del}})$  and  $\varphi_m(t_{\text{del}})$ , the PC can be ambiguously estimated. The PC  $\varphi_s(t_{\text{del}})$  estimation can take two values:  $+90^\circ$  and  $-270^\circ$ .

Starting with this, it is enough to eliminate simply the ambiguity in PC estimation. For this it is enough to monitor its adjacent values and to modify the estimation  $\varphi_s(\hat{t}_{\text{del}})$  as follows. Let us designate the estimation  $\varphi_s(\hat{t}_{\text{del}})$  calculated according to (4.38) as  $\varphi'_s(\hat{t}_{\text{del}})$ . The estimation  $\varphi_s(\hat{R}_n)$  can be formed by the following evident way recounting the delay time into the range:

$$\varphi_s(\hat{R}_n) = \begin{cases} \varphi'_s(\hat{R}_n) + 360^\circ & \text{if } \varphi'_s(\hat{R}_{n-1}) > \varphi'_s(\hat{R}_n) \\ & \text{and } \varphi'_s(\hat{R}_{n-1}) - \varphi'_s(\hat{R}_n) > \Delta\varphi \\ \varphi'_s(\hat{R}_n) + 360^\circ & \text{if } \varphi'_s(\hat{R}_{n-1}) < \varphi'_s(\hat{R}_n) \\ & \text{and } \varphi'_s(\hat{R}_{n-1}) - \varphi'_s(\hat{R}_n) < \Delta\varphi \end{cases} \quad (4.39)$$

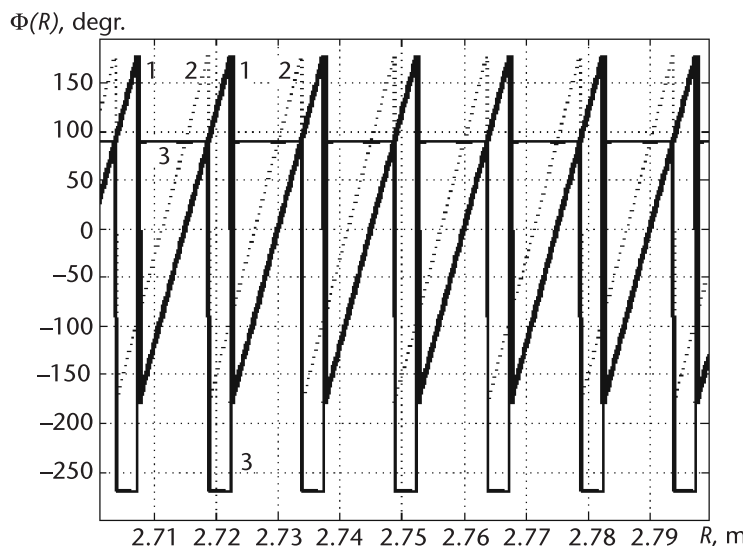


**Figure 4.6** Plots of phase characteristics: 1 is the DFS initial phase, 2 is the function  $\varphi_m(ct_{\text{del}}/2)$ , and 3 is the PC calculated using the DFS initial phase and the function  $\varphi_m(ct_{\text{del}}/2)$ .

where  $\Delta\varphi$  is some threshold of comparison and  $n$  and  $n - 1$  are the numbers of PC measurements displaced in the range with the step  $\Delta$ .

Because the outburst value at PC estimation is equal about  $360^\circ$ , the choice of  $\Delta\varphi$  value in noise absence is arbitrary in the general case:  $\Delta\varphi$  may lie about within the limits of  $10^\circ < \Delta\varphi < 350^\circ$ . The main point is that  $\Delta\varphi$  value is less than the outburst value. As the outburst value does not practically depend upon the step  $\Delta$ , then  $\Delta\varphi$  does not practically depend upon the  $\Delta$  value.

Figure 4.7 shows the PC estimation obtained according to (4.38) and (4.39). At simulation PC is specified by the following equation:

$$\varphi_s(R_n) = 360\{\sin[\pi(n\Delta + R_{\text{init}})/2R_{\text{final}}]\}^4, \quad n = 1, 2, 3\dots \quad (4.40)$$

where  $R_{\text{init}} = 0.3$  m and  $R_{\text{final}} = 30$  m are the initial and final values of the range to the reflecting surface and  $\Delta$  is the displacement step of the reflecting surface (it is accepted as 3 mm at simulation). The carrying FMCW RF frequency is 10 GHz, and the carrier FM sweep is 500 MHz.

The characteristic 1 corresponds to the FMCW RF FC specified according to (4.40). The curve corresponds to the PC  $\varphi_s(\bar{R})$  calculated according to (4.38). It is seen that the PC  $\varphi_s(\bar{R})$  is ambiguously defined due to the outburst presence. The outburst value is about  $360^\circ$ . Curve 2 corresponds to modified PC  $\varphi_s(\bar{R})$  according to (4.39). Obtaining the functions, we assumed that  $\varphi_{\text{rf}} = 30^\circ$ ; therefore, the function  $\varphi_s(\bar{R})$  is raised a bit by  $30^\circ$ . At the beginning of curve 2, we can see oscillations of the PC estimation caused by the influence of the DFS spectrum SLs located at  $\omega < 0$ . The application of (4.39) allows for the elimination of PC definition ambiguity, that is, obtaining curve 2 as a result of the calculation presented in Figure 4.7.

The estimation of PC values at DFS reception on the background of the noisy interference has specific features. At the small ratio  $q$ , the application of (4.39) does not avoid the sharp PC variation by  $360^\circ$ . It is caused by the fact that in a noninterference situation (a very large ratio of signal to noise), the PC  $\varphi_s(\bar{R})$  changes by  $360^\circ$

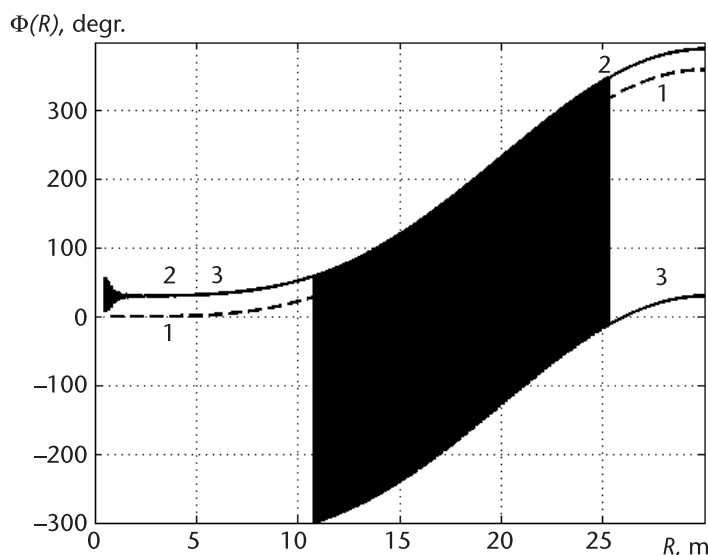


**Figure 4.7** Typical plots of phase characteristics with estimation results correction and without correction.

(or by a close enough value) at two adjacent calculations. The presence of noisy interference leads to the fact that there is a nonzero probability that the PC  $\varphi_s(t_{\text{del}})$  variation by  $360^\circ$  will happen during several adjacent calculations. Therefore, the separate PC variations will be less than the  $\Delta\varphi$  value. The condition (4.39) will not be carried out; therefore, the PC will be displaced by  $360^\circ$ . This PC position can be stable. The PC will return to the initial position when the PC variation by  $360^\circ$  will again occur during several adjacent calculations. The PD definition ambiguity elimination can be provided by supplementing (4.39) by the following condition.

$$\text{if } |\varphi_s(\hat{R}_{n-1}) - \varphi_s(\hat{R}_n)| > \Delta\varphi_1, \text{ then } \varphi_s(\hat{R}_n) = \varphi_s(\hat{R}_{n-1}) \quad (4.41)$$

where  $\Delta\varphi_1$  is some comparison threshold. The condition (4.41) limits the PC outburst values owing to the noise influence.

The values of comparison thresholds  $\Delta\varphi$  in (4.39) and  $\Delta\varphi_1$  in (4.41) should be selected in general by some optimal way, for instance, using the MSD minimization criterion caused by noise influence. However, the strict selection of optimal values of  $\Delta\varphi$  and  $\Delta\varphi_1$  will meet the essential difficulties of mathematical character. Therefore, the values of  $\Delta\varphi$  and  $\Delta\varphi_1$  are selected empirically on the basis of both the statistical simulation results and signal processing obtained using the industrially manufactured FMCW RF Bars-351. As a result of multiple inspections, the comparison threshold value  $\Delta\varphi$  is selected equal to  $250^\circ$  and the value  $\Delta\varphi_1 = 120^\circ$ . The supplement of condition (4.39) by the condition (4.41) is expedient at low ratios  $q$ . Beginning from the ratio  $q = 60$  dB, it is enough to limit by (4.39). We should note that the program unwrap, which is in the MATLAB software medium and is intended for elimination of PC outbursts, showed at small  $q$  worse results than the above-suggested procedure. The typical results of PC estimation with the help of the above-described procedure (plot 1) and the program unwrap (plot 2) are presented in Figure 4.8. We see from Figure 4.8 that for the application of unwrap

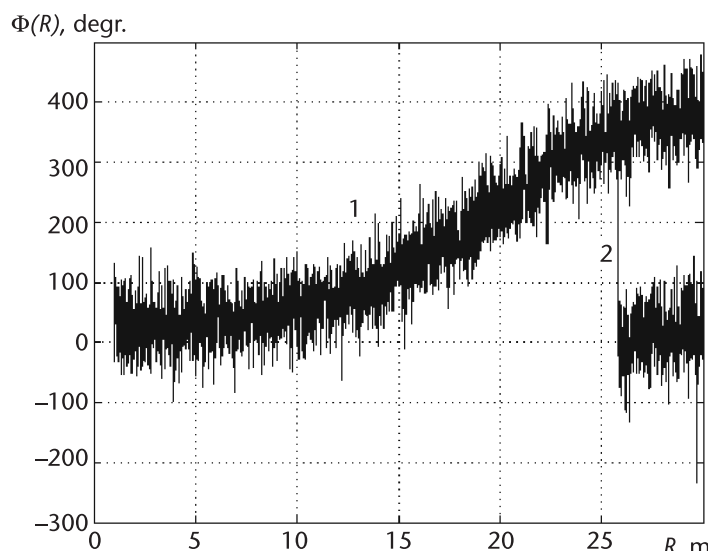


**Figure 4.8** Plots of phase characteristic estimation using the unwrap program and the considered modified estimation.

program the jump is observed in the plot of PC estimation versus the range. Functions are obtained for  $q = 45$  dB. Before the jump, two plots are fully coincided.

We note that the estimation variance  $\varphi_{\text{init}}(\bar{R})$  is essentially less than the estimation variance  $\varphi_s(\bar{R})$  by the value equal to  $12\omega_0^2/\Delta\omega^2$  that follows from (4.9) and (4.13). It can be easily explained because  $\varphi_s(\bar{R})$  is determined with range estimation. For  $f_0 = 10^{10}$  Hz and the carrier FM sweep  $\Delta f = 5 \times 10^8$  Hz, the estimation variance of the initial phase is less than the estimation variance of  $\varphi_s(\bar{R})$  by the value  $1.2 \times 10^3$ .

Besides the noisy interference influence, the truncation error caused by the spectrum SLs' influence (located at  $\omega < 0$ ) upon the main lobe calculated at  $\omega > 0$  leads to errors at PC determination. This was already mentioned at the analysis of Figure 4.7.

The total truncation error of  $\varphi_s(\bar{R})$  estimation according to (4.35) is determined by the truncation error  $\Delta\Phi_n(R)$  at the definition of the  $\varphi_s(\bar{R})$  initial phase and the truncation error  $\Delta\Phi_n(R)$  of estimation of the phase addition  $\omega_0 2\bar{R}/c$ .

At the determination of the truncation error  $\varphi_{\text{init}}(\bar{R})$ , we first consider the case in which the DFS frequency is known. Using (4.36) and assuming that the DFS frequency  $\omega_R$  is equal to the reference frequency of quadratic channels, we provide the simple trigonometric transformations and integration supposing that the noisy interference is absent, we can represent the truncation error  $\Delta\Phi_n(R)$  of calculation of the initial phase  $\varphi_{\text{init}}(R)$  in the following form:

$$\Delta\Phi_n(R) = \varphi_{\text{init},\text{true}}(2R/c) \quad (4.42)$$

$$- \arctan \frac{[-2 \sin(z/2) \sin(-2\Delta\omega R/c)]/z_1 - \sin[\omega_0 2R/c + \varphi_s(2R/c)]}{[2 \cos(z/2) \sin(2\Delta\omega R/c)]/z_1 + \cos[\omega_0 2R/c + \varphi_s(2R/c)]}$$

where  $\varphi_{\text{init},\text{true}}(2R/c)$  is the true initial phase,  $z = 2R(\omega_0 + \Delta\omega)/c + \varphi_s(2R/c)$ , and  $z_1 = 4\Delta\omega R/c$ .

The maximal error value  $\Delta\Phi_{n\max}(R)$ , that is, the envelope of the function  $\Delta\Phi_n(R)$  in degrees, is defined as:

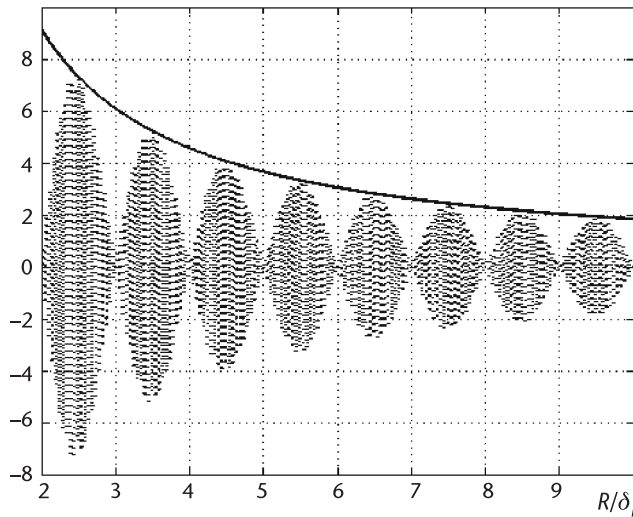
$$\Delta\Phi_{n\max}(R) = c180^\circ/(2\Delta\omega R\pi) \quad (4.43)$$

Figure 4.9 shows the function of instantaneous error of DFS initial phase determination versus the relative frequency at known DFS frequency and its envelope calculated in accordance with (4.42) and (4.43).

Simulation results are completely correlated with plots presented in Figure 4.9. At simulation, the true range was substituted in formulas determining the PC estimation.

We see that the truncation error of DFS initial phase determination has oscillating character. The period of high-frequency oscillations is  $\lambda/4$ . The PC  $\varphi_s(R)$  does not affect the error  $\Delta\Phi_n(R)$ . Its influence manifests itself in the value of initial phase of high-frequency oscillations. The envelope of the instantaneous error determines the maximal error of initial phase estimation.

$\Delta\Phi_n(R/\delta_R)$ , degr.



**Figure 4.9** The plot of truncation error of initial phase estimation versus the relative range for known DFS frequency and its envelope.

To determine the truncation error of initial phase estimation at the unknown DFS frequency, we assume that the reference frequency in the quadratic channels is different from DFS frequency. Performing transformations according to (4.36), we determine that at an unknown DFS frequency the truncation error can be presented in the form:

$$\Delta\Phi_{nn}(R) \approx \varphi_{\text{init},\text{true}}\left(\frac{2R}{c}\right) - \arctan \frac{\frac{\sin\left(\frac{z}{c}\right)\sin\left(\Theta - \frac{z}{c}\right)}{\sin\left(\frac{z}{c}\right)\cos\left(\Theta + \frac{z}{c}\right)} - \frac{\sin\left(\frac{-z+z_1}{c}\right)\sin\left(\frac{z+z_1}{c} + \Theta\right)}{\sin\left(\frac{z+z_1}{c}\right)\cos\left(\frac{z+z_1}{c} + \Theta\right)}}{z - z_1}$$
(4.44)

where  $z = \Delta\omega\Delta R/2$ ;  $z_1 = 2\Delta\omega R$ ;  $\Theta = \omega_0 2R/c + \varphi_s(2R/c)$ ,  $\Delta R$  is the truncation error at range measurement. When determining (4.44), we supposed the only assumption, that  $\Delta R/R$  is negligibly small.

The function obtained according to (4.44) is shown by a thin dotted line in Figure 4.10. The appropriate DFS simulation was performed with this aim using the algorithm (3.4) and the range was estimated and the error  $\Delta R$  was determined, which was substituted in (4.44). Simulation results and calculations according to (4.44) practically completely correlate.

The behavior of truncation errors of initial phase estimations for known and unknown DFS frequency has a different character. First, the high-frequency oscillation estimation scope for an unknown frequency is about three times more than the high-frequency oscillation estimation scope for DFS phase with a known signal frequency. Second, there are no clearly expressed nodes, which are observed

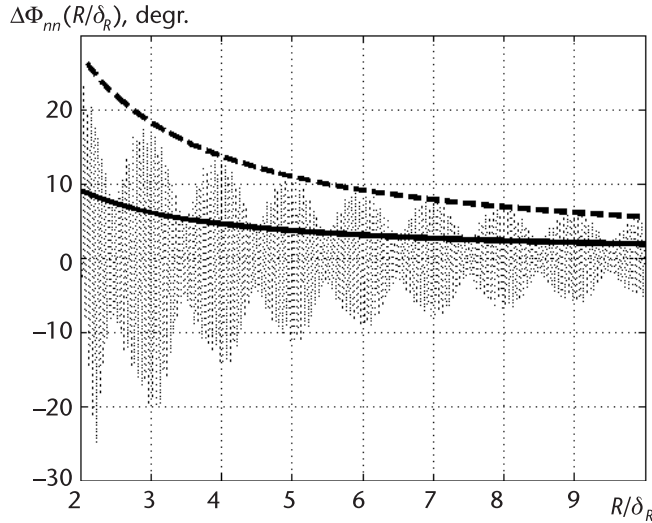


**Figure 4.10** Plots of the truncation errors of initial phase determination versus the relative range at unknown DFS frequency.

in Figure 4.9, in the plot of the truncation error of initial phase estimation with unknown frequency. The period of high-frequency oscillations is  $\lambda/4$  as before.

The maximal error value (the high-frequency oscillation envelope of initial phase estimation) is defined by the following equation (in degrees):

$$\Delta\Phi_{nn_{\max}}(R) \approx 3(180^\circ)/(2\pi\Delta\omega R) \quad (4.45)$$

This function is shown in Figure 4.10 by the thick dotted line. The minimal value of the truncation error of the DFS initial phase determination for an unknown frequency can be determined according to (4.43) and it is shown in Figure 4.10 by the thick solid line.

From Figure 4.10 we see that the truncation error of initial phase estimation monotonically decreases with the relative range increase. At an unknown signal frequency, the truncation error of initial phase determination on relative range equal to 5 is the value of about  $10^\circ$ .

The characteristics presented in Figures 4.9 and 4.10 were obtained without using WF. Having not described the bulky mathematical transformations, we indicate that WF application, in particular, the Blackman WF, allows for the reduction of the truncation error of the DFS initial phase estimation by about the order.

Now we compare the truncation error of initial phase determination and the error of PC determination  $\varphi_s(\hat{t})$ .

Figure 4.11 shows the characteristic corresponding to the truncation error  $\Delta\Phi_s(R)$  of PC estimation  $\varphi_s(\hat{R})$  versus the relative range. To obtain this curve at discrete range variation with the step 0.0001 m, we simulated DFS on the basis of the algorithm (3.6) and estimated the range, and then, on the basis of this approach, we determined the PC and calculated the error according to the formula:

$$\Delta\Phi_s(R) = [\varphi_{\text{init}}(\hat{R}) - 2\omega_0\hat{R}/c] - \varphi_{s,\text{true}}(R) \quad (4.46)$$

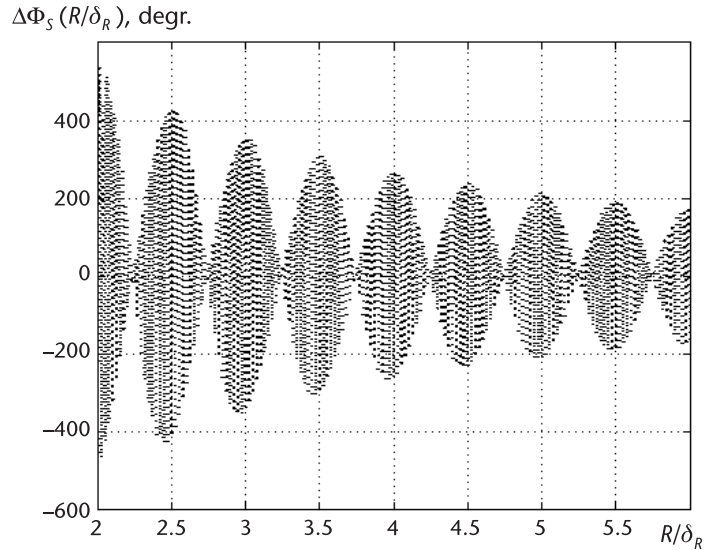


**Figure 4.11** The plot of the truncation error of PC determination of FMCW RF without WF.

where  $\varphi_{s,\text{true}}(R)$  is the true PC. Simulation was performed at the carrier frequency 10 GHz and for the FM sweep at 500 MHz.

From Figure 4.11 it can be seen that the truncation error of the PC estimation significantly exceeds the error of initial phase estimation. Taking into consideration that the 1-mm range measurement error gives inaccuracy in the PC determination by  $24^\circ$ , which is caused by the item  $\omega_0 2\hat{r}/c$  that is used for PC estimation, we can make a conclusion that the error of range estimation has the main contribution in the PC estimation error. Evidently, it is impossible to use PC with such a truncation error for generation of the algorithm's reference signal on the basis of MLM. To decrease the truncation error, we use the Blackman WF. Simulation results obtained using the Blackman WF are presented in Figure 4.12.

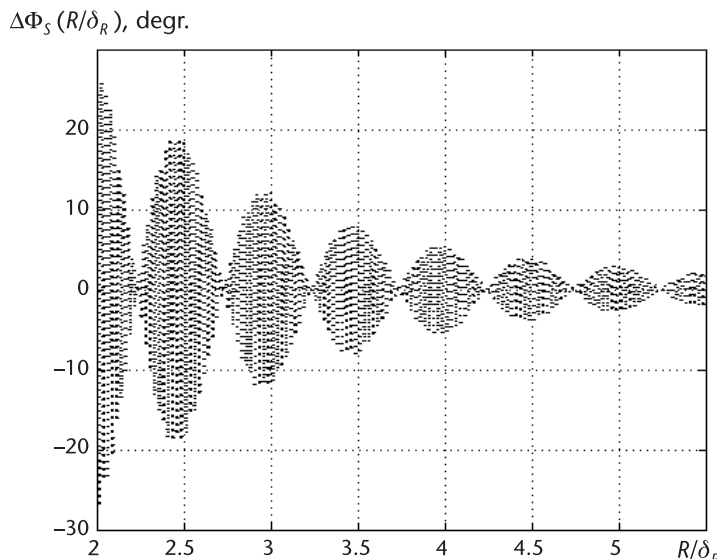


**Figure 4.12** The plot of the truncation error of FMCW RF PC determination using WF.

Taking into account the results of Chapter 3, we may notice that the truncation error of PC determination decreases practically proportionally to the reduction of the range determination error, at which the value of  $\Delta\Phi_s(R)$  decreases quickly enough. From Figure 4.12 we see that for the relative range equal to 5, the value truncation error of PC determination is equal to about  $8^\circ$ . For the relative range equal to 10, this error is equal to about  $3^\circ$ . Taking into consideration that the PC determination error by  $10^\circ$  leads to a range measurement error of 0.406 mm, we may recommend executing the PC estimation with the Blackman WF beginning from relative ranges equal to 8 to 10. Such relative frequencies correspond to a measuring range of 1.2 to 1.5 m (for a FM sweep of 1 GHz).

It is necessary to note that the application of methods described in Chapter 3 allows reduction of the PC error on lesser ranges until the accepted level. Because the error of PC determination essentially depends upon range determination error, then the above-mentioned conclusion about frequency estimation is true for PC estimation. Namely, for relative frequencies larger than 4 to 5, the main contribution (for ratio  $q = 70$  dB and less) into the total error (4.32) is made by the noisy interference. To evaluate the range estimation accuracy, which is used for PC estimation, we use (4.28). After transformations, neglecting the second order of smallness, we obtain that in the first approximation the PC estimation error  $\delta\varphi$  is connected with range estimation error  $\delta R$  as  $\delta\varphi = 720^\circ \delta R / \lambda$ . In the future, we use the PC estimation obtained using the WF for generation of the reference signal phase of the frequency estimation algorithm on the basis of the MLM.

In [1–4], it is shown that in the general case maximal likelihood estimates have distributions, which differ from the normal one. Nevertheless, the conditional distributions of estimation error (i.e., for fixed value of estimating parameter) will approach asymptotically to the normal one with an increase in  $q_{s/n}$  [1]. It follows from (4.36) and (4.37) that PC estimation is obtained using algorithms, which realize the MLM. Therefore, we shall assume that the distribution  $\hat{\varphi}_c(t_{\text{del}})$  is normal with the mean value  $\varphi_c(t_{\text{del}})$ .

## 4.6 Simulation of the Range Estimation Algorithm

The aim of simulation is an estimation of the realistic benefit in accuracy of range measurement using MLM with the known DFS phase. The error analysis performed above showed that two reasons mainly contribute to the resulting error. The first one is the difference of PC used in the reference signal from its true value. The second one is the difference of carrier frequency of the transmitter from its rated value. At the simulation performance, we assume that the carrier frequency  $\omega$  of the FMCW RF is not equal to the frequency  $\omega_{\text{ref}}$  of the reference signal. The difference of frequencies  $\omega$  and  $\omega_{\text{ref}}$  will lead to offset of range estimation, which can be considered at the analysis of simulation results.

Determining the PC according to the above-described approach assumes the estimations of the DFS initial phase and delay time in the whole measuring range interval with the step  $\Delta$ . At each fixed value of the range, the single measurement of the DFS phase is carried out for each value. The application of such a PC in the reference signal, as we already mentioned, does not lead to decrease of estimation

variance compared with algorithms, which do not take into account the signal phase. To determine the PC estimation with a lesser variance, the averaging operation is necessary either over a DFS ensemble or inside some small range interval. The last requires the reflecting surface displacement with respect to the FMCW RF.

#### 4.6.1 Simulation Results at a Known Phase Characteristic

Now let us find out the range measurement errors depending on the relative range for the case when reference signal parameters correspond to DFS to delay accuracy. Figure 4.13 shows functions of the relative error logarithm versus the relative range obtained using simulation. The two-stage procedure was simulated described in Section 4.3. At the first stage, we used the Blackman weighting function. The useful reflector was moved with the 1-mm step. The relative MSD was calculated in the 15-cm range interval. Results were obtained for three values of SNR (20 dB, 60 dB, and 100 dB).

The comparison with Figures 3.24 and 3.25 allows the statement that MLM permits essentially decreasing the noise influence on the range estimation result.

#### 4.6.2 Simulation Results at the Unknown Phase Characteristic: The Approach to Practical Estimation of the Phase Characteristic

We assume that the PC of the FMCW RF and dielectric properties of the reservoir contents determining the phase  $\varphi_{rf}$  are unknown. The PC of FMCW RF will be determined at its mounting on the object. Here some explanations are necessary. After the FMCW RF mounting on the object, as a rule, we have no information about the reflecting surface condition (at the discharge, the loading is performed, or the reflecting surface is fixed). The results of range measurement with the help of the algorithm (3.4) can serve as the criterion of reflecting surface condition. At the fixed position of reflecting surface with respect to the FMCW RF, the PC estimation determined over the ensemble DFS realizations can be displaced as PC estimation has an oscillating character depending on the range. The displacement of the PC

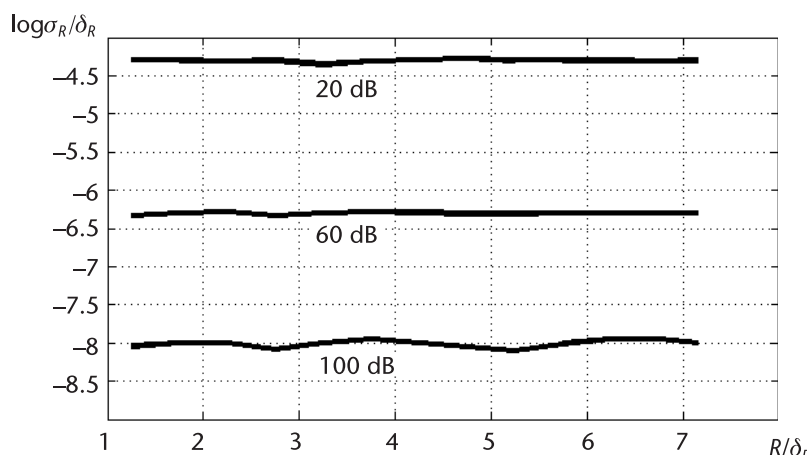


Figure 4.13 The function of relative MSD for MLM versus the relative range for three SNRs.

estimation will lead to the additional error of range measurement. The average values of PC estimations obtained at different ranges from FMCW RF over DS ensembles should be approximate (using software) by some deterministic function (at autonomous operation of the device) with the purpose of the reference signal PC generation for the MLM.

Therefore, the following procedure of PC estimation obtained with a lesser variance seems to be more suitable. Let us carry out PC averaging inside the range interval that is small enough. We designate the PC estimation  $\varphi_s(R)$  as:

$$\bar{\varphi}_s(R) = \varphi_s(R) + \Delta\varphi_s(R) \quad (4.47)$$

where  $\Delta\varphi_s(R)$  is the estimation span with respect to PC mean value, that is, with respect to  $\varphi_s(R)$ . The variance of the random variable  $\Delta\varphi_s(R)$  with a zero mean value is equal to the estimation variance  $\varphi_s(R)$  and it can be determined by (4.9). To obtain a PC estimation with a lesser variance, we average  $\bar{\varphi}_s(r) = \varphi_s(r) + \Delta\varphi_s(r)$  in accordance to the equation:

$$\bar{\varphi}_s(\bar{R}_n) = \frac{1}{N} \sum_{i=1+n}^{N+n} \bar{\varphi}_s(\bar{R}_i) = \frac{1}{N} \sum_{i=1+n}^{N+n} \varphi_s(R_i) + \frac{1}{N} \sum_{i=1+n}^{N+n} \Delta\varphi_s(\bar{R}_i) \quad (4.48)$$

where  $N = R_{\text{int}}/\Delta$ ;  $R_{\text{int}}$  is the range interval in which PC averaging is performed,  $\Delta$  is the range increment to reflecting surface at each measurement, and  $\bar{R}_i$  is the  $i$ th range estimation on the  $i$ th DFS obtained with the help of the algorithm (3.4). For checking the level displacement, we need to use the algorithm of range measurement on the basis of (3.4).

Averaging in accordance with (4.48) corresponds to PC averaging inside the sliding rectangular window. At such averaging, the PC estimation variance will decrease by  $N$  times. However, the PC displacement  $\varepsilon_\varphi$  arises, which can be defined as:

$$\varepsilon_\varphi(R) = \varphi_s(R) - \bar{\varphi}_s(R) = \varphi_s(R) - \int_{R_1}^{R_2} \varphi_s(R)dR/R_{\text{int}} \quad (4.49)$$

where  $R_1$  and  $R_2$  are the initial and final values of the  $R_{\text{int}}$  interval, which leads to displacement of the range estimation due to PC difference of the reference signal and DFS. The value of  $\varepsilon_\varphi$  displacement depends on  $R_{\text{int}}$  and on the behavior of the function  $\varphi_s(R)$  inside the interval  $R_{\text{int}}$ . For a practically important case when the FMCW RF PC is the linear function of range

$$\varphi_s(R) = kR + b \quad (4.50)$$

where coefficients  $k$  and  $b$  are unknown, the PC displacement will be determined as:

$$\varepsilon_\varphi = [\varphi_s(R_2) - \varphi_s(R_1)]/2 \quad (4.51)$$

For simultaneous reduction of displacement  $\varepsilon_\varphi$  and PC estimation variance, it is necessary to take into consideration that the displacement  $\varepsilon_\varphi$  decreases at  $R_{\text{int}}$

reduction, and the variance of PC estimation at fixed  $\Delta$  increases. It is very difficult to determine analytically the optimal value of  $R_{\text{int}}$  at simultaneous minimization both displacement and estimation variance. Nevertheless, it is evident that the interval length  $R_{\text{int}}$  should be multiple of  $\lambda/2$ . Such a choice of  $R_{\text{int}}$  allows minimization the displacement error caused by oscillating character of the function of PC estimation versus range.

Now we determine of achieved estimation using simulation. We require that the displacement error due to PC estimation displacement would be essentially less than the displacement  $\Delta R_\omega$  due to carrier frequency instability of the transmitter determined according to (4.28). We shall assume that FMCW RF PC is the linear function of the range (4.50), where  $k = 4\pi/R_{\text{max}}$  ( $R_{\text{max}}$  is the maximal measuring range). The coefficient  $b$  can be considered as zero since the estimation displacement  $\Delta R_\varphi$  does not depend upon it. The choice of  $R_{\text{int}}$  is caused by the variation speed of the reflected surface. We select  $R_{\text{int}} = 15$  mm. The displacement calculation according to (4.51) with a recount to the range will lead to displacement  $\Delta R_\varphi = 0.0075$  mm at PC averaging in accordance with (4.48). The value of  $\Delta R_\varphi$  depends only upon  $R_{\text{int}}$  at PC approximation by the linear function. The range variation speed to the reflecting surface can be accepted as 1 m/min. We assumed at simulation that the transmitter frequency drift of FMCW RF is maximal: 10 kHz. To minimize the truncation error caused by PAM, the Blackman WF is used.

The simulation results are presented in Figure 4.14 in the form of the total measurement error calculated according to (4.27) versus the measuring range.

Curve 1 corresponds to the range estimation error when using the algorithm (3.4), and other curves correspond to the MLM with the PC averaging inside the sliding window according to (4.49) for  $N$  equal, respectively, to 10, 20, and 100. With an increase of the range from FMCW RF, the reduction of the benefit in measurement accuracy is observed compared to the algorithm (3.4). This can be explained by the fact that at the calculation of the total error we took into account the range estimation displacement caused by the frequency difference of DFS and the reference signal (i.e., the phase difference of DFS and the reference signal).

The choice of  $N$  at averaging is determined by processor operating speed, which realizes the necessary calculation operations for MLM implementation. For the range variation speed to the reflecting surface for  $N$ , equal, respectively, to 10, 20, and 100, it is necessary to have the processor performing calculations necessary for a practical MLM implementation during approximately 0.7, 0.14, and 0.07 second.

The reduction of the total error when using the MLM with an account of the PC, as it follows from Figure 4.13, depends on the measured range. If for the 30-m range the error reduction (depending on  $N$ ) is two to three times larger, then for the 5-m range the benefit in accuracy is from 3 to 7. Besides error reduction caused by the noisy interference, the MLM essentially allows a decrease in the measurement error of small range measurement. Because of narrow LLF maxima, its component with the doubled frequency does not influence as strongly as SL the DFS spectrum for  $\omega < 0$ .

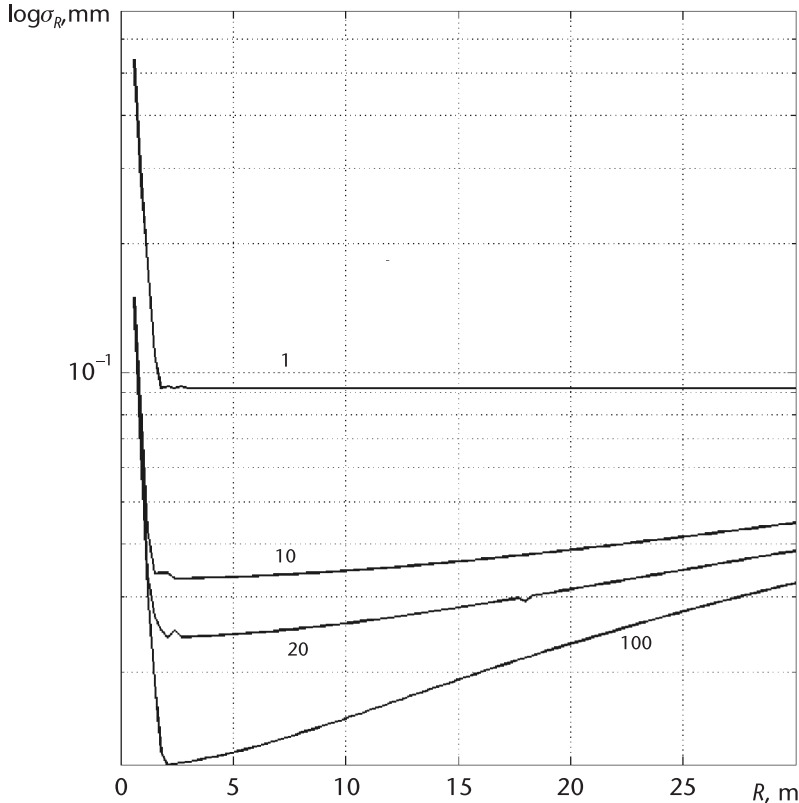


**Figure 4.14** Plots of total error functions of the range measurement by the MLM with PC averaging.

#### 4.6.3 Reduction of the Noise Influence on the Accuracy of the Phase Characteristic Estimation

The benefit in accuracy at using the MLM taking into account the signal phase compared with the algorithm (3.4) can be increased owing to the reduction of the total error component in (4.32) caused by noise influence and displacement of PC estimation caused by PC averaging inside the sliding window. For this, it is necessary to carry out the FMCW RF PC estimation on the special measuring bench, which is desirable in the anechoic box. For each fixed range  $R_i$  in the whole range of measuring ranges with some step  $\varepsilon_R$ , it is necessary to perform PC estimation over  $N$  DFS realization and then to average in accordance with

$$\bar{\varphi}_s(R_i) = \sum_{i=1}^N \hat{\varphi}_s(R_i)/N \quad (4.52)$$

It is clear that the variance of average PC  $\bar{\varphi}_s(R_i)$  will be  $N$  times less than the variance  $\bar{\varphi}_s(R_i)$ .

At the next stage, it is necessary to approximate the discrete sequence  $\bar{\varphi}_s(R_i), i = 1, 2, \dots$  by the continuous function  $\varphi_s(R_i)$  using the known methods of approximation. The similar approximation can be carried out simply enough because range finders have described PC as the function that is closed to linear.

The range, at which the value of  $\varphi_s$  is defined, must be selected from the condition of minimization of spectrum SLs' influence for negative frequencies upon the result of PC calculation.

## 4.7 Conclusions

Relations allowing for the determination the potential accuracy of the range estimation at DFS processing on the background, the white normal noise as a function from SNR, the frequency of the carrying oscillation, and its FM sweep are given. The MLM application at an a priori known phase of DFS allows the reduction of the variance of range estimation by about three orders compared with algorithms, which do not take the signal phase into consideration.

The main components of the error affecting the range estimation error by the MLM method are determined. It is shown that, in the first place, PAM can be attributed to the DFS phase estimation error, differences in the carrying oscillation of DFS, and the reference signal. The calculation expressions are given, allowing the determination of the range calculation error as a function of these factors. It is shown that the error caused by PAM can be eliminated with the help of the WF application. However, the WF application leads to an increase of the variance of range estimation.

The equation is obtained allowing the determination of the appearance probability of anomalous errors multiple to the half-wavelength of the carrying oscillation depending on SNR at the search of the global maximum of the likelihood function in the wide range.

The two-stage procedure of the range estimation by the maximal likelihood method is offered, which permits refusal from the global maximum search in the wide a priori range interval. In the first stage, the preliminary range estimation is determined on the basis of the algorithm searching the maximal spectral component of DFS. In the second stage, the global extremum of the likelihood function is determined in the narrow range equal to the wavelength of carrying SHF signal, which allows practically complete elimination in the upshot of the anomalous measurement errors and a decrease in the computation expenses.

The approach of determination of the phase-frequency characteristic of FMCW RF on the basis of DFS obtained during calibration on the measuring bench is discussed. The simple and effective method of outburst elimination at DFS phase estimation is offered based on the comparison of calculated PC values for two adjacent calculations.

Relations are obtained allowing determination of the truncation errors of DFS phase estimation at known and unknown signal frequency. It is shown that the main component of the truncation error of DFS phase estimation is defined by the truncation error of the range estimation.

The Rao-Cramer boundary is defined for the variance of DFS phase estimation. The equation for determination of the correlation coefficient between DFS phase estimation and the delay time is obtained.

The procedure is described allowing MLM realization at an unknown FMCW RF PC and offering averaging application of calculated values of PC estimation

inside the window sliding on the range axis. Such a procedure requires RF displacement.

It is shown that the total error of the range error, which takes into account the estimation variance and the truncation error, depends on the measuring range with consideration of frequency instability of carrying oscillation and PAM. To reduce the total error, it is necessary to increase frequency stability of carrying oscillation.

The analysis of the signal frequency estimation algorithm presented by the short realization is performed. The received signal having the unknown frequency and initial phase is compared with the set of reference signals, which are calculated on different frequencies and for different initial phases. We assumed that realizations of the received signal have a different scale parameter. With the help of simulation, it is shown that MSD frequency estimations decrease the minimum by two times compared with known algorithms of frequency estimation of the signal presented by short realization. The offered algorithm permits to provide the measurement not only of frequency but the initial signal phase as well, in contrast to the known algorithms.

## References

- [1] Tikhonov, V. I., *Optimal Reception of Signals*, Moscow, Russia: Radio i Sviaz Publ., 1983. [In Russian.]
- [2] Sosulin, Y. G., *Stochastic Signal Detection and Estimation Theory*, Moscow: Sovetskoe Radio Publ., 1978, 320 pp. [In Russian.]
- [3] Kulikov, E. I., and A. P. Trifonov, *Signal Parameter Estimation against Interference Background*, Moscow: Sovetskoe Radio Publ., 1978, 296 pp. [In Russian.]
- [4] Berezin, L. V., and V. A. Veitsel, *Theory and Design of Radio Systems*, Moscow: Sovetskoe Radio Publ., 1977, 448 pp. [In Russian.]
- [5] Jenkins, G. M., and D. G. Watts, *Spectral Analysis and Its Applications*, San Francisco, Cambridge, London, Amsterdam: Holden-Day, 1969.

# Effects of FM Nonlinearity

## 5.1 Introduction

In frequency-modulated range-finding, one of the significant factors influencing the main error of range measurement is linearity on the modulation characteristics of the SHF transmitter. At present, the methods of the MC linearity provision with the help of digital frequency synthesis using the phase-locked loop (PLL) system are known [1]. The synthesis usually performs on a comparatively low carrier frequency and, after that, frequency multiplication to the required value and the amplification of the obtained signal is performed. These methods allow us to obtain good linearity and a wide FM sweep of the oscillator; however, their implementation is relatively expensive and complicated. Therefore, the problem of required accuracy ensuring the range measurement by simpler and cheaper methods at MC nonlinearity is worth investigating.

To solve this problem, it is necessary to develop a model of oscillator MC, to investigate the influence of MC nonlinearity on results of range measurement, and to offer methods allowing for the reduction of the error.

## 5.2 The Mathematical Model of the Modulation Characteristic

In this case, we are speaking about the model  $\omega(u_{\text{mod}})$  representing external characteristics of the FMCW oscillator influencing range measurement accuracy.

In most cases, the voltage-controlled oscillator (VCO) is used as the source of FMCW oscillations. The varactor (or varicap) is most frequently used as the control element for FM sweep. Its properties are exactly defined as the practical character of frequency variation, which depends upon the linearity of  $\omega(u_{\text{mod}})$ .

The linearity of the FM sweep of the SHF oscillator is one of the main conditions for the achievement of the high accuracy of range measurement. To estimate the MC linearity degree, the analytical MC record in the form of some equation selected with the help of approximation methods is more suitable. For a more complete account of peculiarities of the MC form in our problems, we write the function of the cyclic frequency versus voltage as:

$$f = f_0 + K_{\text{MC}}u_{\text{mod}} + au_{\text{mod}}^2 + \sum_{n=1}^M b_n \sin[d_n(u_{\text{mod}} + U_{\text{init},n})] \quad (5.1)$$

where  $K_{MC}$  and  $a$  define the linear and quadratic component,  $b_n$ ,  $d_n$ , and  $U_{init,n}$  define, respectively, the oscillation amplitude, their frequency on the voltage axis, and the initial bias of each sine items, and  $M$  is a quantity of considering harmonics.

We assume the linear variation of the voltage  $u_{mod}$  in time in this formula:

$$u_{mod} = K_u t \quad (5.2)$$

Therefore, the maximal voltage value at symmetric triangle modulation law (1.4) is

$$U_{mod} = K_u T_{mod}/2 \quad (5.3)$$

This maximal value is defined starting from the specified FM sweep  $\Delta F$  by means of a numerical solution of the nonlinear equation (for one oscillating component):

$$K_{MC} U_{mod} + b \{ \sin[d(U_{init} + U_{mod})] - \sin(dU_{init}) \} = \Delta F \quad (5.4)$$

for the given MC parameters  $K_{MC}$ ,  $b$ ,  $d$ ,  $U_{init}$  and the specified range  $\Delta F$  of FM sweep at FMCW.

To find out all MC parameters in (5.1) based on the experimental data obtained in the table form containing the set of  $N$  pairs of appropriate numbers  $u_{mod}, f_i$ ,  $i = 1, 2, \dots, N$ , we may apply the method of sequential extraction of separate elements described in [2] and developed in [3, 4]. The first three items can be defined on the basis of quadratic regression by means of approximation according to the least-squares method [5].

Figure 5.1 shows (dotted line) one of the MCs of the industrially manufactured oscillator.

The solid line of quadratic regression obtained in the software medium MATLAB 6.5 with the help of typical subprograms polyfit and polyval, which calculate, respectively, regression coefficients and the regression equation, is presented in the plot. After subtraction of the experimentally taken regression line data from the set on the basis of the obtained estimation values of the first three items in (5.1), we arrive to the remainder of the oscillating part in the form of the number set  $u_{mod,i}, \Delta_i$ :

$$\Delta_i = f_i - f_0 - K_u u_{mod} - \hat{a} u_{mod,j}^2, i = 1, 2, \dots, N \quad (5.5)$$

shown in Figure 5.2 by a dotted line.

Because there may be several harmonics in (5.1), we may apply the approach considered in [2], when the sequential extraction of each spectral component is performed.

Taking into account that in this case we are discussing not a time function but the function depending upon the modulating voltage, the method of super-resolution of signals offered in [2] can be described in the following form. It is required to estimate parameters of harmonics, which contain  $\Delta_i$  (amplitude  $b_n$ , frequency  $d_n$ , and phase  $\varphi_n = d_n U_{init,n}$ ) according to measurements obtained with the error.

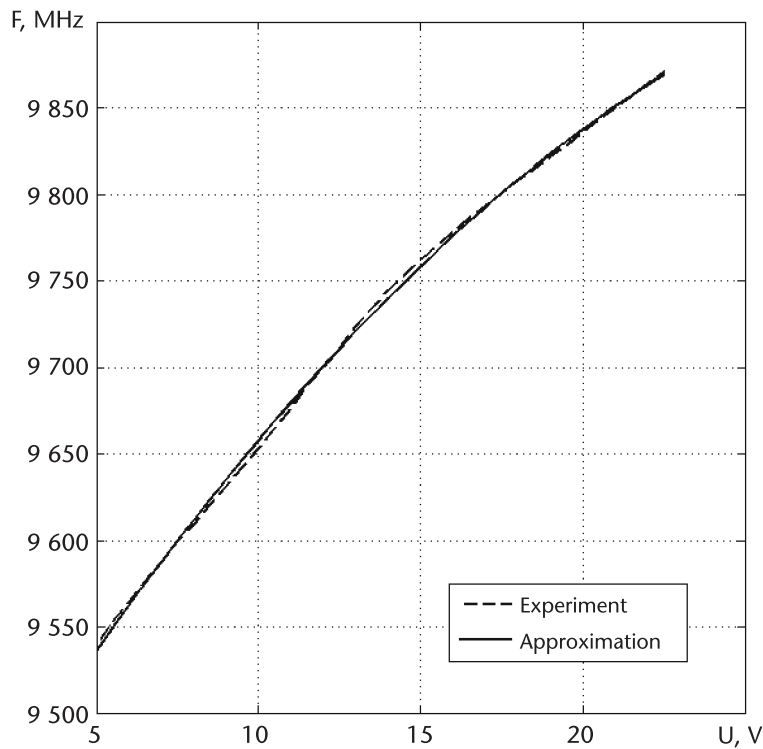


**Figure 5.1** Modulation characteristics of the industrially manufactured oscillator with the quadratic regression line.

For the solution of this problem, one often calculates the square of metric range  $C^2$  between the measured values of  $\Delta_i$  and the model  $f_{\text{osc}}$  of oscillating component with proposed (sorted) parameters

$$C^2 = \sum_{i=1}^M (\Delta_i - f_{\text{osc},i})^2 \quad (5.6)$$

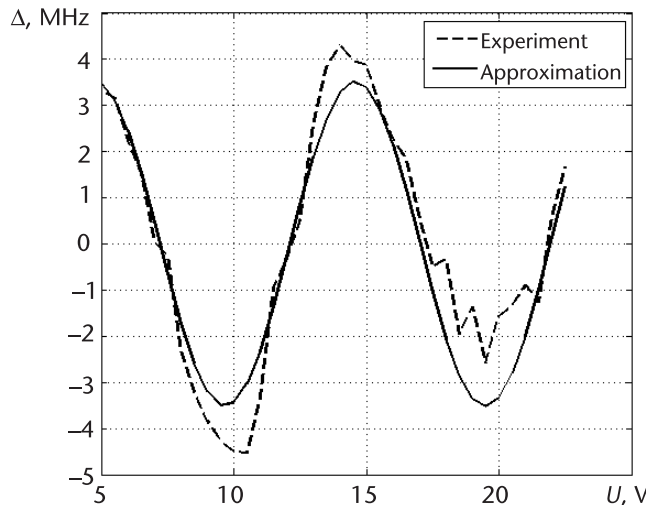


**Figure 5.2** Plots of MC oscillation component with the shown approximate line versus voltage at  $M = 1$ .

The method reduces to the performance of two stages.

- *Stage 1:* The determination of the spectral line coordinates is provided even in the case when they cannot be resolved. This stage consists of two steps:
  - *Step 1:* The peak is searched with maximal amplitude. The parameters of this peak are conferred to relatively parameters of the next spectral line.
  - *Step 2:* The difference is calculated between process values on the previous  $m-1$ th iteration and values of the next extracted spectral line:

$$\Delta_{i,m} = \Delta_{i,m-1} - f_{\text{osc}}(b_n, d_n, \varphi_n) \quad (5.7)$$

Steps 1 and 2 are repeated until the amplitudes of the extracted peaks would be less than the chosen threshold.

- *Stage 2:* The successive specification of all spectral line coordinates is carried out. The stage realizes the estimate performance by the least-squares method at searching of parameters.

The parameters of spectral peaks are specified at the beginning and at subtracting, at which all signals are obtained from the previous step of the initial signal with optimized parameters. The specification of spectral peak parameters is performed until the difference between newly obtained parameters from the previous stage would become less of the value required in advance.

At each step of the second stage, it is expedient to apply the procedure of one-dimensional minimization instead of the three-dimensional one referred to as the method of nonlinear least squares in [6].

As a result, we can reduce the procedure of multidimensional numerical minimization to the procedure of one-dimensional minimization on the frequency  $d_n$ . After finding the minimum, we can calculate the required parameters  $b_n$ ,  $\varphi_n$ , and  $U_{\text{init},n}$ :

$$b_n = \sqrt{b_{cn}^2 + b_{sn}^2} \quad (5.8)$$

$$\varphi_n = \arctan(b_{sn}/b_{cn}) \quad (5.9)$$

$$U_{\text{init},n} = \varphi_n/d_n \quad (5.10)$$

The results of the offered algorithm application for MC approximation presented in Figure 5.1 for  $M$  equal to, respectively, 1, 2, 3, and 4 show that, as  $M$  grows, the approximation error decreases.

The results of the MC parameter determination according to this approach for the series of industrially manufactured oscillators allows the conclusion that the range of possible values of MC parameters is:  $K_u = (40...100)$  MHz/V,  $a = (-3 ... -0.5)$  MHz/V<sup>2</sup>,  $b = (0...100)$  MHz, and  $d = (0, 1, \dots 5)$  rad/V. The parameter  $U_{\text{init}}$  usually lies within the MC limits, but it does not influence later results. The considered example proves great possibilities of the model in (5.1) in the description of different types of MCs.

### 5.3 Effects of FM Nonlinearity for the Counting Method of Frequency Measurement

MC nonlinearity leads to the nonproportional variation of the averaged value of the difference frequency  $F_{R,\text{aver}}$  at variation of the measuring range. As was shown earlier, using the method of DFS phase joining, range variation causes variation of the modulation period and, hence, the modulating voltage amplitude, which leads to variation of the average MC slope. Because range calculation in FMCW RF is carried out under the assumption that this slope is constant, the measurement error arises. The presence of the stepwise slope's variation in moments of DFS phase joining point jump to the next extremum and the smooth variation between these moments is the general property of such measurement. Stepwise variation defines the maximal slope's variation, which accordingly causes the maximal measurement error [7]. To estimate the maximal variation value of  $F_{R,\text{aver}}$ , we use (5.1) with the minimal set of nonlinear parameters with  $M = 1$ .

We assume for concreteness that the triangle symmetric modulating voltage is used. To determine the value of stepwise variation of the averaged slope, it is enough to consider one half-period of modulation. The law of modulating voltage variation is assumed to be linear:

$$u = U_{\text{DC}} + K_u t, t \in [0, T_{\text{mod}}/2] \quad (5.11)$$

where  $U_{\text{DC}}$  is the dc component and  $K_u$  is the slope of voltage increase.

We write the time function of the transmitter frequency substituting (5.11) into (5.1) as:

$$\begin{aligned} f(t) = & f_0 + K_{\text{MC}} U_{\text{DC}} + K_{\text{MC}} K_u t + a U_{\text{DC}}^2 + a K_u^2 t^2 + 2a U_{\text{DC}} K_u t \\ & + b \sin[d(U_{\text{DC}} - U_{\text{init}} + K_u t)] \end{aligned} \quad (5.12)$$

Using the formula (1.10), we obtain the equation for difference frequency:

$$F_{\text{DFS}}(t) = t_{\text{del}} \{ A + 2Bt + C \cos[d(U_{\text{DC}} - U_{\text{init}} + K_u t)] \} \quad (5.13)$$

where  $A = K_{\text{DC}} K_u + 2a U_{\text{DC}} K_u$ ,  $B = a K_u^2$ , and  $C = b d K_u$ .

Now we calculate the averaged difference frequency for the modulation half-period according to (1.11):

$$\begin{aligned} F_{R,\text{aver}} = & 2t_{\text{del}} \{ 0.5A + 0.25BT_{\text{mod}} \\ & + b \sin[d(U_{\text{DC}} - U_{\text{init}} + 0.5K_u T_{\text{mod}})] / T_{\text{mod}} \\ & - b \sin[d(U_{\text{DC}} - U_{\text{init}})] / T_{\text{mod}} \} \end{aligned} \quad (5.14)$$

In the moment of the phase joining point, the half-period  $T_{\text{mod}}/2$  changes by the jump on the value  $T_R/2$  to an increase from its minimal value  $T_{\text{st}}$  to the maximal  $T_{\text{st}} + T_R/2$  with measuring range increasing or vice versa to a decrease from the mentioned maximal value to  $T_{\text{st}}$  at the range reduction. Let us find the maximal variation of the averaged value of difference frequency  $\Delta F_{R,\text{aver}}$  and the jump of measuring range  $\Delta R$  for specific cases.

### 5.3.1 The Quadratic Modulation Characteristic

Substituting  $b = 0$  into (5.12) and the values of time moments  $t = 0$  and  $t = T_{st}$ , we obtain the quadratic equation determining the modulating voltage amplitude according to given frequency FM sweep  $\Delta F_{min}$ :

$$\alpha U_{mod}^2 + (K_{MC} + 2\alpha U_{DC})U_{mod} - \Delta F_{min} = 0 \quad (5.15)$$

where  $U_{mod} = T_{st}K_u$  is the value of modulation voltage and  $\Delta F_{min} = T_{st}K_f$  is the value of the FM sweep forming during time  $T_{st}$ . We obtain the solution of this equation taking into account that  $U_{mod} > 0$ :

$$U_{mod} = \frac{-(K_{MC}/2\alpha + U_{DC})}{+\sqrt{(K_{MC}/2\alpha + U_{DC})^2 + \Delta F_{min}/\alpha}} \quad (5.16)$$

The above-mentioned values of practical MC parameters are such that the first item under the square root is several orders more than the second one. Using the expansion into the Maclaurin series [5] for the square root and limiting by first two series items, we obtain the approximate equation:

$$U_{mod} \approx \Delta F_{min}/(K_{MC} + 2\alpha U_{DC}) \quad (5.17)$$

From (5.17) at  $\Delta T_{mod} = T_R/2$ , we obtain the value of stepwise increment of difference frequency:

$$\Delta F_R = 0.5\alpha K_u^2 T_R t_{del} \quad (5.18)$$

Now taking into consideration (1.25), after simple transformations we obtain the equation for the maximal value of the relative error of range measurement caused by the quadratic MC character:

$$\Delta R_{max,quad}/\delta_{Rst} = \alpha \Delta F_{min} / (K_{MC} + 2\alpha U_{DC})^2 \quad (5.19)$$

At fixed MC parameters and the modulation law, the value of this component of the error does not depend on range and is defined only by the specified FM sweep, MC parameters  $\alpha$  and  $K_{MC}$ , and the value of  $U_{DC}$ . The increase of the FM sweep leads to proportional increase of the relative error. The quadratic coefficient  $\alpha$  is the algebraic quantity; therefore, its influence is ambiguous. Nevertheless, it cannot change in arbitrary limits; its value should not be such, at which the negative slopes will arise in the MC [8], and it must be the increasing function. We may consider as such the extreme value from below for  $\alpha$ , at which there is an MC extremum on the half-period boundary (i.e., at  $t = T_{st}$ ). Therefore, the MC derivative becomes equal to zero:

$$df(u)/du|_{u=U_{mod}} = K_{MC} + 2\alpha(U_{DC} + U_{mod}) = 0 \quad (5.20)$$

In this case the lower boundary for the quadratic coefficient is:

$$\begin{aligned} a &\geq -0.5K_{MC}/(K_UT_{st} + U_{DC}) \\ &= -0.5K_{MC}/(U_{mod} + U_{DC}) \end{aligned} \quad (5.21)$$

In the connection that in the denominator of (5.19), the first item is much more than the second one, the influence of  $U_{DC}$  variation is much more than the second, and the  $U_{DC}$  variation on the error is insignificant. Due to this reason, the function of the measurement error versus  $a$  variation is mainly defined by the numerator of (5.18) and is practically linear. Figure 5.3 shows typical plots of the relative error function of range measurement versus the quadratic coefficient for  $K_{MC} = 50$  MHz/V at three values of  $U_{DC} = 2$  V, 4 V, and 6 V.

If one expresses from (5.19) the absolute value of the measurement error taking into account the mentioned fact, it turns out that the modulus of error quadratic component does not depend upon the FM sweep and is defined by MC parameters only:

$$\Delta R_{max,quad} = 0.25 ac/K_{MC}^2 \quad (5.22)$$

From here we see that variation of MC slope effects significantly on the error value. At the slope increase, the error sharply decreases. This fact allows us to put limitations on the parameters of the nonlinear MC according to the given maximal permissible measurement error.

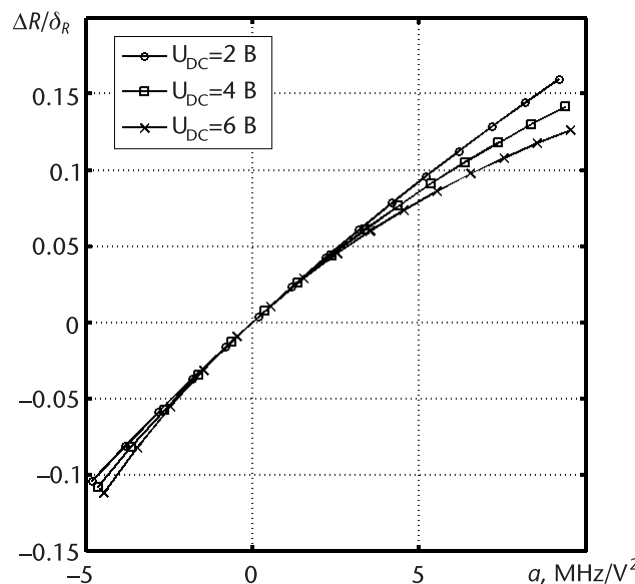


**Figure 5.3** Plots of the function of the normalized measurement error versus the quadratic coefficient for  $K_{MC} = 50$  MHz/V.

### 5.3.2 The Oscillating Modulation Characteristic

The equation for determination of the modulating voltage amplitude can be found out in a similar manner as in (5.15) substituting in (5.12)  $\alpha = 0$  and values of time moments  $t = 0$  and  $t = T_{st}$ :

$$\begin{aligned} K_{MC}U_{mod} + b \sin[d(U_{DC} - U_{init} + U_{mod})] \\ - b \sin[d(U_{DC} - U_{init})] - \Delta F_{min} = 0 \end{aligned} \quad (5.23)$$

This transcendent equation can be solved by a numerical way only. However, as for the quadratic case, we may put on limitations on MC parameters, at which we cannot meet decaying parts:

$$df(u)/du = K_{MC} + bd \cos[d(U_{DC} - U_{init} + u)] \geq 0 \quad (5.24)$$

The worst case will be when the function  $\cos(*)$  in this equation becomes equal to  $-1$ . From this we obtain the limit expression for MC parameters:

$$bd \leq K_{MC} \quad (5.25)$$

Assuming in (5.14) that  $\alpha = 0$ , we obtain the value of stepwise variation of averages difference frequency at transition of the phase joining point by the value of  $\Delta T_{mod} = T_R/2$ :

$$\begin{aligned} \Delta F_R = \frac{2t_{del}b}{(T_{st} + 0.5T_R)} \{ [d(U_{DC} - U_{init} + K_u T_{st} + K_u T_R/2)] \\ - \sin[d(U_{DC} - U_{init})] \} - \frac{2t_{del}b}{T_{st}} \{ \sin[d(U_{DC} - U_{init} + K_u T_{st})] \\ - \sin[d(U_{DC} - U_{init})] \} \end{aligned} \quad (5.26)$$

From here we obtain after transformations:

$$\begin{aligned} \Delta F_R = \frac{xb}{\Delta F_{min} T_{st}} \{ K_Y \sin[D + dU_{mod}/K_Y] \\ - \sin[D + dU_{mod}] - (1 - K_Y) \sin D \} \end{aligned} \quad (5.27)$$

where  $D = d(U_{DC} - U_{init})$ ,  $K_Y = R/(R + \delta_{Rst})$ .

Now we can write the value of stepwise variation of measuring range:

$$\begin{aligned} \frac{\Delta R_{max,osc}}{\delta_{Rst}} = \frac{xb}{\Delta F_{min}} \{ K_Y \sin[D + dU_{mod}/K_Y] \\ - \sin(D + dU_{mod}) - (1 - K_Y) \sin D \} \end{aligned} \quad (5.28)$$

As we see from these equations, the measurement error depends rather complicated upon the range, modulation parameters, and position of the operating point on the MC. The strongest influence is upon the character of the error function versus the range that the parameter  $d$  has.

For the quantitative estimation of possible error values, we transform (5.28) for limit values of the measured range. At small ranges when  $R \rightarrow \delta_{Rst}$ , substituting  $R = \delta_{Rst}$  in (5.28) and transforming the sum of two trigonometric functions, we obtain:

$$\begin{aligned} & \left. \Delta R_{\max, \text{osc}} / \delta_{Rst} \right|_{R=\delta_{Rst}} \\ &= \frac{b}{\Delta F_{\min}} \sin[d(U_{DC} - U_{\text{init}} + U_{\text{mod}})][\cos(dU_{\text{mod}}) - 1] \end{aligned} \quad (5.29)$$

At large ranges for  $R \rightarrow \infty$ , we can use a change of variables  $x = K_Y/(1 - K_Y)$ , which follows from designations in (5.27), and from the L'Hospital rule to overcome uncertainty, we obtain from (5.28) the maximal value of the relative oscillating error:

$$\begin{aligned} & \left. \frac{\Delta R_{\max, \text{osc}}}{\delta_{Rst}} \right|_{R \rightarrow \infty} \\ &= \frac{b}{\Delta F_{\min}} \left\{ \sqrt{(dU_{\text{mod}})^2 + 1} \sin[\arctan(dU_{\text{mod}}) - D - dU_{\text{mod}}] - \sin D \right\} \end{aligned} \quad (5.30)$$

From (5.29) and (5.30), the conclusion is offered that by changing voltages  $U_{DC}$  and  $U_{\text{mod}}$ , we can minimize errors right up to zeroing. Nevertheless, this is not so as these voltages are included in (5.23) defining the value of  $\Delta F_{\min}$  inside the time interval  $T_{st}$ . Due to the fact that  $\Delta F_{\min}$  is fixed with the help of any external circuits, it is impossible to arbitrarily change simultaneously  $U_{DC}$  and  $U_{\text{mod}}$ . At variation of  $U_{DC}$  from (5.23), we obtain the rigidly connected value of  $U_{\text{mod}}$ .

Let us find maximal possible values of stepwise variations of measurement results.

The maximal values of the error modulus can be found by sorting out the worst combinations of limit values of trigonometric functions included in (5.29) at a small range ( $R = \delta_{Rst}$ ):

$$|\Delta R_{\max, \text{osc}} / \delta_{Rst}|_{R=\delta_{Rst}} \leq 2b/\Delta F_{\min} \quad (5.31)$$

and at a large range ( $R \rightarrow \infty$ ):

$$|\Delta R_{\max, \text{osc}} / \delta_{Rst}|_{R \rightarrow \infty} \leq b \left[ 1 + \sqrt{(dU_{\text{mod}})^2 + 1} \right] / \Delta F_{\min} \quad (5.32)$$

These formulas allow the estimation of possible error values according to known MC parameters.

It follows from these expressions that an increase of the FM sweep gives a serious positive effect at small ranges only. It is well seen in Figure 5.4, where the solid line shows the calculation results of the relative error function versus the FM sweep according to the accurate formula (5.29) for  $R/\delta_{Rst} = 1$  and the dotted line shows the same results obtained according to (5.31).

Accurate calculation results strongly oscillate at the variation of the FM sweep; however, the modulus of the accurate error value does not exceed the approximated value determined according to (5.31) at any values of parameters. Both equations show the essential error variation at the changing of the frequency FM sweep.

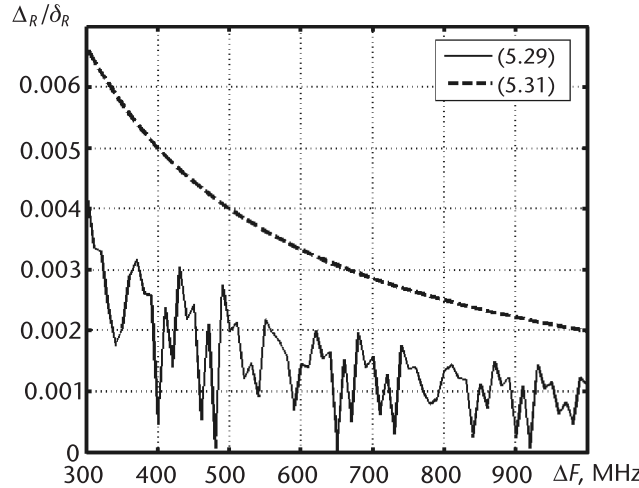


**Figure 5.4** Plots of the function of normalized measurement error versus the frequency FM sweep for  $d = 5 \text{ rad/V}$ ,  $b = 1 \text{ MHz}$ ,  $U_{\text{init}} = 0V$ ,  $U_{\text{DC}} = 5V$ , and  $\Delta R/\delta_{\text{Rst}} = 1$ .

There is a multiplier in (5.32) for large ranges, whose value depends upon the product  $dU_{\text{mod}}$ . This value is mainly proportional to the frequency FM sweep; therefore, it partially compensates the denominator influence of this formula. The degree of compensation depends on  $d$ . The effect of  $U_{\text{mod}}$  is weak at small  $d$  only and, therefore, the measurement error decreases for large ranges with increasing of the FM sweep as it is shown in Figure 5.5 drawn for  $d = 0.3 \text{ rad/V}$ .

Increasing  $d$  leads to a strengthening of the  $U_{\text{mod}}$  effect and, hence, to a decrease of the FM sweep influence on the error. It can be seen in Figure 5.6, where functions similar to Figure 5.5 but at  $d = 5 \text{ rad/V}$  are shown. Because  $dU_{\text{mod}}$  can be much more than 1, at a large range and for large  $d$ , the error very weakly depends upon the FM sweep and aspires to the value:

$$\left| \Delta R_{\max, \text{osc}} / \delta_{\text{Rst}} \right|_{R \rightarrow \infty} \leq bd/K_{\text{MC}} + b/\Delta F_{\min} \quad (5.33)$$

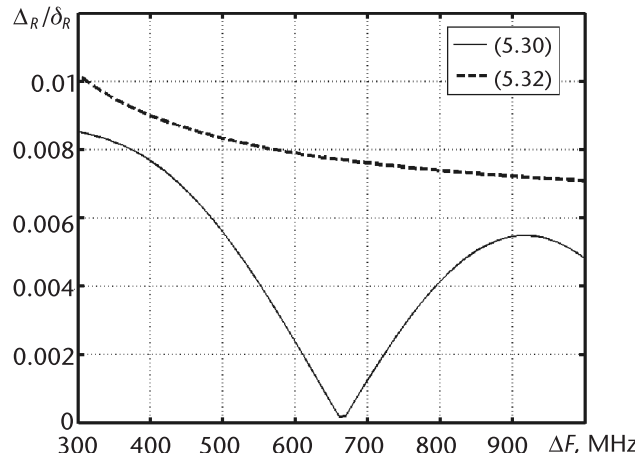


**Figure 5.5** Plots of the function of the relative measurement error versus the frequency FM sweep for  $d = 0.3 \text{ rad/V}$ ,  $b = 1 \text{ MHz}$ ,  $U_{\text{init}} = 0V$ ,  $U_{\text{DC}} = 5V$ , and  $\Delta R/\delta_{\text{Rst}} = 200$ .

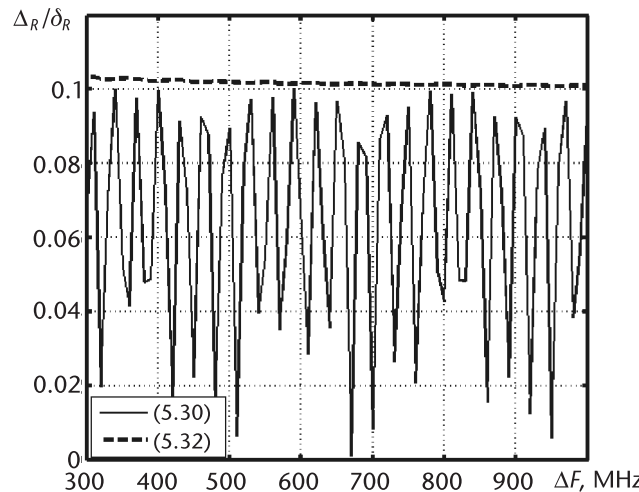


**Figure 5.6** Plots of the function of the relative measurement error versus the frequency FM sweep for  $d = 5 \text{ rad/V}$ ,  $b = 1 \text{ MHz}$ ,  $U_{\text{init}} = 0V$ ,  $U_{\text{DC}} = 5V$ , and  $\Delta_R/\delta_R = 200$ .

that is, it is mainly defined by the MC parameters only because the second item is significantly less than the first one. Thus, in Figure 5.6, the variation of maximal error does not exceed of units of percent from its absolute value.

### 5.3.3 The Quadratic Modulation Characteristics with the Oscillating Component

This is the most general case. The performed analysis allows the recording in this case for the total measurement error as a sum of two considered components. In practice, the limit error value is more interesting. We can write it combining (5.22) and (5.33):

$$|\Delta R_{\max}/\delta_{Rst}|_{R \rightarrow \infty} \leq bd/K_{\text{MC}} + |a|\Delta F_{\min}/K_{\text{MC}}^2 \quad (5.34)$$

Therefore, the presence of quadratic component leads simply to a displacement of the oscillating component plot upward or downward in accordance with a sign of quadratic item. All conclusions concerning the error behavior at the variation of modulation parameters and the MC remain true.

## 5.4 Effects of FM Nonlinearity for the Weighting Method of Difference Frequency Averaging

The estimation of MC nonlinearity influence on the range measurement error is carried out with the help of computer simulation at different types of MC nonlinearity. In the simplest case of a quadratic MC, the calculations show that for different WF the general view of error plots versus range is approximately the same and it looks like the curves presented in Figures 2.4.

Figure 5.7 shows the typical function of the relative error versus normalized range for algebraic WF at  $n = 1$  and  $a = -2 \text{ MHz/V}^2$ .

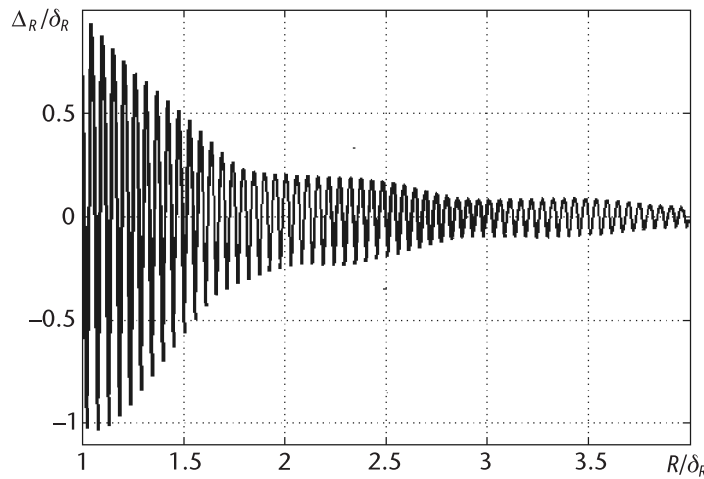


**Figure 5.7** Plots of the function of the normalized measurement error versus normalized range for  $n = 1$  and  $a = 2 \text{ MHz/V}^2$ .

Quadratic nonlinearity leads to the fact that nodal points are eliminated from the error plots and the total error level increases, and therefore, the more  $n$  (the more complicated shape of the algebraic WF), the stronger the nonlinearity influence. The total function character remains the same (i.e., slow and fast error oscillations are observed). The fast oscillation period, as usual, is equal to a quarter-wavelength of the carrying oscillation. The amplitude of these oscillations decreases monotonically with increasing range. Slow oscillations are expressed as weaker and for a significant nonlinearity increase they have disappeared.

Figure 5.8 shows the function of the normalized error  $\sigma_\Delta$  averaged according to (2.23) versus the normalized range at different coefficients of the quadratic nonlinearity for  $n = 1$ .

The increase of quadratic nonlinearity degree leads to increase of the total error level. The specific form of such plots is strongly varied at changing of the WF form. The strongest variations are observed for more complicated WF.

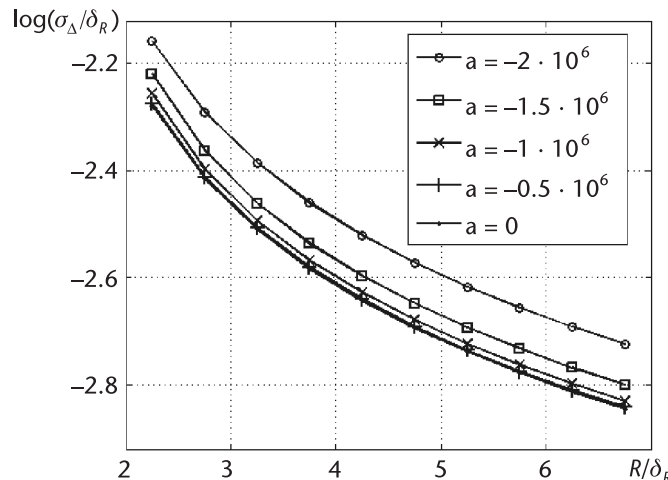


**Figure 5.8** Plots of the function of the normalized average error at different coefficients of quadratic nonlinearity for  $n = 1$ .

Let us consider the influence of the oscillating process of the nonlinear MC for the simplest case: the presence of one harmonic only. The analysis of the formula (5.1) shows that MC slope variation in this case is defined by the product  $bd$ . Therefore, the maximal slope is  $S_{\max} = K_{MC} + bd$ , and minimal slope is  $S_{\min} = K_{MC} - bd$ . Calculations show that the character of the error function versus range depends on WF shape and MC parameters  $d$ ,  $b$ , and  $U_{\text{init}}$ . The analysis of calculation results allows the following conclusions:

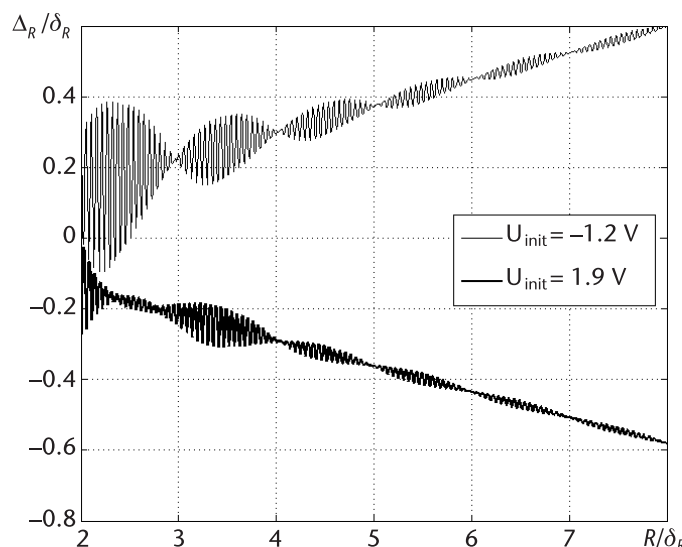
- As usual, two types of periodicity are observed to be connected with the wavelength of the carrying oscillation and with QI value.
- The linear trend rises, which has the slope value and the slope sign dependent in a complicated manner upon the product  $bd$  and the initial phase of oscillating component  $dU_{\text{init}}$ .
- At the variation of initial phase, the trend slope varies within the limits from some minimal negative value to the positive maximal value.

Figure 5.9 shows typical functions of the relative range measurement error versus normalized range for  $n = 1$ ,  $d = 1 \text{ rad/V}$ , and  $b = 10 \text{ MHz}$  and two extreme values of  $U_{\text{init}}$  defining the extreme value of the linear trend.

If trend parameters are known, we can consider them at the range calculation. The functions of measurement error with eliminated trend remind the plot shown in Figure 5.7.

The linear trend slope depends on the MC parameters. The functions of slope versus  $U_{\text{init}}d$  at different parameters  $b$  and  $d$  obtained with the help of simulation are presented in Figure 5.10.

The dependence on the initial phase  $U_{\text{init}}d$  has a sine shape. Functions versus  $b$  and  $d$  parameters are more complicated. The linear trend from the error plot can be



**Figure 5.9** Plots of the function of normalized range measurement versus normalized range for  $n = 1$ ,  $d = 1 \text{ rad/V}$ ,  $b = 10 \text{ MHz}$ , and two values of  $U_{\text{init}}$ .

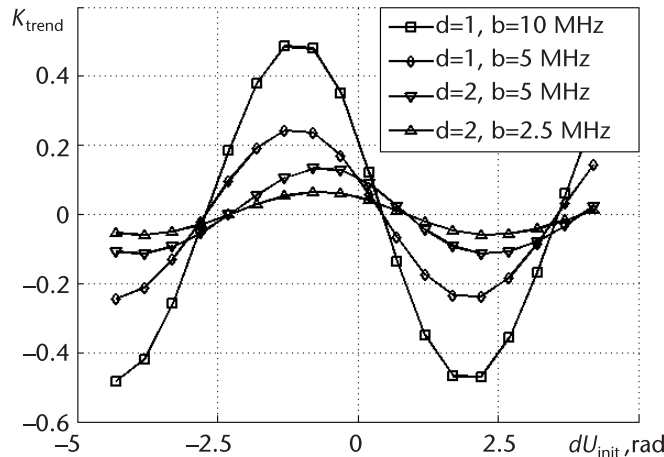


**Figure 5.10** Plots of slope coefficient of the linear trend versus initial phase of MC oscillating component.

easily eliminated by variation of the coefficient  $K_{WF}$ , whose value depends upon the parameters of the MC oscillating component and the WF form.

After trend elimination, it turns out that the error oscillating component MSD depends weakly upon the MC nonlinearity parameters. It is well seen from plots presented in Figure 5.11.

Thus, the obtained results allow the conclusion about the possibility of result corrections of range measurement according to the known MC nonlinearity parameters. To solve this problem, it is necessary to determine the functional connection between MC nonlinearity parameters and the coefficient  $K_{WF}$ , included in the calculation formula (2.5) for the correction of measurement results. Moreover, it is necessary to have the possibility of defining MC nonlinearity parameters according to the operating DFS to carry out the urgent correction of results.

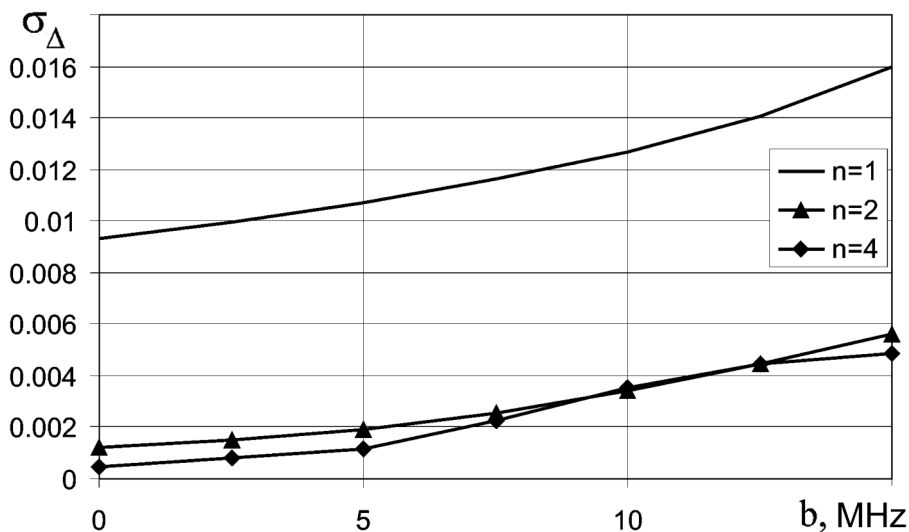


**Figure 5.11** Plots of range measurement MSD versus amplitude of the MC oscillating component for  $dU_{init} = 1$  and  $R/\delta_R = 6$ .

## 5.5 Connection of the Correction Coefficient with Nonlinearity Parameters of the MC

To obtain a connection of the coefficient  $K_{WF}$  with nonlinearity parameters, it is necessary to calculate the integral from (2.4) having substituted in it the expression for WF in (2.9) and the equation for difference frequency in (1.10). We consider separately the case of quadratic MC nonlinearity and the oscillating nonlinearity.

### 5.5.1 Quadratic Nonlinearity of Modulation Characteristics

Taking into consideration (5.1), at the quadratic MC nonlinearity, the difference frequency from (1.10) is defined by the equation:

$$F_{DFS}(t) = t_{\text{del}} \left( k k_U + 2 a k_U^2 t \right) \quad (5.35)$$

Then

$$S = K_W 2 t_{\text{del}} \int_0^{T_{\text{mod}}/2} \sum_{m=0}^K A_m \cos \left( 4\pi m \frac{1}{T_{\text{mod}}} \right) \left( K_{MC} k_U + 2 a k_U^2 t \right) dt \quad (5.36)$$

After transformations and changing the variables, we obtain:

$$\begin{aligned} S &= \frac{T_{\text{mod}}}{\pi} K_W K_{MC} k_U t_{\text{del}} \sum_{m=0}^K A_m \int_0^{\pi} \cos(2mx) dx \\ &\quad + \frac{T_{\text{mod}}^2}{(2\pi)^2} K_W 4 t_{\text{del}} a k_U^2 \sum_{m=0}^k A_m \int_0^{\pi} x \cos x (2mx) dx \end{aligned} \quad (5.37)$$

where  $x = 2\pi t/T_{\text{mod}}$ .

Using the table integral from [9], we obtain:

$$S = T_{\text{mod}} K_W K_{MC} k_U t_{\text{del}} A_0 + \frac{T_{\text{mod}}^2}{2} K_W t_{\text{del}} a k_U^2 A_0 \quad (5.38)$$

Taking into account that  $k_U T_{\text{mod}}/2 = U_{\text{mod}}$ , we can write:

$$S = 2 t_{\text{del}} \left( U_{\text{mod}} K_{MC} + U_{\text{mod}}^2 a \right) = 2 t_{\text{del}} \Delta F \quad (5.39)$$

Thus, we see that at the quadratic MC nonlinearity the coefficient  $K_W = 1$ , which coincides with simulation results described in the previous section.

### 5.5.2 Oscillating Nonlinearity of the Modulation Characteristic

Taking into account (5.1), at the oscillating MC nonlinearity, the difference frequency from (1.10) is defined by the equation:

$$F_{DFS}(t) = t_{\text{del}} \{ K_{MC} k_U + b d k_U \cos[d(k_U t + U_{\text{init}})] \} \quad (5.40)$$

From here

$$S = K_W 2t_{\text{del}} \sum_{m=0}^K A_m \int_0^{T_{\text{mod}}/2} \cos\left(2\pi m \frac{2t}{T_{\text{MOD}}}\right) \{K_{\text{MC}} k_U + bdk_U \cos[d(k_U t + U_{\text{init}})]\} dt \quad (5.41)$$

After transformations and changing the variables, we obtain:

$$\begin{aligned} S &= T_{\text{mod}} K_W K_{\text{MC}} k_U t_{\text{del}} A_0 + K_W t_{\text{del}} bdk_U \frac{T_{\text{mod}}}{\pi} \\ &\times \sum_{m=0}^K A_m [\cos(dU_{\text{init}}) \int_0^\pi \cos(2mx) \cos(vx) dx - \sin(dU_{\text{init}}) \int_0^\pi \cos(2mx) \sin(vx) dx] \end{aligned} \quad (5.42)$$

where  $v = dk_U T_{\text{mod}}/(2\pi)$  and  $x$  is defined as in (5.37).

As a result of integration and simple transformations, we obtain:

$$\begin{aligned} S &= 2K_W U_{\text{mod}} t_{\text{del}} \left\{ K_{\text{MC}} A_0 + bd \{\sin[d(U_{\text{init}} + U_{\text{mod}})] - \sin(dU_{\text{init}})\} \right. \\ &\left. \times \sum_{m=0}^K A_m \frac{dU_{\text{mod}}}{(dU_{\text{mod}})^2 - (2\pi m)^2} \right\} \end{aligned} \quad (5.43)$$

where  $U_{\text{mod}}$  is the amplitude of saw-tooth voltage defined according to (5.4).

Taking into account (2.4), from (5.43) we can obtain that

$$\begin{aligned} K_{\text{WF}} &= \frac{K_W U_{\text{mod}}}{\Delta F} \left\{ K_{\text{MC}} A_0 + bd \{\sin[d(U_{\text{init}} + U_{\text{mod}})] \right. \\ &\left. - \sin(dU_{\text{init}})\} \times \sum_{m=0}^K A_m \frac{dU_{\text{mod}}}{(dU_{\text{mod}})^2 - (2\pi m)^2} \right\} \end{aligned} \quad (5.44)$$

In this case the coefficient  $K_{\text{WF}}$  depends in a complex manner upon parameters of oscillating MC components and WF parameters. Calculations of this coefficient according to (5.44) with the parameters of the MC nonlinearity, which were used at simulation of DFS processing in Section 5.3, allows the construction of plots, as shown in Figure 5.10. This confirms the correctness of the obtained formulas and allows a conclusion about the practical possibility of the coefficient correction  $K_{\text{WF}}$  included in (2.5) for measuring the range at the known parameters of the MC nonlinearity.

### 5.5.3 Quadratic and Oscillating Nonlinearity of the Modulation Characteristic

Repeating computations used at derivation of (5.39) and (5.44), we may obtain the following equation:

$$\begin{aligned} K_{\text{WF}} &= \frac{K_W U_{\text{mod}}}{\Delta F} \left\{ A_0 (K_{\text{MC}} + aU_{\text{mod}}) \right. \\ &\left. + bd \{\sin[d(U_{\text{init}} + U_{\text{mod}})] - \sin(dU_{\text{init}})\} \frac{\sum_{m=0}^K A_m dU_{\text{mod}}}{(dU_{\text{mod}})^2 - (2\pi m)^2} \right\} \end{aligned} \quad (5.45)$$

From this we can see that in this case all parameters of the MC nonlinearity influence the value of  $K_{WF}$ .

## 5.6 Estimation of the Correction Coefficient According to the Operating Difference-Frequency Signal

The time function of the difference frequency at presence in MC of quadratic and one oscillation component has a view:

$$F_{DFS} = t_{del} \left\{ K_{MC} k_U + 2ak_U^2 t + bdk_U \cos[d(k_U t + U_{init})] \right\} \quad (5.46)$$

This formula looks like (5.1) on its structure. The difference is that the quadratic component is absent and the multiplication  $t_{del}$  defined by the measuring range is present. Therefore, we suggest using the algorithm of the MC parameter determination according to the measured time function of the difference frequency on the basis of the method described in Section 5.1.

### 5.6.1 The Algorithm Sequence

The algorithm sequence is the following:

- *Step 1:* According to the measured DFS, the function of the difference frequency period  $T_{DFS}$  versus time is determined.
- *Step 2:* The translation of the period into the difference frequency  $F_{DFS} = 1/T_{DFS}$  is provided.
- *Step 3:* According to the found function, on the basis of linear regression, with the help of the approximation on the least-square method [5], the parameters of the linear trend (dc component  $f_{DC}$  and the slope coefficient  $k_f$ ) are obtained.
- *Step 4:* The parameters of linear and quadratic MC components are determined with the help of equating the appropriate items in (5.47) to the found parameters of the linear trend

$$K_{MC} = f_{DC} / (t_{del} k_U) \quad (5.47)$$

$$a = k_f / (2t_{del} k_U^2) \quad (5.48)$$

- *Step 5:* The linear trend is subtracted from the obtained time function of the difference frequency.
- *Step 6:* The frequency  $F$ , the oscillation amplitude  $\Delta F_{osc}$ , and the phase  $\varphi$  are determined from the obtained oscillating component of time function of difference frequency using the method described in Section 5.1.
- *Step 7:* MC oscillating component parameters are obtained according to the determined parameters:

$$d = 2\pi F/k_U \quad (5.49)$$

$$b = \Delta F_{\text{osc}}/(dk_U t_{\text{del}}) \quad (5.50)$$

$$U_{\text{init}} = (\varphi + 0.5\pi)/d \quad (5.51)$$

The unknown parameter  $t_{\text{del}}$  is included in these formulas. Therefore, similar calculations can be performed only at the calibration of the device for range known in advance and use these parameters for the correction coefficient  $K_{\text{WF}}$  included in (2.5).

However, a possibility to estimate the MC nonlinearity parameters and their consideration in the operating mode has a practical interest at each range measurement. In this case the measuring range and, hence,  $t_{\text{del}}$ , is unknown. It is expedient to determine such a formula for the estimation of  $K_{\text{WF}}$ , in which  $t_{\text{del}}$  is absent. The value of the FM sweep  $\Delta F$  is included in the denominator of (5.45). Using (5.1), we connect the FM sweep with nonlinearity parameters:

$$\begin{aligned} \Delta F &= K_{\text{MC}} U_{\text{mod}} + a U_{\text{mod}}^2 \\ &+ \sum_{n=1}^M b_n \{ \sin[d_n(U_{\text{mod}} + U_{\text{init},n})] - \sin(d_n U_{\text{init},n}) \} \end{aligned} \quad (5.52)$$

Substituting this equation into (5.45) and using estimations (5.47) to (5.51) as the parameters of the MC nonlinearity, we can obtain the following formula for  $K_{\text{WF}}$ , which in our case of the quadratic and one MC oscillating component has the view:

$$K_{\text{WF}} = \frac{K_{\text{W}} \bar{F} \left\{ A_0(2\bar{f}_n + \bar{k}_f) + 2\bar{F}\Delta\bar{F}_{\text{osc}} [\sin(\bar{F} + \varphi) - \sin \varphi] \sum_{m=0}^N \frac{A_m}{\bar{F}^2 - (2\pi m)^2} \right\}}{\bar{F}(\bar{f}_n + \bar{k}_f) + 2\Delta\bar{F}_{\text{osc}} [\sin(\bar{F} + \varphi) - \sin \varphi]} \quad (5.53)$$

where  $\bar{F} = FT_{\text{mod}}/2$ ,  $\bar{f}_{\text{osc}} = f_{\text{osc}}T_{\text{mod}}/2$ ,  $\bar{k}_f = k_f(T_{\text{mod}}/2)^2$ ,  $\Delta\bar{F}_{\text{osc}} = \Delta F_{\text{osc}}T_{\text{mod}}/2$  are normalized estimations. This expression can be used for the correction of the results at each range measurement.

The effectiveness of such a correction was checked with the help of simulation. Figure 5.12 shows the functions of the logarithm of averages error square versus normalized range for hypothetical case of completely known MC nonlinearity parameters, that is, obtained using the accurate value of  $K_{\text{WF}}$  calculated according to (5.46), and the noncorrected results.

### 5.6.2 Simulation Conditions

The simulation conditions are the following:

1. The MC nonlinearity parameters  $K_{\text{MC}} = 70 \text{ MHz/V}$ ;  $a = 2 \text{ MHz/V}^2$ ,  $b = 2 \text{ MHz}$ ,  $d = 2 \text{ rad/V}$ ,  $U_{\text{init}} = 3 \text{ V}$ ;
2. WF (2.19) for  $n = 1, 2$ , and  $4$ ;
3. MC parameter estimation and calculation of  $K_{\text{WF}}$  according to (5.53) were provided at each measurement.

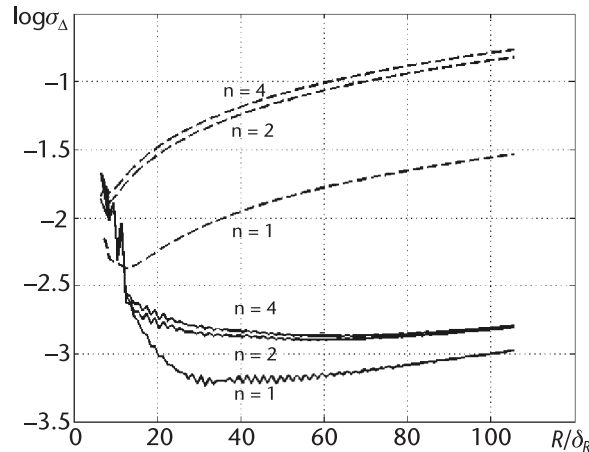


**Figure 5.12** Plots of the logarithm of the average error square versus normalized range. The dotted line is the noncorrected error, and the solid line is the corrected error.

We see that for each WF there is a minimal range beginning from when it is expedient to provide a correction. At a large range, the error decreases from units to tens of units depending on the WF type and the achieved error corresponds to the requirement for this equipment.

## 5.7 Compensation of Modulation Characteristic Nonlinearity

Let us show a possibility for adaptive linearization of the MC of the SHF oscillator for FMCW RF on the basis of parameter analysis of received signals [10] and determine the quantitative estimation of linearization quality. This can be done by relying on the fact that we are discussing the measurement of small ranges, when the signal delay  $t_{\text{del}}$  is a negligible quantity compared with the modulation period  $T_{\text{mod}}$ . Using (1.8), we can write the difference signal phase  $\varphi_{\text{dif}}(t)$  at the output of the FMCW RF mixer in the form:

$$\varphi_{\text{dif}}(t) = 2\pi f_0 t_{\text{del}} + 2\pi f(t)t_{\text{del}} \quad (5.54)$$

Thus, there is the function of frequency variation of the oscillator in the phase of the difference signal. Therefore, analyzing the difference signal, we can reveal deviations of the practical function of the frequency variation from the required function. After that, we can calculate the correcting voltage  $u_{\text{corr}}(t)$  according to this deviation, which changes in such a manner to compensate unwanted variations and to provide correction of modulating voltage  $u_{\text{mod}}(t)$ , adding the correcting value to this.

Let us present the MC of the oscillator as a sum of linear  $f_l(u)$  and nonlinear  $f_{\text{nl}}(u)$  parts:

$$f(u) = f_l(u) + f_{\text{nl}}(u) = K_{\text{MC}}u + f_{\text{nl}}(u) \quad (5.55)$$

According to this, the modulating voltage can be presented as:

$$u_{\text{mod}}(t) = u_l(t) + u_{\text{corr}}(t) = K_u t + u_{\text{corr}}(t) \quad (5.56)$$

where  $K_u = 2U_{\text{mod}}/T_{\text{mod}}$  is the slope of linear part increase of the modulating voltage and  $U_{\text{mod}}$  is the amplitude of modulating voltage.

Equation (5.55) can be rewritten in the form [10–12] taking into consideration (5.56):

$$f(u) = [K_{\text{MC}}u_{\text{corr}}(t) + f_{\text{nl}}(u) + f'_{\text{nl}}(u)u_{\text{corr}}(t)] + K_{\text{MC}}u_l(t) \quad (5.57)$$

In this equation the nonlinear MC part is presented in the form of first expansion items in a series in vicinity the point  $u(t)$ . To change the frequency linearly, it is necessary that the expression in the square brackets of (5.57) would be equal to zero. From this we obtain:

$$u_{\text{corr}}(t) = -f_{\text{nl}}(u)/K_{\text{MC}} + f'_{\text{nl}}(u) \quad (5.58)$$

Taking (1.10) into account, we can present the instantaneous period of the difference signal  $T_{\text{DFS}}(t)$  using the similar expansion in a series as:

$$\begin{aligned} T_{\text{DFS}}(t) &= \frac{1}{F_{\text{DFS}}(t)} = \frac{1}{[f_l(t) + f'_{\text{nl}}(t)]t_{\text{del}}} \\ &\approx \frac{1}{f_l(t)t_{\text{del}}} - \frac{f'_{\text{nl}}(t)}{[f_l(t)]^2 t_{\text{del}}} = T_{\text{DFS},l} + \Delta T_{\text{DFS}}(t) \end{aligned} \quad (5.59)$$

where  $T_{\text{DFS},l}$  is the period of DFS caused by the linear MC part,  $\Delta T_{\text{DFS}}(t)$  is the DFS variation caused by the nonlinearity of the modulation characteristics.

Using (5.55) and (5.56), we can rewrite (5.59) as:

$$T_{\text{DFS}}(t) = \frac{1}{K_{\text{MC}}K_u^2 t_{\text{del}}} - \frac{1}{K_{\text{MC}}^2 K_u^2 t_{\text{del}}} \frac{df_{\text{nl}}}{dt} \quad (5.60)$$

From (5.59) and (5.60), we can obtain:

$$\frac{df_{\text{nl}}}{dt} = f'_{\text{nl}}(t) = -\Delta T_{\text{DFS}}(t)K_{\text{MC}}^2 K_u^2 t_{\text{del}} \quad (5.61)$$

From this we have:

$$f_{\text{nl}}(t) = -K_{\text{MC}}^2 K_u^2 t_{\text{del}} \int_0^t \Delta T_{\text{DFS}}(t) dt \quad (5.62)$$

We should note the voltage derivative of the nonlinear MC part is included in (5.57), and the time derivative is included in (5.61). Replacing approximately the modulation voltage derivative by the constant quantity equal to the average slope  $K_u$ , we obtain:

$$f'_{\text{nl}}(t) = -K_{\text{MC}}^2 K_u t_{\text{del}} \Delta T_{\text{DFS}}(t) \quad (5.63)$$

Having substituted (5.61) and (5.63) in (5.57), we obtain:

$$u_{\text{corr}}(t) = \frac{K_{\text{MC}}K_u^2 t_{\text{del}} \int_0^t \Delta T_{\text{DFS}}(t) dt}{1 - K_{\text{MC}}K_u t_{\text{del}} \Delta T_{\text{DFS}}(t)} \quad (5.64)$$

It follows from this equation that to form the correcting voltage it is necessary to know the wanted averaged MC slope, the average slope of modulating voltage increase, and the measuring range. The necessity of the current range consideration complicates this procedure; however, we can eliminate it if introducing the normalized value of irregularity of the difference frequency period  $\eta(t)$ , which can be rewritten from (5.58) and (5.59) as:

$$\eta(t) = \Delta T_{\text{DFS}}(t)/T_{\text{DFS},I} = K_{\text{MC}} K_u t_{\text{del}} \Delta T_{\text{DFS}}(t) \quad (5.65)$$

In this case, (5.64) can be simplified:

$$u_{\text{corr}}(t) = \frac{K_u \int_0^t \eta(t) dt}{1 - \eta(t)} \quad (5.66)$$

The quantity  $\eta(t)$  is less than 1 and for small values of irregularity we can neglect the second item in the denominator of (5.66). These equations are approximate due to accepted assumptions. Due to this reason, it is impossible to compensate the MC nonlinearity by the one-pass calculation of  $u_{\text{corr}}(t)$ .

The procedure of modulating voltage formation is recurrent and is performed by several iterations. During an irregularity decrease of the difference signal periods, the accuracy of (5.66) increases. Therefore, the minimum search of the following functional is provided:

$$S = \max[\eta(t)] \quad (5.67)$$

at the limitations  $\Delta F = \text{const}$ ,  $T_{\text{mod}} = \text{const}$  and for formation of modulating voltage as:

$$u_{\text{mod},k}(t) = u_l(t) + \alpha u_{\text{corr},k}(t) \quad (5.68)$$

where  $u_l(t) = U_{\text{DC}} + K_u t$ ,  $u_{\text{corr},k}(t) = u_{\text{corr},(k-1)}(t) + \Delta u_{\text{corr},k}(t)$  is the correcting voltage obtained at the  $k$ th iteration,  $u_{\text{corr},(k-1)}(t)$  is the correcting voltage obtained at  $k-1$ -th iteration,  $\Delta u_{\text{corr},k}(t)$  is an increment of the correcting voltage calculated according to (5.66) on the  $k$ th stage, and  $\alpha = 0 \dots 1$  is the smallness parameter.

The practical implementation of this procedure assumes microprocessor application in the processing equipment and has some peculiarities. In particular, at the experimental determination of the function  $T_{\text{DFS}}(t)$ , the discrete function  $T_{\text{DFS},i}$  is determined by the measurement of current time intervals between adjacent DFS zeroes  $T_{\text{zero},i}$ :

$$T_{\text{DFS},i} = T_{\text{zero},i} - T_{\text{zero},i-1} \quad (5.69)$$

is the duration of the  $i$ th instantaneous DFS period.

Owing to the fact that the DFS frequency is changing continuously, discrete samples  $T_{\text{DFS},i}$  represent some average quantity. Therefore, these samples and, hence, samples of correcting voltage  $u_{\text{corr},i}$  are reasonable to correlate with the correction moments  $T_{\text{corr},i}$  located in the middle of the appropriate interval between two zeroes:

$$T_{\text{corr},i} = [T_{\text{zero},i} + T_{\text{zero},i-1}]/2 \quad (5.70)$$

Here  $T_{\text{corr},i}$  is a time moment, at which calculation of the correcting voltage is performed.

It is advisable to provide the modulation in such a manner that beyond the limits of time interval interesting for us that we call the analysis interval  $T_{an}$  the two DFS zeros minimum would be formed. It is necessary for the fact that beyond the limits of the analysis interval the one correction point at least will be formed reliably from each side. Therefore, the FM sweep of the SHF oscillator becomes more than the required FM sweep  $\Delta F$ ; however, we suppose that inside the analysis interval the FM sweep is provided by the value  $\Delta F$ . At the origin of time reckoning, we attach to the beginning of this interval, which can be done using frequency marks formed with the help of dielectric resonators [13]. As a result, the discrete function (5.69) contains  $N$  DFS zeros:

$$N = \text{int}\left(\frac{4\Delta FR}{c}\right) + 4 \quad (5.71)$$

At the maximal range,  $N$  can achieve the values of 200 to 300.

For each new  $k$ th iteration, the position of  $i$ th correction point  $T_{\text{corr},k,i}$  on the time axis may differ from the  $i$ th point  $T_{\text{corr},k-1,i}$  obtained on the previous ( $k - 1$ ), the iteration as the modulation voltage variation occurs. Therefore, beginning from the second iteration, it is necessary to provide translation of the correcting voltage from points of the previous step to points of the current step using the interpolation and extrapolation formulas:

The total correcting voltage can be obtained by summation in new time points of correction  $T_{\text{corr},k,i}$  of old and new values:

$$\begin{aligned} u_{\text{corr},k}(T_{\text{corr},k,i}) &= \bar{u}_{\text{corr},(k-1)}(T_{\text{corr},(k-1),i}) \\ &\quad + \Delta u_{\text{corr},k}(T_{\text{corr},k,i}) \end{aligned} \quad (5.72)$$

where  $\Delta u_{\text{corr},k}(T_{\text{corr},k,i})$  is the correcting voltage on  $k$ th iteration calculated according (5.66), which can be written in the discrete form:

$$\Delta u_{\text{corr},i} = \frac{K_u \sum_{i=1}^N \eta_i T_{\text{DFS},i}}{1 - \eta_i} \quad (5.73)$$

where  $\eta_i = (T_{\text{DFS},i} - T_{\text{DFS,aver}})/T_{\text{DFS,aver}}$  and  $T_{\text{DFS,aver}} = \sum_{i=1}^N T_{\text{DFS},i}/N$ .

After similar translation at each iteration, it is necessary to provide variation of correcting voltage in such a manner to remain the boundary tuning frequencies of SHF oscillator. These values of modulating voltage should remain unchanged in extreme points of the modulation interval. Variation is provided with the help of elimination of the constant value  $u_{\text{corr},k}(0)$  from the correcting voltage, which is equal to the value and further multiplication of the voltage [calculated according to (5.68)] by the correcting coefficient:

$$K_{\text{corr}} = U_{\text{span}} / [U_{\text{span}} + u_{\text{corr},k}(T_{\text{span}})] \quad (5.74)$$

Here  $U_{\text{span}}$  is the span of the linear part of modulation voltage in time interval  $T_{\text{span}}$ .

The formation of the transmitted signal is already provided according to the new modulation voltage. Therefore, the generation of this voltage is carried out by the digital approach using a digital-analog converter on the basis of interpolation formulas.

The correction process may be not driven to obtain the accurate minimum of (5.67). It can be interrupted at the irregularity reduction of difference signal periods to the accepted value, which is defined by a sensitivity level to the residual nonlinearity of the chosen method of DFS processing. The iteration process of modulating voltage calculation can be presented as the following algorithm.

### The Correction Algorithm

The correction algorithm is as follows:

- *Step 1:* The linear modulating voltage is formed on the basis of (5.3). The modulating voltage amplitude is chosen in such a manner to form two zeros at each of side beyond the limits of time interval of DFS analysis  $T_{\text{an}}$ . Then the correcting voltage is equal to zero.
- *Step 2:* Based on the received signal, zeros  $T_{\text{zero},i}$  of DFS are determined.
- *Step 3:* Correction points are calculated according to (5.70) and DFS periods based on (5.69).
- *Step 4:* Increments of correcting voltage are calculated according to (5.73).
- *Step 5:* Using the interpolation and extrapolation formulas, the translation of the earlier calculated correcting voltage to the new correction points is performed.
- *Step 6:* The correction of modulating voltage is provided to keep the unchanged FM sweep using the correction coefficient (5.74).
- *Step 7:* The maximal absolute value of relative irregularity  $\eta_{\text{max}}$  is determined and is compared with the threshold value  $\eta_{\text{thr}}$ . If  $\eta_{\text{max}} > \eta_{\text{thr}}$ , the return to Step 2 is performed, and repeat of all steps until the reverse relation would be ensured.

As time goes by, MC nonlinearity can change, for instance, due to the variation of the environment. That is why it is expedient to perform regularly the new correction of nonlinearity using the current results of range measurement. Nevertheless, such a correction should be performed in the case only when there are a sufficient number of discrete points (not less than 10) in the estimating function  $T_{\text{DFS}}(t)$ . It is advisable that this procedure would be possible at any measured range inside the operating range of FMCW RF. With this purpose, it is necessary to choose the FM sweep in such a manner that at the least range during the modulation period, the necessary number of periods of DFS would be realized.

The effectiveness of such compensation and opportunities of its practical application was checked with the help of simulation of the range measurement

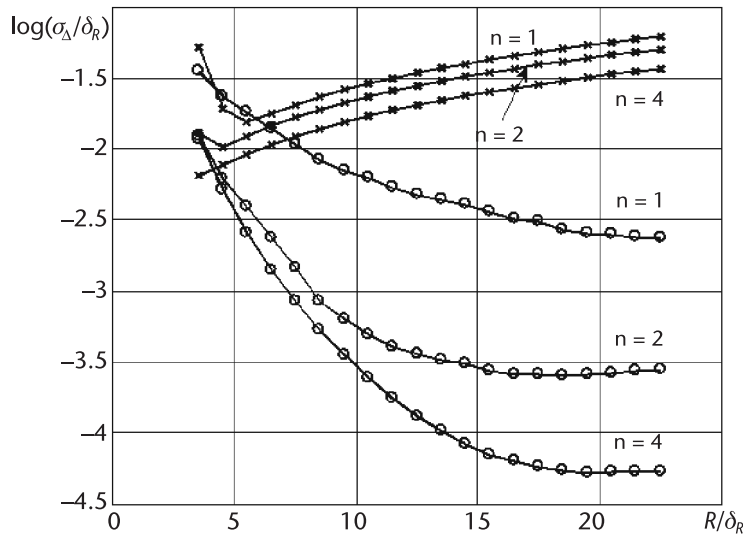


**Figure 5.13** Plots of the logarithm of rms error versus the normalized range for nonlinearity compensation (round marks) and without compensation (cross-shaped marks) for  $b = 10$  MHz and  $a = 2$  MHz/V<sup>2</sup>.

process with achieved irregularity levels and of comparison with results obtained without compensation for the same values of MC nonlinearity parameters. Simulation was performed at  $K_{MC} = 70$  MHz/V for three WFs, which were used earlier. The calculation of the compensating voltage was provided at the same range and samples of this voltage were stored. Then range measurement was simulated in the range from 4 to 23 discrete errors with the 1-mm step. At that simulation, generation of modulating voltage and, relatively, DFS was carried out using obtained samples of the correcting voltage. As a result of simulation, it is determined that for purely quadratic nonlinearity it is inexpedient to perform compensation because, as a result of this, instead of the smooth nonlinearity, the chaotic nonlinearity of the correcting voltage arises with some small level with the large frequency leading to an error increase.

In the worst case of the quadratic and oscillating nonlinearity presence, the benefit about two orders remains when using compensation, as we see from Figure 5.13. Therefore, there is a relative range, which is individual for different WFs, and if the range is less, the benefit will not be ensured.

A two-times increase of the FM sweep leads to a reduction of the total error level by four times.

Thus, the performed calculations prove the high effectiveness of the suggested algorithm of MC nonlinearity compensation.

## 5.8 Consideration of Modulation Characteristic Nonlinearity at Range Calculation

The consideration of the MC nonlinearity at calculation of range is possible by a means of measurement of appearance moments of DFS typical points inside of the modulation period. For this purpose, the additional formation of two pulse

signals (frequency marks) were provided in coinciding moments of the transmitted signal frequency with the lower  $F_{st1}$  and upper  $F_{st2}$  reference frequencies and measurement of its appropriate position  $t_{st1}$  and  $t_{st2}$ . Reference frequencies can be specified, for instance, with the help of high-Q dielectric resonators [13]. Control by modulating voltage is provided in such a manner to form one typical point beyond the analysis interval, which is equal to  $T_{an} = t_{st2} - t_{st1}$ . Two variants of processing these measurement results are possible [11, 12].

### 5.8.1 Estimation of Extreme Period Parts

The first variant of the MC nonlinearity consideration at range calculation can be suggested based on the method described in [14], where range is calculated according to the formula:

$$R = \frac{c}{2\Delta F}(k + x) \quad (5.75)$$

where  $k$  is a number of integer DFS periods inside the analysis interval and  $x$  is an additional amendment that is a reminder of the DFS half-period.

In contrast to [14], a sum of the integer number of DFS half-periods and the additional amendment will be calculated as [11, 12]:

$$k + x = \frac{2}{K_{WF}} \sum_{j=0}^k \alpha \left( \frac{2\pi t_{cal,j}}{T_{an}} \right) \quad (5.76)$$

where  $t_{cal,j} = (j + 1 - x_1)T_{aver}$  is calculated at the  $j$ th moment of DFS typical point appearance with the averaged period  $T_{aver}$  counting from the beginning of the analysis

interval,  $T_{aver} = \frac{T_{an}}{k - x_1 + x_2}$  is the average DFS period,  $T_{an} = t_{st2} - t_{st1}$  is the duration

of the analysis interval,  $x_1$  and  $x_2$  are normalized positions of extreme points of the analysis interval with respect to left boundaries of the appropriate DFS half-periods, and  $K_{WF}$  is the constant coefficient depending on the type of weighting function.

Let us designate through  $t_0, t_1, \dots, t_N$  and  $t_{N+1}$  the measured positions of typical points assuming that  $t_{st1}$  is located between  $t_0$  and  $t_1$ , and  $t_{st2}$  is between  $t_N$  and  $t_{N+1}$ . Using these designations, the normalized positions of the boundary points  $x_1$  and  $x_2$  can be calculated according to the values of  $t_{st1}$  and  $t_{st2}$  in different ways:

1. Linear extrapolation with the application of two typical point positions nearest to the lower and upper frequency marks used in [15];
2. Linear interpolation with the application of two typical point positions, between which the upper and lower marks are located;
3. Quadratic interpolation with the application of three typical point positions, between which the upper and lower marks are located;
4. Cubic spline interpolation.

A comparison of these variants was carried out using numerical simulation. The FM sweep of 500 MHz and  $K_{MC} = 70$  MHz/V are used for simulation. Typical plots are presented in Figure 5.14.

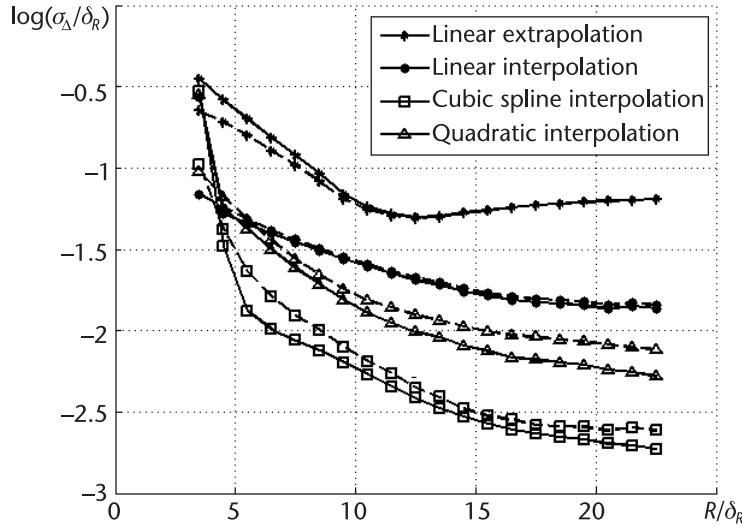


**Figure 5.14** The plot of the logarithm of normalized rms error versus normalized range for different variants of calculation of phase amendments for  $b = 1$  MHz,  $a = -1.5$  MHz/V<sup>2</sup>, and for various WFs (solid curve  $n=4$ , dotted curve  $n=1$ ).

We can note that for all variants of phase amendment calculation the absolute error level decreases at range grows. The worst results are achieved at application of the linear extrapolation of these amendments. The total error level ensured by each variant of phase amendment calculation may be changed by the order at the variation of nonlinearity parameters. The cubic spline interpolation method is strongly sensitive to nonlinearity parameters; however, it ensures on average the best result. The variant of quadratic interpolation has the less sensitivity and the linear interpolation has insignificant yields.

In the most cases, WF shape complication leads to error decrease. The degree of decrease oscillates from two to three to 10 to 15 times depending on the variant of phase amendment calculation and the sign of the parameter of quadratic nonlinearity. Most improvement is achieved at the spline interpolation and the positive values of the quadratic nonlinearity parameter.

Thus, the considered approach allows the consideration of the MC nonlinearity without the essential complication of FMCW RF structure at range calculation based on measurement results of DFS typical points position inside the modulation period.

### 5.8.2 Approximation of the Time Function of Signal Periods

In this variant, we consider that at fixed measured range and any external conditions the transmitter is tuned on the same frequency value  $\Delta f_m$  [11, 12] during time-keeping within any adjacent typical points of the beating signal. It can be explained by the fact that DFS phase increment  $\Delta\Phi$  is equal to  $\pi$  at transition from the one typical point to another (adjacent), that is, through one half-period, and for transition through  $m$  half-periods:

$$\Delta\Phi = 2\pi\Delta f_m t_{\text{del}} = 2\pi m \Delta f_1 t_{\text{del}} = m\pi \quad (5.77)$$

From this we obtain the calculation formulas for the measuring range:

$$R = \frac{vm}{4\Delta f_m} \quad (5.78)$$

where  $v$  is the speed of electromagnetic wave propagation under monitored surface.

To calculate  $\Delta f_m$  based on DFS, we can use the approximation of the time function of the transmitted signal by some function. The solution in the final form that we may obtain if we use the polynomial of  $n$  order is used for  $F(t)$  approximation:

$$F = \sum_{i=0}^n a_i t^i \quad (5.79)$$

where  $n + 1$  is a number of typical DFS points inside the modulation period used at the calculation and  $a_i$  are constant coefficients.

Using the measurement results of the function of appearance moments  $t_i$  of typical DFS points versus time and time positions  $t_{st1}$  and  $t_{st2}$  of two pulse signals obtained in the coincidence moments of reference and radiated frequencies, we can form the system of three linear equations with respect to  $n + 1$ th unknown coefficients  $a_i$ , the frequency of appearance of the first typical point  $F_1$  of DFS, and the FM sweep  $\Delta f_1$  between two adjacent typical DFS points.

In the matrix form this system has the form:

$$\begin{array}{cccccc|c|c} 1 & 0 & -1 & -t_0 & \dots & -t_0^n & F_1 & 0 \\ 1 & m_1 & -1 & -t_{m_1} & \dots & -t_{m_1}^n & \Delta f_1 & 0 \\ 1 & m_2 & -1 & -t_{m_2} & \dots & -t_{m_2}^n & a_0 & 0 \\ 1 & m_3 & -1 & -t_{m_3} & \dots & -t_{m_3}^n & a_1 & 0 \\ & \dots & & & & & \dots & \dots \\ 1 & m_n & -1 & -t_{m_n} & \dots & -t_{m_n}^n & a_{n-2} & 0 \\ 0 & 0 & 1 & t_H & \dots & t_{st1}^n & a_{n-1} & F_{st1} \\ 0 & 0 & 1 & t_B & \dots & t_{st2}^n & a_n & F_{st2} \end{array} \times = \quad (5.80)$$

where  $m_1, m_2, \dots, m_n$  are numbers of typical points used at calculation.

From this system we have:

$$\Delta f_1 = \frac{A_{n-1,2} F_{st1} + A_{n,2} F_{st2}}{\Delta} \quad (5.81)$$

where  $\Delta$  is the determinant of the coefficient matrix (5.80) and  $A_{i,j}$  is appropriate algebraic complement.

To form the equation system and to find the FM sweep  $\Delta f_1$ , any typical points from the measurement can be used. With measuring range increasing, beginning from minimal amount possible, a number of typical points increase continuously from the minimal value equal to 2. If, therefore, we consider in (5.80) all typical points, the equation system dimension also increases continuously. It is clear

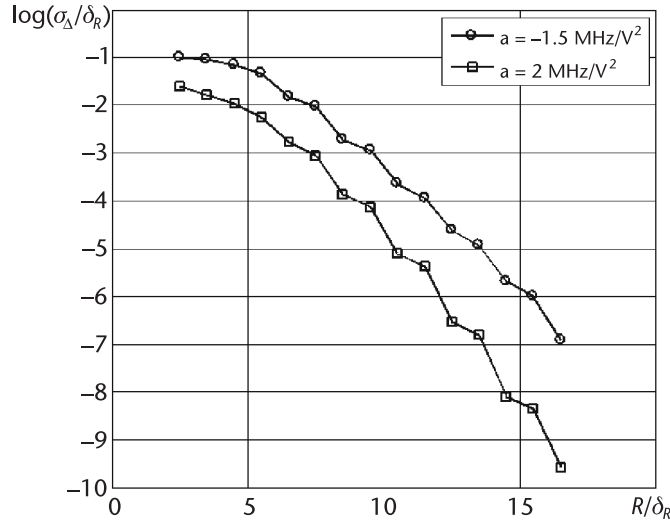


**Figure 5.15** Functions of the logarithm of normalized rms error versus normalized range at the matrix dimension not exceeding 14.

that the range measurement accuracy should increase as well. Nevertheless, simulation results show that the quadratic matrix included in (5.80) with the increasing dimension becomes ill-conditioned. Therefore, it is advisable to limit the dimension of this matrix by the value, at which this property is not noticeable. The simulation shows that the number of considered successively located typical points, at which the reliable solution of (5.80) is still possible, is equal to 14. This corresponds to the matrix dimension equal to 16. At a further range, increasing the matrix dimension is expedient to remaining unchanged.

Figure 5.15 shows the function of the logarithm of the normalized MSD versus the normalized range at the matrix dimension, which does not exceed 14, obtained by simulation of the measurement process based on solution the equation system (5.80). At the simulation we used the FM sweep of 500 MHz. Therefore, we assumed the following nonlinearity parameters:  $K_{MC} = 70 \text{ MHz/V}$ ,  $b = 10 \text{ MHz}$ ,  $d = 1 \text{ rad/V}$ , and  $U_{init} = 0 \text{ V}$ . The value of  $a$  was varied. The system solution in (5.103) is provided with the help of the standard function within the MATLAB system. We see that with the range increasing, the error decreases monotonically at any nonlinearity parameters.

In a practical realization, the matrix dimension can be limited by the value 10 to accelerate calculations. The error level, which can be achieved reliably, corresponds to the requirements typical for devices of this type.

## 5.9 Conclusions

The offered MC model and the method of its parameter determination according to experimental signals allow a performance of the analysis of the MC nonlinearity influence on the range measurement results.

On the basis of this model, formulas are obtained for estimation of the maximal error of the range measurement by means of the counting measurement method

caused by MC nonlinearity. It is shown that the FM sweep has a serious effect on small ranges only. At the measuring range, increasing the error level is determined completely by the MC parameters.

Three variants of the error level reduction are offered and are caused by the MC nonlinearity influence. All variants are based on the analysis of nonlinearity degree on instantaneous periods of operating DFS and they perform directly during the measurement.

The compensation of nonlinearity influence by means of variation of the scaling coefficient consists of the determination of the MC nonlinearity parameters, calculation of the coefficient, and computation of the range using this coefficient. Such a calculation can be carried out sufficiently through some time intervals, during which the nonlinearity degree does not change essentially, for example, at each FMCW RF activation or at a significant change of environment temperature because the nonlinearity degree changes at temperature variation.

The method of the MC nonlinearity compensation according to estimation of irregularity degree of DFS periods allows a reliable reduction of the range measurement error up to the accepted value. It consists of the determination of predistortions introduced in the modulating voltage, storing these predistortions in the device memory, and the performance of measurement, taking into account these values. The periodicity of the compensating voltage upgrade is the same as in the previous point.

The consideration of the MC nonlinearity based on the position of the extreme or all typical points at the range calculation should be carried out for each measurement.

## References

- [1] Levin, O. A., V. N. Malinovskiy, and S. K. Romanov, *Frequency Synthesizers with the System of Pulse PLL*, Moscow: Radio i Sviaz Publ., 1989, 232 pp. [in Russian.]
- [2] Sventkovskiy, R. A., "Super-Resolution of Signals: Possibilities, Restrictions, Non-Autoregression Approach," *Radiotekhnika i Electronika*, Vol. 43, No. 3, 1998, pp. 288–292. [in Russian.]
- [3] Baranov, I. V., and V. V. Ezerskiy, "Digital Spectral Analysis of the Polyharmonic Signal," *Proceedings of 10th Intern. Conf. "Digital Signal Processing and Its Applications" (DSPA-2008)*, 2008, pp. 500–502. [in Russian.]
- [4] Baranov, I. V., V. V. Ezerskiy, and A. Y. Kaminskii, "Measurement of the Thickness of Ice by Means of a Frequency-Modulated Radiometer," *Measurement Techniques*, Vol. 51, No. 7, 2008, pp. 726–733.
- [5] Korn, G., and T. Korn, *Mathematical Handbook for Scientists and Engineers*, New York, Toronto, London: McGraw Hill Book Company, 1961.
- [6] HYPERLINK "<http://link.springer.com/search?facet-author=%22S.+A.+Labutin%22>" Labutin, S. A., HYPERLINK "<http://link.springer.com/search?facet-author=%22M.+V.+Pugin%22>" Pugin, M. V. HYPERLINK "<http://link.springer.com/article/10.1007/BF02503928>" Noise Immunity and Speed of Frequency Measurements of Short Harmonic Signals, *Measurement Techniques*, Vol. 41, No. 9, 1998, pp. 837–841.
- [7] Ezerskiy, V. V., B. V. Kagalenko, and V. A. Bolonin, "Adaptive Frequency-Modulated Level Meter. An Analysis of Measurement Error Components," *Sensors and Systems*, No. 7, 2002, p. 44. [in Russian.]

- [8] Vinitkiy, A. S., *Essay on Radar Fundamentals for Continuous-Wave Radiation*, Moscow: Sovetskoe Radio Publ., 1961, 495 pp. [in Russian.]
- [9] Gradstein, I. S., and I. M. Ryzhik, *Tables of Integrals, Sums, Series and Products*, New York: Academic Press, 1965.
- [10] Ezerskiy, V. V., I. V. Bolonin, and I. V. Baranov, “The Algorithm of Modulation Characteristic Non-Linearity Compensation for FMCW Range Finders,” *Vestnik RGRTA, Ryazan*, No. 10, 2002, pp. 38–42. [in Russian.]
- [11] Patent 2234716 (Russian Federation), INT. CL. G01 S 13/34. Method of Transmitted FMCW Signal Generation for the Range Finder with Periodic Frequency Modulation. / B. A. Atayants, I. V. Baranov, V. A. Bolonin, V. M. Davydochkin, V. V. Ezerskiy, B. V. Kagalenko, V. A. Pronin. No 2003105992/09; Filed 04.03.2003; Published 20.08.2004, Bull. 23.
- [12] Atayants, B. A., V. V. Ezerskiy, V. A. Bolonin, I. V. Baranov, V. M. Davydochkin, and V. A. Pronin, “Influence of Modulation Characteristic Non-Linearity of the Transmitter on Distance Measurement in Short-Range Radar,” *Information-Measurement and Control Systems*, Vol. 1, No. 2–3, 2003, pp. 50–56.
- [13] Ezerskiy, V. V., “Problems of Optimization of Modulation Voltage Control for FMCW Range Finder,” *Vestnik RGRTA*, No. 12, 2003, pp. 44–49. [in Russian.]
- [14] Marfin, V. P., V. I. Kuznetsov, and F. Z. Rosenfeld, “SHF Level-Meter,” *Pribory i Sistemy Upravleniya*, No. 11, 1979, pp. 28–29. [in Russian.]
- [15] Komarov, I. V., and S. M. Smolskiy, *Fundamentals of Short-Range FMCW Radar*. Norwood, MA: Artech House Publishers, 2003, 289 pp.

# Analysis of the Range Measurement Error at the Interference Presence

## 6.1 Introduction

We will consider as clutter any signal distorting the results of useful signal processing, which carries information about range to the UR, which must be measured. The influence of clutter signals formed by spurious reflections (SR) of any kind is the significant factor restricting the accuracy of range measurement. The reasons for these signals' appearance may be the presence of physical SRs in the operation zone of the FMCW RF as well as other factors. When the FMCW RF is used as a level-meter, the typical SRs are reflections from the construction elements, its sidewalls, the bottom, and multiple reflections between the surface of transmitted liquid in the reservoir and its roof. Hence, a variety of electric physical properties of target materials, constructive reservoir implementation, and measuring ranges lead to the fact that the useful signal amplitude can be both larger and smaller than amplitudes of numerous interferences. A significant excess of clutter amplitude over useful signal amplitude is observed at the probe on the nondeep layer of radio-transparent and weakly reflecting liquid on the background of interference from the reservoir bottom.

For example, Figure 6.1 shows the amplitude spectrum of DFS obtained at the level measuring of the strongly reflecting plane surface (metal, water) for the level-meter mounted on the reservoir with the plane metal roof. In this case, the normalized frequency of the useful DFS component is 35. From this spectrum, we see that useful SC is rounded by various SCs with different frequencies, which have amplitudes both lesser and larger than the useful SC amplitude. Moreover, all SCs are saturated by items not resolved in frequency. The presented signal spectrum gives a presentation about the complexity of the problem of ensuring the low error of the range estimation.

We note that restricted reservoir sizes lead to two additional specific components of the error. At large vertically standing reservoirs, the mounting places of industrial automation devices usually locate near the vertical wall of the reservoir. In this case, the intensive interference arises due to waves radiated and received by the antenna in the direction of the angle formed by the vertical reservoir wall and the liquid surface. The second SCs are caused by edge modes due to the restricted sizes of the probing surface. Difference frequencies of both SCs practically coincide and cannot be resolved with the difference frequency of the useful signal. Difference frequencies of these interferences vary synchronously with the difference frequency of the useful signal.

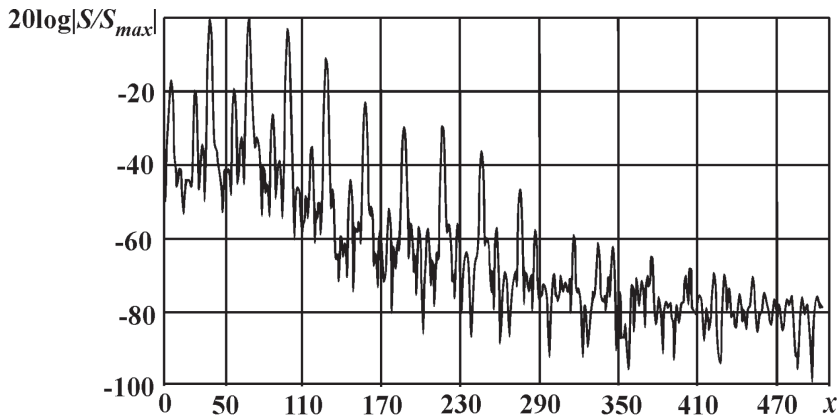


**Figure 6.1** A typical DFS spectrum for a level-meter mounted on a reservoir with a plane metal roof.

At insufficiently deep isolation of transmitting and receiving channels, the echo signal may create the frequency-dependent influence on the operating mode of the probe signal oscillator to cause the parasitic frequency modulation and, as a consequence, the measurement error. This influence should be connected with peculiarities of probing oscillator construction for elimination or reduction of the mentioned component of the measurement error down to accepted level.

One of the significant sources of the error is the transmitted signal reflection from numerous irregularities of the antenna-waveguide path (AWP). Constructive features of AWP are unavoidable due to necessity of its hermetic encapsulation. The reflection from AWP constructive elements always exists due to the impossibility of matching provision in the wide frequency band, and it creates interference with rather stable parameters. Nevertheless, after a time, the material of the probing medium and the water condensate deposits on the antenna and on AWP encapsulation elements, which usually leads to degradation of the matching level achieved earlier and to the appearance of new various combinational interference in the FMCW RF mixer.

The appearance of resonant reflections is possible in AWP caused by excitation of high types of waves and leading to a rise in clutter of the pulse character in DFS. The need for AWP encapsulation predetermines preferable application of waveguide paths with circular waveguides of variable sections, which often are subject to an increase of higher types of waves at parameter variations of encapsulating dielectric inserts due to deposition of evaporation products during operation.

For example, Figure 6.2 shows the DFS plot obtained from the level-meter, in which the dew appears on the encapsulated dielectric insert.

From this figure we see that useful DFS component (sinusoidal with high frequency) is received on the background of pulse and quasi-sinusoidal (slowly changing) interference due to reflections from AWP elements and is distorted by PAM, which usually accompanies the generated FMCW signal. PAM may appear as well due to frequency-dependent reflections from both the useful product and SR. In the latter case, functions characterizing PAM will be different for various objects.

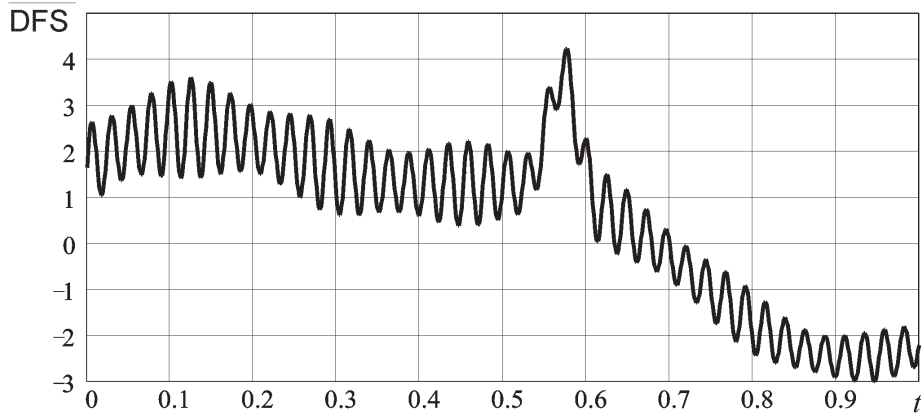


**Figure 6.2** DFS with pulse and quasi-sinusoidal interference caused by a reflection from AWP elements.

A variety of elements used in construction of a reservoir create a variety of scattered *electromagnetic waves* (EMW) and DFS components. Mathematical models of scattered EMW are obtained with a sufficient degree of conformity to real EMWs for some simple geometrical shapes only (for example, a sphere, a disk, or a dipole). At the same time, many regularities of the SR influence can be adequately described under assumption of delay time  $t_{\text{del},i}$  independence upon the transmitted signal frequency. Such assumption allows application for analysis the signal model in the form of a sum of useful and spurious components with PAM:

$$\begin{aligned} u_{\text{res}} = & U_{\text{us}}(t) \cos[\omega(t)t_{\text{del},\text{us}} - \varphi_{\text{us}}(t)] \\ & + \sum_{i=1}^M U_i(t) \cos[\omega(t)t_{\text{del},i} - \varphi_i(t)] + \xi(t) \end{aligned} \quad (6.1)$$

where  $M$  is the interference number created by SR with mentioned properties, the index “us” is the useful reflector,  $U_i(t)$  is the function characterizing PAM of the appropriate partial DFS, and  $\xi(t)$  is the white normal noise.

In particular, the time function of amplitude  $U_i(t)$  of the  $i$ th SC can be described in the form of a pulse with arbitrary duration  $T_p$  arising in the moment  $t_p$ ,  $U_i(t) \neq 0$  for  $t_p \leq t \leq t_p + T_p$  and  $U_i(t) = 0$  for  $t < t_p$ ,  $t > t_p + T_p$ . In this case the carrier frequency of radio pulse  $U_i(t) \cos [\omega(t)t_{\text{del},i} - \varphi_i(t)]$  is defined by electrical range to the  $i$ th source of reflection, and a phase is defined by frequency-dependent of the reflection coefficient.

This list does not cover all types of clutter, which affect the FMCW RF error; however, it shows the necessity of a DFS processing method search, which has sufficient resolving capability and allows estimation of potential opportunities of both traditional and original methods of difference frequency estimation.

The spectrum of any signal has a variety of damping SLs in the frequency domain. They superimpose on the main lobe of UR spectrum, distort its shape and maximum position, and, under definite conditions, may completely mask it.

Therefore, any method of frequency estimation leads to an increase in additional measurement error, in which the value decreases and the range increases between UR and SR under the condition of a small SL influence.

At DFS processing in the time domain due to the influence of spurious signal, there is inevitably an increase in DFS zero displacement and even the appearance of new ones. As a result, the range measurement error increases, in which the value depends upon the SR level and the range between UR and SR.

In all cases it is important to estimate the degree of range measurement accuracy decrease caused by interference influence and to formulate requirements to the admissible SR level.

Later we consider the normal probe of the object with the plane surface, for which the main radar equation [1] takes the extremely simple form:

$$P_{\text{rec}} = P_{\Sigma} |\dot{\Gamma}|^2 G^2 \eta_{\text{rec}} \eta_{\Sigma} \lambda^2 / (4\pi R)^2 \quad (6.2)$$

where  $P_{\text{rec}}$  is a power of the received signal,  $P_{\Sigma}$  is a power of the transmitted signal,  $\dot{\Gamma}$  is the reflection coefficient of EMW from the material of probing surface,  $G$  is the antenna gain (we assume that in transmitting and receiving modes these coefficients are equal),  $\eta_{\text{rec}}$ ,  $\eta_{\Sigma}$  are the efficiency of receiving and transmitting AWP, and  $\lambda$  is the wavelength of the carrying oscillation.

## 6.2 The Error Caused by the Single Spurious Signal of the Difference Frequency

### 6.2.1 Error Estimation According to the DFS Spectrum Maximum Position

Let us consider the range measurement error according to the difference signal frequency weighted with the help of the WF  $w(t)$ . Taking into consideration that all WF types, including those that are not expressed via elementary functions, can be represented or approximated by AWF, we perform analysis using AWF and general equations (A.15) to (A.18) for the SD, keeping the generally accepted names of the approximating functions.

Now we consider an effect of one spurious item on the range estimation error, neglecting by both a noise and the other interference. In the future, depending on signal/interference ratio (SIR), we use those pairs of (3.14) and (3.15) or (3.16) and (3.17), which ensure negligible errors of accuracy determination, for theoretical calculations of range measurement errors.

Figure 6.3 shows the results of the error calculation of the range estimation by a range finder with the 1,000-MHz FM sweep, the carrier frequency at 5 GHz, and the application of WF (2.19) with  $n = 1$  for two values of SIR.

The functions of the current measurement error  $\Delta R$  versus the range difference  $R_1 - R_2$  between UR and SR for  $q_{s/i} = 20$  dB and  $q_{s/i} = 30$  dB, respectively, are shown in Figure 6.3 by solid thin and bold lines. We see that in the SR vicinity there is an *increased error zone* (IEZ) symmetric with respect to its position. The IEZ width is connected with the width of the SD main lobe of used WF. The oscillating plot character is similar to Figure 3.2; however, the period of fast and slow oscillations is now twice more. The period of fast oscillations is equal to half of the average

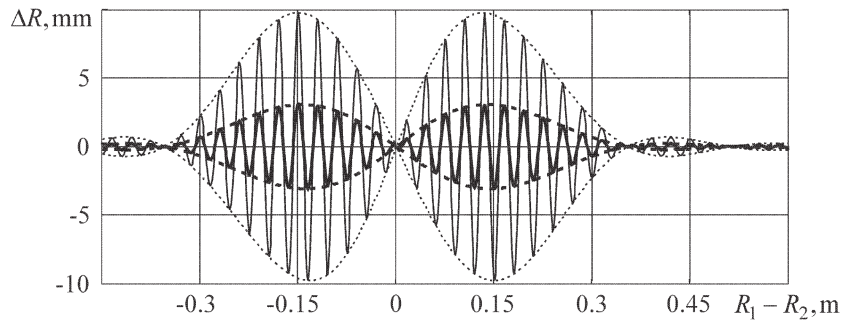


**Figure 6.3** Plots of the measuring error versus the range between UR and SR using the WF (2.19) with  $n = 1$ .

wavelength of the radiated signal, and the position of the zero error values depends upon the phase difference of reflection coefficients from UR and SR. The period of slow oscillations, which is independent on UR and SR properties, is connected with the periodicity of WF SL used at the DFS spectral analysis. At the high level of the SIR, the reduction of interference level does not lead to a proportional error decrease. If we assume that  $\cos[\omega_0(\tau_2 - \tau_1) - (\varphi_2 - \varphi_1)] = \pm 1$ , then, based on (3.14), (3.15), (3.16), and (3.17), we obtain the envelopes of fast *error oscillation* (EE), which are shown by dotted thin and bold lines, respectively, in Figure 6.3. These curves correspond to functions of the current measurement error. We mainly show the EE functions in the figures.

To illustrate the EE shape variation at the WF changing and FM sweep, Figure 6.4 shows the calculation results of logarithm of the envelope modulus of the normalized measurement error  $\log|\Delta x_{\text{EE}}|$  versus the range difference  $R_1 - R_2$  between the target and clutter using the Blackman WF (solid bold lines) and the Hamming WF (dotted lines) for  $q_{\text{SA}} = 10$  dB and the FM sweep  $\Delta f = 500$  MHz.

The functions of EE  $\Delta R_{\text{EE}}$  and  $\log|\Delta x_{\text{EE}}|$  have two main lobes caused by the interaction of signal SPD main lobes and clutter SPD, and a sequence of SL. In the point of range equality to the UR and SR, that is, for  $R_1 - R_2 = 0$ , the measurement error is equal to zero. At the unchanged SIR, the positions of the maxima of main

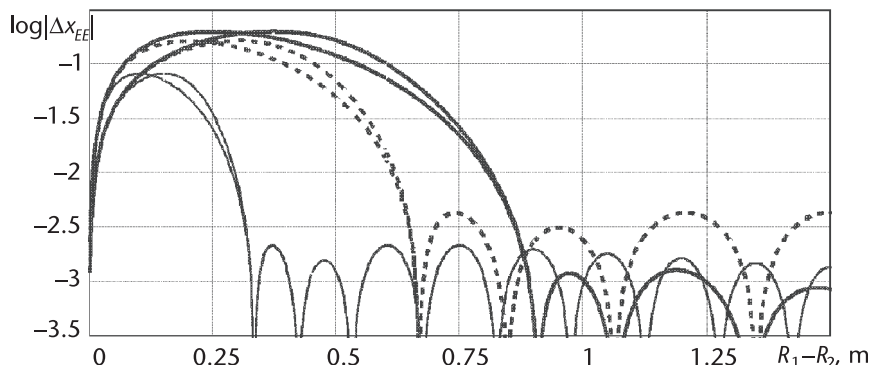


**Figure 6.4** Plots of the envelope modulus logarithm of the normalized error versus the range difference between UR and SR using the Blackman WF (solid bold lines) and the Hamming WF (dotted lines) for  $\Delta f = 500$  MHz and the Hamming WF for  $\Delta f = 1,000$  MHz (solid thin lines).

lobes, its level, and a width of main lobes as well as the EE SLL are connected with the width of the main lobe and of the EE SLL of the used WF. It is important to note that a decrease in the EE main lobe maxima is possible owing to a narrowing of the SD main lobe of used WF; however, at that EE, SLL usually grows. It is seen from a comparison of Figures 6.4 and 6.5.

In the range area corresponding to interaction of main lobes of signal and clutter spectra, the EE are nonsymmetrical with respect to an abscissa axis. EE asymmetry clearly becomes apparent for small SIR, which is demonstrated by Figure 6.5 for  $q_{s/i} = 0.4455$  dB,  $\Delta f = 1000$  MHz and for using of the uniform WF (solid curves) and the Blackman WF (dotted curves).

With  $q_{s/i}$  increasing, the asymmetry degree decreases (compare Figures 6.3 and 6.5) and for  $q_{s/i} \gg 1$  EE becomes practically symmetric with respect to the abscissa axis, and the maximal error decreases practically proportional to  $q_{s/i}$ . The increase of the FM sweep leads to an inverse proportional decrease of the maximal error and the width of both EE main and EE SL. The EE shape remains unchanged, and the function scale changes proportional to variation of FM sweep. Nevertheless, the shape of the instantaneous range measurement error function changes because in addition, a number of error oscillations in intervals between the EN change inversely proportionally.

### 6.2.2 Error Estimation at Signal Processing in the Time Domain

Let us consider the SR influence on the method of weighting average of difference frequency. At that, we take into account results of investigations of SR influence on the counting method of difference frequency estimation performed in [2]. This publication shows that the SR located near the UR creates a displacement of the DFS zero positions. The SR located far from the UR causes in some cases the increase of additional false zeros. The appearance of such zeros causes a large error and therefore it is not interesting from practical and theoretical points of view. In these cases, it is necessary to take additional measures on DFS filtering with the

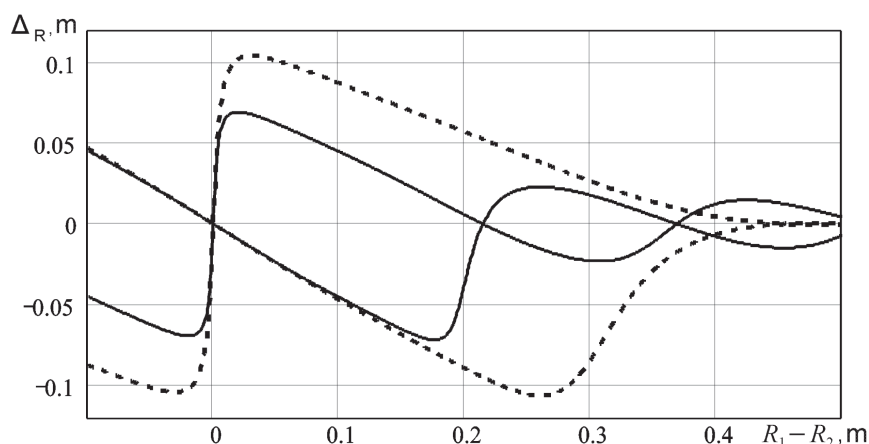


**Figure 6.5** Plots of EE versus range difference between UR and SR for  $q_{s/i} = 0.4455$  dB,  $\Delta f = 1,000$  MHz at the uniform WF (solid curve) and the Blackman WF (dotted curve).

purpose of decreasing the interference influence on measurement results. Therefore, we will only consider the situation in which interference leads to a displacement of the zero position.

The measurement error, as in Chapter 2, caused by influence of DFS zero displacement can be presented by (2.46). To use this equation in this case, it is necessary to determine the DFS zero displacement under interference action. Assuming that SIR is rather large, zero displacement is small, and expanding in the Taylor series the instantaneous value of the signal  $u_s(t)$  and interference  $u_{\text{int}}(t)$  in the DFS zero point  $t_i$ , we can write the equation for the zero displacement  $\Delta t_i$  determination:

$$u'_s(t_i)\Delta t_i + u_{\text{int}}(t_i) + u'_{\text{int}}(t_i)\Delta t_i = 0 \quad (6.3)$$

The solution of (6.3) is

$$\Delta t_i = \frac{-u_{\text{int}}(t_i)}{u'_s(t_i) + u'_{\text{int}}(t_i)} \quad (6.4)$$

For instantaneous values of the signal and interference, we can write:

$$\begin{aligned} u_s(t) &= A_s \cos[\omega_0 t_{\text{del},s} + \omega(t)t_{\text{del},s} + \varphi_s] \\ u_{\text{int}}(t) &= A_{\text{int}} \cos[\omega_0 t_{\text{del,int}} + \omega(t)t_{\text{del,int}} + \varphi_{\text{int}}] \end{aligned} \quad (6.5)$$

where  $A_s$ ,  $\varphi_s$ , and  $t_{\text{del},s}$  are, respectively, DFS amplitude, initial phase, and delay time caused by the UR;  $A_{\text{int}}$ ,  $\varphi_{\text{int}}$ , and  $t_{\text{del,int}}$  are, respectively, DFS amplitude, initial phase, and delay time caused by the SR.

Calculating the derivatives of (6.5) and substituting them into (6.4), we obtain after transformations:

$$\Delta t_i = \frac{\cos \psi_{\text{int}}(t_i)}{\omega'(t)\{q_{s/i} t_{\text{del},s} \sin \psi_s(t_i) + t_{\text{del,int}} \sin \psi_{\text{int}}(t_i)\}} \quad (6.6)$$

where  $\psi_s(t_i) = \omega_0 t_{\text{del},s} + \omega(t_i)t_{\text{del},s} + \varphi_s$ ;  $\psi_{\text{int}}(t_i) = \omega_0 t_{\text{del,int}} + \omega(t_i)t_{\text{del,int}} + \varphi_{\text{int}}$ ;  $q_{s/i} = A_s/A_{\text{int}}$ .

Future calculations are possible for specific WFs. We consider the WF in (2.9). Assuming that the FMCW is carried out under the symmetric triangle law, we obtain an equation for the normalized interference component of the range measurement error  $\Delta_{S,\text{int}}$ :

$$\Delta_{S,\text{int}} = -2\pi K_W \sum_{m=1}^K m A_m \sum_{i=1}^N \sin(2\pi m t_{\text{norm},i}) \Delta t_{\text{norm},i} \quad (6.7)$$

where  $\Delta t_{\text{norm},i} = \frac{\cos \psi_{\text{int}}(t_{\text{norm},i})}{2\pi \Delta F \{q_{s/i} t_{\text{del},s} \sin \psi_s(t_{\text{norm},i}) + t_{\text{del,int}} \sin \psi_{\text{int}}(t_{\text{norm},i})\}}$ ;

$\psi_{\text{int}}(t_{\text{norm},i}) = t_{\text{del,int}}(\omega_0 + \Delta \omega t_{\text{norm},i}) + \varphi_{\text{int}}$ , and  $\psi_s(t_{\text{norm},i}) = t_{\text{del,s}}(\omega_0 + \Delta \omega t_{\text{norm},i}) + \varphi_s$ .

Calculations according to this formula at a relative range to interference equal to  $10\delta_R$ ,  $q_{s/i} = 20$  dB, 10-GHz carrier frequency, and 2-GHz FM sweep are represented in Figure 6.6 by the solid bold curve.

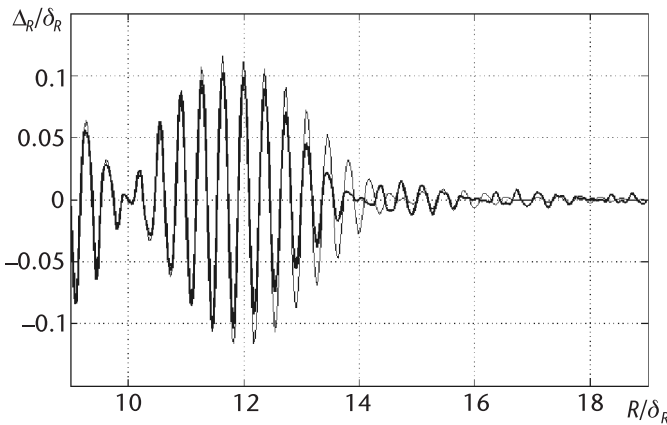


**Figure 6.6** The plot of the normalized interference error versus the relative range to the UR for  $n = 1$ .

For comparison, the normalized error at DFS processing in the spectral domain obtained under the same conditions is presented in this figure by a thin curve. It follows from Figure 6.6 that using two similar WFs for DFS processing on spectral and time domains, the shape of the normalized errors has the same character, but there are quantitative differences. At DFS processing in the spectral domain, the EE main lobe maximum is 10% higher and its width on the zero level is greater, but at that EE, the SLL is lower.

Both methods of the DFS processing acceptable for practice levels of the interference error, which can be neglected, are achieved at SIR of 40 to 45 dB.

### 6.3 The Error Caused by the Influence of Spurious Reflectors in the Antenna-Waveguide Path and in the Operating Zone of the FMCW Range-Finder

#### 6.3.1 Influence of the Frequency-Independent Spurious Reflectors in the AWP and in the Operating Zone of the FMCW RF

Let us analyze the influence of reflection from the single frequency-independent irregularity in the AWP and from the SR located in the FMCW RF operating zone assuming that amplitude of any DFS item is proportional to the SHF signal at the AWP input. Taking into consideration that the FMCW RF waveguide path length usually does not exceed some tens of centimeters, we can think that losses in it do not influence the SIR. In this case, we obtain that the amplitude of the DFS item created by an irregularity in the AWP is proportional to the reflection coefficient modulus  $|\dot{\Gamma}_{AWP}|$  from the AWP irregularity:

$$U_{AWP} = G_{s1} |\dot{\Gamma}_{AWP}| \sqrt{P_{inc}} \quad (6.8)$$

where  $G_{s1}$  is a coefficient of proportionality and  $P_{inc}$  is the power of incident electromagnetic wave in the AWP.

On the basis of (6.1), we determine the amplitude of the DFS item from the useful reflector  $U_s$ :

$$U_s = G_{s1} \sqrt{(1 - |\dot{\Gamma}_{AWP}|^2) P_{rec}} = G_{s1} G |\dot{\Gamma}| \lambda \sqrt{(1 - |\dot{\Gamma}_{AWP}|^2) \eta_{rec} \eta_{\Sigma} P_{\Sigma}} / 4\pi R_{ant} \quad (6.9)$$

where  $R_{ant}$  is range from the antenna phase center to the UR. Taking into consideration that AWP is performed in a rather well-matched way, we can think that  $(1 - |\dot{\Gamma}_{AWP}|^2) \eta_{rec} \eta_{\Sigma} P_{\Sigma} \approx P_{inc}$ . Then SIR  $q_{s/i,ant}$  can be written as:

$$q_{s/i,ant} = \frac{G |\dot{\Gamma}| \lambda}{4\pi R_{ant} |\dot{\Gamma}_{AWP}|} \quad (6.10)$$

Values of  $|\dot{\Gamma}_{AWP}|$  of the industrially manufactured FMCW RFs are 0.05 to 0.1. Evidently, the maximal possible value of  $q_{s/i,ant} \approx |\dot{\Gamma}| / |\dot{\Gamma}_{AWP}|$  will be, when on the minimal possible range (restricted by antenna size), the whole useful reflected signal received by the antenna. Values of  $|\dot{\Gamma}|$  are varied most frequently within the limits 0.17 to 1. Depending on the achievable AWP matching level and the reflection level from the UR, the maximal value of  $q_{s/i,ant}$  can be from 4.6 dB to 26 dB. However, at the necessity of the level measurement of weakly reflected liquids, for instance, cryogenic,  $q_{s/i,ant}$  can be significantly less than 0 dB at all ranges beginning from the antenna aperture with the encapsulated radome.

A proportional decrease of  $q_{s/i,ant}$  with the range increasing to the UR leads to the fact that beginning from some range,  $q_{s/i,ant} \ll 1$  at the input of the circuit for analogous signal processing. Because of this, in spite of the fact that with range increasing the useful signal and clutter are easily resolved, it is necessary to take clutter influence into consideration at the analysis of any of the methods used in DFS processing.

It is known that the problem of detection of resolving weak signals of the SD SL background of the strong signal is easily implemented using the WF  $w(t)$  [3]. In the case under consideration, there are some peculiarities. In particular, at the loading-level measurement in reservoirs, the function of echo-signal values versus the range defined by (6.2) significantly differs from the function of echo-signal values in traditional radar technology. That is why widely used WFs can be nonoptimal in the velocity  $C_s$  of the SD SL decrease, because redundant  $C_s$  inevitably increases the range measurement error at interference present.

Figure 6.7 shows calculated functions of the normalized EE for range measurement versus normalized range to probing plane surface at presence of single irregularity located in antenna aperture. The relative AWP length is assumed to be equal to 4; the antenna phase center coincides with its aperture; the reflection coefficient modulus from irregularity is equal to 0.2, and from the probing surface it is equal to 1. The SIR at the coincidence of the probing surface with antenna aperture is equal to 5. In calculations we used the AWF in (A.13) and (A.14) with  $N = 2$ . The varied zeros for two AWFs in (A.13) and one AWF in (A.14) are equal, respectively, to  $(b_1 = 2.014044, b_2 = 2.628)$ ,  $(b_1 = 2.06438, b_2 = 2.06438)$ , and  $(b_1 = 1.15122228, b_2 = \infty)$ . The EE SLL decrease speeds are equal, and that, respectively, 6 dB/oct is denoted by a dotted curve, 18 dB/oct is denoted by a solid thin curve, and 12 dB/oct is denoted by a solid bold curve.

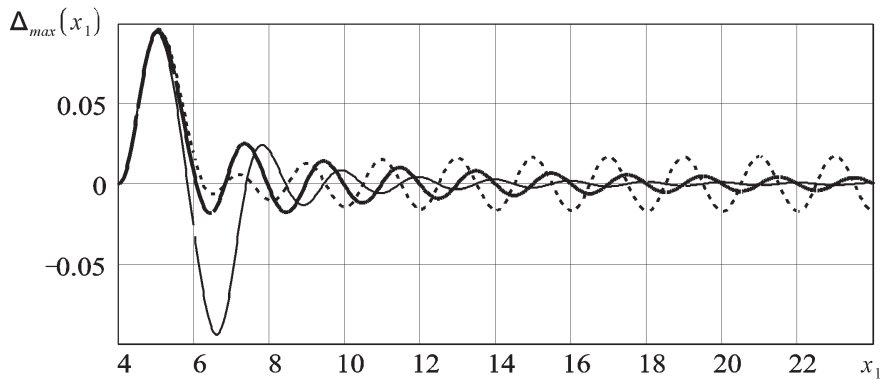


**Figure 6.7** Plots of the envelope of the normalized range estimation error caused by reflection from irregularity in the antenna aperture.

From Figure 6.7 we see the nondamping (with the range) EE character at the WF application with  $C_s = 6 \text{ dB/oct}$  with the lowest first SL of the EE function. When using the WF with  $C_s = 18 \text{ dB/oct}$ , the EE oscillations have fast damping but the first SL is commensurable in amplitude with the main lobe. Such a large level of the first SL is caused by the fact that at  $C_s = 18 \text{ dB/oct}$  the tendency of the decrease in the EE maximum  $F_{\text{env},\text{max}}$  up to 1.25 leads to the necessity of essentially narrowing the WF SD main lobe, due to which the first SD SL is sharply increased and, hence, the first EE SL. The application of the WF with  $C_s = 12 \text{ dB/oct}$  provides a damping character of the EE oscillations at a relatively small initial level.

At the application of the WF with  $C_s = 6 \text{ dB/oct}$ , the nondamping (with the range) character of this EE component caused by the reflection from the irregularity located in the AWP is reported on the range estimation error near the SR located far from the antenna in the measurement region. Calculation error functions under conditions similar to those shown in Figure 6.7 and with the same designations are shown in Figure 6.8 but, at present, of the SR in the measurement region at relative range 20. The SIR on the SR  $q_{s/i}$  at the range equality to the UR and the SR is equal to 10.

We see from Figure 6.8 that the nondamping oscillations of the range estimation error introduce the most additional error in the measurement result. At the

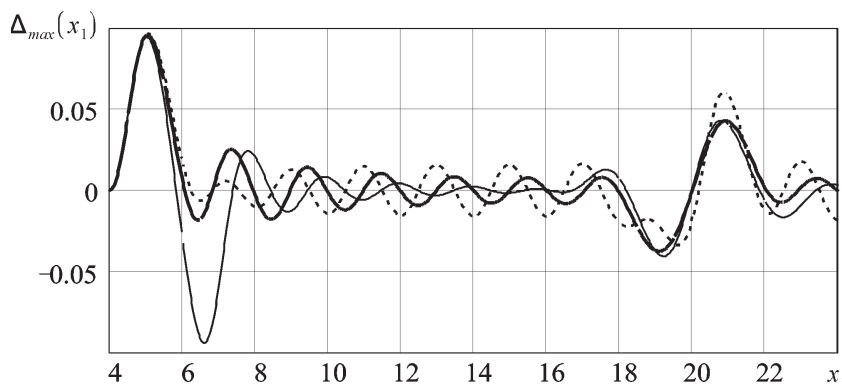


**Figure 6.8** Plots of envelopes of the normalized range estimation error caused by a reflection from irregularity in the antenna aperture and from the spurious reflector in the measurement region.

application of the WF with  $C_s = 12$  dB/oct and with  $C_s = 18$  dB/oct, the additional error is significantly less.

A choice of fixed WF parameters is usually made starting from the compromise between the width of the EE main lobe, the level of the maximal error, and the EE SLL. It should be noted that the AWF family in (A.14) in many problems of the range estimation to the plane surface can ensure the noticeable advantage in the resulting error due to possibility of obtaining an EE maximum that is not large with medium SD sidelobes increasing and, accordingly, EE SLL. At the probing of objects, for which the received signal power is inversely proportional to the fourth order of the range [1], the advantage is ensured by the WF with  $C_s = 18$  dB/oct. Such WFs are obtained from the AWF family in (A.13) by specification of one of the zeros on infinite relative frequency. In general, the probing object geometry and damping factor of the EMW in the space influence upon dependence of received signal power versus range. In this connection, a choice of the AWF family in (A.13) or (A.14) and specification of  $C_s$  in the real situation must be made on the basis of the speed analysis of the decrease of the received signal power.

### 6.3.2 Influence of the Spurious Reflection of the Pulse Character

In this case, it is not the nature of the increase in pulse interference that is interesting but the influence of the pulse parameters on the range measurement error; therefore, we use for analysis the pulse interference approximation, which allows us to obtain SAD analytical equations. We use the product of the sinusoidal function and the AWF as the signal mathematical model. Therefore, the pulse radio signal can be presented as:

$$u(t) = \begin{cases} q_{s/i} \cos \left[ (\omega_0 - \omega_{\text{dev}}) \tau_{\text{wg}} + 2\omega_{\text{dev}} \tau_{\text{wg}} \frac{t}{T_{\text{an}}} - \varphi_{\text{wg}}(t) \right] \times \\ \left\{ 1 + \sum_{n=1}^N C_{sn}(b_{11}, \dots, b_{1N}) \cos \left[ 2\pi n \left( \frac{t - t_p}{T_p} - 0.5 \right) \right] \right\} & \text{at } t_p \leq t \leq t_p + T_p \\ 0 & \text{at } t \leq t_p, t > t_p + T_p \end{cases} \quad (6.11)$$

where  $\omega_{\text{dev}} = \Delta\omega/2$  is the frequency deviation.

The signal CSD in (6.11) looks like this:

$$\begin{aligned} S(x) \frac{1}{q_{s/i}} &= e^{-j\Omega \left( t_p + \frac{T_p}{2} \right)} \frac{T_p}{2} \\ &\times \left\{ e^{j\varphi_{\text{wg}}} \operatorname{sinc}(\pi x_-) \left[ 1 + \sum_{n=1}^N C_{sn}(b_{11}, \dots, b_{1N}) \cos \left( n\pi \frac{x_-^2}{x_-^2 - n^2} \right) \right] \right. \\ &\left. + e^{-j\varphi_{\text{wg}}} \operatorname{sinc}(\pi x_+) \left[ 1 + \sum_{n=1}^N C_{sn}(b_{11}, \dots, b_{1N}) \cos \left( n\pi \frac{x_+^2}{x_+^2 - n^2} \right) \right] \right\} \end{aligned} \quad (6.12)$$

where  $\varphi_{\text{WG}} = (\omega_0 - \omega_{\text{dev}})\tau_{\text{WG}} - \varphi_{\text{WG,irr}}(t) + \Omega_{\text{WG}}(t_p + T_p/2)\}$ ,  $t_p$  is a moment of pulse start with duration  $T_p$ ,  $x_- = (x - x_{\text{WG}})/Q_{\text{off}}$ ,  $x_+ = (x + x_{\text{WG}})/Q_{\text{off}}$ ,  $x_{\text{WG}} = \Omega_{\text{WG}}T_{\text{an}}/2\pi$  is the normalized range to irregularity in the waveguide,  $Q_{\text{off}} = T_{\text{an}}/T_p$  is the off-duty factor of the pulse signal,  $T_{\text{an}}$  is the duration of the analysis interval (a half-modulation period at triangle law),  $\text{sinc}(\pi x) = \sin(\pi x)/\pi x$ ,  $\tau_{\text{WG}}$  and  $\varphi_{\text{WG,ref}}(t)$  is the delay of the transmitted wave at propagation in the waveguide to irregularity and back and the phase of reflected wave in the waveguide, respectively,  $\Omega_{\text{dif}} = 2\omega_{\text{dev}}\tau_{\text{WG}}/T_{\text{an}}$  is the difference frequency of the signal with the pulse envelope, and  $b_{11}, \dots, b_{1N}$  are specified AWF zeros, which approximate the envelope of the radio pulse signal.

We should pay attention to some SR peculiarities of the pulse character and its CSD, which are illustrated by (6.11) and (6.12). Because the duration  $T_p$  of the pulse character interference is essentially less than the FM period, and the SAD main lobe is significantly wider than useful signal SAD and is in conjunction with the fact that AWP length does not usually exceed some tens of centimeters, the modulus maximum of pulse interference SAD is the most used, located very close to zero frequency. Therefore, the AWP length has a significant effect on the SAD amplitude of the pulse interference due to the interaction of the SAD items from the areas  $\omega > 0$  and  $\omega < 0$ . This influence is illustrated by Figure 6.9, in which the CSD modulus in (6.7) is shown with  $Q_{\text{off}} = 20$  when using for the mathematical model of the pulse radio signal in (6.6) for  $N = 2$  and  $b_{11} = b_{12} = 2$ . The SD modulus of radio pulses are shown by the solid, dotted, and chain curves obtained in the AWP with the relative electric length to irregularity created the pulse interference equal to, respectively, 1.3827, 1.395, and 1.40741.

We see from Figure 6.9 more than tenfold variation of the SAD maximum of the radio pulse at variation of normalized range (position) to irregularity by 0.02471 (these irregularity positions are selected according to the influence maximum). The maximum of the SAD pulse is located on zero frequency if the doubled relative electric range is less than that resolving for the pulse of specified duration and shape. However, there are narrow zones of range to irregularity, when CSD items for  $\omega > 0$  and  $\omega < 0$  are antiphase and the CAD extreme is formed on zero frequency for a positive second derivative. The same figure shows by a thin solid curve the SAD of a radio pulse created by irregularity in AWP with relative electric length to irregularity equal to 40. The interaction of CSD items from areas  $\omega > 0$  and  $\omega < 0$  is weakened and the maximal value of SAD modulus is stable.

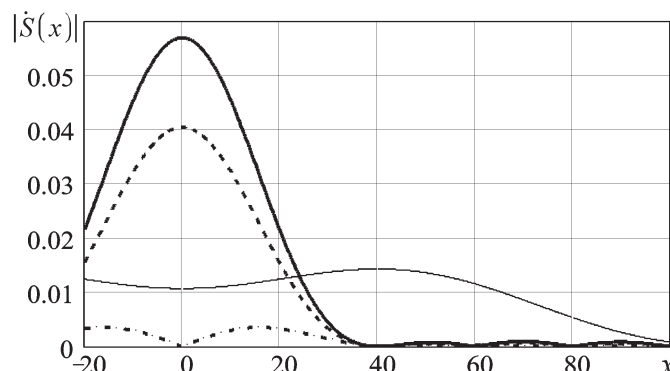
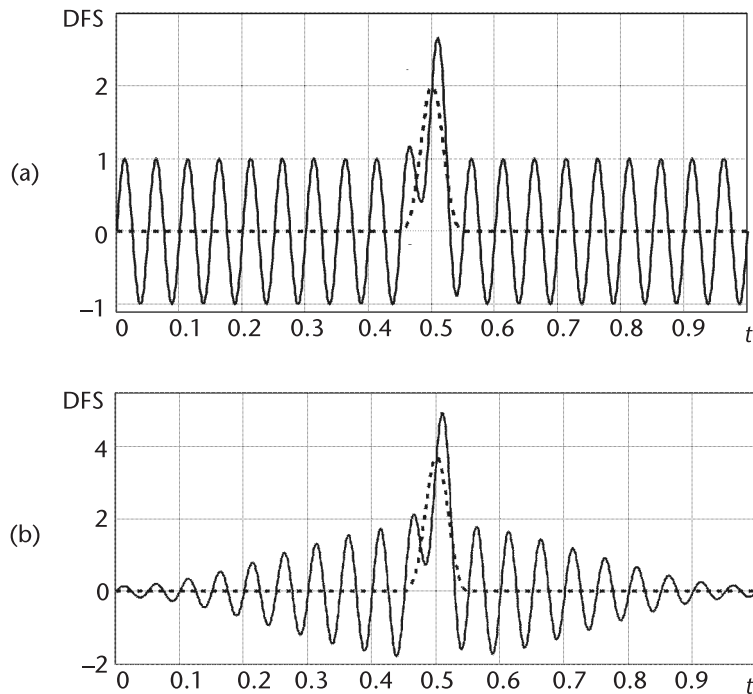


Figure 6.9 SAD of the radio pulse signal.



**Figure 6.10** Pulse interference and resulting DFS: (a) before WF processing and (b) after WF processing.

Let us consider the influence of the radio pulse (6.11) on the range estimation error.

We note that with the increasing moment of pulse interference defined by the coincidence of the generated frequency of the FM oscillator with resonant frequency of AWP irregularity, the inside of the analysis interval  $T_{an}$  can be arbitrary. Therefore, due to the multiplication of DFS and the pulse interference sum with the smoothing WF, the interference influence on processing result will be maximal if the pulse interference arises in the area of the WF maximum; that is, in the center of the  $T_{an}$  interval. Therefore, we give the calculation results assuming that the moment of pulse interference arising is in the center of  $T_{an}$  interval.

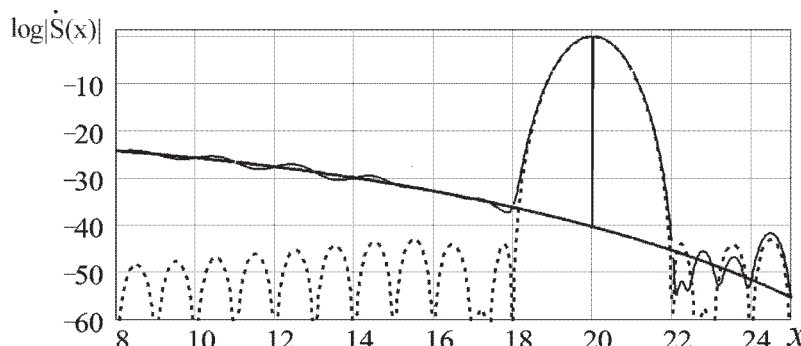


**Figure 6.11** SAD on pulse interference (curve 1), of useful DFS item (curve 2) and of the resulting signal (curve 3).

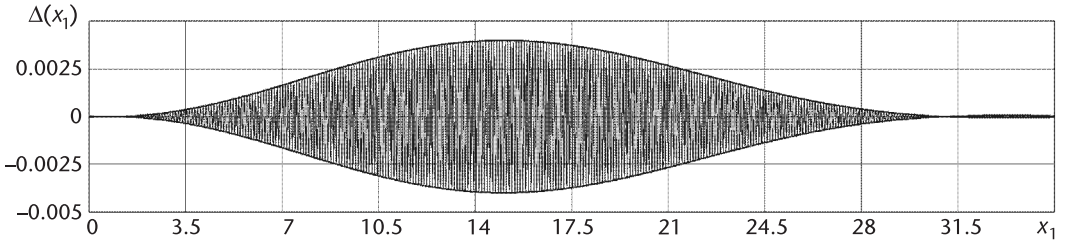


**Figure 6.12** Plots of the measurement error and its envelopes versus range to UR.

The resulting signal is processed by the AWF in (A.13), which is optimal on the EE SLL with  $F_{\text{env},\max} = 1.25$  and  $b_1 = 2.014044$ ,  $b_2 = 2.628$ . SIR defined according to the amplitude values of the signal and interference is equal to  $q_{\text{s/i}} = -6$  dB. The normalized range to the useful reflector is 20, and the normalized range to spurious irregularity in AWP is 1. The duration of the interference pulse is  $T_p = 0.1T_{\text{an}}$ . The bell shape of the pulse is specified by (6.11) with  $N = 2$  and  $b_{11} = \sqrt{28/3}$ ,  $b_{12} = \infty$ .

SAD of interference and useful DFS items and SAD of the resulting signal, shown in Figure 6.10, are presented in Figure 6.11.

DFS processing by the weighting function at the narrow pulse does not practically influence on its shape and, accordingly, does not influence SAD. The SAD shape of the useful item can be widely varied by the WF parameter changing.

Using (3.17) and (6.12) for the above-mentioned conditions, we calculate the measurement error function versus range to the UR and its envelopes at the 1-GHz FM range and the 10-GHz carrier frequency. These functions are presented in Figure 6.12.

As before, the plot character contains fast and slow oscillations. The period of fast oscillations is equal to half of the average wavelength of the radiated signal, and the position of the zero error values depends on the phase difference of reflection coefficients from useful and spurious objects. The period of slow oscillations is connected with pulse interference SAD SL periodicity and it caused by its duration and shape. The position of the envelope maximum, which is defined mainly by the maximum position of the first derivative of the pulse SAD, is connected with the duration and shape of the pulse interference. The application of the AWF in (A.13)

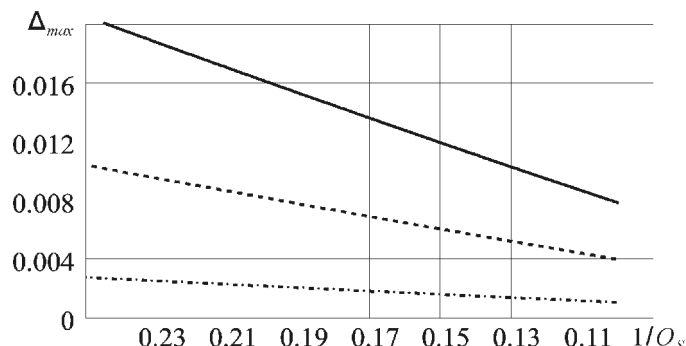


**Figure 6.13** Plots of the maximal error values versus the pulse duration.

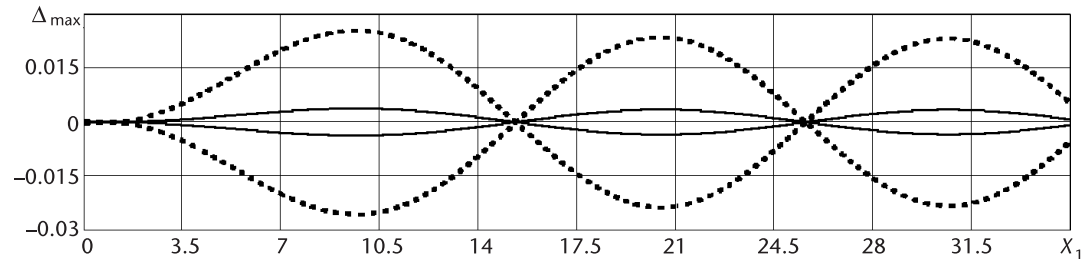


**Figure 6.14** Envelopes of the normalized error of range estimation caused by the pulse interference.

with  $N = 2$  and  $b_{11} = \sqrt{28/3}$ ,  $b_{12} = \infty$ , which has an SLL less than  $-58$  dB, for pulse shape approximation, defines the low WF SLL not shown in the plot.

We examine the relatively low error level even for low  $q_{S/I} = -6$  dB and the very wide main lobe of the error. Both factors are caused by the wide main lobe of spurious item's SAD. In turn, the width of the SAD main lobe of the spurious item is connected with the pulse duration and shape. Pulse duration influence on the frequency estimation error is illustrated in Figure 6.13, in which the functions of maximal error values  $\Delta x_{EE,\max}$  are shown at the DFS processing by the Blackman WF (solid line), by the above-mentioned AWF in (A.13) optimal on the EE SLL with  $F_{EE,\max} = 1.25$  and  $b_1 = 2.014044$ ,  $b_2 = 2.628$  (dotted line) and by the uniform WF (dashed-dotted line).

A strong influence of the pulse interference shape on the value and shape of envelope can be seen from a comparison of Figures 6.12 and 6.14. Figure 6.14 shows the EE for the above-mentioned conditions but at the effect of the rectangular pulse. Error envelopes for the application of the Blackman WF for the DFS processing (dotted line) and the AWF in (A.13) with  $b_1 = 1.1512$ ,  $b_2 = \infty$  (solid line) are presented in this figure. At the influence of the rectangular pulse, the EE character becomes nondamping with the lesser width of the main lobe. Independently on WF used for DFS processing, the EE function character is saved, but the scale of error axis strongly changes. The reduction of the main lobe width by 2.6 times for the AWF in (A.13) with fixed zeros compared with the Blackman WF leads to an error decrease by 6.6 times.

These figures show that some tasks of the precision range estimation on the background of the pulse interference can be solved with the error, which does not exceed the specified value, by an efficient WF choice.

## 6.4 The Error Caused by the Signal Reflection from the Corner Formed by the Reservoir Vertical Wall and the Liquid Surface

Let us consider the error component, which arises due to waves radiated and received by an antenna in the direction of the corner formed by the reservoir vertical wall and the liquid surface. In this case, the UR and SR are not usually resolved in the range. In connection with the fact that the UR and SR represent different parts of the same liquid, the SIR can decrease to 1.

Usually at mounting, the level meter is located in such a manner that the directional pattern (DP) axis of an antenna would be oriented on normal to the probing plane liquid surface. We assume that the reservoir base radius exceeds by many times

the range from the place of the FMCW RF mounting to the wall. We may consider that the interference is created by the waves' reflection from the two-sided corner formed by the vertical wall tangent to the reservoir wall and the liquid surface. Assuming also that all ranges allow the application of the geometrical optic approximation for the determination of amplitude-phase relations of useful and spurious signals, we obtain that the amplitude of the useful signal is defined by the range to the liquid surface and the reflection coefficient from the probing liquid at the normal wave incidence on it. The spurious signal amplitude is defined by the range to the corner formed by the reservoir vertical wall and the liquid surface, by the antenna DP in the direction of the corner, and by orientation of the vector of electrical field intensity with regard to the incidence plane and the wave reflection coefficient at inclined incidence. The main peculiarity of the EMW reflection from the two-sided corner consists of the cross-polarized reflected electromagnetic field [4] if the vector of electrical field intensity of the incident wave  $\vec{E}_{\text{inc}}$  is nonperpendicular or nonparallel to the edge of the two-sided corner. In the case if the vector of the linear-polarized field  $\vec{E}_{\text{inc}}$  is oriented under angle  $\pi/4$  to the edge of two-sided corner, the reflected field is orthogonally polarized with regard to the incident wave field and is not received by the transmit-receive antenna. As a result, the interference amplitude will be zero. In a similar way, we may eliminate the interference signal using the field with circular polarization. In general, under the above-mentioned conditions, the SIR may take values from close to 1 to  $\infty$ .

At first, we analyze the case when the SIR is close to 1; that is, when the vector  $\vec{E}_{\text{inc}}$  is oriented in parallel to the edge of two-sided corner. The error function character versus range to the liquid surface is defined by the range difference between the UR and SR  $\Delta r = \sqrt{R^2 + b^2} - R$  and the antenna DP shape. In these equations,  $b$  is range from the phase center of the FMCW RF to the vertical wall of the reservoir and  $R$  is the range from the antenna phase center to the liquid surface. Hence, DFS without account of the noise

$$u_{\text{dif}} = U_0(t) |\dot{\Gamma}_{\text{ref}}(0)| \left\{ \cos[\omega(t)t_{\text{del,int}} - \varphi_s] + \frac{|\dot{\Gamma}_{\text{ref}}(\Theta)|}{|\dot{\Gamma}_{\text{ref}}(0)|} \frac{F^2(\Theta)}{F^2(0)} \frac{R^2}{R^2 + b^2} \cos[\omega(t)(t_{\text{del,int}} + \Delta t_{\text{del}}) - \varphi_s] \right\} \quad (6.13)$$

where  $F(\Theta)$  is a characteristic of antenna directivity,  $|\dot{\Gamma}_{\text{ref}}(\Theta)|$  is reflection coefficient from the probing surface for the wave incidence angle equal to  $\Theta$ ,  $|\dot{\Gamma}_{\text{ref}}(0)|$  is the reflection coefficient from the probing surface for wave incidence angle equal to zero,  $\Delta t_{\text{del}} = 2\Delta r/c$ . In the considered case of the vector  $\vec{E}_{\text{inc}}$  orientation in parallel to the edge of a two-sided corner,

$$|\dot{\Gamma}_{\text{ref}}(\Theta)|/|\dot{\Gamma}_{\text{ref}}(0)| \approx 1 \quad (6.14)$$

Because the WF influence on the range estimation error was considered in Section 6.2, we do not focus attention on the peculiarities of error variation at the WF variation and in all cases we use the AWF with a normalized half-width of the SAD main lobe  $b_1 = 2$ .

Figure 6.15 shows in absolute units the measurement errors as a function of range to liquid surface  $R$  during M RF mounting, relatively, at range  $b = 0.4$  m and

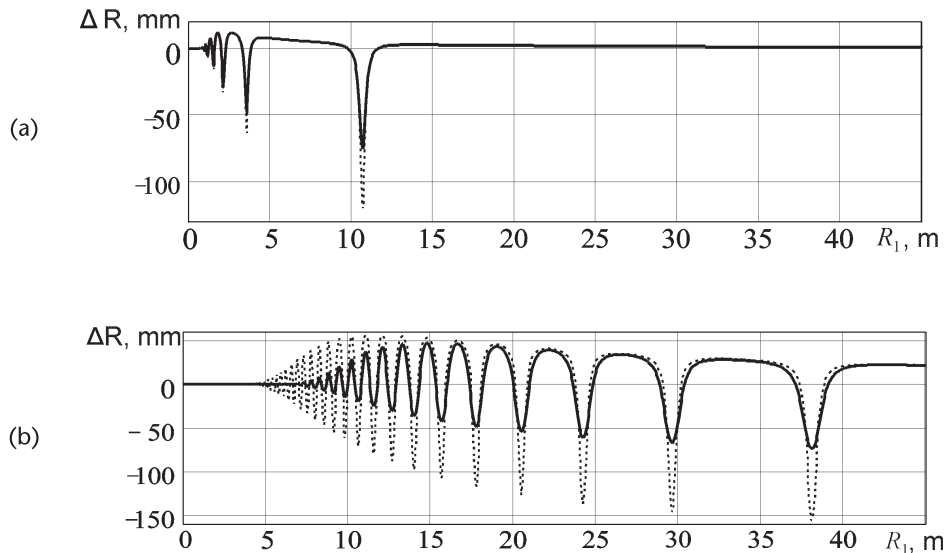


**Figure 6.15** Plots of the measurement error by the range-finder, which is mounted at the range (a) 0.4 m and (b) 2 m from the reservoir wall.

$b = 2$  m from the wall using an antenna with the DP width  $15^0$  on level  $-3$  dB for a 10-GHz carrier frequency. The solid curves correspond to the FM sweep at FM  $\Delta f = 1$  GHz, and dotted curves to  $\Delta f = 500$  MHz.

We see from Figure 6.15 that the measurement error has an oscillating character with narrow parts with the high measurement error, on which the measurement result is underestimated, and with more wide parts with the much lesser error, on which the measurement result is overestimated. A comparison of figures shows that the number and relative portion of parts with the high error do not practically depend upon the FM sweep and is determined by range to the reservoir wall. The FMCW RF approach to the reservoir wall allows error reduction, especially in wide parts with the overestimated measurement result. Moreover, in this case the last outermost part with high error approaches to the FMCW RF, and then the error monotonically decreases to zero. At that, at the near range from the wall in the parts with the overestimated measurement result, the measurement error does not practically depend upon the FM sweep. At these parts, the error functions corresponding to  $\Delta f = 1000$  MHz and  $\Delta f = 500$  MHz are indistinguishable in Figure 6.15. In the zones of high error, its value is practically proportional to the FM sweep.

One can eliminate the interference signal using orthogonally polarized waves reflected from the corner. The reduction of interference amplitude to 5 to 10 times is practically possible in such a way. As a result, the measurement error essentially decreases. The functions of the measurement errors versus the range to the liquid surface for the above-mentioned conditions are presented in Figure 6.16 but for the interference signal elimination by 14 dB.

As a result, the measurement error level is not only essentially decreased but the type of its range dependence is changed. Distribution of parts with overestimated and underestimated measurement results becomes practically uniform, and at the small range from the wall (0.4 m and less), the dependence of the measurement error on the FM sweep practically disappears. At the FMCW RF mounting for the range

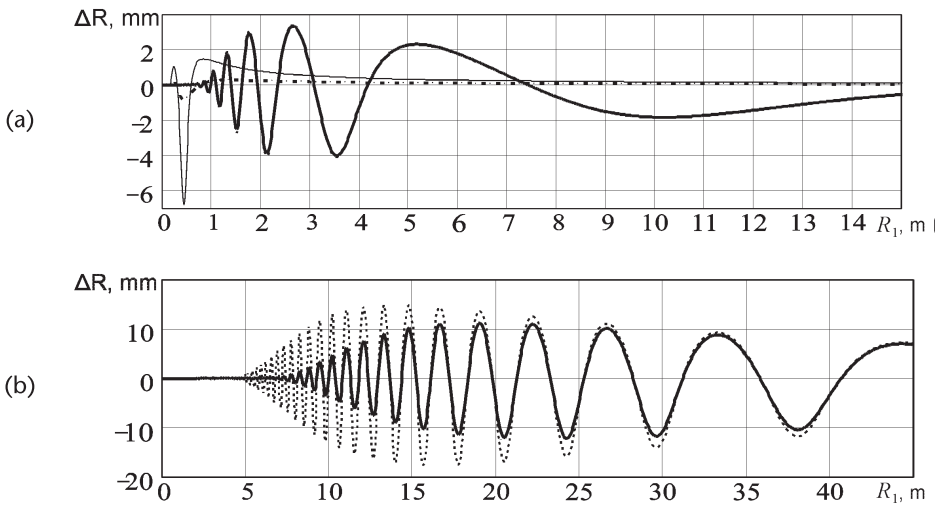


**Figure 6.16** Plots of the measurement error by the range-finder mounted from the reservoir wall at range: (a) 0.4 m and 0.08 m and (b) 2 m.

2 m from the wall in the initial part of the error function, its value strongly depends upon the FM sweep and with the range increasing to the liquid, the amplitude error values for  $\Delta f = 1000$  MHz and  $\Delta f = 500$  MHz become practically equal. Figure 6.16(a) shows by the thin line the function of measurement error by the FMCW RF, in which the antenna is mounted almost right against the reservoir wall. The antenna with DP width 15° on the level of -3 dB with the aperture radius 0.075 m used earlier is mounted at range  $h = 0.08$  m from the reservoir wall. The insignificant error increase is seen only at the near range.

These results are evidently true for the range-finder mounted near the smooth reservoir wall in the absence of the SR in the form of wall irregularities. Under such conditions, the radical method of error decrease is an extremely close antenna location near the reservoir wall.

## 6.5 Influence of the Edge Modes Caused by the Restricted Sizes of the Probing Object

The representation of DFS from the probing object in the form of the first item of (6.1) assumes that this object is an infinite plane reflector. Nevertheless, in reality the probing object has always been the restricted sizes, which can lead to measurement errors.

Let us suppose that the plain reflector is mounted at a range  $R_1$  perpendicular to the direction to the FMCW RF (Figure 6.17). We need to estimate the influence of reflector configuration. We assume that the angular reflector's sizes with regard to the point of FMCW RF antenna location are small, and linear sizes exceed the wavelength many times. In this case, we can neglect by the function of the reflection coefficient versus the incident angle, and to determine of complex amplitude of the reflected field (in arbitrary point A), we may use the scalar Kirchhoff approximation [5]:

$$\dot{U}_{\text{ampl}} = \dot{U}_0 \frac{jk}{2\pi} \int_{s_0} F(\Theta) \frac{e^{-j2kr_s}}{r_s^2} \cos(\vec{n}, \vec{r}^0) ds \quad (6.15)$$

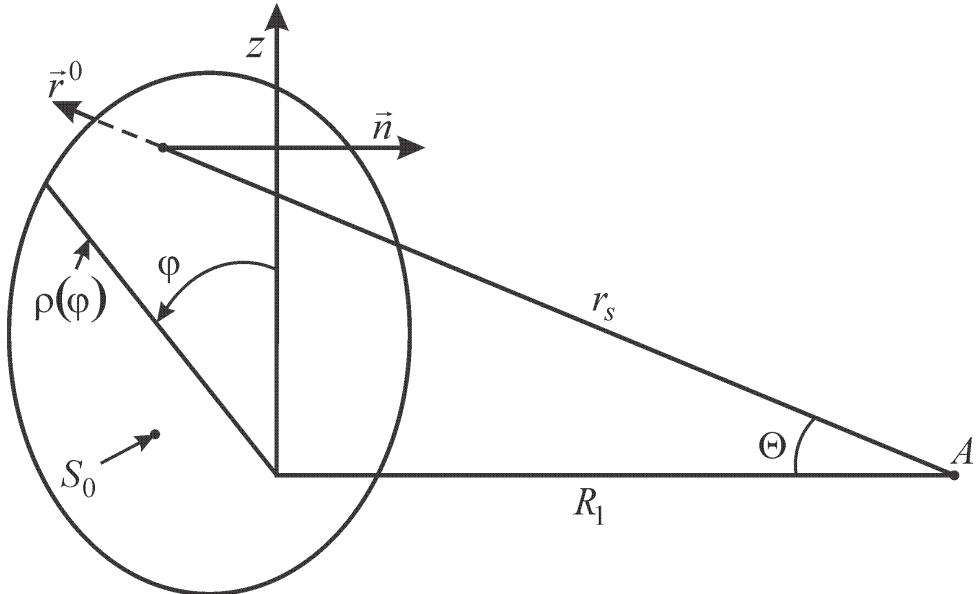


Figure 6.17 The calculation of the field reflected by the plane reflector of finite sizes.

where  $F(\Theta)$  is the characteristic of antenna directivity and  $\dot{U}_0$  is the complex amplitude of the wave falling to the reflector,  $k = 2\pi/\lambda$ . Other designations are clear from Figure 6.17.

Equation (6.15) can be presented by asymptotic expansion

$$\begin{aligned} \dot{U}_{\text{ampl}} = & \dot{U}_0 F(0) \frac{e^{-j2kR_1}}{2R_1} \left\{ 1 + \frac{R_1^2}{F(0)} e^{j2kR_1} \sum_{m=1}^{N-1} \left( \frac{1}{j2k} \right)^m \frac{d^m}{dr^m} \left[ \frac{1}{R_1^2} \cdot F(0) \right] \right\} - \\ & - \dot{U}_0 \frac{R_1}{4\pi} \int_0^{2\pi} F(\Theta) \frac{e^{-j2kr}}{r^2} \left\{ 1 + \frac{r^2}{F(\Theta)} e^{j2kr} \sum_{m=1}^{N-1} \left( \frac{1}{j2k} \right)^m \frac{d^m}{dr^m} \left[ \frac{1}{r^2} \cdot F(\Theta) \right] \right\} d\varphi \quad (6.16) \end{aligned}$$

where  $r = \sqrt{R_1^2 + \rho^2(\varphi)}$ ,  $\rho(\varphi)$  is the reflector configuration.

At  $kR_1 \gg 1$ , it is possible to limit by the first items of a series and then

$$\dot{U}_{\text{ampl}} = \left[ \frac{\dot{U}_0 e^{-j2kR_1} F(0)}{2R_1} - \dot{U}_0 \frac{R_1}{4\pi} \int_0^{2\pi} F(\Theta) \frac{e^{-j2kr}}{r^2} d\varphi \right] \quad (6.17)$$

The item  $\frac{\dot{U}_0 e^{-j2kR_1}}{2R_1} F(0)$  corresponds to the complex amplitude of the field reflected by the infinite plane reflector and its electrodynamical range coincides with the geometric one. Thus, the reflected field represents by the field sum from the infinite plane reflector and the interference caused by finite reflector sizes:

$$\dot{U}_{\text{int}} = \dot{U}_0 \frac{R_1}{4\pi} \int_0^{2\pi} F(\Theta) \frac{e^{-j2kr}}{r^2} d\varphi \quad (6.18)$$

The complex amplitude of interference field can be normalized to the complex amplitude of the infinite reflector  $\dot{U}_\infty$ :

$$\dot{U}_{\text{int,norm}} = \frac{\dot{U}_{\text{int}}}{\dot{U}_\infty} = \frac{1}{2\pi} \int_0^{2\pi} \frac{F(\Theta)}{F(0)} \frac{R_1^2}{r^2} e^{-j2k(r-r_0)} d\varphi \quad (6.19)$$

In general, the interference field distribution depends on the shape, the range to the reflector, and frequency, and the measurement error depends on the distribution of the field intensity, the sizes of the used antennas, and the methods of signal processing. It is impossible to obtain the general analytical solution for the error under the conditions described above. We prove the significance of the above-mentioned type of interference on the range estimation error in an example of a circular disk with the radius  $b$ , which is probed from the axial FMCW RF direction, in which the axis of the axis-symmetric antenna DP is oriented on the disk center. We assume that the measuring range and disk sizes are so large that the field distribution in vicinity of axis within the sizes of the used antenna is constant. In this case, the equation for a normalized complex amplitude of the interference field takes the simplest view:

$$\dot{U}_{\text{int,norm}} = \frac{F(\Theta)}{F(0)} \frac{R_1^2}{r^2} e^{-j2k(r-R_1)} \quad (6.20)$$

The interference field is created by the toroidal wave from the reflector edge. It is reasonable to assume that the complex amplitude of interference at antenna output  $\dot{U}_{\text{ant,int,norm}}$  will be proportional to the antenna DP in the direction to the reflector edge:

$$\dot{U}_{\text{ant,int,norm}} = \frac{F^2(\Theta)}{F^2(0)} \frac{R_1^2}{r^2} e^{-j2k(r-R_1)} \quad (6.21)$$

Hence, the DFS without account of the noise is:

$$u_{\text{dif}} = U_0(t) \times \left\{ \cos[\omega(t)t_{\text{del,int}} - \varphi] + \frac{F^2(\Theta)}{F^2(0)} \frac{R_1^2}{R_1^2 + b^2} \cos[\omega(t)(t_{\text{del,int}} + \Delta t_{\text{del}}) - \varphi] \right\} \quad (6.22)$$

where  $\Delta t_{\text{del}} = 2\Delta r/c$ ,  $\Delta r = \sqrt{R_1^2 + b^2} - R_1$ .

Equation (6.22) for the DFS obtained when illuminating the circular disk with the radius  $b$  under the above-mentioned simplifications coincides in its structure with (6.13), from which it follows that in this case the range estimation error to the circular disk coincides with the range estimation error to the half-infinite probing object restricted by the vertical wall at the range  $b$  from the RF antenna and, as it follows from Figure 6.15, can achieve significant value. Looking ahead, we note that the theoretical and experimental functions of the range measurement error to the circular disk are discussed in Chapter 9.

## 6.6 Influence of Reflected Waves on the Measurement Error of the FM Range-Finder

### 6.6.1 Influence of Echo Signals on the Operating Mode of the SHF Oscillator

It is known that load mismatching of the directing system (DS) causes reflected waves, which lead to a variation of the operating mode of FM oscillator and to distortions of the FM law [6]. Therefore, the presence of reflected echo waves both from the target and from spurious reflectors must lead to error increase of range measurement by the FMCW RF.

We consider the general case [7], when the FM oscillator is connected to the transmitting antenna of DS containing isolation devices (isolators, buffer amplifiers, and so forth) with the finite deepness of the suppression  $D$  of echo waves. The frequency of generated oscillations can be determined from the phase balance condition [6, 8]:

$$\operatorname{Im} \left( \dot{Y}_{\text{osc,s}} + \eta^2 \sum_{i=1}^M \dot{Y}_{\text{in},i} \right) = 0 \quad (6.23)$$

where  $\dot{Y}_{\text{osc,s}} = G_{\text{res}}[1 + j(\omega^2 - \omega_{\text{res}}^2)Q]/(\omega\omega_{\text{res}})$  is the conductance of loaded oscillating system with connected active and modulating elements without influence of echo waves,  $G_{\text{res}}$  is the equivalent conductance of the parallel oscillating circuit of the resonance frequency,  $Q$  is the Q-factor,  $\omega_{\text{res}}$  is the resonance frequency,  $\eta^2 = Y_{\text{in}}/G_{\text{res}} \ll 1$  is the load turn-on ratio in the circuit,  $M$  is the total number of reflectors, in which echo waves arrive to the input of the transmitting antenna,  $\dot{Y}_{\text{in},i} = Y_{\text{ch}}(1 - \dot{\Gamma}_{\text{in},i})/(\dot{\Gamma}_{\text{in},i})$ ,  $Y_{\text{ch}}$  is the characteristic conductance of the transmission line connected to the oscillator output, and  $\dot{\Gamma}_{\text{in},i}$  is the reflection coefficient for each reflected  $i$ th wave on the load input. Then we suppose that  $i = 1$  corresponds to the UR, and all others are spurious; therefore, SR may be absent.

We assume that in the FM process the resonant circuit frequency should change according to the specified law  $\omega_{\text{res}}(t)$ , and owing to the influence of the echo waves, the frequency changes according to another law

$$\omega(t) = \omega_{\text{res}}(t) + \sum_{i=1}^M \delta\omega_i(t) = \omega_{\text{res}}(t) + \delta\omega(t) \quad (6.24)$$

The phase balance condition (6.23) can be rewritten as

$$\begin{aligned} & QG_{\text{res}}[\omega^2(t) - \omega_{\text{res}}^2(t)]/[\omega(t)\omega_{\text{res}}(t)] \\ & + 2Y_{\text{ch}}\eta^2 \sum_{i=1}^M \Gamma_i \sin[\tau\omega(t) + \varphi_i]/D = 0 \end{aligned} \quad (6.25)$$

Taking into consideration that  $D \gg 1$  and for  $|\dot{\Gamma}_{\text{in},i}| \ll 1$  the condition  $\delta\omega(t) \ll \omega_{\text{res}}(t)$  will be satisfied, we obtain the equation for the FM law distortion:

$$\delta\omega(t) = \omega_{\text{res}}(t)A \sum_{i=1}^M \Gamma_i \sin[\tau_i \omega_{\text{res}}(t) + \varphi_i] \quad (6.26)$$

where  $A = Y_{\text{ch}}\eta^2/G_{\text{res}}QD$  is a coefficient depending only upon properties of the transmitting-receiving module (TRM). Usually, values of  $A$  of the industrially

manufactured TRM for the FMCW RF do not exceed 0.0005. The modulation law (6.26) error is a sum of periodic functions of two variables: time and range.

We note that an essential difference between propagation time  $\tau_i$  in (6.26) and delay time  $t_{\text{del}}$  in (6.1) caused the necessity in a different letter designation of, at first glance, the same variables. The range variation between SHF oscillator and the directional coupler (DC) of the local oscillator signal leads to  $\tau_i$  variation, but does not manifest itself on the  $t_{\text{del}}$  value.

Because the ratio of the received and radiated power is included into the equation for the reflection coefficient, evidently the influence on the oscillator frequency of the conditions of radio-wave propagation, the sizes and the shape of probing objects, and their electrical-physical parameters takes place. We consider next the most widespread cases of object probing (represented by the plane or by a set of point reflectors) in the free space and reflectors in the directing system.

We assume that gain of the antenna does not depend upon frequency within the limits of modulation range. Then it follows from [1] that at the normal probing of the plane reflector

$$\Gamma_i = c\Gamma_{\text{mat},i}G_{\text{ant}}/4\omega(t)R_{\text{free},i} \quad (6.27)$$

$G_{\text{ant}}$  is the antenna gain,  $\Gamma_{\text{mat},i}$  is modulus of the reflection coefficient from the material, and  $R_{\text{free},i}$  is range to probing surface.

At the probing of the plane reflector

$$\Gamma_i = cG_{\text{ant}}F^2(\xi,\zeta)\sqrt{\sigma/\pi}/4\omega(t)R_{\text{free},i}^2 \quad (6.28)$$

$\sigma$  is the effective scattering area of the point reflector,  $F(\xi,\zeta)$  is the normalized antenna DP characteristic, and  $\xi,\zeta$  are angular coordinates of the reflector in polar coordinates with a center in the antenna phase center and the polar axis coinciding with the DP axis.

At reflector probing in the directing system [9]

$$\Gamma_i = \Gamma_{i0} \exp\{-\alpha[\omega(t)]2L_i - j[\beta(\omega)2L_i + \varphi_i]\} \quad (6.29)$$

$\Gamma_{i0}$  is the modulus of reflection coefficient from probing object in DS,  $L_i$  is the object longitudinal coordinate, and  $\beta(\omega)$  and  $\alpha(\omega)$  are frequency-dependent coefficients of phase and damping, respectively.

### 6.6.2 Influence of the Wave Reflected from the Useful Reflector on the Range Measurement Error

To calculate the range  $R$ , we use (1.17). In this case, at signal processing, the range measurement error arises due to the fact that the used value of the FM range  $\Delta\omega$  does not coincide with the instantaneous value  $\Delta\omega_{\text{inst}}$  differing from the specified one due to the distortion presence in (6.26):

$$\Delta\omega_{\text{inst}} = \Delta\omega + \delta\omega(T_{\text{mod}}/2) - \delta\omega(0) \quad (6.30)$$

where  $\delta\omega(T_{\text{mod}}/2)$ ,  $\delta\omega(0)$  is the oscillator frequency deviation from the specified outermost point of the analysis interval.

Based on (6.30), (6.26), and (1.17), the normalized error is

$$\frac{\Delta R_{\text{int}}}{\delta_R} = \frac{R_{\text{int}}}{\delta_R} A \times \left\{ \left( 1 + \frac{\Delta\omega}{\omega_0} \right) \Gamma_{\text{int,T}} \sin[\tau_{\text{int}}(\omega_0 + \Delta\omega) + \varphi_{\text{int}}] - \Gamma_{\text{int,0}} \sin(\tau_{\text{int}}\omega_0 + \varphi_{\text{int}}) \right\} \quad (6.31)$$

where  $\Gamma_{\text{int,T}}$ ,  $\Gamma_{\text{int,0}}$  are defined by (6.27) through (6.29) on the frequencies  $\omega_0 + \Delta\omega$  and  $\omega_0$ , respectively.

Taking into consideration that  $(\omega_0 + 0.5\Delta\omega)\tau_{\text{int}} = 4\pi R_{\text{int}}/\lambda_{\text{aver}}$ , where  $\lambda_{\text{aver}}$  is the wavelength of the carrying oscillation corresponding to the average frequency of the FM sweep and  $0.5\Delta\omega\tau_{\text{int}} = 4\pi R_{\text{int}}/\delta_R$  for two types of reflectors on the free space, we obtain the relative measurement error

$$\frac{\Delta_R}{\delta_R} = \frac{G_{\text{ant}}A}{\pi} V \cos\left(4\pi \frac{R}{\lambda_{\text{aver}}} + \varphi_{\text{int}}\right) \sin\left(\pi \frac{R}{2\delta_R}\right) \quad (6.32)$$

where  $V = \Gamma_{\text{int,0}}$  for the plane reflector and  $V = F^2(\xi, \zeta)\sqrt{\sigma/\pi}/R$  for the point reflector.

Similarly, for the reflector located in the DS at the range  $L$ , we have:

$$\begin{aligned} \frac{\Delta_L}{\delta_R} = & \Gamma_{\text{int,0}} \frac{L}{k\delta_R} A \left[ B \sin\left(4\pi \frac{L}{\lambda_2} + \varphi_{\text{int}}\right) \right. \\ & \left. - \sin\left(4\pi \frac{4L}{\lambda_1} + \varphi_{\text{int}}\right) \right] \exp(-\alpha_0 2L) \end{aligned} \quad (6.33)$$

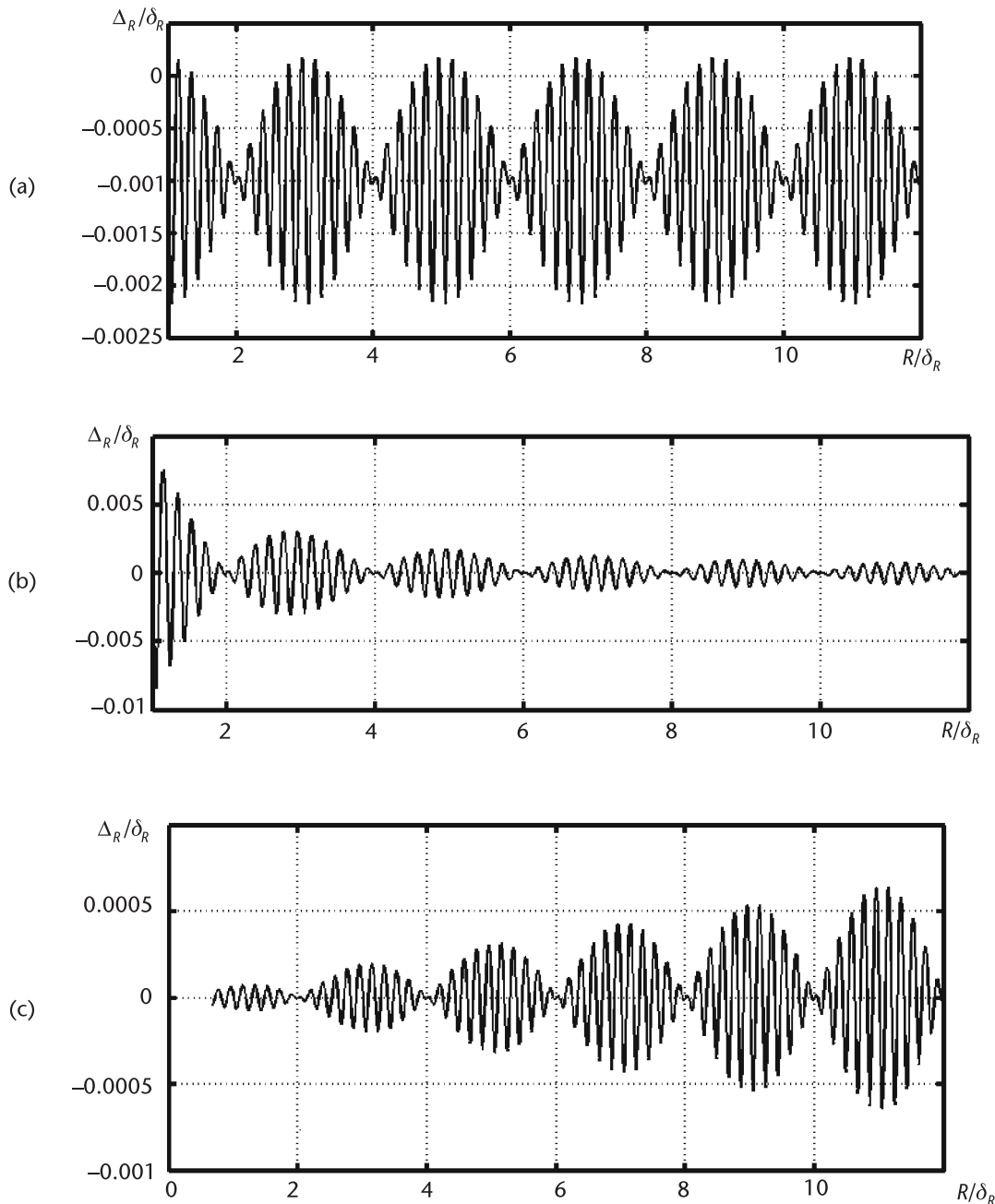
where  $k = \Delta\omega/\omega_0$ ;  $B = (k + 1)\exp(-\alpha k 2L\gamma)$ ;  $\lambda_2$  and  $\lambda_1$  are wavelengths of carrying oscillation corresponding to the upper  $\omega_0 + \Delta\omega$  and lower  $\omega_0$  frequencies of the range.

Figure 6.18 shows the relative measurement error function versus the relative range  $R/\delta_R$  or  $L/\delta_R$  for the three mentioned variants of reflection at  $G_{\text{ant}} = 21$  dB,  $A = 0.0003$ ,  $k = 0.1$ ,  $\Gamma_{\text{int,0}} = 0.2$ ,  $\gamma = 1$ ,  $\lambda_{\text{aver}} = 0.03$  m,  $\Delta F = 1$  GHz,  $\sigma = 0.01$  m<sup>2</sup>,  $F(\xi, \zeta) = 1$  and  $\alpha = 0.2$  dB/m.

In all cases, the measurement error function versus the measured range has an oscillating character with double periodicity. Therefore, a plane reflector probing the maximal value does not depend on the range [Figure 6.18(a)]. At the point object probing [Figure 6.18(b)], the maximal error values are inversely proportional to the range. At the object probing in the DS [Figure 6.18(c)], the maximal values of the oscillating error with the range increasing at first increases to the value

$$\frac{\Delta_L}{\delta_R} \approx \Gamma_{\text{int,0}} A (B + 1) / (k \delta_R 2 \alpha_0 e) \quad (6.34)$$

at the range  $L \approx 1/2\alpha_0$  and then decreases monotonically. Figure 6.18(c) shows the part with decreasing error amplitude, which is located beyond the right boundary of the plot, due to the smallness of the damping factor  $\alpha_0$ .



**Figure 6.18** Plots of the normalized measurement error versus the relative range: (a) the plane reflector, (b) the point reflector, and (c) the reflector in the DS.

### 6.6.3 Simultaneous Influence of Waves Reflected from the Useful and Spurious Reflectors on the Range Measurement Error

In the situation when at the reflector probing located in the free space at the range  $R_{\text{int}}$  there is a single irregularity in the AWP at the range  $R_{\text{ant}}$  from the oscillator, which is extremely important. It is caused by insufficient good matching of separate

units (for instance, the encapsulation device in the AWP). We can write from (6.26) the resulting relative error as:

$$\frac{\Delta_R}{\delta_R} = \frac{G_{\text{ant}} A}{\pi} V \cos\left(4\pi \frac{R_{\text{int}}}{\lambda_{\text{aver}}} + \varphi_{\text{int}}\right) \sin\left(\pi \frac{R_{\text{int}}}{2\delta_R}\right) - \frac{R_{\text{int}}}{\delta_R} \frac{2\Gamma_{\text{AWP}} A}{k} \exp(-\alpha_0 2L) \cos\left(4\pi \frac{R_{\text{ant}}}{\lambda_{\text{aver}}} + \phi_{\text{AWP}}\right) \sin\left(\pi \frac{R_{\text{ant}}}{2\delta_R}\right) \quad (6.35)$$

where  $\Gamma_{\text{AWP}}$  and  $\phi_{\text{AWP}}$  are, respectively, the modulus and phase of the reflection coefficient from irregularity in the AWP,  $V = \Gamma_{\text{mat}}$  for the plane reflector,  $V = \sqrt{\sigma/\pi}/R_{\text{int}}$  for the point reflector, and  $V = 2\pi\Gamma_{\text{int},0}x_{\text{int}}\exp(-\alpha_0 2R_{\text{int}})/k$  for DS.

The error is defined by two items. The second item in (6.35) defines the fast oscillating error component, and the first item defines the direct current of the error depending on the UR position and the reflection coefficient phase.

At the variation of the UR position and for unchanged  $R_{\text{ant}}$ , the oscillating component is summed with the linear-changed component generated by the SR, by the second item in (6.35). The tilt angle tangent of the linear-changed component is defined by the modulus  $\Gamma_{\text{AWP}}$  and phase  $\phi_{\text{AWP}}$  of the reflection coefficient from irregularity in the AWP, its coordinates, and inverse proportion to the coefficient  $k = \Delta\omega/\omega_0$ . The variation of the irregularity coordinate  $R_{\text{ant}}$  in the AWP causes a slope variation of the linear measurement error in the sector  $\pm \frac{R_{\text{int}}}{\delta_R} \arctan\left[\pi \frac{\Gamma_{\text{AWP}}}{k} \exp(-\alpha_0 2R_{\text{ant}})\right]$ . This is shown

in Figure 6.19, where the function of the total normalized measurement error versus the relative range to the UR at the specified parameters and for two SR positions in the AWP corresponding to boundaries of the mentioned sector. At the range increase, this error component may exceed the error caused by all other factors.

For the fixed SR parameters in the AWP, the item of the measurement error caused by these reflectors is stable as well. Therefore, this component can be taken into account at device calibration. The instability of the SR parameters, for example, under the influence of temperature or dust and moisture settling, leads to error variation.

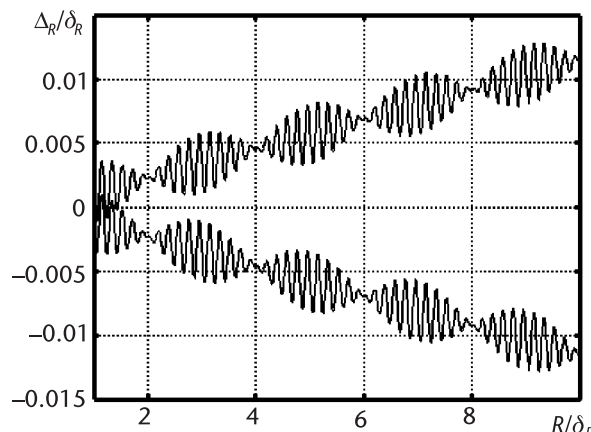


**Figure 6.19** Plots of limited values of the normalized measurement error versus the relative range to the reflector in the free space at the SR presence in the AWP.

## 6.7 Influence of Combination Components in the Mixer of the FMCW RF on the Measurement Error

### 6.7.1 Virtual Reflectors

Substantively existing varied clutter creates new interference due to the inevitable increase in combination components in the FMCW RF mixer [10, 11], in which the amplitude is connected with both the amplitude of spurious signals and the amplitude of the useful signal.

In general, the large number of waves reflected from AWP irregularities and the constructive elements of the reservoir and multiple-reflected waves are applied to the mixer input of the FMCW RF receiver. Nevertheless, the amplitude of multiple-reflected waves decreases quickly with the increase of the number of consecutive reflections; therefore, we can usually neglect them. In this case, we can assume that the probing object is radiated by the generated wave and by accompanying flow of waves (AFW) containing items arising owing to single reflections from AWP irregularities.

The local oscillator signal may contain a series of items arising due to reflections between the mismatched mixer input (on the local oscillator side) and the output of the circuit of local oscillator signal extraction. These items created interference as well.

As a result of interaction of input signals, at the mixer output, the signal is formed containing an item with a multiplier  $\cos([\tau_s \omega(t) - \varphi_s])$  carrying information about range to the probing surface, and a variety of items  $A_{n,int} \cos[(\tau_s \pm n\tau_{int})\omega(t)]$  of a significant amplitude with delays, which are more and less than the delay of informational item.

Low-frequency components  $\cos([\tau_s \omega(t) - \varphi_s])$  and  $\cos[(\tau_s \pm n\tau_{int})\omega(t)]$  usually cannot be resolved, as  $\tau_{int}$  is usually less than the resolving capacity of the FMCW RF. These items are extracted in the form of an unresolved sum  $A_s \cos[\tau_s \omega(t) - \varphi_s] + A_{n,int} \cos[(\tau_s \pm n\tau_{int})\omega(t)]$ . Therefore, low-frequency components  $A_{n,int} \cos[(\tau_s \pm n\tau_{int})\omega(t)]$  are spurious, which can be considered as the appearance of additional virtual clutter [10], in which the number essentially exceeds the number of irregularities in the AWP and in the nearest vicinity of the antenna. Accepting such a consideration, we may assume that the probing object is covered by a variety of closely located virtual reflectors, the number of which depends not only upon a number of irregularities in AWP but also upon the mixer structure.

We can note that virtual clutter, in which the delay is proportional to  $2\tau_{int}$ , passes without suppression to the output of the balanced mixer even at ideal symmetry (currents of both arms of the balanced mixer are summed in-phase), while virtual interference, in which the delay is proportional to  $\tau_{int}$  and  $3\tau_{int}$ , is completely suppressed. This important result tells us that we cannot completely eliminate the measurement error caused by virtual interference.

Virtual reflectors surround the SR from two sides and the AFW creates additional interference, in which the frequency is more than the frequency of the informational item. Thus, in the frequency band exceeding the frequency of informational item, the combination interference and the interference caused by the AFW are formed.

Amplitudes and phases of virtual interference depend upon the amplitudes of the signal and interference and, hence, upon the measured range. Even for unchanged reflections from the AWP irregularities and stable parameters of generated signal, the

SIR for virtual interference depends on the signal amplitude and measured range, and therefore the degree of this dependence is defined by the power level of the radiated signal.

Virtual clutter leads to the appearance of interference with thermal-dependent amplitude and phase. The dependence of this interference upon temperature arises due to the temperature function of volt-ampere characteristic of the nonlinear element. The degree of this function is defined by the ratio of received signal power and the signal of the local oscillator. The mixer operation at the commensurable powers of the signal and the local oscillator leads to a strong temperature dependence of the error [11].

Virtual reflectors situated near the useful reflector distort its spectrum and, as a consequence, lead to measurement errors.

### 6.7.2 Influence of Virtual Clutter on the Range Estimation Error

The results presented in Chapter 3 are applicable to error analysis created by virtual interference. It follows from these results that if there is a single irregularity in the AWP, the function of frequency estimation error versus irregularity position has an oscillating character with fast oscillations, in which the period is connected with the average wavelength of the radiated signal, and slow oscillations, in which the view is defined by the used WF.

The difference is manifested in the fact that oscillating plot is displaced from a zero level by a constant, which is defined by the range between the SR and virtual reflectors and by the ratio of amplitude and phase of considered signals.

Figure 6.20 shows the function of the normalized measurement error versus the range between the virtual reflector and the UR equal to the range from the mixer to the single irregularity in the AWP.

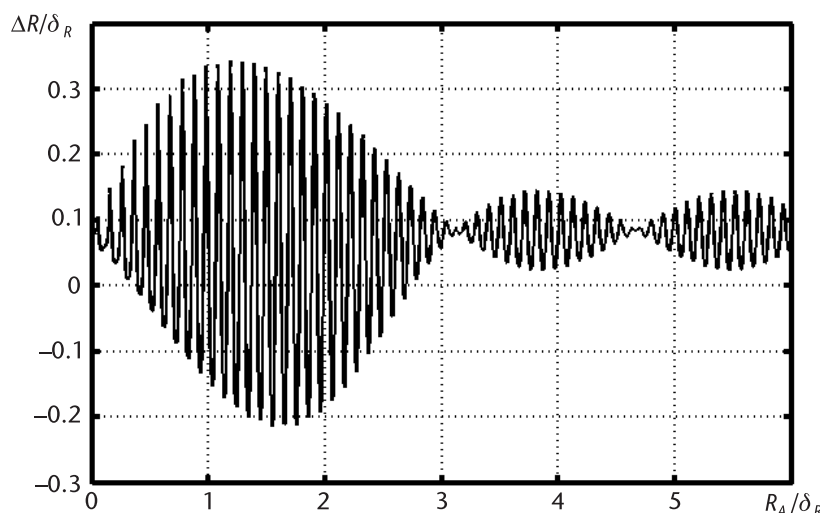


**Figure 6.20** The plot of the normalized measurement error versus the normalized range between the virtual reflector and the UR.

The signal amplitude from the virtual reflector was  $-10$  dB from the amplitude of the useful signal. At the DFS processing, the DC WF was used with the parameter  $Q = 30$  dB.

The periodic character of the plot at the range variation is kept; however, there is the constant displacement of the plot equal to the truncation measurement error corresponding to the analyzed range to the UR.

At the unchanged reflection from the antenna, the measurement error component caused by virtual clutter can be taken into account at calibration. The necessity of its elimination arises at the variation of reflection conditions and at the variation on the useful signal power and the signal caused by the virtual reflector.

## 6.8 Conclusions

In the range-finders of the industrial application, the ratios between levels of the signal, interference, and noise are such that the main contribution into the measurement error is made by interference, which may be created by the device itself and be received from the measurement region. Therefore, the error levels in the most practical situations exceed the admissible value, and it is impossible to eliminate interference in the general case.

We gave a list of the most typical interference acting on the FMCW RF when using it as a level-meter. In most practical applications, the level-meters operate under the conditions of the combined interference influence, and their negative effect on the measurement error is intensified by the presence of the larger number of the combination interference. We can achieve the combination interference level reduction due to the selection of the mixer operation mode.

The analysis of the measurement error function versus the single SR influence showed that the measurement error as a function of the range difference between the UR and the SR has an oscillating character (as the truncation error) but with doubled periods of fast and slow oscillations. Fast oscillations are limited by two envelopes, which form the slow oscillations. The analogy of the error behavior caused by interference and the truncation error allows the adaptation of minimization algorithms of the truncation error to minimize the measurement error caused by interference. However, we should preliminarily estimate the possibility of its application according to the results of interference situation analysis.

The plot of the measurement error is symmetric with regard to the point corresponding to the zero range difference between the UR and the SR. The EE plot has two main lobes and the sequence of the SL. The SLL of the measurement error is practically proportional by the SIR and the SD SLL of the used WF. At the large SIR, the amplitude of main lobes is proportional to this SIR and depends upon the width of the WF SD main lobe as well. Narrowing of the SD main lobe of the used WF allows reduction and main lobe amplitudes of the measurement error function, but, at that, the SLL increases for the measurement error, which can lead to increase of resulting error under the influence of the combined interference. Therefore, the WF parameter choice is expedient to provide starting from an analysis of the interference situation.

The function of the measurement error versus the range difference between the UR and the SR shows that at ranges between the UR and the SR, less than 0.3 from the QI value the error values limited by envelopes do not depend upon the FM range and the type of the used WF and are defined by the SIR only. The range increase between the UR and the SR more than QI leads to the situation that maximal error values become strongly dependent upon the FM range and the type of the WF used. In these cases, the expansion of the FM range leads to an error decrease due to the action of most of the interference.

The reduction of the interference error component due to a significant expansion of the FM range is confronted not only with engineering difficulties, but also with problems of electromagnetic compatibility. Within this framework, the search for signal processing methods that allow error reduction is necessary.

## References

- [1] Cherenkova, E. L., and O. V. Chernushov, *Radio Wave Propagation*, Moscow: Radio i Sviaz Publ., 1984, 272 pp. [In Russian.]
- [2] Levin, O. A., and S. K. Romanov, *Frequency Synthesizers with the System of Pulse PLL*, Moscow, Russia: Radio i Sviaz Publ., 1989. [In Russian.]
- [3] Parshin, V. S., “Estimation of Pulse Interference Influence on Stationary Signal Recognition in the Spectral Domain,” *Radio Elektronika*, Vol. 42, No. 3, 1999, pp. 73–79. [In Russian.]
- [4] Kobak, V. O., *Radar Reflectors*, Moscow: Sovetskoe Radio Publ., 1975, 248 pp. [In Russian.]
- [5] Born, M., and E. Wolf, *Principles of Optics*. 4th edition. Oxford, London, Edinburgh, New York, Paris, Frankfurt: Pergamon Press, 1968.
- [6] Dvorkovich, A. V., “Once More About One Method for Effective Window Function Calculation at Harmonic Analysis with the Help of DFT,” *Digital Signal Processing*, No. 3, 2001, pp. 13–18. [In Russian.]
- [7] Davydochkin, V. M., and V. V. Ezerskiy, “Influence of Reflected Waves upon the Distance Measurement Error by FMCW Range Finder,” *Vestnik RGRTA, Ryazan*, No. 17, 2005, pp. 32–39. [In Russian.]
- [8] Ezerskiy, V. V., I. V. Bolonin, and I. V. Baranov, “The Algorithm of Modulation Characteristic Non-Linearity Compensation for FMCW Range Finders,” *Vestnik RGRTA, Ryazan*, No. 10, 2002, pp. 38–42. [In Russian.]
- [9] Goldshtein, L. D., and N. V. Zernov, *Electromagnetic Fields and Waves*. 2nd edition. Moscow: Sovetskoe Radio Publ., 1971, 664 pp. [In Russian.]
- [10] Atayants, B. A., V. M. Davydochkin, and V. V. Ezerskiy, “Consideration of Antenna Mis-matching Effects in FMCW Radio Range Finders,” *Antennas*, No. 12(79), 2003, pp. 23–27. [In Russian.]
- [11] Davydochkin, V. M., “Virtual Interference Influence on the Error of Difference Frequency Estimation in FMCW Range Finder,” *Vestnik RGRTU, Ryazan*, No. 20, 2007, pp. 47–54. [In Russian.]



# Reduction of the Measurement Error at Interference Presence Using Adaptable Weighting Functions

## 7.1 Introduction

An important feature of the FMCW RF of industrial application is an absence of intentional masking or withdrawing interference. The location and properties of the most interference can be defined in advance before the operation mode starts and therefore we can provide learning or make predictions according to the engineering specifications of those objects on which an FMCW RF is mounted.

A priori information about the interference situation in the FMCW RF operating zone is often used to decrease the range estimation error to the useful reflector. Before measurement performance during FMCW RF mounting on a specific object, one can perform estimation of amplitude and frequency of interference and record them in the memory of the FMCW RF computing device. In many cases, the necessary data can be obtained only on the basis of mathematical models of signals and interference adequate to relevant situations. It is clear that accurate determination of interference parameters would permit complete elimination of the range estimation error to the useful object. Nevertheless, accurate estimation is practically unrealizable and, moreover, interference parameters are unstable and often do not completely correspond to the mathematical model in the form of the finite sum of sinusoidal components (6.1). Therefore, the possibility of decreasing errors significantly depends on the interference situation.

In any case at a range-finder operation under interference conditions, we need to answer to the following questions:

1. Is there an interference influence and how much is it?
2. How do we determine the displacement value caused by interference?
3. How do we make corrections of range indication by the value of the calculated error?

In addition, it is important that the answer to the first question allows the use of a sign of correct orientation of FMCW RF position during its mounting.

Practice shows that, depending on the SR source, the SIR can be changed in wide limits. For instance, at the FMCW RF using the liquid level measurement near the reservoir bottom, the value  $q_{s/i}$  (depending on dielectric properties of the material) can be significantly less than 1. For the reflection intensity from the reservoir

construction elements, its sidewall is such that  $q_{s/i} > 0$  dB. At the range measurement in the loaded reservoir, reflections take place between the reservoir roof, the level-meter case, and the reflecting surface, in this case,  $q_{s/i} > 6$  to 20 dB.

The SR presence leads to the appearance of two additional components of measurement errors:

1. The frequency of the beating signal will be defined with the error, whose value, as shown in Chapter 6, is defined by the degree of the mutual influence of the main lobes and sidelobes of useful and interference signal spectra.
2. The spurious signal can be accepted as the useful signal, which leads to anomalous measurement errors.

Therefore, at the range measurement on the SR background, it is necessary to solve two problems:

1. The problem of choice from the SC's assembly of this component, which is calculated according to the signal (6.1) and corresponds to the useful signal;
2. The problem of the DFS influence on the useful signal minimization corresponding to the SR.

Both problems can be solved in general by means of minimization of some goal function  $F\{S(t), S_M(t)\}$ , where  $S_M(t)$  is some model signal. For minimization of the function  $F\{S(t), S_M(t)\}$  for all  $3M$  parameters (delay time, phases, and amplitudes of  $M$  DFS components), it is necessary to use methods of multiparameter optimization, which require large computing expenses and do not allow us to obtain an unambiguous solution. Therefore, in this chapter and Chapters 8 and 9, we consider the methods and algorithms of the SR influence minimization in various situations and on the basis of different approaches. Therefore, it is advisable to divide these methods into two groups.

To the first group we attribute methods with a classical approach to problem solving based on the reduction of the measurement error by control of the WF shape with the purpose of decreasing the SR spectrum and SL influence on the useful signal or at the analysis of such influence for a different WF shape, and introducing the correcting amendment. These methods will be discussed in this chapter.

In the second group we include methods that are connected (in varying degrees) with the construction of the model and with the application of parameter control of this model for the estimation of the measured range including a situation when the useful and spurious signal are not resolved. We call these methods *parametric* and they will be described in Chapter 8.

## 7.2 Estimation of the Interference Situation

The application of software methods to decrease the measurement error requires an analysis of the interference situation in the FMCW RF operating zone. Therefore, it is required to detect the useful DFS on the SR background. The task becomes complicated by the fact that useful DFS and DFS generated by SR are identical in

their structure and differ by amplitude and frequency only. In the situation when the useful DFS exceeds the signal from the SR in amplitude, the task of detection has no problems, but everything becomes complicated in the situation when the useful DFS becomes less than the signal from the SR. We can solve the task of detection of useful DFS of the background of SL of SAD of the spurious reflection at its resolution and the account of a priori information about all the SR positions. Moreover, the account of such information is necessary for some algorithms decreasing interference influence. Thus, the problem of FMCW RF learning under conditions when the useful reflector is absent in the operating zone is important. Therefore, it is necessary to determine a number of SRs to estimate their location in the FMCW RF operating zone and SIR  $q_{s/i}$  for each of them. This will allow the determination of IEZ boundaries and the selection of the most suitable method of DFS processing, permitting the minimization of the range estimation error. Obviously, for the FMCW RF, such a problem can be solved in the simplest manner in the spectral domain.

At the SR detection in the learning mode, it is necessary to solve the following tasks:

1. Because the SR detection is carried out on the background of noisy interference, it is necessary to minimize the probability of acceptance instead of the noise overshoots (i.e., minimizes the probability of false alarm).
2. To eliminate possibility of the SL spectra acceptance of adjacent reflectors as the spurious reflector.
3. To estimate the frequency corresponding to each SR position.
4. To estimate the SC amplitude for each SR.

SR detection is advisable to perform the classical method used at detection in the spectral domain of separate harmonic components presenting in the signal specified on the finite time interval. Such a task is successfully solved with the help of the WF [1], when the standard procedure of a weak signal detection is used on the background of the strong signal.

It is usually necessary to achieve the accepted measurement accuracy that the FMCW RF noise level is essentially less than a level of the weak useful signal. The applied WF should have the minimal SAD SLL at the specified width of the main lobe and at the specified SL decreased speed (optimal WFs). At the detection of the near located weakly reflected object on the background of strong spurious signal, the useful SAD item with the frequency  $x_1$  is significantly less than the spurious item with frequency  $x_2$  and is distorted mainly by the SL of two spurious SAD items  $S_2$  with frequencies  $x_2$  and  $-x_2$  (for  $\omega > 0$  and  $\omega < 0$ ), and the influence of the item  $S_1$  with the frequency  $-x_1$  from the area  $\omega < 0$  is insignificant. It is known that a choice of large values of WF  $C_s$  at the specified width of the main lobe leads to an inevitable increase of SL of each SAD item closed to the main lobe. In this situation, the increase of SL leads to a larger distortion of the main lobe of the SAD useful item. Therefore, to solve the problem, we should select the WF with a minimal value of  $C_s$ , at which the possibility to obtain the minimum SLL is ensured at the specified width of the mail lobe.

One SR, which is always present in the short-range FMCW RF, is the reflection from the AWP elements. Under the conditions of a long effect of environment with

high contents of dust and moisture on AWP elements, the reflection coefficient of EMW from them due to deposits can increase to the value approaching unity. From (6.2), we can determine that for the most frequently used antennas with the gain about 20 dB, the SIR can decrease to  $-40$  dB already at ranges between the antenna and the probing object corresponding to 3 and more in the frequency domain (at the FM sweep more than 500 MHz). Because the larger value of SIR simplifies signal detection, in the examples we shall use the value equal to  $-40$  dB.

The specification of SLL and the width of the WF main lobe for the first estimation of ranges to UR and SR are defined by the ratio of SD item levels corresponding to probing objects and the range difference to UR and SR. For example, for the DC WF, the SLL  $Q^{-1}$  and a half-width of the main lobe on the zero level  $x_0$  are connected by the relation:

$$x_0 = \sqrt{0.25 + \ln^2(Q + \sqrt{Q^2 - 1})/\pi^2} \quad (7.1)$$

Evidently, to detect the SR with the rough estimation of its parameters on the background of strong interference, the relative SLL of the used WF should be essentially less than the minimal possible SIR with an account of coherent SL summation for  $\omega > 0$  and  $\omega < 0$ . In the considered case, the SLL must be essentially less than  $-46$  dB. The restriction of  $Q$  is defined by the above-mentioned minimal possible range between the positions of SR and UR limiting the width of the WF main lobe. For the DC WF with  $x_0 = 0.625 \dots 0.69 (x_1 - x_2)$  for any  $x_1$  theoretically signals are already absolutely resolved at  $x_1 - x_2 \geq 4$  with a minimal value of SAD dip between signal frequencies  $x_1$  and  $x_2$  more than 6 dB lower than the SAD item level of the weak signal.

At the application of the optimal WF obtained on the basis of AWF (see the Appendix), taking into consideration of above-mentioned recommendations in the problem under consideration, we should use the WF with  $C_s = 6$  dB/oct. From the Appendix, it follows that at the specified value of the AWF main lobe width, an increase of  $N$  allows for the SL reduction. The limit is the DC WF SLL. However, the AWF with  $C_s = 6$  dB/oct at the minimal possible  $N$  for the specified  $Q$  essentially exceeding 46 dB loses to the DC WF in SLL only by 3 to 6 dB. Therefore, to solve the SR detection problem with roughly estimating its parameters on the background of strong interference, we may use the AWF beginning from  $N = 2$  at the same value of the main lobe width as for the DC WF  $b_1 = 0.625 \dots 0.69 (x_1 - x_2)$ .

For example, Figure 7.1 shows the resulting signal SAD by solid bold lines relatively using the DC WF and the AWF with  $C_s = 6$  dB/oct. The amplitude of the useful signal item with the relative frequency  $x_1 = 7$  is 40 dB less than amplitude of the spurious signal with the relative frequency  $x_2 = 3$ . The SAD of the useful signal item with  $\omega > 0$  is shown by the solid thin line. In the scale that is shown, the SLs of the spurious SAD item with the frequency  $x_1 = -7$  from the area  $\omega < 0$  are not seen. The spurious SAD items for  $\omega > 0$  and  $\omega < 0$  from the spurious signal item are shown by the dotted and chain lines, respectively. Both WFs have the same width of the main lobe on the zero level equal to 5.5. The SLL of the DC WF SAD is  $-67.67$  dB, and the SLL of the AWF SAD with  $C_s = 6$  dB/oct,  $N = 2$ ,  $b_1 = 2.75$ , and  $b_2 = 4.2111$  is  $-61.7$  dB.

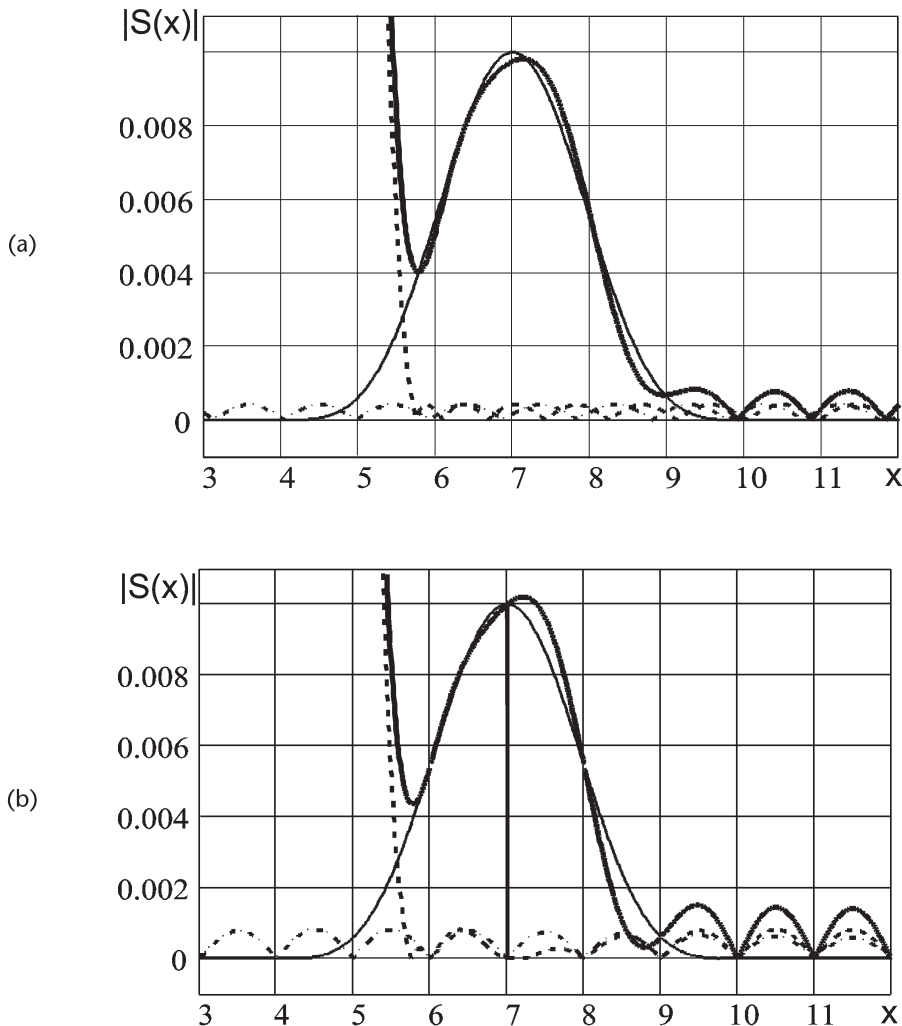


**Figure 7.1** (a, b) The modulus of resulting signal SD and the modulus of its items with the respective frequency  $x_1 = 7$  and  $x_2 = 3$ .

We see from Figure 7.1 that both WFs ensure the extraction of the weak signal on the background of strong interference; therefore, the WF parameter choice shown provides a significant excess of SAD of the weak DFS item over the SL of the strong item. The application of the algorithm (3.4) in the range of the relative frequencies 6 to 8 after the UR detection leads to the normalized relative range errors weakly reflecting the UR equal to 0.136 using the DC WF and 0.2078 using the AWF with  $N = 2$  and  $C_s = 6 \text{ dB/oct}$ .

The SR detection in the FMCW RF operating zone has peculiarities. We consider the case when the SR location is a priori unknown. We analyze the situation when there is a possibility of obtaining the DFS SAD at the UR absence or at its location in the very far point of the operating volume. It is clear that in this case the items from all SRs will be present in the resulting SAD, including reflections from the AWP.

We assume that the SRs, for which the ratio  $q_{i/n,i} = G_{\text{int}}(\omega_i)/N_0$  is large enough ( $q_{i/n,i} > 30 - 40 \text{dB}$ ), are detected with Probability 1, and that probabilities of the false alarm are equal to zero. This case corresponds to the situation in which the SR amplitude is commensurable with the amplitude of the useful signal.

For the SR detection of small intensity in the learning mode, it is necessary to provide acceptable detection characteristics and to eliminate the possibility of accepting the SD sidelobes of the reflection from the AWP as the SR. For this purpose, we may use the optimal detector [2] with some modifications. Using the distribution law (3.49) and assuming that the distribution of the SD estimation of the white noise is exponential with the parameter  $N_0$ , we obtain the likelihood ratio for the  $i$ th SC:

$$\Lambda_i = \exp[-G(\omega_i)/N_0] I_0\left(\sqrt{\hat{G}(\omega_i)G(\omega_i)}/N_0\right) \quad (7.2)$$

where  $\hat{G}(\omega_i)$  is the estimation of the DFS SC  $G(\omega_i)$  on the  $i$ th frequency.

Because the functions  $I_0(z)$  and  $\sqrt{z}$  are monotonic, after taking the logarithm of (7.2), we may obtain the decisive rule:

$$\hat{G}(\omega_i) \geq b \quad (7.3)$$

where  $b$  is the comparison threshold selecting from the Neyman-Pearson criterion [3]:

$$b = b_0 N_0 / q_{i/n,i} \quad (7.4)$$

$b_0 = \ln(1/F)/q_{i/n,i}$  is the normalized threshold being the solution of the equation  $\int_{b_0}^{\infty} W_1(x) dx = F$ ,  $W_1(x)$  is the distribution law of noise PSD, and  $F$  is the probability of false alarm.

To eliminate the possibility of mistaken acceptance of the SL reflection from the AWP as the SR, it is advisable to determine the SLL  $b_{\text{SLL}}$  of the PSD of the reflection from the AWP according to the calculated spectrum and the used WF. Then we may determine the SCs, which in the electric range interval from the minimal to maximal correspond to the simultaneous performance of (7.3) and:

$$\hat{G}(\omega_i) \geq b_{\text{SLL}} \quad (7.5)$$

All determined SCs can be considered as SRs.

To calculate the quality performance for detection, we may recommend multiplying the SC of the white noise and the SC of the DFS by the nonrandom variable  $G_{\text{int}}(\omega_i)$  (i.e., by the average value of the SR SD estimation). As a result of such a functional transformation, the exponential SC distribution of the PSD estimation of the white noise, and the distribution (3.56), we rewrite respectively in the form:

$$\begin{aligned} W_1(x) &= q_{i/n,i} \exp(-q_{i/n,i}x), \\ W_2(x) &= q_{i/n,i} \exp[-q_{i/n,i}(x+1)] I_0\left(2q_{i/n,i}\sqrt{x}\right) \end{aligned} \quad (7.6)$$

The calculated probabilities of the true detection  $D$  depending on the  $q_{i/n,i}$  at different values of  $F$  are presented in Figure 7.2. From the curves of this figure,

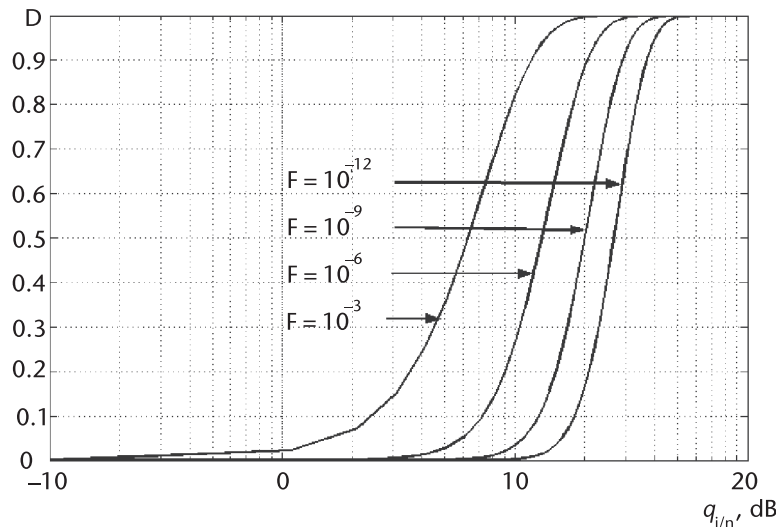


**Figure 7.2** Detection characteristics of the SR.

we may make a conclusion that the SR is detected with the probability practically equal to 1 at the probability of false alarm  $F = 10^{-10}$  in the case in which its intensity exceeds the noise level by not less than 18 dB.

The probabilities of false alarm, at which the functions in Figure 7.2 are calculated, correspond to the SR detection at each of frequencies, where the DFS spectrum is computed. The resulting probability of false alarm  $F_{fa}$  for frequencies  $\omega_i$  where  $1 \leq i \leq I$  and  $I$  is the number of frequencies at which SR detection occurs is determined as:  $F_{fa} = 1 - (1 - F)^I$ . For  $F = 10^{-12}$  at the DFS representation in the time domain by 1,024 samples, the variable  $F_{fa} = 5.12 \times 10^{-12}$  is the case when all SCs are used for SR detection. It is clear that we cannot consider such a probability of false alarm.

In the specific case of the FMCW RF application as a level-meter for liquid products, approaching the reflected surface level to the reservoir bottom leads to the fact that the SIR becomes less than 1. For instance, for some types of mineral oil, the intensity of the reflection from the bottom becomes more than the intensity of the useful signal at the range of 2 m to 3 m from the bottom (for carrying the signal frequency of 10 GHz). Nevertheless, this circumstance does not introduce significant peculiarities in the DFS frequency measurement in the case when spectra are nonresolvable in frequency. The electrical range to the bottom is always more than the true range, which allows simply enough to identify the reflection source as the maximal SC of the useful DFS spectrum is always located on a frequency less than the maximal SC of the DFS spectrum corresponding to the reflection from the bottom. Challenges with DFS frequency measurement arise in the case when the spectra of useful and interference signals are not resolvable.

After the SR detection, we need to determine the IEZ value. In the case when one SC detection threshold exceeds the IEZ boundary (see Chapter 6), we may choose (with recalculation into the range) in the size  $R_{int,i} \pm 9\delta_R$ , where  $R_{int,i}$  is the range to the  $i$ th SR calculated according to the SC frequency estimation satisfying (7.3) and (7.5). In the case when several adjacent SCs satisfy the conditions (7.3) and (7.5), IEZ size will be determined by the frequency range, on which there are detected SCs increased in each side by the value  $9\delta_R$ .

In the operating mode of the range measurement to the UR at the SR presence, the signal from which exceeds the UR level, its detection is provided on the basis of the same algorithms (7.3) and (7.5), but beyond IEZ only.

## 7.3 Error Minimization of Frequency and Amplitude Estimation of the Weak Signal on the Background of Resolvable Single Interference

### 7.3.1 Introduction

Interference properties (see Chapter 6) can significantly differ, but it is most important to estimate the range to probing the surface, the resolving of interference, and the probing object and to determine which algorithm ensures less error in the specific case. Therefore, independently on the interference type, we consider the possibility of decreasing the error caused by the resolvable interference at difference frequency estimation according to the spectrum maximum supposing that the main EE SD lobe exceeds the SLL of interference. At the estimation of the DFS, useful item parameters on the background of single interference two items remain in (6.1).

In the case of the FMCW RF application as the level-meter for weakly reflecting liquids, the amplitude of the useful signal can be essentially less than the amplitude on the interference created by encapsulation inserts in an antenna or by the reservoir bottom. In such a case, it is advisable to analyze the possibility of the range estimation error reduction both to the UR and to the SR. On the basis of range estimation results to the SR and the amplitude-phase parameters of spurious SC, the correction of the measured range to the UR is possible as well as the estimation of the device's state, for instance, estimation of antenna dirtying degree [4]. The approximate SR position in the AWP can be estimated at the calibration stage or during the device's learning.

The range to the reservoir bottom and the relative estimation of this range may change due to reservoir deformation owing to temperature variation, pressure variation inside the reservoir, mechanical influence of the material to the reservoir walls, and other factors. In addition, the dielectric permeability of the probing product can be changed as well as the electrical range to the reservoir bottom.

In any case, due to the interference of a large level, before the range measurement to the UR, the above-mentioned problem of the DFS SC detection corresponding to the useful and spurious SAD items with rough estimation of their parameters should be solved. As a result, the useful and spurious SAD items with the maximal SCs  $\hat{S}_1$  and  $\hat{S}_2$  on the frequencies  $\hat{x}_1$  and  $\hat{x}_2$  will be detected.

### 7.3.2 Minimization of the Range Measurement Error for Weakly Reflecting Liquids

This task arises at the interference presence of the large level from the encapsulating insert in the AWP. We assume that the approximate SR position in the AWP is known. From the operation conditions of the reservoir, the loading liquid and the maximal level of its loading are usually known. From these conditions, the necessary height of the FMCW RF mounting is determined to ensure resolution in the frequency of DFS items caused by the reflection from the AWP and from the liquid surface at the maximal possible loading of the reservoir. The minimal possible measuring range,

the reflection coefficient of EMW from the liquid surface, and, hence, on the basis of (6.2), the minimal possible SIR, become known as well. Therefore, each item in (6.1) plays the part of deterministic interference at the parameter estimation of the other DFS item. Then the error is due to the noise and the SL of three DFS SCs, from which one spurious item is located at  $\omega > 0$  and two items in the area  $\omega < 0$ .

We suppose that the detection problem of DFS SC and parameter estimation is solved in advance and, as a result, the spurious and useful SAD items with maximal SCs  $\hat{S}_1^{(0)}$  and  $\hat{S}_2^{(0)}$  on frequencies  $\hat{x}_1^{(0)}$  and  $\hat{x}_2^{(0)}$  are detected.

Let us determine the possibility of error reduction for the normalized range  $x_1$  and  $x_2$  estimation by the algorithm, which is similar to that analyzed in Chapter 3: the minimization algorithm for the truncation error. We assume that the DFS contains two items, one with the normalized frequency  $x_1 = 3$  and the unitary amplitude, and the other one with an amplitude lesser by 40 dB, corresponding to the UR with a normalized frequency  $x_2 = 10$ .

The process of the necessary WF parameter determination is iterative with a multiple repeat of calculations and specification of values  $b_1, b_2, \dots, b_n$  on each iteration to decrease the absolute value of difference between newly received values  $\hat{x}_1^{(n)}$  and  $\hat{x}_2^{(n)}$ , and previous values  $\hat{x}_1^{(n-1)}$  and  $\hat{x}_2^{(n-1)}$  lower than specified in the advance value  $|\hat{x}_1^{(n)} - \hat{x}_1^{(n-1)}| \leq \Delta_{x1}$  and  $|\hat{x}_2^{(n)} - \hat{x}_2^{(n-1)}| \leq \Delta_{x2}$ . In general,  $\Delta_{x1}$  and  $\Delta_{x2}$  may be different.

The frequency estimations of all SAD parameters of the model (6.1) displace due to its mutual influence. To minimize the frequency estimation error of any items, the applied AWF should ensure obtaining zero SAD with an order of not less than 2 on four frequencies corresponding to the difference of the estimated positions of the SAD item maxima. Therefore, all SAD items should be resolvable in frequency. In the considered example, this algorithm gives a zero error component caused by the mutual influence of the UR and SR SAD items at any  $x_1$ , but for  $\Delta\hat{x}_1^{(0)} = \hat{x}_2^{(0)} - \hat{x}_1^{(0)} \geq 6.5$ .

Figure 7.3 shows the SAD of the useful DFS item with the frequency  $x_1 = 10$  identified by the thin solid line, the SAD of the resulting DFS with the frequency of spurious item  $x_2 = 3$  identified by the solid bold line using the AWF with  $C_s = 6$  dB/oct,  $N = 8$  and  $b_1 = b_2 = 6, b_3 = b_4 = 7, b_5 = b_6 = 13$ , and  $b_7 = b_8 = 20$ , and the SAD difference (multiplied by 1,000) of the resulting and useful signals identified by the dotted line.

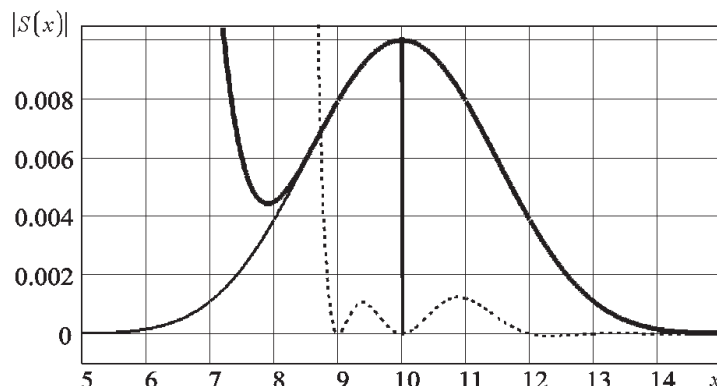


**Figure 7.3** The SAD of the useful signal with the relative frequency  $x_1 = 10$  (thin solid line), the resulting signal with interference on the frequency  $x_2 = 3$  (bold solid line) and multiplied by 1,000 modulus of SAD difference of resulting and useful signals (dotted line).

It follows from Figure 7.3 that at  $x_1 - x_2 = 7$  the AWF with the mentioned parameters ensures the accurate frequency and amplitude estimation of the weak signal on the background of strong interference due to the distortion absence by the interference SAD item on this frequency.

### 7.3.3 Action Sequence at the Level Measurement of the Weakly Reflecting Material Near an Antenna

The action sequence is the following:

- *Step 1:* According to the signal samples recorded in the memory, we calculate the SAD for the chosen AWF and determine the maximum positions of the spectrum modulus, the zero approximation for  $\hat{x}_1^{(0)}$  and  $\hat{x}_2^{(0)}$ , and the ratio of intensities of the DFS items.
- *Step 2:* The zero approximations for  $\Delta\hat{x}_1^{(0)} = \hat{x}_1^{(0)} - \hat{x}_2^{(0)}$ ,  $\Delta\hat{x}_2^{(0)} = 2\hat{x}_1^{(0)}$ ,  $\Delta\hat{x}_3^{(0)} = 2\hat{x}_2^{(0)}$ , and  $\Delta\hat{x}_4^{(0)} = \hat{x}_2^{(0)} + \hat{x}_1^{(0)}$  are calculated.
- *Step 3:* The values of  $b_1^{(0)} = b_2^{(0)} = \Delta\hat{x}_1^{(0)}$ ,  $b_3^{(0)} = b_4^{(0)} = \Delta\hat{x}_2^{(0)}$ ,  $b_5^{(0)} = b_6^{(0)} = \Delta\hat{x}_3^{(0)}$ , and  $b_7^{(0)} = b_8^{(0)} = \Delta\hat{x}_4^{(0)}$  are specified.
- *Step 4:* According to the signal samples recorded in the memory, we calculate the next and  $n$ th approximations  $\hat{x}_i^{(n)}$  at the specified AWF parameter values  $b_i^{(n-1)} = b_{i+1}^{(n-1)} = \Delta\hat{x}_{(i+1)/2}^{(n-1)}$ .
- *Step 5:* Steps 2 to 4 are repeated before the performance of the condition  $|\hat{x}_1^{(n)} - \hat{x}_1^{(n-1)}| \leq \Delta_x$  and  $|\hat{x}_2^{(n)} - \hat{x}_2^{(n-1)}| \leq \Delta_x$ .
- *Step 6:* Amplitudes and phases of each item are estimated.

If  $N = 8$ , all SAD items can be resolved in frequency and in four frequencies corresponding to the difference of the estimated positions of the SAD item maxima, and this ensured obtaining the SAD zero with an order of not less than 2. In this case, the algorithm shown theoretically allows without noise obtaining the zero error for  $2 \leq x_1 \leq 4$  and  $x_1 - x_2 \geq 6$ . If  $x_1 > 4$ , and then the algorithm ensures error minimization at  $x_1 - x_2 > 6.5$ .

However, there are a variety of problems when it is required to estimate the range to the weakly reflecting object located essentially closer to the antenna. In this case, it is necessary to neglect the weak SAD item influence from the area  $\omega < 0$  with the coordinate  $-x_1$  upon the error estimation of the weak SD item from the area  $\omega > 0$  with the coordinate  $x_1$  to increase the zero order of the SD item with the coordinate  $x_2$  in the area  $x = x_1$ . In the Appendix it is shown that an increase of a number of items  $N$  of the AWF at the specified values  $b_1 < N - 1$  and  $b_1 - b_2 > 1$  can lead to an SL increase in the interval  $[b_1, b_2]$  and relatively to an increase of the estimation error. This is especially true with a difference frequency estimation of the DFS weak item on the background of a strong item near a resolution boundary in the range. In this case, it is important to decrease the error at minimal  $N$  or to determine  $N$  at an admissible error level in the range interval from the minimal possible to  $\Delta\hat{x}_1^{(0)} = \hat{x}_1^{(0)} - \hat{x}_2^{(0)} \geq 6.5$ , when we can use the above-mentioned algorithm of accurate frequency estimation. Then we consider only the task of determining  $N$  in the interval  $4 \leq \Delta\hat{x}_1^{(0)} = \hat{x}_1^{(0)} - \hat{x}_2^{(0)} \leq 7$ .

Varying  $N$ , we determine the admissible error level of the normalized range estimation of  $x_1$  and  $x_2$  according to the DFS, one item with fixed normalized frequency  $x_2 = 3$  and unitary amplitude corresponding to the reflection from the antenna, and the other item with amplitude by 40 dB less corresponding to the SR with normalized frequency varying from  $x_1 = 7$  to  $x_1 = 10.5$ .

Taking into account the coincidence shown earlier of theoretical results with numerical experiments in the task under consideration, we give the simulation results only. Among the known WFs, the KB WF is the best for the resolution of two signals and for parameter estimation of signal items at an increase of  $x_1$ . Therefore, we give for comparison the calculation results using the AWF and KB WF on the basis of developed iterative procedures ensuring the error minimum. The results obtained in accordance with an approach similar to the above-mentioned one for the AWF with different  $N$  from 3 to 8 and a different distribution of specified zeros are shown in Figure 7.4.

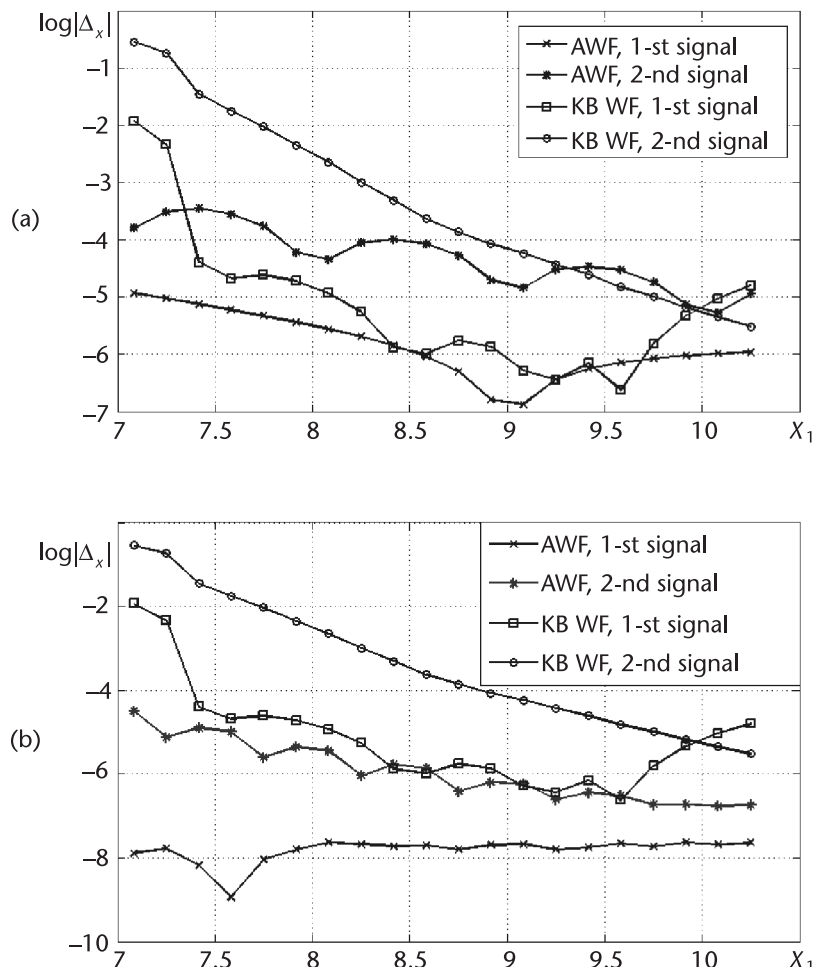


**Figure 7.4** Plots of the normalized MSD logarithm of the estimation DFS error weighted by the KB WF and AWF: (a)  $w_s(\hat{x}_1 - \hat{x}_2, \hat{x}_1 - \hat{x}_2, \hat{x}_1 + \hat{x}_2)$  with  $N = 3$  and (b)  $w_s(\hat{x}_1 - \hat{x}_2, \hat{x}_1 - \hat{x}_2, \hat{x}_1 - \hat{x}_2, \hat{x}_1 - \hat{x}_2, 2\hat{x}_2, 2\hat{x}_2, \hat{x}_1 + \hat{x}_2, \hat{x}_1 + \hat{x}_2)$  with  $N = 8$ .

The application of the AWF with a minimal number of varied parameters  $N = 3$  [Figure 7.4(a)] provides an advantage on the level of the frequency estimation error of the DFS items over the KB WF achieving several orders only near the signal resolution boundary  $x_2 - x_1 < 6$ . The increase of frequency of the weak item leads to practically the same results of the DFS item frequency estimation for both WFs. The increase of the AWD-varying parameter number  $N$  [Figure 7.4(b)] allows some more reduction of the estimate error. From a comparison of Figure 7.4, we see that the frequency estimation error of the weak signal near the resolution boundary ( $x_2 - x_1 \approx 4.5$ ) decreases by more than three orders with the number increasing the varied parameters of  $N$  from three to eight. We note that in accordance with the above-mentioned notes the AWF zero order in the frequency area  $b_1 = b_2 = b_3 = b_4 = \hat{x}_1 - \hat{x}_2$  was increased to 4 owing to the elimination of the varied zeros on the frequency  $2\hat{x}_1$  to obtain Figure 7.4(b). At a reliable signal resolution ( $x_2 - x_1 \approx 7$ ), the benefit with an increase of a varied parameter number decreases to 1.5 orders.

The noise presence in the signal does not exclude the possibility of adaptive reduction of estimation errors both for the KB WF and AWF. However, the difference of the minimal achievable levels of error decreases near the boundary of signal resolution and for reliable signal resolution  $x_1 - x_2 > 6$ . Therefore (depending on the noise level), results are varied for the AWF application with a different number of varied parameters (Figure 7.5). For a relatively high noise level ( $q_{s/i} = 20$  dB for a weak signal item), the AWF advantage is demonstrated with small ( $N = 3$ ) number of varied parameters (Figure 7.5), forming about 100 times near the boundary of signal resolution, which decreases to 1 at the frequency difference of the signal items  $x_2 - x_1 \approx 5$  and slowly increases to 1.25 at a further increase of the difference frequency to 7. Under these conditions, the AWF with a number of varied parameters equal to 8 has an advantage over the KB WF only near the resolution boundary  $x_2 - x_1 \leq 4.5$  (figure is not shown).

Such a function of the resulting error is caused by prevailing influence of truncation component at a small frequency difference and by prevailing the noise component at a large frequency difference. At a noise level reduction up to  $-60$  dB with

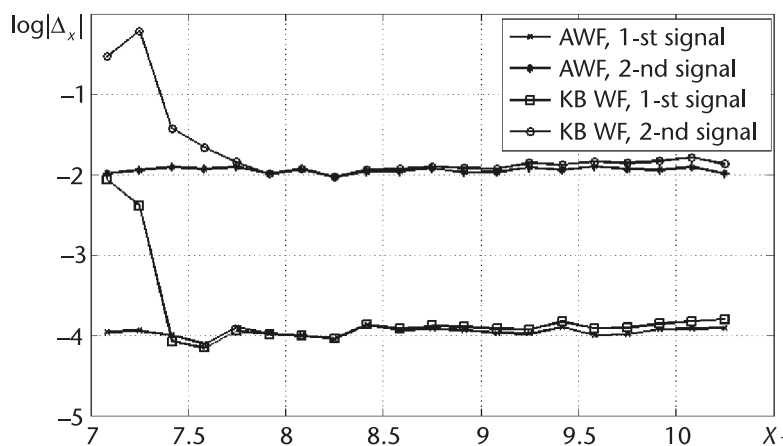


**Figure 7.5** Plots of the normalized MSD logarithm of the estimation error of the difference frequencies of the DFS weighted by the KB WF and AWF  $w_s$  ( $\hat{x}_2 - \hat{x}_1, \hat{x}_2 - \hat{x}_1, \hat{x}_2 + \hat{x}_1$ ) with  $N = 3$ :  $q = 20$  dB.

regard to a weak DFS item, the AWF advantage begins to increase, especially near the boundary of signal resolution.

At the amplitude estimation of signal items, the application of the AWF even with a small item number  $N = 3$  allows the reduction of the truncation component of the error up to 6 orders near the resolution boundary compared to the KB WF [Figure 7.6(a)]. The growth of the number of items increases the AWF advantage. The rela-

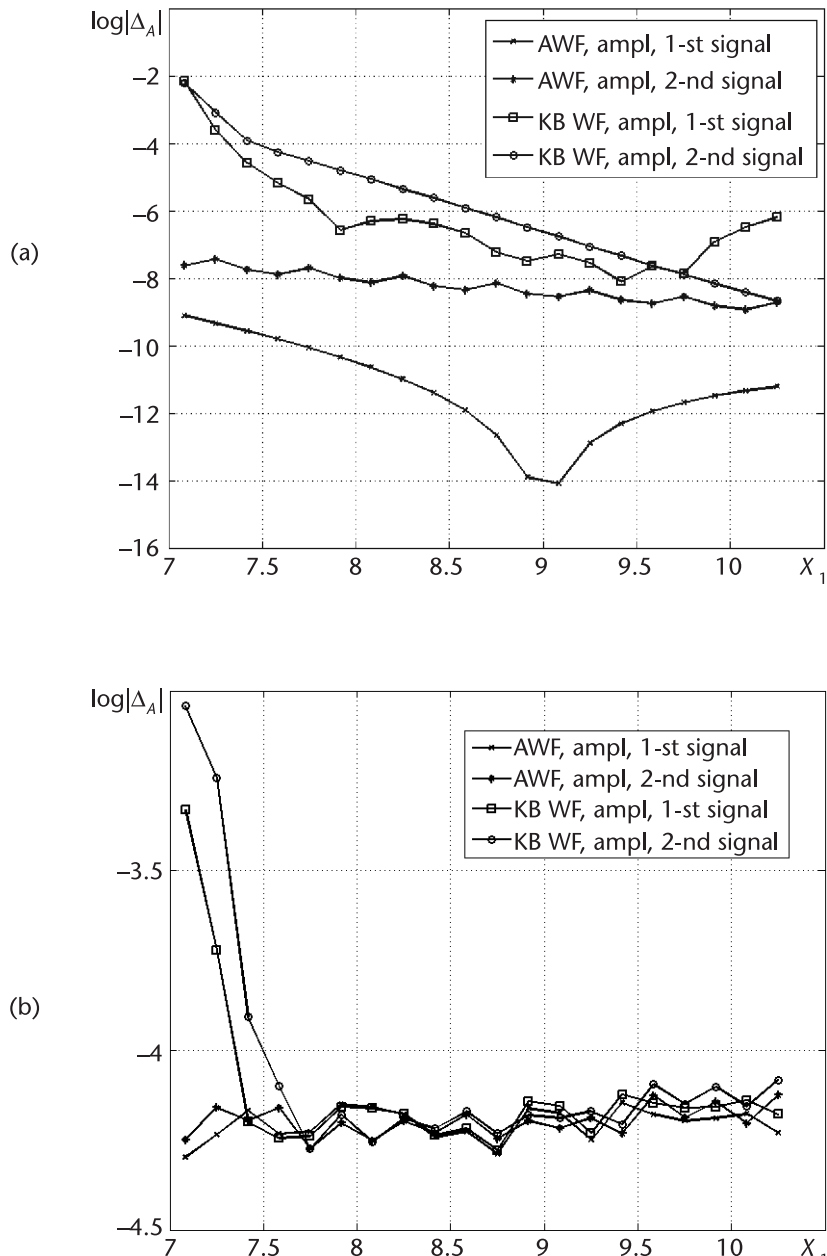


**Figure 7.6** Plots of the normalized MSD logarithm of amplitude item estimation of the DFS weighted by the KB WF and AWF  $w_s(\hat{x}_2 - \hat{x}_1, \hat{x}_2 - \hat{x}_1, \hat{x}_2 + \hat{x}_1)$  with  $N = 3$ : (a) without noise and (b) with a noise of 20 dB.

tively high noise level ( $q_{s/i} = 20$  dB with regard to the weak DFS item) decreases the AWQF advantage from 10 times near the resolution boundary to 1 at the frequency difference of DFS items  $x_2 - x_1 \approx 5$ , which then slowly increases about to 1.1 for a further increase of the difference frequency of the DFS items to 7 [Figure 7.6(b)].

### 7.3.4 Range Measurement on the Background of Strong Reflection from a Reservoir Bottom

It follows from the results of Chapter 6 that at range measurement to the surface of the weakly reflecting radio transparent liquid on the background of strong reflection from a reservoir bottom, the WF ensuring  $C_s = 12$  dB/oct is the best option. It is caused by significant reduction of the SAD item SL with frequencies  $-x_2$  and  $-x_1$  from the area  $\omega < 0$ . In this case, algorithm simplification is possible for signal parameter estimation and reduction of varied parameter number due to the natural decrease of the SLL of spectrum items on the frequencies  $\omega < 0$  for  $x_1 \gg 1$  and  $x_2 \gg 1$ . As an example, we may give parameters of the optimal WF with  $C_s = 12$  dB/oct,  $N = 2$ ,  $b_1 = 2.75$ , and  $b_2 = 3.37145$ . For the maximal SAD SLL equal to  $-60.7$  dB, this WF on the relative frequency ensures about  $-98$  dB.

Because in this case we may neglect the spectrum items for  $\omega < 0$ , the estimation of the signal component frequency can be carried out by algorithms (considered in Chapter 3) of minimization of the truncation error of the range estimation on the noise background. The difference consists in the determination of the specified AWF parameter  $b_N^{(0)} = |\hat{x}_2^{(0)} - \hat{x}_1^{(0)}|$  and its further specifications  $b_N^{(n)} = |\hat{x}_2^{(n)} - \hat{x}_1^{(n)}|$ .

If the maximum SLL of WF is commensurable with the SLL of the WF on the difference of relative frequencies  $2|x_2 - x_1|$ , we cannot completely neglect the spectrum items in the negative frequency area. If, at that, the relative range essentially exceeds 1, then the previous algorithm of error decrease due to the SL of one SD item is added by the procedure of the SD SL item suppression for  $\omega < 0$  determined according to the initial estimation considered above. In this case, frequency increase of signal items provides additional reduction of estimation errors practically to the level of the truncation error analyzed in Chapter 3. Therefore, it is enough to have three varied AWF parameters, two of which  $b_1^{(n)} = b_2^{(n)} = |\hat{x}_2^{(n)} - \hat{x}_1^{(n)}|$ , and the third of which  $b_3^{(n)} \approx \hat{x}_2^{(n)} + \hat{x}_1^{(n)} + |\hat{x}_1^{(n)} - \hat{x}_2^{(n)}|A_1/(A_1 + A_2)$  for  $x_1 \geq x_2$  or  $b_3^{(n)} \approx \hat{x}_2^{(n)} + \hat{x}_1^{(n)} + |\hat{x}_1^{(n)} - \hat{x}_2^{(n)}|A_2/(A_1 + A_2)$  for  $x_2 > x_1$ .

## 7.4 Error Reduction of Difference Frequency Estimation of the Signal Received on the Background of Nonresolvable Interference

### 7.4.1 The Situations Most Often Met in Practice

The situations most often met in practice are the following:

1. Consideration of synchronous range variation to the SR and to the UR is typical for the FMCW RF application for level measurement on objects within the oil-chemical industry in the case of the FMCW RF mounting near a reservoir wall, which was analyzed in Chapter 6.

2. Widespread application of the industrial FMCW RF is the level measurement in takeoff lines or directing tubes of pontons, which play the role of multimode waveguides for the FMCW RF. In this case, waves of higher modes influence the range estimation error due to different phase velocities. As in the previous example, connections between useful signal delays and manifold interference can be determined with a small error. However, phases and amplitudes of higher modes depend on whether the condition of the internal surface of tubes are unstable.
3. Fixed positions of interference can be estimated and recorded into the FMCW RF memory at the stage of learning. However, interference parameters do not remain constant during the operation process and therefore we should take into account their instability.

#### 7.4.2 The Method of Error Decrease

The unambiguous connection of ranges to the UR and SR and the interference amplitude and shapes of WF SAD with the range estimation error to the useful object at range measurement according to SAD maximum are determined by (3.16) and (3.17), considered in Chapter 3. This connection gives the possibility of formulating the inverse problem according to the specified set of WF parameters, of which the SAD is known, and according to the estimated ranges corresponding to this set of WF parameters to determine the range to the useful object. In such a formulation, (3.16) and (3.17) give a system of nonlinear equations, for which an analytical solution cannot be possible in the closed form.

To reduce errors, we note that the dependence of (3.16) and (3.17) versus the range to the UR and SR has an oscillating character and passes through the sequence of points in which the estimation error is absent.

Figure 7.7 illustrates the theoretical functions of the range estimation error and the error envelopes versus measured range. The signal is weighted by the uniform

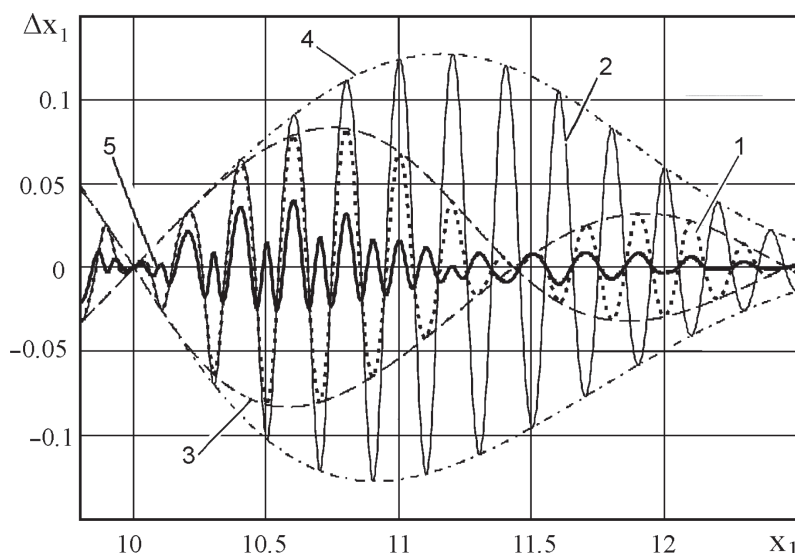


Figure 7.7 Envelope curves and range estimation errors.

WF (curve 1) and the Blackman WF (curve 2). The functions of error envelopes are curves 3 and 4, respectively. In Figure 7.7, the normalized range to the SR is equal to 10 and  $q_{s/i} = 14$  dB.

At high SIR ( $q_{s/i} \geq 14$  to 20 dB), the positions of points of accurate range estimation do not depend practically upon the WF SAD shape. Between these points, the error value is defined by the range difference between the UR and SR, the ratio of their amplitude and properties of the used WF. Narrowing of the WF SAD main lobe allows the error reduction caused by a nonresolvable object (in range) but at the expense of an error increase caused by the distant SR.

Differences in range estimation according to the signal processed by the WF with a different width of the main lobe are a sign of interference influence on the range estimation. The application of this sign allows us to obtain the equation for the result correction of the range estimation from (3.16) and (3.17).

The variation of the WF SAD shape leads to the variation of the estimation result  $x_{\text{est}1}(*)$  and  $\Delta x_{\text{est}2}(*)$  by the value

$$\begin{aligned}\Delta x_{\text{est}}(x_1, x_2, b_1, \dots, b_m, q_{s/i}) &= x_{\text{est}1}(x_1, x_2, b_1, \dots, b_m, q_{s/i}) \\ &\quad - x_{\text{est}}(x_1, x_2, b_{m+1}, \dots, b_m, q_{s/i})\end{aligned}\quad (7.7)$$

where  $b_1, \dots, b_m$  and  $b_{m+1}, \dots, b_m$  are sets of specified normalized ranges in the AWF,  $x_{\text{est}1}(*)$  and  $x_{\text{est}2}(*)$  are the results of the range estimation to the useful object, respectively, with the first and second sets of the AWF parameters, and  $x_1$  and  $x_2$  are the ranges to the UR and SR, respectively. The recommendations for choosing the AWF parameter set are given next.

Thanks to an adequately stable position of points in which the estimation error is absent (on the level of  $q_{s/i} \geq 14$  to 20 dB), the range error variation is proportional to the EE variation.

Hence, using range estimation variation with different WFs and a priori information about interference position and theoretical functions of the EE variation, we can obtain an approximate value of the correcting amendment of the range estimation

$$\begin{aligned}\Delta x_{\text{corr}}(x_1, x_2, \hat{x}_1, \hat{x}_2, b_1, \dots, b_m, q_{s/i}) &= \Delta x_{\text{est}}(x_1, x_2, b_1, \dots, b_m, q_{s/i}) \\ &\quad \times K(\hat{x}_1, \hat{x}_2, b_1, \dots, b_m, q_{s/i})\end{aligned}\quad (7.8)$$

where

$$K(\hat{x}_1, \hat{x}_2, b_1, \dots, b_m, q_{s/i}) = \Delta \frac{\Delta x_{2\text{est},\text{th}}(\hat{x}_1, \hat{x}_2, b_{m+1}, \dots, b_m, q_{s/i})}{\Delta x_{1\text{est},\text{th}}(\hat{x}_1, \hat{x}_2, b_1, \dots, b_m, q_{s/i}) - \Delta x_{2\text{est},\text{th}}(\hat{x}_1, \hat{x}_2, b_{m+1}, \dots, b_m, q_{s/i})}$$

is the correction coefficient and  $\Delta x_{1\text{est},\text{th}}(\hat{x}_1, \hat{x}_2, b_1, \dots, b_m, q_{s/i})$  and  $\Delta x_{2\text{est},\text{th}}(\hat{x}_1, \hat{x}_2, b_{m+1}, \dots, b_m, q_{s/i})$  are the theoretical EE of the range estimation with the first and second sets of the AWF parameters calculated using estimations.

The EE asymmetry of positive and negative values leads to the necessity of envelope choice depending on a sign of estimation difference. To simplify the algorithm, we may sacrifice an achievable minimum of the resulting error and assume that the denominator of the correcting coefficient is equal to the average value of envelope difference modulus

$$\Delta x_{\text{est,th}} = 0.5 \left\{ \left| \Delta x_{1\text{est,th+}}(\hat{x}_1, \hat{x}_2, b_1, \dots, b_m, q_{s/i}) - \Delta x_{2\text{est,th+}}(\hat{x}_1, \hat{x}_2, b_{m+1}, \dots, b_{2m}, q_{s/i}) \right| + \left| \Delta x_{1\text{est,th-}}(\hat{x}_1, \hat{x}_2, b_1, \dots, b_m, q_{s/i}) - \Delta x_{2\text{est,th-}}(\hat{x}_1, \hat{x}_2, b_{m+1}, \dots, b_{2m}, q_{s/i}) \right| \right\} \quad (7.9)$$

where  $\Delta x_{1\text{est,th+}}(*)$ ,  $\Delta x_{2\text{est,th+}}(*)$ ,  $\Delta x_{1\text{est,th-}}(*)$ , and  $\Delta x_{2\text{est,th-}}(*)$  are the positive and negative values of the theoretical EE functions. Therefore, we write the approximate value of correcting coefficient as:

$$K = \left| \frac{\Delta x_{2\text{est,th}}(\hat{x}_1, \hat{x}_2, b_{m+1}, \dots, b_{2m}, q_{s/i})}{\Delta x_{\text{est,th}}} \right| \quad (7.10)$$

The resulting error and estimation of normalized range will be defined, respectively, by the following equations:

$$\begin{aligned} \Delta x_{\Sigma}(x_1, x_2, \hat{x}_1, \hat{x}_2, b_1, \dots, b_{2m}, q_{s/i}) &= \Delta x_{\text{est}}(x_1, x_2, b_1, \dots, b_m, q_{s/i}) \\ &\quad - \Delta x_{\text{corr}}(x_1, x_2, \hat{x}_1, \hat{x}_2, b_1, \dots, b_{2m}, q_{s/i}) \end{aligned} \quad (7.11)$$

$$\hat{x}_1 = x_{\text{est}}(x_1, x_2, b_{m+1}, \dots, b_{2m}, q_{s/i}) - \Delta x_{\text{corr}}(x_1, x_2, \hat{x}_1, \hat{x}_2, b_1, \dots, b_{2m}, q_{s/i}) \quad (7.12)$$

The possibility of an error decrease is illustrated in Figure 7.7 by curve 5 for  $q_{s/i} = 14$  dB and by curve 1 in Figure 7.8 for  $q_{s/i} = 34$  dB, in which the functions of the corrected estimation errors are presented in the assumption of the fixed range to interference knowledge performed at the learning stage.

The typical feature of the range estimation result correction is the progressive error decrease with  $q_{s/i}$  increasing, which is seen from the comparison of Figures 7.7 and 7.8, in which curve 2 corresponds to the noncorrected range estimation error.

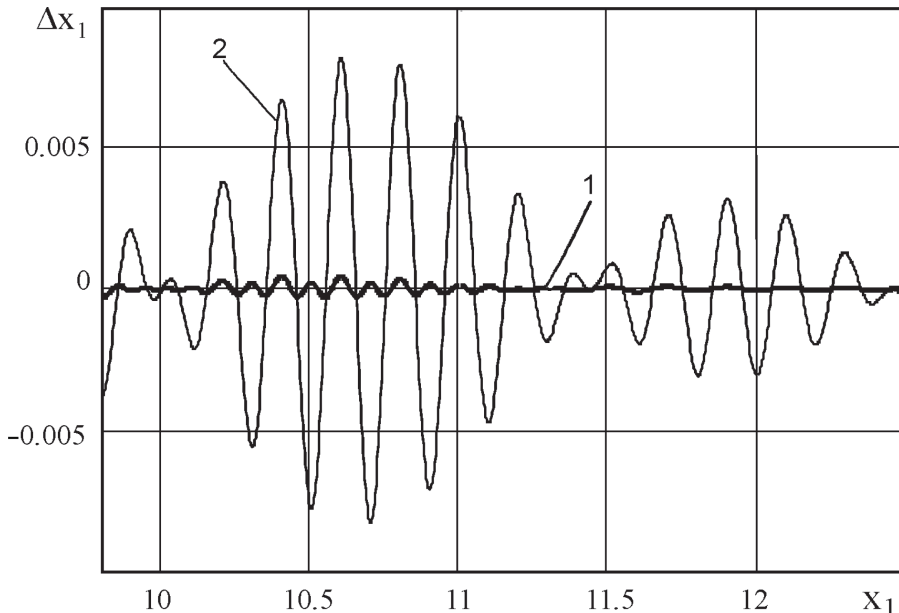


**Figure 7.8** The plots of the noncorrected range estimation error according to the signal weighted by the uniform WF (curve 2) and corrected estimation (curve 1) for  $q_{s/i} = 34$  dB.

This method of correction at the noise presence cannot fully eliminate the interference influence on the range estimation error due to the solution instability in the vicinity of the range coincidence point to the UR and SR, when range estimations do not necessarily depend on the WF shape. Moreover, the range estimation differs from the exact value. Therefore, as mentioned earlier, the possibility of error decrease significantly depends on the following interference situations:

- *Situation 1:* Liquid level variation in the reservoir accompanies the synchronous variation of ranges to the UR and SR and the difference range measurement error for them is insignificant. If neglecting the antenna PC distortions, the range estimation difference to the UR and SR will be determined by the evident equation

$$\Delta x \approx (x_L + \Delta x_L)^2 / 2(x_1 + \Delta x_1) \quad (7.13)$$

where  $x_L$  and  $\Delta x_L$  are the normalized range from an antenna to the reservoir wall and the error of its determination.

In this case, the error of the correcting amendment determination is insignificant and is defined by the range estimation error to the reservoir wall  $\Delta x_L$  (a small value as  $x_L$  can be measured with a standard application) and the range estimation error to the UR  $\Delta x_1$ . If we do not take into account the antenna DP, the resulting error in the scale used in Figures 7.7 and 7.8 is indistinguishable with the error obtained in the assumption of a known range to the SR.

- *Situation 2:* The error of correcting amendment determination is also insignificant due to a practically deterministic connection of delays of the main and higher modes.
- *Situation 3:* Under interference influence, the ranges  $\hat{x}_1$  and  $\hat{x}_2$  are determined with the error and it results in the estimation error  $\hat{K}$  appearance. Figure 7.9 shows the estimation  $\hat{K}$  function versus the range to the UR  $x_1$  with an account of the error of its determination for  $x_2 = 10$  and  $q_{s/i} = 14$  dB (solid line) and for  $q_{s/i} = 34$  dB (dotted line).

We see that the error of the correcting amendment determination increases at the approach of the UR and SR and therefore it has a sharply oscillating character. As a result, the range error to the UR is not specified at the effect of the interference closed in range. In the  $x_1$  area less than 10.52, the narrow error overshoots are observed in Figure 7.10 corresponding to overshoots in the plot of the correction coefficient in Figure 7.9. Significant range specification begins for  $x_1 - x_2 \geq 0.55$ .

The essential error of the correcting amendment determination defines the limitations on the application area of the method of correction results by the range difference to the UR and SR  $\Delta x \geq 0.5$  for  $q_{s/i} \leq 26$  dB. At  $q_{s/i} > 32$  dB, the limitations on the application area of the correction method are taken away. Looking ahead, we note that if we introduce limitations on  $K$ , the correction of range estimation results can also be used at a large interference level. The application of correction

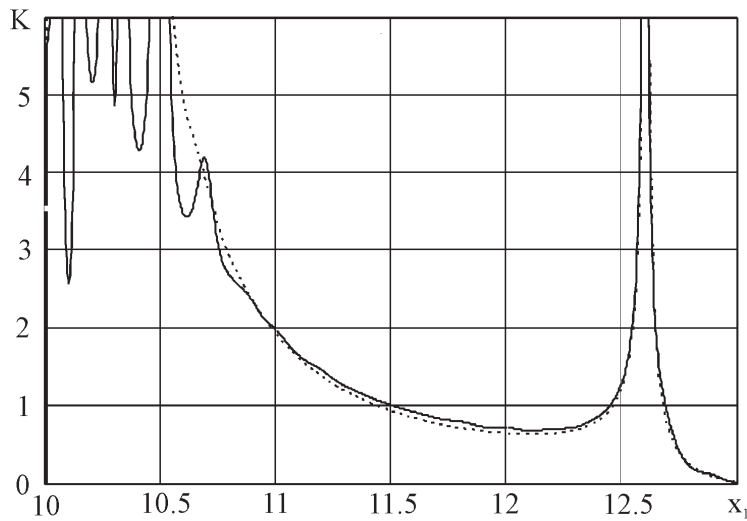


**Figure 7.9** Plots of the correction coefficient estimation versus the range to a useful object  $x_1$  with an account of the error of its determination for  $x_2 = 10$  for  $q_{s/i} = 14$  dB (solid line) and for  $q_{s/i} = 34$  dB (dotted line).

for experimental data processing (Chapter 9) gives positive results for  $q_{s/i} = 14$  dB. In this case, anomalous large errors of the corrected estimation are limited inside the range  $\Delta x \leq 0.5$  by the level of noncorrected estimation. The correction coefficient should be limited on the level of 2.5 to 4.

From theoretical results, it follows that due to low sensitivity to errors of SIR determination under conditions, which are adequate for the first and second situations, the range estimation error reduction can ensure the following algorithm.

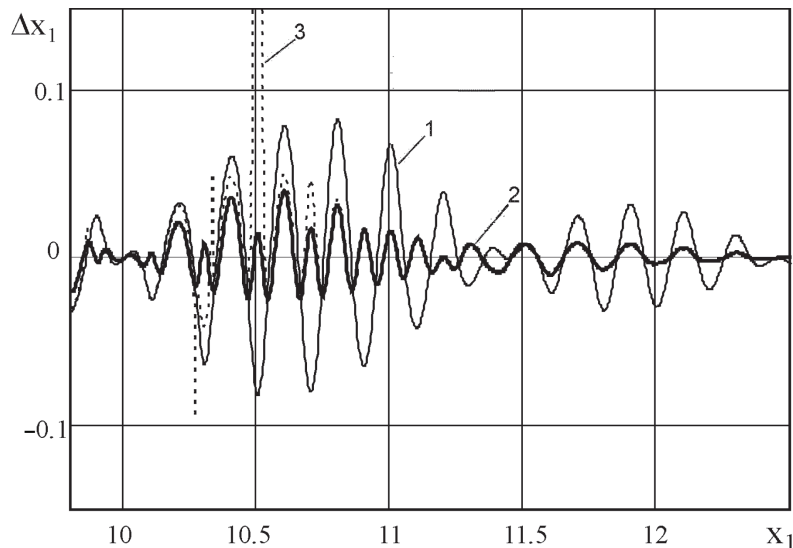


**Figure 7.10** Plots of the noncorrected range estimation error according to the signal weighted by the uniform WF (line 1) and the corrected estimation using the exact value of  $K$  (line 2) and the estimation of  $k$  (line 3) for  $q_{s/i} = 14$  dB.

### 7.4.3 The Algorithm of Estimation Error Reduction: The Sequence of Actions to Decrease the Range Estimation Errors

The following are the steps to decrease the range estimation errors:

- *Step 1:* Estimation of the normalized range  $x_{\text{est}}(x_1, x_2, b_1, \dots, b_m)$  according to the spectrum maximum with the first set of AWF parameters.
- *Step 2:* Estimation of the normalized range  $x_{\text{est}}(x_1, x_2, b_{m+1}, \dots, b_{2m})$  according to the spectrum maximum with the second set of AWF parameters.
- *Step 3:* Determination of range estimation difference  $\Delta x_{\text{est}}(x_1, x_2, b_1, \dots, b_{2m}, q_{\text{s/i}}) = x_{\text{est}}(x_1, x_2, b_1, \dots, b_m, q_{\text{s/i}}) - x_{\text{est}}(x_1, x_2, b_{m+1}, \dots, b_{2m}, q_{\text{s/i}})$ .
- *Step 4:* Determination of the correcting multiplier  $K(\hat{x}_1, \hat{x}_2, b_1, \dots, b_{2m}, q_{\text{s/i}})$  according to envelopes of the theoretical error functions for used WFs.
- *Step 5:* Determination of the correcting amendment (7.8) on the results of steps 3 and 4.
- *Step 6:* Calculation of the corrected range (7.12).

The actual correction method is based on the estimation result variation. Because the estimation range difference is included in the denominator of the correcting multiplier, it is clear that the WFs should be chosen from the condition of maximal differences of two range estimations for any nonresolvable values of  $x_1$  and  $x_2$  for the maximal differences in the shape of the WF SAD main lobe. It follows from the AWF properties that for specified  $N$  and the given width of the WF SD main lobe on the zero level, the differences in SAD shape are defined by the width of the main lobe on any level that is not equal to zero. It follows from here that the WFs should be maximally differed by a specified speed of the SL decrease  $C_s$  and, hence, by the distribu-

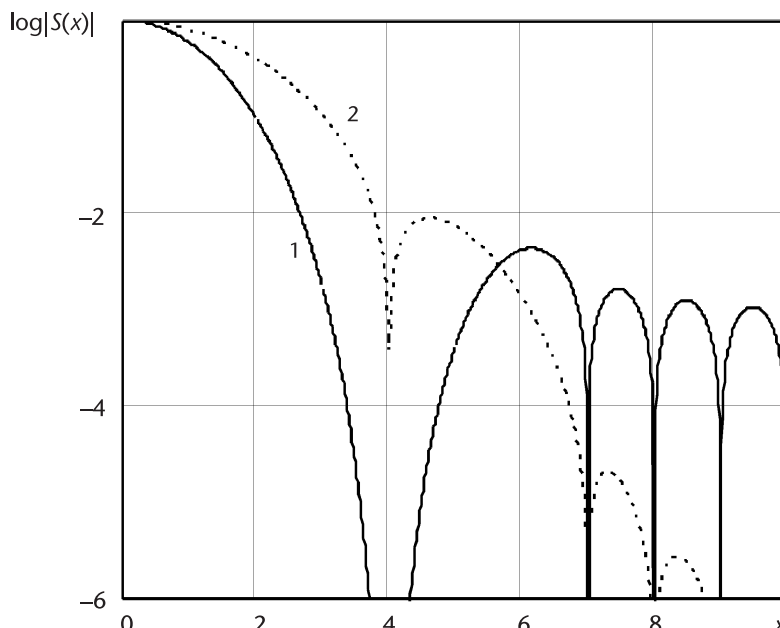


**Figure 7.11** Plots of the logarithm modulus of the AWF SD: 1 denotes  $w_s(t, 4, 4, 4, 4, 4, 4)$  and 2 denotes  $w_s(t, 4, \infty, \infty, \infty, \infty, \infty)$ .

tion of the specified AWF. Figure 7.11 shows the modulus of the SAD logarithms of two AWFs with  $N = 6$  satisfying this condition. For one measurement, the positions of six varied AWF zeros are specified on normalized frequency 4 and for the second measurement, the position of one varied zero is specified on frequency 4 and the position of five other zeros is specified on an infinite frequency. Therefore, for a given  $N = 6$  and for the specified width of the main SAD lobe on the zero level equal to 8, the differences in the main lobe SAD shapes are maximal.

For a situation with fixed interference position, the application of a specific algorithm is possible at a difference of the normalized range to the UR and SR  $x_1 - x_2 \geq 0.5$ .

Thus, the variation of range indications at the frequency calculation according to the similar recorded data array with different WFs provides answers to the following questions:

1. How is the interference influenced?
2. How do we estimate the displacement value caused by interference?
3. How do we correct the range estimation of the FMCW RF position on the value of the calculated error?
4. How do we use a sign of range estimation variation for the correct orientation of the FMCW RF position at its mounting?

The answers to the first and fourth questions can be obtained at  $q_{s/i} \geq 6$  dB, and the answers to the second and third questions can be obtained at  $q_{s/i} \geq 14$  dB.

## 7.5 Error Decrease Caused by the Virtual Reflector

We can eliminate the increased error caused by the virtual reflector with the help of the method described in Chapter 3, adaptive control of modulation parameters and WF, which neutralizes influence of the virtual reflector. Its validity follows from Figure 6.3, in which we see the presence of envelope nodes of fast error oscillations at a range variation between the UR and the virtual reflector. We may significantly decrease the influence of the virtual reflector at any values of parameters we superpose its position on the axis of the normalized range between reflectors with the position of the envelope node of fast error oscillations.

Using the results of Chapter 3, for this case the measurement error will be equal to zero under the condition of the coincidence of SL spectrum maxima  $S_{WF}(x_{\Sigma us}/2)$ ,  $S_{WF}(x_{\Delta v}/2)$ , and  $S_{WF}(x_{\Sigma v}/2)$  with extremes of the main lobe of spectrum  $S_{WF}(x_{\Delta}/2)$ :

$$\frac{d}{dx} S_{WF}(x_{\Sigma us}/2) \Big|_{x_{\max} = x_R} = 0 \quad (7.14)$$

$$\frac{d}{dx} S_{WF}(x_{\Delta v}/2) \Big|_{x_{\max} = x_R} = 0 \quad (7.15)$$

$$\frac{d}{dx} S_{WF}(x_{\Sigma v}/2) \Big|_{x_{\max} = x_R} = 0 \quad (7.16)$$

where the indexes “us” and “v” correspond to the useful and virtual reflectors and  $x_{\Delta} = x - x_R$  and  $x_{\Sigma} = x + x_R$ .

Further analysis is possible in conformity with the specific WF. We consider the DC WF. In this case, (7.14) through (7.16) lead to the conditions:

$$L^2 - (\pi x_{\text{int}})^2 = \pi^2 N_1^2 \quad (7.17)$$

$$L^2 - [0.5\pi(x_{\text{int}} - x_{\text{ant}})]^2 = \pi^2 N_2^2 \quad (7.18)$$

$$L^2 - [0.5\pi(2x_{\text{int}} - x_{\text{ant}})]^2 = \pi^2 N_3^2 \quad (7.19)$$

where  $x_{\text{ant}}$  is the normalized range from a mixer to an antenna,  $N_1$ ,  $N_2$ , and  $N_3$  are, respectively, the numbers of the SL spectra  $S_{\text{WF}}(x_{\Sigma \text{int}}/2)$ ,  $S_{\text{WF}}(x_{\Delta v}/2)$ , and  $S_{\text{WF}}(x_{\Sigma v}/2)$  coinciding with the main lobe of the spectrum  $S_{\text{WF}}(x_{\Delta \text{us}}/2)$ .

We may achieve simultaneous performance of these conditions with the help of control by the FM sweep and by WF parameters. There are three conditions but only two varying parameters. In this case, we may use the compromise solution allowing the performance of two of these conditions and agreement with the value of the additional measurement error arising due to a violation of the third condition. Therefore, for the optimization of the above-mentioned parameters, we choose the most affecting spectra  $S_{\text{WF}}(x_{\Sigma \text{us}}/2)$  and  $S_{\text{WF}}(x_{\Delta v}/2)$ ; that is, conditions (7.17) and (7.18). Solving this equation system, we obtain relations for the optimal values of ED:

$$\delta_{R \text{ opt}} = \frac{1}{2} \sqrt{\left(4R_{\text{PR}}^2 - R_{\text{ant}}^2\right) / \left(N_1^2 - N_2^2\right)} \quad (7.20)$$

and the coefficient  $L$ :

$$L_{\text{opt}} = \pi \sqrt{(0.5R_{\text{PR}}/\delta_{R \text{ opt}})^2 - N_1^2} \quad (7.21)$$

connected with the DC WF parameter  $Q$  by the equation given in the designations of (3.23).

The values of the ranges to the UR  $R_{\text{PR}}$  and to an antenna  $R_{\text{ant}}$  and the SL spectrum numbers  $N_1$  and  $N_2$  are included in (7.20) and (7.21). Because at range measurement  $R_{\text{ant}}$  is the only known value, the measurement procedure should be iterative with the estimation of unknown values and with the calculation of necessary parameters at each step.

It is clear that for the KB WF the similar formulas may be obtained. However, instead of an SL number, the number of a root corresponding to the error envelope node of (3.28) will appear in them.

### 7.5.1 Action Sequence for the Influence Reduction of the Virtual Reflector

The following steps comprise the action sequence for the influence reduction of the virtual reflector [5]:

- *Step 1:* DFS samples measurement and recording in the memory are carried out in a modulation half-period at the initial value of the FM sweep  $\Delta F$ .

- *Step 2:* Using the initial value of the WF parameter according to a DFS spectrum maximum by the methods described in Chapter 3, the zero estimation of range to the useful reflector  $\hat{R}_{\text{PR}}^{(0)}$  is determined.
- *Step 3:* The estimation of SL numbers of spurious spectra  $\hat{N}_1$  and  $\hat{N}_2$  is calculated:

$$\hat{N}_1 = \text{int} \left[ \sqrt{(\hat{R}_{\text{PR}}/\delta_R)^2 - (L/\pi)^2} \right]$$

$$\hat{N}_2 = \text{int} \left[ \sqrt{(R_{\text{ant}}/\delta_R)^2 - (L/\pi)^2} \right]$$

- *Step 4:* The zero approximation of the optimal QI value  $\delta_{R \text{ opt}}^{(0)}$  is calculated in (7.20) and zero approximation of the optimal value of the FM sweep  $\Delta F_{\text{opt}}^{(0)}$  is:

$$\Delta F_{\text{opt}}^{(0)} = c / (4\delta_{R \text{ opt}}^{(0)}) \quad (7.22)$$

- *Step 5:* According to (7.21), the zero approximation of the coefficient  $L_{\text{opt}}^{(0)}$  and the DC WF parameter are obtained:

$$Q_{\text{opt}}^{(0)} = \left[ \left( B_{\text{opt}}^{(0)} \right)^2 + 1 \right] / (2B_{\text{opt}}^{(0)}) \quad (7.23)$$

where  $B_{\text{opt}}^{(0)} = \exp(\pi L_{\text{opt}}^{(0)})$ .

- *Step 6:* A new measurement and the DFS sample recording with obtained value of the FM sweep are performed.
- *Step 7:* Using the current value of the WF parameter according to the DFS spectrum maximum, the current range estimation to the UR  $\hat{R}_{\text{PR}}^{(i)}$  is obtained.
- *Step 8:* The current  $i$ th approximation of the optimal QI value  $\delta_{R \text{ opt}}^{(i)}$  is calculated in (7.20) and from (7.22) the  $i$ th approximation of the optimal value of the FM sweep  $\Delta F_{\text{opt}}^{(i)}$  is calculated.
- *Step 9:* According to (7.21), the current  $i$ th approximation  $L_{\text{opt}}^{(0)}$  is calculated and in (7.23) we obtain the current  $i$ th approximation of the DC WF parameter  $Q_{\text{opt}}^{(i)}$ .
- *Step 10:* Steps 6 through 9 are repeated until the new obtained value or the normalized range  $\hat{R}_{\text{PR}}^{(i)} / \delta_{R \text{ opt}}^{(i)}$  will not satisfy the condition (3.31).

The simulation results of the above-mentioned procedure of influence minimization of virtual reflector on the range measurement results are presented in Figure 7.12.

At simulation, the ratio of signal amplitudes from the virtual reflector and from the UR was 0.3 and the normalized range to the antenna was  $x_{\text{ant}} = 4$ .

The MSD of the measurement error obtained without the optimization procedure of the DFS generation and processing is presented in Figure 7.12 by a solid bold line, and the MSD of the measurement error obtained with using of offered optimization procedure is shown by solid thin line, and MSD with the result averaging at an additional slow FM with obtained optimal values of frequency deviation and the WF parameter is presented by a dotted line. The increase of the range to

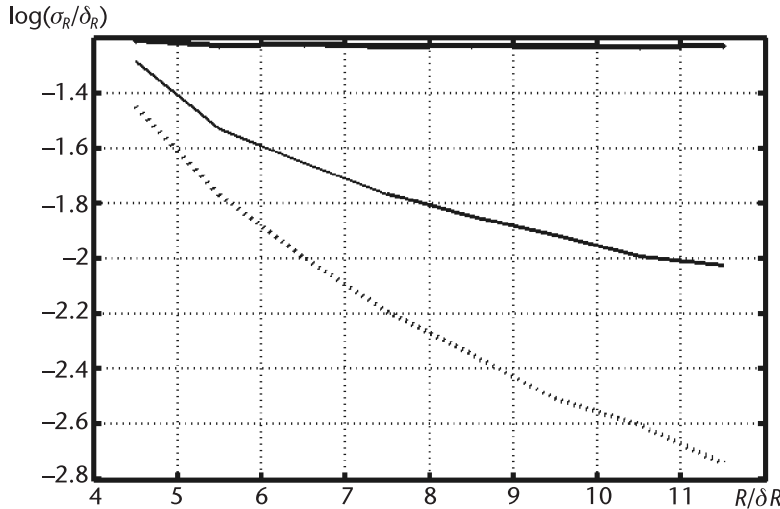


**Figure 7.12** Plots of the normalized MSD logarithm of the measurement error versus the normalized range at the frequency estimation according to the spectrum maximum for the DC WF.

the UR from the possible minimum does not change the first plot, and therefore, two others smoothly decrease and aspire to some steady-state values. We see the advantage of an optimization procedure providing a measurement error decrease from units to hundreds of times. Averaging the results with the help of additional slow FM allows the reduction of the measurement error by 7 to 100 times.

Thus, the proposed method and algorithm of DFS generation and processing optimization allow an essential decrease of the measurement error in conditions leading to the property variation of the virtual reflector. However, they require providing a large volume of calculations and having the possibility of the FM sweep control and the carrier frequency (i.e., they need the large computing and frequency resources of the FMCW RF).

### 7.5.2 Measures Providing a Decrease of the Error Caused by an Echo Signal

The following are measures that provide a decrease in the error caused by an echo signal:

- *Method 1:* The most evident method of a measurement error decrease consists of an increase of suppression deepness of echo waves penetrating to the output of the FM oscillator at the expense of the number and quality increase of isolating devices, application of multiplication circuits, and frequency synthesis with PLL systems.
- *Method 2:* This method allows a reduction of the error component caused by a reflection from the AWP encapsulating device. From (6.28), (6.29) and Figure 6.6, it follows that a decrease of this error is possible at the choice  $R_{\text{ant}} = 2n\delta_R$ ,  $n = 1, 2, \dots$ . In this case, the boundaries of the FM sweep display equally under the effect of echo waves and the error does not arise. This variant can be applied for a length choice of uniform parts of the AWP.

- *Method 3:* This method allows the reduction of the total range measurement error. It takes into consideration the peculiarity of the SHF path construction for the FMCW RF TRM, in which the local oscillator signal is obtained by means of extraction of the transmitter power part by a directional coupler. In this case, the time of signal propagation in (6.6) and (6.10) can be represented in the form of three items:

$$\tau_i = \tau_{i(\text{OSC-DC})} + \tau_{i(\text{DC-A})} + \tau_{i,\text{free}}$$

where  $\tau_{i(\text{OSC-DC})}$  is the time of signal propagation on the SHF path portion between the FMCW oscillator and directional coupler,  $\tau_{i(\text{DC-ANT})}$  is the time of signal propagation between the DC and an antenna, and  $\tau_{i,\text{free}}$  is the time of signal propagation in the free space.

At an unchanged electrical range from the DC to the probing object, the measurement error changes at the variation of the line of electrical length between the FMCW oscillator and the DC (i.e.,  $\tau_{i(\text{OSC-DC})}$ ).

We can decrease the error if in each point of the measured range we provide two measurements corresponding to the variation of a line of electrical length between the oscillator and the DC by means of the controllable phase shifter by a quarter of an average wavelength  $\lambda_{\text{aver}}/4$ , and to average the results of these measurements. Therefore, the measurement error for all components of (6.35) is:

$$\frac{\Delta_R}{\delta_R} = \frac{G_{\text{ant}} A V}{2\pi} \cos\left(4\pi \frac{R}{\lambda_{\text{aver}}} + \varphi_s\right) \cos\left(\pi \frac{R}{2\delta_R}\right) \sin\left(\pi \frac{\lambda_{\text{aver}}}{8\delta_R}\right) \quad (7.24)$$

An error decrease will happen about  $16\delta_R/\pi\lambda_{\text{aver}}$  times. At the above-mentioned FMCW RF parameters, it is about 26.7 times, which is equivalent to increase the SHF oscillator isolation with the other part of the FMCW RF by about 28.5 dB.

The obtained results allow the determination of the required TRM and AWP parameters starting from the admissible measurement.

## 7.6 Conclusions

For an effective struggle against spurious reflections, it is necessary to provide an interference situation analysis in the operating zone of the RF. Therefore, the preliminarily learning of the device allows the determination of the IEZ boundaries.

In the SR number, reflections from AWP irregularities and from the reservoir bottom typical for systems of level measurement and interference caused by reflections from reservoir walls by higher modes in directing systems and the finite UR sizes are included.

In the resolution zone of the UR and SR, one can essentially decrease the measurement error selecting AWF parameters in such a manner that the sidelobe of the SR spectra will be equal to zero. The algorithm of the WF shape control is iterative with the multiple performance of estimation down to an error decrease less than the specified value.

In the case when the UR and SR resolution cannot be implemented, the correction of range estimation according to the results of two consecutive measurements with the WF having significantly different shapes of the main SAD lobe at an equal width on the zero level.

The optimal choice of FM, WF parameters, the constructive implementation of TRM, and AWP allow error reduction caused by the virtual reflector and echo signal to the levels accepted in practice.

The control of line of electrical length between the oscillator and the DC decreases by 26 times the measurement error caused by the effect of the reflected signal on the SHF oscillator.

## References

- [1] Harris, F. J., "On Use of Windows for Harmonic Analysis with the Discrete Fourier Transform," *IEEE Trans. Audio Electroacoust.*, Vol. AU-25, 1978, pp. 51–83.
- [2] Sosulin, Yu. G., *Stochastic Signal Detection and Estimation Theory*, Moscow: Sovetskoe Radio Publ., 1978, 320 pp. [in Russian.]
- [3] Levin, B. R., *Theoretical Fundamentals of Statistical Radio Engineering*. In three volumes. 2nd edition. Moscow: Sovetskoe Radio Publ., 1974, 552 pp. [in Russian.]
- [4] Atayants, B. A., V. M. Davydochkin, and V. V. Ezerskiy, "Consideration of Antenna Mis-matching Effects in FMCW Radio Range Finders," *Antennas*, No. 12(79), 2003, pp. 23–27. [in Russian.]
- [5] Ezerskiy, V. V., "Minimisation of Influence of a Virtual Reflector in a Frequency Range Finder," *Vestnik RGRTU, Ryazan*, No. 18, 2006, pp. 35–39. [in Russia.]

# Parametrical Methods and Algorithms for Increasing the Measurement Accuracy at the Interference Presence

## 8.1 Introduction

Traditional methods for reduction of interference influence were considered based on the optimization of the WF shape used and allowed by a serious decrease of the measurement error in the signal resolution area. Much interest has been generated by an investigation of the error reduction possibility on the interference background not only under the conditions of the UR and SR resolution but also in the areas where they cannot be resolved. In this case, the problem statement is possible when we want to reduce IEZ sizes and decrease the measurement error in this zone up to the accepted level in practice.

One of the directions allowing the reduction of the SR influence is the well-known approach consisting of the estimation of interference signal parameters and in the generation of the cancellation signal on its basis. Therefore, the definition of requirements to the estimation accuracy of such a signal and the definition of the limitations on this method of application are important.

To minimize the SR influence, it is advisable to consider the possibilities of the MLM application.

In many cases, to increase the resolving capability of the spectral analysis, we recommend using algorithms of the frequency determination based on parametric methods of spectral estimation [1] (the Prony method and the method based on the analysis of eigenvectors). That is why it is desirable to investigate the features of this method's application as well the reduction of the SR influence.

Besides the purely measuring methods in the case of clearly expressed local SRs, it is possible to use an approach that considers the peculiarities of a purely industrial FMCW RF application. It is based on the estimation of the UR displacement speed before it enters into the IEZ. We may consider the prediction result with an account of the performed estimation of the UR displacement speed as the range estimation. These tasks are considered in this chapter.

## 8.2 Cancellation of Spurious Reflections

One of the methods allowing a reduction of the DFS interference component influence on measurement results is the cancellation of signals caused by the SRs. The reduction of the SR influence by means of its cancellation is the most clear engineering

solution. Nevertheless, in the known publications, the issues that concern SR cancellation were not practically investigated. Reference [2] is the only exception, but the cancellation mode not thoroughly studied. The recommendations regarding practical application of this mode are absent; there is no information concerning the estimation of the benefit in the accuracy and conditions at which a practical implementation of the SR cancellation mode are not formulated.

We assume that the range to SR is known. The cancellation mode can be used for the range to the SR measurement in free space. We are limited by the specific case of the FMCW RF application as level-meters for the estimation of closed reservoir filling. This assumption supposes the cancellation application in the case when the SR is not shut by the layer of the reservoir's content during the measurement process. However, the UR can be located in the immediate vicinity from the SR, which will lead to additional errors as well. Figure 8.1 shows the error function for measurement by the algorithm (3.4) for this case at the SIR 6 dB and 20 dB (the carrier frequency and the FM sweep are, respectively, 10 GHz and 500 MHz). The SR is situated on a range of 3 m from the FMCW RF. When the reservoir's contents level fall below the construction element, which is the SR source, the mutual influence of the UR and SR spectra leads to additional errors.

The sign for cancellation mode activation is the performance of the following condition: the measured range  $\hat{R}$  from the FMCW RF to the measured level in the reservoir should be more than the range to the SR. If SR is situated on the range  $R_{SR}$  and its maximal spectral SC does not exceed the maximal SC of the useful signal, for the measured range  $R > R_{SR}$  or  $R < R_{SR}$ , the following conditions are always satisfied:  $\hat{R} > R_{SR}$  or  $\hat{R} < R_{SR}$  (here  $\hat{R}$  is the range estimation and  $R$  is its true value). This statement is true at the application of the algorithm (3.4) and other algorithms of the frequency estimation (i.e., the range) considered in Chapter 3. The cancellation of interference signals can be performed either in the time domain or in the spectral domain. For cancellation in the time domain, it is necessary to estimate the frequency, the initial phase, and the amplitude of the each interference signal and then to generate the signal that is out of phase to the interference. Moreover,

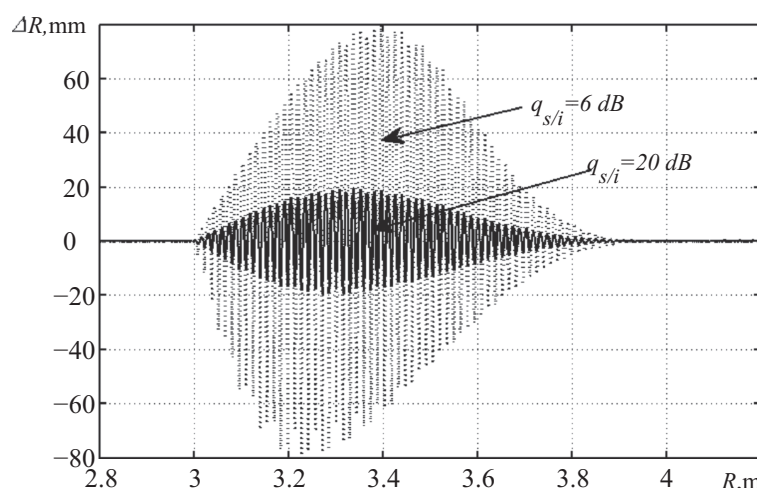


**Figure 8.1** Functions of the measurement error versus the range.

for good cancellation, it is necessary to estimate the PAM level. Because the mutual influence of the UR and SR on the signal shape estimation of the cancellation signal parameters should be performed by calculating the DFS spectrum, the interference cancellation itself is advisable to be performed in the spectral domain. In this case, saving the SR spectra, we can provide cancellation without the estimation of the SR parameters.

The procedure of learning consisting of the following should precede the procedure of interference signal cancellation in the spectral domain:

- *Step 1:* For an empty reservoir, it is necessary to obtain the DFS spectrum

$$S_{\text{tr}}(j\omega) = S_{\text{bot}}(j\omega) + \sum_{l=1}^L S_{l,\text{SR}}(j\omega) \quad (8.1)$$

where  $S_{\text{bot}}(j\omega)$  is the spectrum of the signal reflected from the bottom and  $S_{l,\text{SR}}(j\omega)$  is the signal spectrum corresponding to the  $l$ th SR.

- *Step 2:* It is necessary to detect the main lobes of spectra  $S_{l,\text{SR}}(j\omega), l = \overline{1, L}$ . The main point here is the probability minimization of confusing the SL of the spectrum  $S_{\text{bot}}(j\omega)$  with the main lobes of the signal spectra corresponding to the SRs. Therefore, to detect the SRs, we need to use the calculation of the signal spectrum obtained for the empty reservoir using WF (i.e., to use the standard procedure of detection of the weak signals on the background of the strong signals in the spectral domain, which was mentioned in Chapter 7).
- *Step 3:* After detection of the SR spectra, we can determine the boundaries of the frequency range  $\omega_{\text{low},l} - \omega_{\text{high},l}$  of each  $l$ th SR corresponding to the width of the main lobe of the used WF.
- *Step 4:* In frequency ranges  $\omega_{\text{low},l} - \omega_{\text{high},l}$  and  $l = \overline{1, L}$ , the samples of the SR spectra are saved, which will be used for interference cancellation at the FMCW RF operation.

As a result of the cancellation, the DFS spectrum can be presented as

$$S_{\text{comp}}(j\omega) = S_{\text{PR}}(j\omega) + \sum_{l=1}^L S_{l,\text{int}}(j\omega) - \sum_{l=1}^L S_{l,\text{SR}}(j\omega) \quad (8.2)$$

where  $S_{\text{PR}}(j\omega)$  and  $S_{l,\text{int}}(j\omega)$  are the spectra of signals reflected from the UR, the range to which they are measured, and from  $l$ th interference calculated according to DFS.

At the FMCW RF operation, amplitudes and initial phases of signals corresponding to the SRs may change. The reason for this is the possible deposition on SRs of liquid and solid substances contained in the environment. Moreover, due to the deformation of temperature expansion of constructive elements the range from the FMCW RF to the SR source may be changed. As a result, the complete cancellation will not occur and the following noncompensated remainder of the SR spectrum will arise:

$$\Delta(j\omega) = \sum_{l=1}^L S'_{l,\text{int}}(j\omega) - \sum_{l=1}^L S_{l,\text{SR}}(j\omega) \neq 0 \quad (8.3)$$

where  $S'_{l,\text{int}}(j\omega)$  is the spectrum  $l$ th SR taking into account variations caused by operation conditions of the FMCW RF. This remainder will lead to an increase of the range measurement error to the SR due to the influence of the main lobe and the SL of the spectrum  $\Delta(j\omega)$  upon the useful signal spectrum.

Furthermore, in this section we estimate the possibility of the SR cancellation using both DFS CSD [3] and its PSD.

### 8.2.1 Using the Complex Spectral Density for Cancellation

For estimation of the cancellation quality, the numerical simulation was carried out for the procedure of the material reservoir's level measurement using CSD for cancellation. At simulation, we assumed that there is one SR located at the range of 3 m. At analysis, the SIR was equal to  $q_{s/i} = 6$  dB and the SNR and interference/noise ratio after cancellation were, respectively, 70 dB and 64 dB. The spectrum of compensating signal was obtained at the learning stage. The carrying signal frequency and the FM sweep are 10 GHz and 500 MHz. To decrease the influence of the DFS spectrum SLs, we used the Blackman WF.

To estimate the cancellation quality, the rms criterion was used as reduced to the range interval equal to the wavelength of the carrying oscillation:

$$\sigma_{\text{comp}} = \left[ \frac{1}{m} \sum_{i=1}^m (\hat{R}_i - R_i)^2 \right]^{0.5} / \lambda \quad (8.4)$$

where  $\hat{R}$  and  $R$  are, respectively, the range estimation and its true value and  $m$  is a number of calculating points in the range interval  $\lambda$ .

Figure 8.2 shows the function of the error  $\log \sigma_{\text{comp}}$  for the equality of the compensating spectrum and the spectrum of the corresponding RS (curve 1). At calculation it was assumed that  $m = 10$ . Curves are obtained for averaging on 500 DFS realizations.

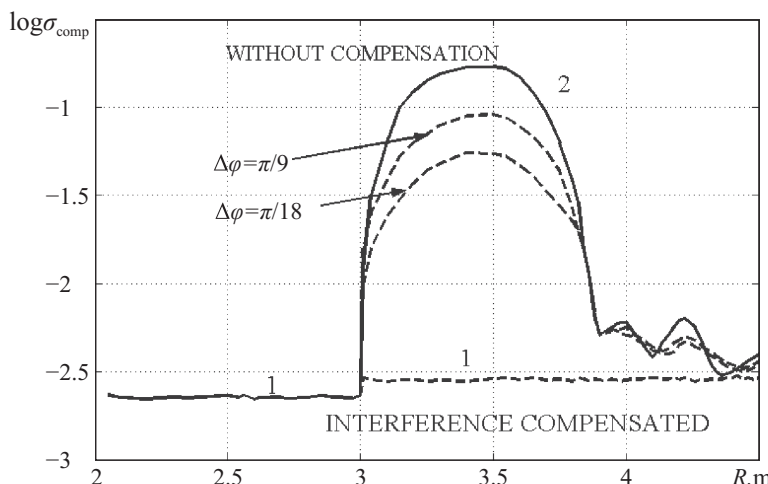


**Figure 8.2** Functions of the range measurement error using the complex spectrum for the SR cancellation.

As we see, the SR influence is completely eliminated. The increase of the measurement error at a range more than 3 m is caused by the noise influence obtaining the compensating spectrum. It follows from Figure 8.2 that the measurement error will be defined mainly by the noise interference at the equality of the parameters of compensating and interference signals. Other curves in Figure 8.2 are obtained at the cancellation absence (curve 2) and for the difference in phases  $\Delta\varphi$  of compensating and interference signals by  $10^\circ$  and  $20^\circ$ . We see from Figure 8.2 that this misphasing leads to a significant increase of the measurement error. The influence of the SL of the DFS spectrum is noticeable: the error caused by them at moving the UR away from the SR aspires to the error value defined by the noise interference.

Instantaneous functions of the measurement error without cancellation and for the difference in phases  $\Delta\varphi$  of interference and compensating signals of  $20^\circ$  are presented in Figure 8.3. The  $q_{s/i}$  ratio is 6 dB.

We see that difference in phases between compensatory and compensating signals by  $20^\circ$  leads to an error increase of about up to 30 mm.

These figures show that for the achievement of small measurement errors at CSD, using it is necessary to provide the phase equality of compensating and interference signals. In practice, this means that the learning mode should be ensured at each discharge (or loading) of the reservoir. However, at a high-specific-density product, the signal phase, which reflects from the SR, will change in time because the thickness of the deposition layer on the SR will be changed as well.

The plots presented allow the determination of the error increase as well at cancellation caused by the range variation from the FMCW RF case to the reflector owing to, for example, temperature variation. At a wavelength of 3 cm, the variation of this range by 1 mm is equivalent to the phase variation of the compensating signal by  $24^\circ$ . We note that the frequency difference of the DFS compensating signal and DFS caused by the SR may influence this case on the measurement error.

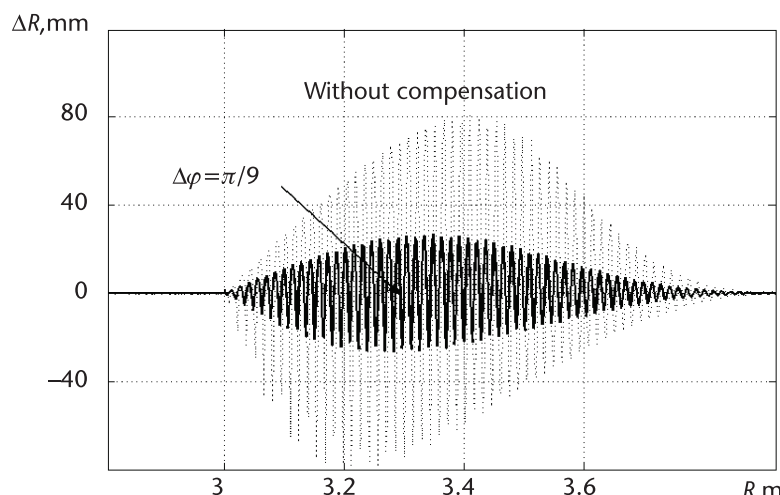


**Figure 8.3** Plots of instantaneous error of the range measurement when using the complex spectrum for cancellation.

Taking the above-mentioned factors into consideration, we can conclude that the cancellation at CSD does not allow a performance of the sufficient measurement accuracy. The main limitation at using CSD for cancellation is the inaccurate determination of the CSD phase (or its variation during the FMCW RF operation).

### 8.2.2 Using Spectral Power Density for Cancellation

At first, we consider the possibility of using the DFS SPD for the SR cancellation presented in the classical form. We are limited by the case when there is the only one SR. Let us represent the SPD of a sum of two signals (the useful signal and the signal corresponding to SR) in the form:

$$\begin{aligned} |S(j\omega)|^2 = & \frac{2}{T_{\text{mod}}} |S_{\text{PR}}(j\omega)|^2 + \frac{2}{T_{\text{mod}}} |S_{\text{SR}}(j\omega)|^2 \\ & + \frac{2}{T_{\text{mod}}} |S_{\text{PR}}(j\omega)| |S_{\text{SR}}(j\omega)| \Phi(\omega_{\text{var}}, \Delta t, \Delta\phi) \end{aligned} \quad (8.5)$$

where  $\Phi(\omega_{\text{var}}, \Delta t, \Delta\phi) = \cos(\omega_{\text{var}} \Delta t + \Delta\phi)$ ,  $\omega_{\text{var}}$  are values of a varied carrier frequency,  $\Delta t = t_{\text{del}} - t_{\text{del,SR}}$ ,  $\Delta\phi = \varphi_1(t_{\text{del}}) - \varphi_2(t_{\text{del,SR}})$ , and  $\varphi_1(t_{\text{del}})$  and  $\varphi_2(t_{\text{del,SR}})$  are values of DFS phases on beating frequencies corresponding to delays  $t_{\text{del}}$  of the useful signal and  $t_{\text{del,SR}}$  of the signal from SR.

As a result of cancellation, assuming that  $S_{\text{SR}}(j\omega) = S_{\text{tr}}(j\omega)$ , we see that the spectrum  $|S_{\text{comp}}(j\omega)|^2$  of the compensated signal is equal:

$$\begin{aligned} |S_{\text{comp}}(j\omega)|^2 = & \frac{2}{T_{\text{mod}}} |S_{\text{PR}}(j\omega)|^2 \\ & + \frac{2}{T_{\text{mod}}} |S_{\text{PR}}(j\omega)| |S_{\text{SR}}(j\omega)| \Phi(\omega_{\text{var}}, \Delta t, \Delta\phi) \end{aligned} \quad (8.6)$$

The second item in (8.6) is the mutual spectrum of the useful signal and the signal corresponding to the SR. We note again that the mutual spectrum depends upon the phases of these signals.

It follows from (8.6) that the SR influence on the measurement result will be eliminated only in cases when

$$\Phi(\omega_{\text{var}}, \Delta t, \Delta\phi) = 0 \quad (8.7)$$

This condition is satisfied if

$$\omega_0(t_{\text{del}} - t_{\text{del,SR}}) + \varphi_1(t_{\text{del}}) - \varphi_2(t_{\text{del,SR}}) = (0.5 + k)\pi, \quad k = 0, 1, 2, \dots$$

Equation (8.6) can be laid as a basis of the cancellation algorithm of SR influence on measurement results. For this, varying the carrier frequency within some limits, it is necessary to achieve the condition performance in (8.7). The FM sweep at the performing measurement on each value  $\omega_{\min} \leq \omega_{\text{var}} \leq \omega_{\max}$  ( $\omega_{\min}, \omega_{\max}$  are limits of carrier frequency variation) should remain unchanged.

To estimate the cancellation quality, we may use the functional

$$A_1[\Phi(\omega_{\text{var}}, \Delta t, \Delta\phi)] = \int_0^\infty |S_{\text{comp}}(j\omega)|^2 d\omega \quad (8.8)$$

Calculations show that  $A_1[\Phi(\omega_{\text{var}}, \Delta t, \Delta\varphi)]$  has an oscillating character because the value  $[\Phi(\omega_{\text{var}}, \Delta t, \Delta\varphi)]$  during the varying process changes within the limits  $-1 \div +1$ . To compensate the SR, it is necessary to determine the frequencies  $\omega_1$  and  $\omega_2$ , at which the adjacent maximal  $A_{\max}$  and minimal  $A_{\min}$  values of the function (8.8). The vicinities of the average frequency values correspond to  $A_{\max}$  and  $A_{\min}$ , that is,  $\omega_{\text{opt}} = (\omega_1 + \omega_2)/2$  correspond to those  $\omega_{\text{opt}}$ , at which the following equality is performed:

$$\frac{2}{T_{\text{mod}}} |S_{\text{PR}}(j\omega)| |S_{\text{SR}}(j\omega)| |\Phi(\omega_{\text{opt}}, \Delta t, \Delta\varphi)| \approx 0 \quad (8.9)$$

Therefore, the SR influence will be compensated, which follows from (8.6).

At a practical implementation of the cancellation mode with the help of tuning the transmitter carrier frequency, it is convenient to represent the SPD of the compensated signal through the SAD of the DFS and the compensating signal. We write the modified spectrum  $|S_{\text{comp},m}(j\omega)|^2$  obtained as a result of cancellation in the form:

$$|S_{\text{comp},m}(j\omega)|^2 = \{ |S_{\text{PR}}(j\omega)| + |S_{\text{SR}}(j\omega)| - |S_{\text{tr}}(j\omega)| \}^2 \quad (8.10)$$

After transformations, we obtain that it will be determined as:

$$\begin{aligned} |S_{\text{comp},m}(j\omega)|^2 &= \{ |S_{\text{PR}}(j\omega)|^2 + |S_{\text{SR}}(j\omega)|^2 + |S_{\text{tr}}(j\omega)|^2 \\ &\quad - 2|S_{\text{tr}}(j\omega)| [ |S_{\text{PR}}(j\omega)|^2 + |S_{\text{SR}}(j\omega)|^2 \\ &\quad + 2|S_{\text{PR}}(j\omega)||S_{\text{SR}}(j\omega)|\Phi(\omega_{\text{var}}, \Delta t, \Delta\varphi) ]^{1/2} \\ &\quad + 2|S_{\text{PR}}(j\omega)||S_{\text{SR}}(j\omega)|\Phi(\omega_{\text{var}}, \Delta t, \Delta\varphi) \} \end{aligned} \quad (8.11)$$

The maximal values of the functional

$$A_2[\Phi(\omega_{\text{var}}, \Delta t, \Delta\varphi)] = \int_0^\infty |S_{\text{comp},m}(j\omega)|^2 d\omega \quad (8.12)$$

as it follows from (8.11), correspond to the condition  $\Phi(\omega_{\text{var}}, \Delta t, \Delta\varphi) = 1$ . In this case, the SR cancellation occurs. As well, it follows from (8.11) that the complete SR cancellation will take place when spectra  $|S_{\text{SR}}(j\omega)|$  and  $|S_{\text{tr}}(j\omega)|$  will be equal.

It is much more economical to determine the maximums of the functional  $A_2[\Phi(\omega_{\text{var}}, \Delta t, \Delta\varphi)]$  than the transitions of the functional  $A_1[\Phi(\omega_{\text{var}}, \Delta t, \Delta\varphi)]$  through the line equal to  $\int_0^\infty |S_{\text{comp}}(j\omega)|^2 d\omega$ . The range  $\Delta f$  of the transmitter carrier frequency varying depends on the delay difference  $\Delta t_{\text{del}} = t_{\text{del}} - t_{\text{del,SR}}$  and the values of phases  $\varphi_1(t_{\text{del}})$  and  $\varphi_2(t_{\text{del,SR}})$ . This range, which is necessary for the cancellation of the SR influence, is easy to determine if we take into consideration that varying should be provided by the phase variation of the function  $\Phi(\omega_{\text{var}}, \Delta t, \Delta\varphi)$  not less than by  $\pi$ . Carrying out the transformation of the function  $\Phi(\omega_{\text{var}}, \Delta t, \Delta\varphi)$ , we obtain:

$$\Delta f = c/2\Delta l \quad (8.13)$$

where  $\Delta l$  is the range between the SR and UR, at which the complete SR cancellation takes place. From this, we see that it is impossible to ensure the complete interference cancellation in the whole range by this approach. We can only speak about the decrease of the IEZ.

At the IEZ value  $\Delta l$  equal to 2 cm, the range of varying is  $\Delta f \approx 7.5$  GHz. It is impossible to provide such a variation of the carrier frequency in the centimeter range. With  $\Delta l$  increasing, that is, with the IEZ increasing up to 20 cm and 40 cm, the value  $\Delta f$  decreases relatively to 1,500 MHz and 750 MHz, which can be provided in practice as these values are comparable with the FM sweep value of the modern FMCW RF of the centimeter range.

Figure 8.4 shows the error behavior  $\log \sigma_{\text{var}}$  of the range measurement calculated with the help of (8.4) at an equality of the SR and compensating signal amplitudes. At simulation, the SIR was 6 dB, and the SNR is 70 dB. The FM sweep was 500 MHz, and the frequency of carrying oscillation was  $\pm 750$  MHz. The function shown in Figure 8.4 was obtained by averaging for 500 DFS realizations.

A comparison with Figure 8.3 allows the assertion that the IEZ essentially decreased. The simulation showed that the phase difference of compensating and interference signals does not influence the IEZ sizes. Its sizes are defined by the range of the transmitter carrier frequency variation.

The error behavior  $\log \sigma_{\text{var}}$  has a practical interest in the case of the amplitude difference of the compensating signal and the signal corresponding to the SR. The behavior of the error  $\log \sigma_{\text{var}}$  is shown in Figure 8.5 for the difference of these amplitudes. The conditions of the simulation performance remain the same as for Figure 8.4.

The differences in amplitudes of compensating and interference signals lead to a deterioration of cancellation quality (i.e., to the IEZ and measurement error increase).

Figure 8.6 shows the instantaneous error of range measurement at the equality of amplitudes of interference and compensating signals and for different amplitudes obtained under the above-mentioned conditions. We see that the IEZ is significantly

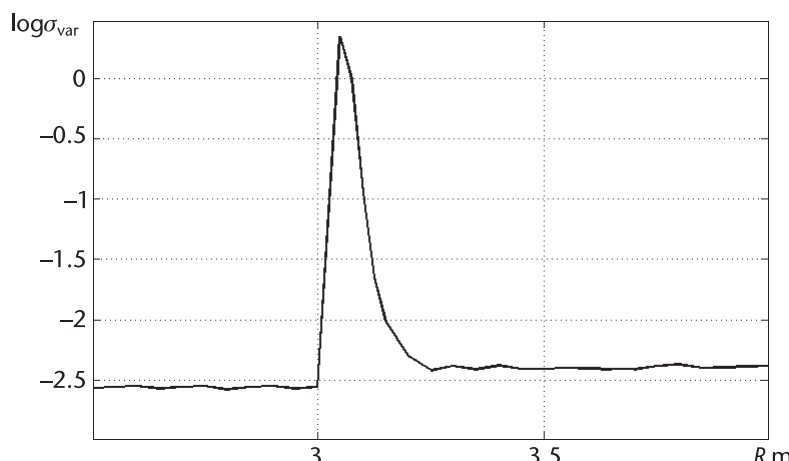
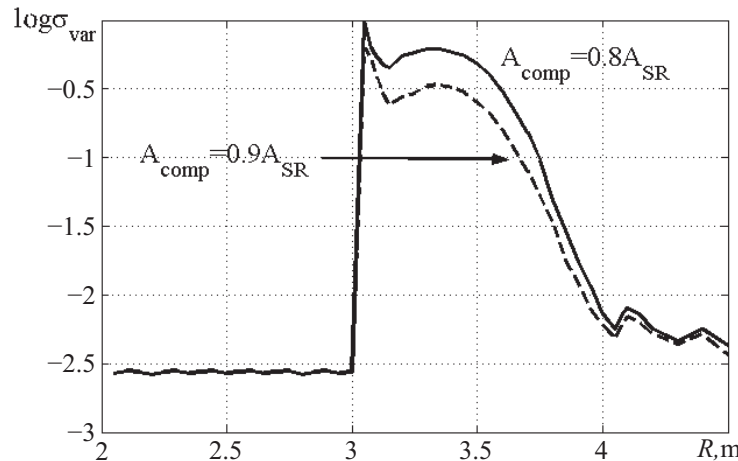


Figure 8.4 The plot of measurement error using the SPD for the SR cancellation.



**Figure 8.5** Plots of functions of measurement error using the SAD for the SR cancellation and at the inequality of the interference amplitude ( $A_{\text{SR}}$ ) and the compensating signal ( $A_{\text{comp}}$ ).

less than when using the algorithm (3.4). However, at differences of amplitudes of interference and compensating signals, the IEZ increases. We have already noted that compensating signals are obtained at the learning stage. Therefore, the difference in amplitudes of compensating and interference signals can be reduced to a small value. We would also like to note that, in spite of this difference, the measurement error decreases about four to eight times compared to the algorithm (2.4).

The conclusion, which can be made from the analysis of Figures 8.5 and 8.6, is that the cancellation of interference signals can be implemented in practice only by using SPD and varying the transmitter carrier frequency. The zone, when the increased measurement error is observed, depends on the variation range and is determined by (8.13). If we choose the maximal value of the variation range of

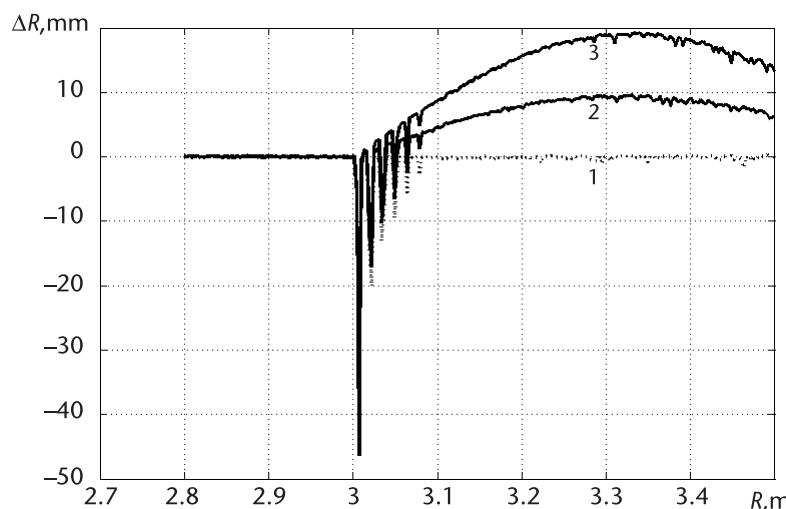


**Figure 8.6** Instantaneous range measurement errors. Curve 1 corresponds to the equality of amplitudes of compensating and interference signals. Curves 2 and 3 correspond to amplitude difference equal to 10% and 20%.

$\pm 750$  MHz, the increased error is observed at a range 20 cm from the SR (at the equality of amplitudes of compensating and interference signals and for the FM sweep of 500 MHz). Compared to the application of the algorithm (3.4), the IEZ width decreases about five to six times. At range more than 20 cm from the SR, the measurement error is defined by the noise influence only and the accuracy of finding the extremes of the function  $A_2[\Phi(\omega_{\text{var}}, \Delta t, \Delta\phi)]$ .

### 8.3 Reduction of Spurious Reflector Influence on the Accuracy of the Range Estimation by the Maximal Likelihood Method

The DFS LLF is an oscillating function with a period of likelihood  $T_{\text{like}} = \lambda/2c$ . The envelope of this function coincides (with accuracy to the constant multiplier) with the spectrum shape of the single pulse with the duration  $T_{\text{mod}}/2$ . At the DFS frequency estimation with the help of the MLM, when the signal is received on the background of the noise interference, the variance of frequency estimation will coincide with the lower variance boundary defined by the Rao-Cramer inequality. Therefore, an investigation of the application possibility for the DSF frequency estimations received on the SR background of algorithms constructed on the basis of the LF has a practical interest. The fast oscillating LF view allows the assumption that the displacement of its extremes under the SR influence will be significantly less than the displacement of the LF envelope extreme, that is, at the DFS frequency measurement according to the position of its spectrum maximum.

#### 8.3.1 The Tracking Range Measuring System

Before the material presentation, in this section we change the designation of some variables. Here we designate as  $t$ , by the letters  $\tau$  for the LF argument,  $\tau_{\text{del}}$  for the delay time corresponding to the useful signal, and  $\tau_{\text{del},\text{SR}}$  for the delay time corresponding to SR.

Limiting the case of a single SR, we can write the modified function of likelihood  $\ln l_m(\tau)$  as:

$$\begin{aligned} \ln l_m(\tau) = & \frac{1}{N_0} \int_0^{T_{\text{mod}}/2} \left\{ 2y(t)A_{\text{ref}} \cos \left[ \omega_0 \tau_{\text{del},\text{ref}} + \frac{2\Delta\omega \tau_{\text{del},\text{ref}} t}{T_{\text{mod}}} + \varphi_{\text{ref}}(\tau_{\text{del},\text{ref}}) \right] \right. \\ & \left. - A_{\text{ref}}^2 \cos^2 \left[ \omega_0 \tau_{\text{del},\text{ref}} + \frac{2\Delta\omega \tau_{\text{del},\text{ref}} t}{T_{\text{mod}}} + \varphi_{\text{ref}}(\tau_{\text{del},\text{ref}}) \right] \right\} dt \end{aligned} \quad (8.14)$$

$$\begin{aligned} \text{where } y(t) = & A_{\text{dif}} \cos \left[ \omega_0 \tau_{\text{del}} + \frac{2\Delta\omega \tau_{\text{del}} t}{T_{\text{mod}}} + \varphi_s(\tau_{\text{del}}) \right] \\ & + A_{\text{SR}} \cos \left[ \omega_0 \tau_{\text{del},\text{SR}} + \frac{2\Delta\omega \tau_{\text{del},\text{int}} t}{T_{\text{mod}}} + \varphi_s(\tau_{\text{del},\text{SR}}) \right] + \xi(t) \end{aligned}$$

where  $A_{\text{ref}}$ ;  $\tau_{\text{del},\text{SR}}$ ;  $\varphi_{\text{ref}}$   $\tau_{\text{del},\text{SR}}$  are the amplitude, delay time, and phase of the reference signal.

The function

$$q_m(\tau_{\text{del}}) = \frac{2}{N_0} \int_0^{T_{\text{mod}}/2} \left\{ A_{\text{dif}} \cos \left[ \omega_0 \tau_{\text{del}} + \frac{2\Delta\omega \tau_{\text{del}} t}{T_{\text{mod}}} + \varphi_s(\tau_{\text{del}}) \right] \right. \\ \left. + A_{\text{SR}} \cos \left[ \omega_0 \tau_{\text{del},\text{SR}} + \frac{2\Delta\omega \tau_{\text{del},\text{SR}} t}{T_{\text{mod}}} + \varphi_s(\tau_{\text{del},\text{SR}}) \right] \right\} \\ \times A_{\text{ref}} \cos \left[ \omega_0 \tau_{\text{del},\text{ref}} + \frac{2\Delta\omega \tau_{\text{del},\text{ref}} t}{T_{\text{mod}}} + \varphi_{\text{ref}}(\tau_{\text{del},\text{ref}}) \right] dt \quad (8.15)$$

will fully define the time delay measurement error at the SR presence with accuracy to the integral value

$$A[\tau_{\text{del},\text{ref}}, \varphi_{\text{ref}}(\tau_{\text{del},\text{ref}})] \\ = \frac{1}{N_0} \int_0^{T_{\text{mod}}/2} A_{\text{ref}}^2 \cos^2 \left( \omega_0 \tau_{\text{del},\text{ref}} + \frac{2\Delta\omega \tau_{\text{del},\text{ref}} t}{T_{\text{mod}}} + \varphi_{\text{ref}}(\tau_{\text{del},\text{ref}}) \right) dt$$

Calculating the integral in (8.14) and neglecting items with the doubled frequency, we obtain:

$$q_m(\tau_{\text{del}}) = q_{\text{dif}}(\tau_{\text{del}}) + q_{\text{SR}}(\tau_{\text{del}}) \\ = \frac{T_{\text{mod}}}{2N_0} \left\{ A_{\text{dif}} A_{\text{ref}} \cos[\Phi(\omega_0, \Delta t_1, \Delta\varphi_1)] \frac{\sin[\Delta\omega(\tau_{\text{del}} - \tau_{\text{del},\text{ref}})/2]}{\Delta\omega(\tau_{\text{del}} - \tau_{\text{del},\text{ref}})/2} \right. \\ \left. + A_{\text{SR}} A_{\text{ref}} \cos[\Phi(\omega_0, \Delta t_2, \Delta\varphi_2)] \frac{\sin[\Delta\omega(\tau_{\text{del},\text{SR}} - \tau_{\text{del},\text{ref}})/2]}{\Delta\omega(\tau_{\text{del},\text{SR}} - \tau_{\text{del},\text{ref}})/2} \right\} \quad (8.16)$$

where  $\Delta t_1 = \tau_{\text{del}} - \tau_{\text{del},\text{ref}}$ ;  $\Delta\varphi_1 = \varphi_s(\tau_{\text{del}}) - \varphi_s(\tau_{\text{del},\text{ref}})$ ;  $\Delta t_2 = \tau_{\text{del},\text{SR}} - \tau_{\text{del},\text{ref}}$ ;  $\Delta\varphi_2 = \varphi_s(\tau_{\text{del},\text{SR}}) - \varphi_s(\tau_{\text{del},\text{ref}})$ .

We consider the functions  $q_{\text{dif}}(\tau_{\text{del}})$  and  $q_{\text{SR}}(\tau_{\text{del},\text{int}})$  as SF, respectively, for the useful signal and for the signal corresponding to the SR.

The function  $q_m(\tau_{\text{del}})$  shape is defined by the sum of two oscillations with the same frequencies and, in general, with different initial phases and amplitudes with envelopes defined by the multiplier of type  $\sin z/z$ .

To determine the accuracy of the time delay estimation, we first determine the deviation  $\Delta\tau(\tau_{\text{del}})$  of the function  $q_m(\tau_{\text{del}})$  extremes arising under the SR influence at a different  $q_{\text{sf}}$  ratio and different values of phases  $\varphi_s(\tau_{\text{del}})$ ,  $\varphi_s(\tau_{\text{del},\text{SR}})$ , and  $\varphi_s(\tau_{\text{del},\text{ref}})$ . A variation of the high-frequency oscillation phase of the function  $q_{\text{dif}}(\tau_{\text{del}})$  under the influence of the same oscillations of the function  $q_{\text{SR}}(\tau_{\text{del}})$  is the reason for the deviation  $\Delta\tau(\tau_{\text{del}})$  appearance. The oscillation  $q_{\text{SR}}(\tau_{\text{del}})$  phase will also change under influence of oscillations  $q_{\text{dif}}(\tau_{\text{del}})$ , but this variation will not lead to a measurement error increase.

It is necessary to note that the deviation of the function  $q_m(\tau_{\text{del}})$  extremes takes place under the effect of the SF component on a doubled difference frequency. Nevertheless, this deviation has a second smallness order compared to  $\Delta\tau(\tau_{\text{del}})$  and, therefore, we can neglect them.

Calculating the partial derivative  $\partial q_m / \partial \tau_{\text{del}}$  and carrying out the necessary transformations, we can determine the deviations of the function  $q_m(\tau_{\text{del}})$  maxima

(including the main) according to the following formula under the SR effect for  $A_{SR} \leq A_{dif}$  [4]:

$$\Delta\tau(\tau_x) = \tau_{del} - \arctan \left\{ \frac{A_{dif} \sin[z_1] + A(\tau_x) \sin[z_2]}{A_{dif} \cos[z_1] + A(\tau_x) \cos[z_2]} \right\} \frac{1}{\omega_0} \quad (8.17)$$

where  $A(\tau_x) = A_{SR} \frac{\sin[\Delta\omega(\tau_{del,SR} - \tau_x)/2]}{\Delta\omega(\tau_{del,SR} - \tau_x)/2}$  is the value of the SF envelope  $q_{SR}(\tau_{del})$  at the range  $R_x = 2\tau_x/c$  from the SR;  $z_1 = \omega_0 \tau_{del} + \varphi_s(\tau_{del}) - \varphi_s(\tau_{del,ref})$ ;  $z_2 = \omega_0 \tau_{del,SR} + \varphi_s(\tau_{del,SR}) - \varphi_s(\tau_{del,ref})$ .

When obtaining (8.17), we assumed that the displacement  $\Delta\tau(\tau_x)$  is small and therefore, it is accepted that  $\frac{\sin[\Delta\omega(\tau_{del} - \tau)/2]}{\Delta\omega(\tau_{del} - \tau)/2} = 1$ .

At the range difference  $R_x$  between the reflecting surface and the SR equal to  $m\lambda/4$  ( $m$  is an integer number), and for the performance of the condition  $\varphi_s(\tau_{del}) = \varphi_s(\tau_{del,SR}) = \varphi(\tau)$ , the range measurement error (displacement of the extreme positions  $\Delta\tau$ ) is defined by the noise interference only. The SR has no influence. It can be explained by the fact that high-frequency oscillations of functions  $q_{dif}(\tau_{del})$  and  $q_{SR}(\tau_{del})$  are summed either with the same phases or with phases that differ by  $180^\circ$ . The condition  $A_{SR} \leq A_{dif}$  is a guarantee that the required range (delay) corresponds to one of the maxima of the function  $q_m(\tau_{del})$ . An error increase is observed in the case when the range  $r_x$  is not a multiple to the value  $m\lambda/4$ .

The functions of the displacement  $\Delta\tau$  of the function  $q_m(\tau_{del})$ , which is recalculated into the range at the ratios  $q_{s/i} = 2, 6, 20$  dB, for the FM sweep of 500 MHz and the carrier frequency of 10 GHz calculated according to (8.17), are presented in Figure 8.10 ( $R_x = R - R_{SR}$ ).

We see that the presented functions have a fast oscillating character (the oscillation period is  $\lambda/2$ ) with envelopes defined by the spectrum shape of the single pulse, which corresponds to the LLF character. A comparison of Figure 8.7 with the figures presented in Chapter 6 and with the results of calculations on (8.24) shows that the maximal DFS frequency measurement error is essentially about 82 times

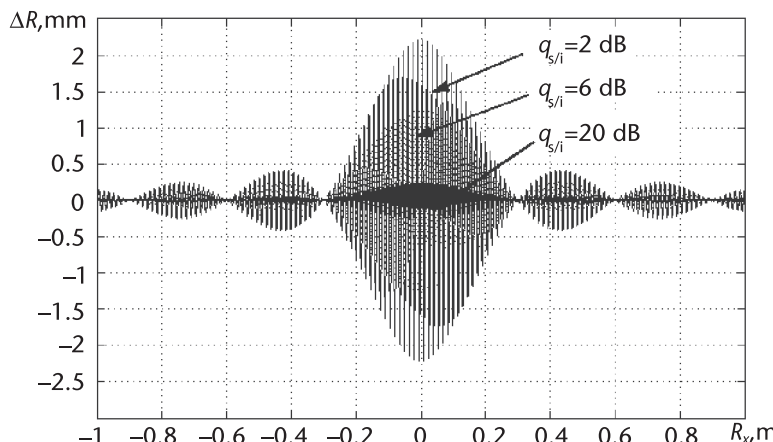


**Figure 8.7** Plots of extreme displacement function  $q_m(\tau_{del})$  versus the range between the UR and SR for different SIR for the FM sweep of 500 MHz.

less than when using the algorithm (3.4) for the DFS frequency estimation. Calculations according to (8.17) show that the phase difference of  $\varphi_s(\tau_{\text{del}})$  and  $\varphi_s(\tau_{\text{del,ref}})$  leads to the displacement of extreme positions  $q_m(\tau_{\text{del}})$ ; that is, to the measurement truncation error, which is defined by (4.27). The phase value  $\varphi_s(\tau_{\text{del,ref}})$  does not influence the value of the truncation error and its effect consists of the initial phase variation of the fast oscillating component of functions in Figure 8.10, and hence, the oscillation envelope does not change.

Figure 8.8 shows the the functions of the displacement  $\Delta\tau$  of  $q_m(\tau_{\text{del}})$  extremes recalculated into the range for the FM sweep  $\Delta F = 1$  GHz at ratios  $q_{s/i} = 2, 6, 20$  dB.

We see that compared with Figure 8.7 the maximal value of the displacement  $\Delta\tau$  remains practically the same. The IEZ decreases proportionally to increase the carrier FM sweep.

The variation of the carrier frequency, as it follows from (8.17), leads to an inverse proportional variation of extreme displacement  $q_m(\tau_{\text{del}})$  at an unchanged value of the FM sweep. To decrease this displacement, it is necessary to increase the carrier frequency of the FMCW RF transmitter. We should note once more that functions, which are presented in Figures 8.7 and 8.8, are calculated according to (8.17). Simulation results completely coincide with calculation data and therefore, we did not discuss them.

The main maximum of the function  $q_m(\tau_{\text{del}})$  at  $A_{\text{SR}} = 0$  coincides with the main maximum of the LF (4.2) and corresponds to the estimating delay time  $\tau_{\text{del}}$ . The SR influence leads to an envelope  $q_m(\tau_{\text{del}})$  variation as the functions  $q_{\text{dif}}(\tau_{\text{del}})$  and  $q_{\text{SR}}(\tau)$  have different amplitudes, phases, and envelopes. Summation of functions  $q_{\text{dif}}(\tau_{\text{del}})$  and  $q_{\text{SR}}(\tau)$  with different amplitudes, phases, and envelopes leads to variations of function  $q_m(\tau_{\text{del}})$  maxima. As a result, the main maximum of  $q_m(\tau_{\text{del}})$  will not correspond to a true delay.

In other words, in spite of insignificant displacements of maxima positions under the influence of the SR the maximum corresponding to the measuring range will not be global. The largest variation of this maximum value will be observed at the spectra overlapping the useful signal and the SR.

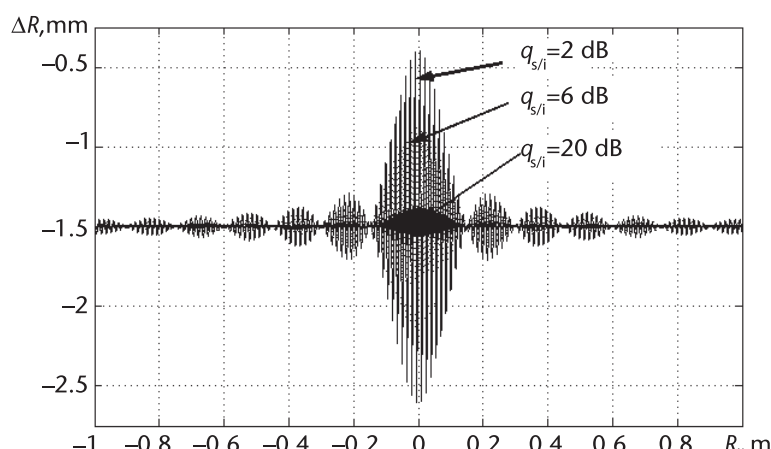


**Figure 8.8** Plots of extreme displacement  $q_m(\tau_{\text{del}})$  versus the range between the UR and SR for different SIR at the FM sweep of 1 GHz.

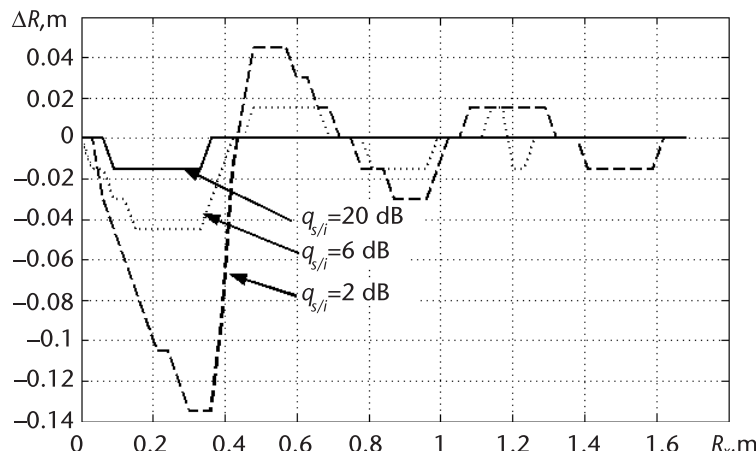
Figure 8.9 shows the functions of the range measurement error using the main maximum of the function (8.16) at the SR presence obtained with the help of simulation. The behavior of  $\Delta R = \lambda(n_m - n_{\tau_{\text{del}}})/2$ , that is, the value of  $\Delta\tau_{\text{del}} = T_{\text{carr}}(n_m - n_{\tau_{\text{del}}})/2$  recalculated into the range (numbers  $n_m$  and  $n_{\tau_{\text{del}}}$  correspond to numbers of the main extreme  $Z_\tau$  corresponding to the delay  $\tau_{\text{del}}$ , and  $T_{\text{carr}}$  is the period of carrying oscillation) is shown in this figure at different ranges  $R_x$  from the SR to UR. Functions are obtained at the performance of equalities  $\varphi_s(\tau_{\text{del}}) = \varphi_s(\tau_{\text{del,ref}}) = \varphi_s(\tau_{\text{del,SR}}) = 0$ .

Figure 8.9 allows a qualitative estimation of the range measurement error using the main maximum of the function  $q_m(\tau_{\text{del}})$ . We see that in spite of small displacements, which follow from (8.17), it is impossible in general to use the function  $q_m(\tau_{\text{del}})$  for the accurate measurement at presence of the SR if providing measurements on the basis of a global maximum search. The second conclusion from Figure 8.9 is that anomalous range measurement errors according to the position of the main maximum take place for large  $R_x$  from SR, especially at small  $q_{s/i}$ . Therefore, for accurate range measurement, it is necessary to realize the tracking procedure for the local extreme  $Z_\tau$  corresponding to the estimating delay [4].

### 8.3.2 Main Stages of the Tracking Procedure After the Local Extreme

The following are the main stages:

- *Stage 1:* It is necessary to determine those range intervals, within which the SR influence is significant, that is, to determine the IEZ boundaries in the whole delay interval ( $\tau_{\text{del}} \in \tau_{\text{del,min}}, \tau_{\text{del,max}}$ ).
- *Stage 2:* The measurement of the delay time in the range intervals, for which the SR influence is insignificant, can be provided with the help of algorithms identifying the position of the maximal SC with the DFS frequency or using for this purpose the algorithm realizing the MLM.
- *Stage 3:* In entering the IEZ, it is necessary to form the delay interval  $\Delta T_{\text{del}}$ , within which is the maximum  $Z_\tau$ , using the previous measured value  $\tau_{\text{del}}$



**Figure 8.9** Plots of the range measurement error according to the position of the main maximum of the function  $q_m(\tau)$  versus the range between the SR and UR.

obtained with the help of the algorithm (3.4). On the inside of the IEZ, the delay interval  $\Delta T_{\text{del}}$  is forming on the basis of the previous measurement of the time delay by the tracking measurer.

- *Stage 4:* To eliminate the error connected with the phase difference of the reference signal and the DFS, according to the PFC, we need to estimate the DFS phase value for the range corresponding to the IEZ boundary using the approach described in Chapter 4.
- *Stage 5:* It is necessary to ensure the displacement of the delay interval  $Z_\tau$ , which corresponds to the measured range.
- *Stage 6:* The measurement of the time delay is carried out according to the position of the maximum, which falls in the delay interval  $\Delta T_{\text{del}}$ .

For a practical implementation of the tracking measurer, it is necessary to define its main parameter, the width of the delay interval  $\Delta T_{\text{del}}$ . The probabilities of the anomalous error appearance (as before, we understand the “jump” to the adjacent maximum as an anomalous error) and the tracking loss (we understand the tracking after one maximum of the function  $q_m(\tau_{\text{del}})$  corresponding to the SR as the tracking loss) will depend upon  $\Delta T_{\text{del}}$ . It is clear that  $\Delta T_{\text{del}}$  should not exceed the value  $\lambda/2c$ . This condition ensures against appearance of anomalous errors as the condition  $\Delta T_{\text{del}} < \lambda/2c$  eliminates falling in the interval  $\Delta T_{\text{del}}$  of two adjacent maxima. In the future, this exact value will be accepted at simulation and at the processing of experiment data.

Tracking after the useful extreme of the function  $q_m(\tau_{\text{del}})$  at the measurement of the range to the SR has peculiarities that do not permit using the known methods [5, 6] based on the application of time discriminators and phase-locked-loop systems. It can be explained by the fact that although the speed of the range to the UR variation in the moments of discharge and loading of the reservoir is rather stable, the speed vector sign is arbitrary. In general, with the same probability in any time moment, the increment of the range to the UR variation may be positive, negative, or equal to zero.

### 8.3.3 Tracking Modes

The following are the tracking nodes:

1. The generation of the initial  $\tau_{\text{del},\text{init}}$  and final  $\tau_{\text{del},\text{final}}$  values of the interval  $\Delta T_{\text{del}}$  on the basis of the previous estimation  $\tau_{\text{del}}$ , that is, values  $\tau_{\text{del},\text{init}}$  and  $\tau_{\text{del},\text{final}}$  will be defined as

$$\tau_{\text{del},\text{int}} = \hat{\tau}_{\text{del},(n-1)} - \lambda/4c \quad (8.18)$$

$$\tau_{\text{del},\text{final}} = \hat{\tau}_{\text{del},(n-1)} + \lambda/4c \quad (8.19)$$

We do not meet anomalous errors in the case if the fall of the maxima of the function  $q_m(\tau_{\text{del}})$  (adjacent to  $Z_\tau$ ) in the interval  $\tau_{\text{del},\text{final}} - \tau_{\text{del},\text{init}} = \lambda/2c$  is eliminated. It can be achieved at the performance of the evident condition:

$$\begin{aligned} \tau_{\text{del},(n-1)} + \Delta\tau_{\text{del},(n-1)} - \lambda/2c &< \tau_{\text{del},n} \\ + \Delta\tau_n &< \tau_{\text{del},(n-1)} + \Delta\tau_{n-1} + \lambda/2c \end{aligned} \quad (8.20)$$

where  $\Delta\tau_{n-1}$  and  $\Delta\tau_n$  are the errors of the previous and future measurements.

Recounting the delay into the range, we obtain from (8.20):

$$-\lambda/4 < \Delta R + \Delta R_n - \Delta R_{n-1} < \lambda/4 \quad (8.21)$$

where  $\Delta R$  is the variation of the range to the reflecting surface for two consequent measurements;  $\Delta R_n$  and  $\Delta R_{n-1}$  are measurement errors of the tracking measurer.

It follows from (8.21) that the following condition should be satisfied:

$$|\Delta R + \Delta R_n - \Delta R_{n-1}| < \lambda/4 \quad (8.22)$$

At a decrease of the  $q_{s/i}$  ratio, the errors  $\Delta\tau_{n-1}$  and  $\Delta\tau_n$  increase, which leads to the necessity of a  $\Delta R$  reduction. The function of an admissible  $\Delta R$  value versus the SIR  $q_{s/i}$  for  $\omega_0 = 10$  GHz calculated using (8.17) and (8.22) is shown in Figure 8.10 (curve 1). Function 1 tends to  $\Delta R = 7.5$  mm (curve 2) with  $q_{s/i}$  increasing. We can see from Figure 8.10 that at  $q_{s/i} = 2$  dB the admissible value of the measuring range increment is equal to about 3 mm from one measurement to another. For a smaller SR intensity corresponding to  $q_{s/i}$ , the increase of  $\Delta R$  is possible.

The variation of the FM sweep does not practically lead to curve 1 variation. However, the reduction of the carrier frequency allows for an increase of  $\Delta R$ . Figure 8.10 shows the function of  $\Delta R$  versus the SIR  $q_{s/i}$  for a carrier frequency of 5 GHz (curve 3), which tends asymptotically to  $\Delta R = 0.015$  m (curve 4) with  $q_{s/i}$  increasing. Nevertheless, an increase of  $\Delta R$  achievable at a carrier frequency reduction is accompanied by a proportional increase of  $\Delta\tau(\tau_x)$ , which follows from (8.17).

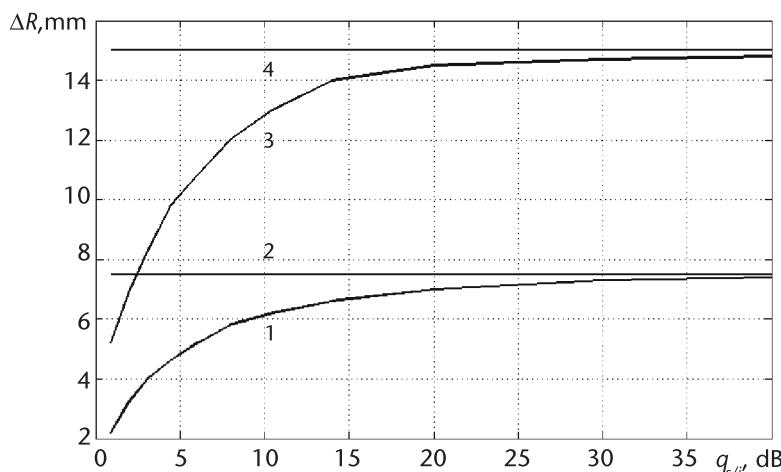


Figure 8.10 Plots of admissible level increment versus the SIR.

We can increase the admissible value of  $\Delta R$  assuming the information application about range increment to the reflecting surface, for which it is necessary to store data obtained at a previous measurement. Restricting storing the results of  $(n - 2)$ -th and  $(n - 1)$ -th measurements, we can write on the analogy of (8.28):

$$-\lambda/4 < \Delta R_n + \Delta R_{n-2} - 2\Delta R_{n-1} < \lambda/4 \quad (8.23)$$

This is equivalent to

$$|\Delta R_n + \Delta R_{n-2} - 2\Delta R_{n-1}| < \lambda/4 \quad (8.24)$$

Hence, the sum of errors at measurement with numbers  $n$ ,  $n + 1$ ,  $n + 2$  should not exceed  $\lambda/4$ . The calculations performed according to (8.17) and (8.24) and the simulation results allow the statement that at uniform UR motion the condition (8.24) is satisfied beginning at  $q_{s/i} \approx 0$  dB. Therefore, the value  $\Delta R$  will be equal to about  $\lambda/5$ .

### 8.3.4 Influence of the Phase Characteristic Estimation Error on the Operation of the Tracking Measurer

The measurement results of the delay time with the help of the tracking measurer will be accompanied by the additional error  $\delta r$  connected with an inaccuracy of the PFC estimation. Entering into the IEZ, this error will be defined in accordance with (4.27) as:

$$\delta R_{\text{int}} = \lambda [\bar{\varphi}(\tau_{\text{del,init}}) - \varphi(\tau_{\text{del,init}})]/[4\pi(1 + \Delta\omega/\omega)] \quad (8.25)$$

where  $\bar{\varphi}(\tau_{\text{del,init}})$  and  $\varphi(\tau_{\text{del,init}})$  are the estimation and the true value, respectively, of the PFC at the input of the IEZ.

At the output from the IEZ, this error is equal to:

$$\delta R_{\text{final}} = \lambda [\bar{\varphi}(\tau_{\text{del,init}}) - \varphi(\tau_{\text{del,final}})]/[4\pi(1 + \Delta\omega/\omega)] \quad (8.26)$$

where  $\varphi(\tau_{\text{del,final}})$  is the true PFC value at the output of the IEZ.

The value  $\delta r_{\text{init}}$  is defined by the PFC estimation error caused by the noisy interference and the mutual influence of the SL of the UR and SR spectra. The value  $\delta r_{\text{final}}$  is defined by the difference of the signal phase values at the beginning and end of the IEZ, the noisy interference, and the SL of the UR and SR spectra. Its value can be decreased by an approximation of the DFS phase within the IEZ limits by the linear function:

$$\varphi(\tau_{\text{del}}) = \frac{\hat{\tau}_{\text{del}} - \hat{\tau}_{\text{del,init}}}{\hat{\tau}_{\text{del,init}} - \hat{\tau}_{\text{del,final}}} [\varphi(\hat{\tau}_{\text{del,init}}) - \varphi(\hat{\tau}_{\text{del,final}})] + \varphi(\hat{\tau}_{\text{del,init}}) \quad (8.27)$$

A choice of this linear function is explained as follows. The phase variation within the IEZ, as the practice shows, is  $20^\circ$  to  $30^\circ$ ; that is, the additional measurement error does not exceed 0.8 to 1.2 mm. Therefore, it is quite inexpedient to use it for the approximation of the more complicated function.

### 8.3.5 Determination of the Conditions at which the Tracking Loss Occurs

The function  $q_m(\tau_{\text{del}})$ , as already mentioned, can be considered as a sum of two SF functions,  $q_{\text{dif}}(\tau_{\text{del}})$  and  $q_{\text{SR}}(\tau_{\text{del}})$ . The shapes of envelopes  $F_{\text{dif}}(\tau_{\text{del}})$  and  $F_{\text{SR}}(\tau_{\text{del}})$  of these fast oscillating functions are the same and are defined by the multipliers of type  $\sin z/z$ . In points where envelopes have zero values, phases of oscillations in the interval equal to  $\lambda/4$  change by  $\pi$ .

The envelope  $F_{\text{envel}}(\tau_{\text{del}})$  square of the function  $q_m(\tau_{\text{del}})$  can be presented in the form:

$$\begin{aligned} F_{\text{envel}}^2(\tau) &= |F_{\text{dif}}(\tau)\exp(-j\omega\tau + \Phi_1) + F_{\text{SR}}(\tau)\exp(-j\omega\tau + \Phi_2)|^2 \\ &= F_{\text{dif}}^2(\tau) + F_{\text{SR}}^2(\tau) + 2F_{\text{dif}}(\tau)F_{\text{SR}}(\tau)\cos(\Phi_1 - \Phi_2) \end{aligned} \quad (8.28)$$

where  $\Phi_1 = \omega\tau_{\text{del}} + \varphi_s(\tau_{\text{del}}) - \varphi_s(\tau_{\text{del,ref}})$  and  $\Phi_2 = \omega\tau_{\text{del,SR}} + \varphi_s(\tau_{\text{del,SR}}) - \varphi_s(\tau_{\text{del,ref}})$ .

The reason for a tracking loss can be explained most clearly at performance of two conditions: phase equality to zero:  $\varphi_s(\tau_{\text{del}}) = \varphi_s(\tau_{\text{del}}) = \varphi_s(\tau_{\text{del,SR,ref}}) = 0$  and for a discrete variation of the range between the SR and the reflecting surface by the value  $m\lambda/4$  ( $m$  is odd). For this case, the envelope square is:

$$F_{\text{envel}}^2(\tau_{\text{del}}) = F_{\text{dif}}^2(\tau_{\text{del}}) + F_{\text{SR}}^2(\tau_{\text{del}}) \quad (8.29)$$

therefore, the zero values of  $F_{\text{envel}}(\tau_{\text{del}})$  correspond to points, in which  $F_{\text{dif}}(\tau_{\text{del}}) = F_{\text{SR}}(\tau_{\text{del}})$ . In the points  $F_{\text{envel}}(\tau_{\text{del}}) = 0$ , the variation of the oscillation phase happens by  $\pi$ . For approaching the UR to the SR (we assume for distinctness that the UR approaches to the SR from the left), the SL of the function  $q_{\text{SR}}(\tau_{\text{del}})$  affects at first the extreme displacement of the function  $q_{\text{dif}}(\tau_{\text{del}})$ . The value of the main maximum  $Z_\tau$  significantly exceeds the maxima of  $q_m(\tau_{\text{del}})$  caused by the SR effect. By overlapping the main lobes of the functions  $q_{\text{dif}}(\tau_{\text{del}})$  and  $q_{\text{SR}}(\tau_{\text{del}})$ , which takes place for their approach by the value  $\Delta\tau < 1/2\Delta\omega$ , the decrease of both the useful maximum and the maximum corresponding to the reflection from the SR occurs as high-frequency oscillations will be summed with phases differs by  $\pi$ . Tracking loss happens when those points  $\tau'$  are in the vicinity of which (in the interval  $\lambda/4c$ ) the phase variation of high-frequency oscillations by  $\pi$  occurs in the delay interval  $\Delta T_{\text{del}}$ . In this point  $F_{\text{envel}}(\tau') = 0$  and in its vicinity, the maxima of the function  $q_m(\tau_{\text{del}})$  take minimal values. To the left of the point  $\tau'$ , the maxima positions of functions  $q_m(\tau_{\text{del}})$  and  $q_{\text{DFS}}(\tau_{\text{del}})$  coincide. From the right side, they coincide with maxima positions of the function  $q_m(\tau_{\text{del}})$ . The last statement is true when the condition  $A_{\text{dif}} < A_{\text{SR}}$  is carried out. Thus, when the UR passes the point  $\tau'$ , the maximum of the function  $q_m(\tau_{\text{del}})$  coinciding with the maximum of the function  $q_{\text{SR}}(\tau_{\text{del}})$  falls inevitably in the interval  $\Delta T_{\text{del}}$ . At a further UR moving (to the right of the point  $\tau'$ ) and at the performance of the condition  $A_{\text{dif}} < A_{\text{SR}}$ , the measurer will track after a fixed maximum of the function  $q_m(\tau_{\text{del}})$ ; that is, tracking loss will occur. It is explained by the fact that initial  $\tau_{\text{del,init}}$  and final  $\tau_{\text{del,final}}$  values of the interval  $\Delta T_{\text{del}}$  will be formed on the basis of range measurement to the fixed maximum. In general, we can determine the range  $R_{\text{tr},1}$  to the SR, at which the tracking loss occurs, from the equation:

$$A_{\text{DFS}} < A_{\text{SR}} \sin[\Delta\omega(\tau_{\text{SR}} - \tau)/2]/[\Delta\omega(\tau_{\text{SR}} - \tau)/2] \quad (8.30)$$

In other words, tracking loss happens when the maximal envelope value of the function  $q_s(\tau_{\text{del}})$  becomes less than the envelope of the function  $q_{\text{int}}(\tau_{\text{del}})$ . Expanding  $\sin z$  into the Taylor series, being limited by two series items and presenting a delay through range, we can find the solution of (8.30) in the following form:

$$R_{\text{tr},l} \geq \left[ 6 \left( 1 - \sqrt{q_{s/i}} \right) \right] c / \Delta\omega \quad (8.31)$$

Functions showing the connection of the range  $R_{\text{tr},1}$  with  $q_{s/i}$  are presented in Figure 8.11. At simulation,  $q$  is 70 dB.

The upper plots for the FM sweeps of 10 GHz and 500 MHz obtained by simulation correspond to the first tracking mode, and the lower plots correspond to the second mode, that is, with account of reflector motion speed. From Figure 8.11 we can conclude that the calculation results according to (8.31) coincide satisfactorily with simulation results.

The main conclusion from the presented functions is that tracking loss occurs under the condition  $q_{s/i} < 0$ ; however, tracking after a locked extreme (at the IEZ boundary) of the function  $q_m(\tau_{\text{del}})$  can be provided in some cases at  $q_{s/i} < 0$ . This statement requires explanation. Preliminary targeting for the tracking algorithm is provided using the algorithm (3.4). If  $q_{s/i} < 0$ , then, with the help of this algorithm, the frequency variation will occur corresponding to the range to the SR. In the specific case of the FMCW RF as a level-meter, when the SR with  $q_{s/i} < 0$  corresponds to the reflections from the reservoir bottom, and the range to the bottom, as a rule, is known, the seemingly measured range to the SR will be more than a range to the reservoir bottom. It occurs due to an increased signal delay in the layer located over the bottom. This is a sign for the SR selection with  $q_{s/i} < 0$ .

Calculated functions rather accurately coincide with simulation results. The functions presented in Figure 8.11 correspond to the tracking mode, at which the range increment estimation is provided according to two previous measurements.

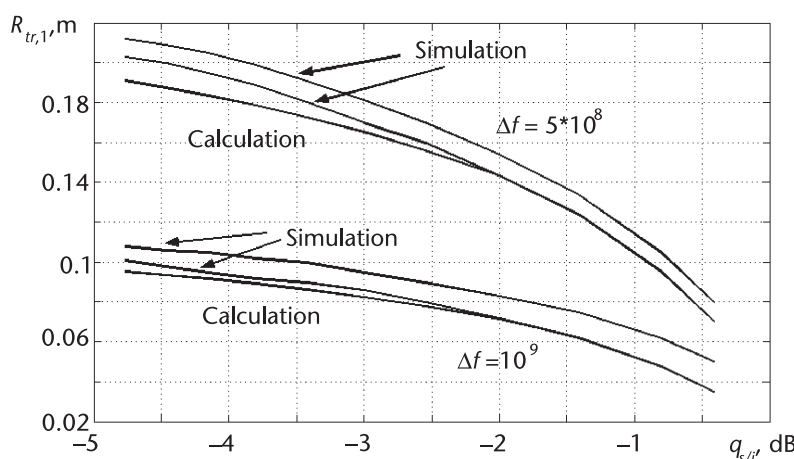


**Figure 8.11** Plots of the range to the SR, at which tracking loss occurs, versus the SIR.

In the case when tracking is arranged without consideration of the range increment estimation, the tracking loss occurs at some larger range from SR. If  $\Delta R = 0.003$  m,  $R_{tr,1}$  increases about 0.02 m. For  $\Delta R = 0.005$  m,  $R_{tr,1}$  increases by 0.03 m. Calculations are presented for  $\lambda = 3$  cm.

### 8.3.6 Range Measurement at the Presence of the Spurious Reflectors of Small Intensity

The MLM application for range estimation, as already mentioned, leads to the necessity of using a two-stage procedure: the first stage is the preliminary estimation  $\hat{R}$  of the range with the help of the algorithm (3.4) ensuring the fall in the vicinity of the main LLF maximum, and the second stage is the specification of the estimation provided, that is, the position of the main LLF maximum is searched. SRs lead to an error increase of the range measurement by the algorithm (3.4), which is illustrated in figures in Chapter 6. Therefore, the maximum not corresponding to measured range will fall in the range interval  $-\lambda/4 < \hat{R} - R < \lambda/4$ . The MLM application in this case leads to anomalous errors, which value is multiplied to  $\lambda/2$ .

Let us call such SR the SR of small intensity, which leads to the error  $\Delta R$  of the range estimation  $R$ , which is less than  $\lambda/4$  using the algorithm (3.4). In this case, the LLF extreme corresponding to a measured range with a probability practically equal to 1 will be located in the range interval  $-\lambda/4 < \hat{R} - R < \lambda/4$ . Therefore, a possibility is opened to decrease the measurement errors using the MLM with the known DFS phase not resorting to the tracking algorithm. Calculations according to (8.17) confirmed by simulation results show that SRs of small intensity are such SRs, for which the range measurement error by the algorithm (3.4) does not exceed  $\lambda/4$ . Such SRs lead to a lesser error of the range estimation when using the algorithm (3.4) than the value  $\lambda/4$ , which ensures falling in the interval  $-\lambda/4 < \hat{R} - R < \lambda/4$  of the LLF extreme corresponding to the required range. The displacement of the LLF global extreme under the influence of the SR of small intensity, according to (8.17), does not exceed a tenth of a millimeter.

Figure 8.12 shows instantaneous error estimations as a function of the range at the presence of the SR of small intensity obtained with the simulation help (the carrier frequency of 10 GHz and the FM sweep of 500 MHz). The SR with the ratio  $q_{s/i} = 30$  dB is located at a range of 3.5 m. Function 1 corresponds to the range measurement with the help of the algorithm (3.4), and function 2 corresponds to the range measurement of the algorithm on MLM basis.

At the application of the tracking algorithm for the range measurement, the maximal error decreases about 82 times compared with the algorithm (3.4). In contrast to the tracking algorithm, the direct application of the MLM with a known phase for the range measurement for the SR of small intensity does not require limitations on the UR movement speed.

There is practical interest in estimating the possibilities of the MLM application with the known signal phase for the measurement of small ranges. In this case, the spectrum formed at  $\omega < 0$  represents the specific interference, which is impossible to eradicate. The simulation results performed under the conditions that the carrier frequency of the transmitter is 10 GHz and the FM sweep is 500 MHz are

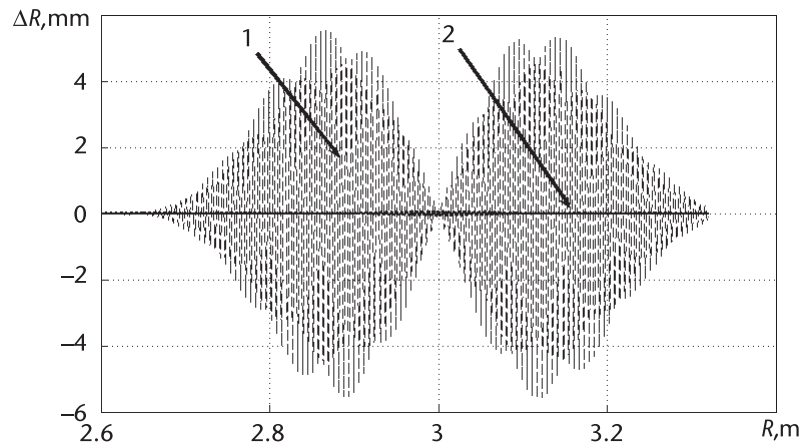


**Figure 8.12** Plots of the range measurement error at a presence of the SR of small intensity.

presented in Figure 8.13. The dotted line corresponds to the measurement using the algorithm (3.4), and the solid line corresponds to the range measurement on the MLM basis. The Blackman WF is used in the algorithm (3.4). If the error of the preliminary range estimation exceeds  $\lambda/4$ , which in this case is observed at a range of 0.41 m, then the maximum adjacent to the global one falls into the range interval  $-\lambda/4 < \hat{R} - R < \lambda/4$ , which leads to anomalous errors.

With the range increasing (an increase of relative frequency), the error of its preliminary estimation decreases down to a value lesser than  $\lambda/4$ , which allows the MLM application and thereby significantly decreases the range estimation error. The application of the MLM with the known phase supposes that the PHC of the FMCW RF is known. Its estimation can be provided according to the procedure described in Chapter 4. Calculations according to (8.17) confirmed by simulation results show that the truncation error of a small range measurement decreases by 82 times compared to the application of the algorithm (3.4).

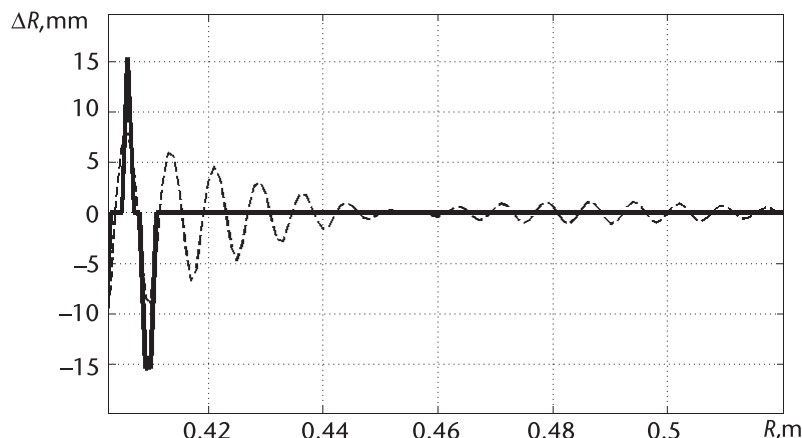


**Figure 8.13** Error plots at the measurement of small ranges using the MLM.

## 8.4 Frequency Measurement Using Methods of the Parametric Spectral Analysis

### 8.4.1 The Algorithm of the Frequency Measurement on the Basis of Eigenvector Analysis in the Noise Subspace

Spectral estimation based on the analysis of eigenvectors in the noise subspace is concerned with methods of parametric spectral analysis (PSA) allowing the best-resolution characteristics and a frequency estimation of narrowband signals [1]. Algorithms of the Pisarenko harmonic expansion (PHE), multiple signal classification (MUSIC), and the eigenvector algorithm (EV) can be concerned with these methods. The significant disadvantage of the PHE algorithm in contrast to the MUSIC and EV algorithms is mentioned in [1] for accuracy degradation of frequency estimation at reduction of analyzing the sequence duration.

The idea of MUSIC and EV methods consists of the fact that  $p - L$  eigenvectors of the noise subspace  $v_{L+1}, \dots, v_p$  of the covariance matrix or modified covariance matrix of data from  $p$  complete eigenvectors and  $L$  main vectors will be orthogonal to vectors of sine signals [1]. Orthogonality property leads to the fact that the linear combination

$$\sum_{k=L+1}^p a_k |e^H(\omega)v_k|^2 \quad (8.32)$$

where  $e(\omega)$  is a vector of the complex sine (the symbol  $H$  means a sign of the complex conjugation of matrix elements and its further transposition) will be equal to zero if the vector  $e(\omega)$ ,  $i = \overline{1, N}$  is one of the vectors of the sine signals.

For the EV and MUSIC methods, we assume the spectrum estimation to be

$$P_{EV}(\omega) = \frac{1}{\sum_{k=L+1}^p a_k |e^H(\omega)v_k|^2} \quad (8.33)$$

The difference of the MUSIC and EV methods consists of the fact that in the EV method coefficients  $a_k$  are considered equal to the value inverse to the eigenvalue of  $k$ th eigenvalue of  $\lambda_k$ , that is,  $a_k = 1/\lambda_k$ . In the MUSIC method, all coefficients  $a_k = 1$ . Therefore, the EV method begets a lesser number of spurious spectral peaks (SSP) caused by the effect of noise interference, and their intensity is significantly less than in the MUSIC method. It is typical for the EV method that in its spectrum the SSPs are absent, which can exceed (in amplitude) the spectral peaks of sine components that are present in the DFS. Therefore, to solve a problem of the DFS frequency estimation, which is received on the SR background, the EV method is preferable because its application allows the practical elimination of the anomalous measurement errors.

Nevertheless, the EV method has a disadvantage typical of all PSA methods. These methods were developed for the determination of a number of narrowband signals and for its frequency estimation in the case that the FFT and DFT algorithms do not allow sufficient resolution. It is necessary to note that the main task at the PSA methods application is the resolution of the narrowband components. The

frequency estimation of these components is the secondary task. The low stability of spectral estimation, of which we understand the inaccurate representation of the power of sine components of the signal, is a fee for the increase of the resolution capability of the spectral estimation. This leads to the fact that in the pseudo-spectrum (8.33) the component with a larger intensity can be represented by the SC with the lesser intensity. In other words, inaccurate representation of the power of separate signal components is demonstrated already on the level of more or less. For the DFS frequency estimation for signals received on the SR background, this circumstance has essential importance since the sign disappeared, for which it is possible to provide a selection of useful and spurious signals.

Publications [7,8] are devoted to a choice of the matrix order  $m$  and the model order  $p$ , which are used to calculate eigenvectors. It is recommended to use the modified covariance matrix or the covariance matrix of data [1] for the calculation of eigenvectors. The first one allows us to ensure a higher resolution (by about 15% to 20%). The dimension of the modified matrix is chosen starting from the sample number of the signal and it should be in the range  $m = 2p + K/2$ . To ensure the more accurate range measurement at the SR presence, it is necessary that  $m$  is chosen to be equal or closed to its maximal possible value. As to the choice of the model order  $p$ , investigations [7,8] showed that the measurement error weakly depends upon the model order already for  $p \geq (2-4)L$ . A further increase of the model order is inexpedient.

Addition of zero samples at calculations leads to increase the DFS frequency estimation accuracy.

However, recommendations described in [7,8] are formulated for the resolution of the sine components. The DFS of the FMCW RF has the above-mentioned specificity, the presence of PAM, which leads to peculiarities at the application of the EV method in the frequency range finding.

In [9], the author uses the EV method for range estimation at the SR intensity, exceeding the intensity of the useful signal, which is typical at measurement of the weakly absorbed material level near the reservoir bottom. As the range to the bottom is known, the SC selection of the EV spectrum corresponding to the reflection from the bottom does not cause difficulties. In this case, when there is a useful signal and one SR is caused by reflections from the bottom, it is necessary to calculate the ranges

$$\hat{R}_{\min,\max} = c\hat{f}_{\min,\max,EV}K/4\Delta f \quad (8.34)$$

where  $\hat{f}_{\min,\max,EV}$  are the values on the minimal and maximal frequencies, at which the SCs of the EV pseudo-spectrum are situated, expressed through the parts of the  $\pi$  number.

As the range estimation to reflecting surface, we need to accept the value of  $\hat{R}_{\min}$  (i.e., the estimation corresponding to the minimal range). Another variant of the SR selection is possible. It is necessary to determine the frequency interval  $\Delta\Omega$ , in which the SCs of the EV pseudo-spectrum, which correspond to the reflection from the bottom, are formed. SCs corresponding to the useful signal should be searched in the frequency range excluding the interval  $\Delta\Omega$ .

Figure 8.14 shows plots of instantaneous errors of range measurement with the help of the algorithm based on EV method using the covariance matrix of data (plot 1) and using the algorithm (3.4) (plot 2) obtained with the help of modulation. Both plots show the distant measurement error versus the material level to the reservoir bottom  $r_x = R - \bar{R}$ . Results are obtained for the FMCW RF with the carrier frequency of 10 GHz and the FM sweep of 500 MHz, and the SNR is equal to 70 dB. At the simulation, in the first approximation, the dielectric properties of reservoir contents are taken into consideration, and the range to the bottom is equal to 15 m. At the material level movement from 14 m to 15 m, the seeming range to the bottom was varied from 15.5 m to 15 m; therefore, the  $q$  ratio varied from  $-3.5$  dB to  $-4.2$  dB. The DFS sample's number was 256, the model order  $p = 8$ . At the calculation of the EV spectrum, the signal period is increased artificially by 64 times. We did not use the SCs of the EV spectrum located far (more than 15 m) from the FMCW RF. The presented plots are obtained at the PAM absence. At the range estimation with the help of the algorithm (2.4), the Blackman WF was used. We see from Figure 8.14 that the algorithm of range estimation on the basis of the EV method allows an essential decrease in the measurement error caused by reflections from the bottom and the reduction of the IEZ. The increased error is observed only at a range of 15 to 20 cm from the bottom; that is, at such a range where the SCs of the EV pseudo-spectrum are stopping to resolve. The algorithm (3.4) shows the increased error at an essentially larger range from the bottom. At the spectra resolution in the Fourier basis, the measurement error is sufficiently small, and at absence of resolution the error sharply increases. To obtain curve 2, the algorithm (3.4) is modified: two maximal SCs (corresponding to the useful signal and the SR) were searched and that SC, which is located close to the FMCW RF, was accepted as the useful one. At the performance of the simulation, the inspection of the spectrum SL was provided. Those SCs, for which the intensity exceeds the intensity of the largest spectrum SL to the left of the maximal SC corresponding to SR, are accepted as the useful SCs. However, the specific DFS distortions are not considered in [9].

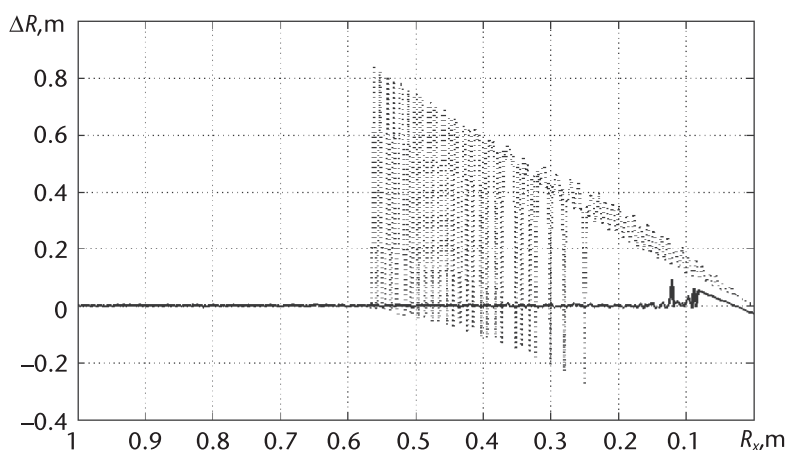


**Figure 8.14** Plots of the instantaneous error of range measurement as a function of reflector removal from the reservoir bottom at using of the covariance data matrix.

The PAM influence upon the application effectiveness of the range measurement on the basis of the EV method causes practical interest. Figure 8.15 shows the function of the PAM deepness influence  $\mu$ , according to (4.31), on the range measurement error. Plots are calculated in accordance to (8.4). Curve 1 corresponds to the application of the algorithm (3.4). The simulation performance conditions are the same as for Figure 8.14. We clearly see that the PAM leads to an increase of measurement error. The error increase is observed at a significant range from the reservoir bottom. However, the benefit in accuracy is significant at the PAM influence on the measurement results. At the UR exit from the IEZ, it is necessary to transfer to the measurement on the basis of the algorithm (3.4), which is not sensible to the PAM.

The functions presented in Figures 8.14 and 8.15 give us reason to state that the algorithm of the range estimation on the basis of the EV method allows error reduction and the IEZ size in the very unfavorable situation when  $q_{sf} < 0$ . However, the increased computational expenses are the fee for the measurement accuracy increase.

#### 8.4.2 The Frequency Measurement Algorithm by the Prony Method of Least Squares

The interest in the Prony method is caused because its application allows us to obtain a resolution close to the resolution of the EV method with much less computational expenses. The sense of the Prony method is described in [1].

We use the signal model in the form of a sum of  $p$  complex exponents:

$$x[n] = \sum_{k=1}^p h_k z_k^{n-1} \quad (8.35)$$

where  $h_k = A_k \exp(j\theta_k)$  is a complex amplitude,  $z_k = \exp[(a_k + j2\pi f_k)\Delta t]$  is the complex exponent,  $A_k$  and  $a_k$  are the amplitude and damping coefficient of the  $k$ th complex

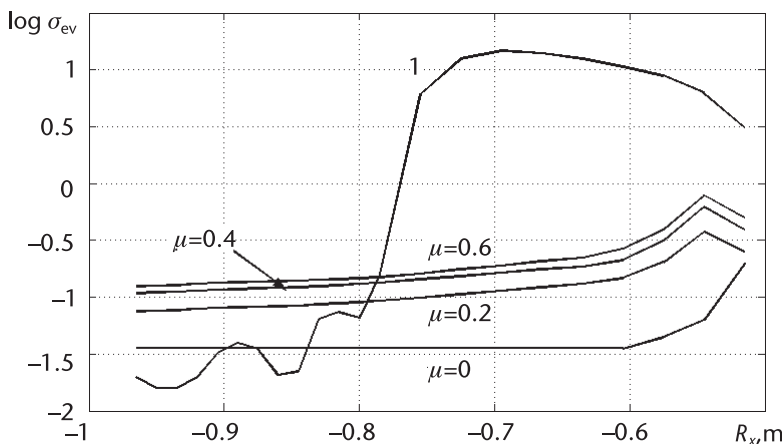


**Figure 8.15** Plots of the function of the relative measurement error MSD versus the PAM deepness using the data matrix.

component,  $f_k$  and  $\theta_k$  are the frequency and the initial phase of the  $k$ th sinusoid,  $\Delta\tau$  is the sample interval in seconds, and  $x[n]$  and  $n = 1, 2, 3, \dots$  are complex samples of the signal. Model parameters are selected in such a manner to fit the model to data samples with maximal accuracy.

At the DFS frequency measurement, the samples' number  $K$  exceeds that minimal number, which is necessary to fit the model from the  $p$  complex exponents (we call this  $p$  the model order). For this case, the specific method was developed, which in the literature [1] is called the Prony method of least squares.

The practical implementation of the frequency estimation algorithm on the basis of the Prony method meets definite complexities. To achieve the maximal resolution of the useful signal corresponding to the SR, it is necessary to define the optimal model order  $p$  and the DFS samples' number. It should be noted that the optimization procedure of the  $p$  value and the DFS samples' number  $K$  is absent. Therefore, we give the recommendation [10], which was obtained during the simulation and experimental investigations.

The model order should be defined starting from the condition  $p \approx K/4$ . At an increase of the model order to this value, we can observe the essential reduction of the range measurement error. A choice of the model order in the range  $p = K/4 \div K/3$  leads also to an accuracy increase; however, the benefit is not significant, and beginning from  $p > K/3$ , the measurement accuracy begins to decrease. The reason for the measurement error increase at small values of the model order  $p$  with respect to sample number  $K$  is connected with the fact that the coefficients  $\alpha_m$  can be calculated insufficiently accurately because the equation systems are strongly overdetermined. At relatively large model orders, the error increase is caused by the fact that the above-mentioned equation systems become ill-conditioned.

Recommendations on a choice on the DFS sample number can be reduced to the following. Their number should not exceed the value  $2K_K$  ( $K_K$  is the DFS sample number determined in accordance with the Kotelnikov theorem). A sample number increase more than  $2K_K$  leads to an error increase for the calculation of coefficients  $\alpha_m$ . It is necessary to attract attention to the fact that the DFS sample number according to Kotelnikov depends on the range to the reflector. Therefore, it is difficult in practice to choose the optimal model order, which leads to the fact that the measurement error becomes a function of the range. The choice of the model order from the condition  $p = K/4 \div K/3$  leads to a spurious SC appearance in the Prony spectrum. Because of the instability of SC amplitudes, the minimal SC will not necessarily correspond to the useful signal.

It is hypothesized in [11] to use the following procedure for the elimination of acceptance of the spurious SC for the spectral peak of the useful signal. Let it be necessary to provide the range measurement on  $N_p$  DFS realizations using the maximal SCs of the Prony spectrum and to determine the  $N_p$  values of the measured range according to (8.35). From the  $N_p$  values of the measured range, it is necessary to reject  $N_M$  maximal and  $N_M$  minimal values. The remaining values of the measured range are averaged. The method eliminated reliably anomalous errors; therefore, the average operation decreases the estimation variance. The two-stage procedure of the range estimation facilitates the reduction of an appearance probability of anomalous errors:

- *Stage 1:* The range estimation is searched with the help of the algorithm (3.4), which allows the reduction of those range intervals, in which the maximal SC of the Prony spectrum is searched.
- *Stage 2:* The above-mentioned procedure of the anomalous error elimination using the DFS  $N_P$  realizations is used.

The typical function of the instantaneous range measurement error is shown in Figure 8.16 when using the Prony least square method obtained under the following conditions. The SR is located at a range of 5.5 m, the ratio of  $q_{s/i}$  dB,  $q = 70$  dB, a DFS sample number of  $K = 64$ , and the model order of  $p = 34$ . The carrier frequency and its FM sweep were, respectively, 10 GHz and 500 MHz. To obtain the plot at each specific range, 10 measurements to the reflector were provided, and two minimal and two maximal were rejected. Other values of the measured range were averaged.

We see from Figure 8.16 that the application of the range measurement algorithm on the basis of the Prony method allows an essential reduction on both the measurement error and the IEZ size compared with the algorithm (3.4). The careful analysis of Figure 8.16 allows the determination that the error begins to insignificantly increase from the range of less than 0.4 m to the SR. At a larger removal from the SR, the measurement error does not exceed the boundaries of  $\pm 1$  mm. A sharp error increase begins from the range  $R_x$  equal to about 0.23 m only. Nevertheless, the maximal error value, as simulation data show, does not exceed 4 to 5 cm.

We note that the above-mentioned plots were obtained at the PAM absence. Let us monitor how the PAM affects the error. Figure 8.17 shows the functions of the range measurement MSD versus the PAM deepness at the application of the Prony least squares method. Functions are obtained under the same condition as in Figure 8.16.

As well as at the application of the EV method, the PAM presence leads to a resolution degradation and to errors of the frequency determination, at which the maximal SC is situated. It follows from Figure 8.17 that the range measurement

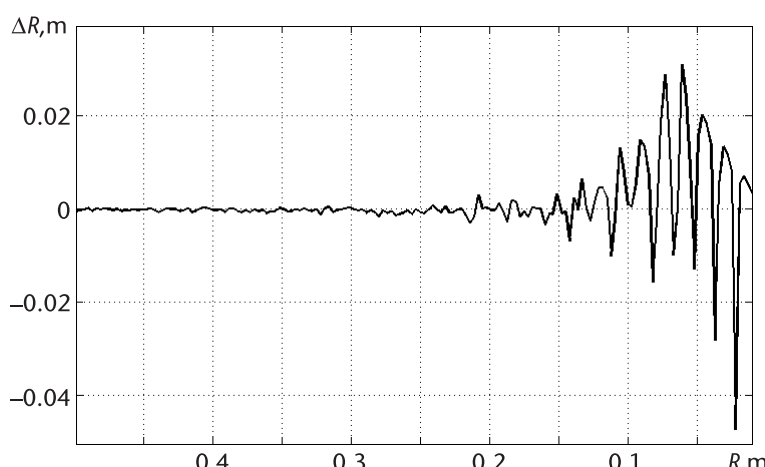


**Figure 8.16** Plots on the instantaneous error of range measurement when using the Prony least squares method.

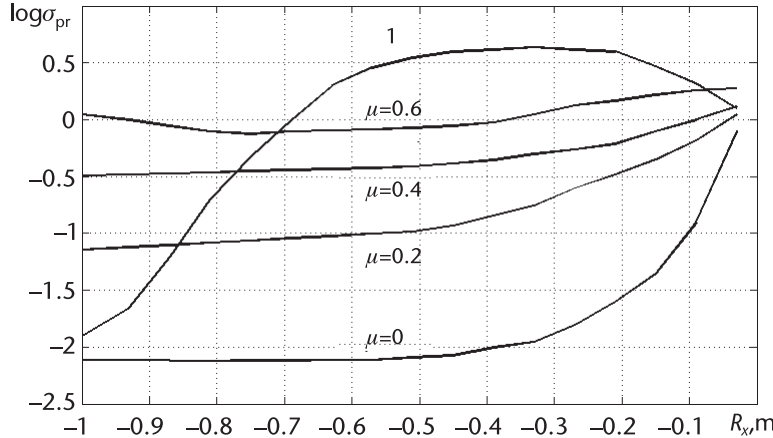


**Figure 8.17** Plots of the relative MSD function of range measurement versus the PAM deepness at the application of the Prony least squares method.

algorithm on the basis on the Prony method is much more sensible to the PAM than the measurement algorithm on the basis of the EV method.

The presented results allow the statement that the frequency estimation algorithms on the basis of the PSA methods permit a decrease in the measurement error by about the order compared with the algorithm (3.4). The IEZ size decreases significantly as well, but these methods are sensible to the DFS distortions caused by the PAM. The PAM presence leads to a noticeable benefit decrease in measurement accuracy.

## 8.5 Range Prediction on the Basis of Consideration of the Movement Speed

Let us consider the variant of the FMCW RF application for the range measurement to the UR under the conditions when a sign of the speed vector movement is known. In conformity to industrial systems, this corresponds to the case when signals corresponding to the approach or removal modes of the useful reflector [12] are applied to the FMCW RF from the automatic control system.

We shall then assume that the UR movement speed is described by some monotonic function and that the locations of all SRs are known as well. Outside the IEZ the range measurement is provided using the algorithm (3.4) through the same time intervals. We consider two situations possible in practice.

### 8.5.1 Uniform Velocity of the Useful Reflector Movement

The velocity of reflector movement will be estimated in some range interval  $\Delta R$  before reflector input in the IEZ. The range prediction in the IEZ will be provided in accordance with the formula:

$$\hat{R}_i = \hat{R}_{i-1} + \bar{V}_{\text{vel}} t_{\text{meas}} \quad (8.36)$$

where  $\hat{R}_i$  and  $\hat{R}_{i-1}$  are, respectively, the current and previous values of measured range,  $\hat{V}_{\text{vel}}$  is an estimation of the reflector movement velocity, and  $t_{\text{meas}}$  is the time interval between two consecutive measurements.

If  $t_{\text{meas}}$  is fixed (not random), it is clear that the measurement error will be defined by the error of the velocity  $V_{\text{vel}}$  estimation. The estimation of velocity at two consequence measurements with numbers  $i - 1$  and  $i$  can be defined as:

$$\hat{V}_{\text{vel},i} = (\hat{R}_{i-1} - \hat{R}_i)/t_{\text{meas}} \quad (8.37)$$

where  $\hat{R}_{i-1}$  and  $\hat{R}_i$  are the estimations of the range to the reflector for two consecutive measurements. The accuracy of velocity estimation is defined by two factors acting independently: noisy interference and the level of sidelobes of the DFS spectrum, that is,

$$\hat{V}_{\text{vel},i} = V + \delta V_{\text{ni},i} + \delta V_{\text{tr,er}} \quad (8.38)$$

where  $\delta V_{\text{ni},i}$  is an error caused by noisy interference and  $\delta V_{\text{tr,er}}$  is a truncation error caused by the DFS SL influence.

The average value of the random variable  $\hat{V}_{\text{vel},i}$  can be defined taking into consideration that the range measurement estimation using the algorithm (3.4) is not asymptotically shifted:

$$M\{\hat{V}_{\text{vel},i}\} = V_{\text{vel}} + \delta V_{\text{tr,er},(i-1)} - \delta V_{\text{tr,er},i} \quad (8.39)$$

The variance of  $\hat{V}_{\text{ni}}$  can be defined as taking into account that the estimation is formed at two consecutive independent measurements:

$$D(\hat{V}_{\text{vel},i}) = 3N_0c^2 / [E(2\Delta\omega)^2 t_{\text{meas}}^2] \quad (8.40)$$

which follows from (4.8).

The errors  $\delta V_{\text{ni},i}$  and  $\delta V_{\text{tr,er}}$  can be decreased averaging  $V_{\text{vel},i}$  in the range interval  $R_{\text{init}} < \Delta l < R_{\text{final}}$ , that is, determining the average value of velocity as

$$\overline{V_{\text{vel}}}(\Delta l, R_{\text{init}}, R_{\text{final}}) = \sum_{i=1}^L \hat{V}_{\text{vel},i}/L \quad (8.41)$$

where  $L$  is a number of measured values  $V_{\text{vel},i}$  in the range interval  $\Delta l$  before the reflector input in the IEZ.

The averaged estimation of velocity in (8.41) is designated as a function of three parameters:  $\Delta l, R_{\text{init}}, R_{\text{final}}$ . The sequence of values  $\hat{V}_{\text{vel},i}$  as a function of  $i$  will have the oscillating character repeating the same character of the measurement error by the algorithm (3.4) with accuracy up to the phase and the span of high-frequency oscillations, which follows from (8.37). It is evident that the velocity estimation error will be minimal in the case if the integer period number of high-frequency oscillations is in the interval  $\Delta l$ . The maximal error of velocity estimation will be when in the interval  $\Delta l$  there is the integer period number plus the high-frequency oscillation half-period and the beginning of the interval  $\Delta l$  will be located in the point corresponding to a maximum of a high-frequency oscillation envelope.

Simulation results of the range estimation procedure at the uniform reflector movement (estimations of velocity are provided with the step at 3 mm) are presented in Figure 8.18.

The experiment was carried out in such a manner: SR is located at a range of 5 m; the FM sweep is 500 MHz; and the frequency of carrying oscillation is 10 GHz. We used the Blackman WF. Before the range of 4.092 m (at this range there is a first node of the high-frequency oscillation envelope) and at a range of more than 6.3 m, the measurement was conducted with the help of the algorithm (3.4). In the range interval of 4.092 to 6.3 m, the range prediction is provided on the basis of consideration of the reflector movement velocity (curves 1 to 4) according to (8.36). The velocity estimation is performed, respectively, for ranges designated by the letters A, B, C, and D in Figure 8.18. Then, the loop centers of the high-frequency oscillation envelope of the error function, the very unfavorable variant was chosen (a number of high-frequency oscillation periods is equal to the integer number plus a half-period). Simulation is conducted at a noisy interference absence and  $q_{s/i} = 2$  dB. It is clearly seen from the figure that the algorithm of velocity account allows an essential reduction of the range measurement error. For example, we can note that at the mentioned  $q$  and the same other condition, the error achieves 18 cm. However, this error depends on the interval  $\Delta l$ . In the very unfavorable case when the interval  $\Delta l$  is chosen from the center of the first loop (point D), the measurement error achieves 27 mm. With  $\Delta l$  increasing, the error decreases rapidly.

Simulation results allow the determination that for the provision of a small error of the range prediction, the velocity estimation should be carried out starting from the range equal to about 1.75 m to the SR (for the very unfavorable case). At an FM sweep  $\Delta F$  variation, the view of the plot presented in Figure 8.18 will noticeably change, but conclusions concerning the interval  $\Delta l$  choice remain the same with the account of  $\Delta F$  variation. For a carrier FM sweep of 1 GHz in the very unfavorable case, to achieve a small error, the velocity account should be done from the range twice less than at the FM sweep of 500 MHz.

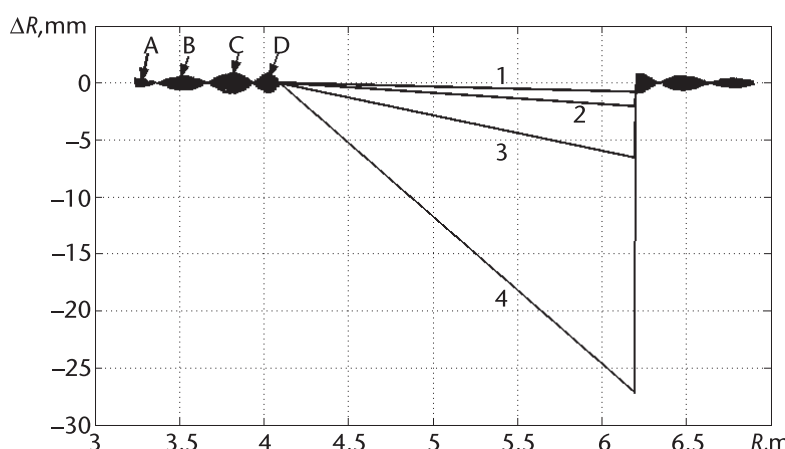


**Figure 8.18** Plots of the instantaneous range measurement error at the uniform velocity of reflector movement.

It should be noted that at the velocity estimation from the range, at which there is a node of a high-frequency oscillation envelope, the velocity estimation error decreases owing to reduction of  $\delta V_{n,\text{inter},i}$ . As an example, we may show that at a velocity estimation, beginning from the second node before the SR, the error of range prediction does not exceed 1 mm and part of a millimeter for the velocity account beginning from the range, at which there is a third envelope node. The variance of a range prediction in the range interval, where the prediction is performed with an account of the velocity estimation, is determined as according to (4.8):

$$D(\hat{R}_{\text{vel}}) = \frac{2.25c^2}{q_{s/n}L(\Delta\omega)^2} \quad (8.42)$$

which is confirmed by the simulation results.

The plots presented in Figure 8.18 are obtained using the Blackman WF and for the FM sweep of 500 MHz. The application of another WF leads to a plot variation. The increase of the FM sweep allows a proportional reduction of the range to the reflector beginning from which it is necessary to take into consideration the velocity of its movement.

### 8.5.2 The Nonuniform Velocity of the Useful Reflector Movement

For practice, this is the most interesting case because by using the FMCW RF as a level-meter, the performance of the pumping equipment can depend both upon the reservoir loading degree and the properties of contents. We assume that the reflector movement velocity can be described by an exponential function with an unknown damping decrement  $\alpha$ ; that is,

$$V(R) = V_{\text{init}}(R) \exp(-\alpha R) \quad (8.43)$$

where  $V_{\text{init}}(R)$  is an initial value of reflector velocity at range  $R$  from FMCW RF to SR.

It is necessary to note that the function choice (8.43) described the velocity variation and the choice of the damping decrement  $\alpha$  (chosen to ensure the velocity variation by 20% at range variation by 2 m) has to a great extent an arbitrary character. Nevertheless, the simulation performed under the above-mentioned assumptions allows us to obtain an answer about the behavior of the range prediction error under conditions when the approximated function has an oscillating character caused by the influence of the spectra SL of the interference and the useful signal.

As usual, we assume that the outside IEZ measurements are conducted using the algorithm (3.4).

It is possible to decrease the error accumulation at the prediction in the case if we can determine some function describing the velocity variation as a function of the number of measurement  $n$ . At input in the IEZ, we form the range estimation on the basis of the found function assuming as usual that  $t_{\text{meas}}$  is not random. It seems simple to determine the approximation of this unknown function (in general) in the form of a polynomial of the order  $K_p$ :

$$\bar{V}_n = \sum_{i=1}^{K_p} b_i(n), \quad n = 1, 2, \dots, N \quad (8.44)$$

where the sequence of polynomial coefficients is chosen by the least squared method, that is, the following function is minimized:

$$Q(b) = \sum_{n=1}^N (V_n - \bar{V}_n)^2 \quad (8.45)$$

Simulation results are presented in Figure 8.19.

Simulation conditions are the same. The only difference is that simulation is carried out at the SNR of 70 dB. In the whole range interval including the IEZ, we used the algorithm (3.4). At its basis, according to (8.44), the velocity is estimated at each  $n$ th measurement. In the IEZ, the calculated value in accordance with the found function  $\bar{V} = f(n)$  described the UR velocity variation versus range is accepted as the range estimation (i.e., the nonlinear function of velocity versus range is considered). At simulation, the function (8.43) is approximated by the polynomial of the second order.

The simulation showed that only the value of the range interval at the input in the IEZ, in which the determination of  $\bar{V} = f(n)$  occurs, influences noticeably on the prediction error. The prediction error depends very little on where the determination  $\bar{V} = f(n)$  occurs: from the node or the loop of envelope. Curve 1 corresponds to the estimation  $\bar{V} = f(n)$  beginning from point D (see Figure 8.18). Curve 2 is the estimation of  $\bar{V} = f(n)$  provided from the range at which there is a ninth node of the oscillation envelope of the error curve (i.e., from a range of about 1.9 m from the IEZ). We see from Figure 8.19 that the prediction error is high enough. The application of the described procedure allows its reduction compared to using the algorithm (3.4) only by three to six times. However, it is necessary to note that the SIR increase leads to a proportional decrease of the range prediction error. In the

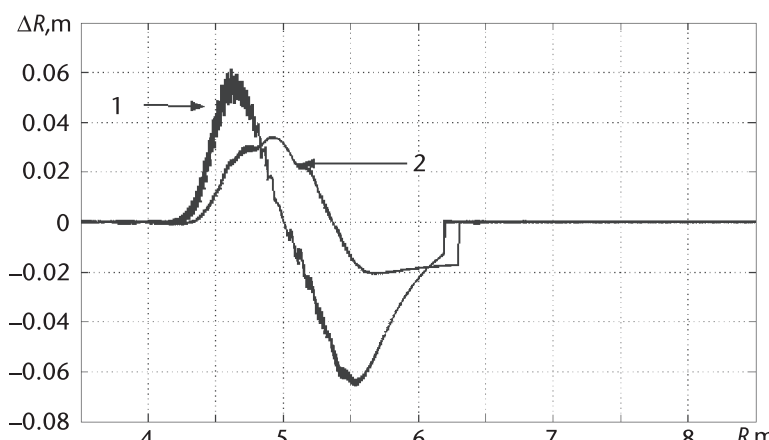


**Figure 8.19** Plots of instantaneous measurement error for the nonlinear velocity variation.

case when the UR velocity is uniform, the prediction error decreases to the values of the order in units of millimeters.

## 8.6 Conclusions

The investigation of different methods allowing reduction of the range measurement error at SR presence permits us to determine the following. SR cancellation is most effective at an offered frequency variation of the FMCW RF-carrying oscillation. In this case, the application of the cancellation mode allows a decrease in the IEZ approximately by the order at the frequency varying of the carrying oscillation within the limits commensurable with the FM sweep of the oscillator frequency, which is quite feasible in practice.

The tracking algorithm allows the reduction of the range measurement error by 82 times compared with algorithms using a spectrum in the Fourier basis. It is proved that the admissible velocity of the reflector movement depends on the SIR. At  $q_{s/i} = 2$  dB, the reflector movement from one measurement to another should not exceed  $\lambda/8$  and may be increased to the value  $\lambda/4$  at the decrease of the SIR. The range to the SR is determined with an intensity exceeding the useful signal intensity at which the tracking loss happens. This range is equal to about  $1.5\delta_R$  at  $q_{s/i} = -4.5$  dB.

The feasibility study of the range estimation algorithm application is performed based on the eigenvector analysis in the noise subspace for the range measurement to the content level in reservoirs. It is shown that the PAM significantly affects the accuracy characteristics of such an algorithm of range estimation. Depending on the PAM deepness, the range measurement error can be reduced approximately by the order.

The algorithm of range estimation is offered based on the application of another PSA method, the Prony method. Depending on the PAM deepness, the range measurement error can be reduced approximately by the order as well. It is shown that the range estimation algorithm on the basis of the Prony method is more sensitive to the PAM influence. We note that the PSA methods do not allow adequate elimination of the SR effect.

The investigation of the range estimation algorithm at the SR presence is provided based on the estimation of the velocity of the reflector movement. It is proved that the velocity estimation accuracy depends upon the range interval at which it is estimated. At the UR movement, the velocity estimation should be provided beginning from the range of about  $10\delta_R$  to the SR. The reduction of the range measurement error in this case is equal to approximately two orders. At the nonuniform SR movement, the range measurement error essentially increased. At other equal conditions, it reduces by about three to six times.

Our experience of working with FMCW range-finders leads us to the conclusion that there is not a universal solution that permits minimizing the SR influence in all practical situations. The conditions of the FMCW RF functioning, especially for range measurement to liquid media, may vary. We must choose this method for the SR influence minimization taking into consideration the peculiarities of the device application, computing resources of the FMCW RF processor, and requirements for its accuracy.

## References

- [1] Marple, S. L., Jr., *Digital Spectral Analysis with Applications*, Englewood Cliffs, NJ: Prentice-Hall, 1987.
- [2] Imada H., and Y. Kawata, "New Measuring Method for a Microwave Range Meter," *Kobe Steel Eng. Repts.*, Vol. 30. No. 4, 1980, pp. 79–82.
- [3] Parshin, V.S.; V. M. Davydochkin, V. S. Gusev, "Compensation of Spurious Reflections' Influence on Distance Measurement Accuracy by FMCW Range Finder," *Digital Signal Processing and Its Application. – Proceedings of RNTORES Named after A.S. Popov.* No. 5, Moscow, Vol. 1, 2003, pp. 261–263. [In Russian.]
- [4] Parshin, V. S. "Tracking Frequency Meter of the Beating Signal of the Radio Range Finder with Frequency Modulation of Radiated Signal," *Digital Signal Processing and Its Application. – Proceedings of RNTORES Named after A. S. Popov.* No. 10, Moscow, Vol. 1, 2008, pp. 395–398. [In Russian.]
- [5] Patent 2410650 (Russian Federation), INT.CL. G01F 23/284, G01S13/34. "Method of Material Level Measurement in a Reservoir," B. A. Atayants, V. S. Parshin, V. V. Ezerskiy. Bull. No 3. Filed November 1, 2008; published January 27, 2011.
- [6] Lindsey, V., *Synchronization Systems in Communication and Control*, Moscow: Sovetskoe Radio Publ., 1978, 600 p. [In Russian.]
- [7] Kavex, M., A. J. Barabell, "The Statistical Performance of the MUSIC and the Minimum-Norm Algorithms for Resolving Plane Waves in Noise," *IEEE Trans. Acoust. Speech Signal Process*, Vol. ASSP-34, April 1986, pp 331–341.
- [8] Wang H., M. Kavex, "Performance of Narrowband Signal-Subspace Processing," *Proceedings of the 1986 IEEE International Conference on Acoustics, Speech, and Signal Processing*, Tokyo, Japan, April 1986, pp. 589–592.
- [9] Wax, M., T. Kailath, "Detection of Signals by Information Theoretic Criteria," *IEEE Trans. Acoust. Speech Signal Process*, Vol. ASSP-33, April 1985, pp 387–392.
- [10] Parshin, V. S., A. A. Bagdagulyan, "Distance Measurement to Material Level in a Reservoir at Presence of Spurious Reflections Exceeding the Useful Signal in Intensity," *Digital Signal Processing and Its Application. – Proceedings of RNTORES Named after A.S. Popov.* No. 8, Moscow, Vol. 1, 2006, pp. 306–308. [In Russian.]
- [11] Parshin, V.S.; V. V. Ezerskiy, "Application of Algorithms of Parametric Spectral Analysis at Distance Measurement with the Help of Radar Range Finders with the Frequency-Modulated Signal," *Digital Signal Processing and Its Application. – Proceedings of RNTORES named after A.S. Popov.* No. 7, Moscow, Vol. 1, 2005, pp. 234–238. [In Russian.]
- [12] Patent 2399888 (Russian Federation), INT.CL. G01F 23/284, G01S13/34. "Method of Material Level Measurement in a Reservoir," B. A. Atayants, V. S. Parshin, V. V. Ezerskiy, S. V. Miroshin. Bull. No. 26. Filed January 26, 2009; published September 20, 2010.

# Testing of Precision Measuring Systems of FM Short-Range Radar and Areas of Its Practical Application

## 9.1 Introduction

Development, testing, calibration, attestation, and verification of FM RF are fulfilled with the help of exemplary installations or test benches, in which the standard reflector can be mounted at a specified distance from the FM RF with a specific accuracy. It was shown in Chapter 6 that sizes and shape of the reflector affect the measurement accuracy. As an example, Figures 9.1(a, b) show the calculated (lines 1 and 2) and experimental (line 3) dependence of the distance measurement error to the disk with a diameter of 530 mm as a function of measuring distance when using the antenna with an aperture diameter of 50 mm (lines 1 and 3) and 145 mm (line 2) in FM RF. The frequency tuning range at FM is 1 GHz with a central frequency of 9.8 GHz. We see here a good correspondence of theoretical and experimental results.

It follows from Figure 9.1 that, using of the disk as the standard reflector, the measurement error is inadmissible largely for any practical tasks and, moreover, this error essentially depends upon the width of the antenna DP used in the FM RF. In this context it is necessary to estimate the possibility of radar reflector development that provides acceptable accuracy.

In addition, we consider in this chapter the possible application areas of the FM RF in industry and in scientific research. Naturally, it is impossible to cover all application areas with a high degree of detail. Nevertheless, we note that the above-mentioned material has a rather general character and can be used in many practical problems, which have been detailed in the Introduction.

## 9.2 Equipment and Approaches for the Experimental Estimation of FM RF Characteristics

For reliable measurements of FM RF characteristics, which have a small error, the plane infinite *radar reflector* (RR) is the ideal standard. However, it is practically impossible to realize the conditions under which RR can be considered to be infinite. From Figure 9.1, we see that when using the circular disk as a standard RR, at the distance reduction the error decreases to a low level, when the RR angular

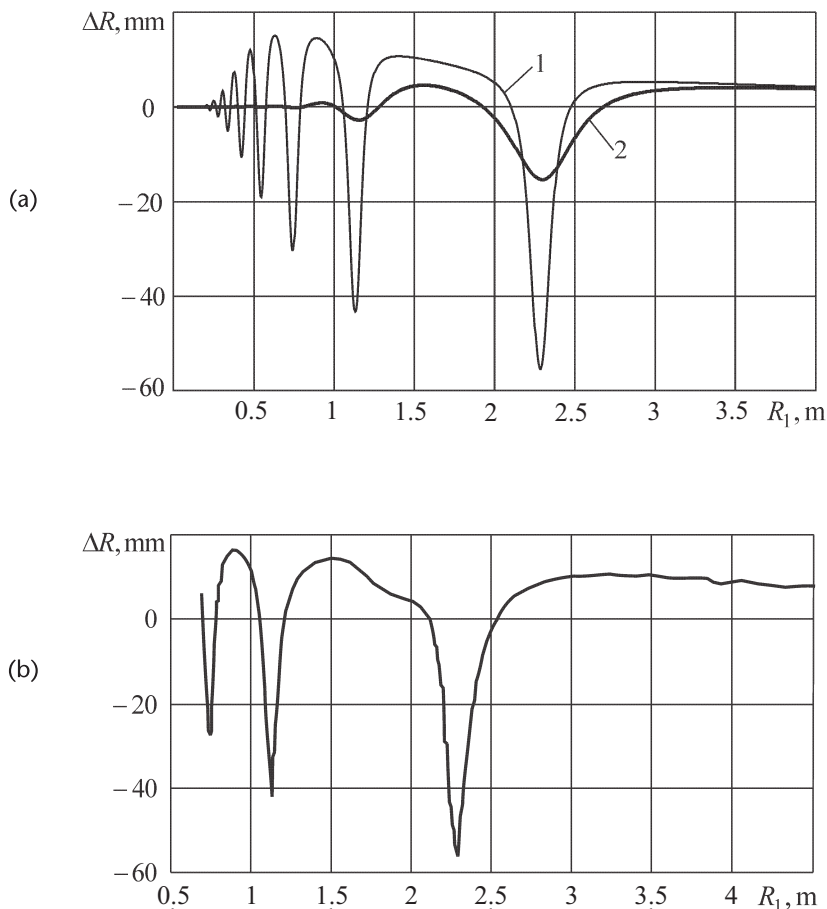


**Figure 9.1** The plot of the distance (to the disk) measurement error versus the measuring distance: (a) calculated results and (b) experimental results.

size becomes commensurable and more than the width of the FM RF antenna DP on the zero level (i.e., when the RR edge is not radiated by the probing wave). Using such an approach to solve the error reduction and for the variety of practical problems that occur with RF antennas, the RR diameter should be commensurable with the length of the FM RF operating zone, which is practically unrealizable. In the context of meteorological FM RF support, the choice of RR geometry is important, as the configuration must be such that at minimal possible sizes it can provide a correspondence of measured geometric and electrodynamic distances. Taking into consideration that for high measurement accuracy in the FM RF the wideband signals are used, the standard RR also must operate in the wide-frequency range. The information presented here shows the importance of standard RR development with specific properties.

The issue of SR reduction to the necessary level in the FM RF operating zone is no less important than the creation (if necessary) of the interference situation with specific features. These conditions can be satisfied most completely in that providing measurements in an anechoic chamber has a necessary level of the SR reduction, in which the standard RR can be located with difference characteristics emulating both the UR and SR. The general requirements for which the anechoic chamber

must be satisfied are described in [1]. Due to the specifics of the FM RF operation, these requirements may be corrected.

### 9.2.1 Synthesis of Radar Reflectors for Precision Measurements

The plane RR is mounted at a distance  $R_1$  perpendicular to the direction on the one-position FM RF (Figure 6.18). Let us choose an RR configuration so that the reflected field in the specified frequency range and in the specified space area would differ as low as possible from the field reflected by the plane infinite reflecting surface. One can formulate several equivalent criteria of RR optimality. In particular, we state the problem of RR creation, which, at specified sizes and a given length of the operating zone, provides in the operating zone a minimum of the complex amplitude of the interference field (a minimal SLL of a complex amplitude modulus of the interference field depending on frequency).

In this sense, we may consider the frequency dependence of a complex amplitude of the RR interference field (frequency response) as optimal and creating RR as optimal.

As we consider the problem of the minimization of RR sizes, we may assume that its angular sizes with regard to the point of the FM RF antenna location are small and that linear sizes often exceed the wavelength. In such a case, to determine the reflected field, we can use the scalar Kirchhoff approximation (6.15).

Equation (6.18) allows the application of known methods of antenna synthesis for RR synthesis. To determine the RR geometry, we can use the classical method of antenna synthesis called the *Dolph-Chebyshev method* [2].

Let us fulfill the RR in such a manner that its edge coincides with the circles of a radius  $\rho_1, \rho_2, \dots, \rho_N$  (Figure 9.2) in sectors  $\Phi_1, \Phi_2, \dots, \Phi_N$ .

Then the normalized complex amplitude of the interference field (6.19) is defined by the following sum:

$$\dot{U}_{\text{int,norm}} = \frac{\dot{U}_{\text{int}}}{\dot{U}_{\infty}} = \sum_{i=1}^N C_i e^{-jk[(i-1)\nu+d]\lambda_0} \quad (9.1)$$

where  $C_i = \frac{F(\theta_i)}{F(0)} \frac{\Phi_i R_1^2}{2\pi r_i^2}$ ,  $r_i^2 = R_1^2 + \rho_i^2$ ;  $d \geq 0$ ;  $\nu\lambda_0$  is the radius variation value of the RR edge, and  $\lambda_0$  is the wavelength of the carrying oscillation on the average frequency of the tuning range. Please note that the sector numeration happens in the order of a radius increase of the RR edge.

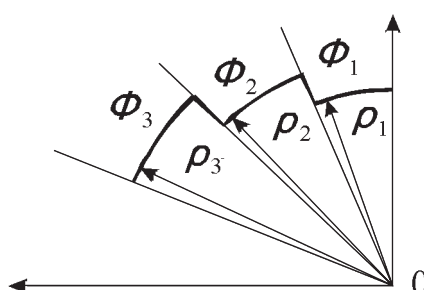


Figure 9.2 The determination of the planar RR shape.

Omitting further transformations, which are similar to [2], we give the equation for the amplitude-frequency response (AFR) of the interference field of the optimal RR. Its AFR is represented by the Chebyshev polynomial

$$U_{\text{int, norm}}(k) = \sum_{i=1}^M 2C_i T_{2i-1}(\cos k\nu\lambda_0/2) = T_{2M-1}\left(\frac{1}{\alpha} \cos k\nu \frac{\lambda_0}{2}\right) \cdot \left[T_{2M-1}\left(\frac{1}{\alpha}\right)\right]^{-1} \quad (9.2)$$

where  $M = N/2$ .

The parameter  $\alpha$  at a known number of sectors defines the frequency range  $|\cos(\pi\nu f/f_0)| \leq \alpha$  and the deepness of the interference field decrease  $Q = T_{2M-1}(1/\alpha)$ .

If a number  $N$  of RR sectors, the value  $\nu$ , the frequency range, and the deepness of the interference field suppression are specified, coefficients  $C_i$  determining the RR geometry will be [3]:

$$C_i = \frac{(2M-1)}{2T_{2M-1}(1/\alpha)} \sum_{\mu=1}^M (-1)^{M-\mu} \left(\frac{1}{\alpha}\right)^{2\mu-1} \frac{(\mu+M-2)!}{(\mu-i)!(\mu+i-1)!(M-\mu)!} \quad (9.3)$$

where  $i = 1, 2, \dots, M$ ;  $M = 0.5N$ .

For an RR with an odd number of sectors:

$$C_i = \frac{M}{T_{2M-1}(1/\alpha)} \sum_{\mu=1}^M (-1)^{M-\mu} \left(\frac{1}{\alpha}\right)^{2\mu} \frac{(\mu+M-1)!}{(\mu-i)!(\mu+i)!(M-\mu)!} \quad (9.4)$$

where  $i = 1, 2, \dots, M$ ;  $M = 0.5(N-1)$ .

Deepness and the range of interference field of the optimal RR are unambiguously connected by the equation

$$\frac{1}{\alpha} = \frac{1}{2} \left\{ \left( Q + \sqrt{Q^2 - 1} \right)^{\frac{1}{N-1}} + \left( Q - \sqrt{Q^2 - 1} \right)^{\frac{1}{N-1}} \right\} \quad (9.5)$$

and the number of RR sectors is defined by the specified values of  $\alpha$  and  $Q$ :

$$N = \frac{\operatorname{arch} Q}{\operatorname{arch} 1/\alpha} + 1$$

For simplification of further formulas, we designate the maximum and minimum frequencies of the tuning range, respectively, as  $f_{\max} = f_{\text{aver}} + \Delta f$  and  $f_{\min} = f_{\text{aver}} - \Delta f$ , where  $\Delta f = \Delta F/2$ ,  $f_{\text{aver}}$  is average frequency of the tuning range. Then  $\cos[\pi\nu(1 + \Delta f/f_{\text{aver}})] = -\alpha$ ,  $\cos[\pi\nu(1 - \Delta f/f_{\text{aver}})] = +\alpha$ . Summing term by term these equalities, we obtain  $\cos\pi\nu \cdot \cos\pi\nu\Delta f/f_{\text{aver}} = 0$ .

In this equation, the constant  $\nu$  should be such that the equality fulfills any values of  $\Delta f/f_{\text{aver}}$ ; hence,  $\nu = 0.5, 1.5, 2.5, \dots$ ; that is, the step value of RR sector is equal to the odd number of Fresnel zones on the average frequency of the tuning range. There will be a minimal RR size in case  $\nu = 0.5$  on the central frequency of the tuning range.

As  $d\lambda$  is not included in the AFR equations, it can be any value. However, at growth of  $d$ , the sizes of RR increase.

Using the above-mentioned approach, we can design RRs with a very different AFR for the suppression of the interference field. For instance, to realize the maximally plane characteristic, the coefficients  $C_i$  defining the RR configuration should be distributed according to the binomial law.

An RR with a smooth edge presents challenges as well. The RR's shape and sizes can be obtained if the number  $N$  of the RR sectors is increased without limit and the step value  $v\lambda_0$  is decreased in such a manner that a maximal RR size  $p_{\max}$  would be constant. Therefore, the equations for AFR in some cases will be simplified and then the AFR of the optimal RR takes a form:

$$U_{\text{int, norm}}(f) = \frac{1}{Q} cb \sqrt{\ln^2(Q + \sqrt{Q^2 - 1}) - \left(\frac{\pi}{2} b \frac{f}{f_{\text{aver}}}\right)^2} \quad (9.6)$$

where  $\sqrt{b} = 2\rho_{\max}/2\sqrt{R_1 0.5\lambda_0}$  is the maximal RR size at  $f = f_{\text{aver}}$  normalized to the diameter of the first Fresnel zone.

The RR configuration realizing the following function of the complex amplitude of the interference field

$$U_{\text{int, norm}}(f) = e^{-j\frac{\pi}{2} b \frac{f}{f_{\text{aver}}}} \sin\left(\frac{\pi}{2} b \frac{f}{f_{\text{aver}}}\right) / \left(\frac{\pi}{2} b \frac{f}{f_{\text{aver}}}\right) \quad (9.7)$$

is defined by the equation

$$F(\Theta) \frac{R_1^2}{r^2} \frac{d\varphi}{dr} = \text{const} \quad (9.8)$$

We note that the RR created according to the specified error of the FM RF in which the antenna with a wide DP is used provides an error reduction compared to the antenna with less DP width. In this context, it is recommended to define the RR shape for the omnidirectional antenna. Then, for a  $kr \gg 1$  equation for the RR configuration with AFR for suppression of the interference field, (9.7) becomes:

$$\rho = \sqrt{R_1 \frac{\varphi}{\pi} b \frac{\lambda_0}{4}} \quad (9.9)$$

The RR configuration in (9.9) is presented in Figure 9.3. For clarity, the first and second Fresnel zones (circles 1 and 2) are shown by a dotted line and a chain line, respectively.

A nonsymmetric RR shape leads to a nonsymmetric distribution of the interference field around the pointing direction to the RR center and to the function of the measurement error upon the mutual orientation FM RF and RR around the antenna axis. To decrease the nonsymmetry degree of the interference field distribution according to presented approach, we can make symmetric multilobe RRs.

It is evident that we can rewrite (6.19) as a sum:

$$\dot{U}_{\text{int, norm}} = \frac{1}{2\pi} \sum_{i=1}^N \int_{\Phi_i}^{\Phi_{i+1}} \frac{F(\theta_i)}{F(0)} \frac{R_1^2}{r^2} e^{-j2k(r-r_0)} d\varphi \quad (9.10)$$

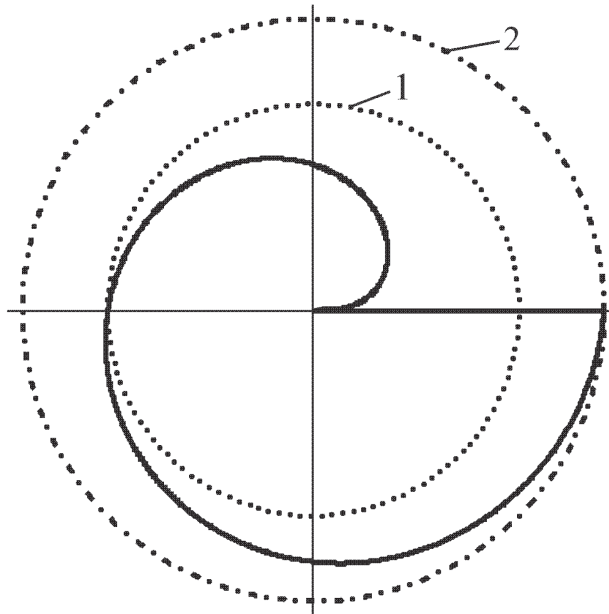


Figure 9.3 RR configuration.

where  $\sum_{i=1}^N (\Phi_{i+1} - \Phi_i) = 2\pi$ . The results of (9.1) through (9.9) are applicable to each item of this sum. Moreover, the expressions presented are invariant to the direction on the angular coordinate counting. It follows from this that this approach can be applied for multilobe, in particular, symmetric doubled-lobe RRs (Figure 9.4). Therefore, (9.9) must be shown as:

$$\rho = \begin{cases} \sqrt{R_1 \frac{4\varphi}{\pi} b \frac{\lambda_0}{4}}, & 0 \leq \varphi < \frac{\pi}{2} \\ \sqrt{R_1 \frac{4(\pi - \varphi)}{\pi} b \frac{\lambda_0}{4}}, & \frac{\pi}{2} \leq \varphi < \pi \\ \sqrt{R_1 \frac{4(\varphi - \pi)}{\pi} b \frac{\lambda_0}{4}}, & \pi \leq \varphi < \frac{3}{2}\pi \\ \sqrt{R_1 \frac{4(2\pi - \varphi)}{\pi} b \frac{\lambda_0}{4}}, & \frac{3}{2}\pi \leq \varphi < 2\pi \end{cases} \quad (9.11)$$

It follows from (9.7) that for deep reduction of interference level caused by the restricted RR size, its size should be not less than two Fresnel zones at a maximum distance from the antenna for  $f = f_{\text{aver}}$ .

The distance measurement error to the reflector has an oscillating character. Figure 9.5 shows the calculated error functions versus distance between RR and an FM RF antenna, where the bold line denotes the RR with configuration (9.11) and maximal value  $\rho = 750$  mm and the thin line denotes the disk with a radius of 750 mm. In the FM RF with a tuning range of 1 GHz and a central frequency of 9.8 GHz, the antenna with an aperture diameter of 50 mm is used.

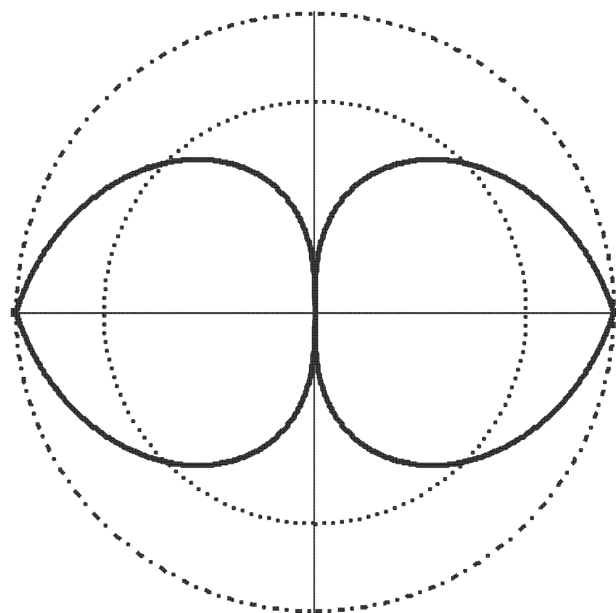


**Figure 9.4** Configuration of double-lobe RRs.

We see from Figure 9.5 that the RR application with the configuration (9.11) provides a reduction of the maximal level of the measurement error to about 2.5 mm; that is, by more than 20 times compared with the equidimensional disk. At  $\rho_{\max}$  growth, further error reduction is possible.

For optimal RRs with the function of the interference field amplitude versus the frequency and distance in (9.6), the distance measurement error  $\Delta r_{\text{err}}$  is defined by given value of  $Q$  in (3.22). Therefore, for the required suppression deepness of the interference field corresponding to the given distance measurement error, the maximal RR size normalized to the diameter of the first Fresnel zone on average frequency and for the maximal distance will be:

$$\sqrt{b} = \sqrt{\frac{2}{\pi} \ln [Q + \sqrt{Q^2 - 1}]} \quad (9.12)$$

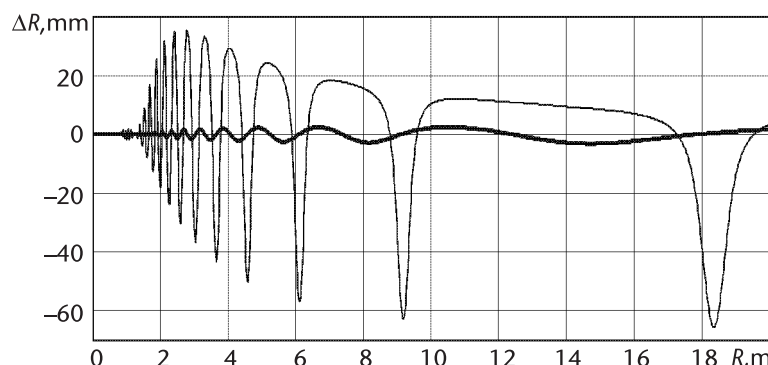


**Figure 9.5** Distance measurement error to the RR.

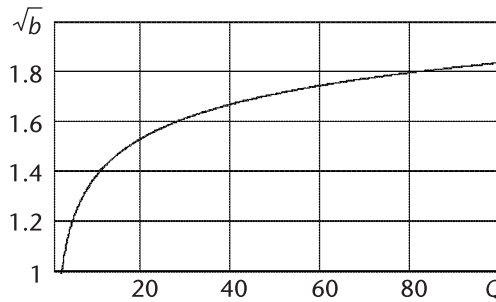


**Figure 9.6** Plot of the normalized maximal size of the optimal RR versus the suppression deepness of the interference field.

This function is shown in Figure 9.6.

From the curve presented, we see that for a specified operating zone, the significant increase of suppression deepness of the interference field by the optimal RR requires an insignificant increase of its geometrical sizes.

### 9.2.2 The Test Bench for the Measurement of the FM RF Parameters

The main constructive signs of a few test benches described in publications are generalized, but at the same time the above-mentioned approach for the RR calculation used at development of the measuring test bench at the company CONTACT-1 allows essential improvement in the main parameters of the test bench (to decrease the error) and widen functional possibilities (to create a specified interference situation) [3, 4].

The measuring test bench MTB-1 (Figure 9.7) is mounted in a room with geometrical sizes  $17 \times 8 \times 3$  m and is called the measuring room (MR). Therefore, the length of the MR operating area is 16 m. All elements of the MR construction potentially capable of creating intensive nonresolvable interference at movement of the standard RR in any point of the operating zone are closed by an absorbing material with a reflection coefficient of  $-30$  dB in the specific wavelength range. The general view of the test bench is shown in Figure 9.8. In contrast to known test benches, here

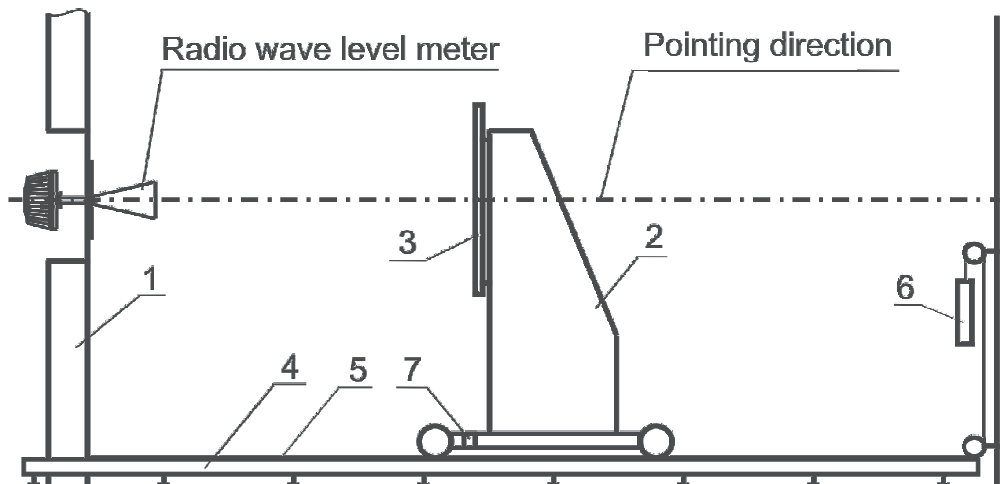


**Figure 9.7** General view of the test bench (the numerical designations are explained in the text).

the standard RR 3 smoothly moves with respect to the FM RF mounted on a special rigid mounting post 1, allowing an accurate positioning of the FM RF. Movement is provided with the help of a lightweight but rigid trolley 7 moving along the directing tubes 4 and supplied by the fixing facility in arbitrary point 3 of the distance. All constructive elements of the trolley are covered by absorbing material.

The weakly reflected post is located on the trolley, which is a support for the standard reflector 3 mounting. The possibility of changing RR is anticipated, emulating different reflecting properties of the target or measuring level. The position of the standard RR is adjusted in three planes. The possibility of mounting in the MR the additional RR is anticipated for the creation of an interference situation with specified properties emulating different reflecting properties of interference.

To determine the electrical distance to the RR, the standard scale 5 with a constant of 1 mm is attached to one of the directing tubes. The scale is stretched by weight 6 suspended on the tape measure attached to the trolley. Distance reading is provided with the help of the Vernier scale 7 located on the trolley. This setup allows for position adjusting of the standard RR with regard to adjusting the plane with an error of not more than 0.2 mm.

Special measures are used to eliminate mirror reflection from the ceiling and the floor of the MR. For this purpose, shields are suspended on the ceiling from absorbing material. To eliminate the reflection from the elements of the trolley construction, the shield from the absorbing material is attached to the front of the trolley.

A practically achieved reduction of the background reflection level can be indirectly estimated on the basis of distribution of the distance measurement error along the MR. The error distribution measured with the help of the level-meter with the frequency tuning range of 0.5 GHz is presented in Figure 9.8. Error distribution without shielding of lower beam is presented by the thin line and shielding of the lower beam (mirror reflection from the floor) is presented by the bold line.

We see that the background reflection is rather large and nonuniformly distributed in the distance. Therefore, it must be taken into account at measuring error estimation and for the FM RF calibration.

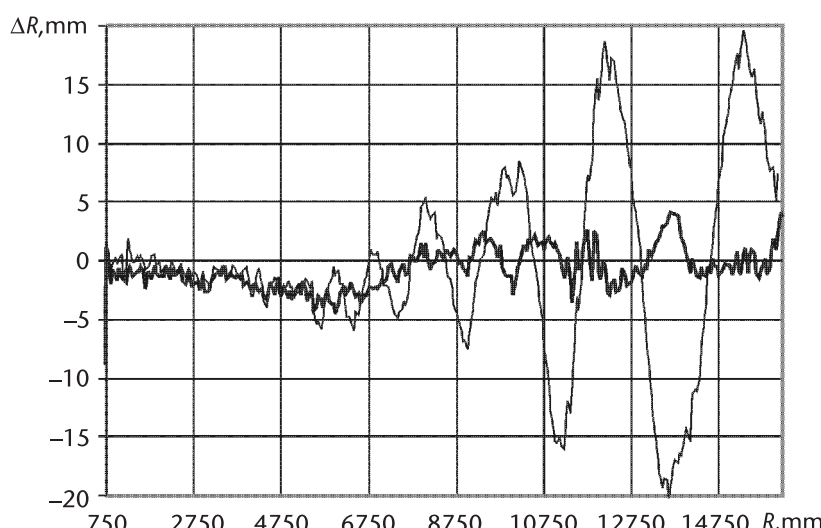


**Figure 9.8** Error distribution for the distance measurement along the MR.

### 9.2.3 The Procedure of Carrying Out Measurements

During testing of an industrially manufactured FM RF, all metrological measurements are provided according to the procedure defined by an appropriate standard. The main error is defined by the results of distance measurement in five uniformly distributed fixed points of the operating distance range. However, this procedure does not take into consideration the presence of an additional spurious background reflection typical for radio-wave measuring devices. It is shown in Chapter 6 that at the SR presence located at a fixed distance from the UR, the plot corresponding to the true distance error is displaced by the value determined by the ratio of the UR and SR parameters. From this the conclusion follows that for unbiased and reliable determination of the main measurement error, it is necessary in each of the above-mentioned distance points to provide the measurement of the error function versus the distance with the step  $\Delta$  that does not exceed that of the octant part of the wavelength of the carrying UHF oscillation during no less than one ED. We can reliably determine the true measurement error of the FM RF according to the oscillation span of this plot.

To fulfill such measurements on the measuring test bench, it is necessary to have equipment that allows us to fix the measured distance and measurement result. In this context, it is advisable to use a personal computer (PC) with special software. All results mentioned later for the specific samples of the FM RF are obtained according to the above-mentioned procedure and using the appropriate software packages, which allowed us to fix all necessary variables in the computer memory.

## 9.3 Experimental Reduction of the Error Caused by Virtual Interference

The influence of practically existing interference signal components on the frequency estimation error in radar systems is investigated in detail in many publications [5–8]. At the same time, the influence of virtual interference has not been analyzed enough. Therefore, researching the practical error level caused by the influence of virtual interference and about the possibility of reducing these errors is appropriate.

### 9.3.1 The Waveguide-Measuring Test Bench

To eliminate the influence of the additional spurious background reflection typical for radio-wave devices, experimental research was conducted on the waveguide-measuring test bench with a serial sample of a level-meter (type BARS 351), in the transmitter of which an attenuator was added to reduce the radiated power. The block diagram of the measuring test bench is shown in Figure 9.9.

The level-meter is connected with a PC with special software for distance estimation according to the spectrum maximum of the weighted DFS. The DFS is formed at the wave reflection from the standard waveguide load.

The pin (in Figure 9.9, irregularity) with adjustable depth of immersion is embedded in the waveguide through the nonradiated slot in the wide wall. The immersion depth of the pin into the waveguide is calibrated on the level of reflection

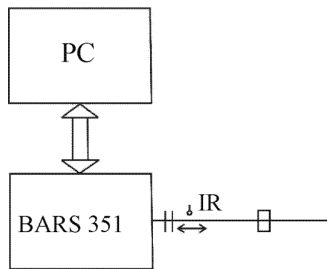


**Figure 9.9** Block diagram of the measuring test bench.

coefficient modulus  $\Gamma$ . The slot length in the waveguide is 800 mm, which allows us to vary the normalized pin position along the waveguide axis within the limits of 3.6 at a frequency tuning range from 9.55 to 10.05 GHz.

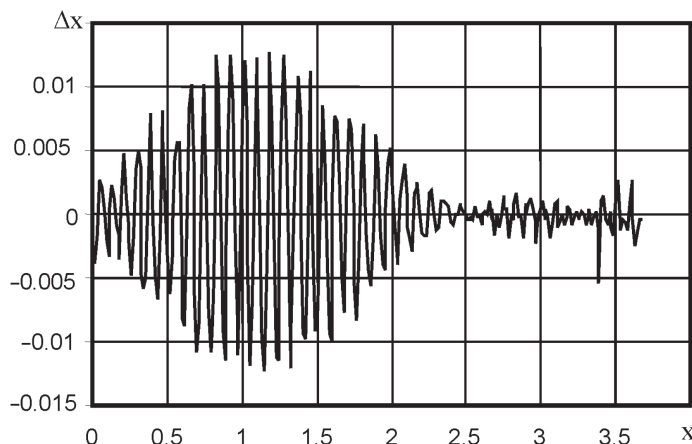
### 9.3.2 Experimental Research on the Possibility of Reducing Virtual Interference Influence

Figure 9.10 shows the normalized measurement results of the distance estimation error versus the pin position along waveguide axis. The presented function is obtained for  $\Gamma = 0.1$ ,  $q_{s/n} = 60$  dB.

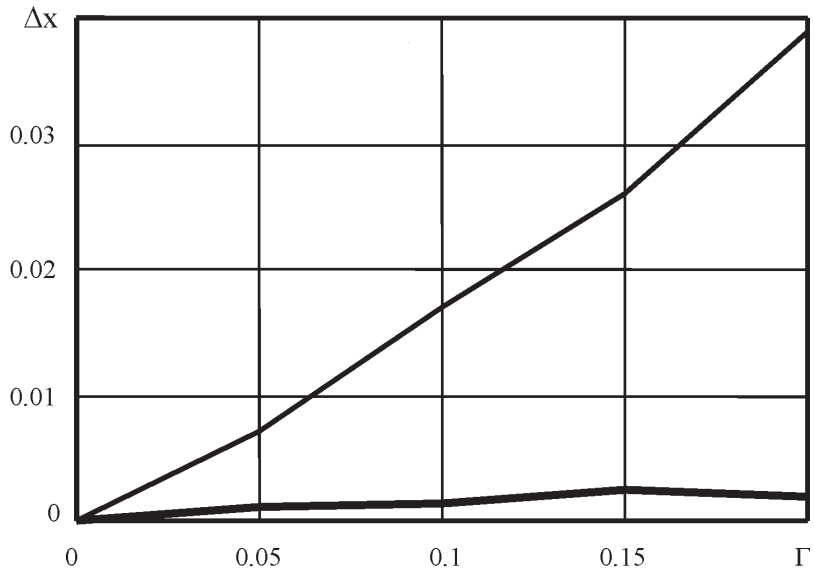
The function of the normalized error of distance estimation to irregularity practically coincides with the theoretical error function versus the distance difference between UR and SR (3.21).

Figure 9.11 shows the normalized distance estimations versus a reflection coefficient modulus from the pin at two fixed normalized pin positions along the waveguide axis:

- $x_1 = b_1 = b_2 = 2.544$  (bold line) when a given AWF zero coincides with a normalized interference position;
- $x_1 = 1.02$ ,  $b_1 = b_2 = 2.544$  (thin line) when a given AWF zero does not coincide with a normalized interference position.



**Figure 9.10** Plot of the normalized error of frequency measurement versus the normalized distance to irregularity in the AWP.



**Figure 9.11** Plot of the normalized error of frequency measurement versus the reflection coefficient modulus from irregularity in the AWP.

In both cases, the estimation error is practically proportional to the reflection coefficient modulus; however, the coincidence of a given AWF zero with a normalized irregularity position in the AWP allows the reduction of the distance measurement error caused by a combination interference from 7.2 to 19.5 times (depending on the reflection coefficient value) compared with the case of a normalized irregularity position specification  $x_1 \approx 0.4 \cdot b_1$  corresponding to the EE maximum for a chosen fixed AWF zero position.

The presented results confirm the results of numerical experiments and theoretical results. From this, it follows that the procedure of a distance estimation error reduction on the background of nonresolvable virtual interference, including the coordinated choice of constructive AWP solutions and algorithms of the difference

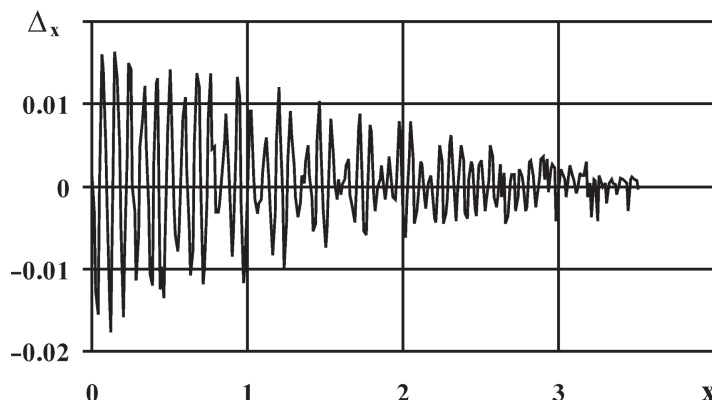


**Figure 9.12** Plot of the normalized error of distance measurement versus the relative irregularity position in the AWP at a radiated power of 20 mW.

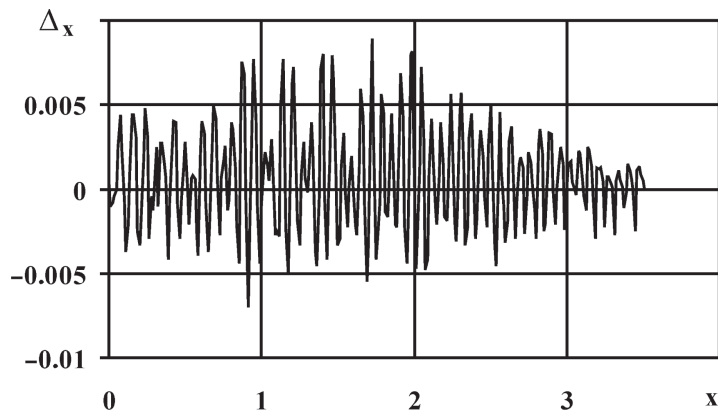


**Figure 9.13** Plot of the normalized error of distance measurement versus the relative irregularity position in the AWP at a radiated power of 2 mW.

signal processing allows an essential reduction of the measurement error under conditions leading to property variations of virtual interference.

### 9.3.3 Influence of Radiated Power Level on the Distance Estimation Error Caused by Virtual Interference Influence

For precision systems of the FM short-range radar, the question about the optimal radiated power level at which the measurement error becomes minimal, is important.

The estimation of theoretical result fidelity is inspected in comparison with the experiment results. Experimental functions of instantaneous values of the relative error of distance  $\Delta x$  estimation versus the relative irregularity position in the AWP similar to theoretical functions (Chapter 6) are presented in Figures 9.12 and 9.13.

It follows from Chapter 6 that the measurement error component caused by virtual interference and the accompanied wave flow significantly depends upon probing signal power and decreases with its reduction, which is confirmed by comparison of experimental results presented in Figures 9.12 and 9.13. As we can see, that admissible reduction degree of radiated power level is defined by the SNR and at probing, for instance, of the plane surface, the optimal level of radiated power is 1 to 2 mW.

## 9.4 Results of the Experimental Reduction of the Distance Measurement Error by the Control of the Adaptable Weighted Function Parameters

In Section 7.4, the rather simple procedure of measurement error reduction on the background of nonresolvable interference is described. Nevertheless, the presence of unstable zones of frequency estimation defined at the theoretical analysis of approach to the error reduction necessitates experimental research to determine the

correspondence of practical achievement results to theoretical ones. As mentioned earlier, experimental investigations are fulfilled at a waveguide test bench as described in Section 9.2. Due to the fact that instability of distance estimations is manifested mainly in the situation of fixed interference position approaching the UR and SR, this situation should be investigated experimentally. In this context, the difference in experiment fulfillment consists of the fact that the interference signal formed by irregularity in the AWP (in this case, the pin) is located at such a fixed distance that does not take into account the rereflections between the device input and formed irregularity. The useful signal is obtained from the moveable short-circuit piston. Electrodynamic distance to spurious irregularity is estimated at the moveable piston replacement by a matched load.

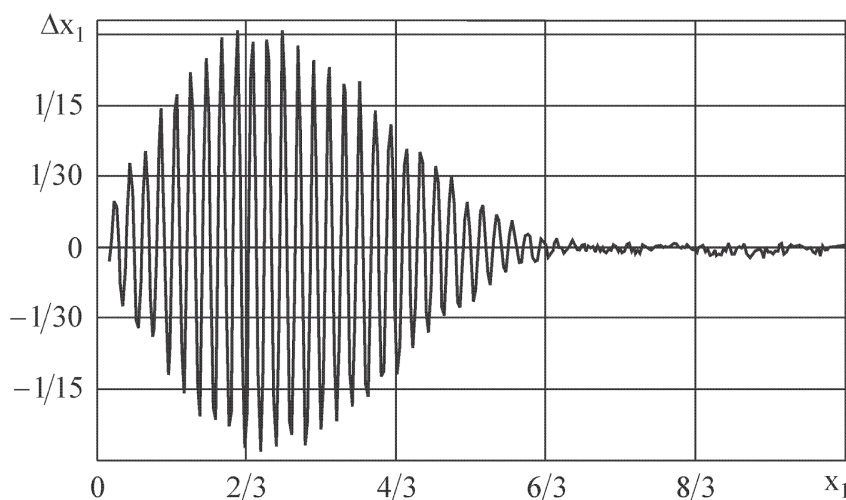
The experimental results presented next are obtained at an interference amplitude of about 0.2 from useful signal amplitude reflected by the moveable piston. In the experiment,  $q_{s/n} = 60$  dB.

Figure 9.14 shows the normalized functions of the distance estimation error versus the normalized distance between the short-circuit piston and the pin using the Blackman WF, and Figure 9.15 shows the normalized functions of the distance estimation error versus the normalized distance between the short-circuit piston and the pin using the uniform WF.

Figure 9.16 shows the normalized functions of the estimation error of the corrected distance using the developed approach of the estimation correction with restriction of the correcting coefficient value in the possible instability zone of the frequency estimation (see Chapter 7).

We see from these figures the good qualitative coincidence of experimental and theoretical results that are described in Section 7.4.

The results of the developed approach application to real signals were compared with the results of the distance estimation during processing of the same array



**Figure 9.14** Plot of the measurement error versus the normalized mutual distance between the pin and the piston using the Blackman weighted window.

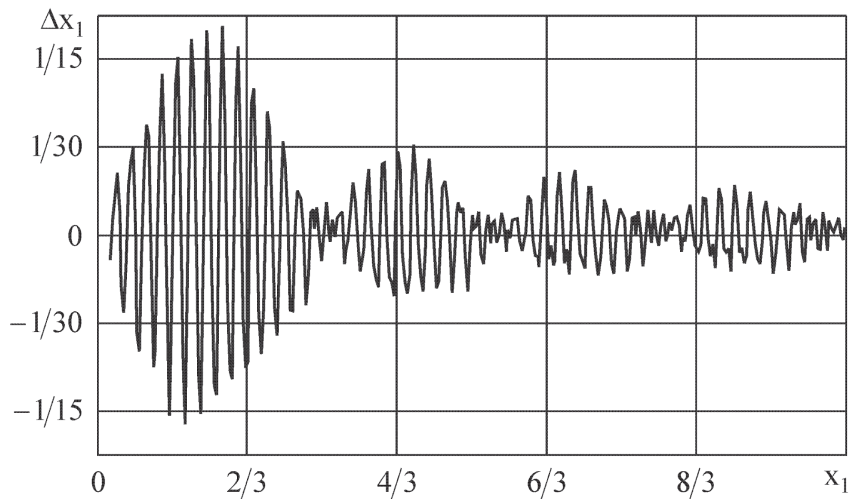


**Figure 9.15** Plot of the measurement error versus normalized mutual distance between the pin and the piston using the uniform weighting window.

of recorded signals by known high-resolution methods, from which the EV method [9] shows the best results. The experimental function of the measuring error versus normalized distance is presented in Figure 9.17 for the EV method.

A comparison of Figures 9.16 and 9.17 shows that the developed approach at a small interference level does not yield to the EV method in the distance measurement error, but essentially gains in computing expenses and in error value, when interference and signals are resolvable.

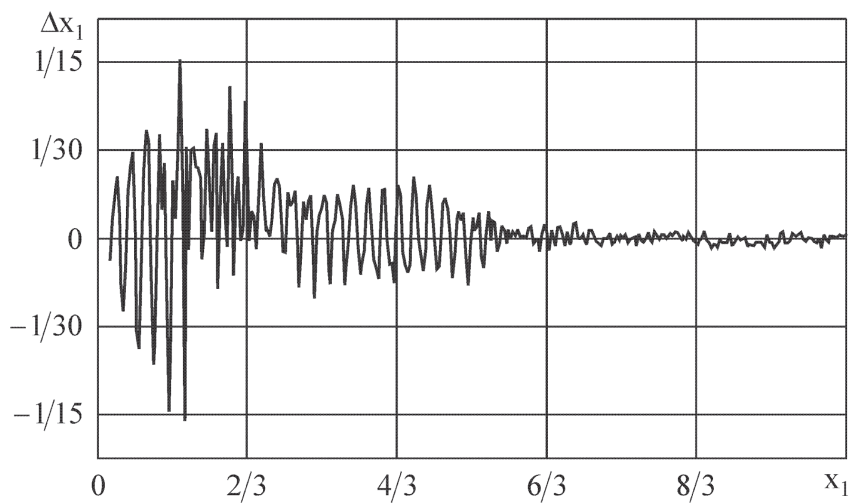


**Figure 9.16** Plot of the error function of the corrected estimation versus the normalized mutual distance between the pin and the piston.

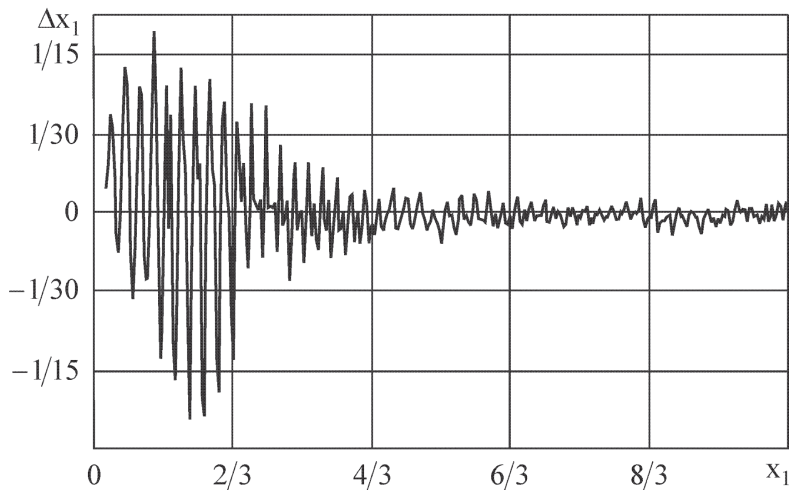


**Figure 9.17** The function of the measurement error using the EV method.

## 9.5 Testing Results of the Parametric Algorithms of the Distance Measurement in the Measuring Test Bench

Experimental data discussed next are obtained using FM RF BARS 351 produced by the Ryazan instrumentation company JSC Contact-1. The testing of algorithms for frequency estimation based on PSA methods was fulfilled at the DFS processing recorded on the measuring test bench equipment for a frequency tuning range of FM RF at 500 MHz. Plots show the distance measurement error using the MLM algorithm, the tracking algorithm, and the algorithm “Prediction” are obtained according to the measurement results using the FM RF. The carrying frequency tuning range is 1 GHz.

### 9.5.1 Algorithms Based on the Methods of Parametric Spectral Analysis

Figure 9.18 shows by a solid line the results of algorithm testing based on the EV method. The SIR is equal to  $-6$  dB. Calculations are fulfilled also with the help of the above-described two-step procedure. During function obtaining, we chose the following parameters: a dimension of the modified covariance matrix is  $m = 80$ , the model order is  $p = 8$ , a number of adding zero samples in the DFS is equal to  $63K$ ; the SR emulating the reservoir bottom is located at a distance of 15 m; and the UR moves with a step of 3 mm. Distance calculation is provided with the help of (8.34). As the useful SC of the EV pseudo-spectrum, we accept the SC that is located nearer to the FM RF.

For comparison, Figure 9.18 shows by a dotted line the distance measurement results when using the algorithm (3.4). A comparative analysis of two plots in Figure 9.18 allows the statement that the application of the distance measurement algorithm on the basis on the EV method essentially decreases the error. However, experimental results coincide well enough with the simulation results (Figure 8.14). Not having given the error plot for the EV method in a larger scale, we may note

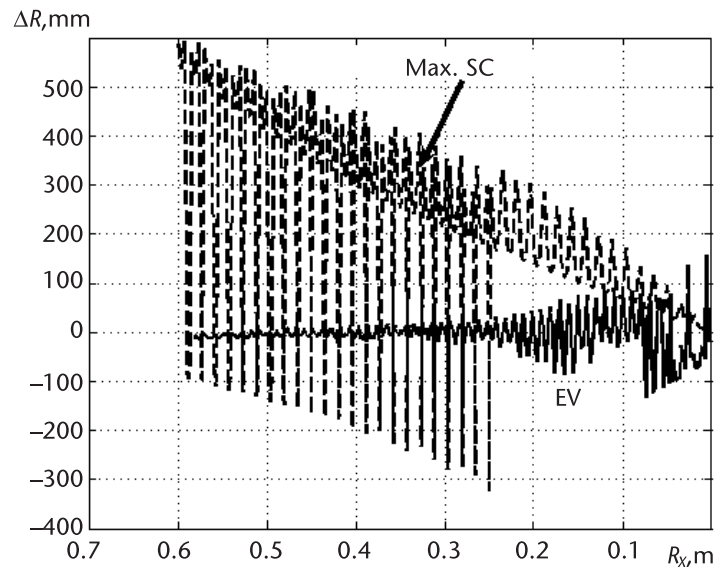


**Figure 9.18** Plot of the instantaneous measurement error versus the reflecting surface distance to the reservoir bottom when using the EV algorithm.

that the increased measurement error ( $2 \div 4$  mm and more) is observed at a considerable distance from the SR.

The results of testing the algorithm based on the Prony least square method are presented in Figure 9.19. At this testing, we chose the following parameters: the model order is  $p = 44$ , a number of DFS samples is 128, and the  $q_{s/i} = 6$  dB. The UR moves with a step of 3 mm with regard to the SR.

The conditions of test conducting did not allow taking several DFS realizations at each distance. Therefore, to decrease the anomalous errors caused by false SCs

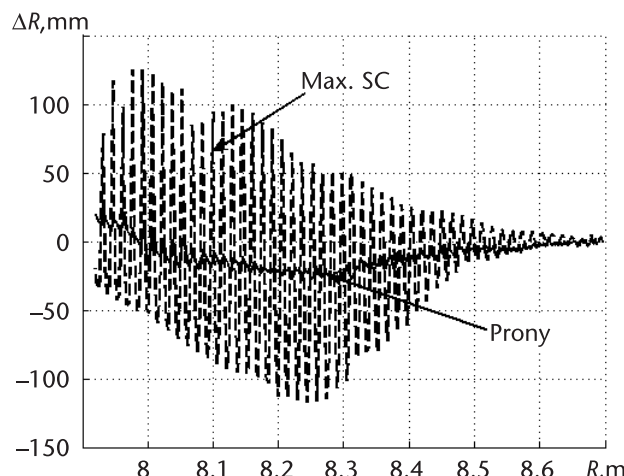


**Figure 9.19** Plots of the instantaneous measurement error as a function of the distance between the reflecting surface and interference when using the algorithm on the basis of the Prony least square method.

of the Prony spectrum, we used the following procedure. The SC corresponding to the measured distance was searched in the distance interval  $R_{\min} < R_x < R_{\max}$  (here  $R_x$  is the distance obtained using (3.4), the values of  $R_{\min} = 0.95 R_x$ , and  $R_{\max} = 1.05 R_x$ ).

The comparison with the distance measurement error confirmed by the algorithm (3.4) produces the statement that the Prony least square method provides an essential error decrease compared with the algorithm (3.4).

### 9.5.2 The Algorithm Based on the Maximal Likelihood Method

It was shown in Chapter 4 that to realize the algorithm providing the MLM, it is necessary to define the PFC of the FM RF. Figure 9.20 shows the typical PFC calculated for the DFS according to the approach described in Chapter 4. The irregularity of PFC behavior is explained by the presence of the SR with small intensity, which is caused by the features of the measuring room and rereflections of various types.

The PFC of one sample of the FM RF is presented in Figure 9.21. We should note that the PFCs of other samples of FM RFs are similar and differences consist only in the various slope of the PFC and its displacement by some value  $\Delta\Phi$ .

The PFC approximation by some function does not present complexity. PFC approximation by the straight segment is shown in Figure 9.21, for which the least square method is used. The distant measurement error using the MLM can serve as the correction criterion of the PFC approximation. The PFC approximation mistake will lead unavoidably to a truncation measurement error appearance.

The distance measurement error for the MR with the MLM application is shown by a solid line in Figure 9.21. At measurement fulfillment, the RR moved discretely with a step of 20 cm. For comparison, the measurement error, which is ensured by the algorithm (3.4), is presented by a dotted line in this figure.

The increased measurement error at the application (3.4) is caused by the same reasons, which cause overshoots in the PFC estimation by reflections from constructive MR elements and rereflections of different types. The application of the

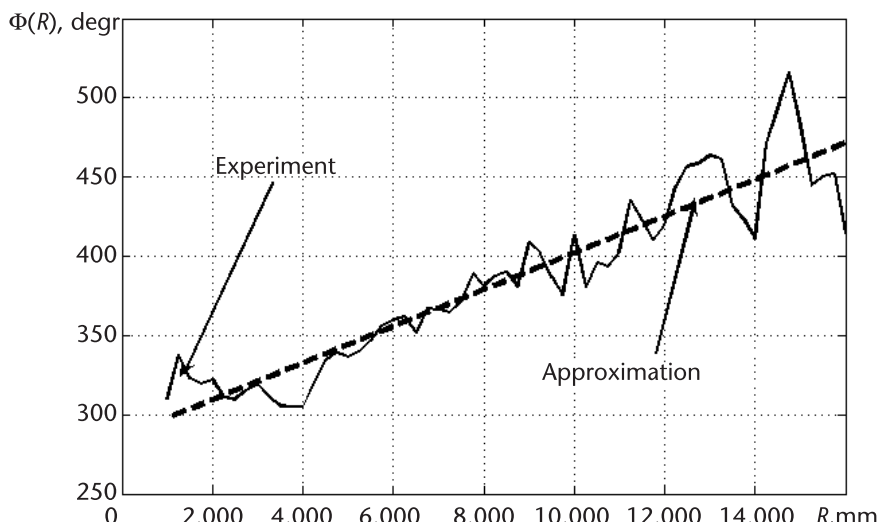
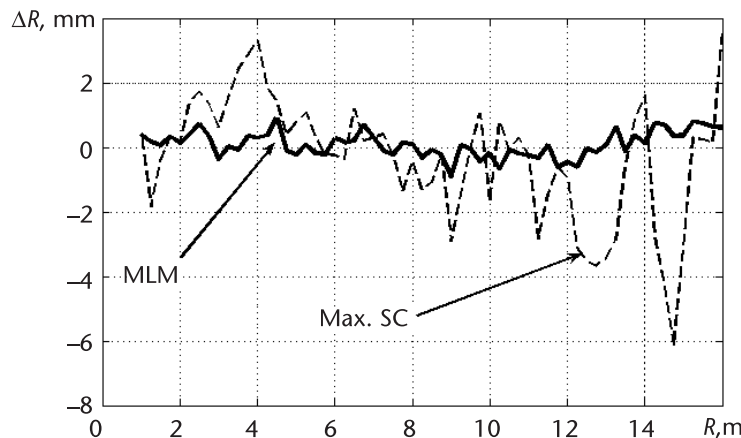


Figure 9.20 Phase characteristics of the FM RF.



**Figure 9.21** Instantaneous distance measurement errors using the MLM.

algorithm on an MLM basis allows an essential reduction of the measurement error at the presentation of rereflections of small intensity. The irregularity of the error plot for the MLM is mainly explained by the inaccuracy of the UR setting. Careful analysis of the error plot for the MLM concludes that, at a distance of more than 13 m, a small truncation error appears. The reason for this is obvious; the small error at the PFC approximation by the straight segment is at a distance of more than 13 m.

### 9.5.3 Testing of the Tracking Distance Meter

Tests of the tracking distance meter were fulfilled on the measuring test bench at the discrete movement of the trolley with the UR. The SR is mounted motionless above the UR in the antenna DP of the FM RF. The mechanism of the SR attachment allowed intensity changing by means of variation of its angular position. It permitted changing the SIR. Typical results, which are ensured by the tracking distance meter, are shown in Figure 9.22. The results presented here were obtained under the following conditions:  $q_{s/i} = 2$  dB and the SR were located at a distance of 5.8 m. At testing fulfillment, the UR moved with respect to the SR with a step of 3 mm; the frequency tuning range was 1 GHz.

At the IEZ boundary the estimation of the PFC  $\Phi(R_{\text{bound}})$  is provided, which is used in the tracking algorithm.

It follows from Figure 9.22 that the tracking meter allows a sharp reduction of the distance measurement error. The obtained results completely coincide with simulation results: the measurement error decreases by 82 times compared with the algorithm (3.4) or with other algorithms, which do not use information about the DFS phase.

### 9.5.4 Testing Results of the Algorithm “Prediction”

Testing of the algorithm “Prediction” was provided in a similar manner but the UR movement was fulfilled smoothly.

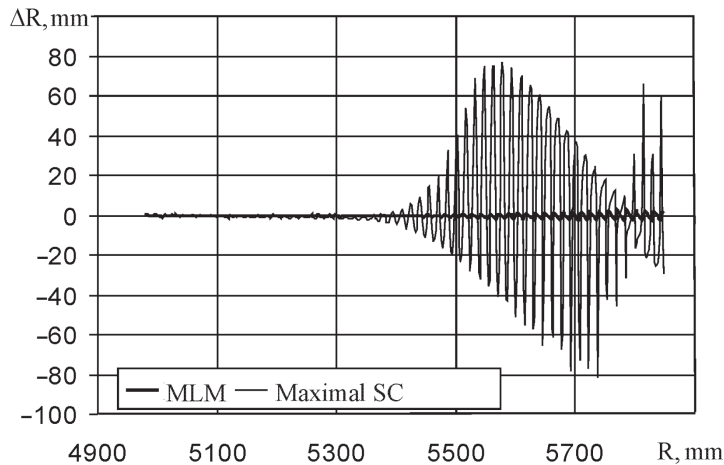


**Figure 9.22** Testing results of the tracking meter.

The emulation of discharge or loading modes was fulfilled with different velocities and for different values of a distant part before the entrance to the IEZ, where movement velocity estimation was provided. The linear movement model with constant velocity was used in the processing algorithm. Testing results were represented in the form of plots of reading the difference of the algorithm “Prediction” and the algorithm (3.4). The SR inside the IEZ was absent in these tests. Therefore, the measurement result by the algorithm (3.4) was considered to be standard and the result obtained by the prediction was compared with it. Examples of similar plots are shown in Figures 9.23 and 9.24. At each plot, the specific reading difference inside the IEZ is presented.

At the exit from the IEZ, a reading jump is observed when the transition from the algorithm “Prediction” to the algorithm (3.4) happens to increase due to error accumulation because of the noncoincidence of the true and estimated velocities of the reflector movement.

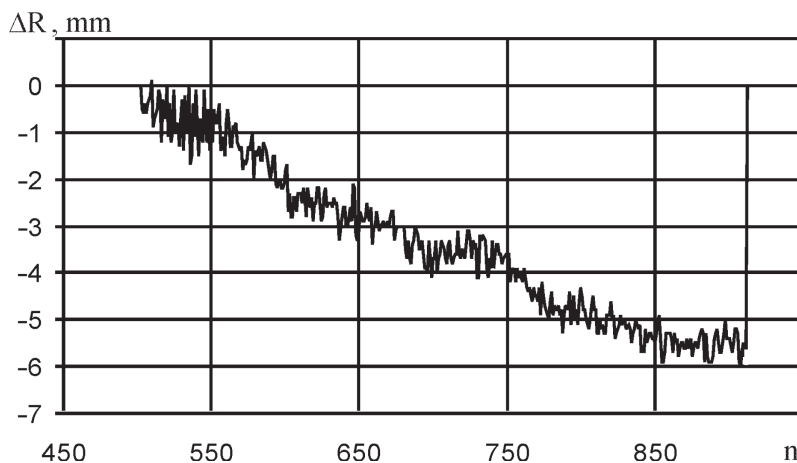


**Figure 9.23** Emulation of discharge at the reflector movement velocity of 10 mm/s.

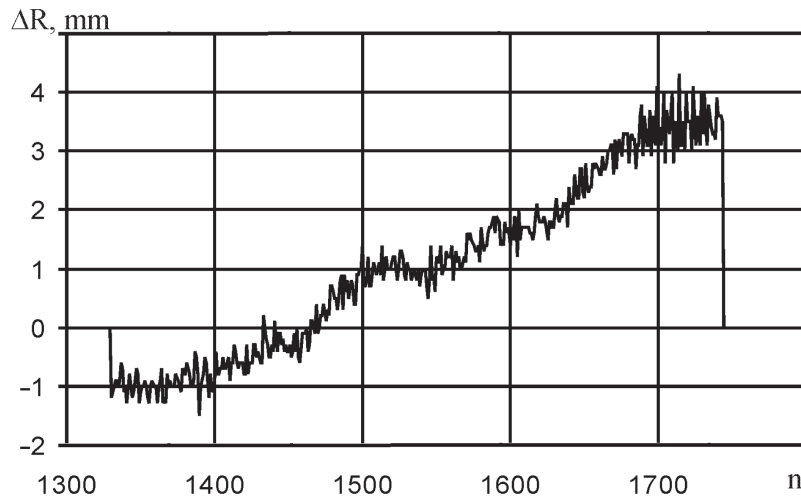


**Figure 9.24** Emulation of loading at the reflector movement velocity of 10 mm/s.

The analysis of these results shows that in a practical application the success of the “Prediction” algorithm operation will be defined by the uniformity of the level variation velocity before the entrance in the IEZ and inside the IEZ.

## 9.6 Areas of Practical Application of the FMCW Radar

The areas of the practical application of the FMCW radar are rather wide [10] due to the following circumstances particular to these devices:

- The possibility of measuring small and ultra small distances to the reflected object;
- The possibility of distancing measurements of the radial velocity determined according to the Doppler frequency shift;
- High accuracy of distance and radial velocity measurement;
- The possibility of measuring the angular coordinates of the target using a scanning antenna pattern;
- The possibility of measuring ultra small distance increments to the reflected object due to high sensitivity to the distance variation;
- The possibility of achieving a high resolving capacity to the distance;
- Signal processing after the mixer in the low-frequency region from hundreds of hertz to hundreds of kilohertz;
- A relatively small level of radiated power;
- Small dimensions, weight, and consumed power.

Due to these features, a huge number of companies around the world develop and manufacture FM range-finders, which are used in the very manifold areas of practical applications. Next we describe briefly only the general properties of those applications where developers use the previously mentioned algorithms and

methods with significant results. We do not recommend specific device types and names of companies based on two reasons:

- It is impossible to list all the companies in the world that deal with such products and we do not want to promote some companies while ignoring others;
- Part of the application is confidential and this information cannot be described in literature.

In some cases, it is necessary to ensure the highest accuracy of measurements for a practical application. In other cases, accuracy may not be as important a requirement as keeping to a minimal cost, which is related directly to the FM range value. Application of the above-described theory allows a successful solution to these problems. We hope that for the considered theoretical problems having enough common characteristics will help experts in dealing with particular areas of practical application and improving their devices in the future.

Let us describe the most distributed applications. We only discuss those problems that are well known to us from the literature. Modern equipment development is progressing at such a rapid pace that it is reasonable to expect exclusively new problems that are not yet known.

#### 9.6.1 Radio Altimeters for Small and Medium Attitudes

This is the most traditional application of the FMCW radar and, at present, radio altimeters and vertical velocity meters find wide application in civil and military aviation and space apparatus [11–13]. In such devices, the FM signal is radiated in a vertical direction from the flying vehicle (FV) downwards to the direction of the surface, of which the distance is necessary to measure. The reflected signal is received on board the FV and is accordingly processed to obtain information on the variations in its attitude and speed.

Such an FMCW provides the following solutions:

- Safe pilotage of airplanes and helicopters at all stages of flight up to a blind landing under complicated meteorological conditions;
- Ensuring automatic control of space apparatus when landing on a planet surface and for the safe attachment of various FVs;
- Automatic control of flight attitude of automatic unmanned objects;
- Height measurement for various industrial applications.

It is evident that in each of these issues there are individual requirements for measurement accuracy, operation speed, and other features.

Accuracy and reliability of measurement depend on the character of the radiated surface. As a rule, the best results can be obtained for a flat surface. The surface irregularity presence (for example, hills or forests) leads to errors. The surface may contain various constructions, for instance, high buildings, towers of electric transmission lines, hills, and mountings, which also distort the measurement results. The correct results are obtained only at a horizontal flight or at a small deviation from this

situation. Otherwise, especially for flat surfaces, the reflected signal can pass and not be received by the antenna. At a relatively high flight attitude, these errors are inessential. The requirements to measurement accuracy increase for the FV landing fulfillment, but in this case, the surface, as a rule, has a uniform character and a flat profile (the landing ground of the airdrome). At helicopter landings in places not prepared in advance, it is important that the surface is approximately the same level directly under the wheels. Therefore, in such applications, it is not desired to integrally check the surface, obtaining the same averaged result, but it is important to check in more detail the fulfilling measurements in three points with the help of three devices or by fulfilling the surface scanning by the antenna pattern.

### 9.6.2 Radio Proximity Fuses

These devices have a purely military application and are intended for activation of an explosive particle for the object intended for destruction falling into the antenna pattern. Activation is made for a minimal distance from the proximity fuse to the object under destruction (airplane or missile) [14]. Such radars are often referred to as the last-mile radar, when the guidance ground-based systems for the missile are switched off and the internal missile radar activates, which controls the movement on the last stage. Initially, such radars were used to activate the artillery shell used in the flaks and for bombing. The antenna pattern shape of the proximity fuse must, as a rule, coincide with the fragments' scattering cone after shell explosion. In some cases, besides the distance measurement, we need to measure the radial velocity of mutual approach. Such problems can be fulfilled ideally by the FMCW radar. Proximity fuses should be maximally simple and cheap but should have high reliability. Their requirements for measurement accuracy are not high, but the measurements should be conducted with high operation speed and reliability. More detailed characteristics of similar devices are device-specific and are not described in many publications.

### 9.6.3 Navigation Radar

Navigation FMCW radars can be used as navigation radars with the range of action up to several kilometers [15]. The FMCW radar may be used with great effectiveness for small distances of tens and hundreds of meters, where there are problems of surveying the sea and river water areas under conditions of bad visibility in terms of distance measurement and the relative velocity of any objects in the port. The important problem is the distance to the wall measurement at the docking of large crafts or at their passage through lock chambers. Besides navigation of large crafts, yacht and small craft navigation under bad visibility conditions is also needed [16] and for this purpose there is a large class of compact FMCW radars.

Navigation radars are wideband devices with FM that allow object resolution with sizes not less than 1m. A frequency range in the area of 10 GHz is used, and radiation levels do not exceed the radiation of a typical mobile cellular phone; therefore, the activity radius is approximately 20 nautical miles.

In all problems of navigation, we must measure not only the distance to the obstacle but also the velocities of the mutual approach.

#### 9.6.4 Transport Radar

In this category of FMCW radars we have two groups. The first group consists of radar for monitoring the situation on roads and for control of transport traffic [17, 18]. Such a radar is mounted on one side of the highway or over it. The action range is some tens of meters. This system determines the number of passing cars and, used the obtained results, calculates the number of passed cars during the time unit, their mean speed, and so forth.

A number of radars are contained in the second group, which ensures the following [18]:

- Safe movement of a transport vehicle on highways;
- Effective braking in case of accident situation detection when approaching another vehicle;
- Facilitation of maneuvering and parking;
- Monitoring of an adjacent strap;
- Movement in blocks following the car ahead and automatic stop and start that can only be controlled by a button pressed by the driver.

There are radars that perform only one of the above-mentioned tasks or perform several at once. For these tasks, the frequency ranges of 24 GHz and 77 GHz are most often used with a probing FM signal. To achieve the required resolution for distance, a range of the frequency tuning of 1.5 to 2 GHz is used. Devices operating in the band of 24 GHz are cheaper. In the 77-GHz band, more advanced devices are distributed that are called adaptive cruise control (ACC).

Ensuring safe movement is done by providing obstacle detection, distance measurement, and the velocities of an obstacle's approach and its angular position. To determine the angular position, the radar must provide scanning of the antenna pattern. It is necessary to ensure that the space surveyed around the car is within the limits of 360°. For this to occur, several radars are mounted on the car, each of which only solves part of the problem, and therefore the minimal radar set consists of four devices with FM [19].

The front radar has a needle-shaped pattern with a width of several angular degrees with the activity radius in a distance of up to 300 to 400 m and with a minimal distance of 20 to 30 cm. The antenna pattern of this radar continuously scans the space in front and provides obstacle detection, its distance measurement, and approach velocity. According to this data, when collision danger is determined, the warning signal is generated, and, if necessary, the braking system is activated.

The back radar has also a needle-shaped antenna pattern and fulfills the same tasks as the front radar. Moreover, it has an additional task arising during parking and during the subsequent backing-up movement when the radar is checking the circular zone just around the car. At this point, we need to check distances from 20 to 30 cm to 2 to 3 m.

Two side radars check zones on the car's sides with a dimension of approximately 10 m and the width, which depends on the car construction, changes from 10° to 20°. The direction of the antenna patterns of these radars is chosen to check the blind zones that are not available to the driver due to the car's constructive features.

Antennas of these radars have minimal sizes and can be easily mounted onto the necessary places of the car body.

### 9.6.5 Level-Meters

Devices allowing the measurement of the filling level of various loaded reservoirs, bunkers, and tankers are referred to as level-meters. The technological and commercial account of various substances can be performed with their help. Radar level-meters are essential parts of checking the measuring equipment of many industrial enterprises in different fields, such as oil extraction, transportation, and the processing, manufacturing, and storage of different types of liquid, viscous, and free-flowing substances at a high pressure and in a wide temperature range [20]. As a rule, such a device is mounted on the reservoir cap over the specially produced hatch or already anticipated reservoir construction. The radar antenna is directed into the hatch. If there is high temperature or redundant pressure inside the reservoir, then the attachment to the reservoir is implemented and arranged through sealing arrangements.

The width of the antenna pattern is usually within the limits of  $10^\circ$  to  $12^\circ$ . The pattern is oriented strictly vertically with respect to the surface of reservoir contents. The FMCW radar measures the distance from its flange, which at calibration is accepted as an origin, to the surface of the product. Because the distance from the reservoir bottom to the FMCW radar's flange is known, we can easily calculate the material level according to the results of the distance measurement to the surface.

The distance measurement error is a very important index for level-meters. As a rule, the absolute error value, depending on level-meter application and on the specific place of its mounting, is changed from several millimeters to even tens of millimeters.

Hundreds of companies around the world deal with production of such devices. They use various frequency ranges: 5 to 6 GHz, 9 to 11 GHz, 24 to 27 GHz, 76 to 77 GHz, and 96 to 98 GHz. Bands of frequency tuning can change from 500 MHz to 2 to 3 GHz.

As it was shown earlier, such parameters allow ensuring the above-mentioned requirements to a level measurement error in an ideal condition of interference absence. However, in reality, there is a great number of various spurious reflections in the reservoir. The approaches that we discuss allow the achievement of the required error in a different interference situation or ensure the required error with a lesser value of the frequency tuning range, which in turn allows a reduction in the complexity and the cost of the equipment.

### 9.6.6 Ice and Snow Blanket Thickness Meters

Such devices are usually referred to as ice-meters [21] and are used for the following purposes:

- Construction of winter ice routes and arranging ice airdromes in the regions of extreme North, Siberia, Alaska, northern regions of Canada and Europe, and temporary ice bridges over freezing rivers;
- Systems for ice frosting and other ice constructions;

- Monitoring of ice blanket thickness near a hydro power station's dams;
- Fulfillment of rescue missions on ice;
- Monitoring of ice obstructions and investigation of ice profiles;
- Safety and quality improvement for fishing;
- Estimation of the fresh ice resource throughout the world;
- Estimation of snow quantity in specific regions and forecast of possible situation at snow melting.

All these situations need urgent, reliable, noncontact, and continuous measurement of ice thickness and determination of environmental character under the ice from ground-based transport vehicles (car, all-terrain vehicles, auto-sledge, tractor), from a helicopter or airplane in the manual pedestrian mode [22, 23]. Moreover, in such investigations, it is necessary to report on the previous measurements and to have a series of other user functions that increase reliability and work comfort. Independently from ice-meter movement at the ice thickness measurement, the transmission of the FMCW signal is provided strictly vertically in the direction of the ice surface. At the reflected signal spectrum, processing the detection of maxima corresponding to the reflection from the upper and lower ice edges is performed and, according to the difference of its delay in time, we can calculate the ice thickness. Furthermore, the relation of signal amplitudes reflected from the upper and lower ice edges allows the determination of the environment character under the ice. In a similar manner, one can measure the snow layer.

The limits for ice thickness measurement are from 5 cm, which is the point at which a person can walk on pond ice, to values of several meters of ice thickness measurement in ponds. The range of frequencies used does not exceed 10 GHz. The higher frequencies are strongly damped in the ice, and the lower frequencies lead to large antenna sizes. The frequency tuning range is defined by the required resolution capability at the smallest ice thickness value and achieves a value of 2 to 3 GHz.

#### **9.6.7 FM Geo-Radar**

Range finders with FMCW signals can be successfully used as geo-radars. These devices are intended to perform the following tasks [24]:

- Searching for promising archeology reliquiae and remainders;
- Preliminary investigation of the fundamental construction design of motor and railway roads, airplane runways, various large buildings, and other construction;
- Performing danger diagnostics in the mining industry in the form of secondary destruction and landslides;
- Localizing underground cellars, galleries, tunnels, and so forth;
- Localizing pipe lines and walls and searching for voids, underground water, and water holes;
- Mine searching in military systems.

As a rule, such devices can find irregularities under the ground located at a depth of 40 to 50 m. The band of frequencies used does not exceed 1.5 GHz. The

FMCW signal is radiated under the ground by the transmitting antenna. The signal reflected from the irregularity is received by the receiving antenna and after amplification and conversion is exposed by spectral transformation. The processing result is extracted to the display. The geo-radar is moved on the ground by a trolley and an underground profile is formed on the display, which can be used for determining the irregular bedding place, its sizes, and its approximate shape.

#### 9.6.8 Atmosphere Sensing Radar

The radio signal of the S-band has the capability of reflecting well from any irregularity of the atmosphere dielectric permittivity caused by atmosphere turbulence, pollution of various air layers by large and small particles, presence of water steam, and small water drops [25, 26]. This reflection represents a combination of coherent reflection from small spatial variations in the index of refraction caused by air turbulence and Rayleigh's reflections from insects, birds, dust, and other formations in which the size is much less than the wavelength of the carrying oscillation. Depending on the application conditions, Rayleigh's reflection from insects can be the interference source during observation of the clear sky and as the useful factor during the observation of layers of transparent air. Because of excellent spatial and temporal resolution, the FMCW radar is able to resolve insects as well and to separate the discrete reflection from particles and from distributed clear air. In this radar, two antennas are usually used to increase sensitivity for the observation of atmosphere conditions. One antenna radiates an FMCW signal vertically upwards and the other antenna is used for the reception of the reflected signal.

#### 9.6.9 Range Finders for Geodesic Research

At measurement fulfillment in the triangulation network, it is necessary to mount passive reflectors in appropriate points, for example, V-shaped, and to conduct distance measurements with the required accuracy with the help of the FMCW radar [14].

Another example of FMCW radar application in such tasks for observing glacier behavior and possible avalanche snow blankets in mountains. For this purpose, angular reflectors are thrown down to the surface from a helicopter or airplane. On the slope or the top of an adjacent mountain, the FMCW radar is mounted, which continuously measures the distance to angular reflectors and transmits the measurement results in automatic mode through a radio line, which results in a pattern of movement dynamics of the monitoring surface.

In a similar manner, one may monitor the displacement of a high building's walls and towers under the influence of various natural phenomena.

All such measurements can be provided in any type of weather, even with a complete absence of visibility.

#### 9.6.10 Birds' Observation Radar

Similar FMCW radars can be used for the prevention of bird collisions with airplanes at the airport and on the flight route, the prevention of bird strikes into the blades

of wind power plants, and for observing bird migration for biological analysis and investigations of habitat [27, 28]. At present, such radars provide continuous 24-hour monitoring in a three-dimensional mode. For this, S-band and X-band frequencies with the possibility of Doppler processing are used. To avoid collisions at airports, FMCW radars are used with an activity radius of 4 to 8 km and resolution on a distance of 2 m, which have horizontal and vertical channels. They allow the separation of bird types and operation in an automatic mode. Usually, a flock or a single-bird position is determined, and the direction of the movement, velocity, and movement trajectory are tracked, recorded, and archived; this information can also be obtained by consumers via a radio channel or through the Internet. Information from bird observation radar can be used by planning experts and consultants as a part of ecological planning when constructing a wind power plant. The operators of the wind power plant can better understand the impact of the birds' movement on the wind power plant and determine when to stop the wind engines if necessary or to activate the means to frighten birds away.

#### 9.6.11 Small Displacement Meters

Such devices are used at the vibration measurement for various machine and mechanism parts. They allow measurement by a noncontact manner of vibration parameters under conditions of significant variation of an operation mode, high temperature, and pressure and in an aggressive environment [14].

The most sensitive method of vibration measurement is the application of phase methods. Nevertheless, it is very difficult to measure the UHF oscillation phase directly. At the same time, as was shown in Chapter 1, when using the FMCW radar, information about the phase angle  $\omega_0 t_d$  is contained in the low-frequency difference frequency signal at the mixer output. This essentially simplifies measurements. At distance variations to the vibrating element by a half-wavelength of the radiated signal, the DS phase varies by  $360^\circ$ . If the wavelength is 8 mm, then the phase variation by  $1^\circ$  corresponds approximately to 10 micrometers of distance variation.

#### 9.6.12 Guarding Systems

FMCW radars find wide applications in various guarding systems that monitor the perimeter of guarded territory or the whole area inside a perimeter for military or civil purposes [29]. The FMCW radars are very suitable for the creation of guarding systems due to small sizes and weight, simplicity in selecting moving targets on the background of fixed objects, the possibility of determining coordinates of moving objects, and small radiated power.

There is a wide variety of such guarding systems, such as portable, mobile, and stationary variants. They detect moved or fixed objects in the monitored zone and generate an audio alarm signal and the signal is then transmitted via a radio channel.

As a rule, guarding radars have high-resolution capability and can operate in an autonomous mode or in the structure of the complicated guarding system. They have an opportunity to classify targets and make their images on the map in the form of

a separate symbol for a visible presentation of the current situation. We can meet combinations with another sensor, for instance, thermal imagers or video cameras.

The distance of target detection changes from hundreds of meters to several tens of kilometers depending on the radar characteristics and type of the target. The error of distance measurement is from 2 to 10 meters and for velocity it is from 0.3 km/hour to 1.5 km/hour. The radiated power is several hundreds of milliwatts. The X frequency band is usually used. To increase functioning reliability and protection from interference, the mode of the continuous change of the carrying frequency is used. Therefore, we can use several tens of such frequencies by randomly choosing the current frequency.

All measurements are linked to the specific coordinates due to the embedded GPS module and the compass.

#### 9.6.13 Robotic Navigation and Mapping Systems

Transport vehicles carrying important loads and fulfilling nonstandard tasks are often used for robotic systems moving on the Earth surface (usual everyday and industrial robots, specific and research robotic systems) through air (piloted and unmanned flying vehicles, military airplanes, robotic missiles), and in outer space. The reference information for these robotic vehicles can be produced by specific radio beacons, guidance systems, and mapping sets, including those recorded in a digital form in specialized processors and memory devices. Frequency ranges of actual navigation robotic radars can be chosen in the bands of 9.4 GHz (see pulse radar), 77 GHz, and 94 GHz (millimeter-wave FMCW radars of surface and aviation types). Robotic autonomous navigation systems are often intended on operation from units of meters to hundreds of meters in range.

Depending upon the specific application of the robotic systems, their actual navigation is fulfilled on the basis of GPS, local landscapes (evident reference points), and clear parts of actual maps. Therefore, the issue of verification of out-of-date maps and finding new ones is important when using robotic systems. Many interesting publications (for example, [30]) have recently been devoted to this issue. The application of robotic autonomous navigation with the help of FMCW radar mounted on the robot together with other sensors (visible light and lasers) is significant. Such radars frequently allow the improvement of mapping and navigation observation performance and the improvement of tracking the robot location.

Therefore, ground-based systems and aviation-based and space-based systems are essentially different from the point of view of the required resolution in the range and angular position, because the navigation error in several meters for ground-based systems (for instance, for standard transport vehicles on the ground) can be absolutely unacceptable compared to the quickly-moving aviation-based and space-based systems, for which the resolution can be much less strict.

FMCW radars are indispensable components of robotic vehicles allowing the detection of landscape parts that are enclosed and invisible to optical and laser systems. In such systems, the operation distance of robotic ground-based devices is from part of a meter to several hundreds of meters, and aviation-based systems require a range of several kilometers.

## 9.7 Conclusions

The problems of reliability ensuring correct estimation error of the FM RF have been considered. The synthesis procedure of the standard RR with minimal sizes is offered for precision measurements. It was shown that it is necessary to use reflectors of a special shape. The results of research of size influence and the reflector shape on the measurement error show that minimal reflector sizes, which allow the correspondence of an electrodynamical distance to a specified geometrical distance (at the admissible error of this correspondence), should exceed two Fresnel zones at a maximal distance from the FM RF. For the most practical problems presented, recommendations permit creating rather easily realizable test benches.

A test bench for the measurement FM RF parameters was developed, manufactured, and certified as the measuring means. The test bench has large universality and provides the possibility of emulating various practical situations. Testing results on this test bench were presented that confirm the suitability of the methods used.

The approach to measurement fulfillment was developed taking into consideration the SR presence, which distorts results. Experimental investigations of many of the above-mentioned algorithms have been fulfilled and good coincidence with the results of the theoretical research and numerical simulation has been obtained. Possible application areas for the FMCW radar were briefly described.

## References

- [1] Emerson, S., "Improved Construction of Anechoic Chamber," *TIIER*, No. 8, 1965, pp. 1227–1229. [In Russian.]
- [2] Markov, G. T., and D. M. Sazonov, *Antennas*, Moscow: Energia Publ., 1975.
- [3] Patent 2207676 (Russian Federation), INT.CL. H01Q 15/14. "Plane Radar Reflector," V. M. Davydochkin. No. 2002111035/09. Bull. No. 18. Filed April 24, 2002; published June 27, 2003.
- [4] Patent 2298770 (Russian Federation), G01S 13/14. "Work-Bench for Adjustment and Testing of Radar Level-Meters," B. A. Atayants, V. M. Davydochkin, V. A. Bolonin, V. V. Ezerskiy, Yu. V. Masalov, S. A. Markin, and D. Ya Nagorny; published May 10, 2007.
- [5] Parshin, V. S., V. M. Davydochkin, V. S. Gusev, "Compensation of Spurious Reflections' Influence on Distance Measurement Accuracy by FMCW Range Finder," *Digital Signal Processing and Its Application. – Proceedings of RNTORES Named after A.S. Popov*. No. 5, Moscow, Vol. 1, 2003, pp. 261–263. [In Russian.]
- [6] Parshin, V. S., "Tracking Frequency Meter of the Beating Signal of the Radio Range Finder with Frequency Modulation of Radiated Signal," *Digital Signal Processing and Its Application. – Proceedings of RNTORES Named after A.S. Popov*. No. 10, Moscow, Vol. 1, 2008, pp. 395–398. [In Russian.]
- [7] Patent 2410650 (Russian Federation), INT.CL. G01F 23/284, G01S13/34. "Method of Material Level Measurement in a Reservoir," B. A. Atayants, V. S. Parshin, V. V. Ezerskiy. Bull. No 3. Filed November 1, 2008; published January 27, 2011.
- [8] Parshin, V. S., and A. A. Bagdagulyan, "Distance Measurement to Material Level in a Reservoir at Presence of Spurious Reflections Exceeding the Useful Signal in Intensity," *Digital Signal Processing and Its Application. – Proceedings of RNTORES Named after A.S. Popov*. No. 8, Moscow, 2006, Vol. 1, pp. 306–308. [In Russian.]

- [9] Parshin, V. S., and V. V. Ezerskiy, "Application of Algorithms of Parametric Spectral Analysis at Distance Measurement with the Help of Radar Range Finders with the Frequency-Modulated Signal," *Digital Signal Processing and Its Application. – Proceedings of RNTORES Named after A.S. Popov.* No. 7, Moscow, 2005, Vol. 1, pp. 234–238. [In Russian.]
- [10] Johanngeorg, O., "Radar Application in Level Measurement, Distance Measurement and Nondestructive Material Testing," *Proc. of 27-th European Microwave Conference*, September 8–12, 1997, pp. 1113–1121.
- [11] Patent 4456911 USA, INT. CI. G01S 13/88, G01S 13/00, G01S 13/04, G01S 13/34. "Frequency Modulated Continuos Wave Altimeter," C. F. Augustine. US 06/198,600; Filed Oct. 20, 1980; date of patent June 26, 1984.
- [12] [http://www.barnardmicrosystems.com/ME4%20files/download/DSTO-TR-1939\\_PR.pdf](http://www.barnardmicrosystems.com/ME4%20files/download/DSTO-TR-1939_PR.pdf).
- [13] Patent 4456911 USA, IPS8 Class AG01S130FI. "High integrity radio altimeter," W. Devensky. No. 20090289834. Filed Jct. 20, 1980; date of patent November 26, 2009.
- [14] Komarov, I. V., S. M. Smolskiy, *Fundamentals of Short-Range FMCW Radar*, Norwood, MA: Artech House Publishers, 2003, 289 p.
- [15] <http://www.simrad-yachting.com/en-US/Products/NSS-Touchscreen-Navigation/NSS12-Navigation-Pack-en-us.aspx>.
- [16] Navico Broadband Radar BR24. Installation Manual.
- [17] Moldovan, E., S. Tatu, T. Gaman, R. Wu K. Bosilio, "New 94-GHz Six-Port Collision-Avoidance Radar Sensor," *IEEE Trans. on MTT*, Vol. 52, No. 3, 2004, p. 751.
- [18] Gresham, I. et al., "SHF-Wideband Radar Sensor for Short-Rang Vehicle Applications," *IEEE Tran. On MTT*, Vol 52, No. 9, 2004, pp. 2105–2122.
- [19] R. Kulke, C. Gunner, S. Holzwarth, J. Kassner, A. Lauer, M. Rittweger, P. Uhlig, P. Weigand, "24 GHz Radar Sensor Integrates Patch Antenna and Frontend Module in Single Multi-layer LTCC Substrate," *EMPS 2005*, June 12–15, Brugge, Belgium.
- [20] Weib, M., and R. Knochel, "A highly Accurate Multi-Target Microwave Ranging System for Measuring Liquid Levels in Tanks," *IEEE MTT-S International Microwave Symposium Digest*, Vol. 3, 1997, pp. 1103–1112.
- [21] Baranov, I. V., V. V. Ezerskiy, A. Yu. Kaminskii, "Measurement of the Thickness of Ice by Means of a Frequency-Modulated Radiometer," *Measurement Techniques*, Vol. 51, No. 7, 2008, pp.726–733.
- [22] Yankielun, N., W. Rosenthal, and R. Davis, "Alpine Snow Depth Measurements from Aerial FMCW Radar," *Cold Reg. Sci. and Tech.*, Vol. 40, No. 1–2, 2004, pp. 123–134.
- [23] Marshall, H. P., and G. Koh, "FMCW Radars for Snow Research," *Cold Regions Science and Technology*, Vol. 52, 2008, pp. 118–131.
- [24] <http://www.ks-analysis.de/groundpenetratingradar/contact.htm>.
- [25] <http://keycom.co.jp/eproducts/pbr/pbr72/page.html> – meteo-radar.
- [26] Ince, T., "FMCW Radar Performance for Atmospheric Measurements," *Radioengineering*, Vol. 19, No. 1, 2010, pp. 129–135.
- [27] <http://www.robinradar.com>.
- [28] <http://www.airporttech.tc.faa.gov/Safety/Downloads/TC-13-3.pdf>.
- [29] <http://www.army-technology.com/contractors/navigation/at-communication/pressat-fmcw-radar-solutions.html>.
- [30] Adams, M., J. Mullane, E. Jose, and Vo Ba-Ngu, *Robotic Navigation and Mapping with Radar*, Artech House. 2012. ISBN 978-1-60807-482-2.



# Conclusion

The materials considered in this book are closely connected with the practical implementation of different devices of short-range FM radar technology. Specific practical needs have encouraged the authors to perform detailed investigations of possibilities to achieve high accuracy in distance measurement under ideal conditions and also with various destabilizing factors.

It is absolutely clear to us that under ideal conditions we can achieve an error of distance measurement that is small enough with the help of any MQIS. In some cases, it can be achieved by WF selection or by adaptive variations of its parameters at distance changing. This is most complicated for measurements of very small distances equaled by parts and units of ED values. Good results can be achieved here by means of optimization of FM parameters. It is expedient to adaptively change the frequency-tuning range of the UHF oscillator in such a manner that the integer number of DFS periods keeps within one modulation period at the symmetric triangle FM law. In this case, DFS takes a form of continuous sine without phase jumps. We can obtain excellent results at any MQIS for such DFS. Supplementing this mode by the smooth DFS phase variation due to slow FM with averaging of the measurement results, we can reduce the measurement error by about an order. Unfortunately, we must pay for the achieved result by increasing the necessary frequency resource of the SHF oscillator and by increasing the processing time. As a whole, we may note that, at present, the substantively achieved measurement accuracy satisfies the practical needs of the industry.

Nevertheless, such results can be obtained for ideal linear FM only. The difference between the MC shape of the SHF oscillator and that of the linear one strongly degrades the distance measurement accuracy. In some cases, we may get good accuracy even at nonlinear MC. This can be achieved by means of the predistortion introduction in the modulating voltage for the comparison of nonlinearity, the correction of calculation results according to the known parameters of MC nonlinearity, or by an account of this nonlinearity at the distance calculation. The most radical struggle against MC nonlinearity is the application of digital frequency synthesizers at the generation of the carrying FM signal.

The most significant factor reducing the accuracy of distance measurements is the presence of noise and spurious signals.

Methods for noise struggle are well known and were almost not considered in this book. Exclusion is the method of maximal likelihood allowing a significant decrease in the variance of the noise component of the distance measurement error.

The problem of how to achieve high measurement accuracy in the presence of spurious signals is most important. In practical applications, there are many reasons for the rise of these signals. First, they have an effect on the measurement accuracy owing to both the DFS shape distortion or its spectrum and the influence on the resonance system of the oscillator and the rise of combination frequencies in the mixer.

Accordingly, there are many methods that struggle. Methods of controllable variation of WF shape and the application of increasing changes as a result of the measurement for the correction of this result are promising. Positive results ensure the compensation of spurious signals or its position account at measurement fulfillment in combination with the most appropriate method of processing, the application of methods for image identification. In some cases, the application of the maximum likelihood method or its various modifications allows the achievement of good results. For example, as it is shown in this book, in the increased error zone near the spurious reflector, tracking of one of the lobes of the signal function is possible. This tracking corresponds to the factual value of the measured parameter, which ensures essential reduction of the measurement error. In most cases, it is impossible to completely solve a problem of elimination of the spurious signal effect by the same method. The combined means are necessary when different methods or their combinations are used at the different measurement and DFS processing stages.

It is possible that some companies use the above-mentioned methods or their modifications under various much-hyped promotional names and even obtain patents on them. We cannot guess what is concealed under these names, but we ourselves analyzed the claims and synthesized suitable algorithms. Frequently, these algorithms are heuristic and sometimes follow strict or approximate theoretical analysis. We appreciate if any readers recognize their own algorithms in some of our solutions and clarify their theoretical possibilities. In any of these situations, when we were aware of publications in Russia or in any other country, we made reference to the relevant publications.

Many of methods and algorithms described in our book are defended by patents on inventions and realized in serially manufactured level-meters of the BARS series.

We realize that we have not described and solved all possible problems. Our task was to designate the most manifest and significant from them and to prove that one may develop practically realizable methods that produce acceptable results. We perfectly understand that there are a variety of problems, especially in the field of interference struggle, reduction of sensitivity to variations of external conditions, a decrease in consuming power, improvement of constructive-technological indices, and cost reduction of these devices.

We appreciate feedback from all interested readers about this book and we hope that our work has helped solve practical or theoretical problems or encouraged readers to use new nonstandard solutions.

# Weighting Functions for Harmonic Analysis and Adjacent Problems

Weighting functions (WFs) are not specific instruments of spectral analysis. They are widely used for many problems and are solved using general mathematical methods.

The development of WFs allow digital signal processing to reduce the signal frequency and amplitude estimation errors on noise and interference background, as well as development of WFs with a minimal SLL of the SD at a specified width of the SD main lobe and specified decrease speed of SLL of SD is promising both for the application in the FMCW RF of the high precision for measurements and for the solution of other problems.

We call the WFs that changing their parameters to obtain the required spectral properties *adaptable* WFs (AWFs). Some AWF properties and methods for obtaining them are described in [1, 2].

## A.1 Analytical Expressions for AWFs

The problem of measurement error elimination of frequencies and amplitudes of signal items on the background of resolvable interference can be solved if there is a WF whose shape is specified by varied parameters in such a manner that on the frequency of each signal item, the SD of other parameters (i.e., spurious items) will be equal to zero, along with the given number of its derivatives. For this, it is necessary that there is a nontrivial solution of the equation system:

where  $\dot{S}(x) = \int_{-\infty}^{\infty} w(t) u(t) \exp(-j2\pi x t) dt$  is the SD of a sum of harmonic signal and

interference segments  $u(t) = \sum_{i=1}^{N_s} U_i \cos[\phi_i(t) + \Phi_i] + \eta(t)$  obtained in the time interval

with duration  $T$  and weighted WF  $w(t)$  symmetric with regard to the time interval center and limited in duration by this interval,  $x = \omega T(2\pi)^{-1}$  and  $t = t_{\text{abs}}/T$  are the normalized signal frequency and the normalized time,  $U_i$  and  $\Phi_i$  are the amplitude

and the DC of the phase of the  $i$ th signal item,  $\eta(t)$  is a noise, and  $b_i$  is a normalized frequency on which the SD or its derivative is equal to zero.

At the consideration of the signal spectrum weighted by the discrete WF, we assume that the transformation from an analog to a digital form is performed without quantization errors and discretization is equidistant. In such a statement, we may speak about truncation errors; that is, about errors peculiar only to the algorithm itself of the Fourier transform of the discrete signal.

Because the signal spectrum shape at accepted assumptions coincides with the WF spectrum shape, it is enough to obtain a solution for the specified frequencies of the WF spectrum. Discretized WFs can be obtained from the continuous WF by using the gating property of the delta function  $\delta(t)$ . Therefore, we obtain  $M_0$  equidistant samples of appropriate WFs with the discretization interval  $T_d = T/M_0$  in the interval  $T$ .

There is a possibility of truncating error elimination that we consider with functions of a type:

$$w(t, b_1, \dots, b_N, M_0) = \left[ 1 + \sum_{n=1}^N C_{sn}(b_1, \dots, b_N) \cos(2\pi n t) \right] \times \sum_{m_0=1-0,5M_0}^{0,5M_0} \delta[t - (m - 0.5)T_d] \quad (\text{A.2})$$

$$w(t, b_1, \dots, b_N, M_0) = \frac{1}{K} \left\{ \cos(\pi t) + \sum_{n=1}^N C_{cn}(b_1, \dots, b_N) \cos[\pi(2n+1)t] \right\} \times \sum_{m_0=1-0,5M_0}^{0,5M_0} \delta[t - (m - 0.5)T_d] \quad (\text{A.3})$$

with unknown coefficients  $C_{sn}(b_1, \dots, b_N, M_0)$  and  $C_{cn}(b_1, \dots, b_N, M_0)$ .

The Fourier transformation of functions (A.2) and (A.3) is expedient to represent in the form infinitely differentiable products of two multipliers with the same coefficients:

$$S_s(x, b_1, \dots, b_N) = \frac{\sin(\pi x)}{M_0 \sin(Mx)} \times \left\{ 1 + \sum_{n=1}^N C_{sn}(b_1, \dots, b_N, M_0) \cos(n\pi) \frac{2 \cos(nM) \cdot \sin^2(Mx)}{\cos(2nM) - \cos(2Mx)} \right\} \quad (\text{A.4})$$

$$S_c(x, b_1, \dots, b_N) = \frac{-\cos(\pi x) \cos(Mx)}{0.5M_0 K} \left\{ \frac{\sin(0.5M)}{\cos(M) - \cos(2mx)} + \sum_{n=1}^N C_{cn}(b_1, \dots, b_N, M_0) \cos(n\pi) \frac{\sin[M(n+0.5)]}{\cos[M(2n+1)] - \cos(2Mx)} \right\} \quad (\text{A.5})$$

where  $M = \pi/M_0$ .

Omitting unwieldy transformations, we give solutions in the general case of the unlimited system (A.1).

At  $N \geq 2$  solutions of the system (A.1) with regard to coefficients, respectively,  $C_{sn}(b_1, \dots, b_N, M_0)$  and  $C_{cn}(b_1, \dots, b_N, M_0)$ , are:

$$C_{sn}(b_1, \dots, b_N, M_0) = \frac{(-1)^{n+1}}{\cos(nM)} \cdot \prod_{i=1}^N \left[ \frac{\cos(2nM) - \cos(2b_i M)}{2\sin^2(b_i M)} \right] \\ \times \prod_{\substack{k=1 \\ k \neq n}}^N \frac{[1 - \cos(2kM)]}{\cos(2nM) - \cos(2kM)} \quad (\text{A.6})$$

$$C_{cn}(b_1, \dots, b_N, M_0) = \frac{(-1)^{n+1} \sin(0.5M)}{\sin[(n+0.5)M]} \\ \times \prod_{i=1}^N \left\{ \frac{\cos[(2n+1)M] - \cos(2b_i M)}{\cos(M) - \cos(b_i M)} \right\} \\ \times \prod_{\substack{k=1 \\ k \neq n}}^N \frac{[\cos(M) - \cos[(2k+1)M]]}{\cos[(2n+1)M] - \cos[(2k+1)M]} \quad (\text{A.7})$$

Then

$$w_s(m, b_1, \dots, b_N, M_0) = 1 + \sum_{n=1}^N C_{sn}(b_1, \dots, b_N, M_0) \cos(2nmM) \quad (\text{A.8})$$

$$w_c(m, b_1, \dots, b_N, M_0) \\ = \frac{1}{K} \cdot \left\{ \cos(mM) + \sum_{n=1}^N C_{cn}(b_1, \dots, b_N, M_0) \cos[(2n+1)mM] \right\} \quad (\text{A.9})$$

for  $N = 1$   $C_{s1}(b, M_0) = \frac{1}{\cos M} \frac{\sin M(b+1) \cdot \sin M(b-1)}{\sin^2 Mb}$ , and  $C_{c1}(b, M_0) =$   
 $\frac{\sin(0.5M)}{\sin(1.5M)} \frac{\cos(3M) - \cos(2Mb)}{\cos(M) - \cos(2Mb)}$ .

In problems of simultaneous estimation of signal frequency and amplitude, the equation for a normalized multiplier is determined from the condition of equality to 1 of the normalized WF SD on zero frequency:

$$K = \frac{-2}{M_0} \\ \times \left\{ \frac{\sin(0.5M)}{\cos(M) - 1} + \sum_{n=1}^N C_{cn}(b_1, b_2, \dots, b_N, M_0) \frac{\cos(n\pi) \sin[M(n+0.5)M]}{\cos[M(2n+1)M] - 1} \right\} \quad (\text{A.10})$$

When the WF is obtained, we assume that signal weighting with regard to the sample center is symmetric. Nevertheless, the signal processing is constructed in such a manner that in the memory of the computing device, the initial number is conferred to the first sample of the signal [3]. In this case, to keep symmetry with regard to the center of signal sample, AWF samples should be displaced and written in the form:

$$w_s(m, b_1, \dots, b_N, M_0) = 1 + \sum_{n=1}^N (-1)^n C_{sn}(b_1, \dots, b_N, M_0) \cos[2n(m+0.5)M] \quad (\text{A.11})$$

$$\begin{aligned} w_c(m, b_1, \dots, b_N, M_0) &= \frac{1}{K} \\ &\times \left\{ \sin[(m+0.5)M] \right. \\ &\left. + \sum_{n=1}^N (-1)^n C_{cn}(b_1, \dots, b_N, M_0) \sin[(2n+1)(m+0.5)M] \right\} \end{aligned} \quad (\text{A.12})$$

Equations for continuous AWFs can be obtained from (A.8), (A.9), (A.11), and (A.12) at  $M_0 \rightarrow \infty$ . Omitting the number of samples  $M_0$  in the designations, we give equations for continuous AWF and their SD:

$$w_s(t, b_1, \dots, b_N) = 1 + \sum_{n=1}^N C_{sn}(b_1, \dots, b_N) \cos(2\pi nt) \quad (\text{A.13})$$

$$w_c(t, b_1, \dots, b_N) = \frac{1}{K} \left\{ \cos(\pi t) + \sum_{n=1}^N C_{cn}(b_1, \dots, b_N) \cos[\pi(2n+1)t] \right\} \quad (\text{A.14})$$

$$w_s(t, b_1, \dots, b_N) = 1 + \sum_{n=1}^N C_{sn}(b_1, \dots, b_N) \cos n\pi \cos(2\pi nt) \quad (\text{A.15})$$

$$w_c(t, b_1, \dots, b_N) = \frac{1}{K} \left\{ \sin \pi t + \sum_{n=1}^N C_{cn}(b_1, \dots, b_N) \cos n\pi \sin[\pi(2n+1)t] \right\} \quad (\text{A.16})$$

$$S_s(x, b_1, \dots, b_N) = \frac{\sin(\pi x)}{\pi x} \cdot \left\{ 1 + \sum_{n=1}^N C_{sn}(b_1, \dots, b_N) \cos(n\pi) \frac{x^2}{x^2 - n^2} \right\} \quad (\text{A.17})$$

$$\begin{aligned} S_c(x, b_1, \dots, b_N) &= \frac{-\cos(\pi x)}{\pi K} \cdot \left\{ \frac{0.5}{x^2 - 0.25} \right. \\ &\left. + \sum_{n=1}^N C_{cn}(b_1, \dots, b_N) \cos(n\pi) \frac{n+0.5}{x^2 - (n+0.5)^2} \right\} \end{aligned} \quad (\text{A.18})$$

with coefficients

$$C_{sn}(b_1, \dots, b_N) = (-1)^{n+1} \cdot \prod_{\substack{k=1 \\ k \neq n}}^N \frac{k^2}{k^2 - n^2} \cdot \prod_{i=1}^N \left( 1 - \frac{n^2}{b_i^2} \right) \quad (\text{A.19})$$

$$C_{cn}(b_1, \dots, b_N) = \frac{(-1)^{n+1}}{2n+1} \prod_{\substack{k=1 \\ k \neq n}}^N \frac{k^2 + k}{(k^2 + k) - (n^2 + n)} \prod_{i=1}^N \left( 1 - \frac{n^2 + n}{b_i^2 - 0.25} \right) \quad (\text{A.20})$$

$$\text{for } N = 1, C_{s1}(b) = \left( 1 - \frac{1^2}{b^2} \right), \text{ and } C_{c1}(b) = \frac{1}{3} \left( \frac{b^2 - 2.25}{b^2 - 0.25} \right).$$

## A.2 Spectral Properties of AWF in DSP Problems

Taking into consideration that the obtained AWFs are rather new, we analyze some spectral properties of AWFs, which influence to the utmost the possibility of truncation error reduction when using algorithms similar to the above-mentioned ones and allow us to obtain the AWFs with optimal parameters.

We note that the positions of the AWF SD zeros are defined by zero positions of two multipliers. Zero positions defined by multipliers  $\sin(\pi x)/\sin(Mx)$  or  $\cos(\pi x)/\cos(Mx)$ , respectively, for the SD (A.4) and (A.17) or (A.5) and (A.18) are periodic and do not depend on positions of specified zeros  $b_1, b_2, \dots, b_N$  determined by the second multiplier. Therefore, for brevity, we call the zero positions of the first multipliers *stationary*, and zero positions of second multipliers *variable*:

1. For the AWF with  $N$  variable zeros besides stationary  $M_0 - 1 - N$  zeros, we can provide a formation of the SD zero values on  $N$  specified zeros  $b_1, b_2, \dots, b_N$ . The coincidence of SD  $m$  zeros on one frequency leads to the formation on this frequency of zeros of  $m - 1$  derivatives. In the problem of measurement of the difference frequency of the beating signal, this property allows us to ensure deep interference suppression on the signal frequency.

The possibility of specifying the SD zeros on any frequencies is illustrated in Figure A.1 with the AWF SD in (A.4) for  $N = 6$  and  $M_0 = 32$  and given zeros of the third order on two relative frequencies.

2. The application of the AWF in (A.11) and (A.12) for the DSP allows the elimination of the sample number influence on the results of the signal parameter estimation. The WF discretization effect on its spectrum is illustrated by Figure A.2 for  $N = 6$  and the specified frequency  $b = 6$ .

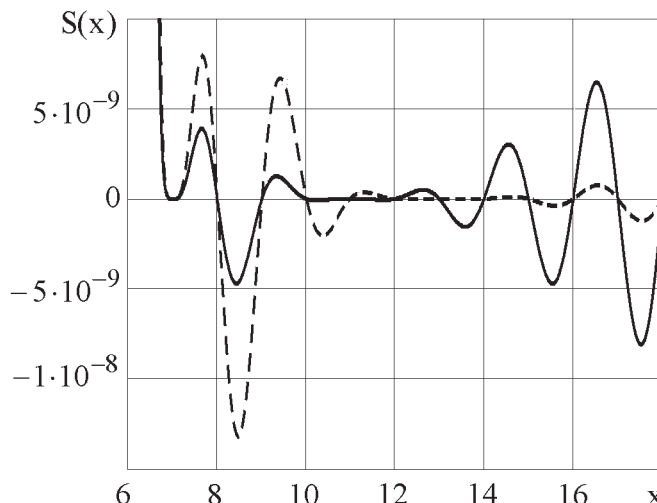


**Figure A.1** The AWF SD in the area of the SL with given zeros of the third order on two relative frequencies: 7 and 11 for the solid curve, and 7 and 13 for the dotted curve.

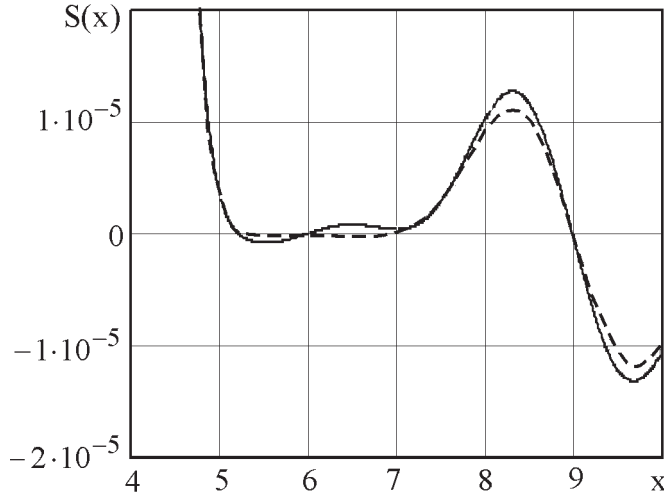


**Figure A.2** The area of the AWF SD zero formation at the DSP.

The dotted curve corresponds to the AWF in (A.11),  $w_s(m, 6, 6, 6, 6, 6, 6, 32)$ , for the analysis of discrete signals containing 32 samples, for which the envelope is defined with an account of the signal sample number. The solid curve corresponds to AWF in (A.13) for  $w_s(t, 6, 6, 6, 6, 6, 6)$  with the envelope obtained at  $M_0 \rightarrow \infty$ , but applied for the DSP containing 32 samples. We see that the DSP by the WF, for which the envelope does not change in accordance with the sample number, leads to spectrum distortions in the SL area. It is clear that for known WFs, the differences in the SD at the analysis of discrete and analog signals are manifested in a similar manner. In problems of signal parameter estimation, these variations restrict the minimal achievable level of the truncation error due to the displacement of specified zero positions on the frequency axis and the reduction of their order.

3. The level of the SD SL unambiguously depends upon the distribution (in frequency) of the variable SD zero values and their order. An interval increase between frequencies of adjacent zeros defining the SL width in this interval leads to SD SLL increase in this interval and influences on the adjacent SL level. This property is illustrated by Figure A.3, where the SD for the WF in (A.14) for  $w_s(t; 1.8; 2.39115; 3.27592; 4.29842)$  (denoted by a thin line) is presented and the minimal possible SLL for this WF is obtained for the main lobe width on the zero level of 3.6.

The frequency increase of one of the variable zeros from 3.27592 to 3.5 led to a level reduction of all lobe with great frequencies (bold line), to increase all SLs with lesser frequencies and to increase the width of the main lobe on any level of all SLs different from zero (not presented in the figure). The frequency decrease of one of the variable zeros leads to the opposite effect. The unambiguous connection of the AWF SD SLL variation with direction of specified zero frequency variation allows the creation of simple algorithms of the WF obtained with specified spectral properties.

4. It may be shown that most of the traditional WFs is the specific case of obtained AWF for fixed values of its parameters. This statement is easily illustrated

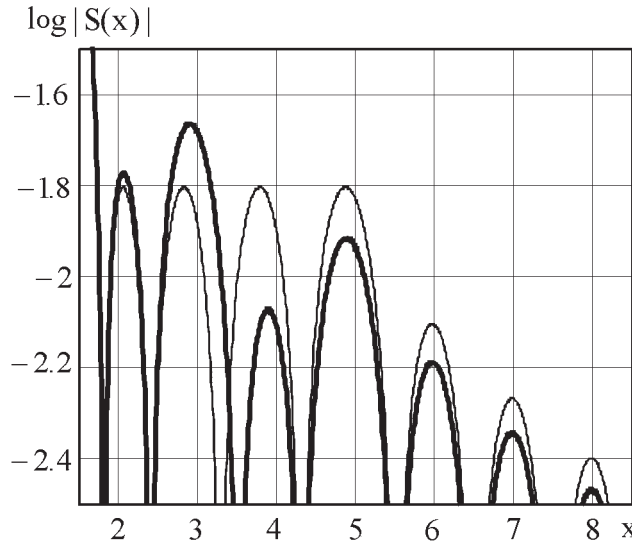


**Figure A.3** The area of sidelobes of the AWF SD.

on a series of widely used WFs. The substitution of the SD zero values  $b_i$  of any known WF presented by the trigonometric series in expression for  $w_s(t, b_1, b_2, \dots, b_N)$  leads to an accurate SD coincidence on a frequency and to an accurate coincidence between a known WF and AWF, and, vice versa, the application of coefficients at appropriate items of the series allows obtaining the frequency values  $b_i$ . For instance, for the popular Blackman WF of the type  $w_s(t, b_1, b_2)$  with the coefficients  $a_1 = 0.5/0.42$  and  $a_2 = 0.08/0.42$ , it is easy to obtain from (A.17) that  $b_1 = \sqrt{28/3}$  and  $b_2 = \infty$ .

Specifying a number of variable parameters for AWF  $w_s(m, b_1, b_2, \dots, b_N, M)$  equal to half of the sample number, and for  $w_c(m, b_1, b_2, \dots, b_N, M)$   $N = 0.5 M_0 - 1$  and specifying zero positions  $b_i$  coinciding with zero positions of the DC WF spectrum [4],

$$b_i = x_{0i} = \frac{M_0}{\pi} \arccos \left[ \left( \operatorname{ch} \frac{\operatorname{arch} Q}{M_0 - 1} \right)^{-1} \left( \cos \pi \frac{2i - 1}{2M_0 - 2} \right) \right] \quad (\text{A.21})$$

we obtain AWF spectra, which completely coincide with the DC WF spectrum. Here  $Q$  is an excess of the spectrum main lobe level over the SLL. In Figure A.4 this coincidence is illustrated by the DC WF spectrum difference

$$ST(x) = \frac{1}{Q} \cdot \operatorname{ch} \left\{ (M_0 - 1) \cdot \operatorname{ach} \left[ \operatorname{ch} \left( \frac{\operatorname{ach} Q}{M_0 - 1} \right) \cdot \cos \left( \pi \frac{x}{M_0} \right) \right] \right\} \quad (\text{A.22})$$

for  $Q = 10^3$  and AWF spectrum, for which the values of  $b_i$  are assumed to be equal to  $x_{0i}$  with rounding in 13 to 15 signs. The difference of the AWF and DC spectra, which does not exceed  $5 \cdot 10^{-15}$ , is defined only by rounding errors. Hence, both WFs obtained from the AWF in such a manner are optimal on the SLL of their spectra (this criterion was suggested by S. L. Dolph), although the forms do not coincide with each other and do not coincide with the Dolph solution [5].

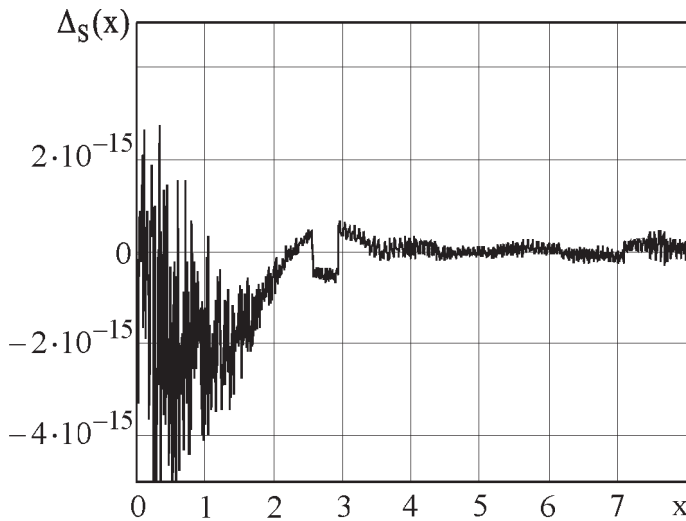


**Figure A.4** The plot of the DC SD and the AWF difference at coinciding with the SD zero distribution.

Describing property allows the AWF application for the WF approximation, which is not expressed by elementary functions, and results in existence limitations to its application. It is known that the DC WF optimality in the energy value in specified frequency band defines this WF attraction. If it is necessary to synthesize the filters with adjustable bandwidth, we use the KB WF approximation [3]. The possibility of obtaining the WF with required spectral properties on the basis of AWF by specification of variable SD zero positions allows the creation of the WF, which cannot be used less successfully in these problems. In particular, to obtain the WF, by approximating the KB WF, it is enough to specify adjustable AWF SD zero positions  $b_i = \sqrt{\alpha^2 - i^2}$ , where  $\alpha$  is the KB WF parameter. A comparison of spectral

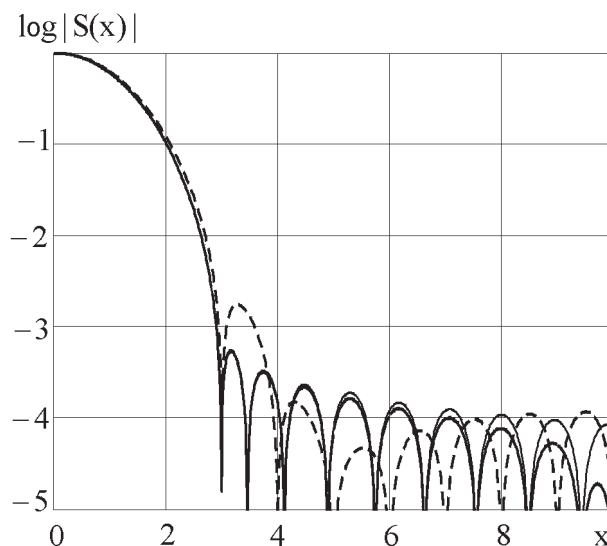


**Figure A.5** Logarithms of the AWF SD and KB WF SD modulus for  $\alpha = 2.82$  and the Harris WF SD modulus logarithm for  $\alpha = 3$ .

properties of such AWF, KB WF, and WF [3] is presented in Figure A.5. The bold curve corresponds to AWF SD modulus logarithm, the thin curve corresponds to the KB WF, and the dotted line corresponds to the J. Harris WF [3]. In a detailed consideration of the AWF SD and KB WF SD, a somewhat lesser width of the AWF SD main lobe on a zero frequency draws attention as well at a somewhat lesser level of the first SLs than for the KB WF. The Harris WF [3] already loses noticeably both to the KB WF and the AWF in the width of the SD main lobe on the zero level at a reduced scale at about 10 dB on the SD SLL.

On the whole, the AWF approximates KB WF essentially better than the known WF [3]. As well, there are no limitations on the specified parameter  $\alpha$  and, hence, on the SD SLL. Therefore, the approximation accuracy increases with  $N$  increasing and for  $N = M_0/2$  AWF exactly coincides with KB WF.

5. At the traditional definition of the asymptotic speed of the SLL decrease  $C_s = 20 \log \lim_{x \rightarrow \infty} |S(2x)/S(x)|$  in the decibel per octave applied to the AWF of

(A.13), (A.15), (A.14), and (A.16), we note that the AWF of the family  $w_s(t, b_1, b_2, \dots, b_N) C_{ss} = (6 + 12N_\infty)$ , and  $w_c(t, b_1, b_2, \dots, b_N) C_{sc} = (12 + 12N_\infty)$ , where  $N_\infty$  is the zero number specified on an infinite frequency. Thereby, these families mutually supplement each other in the asymptotic speed of the SD SLL decrease.

### A.3 SLL Minimization

To date, a variety WFs have been suggested and investigated; therefore, we compare our WF with those WFs that have been adopted as the best for important parameters. We mainly focus on DC, KB, Blackman, and Blackman-Harris WFs [3], as well as WFs developed recently [6–9].

The unambiguous connection of the AWF SD shape with specified zero positions allows on the basis of the AWF to obtain the WFs with spectral properties optimal on known and new criteria. We show the possibility of obtaining the WF according to the SLL minimum criterion at a specified width of the main lobe and the given speed of the SLL decrease, which is similar to a Dolph criterion but with the added requirement of the SD SL decrease with the frequency increasing. We assume that the following parameters are specified: the width of the SD main lobe on the zero level  $\Delta F_0$ , the speed of the SD SLL decrease  $C_s$ , and the number of WF items  $N$ . We need to define variable zero positions  $b_i$  of the AWF SD in such a manner that the SLL would be minimal.

At  $b_i \leq N + 1$ , the value of one of the variable zeros is defined by a specified width of the SD main lobe. In the future, for distinctness, we attribute the number 1 to the minimal value  $b_i = \Delta F_0/2$ . Taking into consideration that the number  $N_\infty$  is defined by a given  $C_s$ , the number of the variable AWF zero positions will be  $N_{\text{var}} = N - (1 + N_\infty)$ . Then, for SLL SD minimization, the objective function can be written in the form:

$$\max S(x, b_2, b_3, \dots, b_{N_{\text{var}}}) \Rightarrow \min_{\Delta F_0/2 \leq b_i \leq 3N} \quad (A.23)$$

Therefore, from all variables  $b_i$ , not more than two may accept values  $b_i \geq N + 1$ .

To solve this problem we can use DC WF SD, for which limiting the values of the ratio of the main lobe width and the SLL are defined by the fundamental property of the Chebyshev polynomial, as a standard in the width of the SD main lobe, in SLL, and in the initial distribution law of the SD zeros. To search optimal values of variable zero positions  $b_i$ , we can use standard software of the multidimension optimization. The unambiguous connection of the SLL with values of the zero positions  $b_i$  described above by property 3 essentially simplifies the search of optimal values of  $b_i$ .

For an effectiveness comparison of known WFs and WFs with the suggested method of the optimal value  $b_i$ , search the main spectral properties of the obtained WFs, DC WF, and some known WFs [6–9], which are the best on the ratio of the width of the SD main lobe and SLL and are presented in Table A.1. At the calculation of optimal AWF parameters on the basis of the AWF in (A.13) and (A.14), the values of  $\Delta F_0$  and  $C_s$  coinciding with  $\Delta F_0$  of the known WFs are considered to be initial.  $F_n$  for the DC WF are calculated for  $M = 32$ .

The frequencies  $b_i$  of the optimal WFs obtained are shown in Table A.2.

It follows from Table A.1 that the SD SLL of the presented optimal WFs are 4.5 to 14.89 dB less than the SD SLL of the best known WFs. In addition, the optimal WFs have a lesser equivalent noise band  $F_n$  and a lesser width on the level minus 6 dB ( $\Delta F_6$ ). To illustrate the advantages of optimal WFs, Figure A.6 shows the logarithms of the SD modulus of the known (dotted line) and optimal (solid line) WF corresponding to lines 1 and 2 from Table A.1. It follows from the AWF spectral properties that with an increase of the necessary values of  $C_s$ , the advantages of the optimal WFs (according to suggested criterion) increase.

The typical SD view of the optimal WFs according to the above-mentioned criterion is constant SD SLL in the interval on a normalized frequency  $x \leq N$  and decreasing SD SLL with the speed  $C_s$  for large  $x$  (Figure A.7, solid bold line and

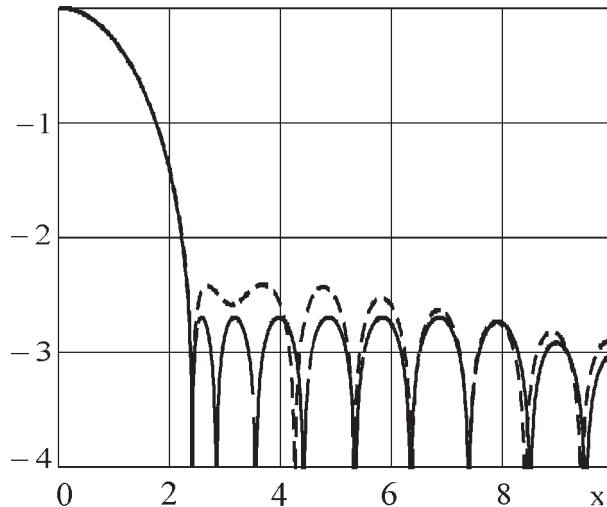
**Table A.1** Comparison of Spectral Properties of Optimal WFs and the Best WFs

WF	$F_n$	SLL, dB	$\Delta F_b$
Algebraic WFs [8] $C_s = (11 - 6)$ dB/oct	1.5344	-48.7	2.04
AWF 1. $C_s = 12$ dB/oct	1.5323	-54.0	2.0375
AWF 2. $C_s = 6$ dB/oct	1.5042	-56.77	1.9998
DC WF for $\Delta F_0 = 4.797745$	1.5073	-58.001	1.9833
WF [6], $C_s = 6$ dB/oct	1.7772	-68.72	2.3653
AWF 3. $C_s = 6$ dB/oct	1.7341	-76.044	2.304
DC WF for $\Delta F_0 = 6.232644$	1.7325	-77.914	2.2841
WF [7] $C_s = 18$ dB/oct	2.0339	-91.1	2.7058
AWF 4. $C_s = 18$ dB/oct	2.018	-95.656	2.6801
DC WF for $\Delta F_0 = 8.0$	1.9677	-102.27	2.6053
WF [7] $C_s = 18$ dB/oct	2.6704	-168.0	3.5503
AWF 5. $C_s = 18$ dB/oct	2.6471	-180.26	3.5133
AWF 6. $C_s = 6$ dB/oct	2.6292	-182.89	3.4895
DC WF for $\Delta F_0 = 13.99936$	2.5587	-184.49	3.4768
WF ( $K_4 \Psi_3$ ), [9]	1.6932	-65.465	2.2234
AWF 7. $C_s = 6$ dB/oct	1.6705	-71.396	2.22
DC WF for $\Delta F_0 = 5.84$	1.6745	-72.482	2.2062
WF ( $\hat{E}_4 \times_{3,5}$ ), [9]	1.8007	-74.952	2.4255
AWF 8. $C_s = 6$ dB/oct	1.7973	-83.149	2.3876
DC WF for $\Delta F_0 = 6.7$	1.7985	-84.369	2.3735

**Table A.2** Frequencies  $b_i$  of Optimal WFs

Number of AWF	Type of AWF
1	$w_c(t; 2.3988727; 2.83204; 3.544289; 4.4047608; 5.346507; 6.34103; 7.39)$
2	$w_s(t; 2.3988727; 2.79835; 3.46185; 4.26824; 5.1512; 6.078; 7.0321; 8.0048; 8.9924)$
3	$w_s(t; 3.1163222; 3.437; 4.0043; 4.7365; 5.5887; 6.808)$
4	$w_s(t; 4; 4.27458; 4.77735; 5.447; 6.23285; 7.1074; \infty)$
5	$w_s(t; 6.99968093; 7.147699; 7.434949; 7.846253; 8.363483; 8.968546; 9.645222; 10.379934; 11.161824; 11.98258; 12.83627; 13.719615; 14.633785; 15.59468; 17.04902; \infty)$
6	$w_s(t; 6.99968093; 7.14364; 7.42322; 7.824; 8.3286; 8.9196; 9.5812; 10.3001; 11.0656; 11.8692; 12.7045; 13.5673; 14.4558; 15.3762; 16.439; 27.405)$
7	$w_s(t; 2.92; 3.252978; 3.833244; 4.567715; 5.39413; 6.27688; 7.19651; 8.14425; 9.1416)$
8	$w_s(t; 3.35; 3.643958; 4.170447; 4.854965; 5.641272; 6.49436; 7.395305; 8.34178; 9.466)$

$\log|S(x)|$

**Figure A.6** Logarithms of the SD modulus of the algebraic WF [10] and AWF SD.

dotted line, respectively, for  $N = 9$  and  $3$ , and  $C_s = 30$  dB/oct). In the specific case, the specification of  $C_s = 0$  leads to the coincidence of AWF SD and DC WF SD (solid thin curve in Figure A.7), for which zero positions are given by (A.21).

We note two regularities in the WF SD property that are optimal according to the suggested criterion. At first, the SD SLL decreases at an increase of the item number of the optimal WFs and asymptotically aspires to the SSL of the DC WF SD. Then the width of the SD main lobe on any level different from zero decreases with an increase of the item number of the optimal WF and asymptotically aspires to the width of the SD main lobe of the DC WF, although at small  $N$  the function is not monotonic for all cases. Therefore, the significant disadvantage DC WF is a nondamping SD SLL and, accordingly, the presence of  $\delta$  functions at the end of the time interval in the optimal WFs (according to the above-mentioned criterion) is eliminated. Figure A.8 shows a view of optimal WFs corresponding to the SD of Figure A.7.

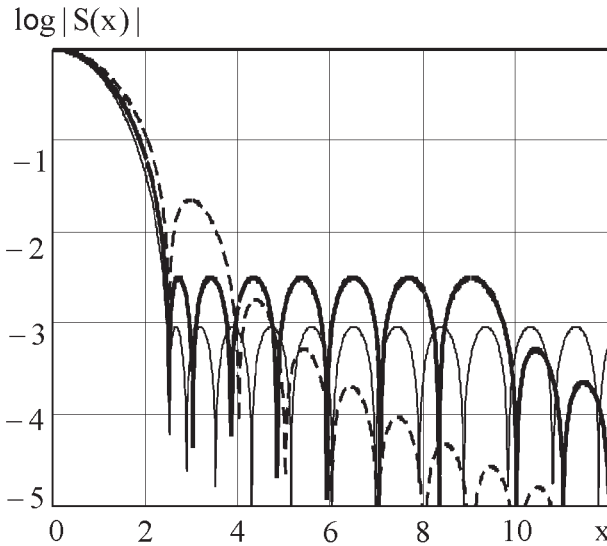


**Figure A.7** Logarithms of the SD modulus of optimal WFs.

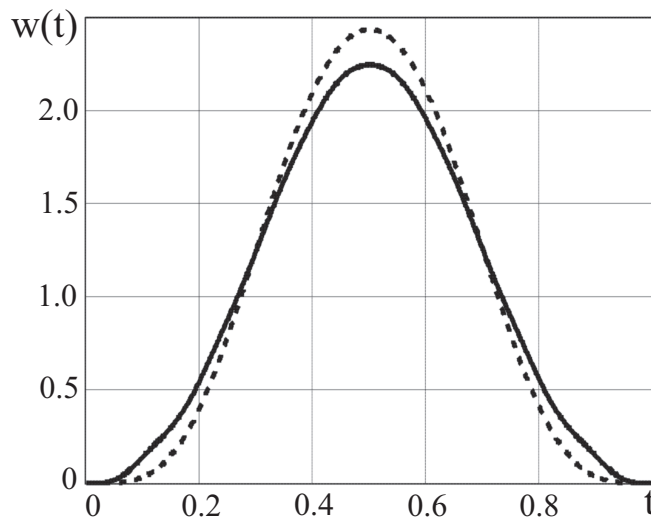


**Figure A.8** Shapes of optimal WFs.

The suggested method of the WF parameter calculation is applicable for discretized WF as well. Therefore, it is recommended to use the WF parameters for continuous signals as initial data because zero positions of its SD are close enough to the required zero positions of the WF SD for discrete signals. As a result of optimization of discretized WFs containing, respectively, 16 and 32 samples, the improvement of the SD SLL achieves 1 dB and 0.2 dB compared to the initial zero distribution of the WF SD for continuous signals.

The details of variable parameters  $b_i$  of optimal WFs with a minimal SLL at the specified width of the main lobe and the specified speed of SLL reduction are presented in Tables A.3 through A.7.

**Table A.3** WF  $w_s(t, b_1, b_2, \dots, b_N)$ ,  $C_{ss} = 6$  dB/oct,  $N_\infty = 0$ 

Number of Parameters	Frequency $b_i$	SLL, dB	$\Delta F_6$
2	1.4; 2.0632	-27.09	1.485922
3	1.4; 2.054043; 2.964663	-27.33723	1.483112
4	1.4; 2.044424; 2.939971; 3.928099	-27.63714	1.47939
2	1.6; 2.208305	-32.97952	1.605812
3	1.6; 2.182227; 3.032195	-33.36247	1.603638
4	1.6; 2.178836; 3.023188; 3.973943	-33.48996	1.602056
2	1.8; 2.404129	-38.26729	1.716504
3	1.8; 2.32694; 3.1405	-39.20138	1.714046
4	1.8; 2.321622; 3.114431; 4.024624	-39.387	1.712335
2	2; 2.6491486	-43.18756	1.818843
3	2; 2.487429; 3.299383	-44.7345	1.817976
4	2; 2.475827; 3.22575; 4.11802	-45.13832	1.815275
2	2.25; 3.04927	-49.421	1.936779
3	2.25; 2.7035993; 3.572	-51.26484	1.940396
4	2.25; 2.682512; 3.39257; 4.30566	-52.02798	1.937086
2	2.5; 3.722585	-56.68243	2.05184
3	2.5; 2.926706; 3.937952	-57.63658	2.054632
4	2.5; 2.899511; 3.579703; 4.56725	-58.6678	2.052087
3	3; 3.352432; 5.32897	-71.48284	2.263773
4	3; 3.348071; 3.97259; 5.410485	-71.66952	2.263569
3	3.5; 4.0431151; 6.7356365	-83.77358	2.44219
4	3.5; 3.800474; 4.367091; 7.052055	-85.40866	2.45274
4	4; 4.280334; 5.089298; 8.71832	-98.17392	2.624308
4	4.5; 4.858; 6.093; 10.661	-110.9039	2.779906

**Table A.4** WF  $w_c(t, b_1, b_2, \dots, b_N)$ ,  $C_{sc} = 12$  dB/oct,  $N_\infty = 0$ 

Number of Parameters	Frequency $b_i$	SLL, dB	$\Delta F_6$
3	1.4; 2.157665; 3.1993	-24.1852	1.52652
4	1.4; 2.12117; 3.10649; 4.20172	-25.1503	1.5138298
2	1.6; 2.3355	-28.30025	1.6731
3	1.6; 2.2818; 3.266	-29.68614	1.65569
4	1.6; 2.251815; 3.18716; 4.24754	-30.6118	1.624943
2	1.8; 2.45137	-34.11852	1.7843
3	1.8; 2.414494; 3.339252	-35.247	1.77066
4	1.8; 2.39115; 3.27592; 4.29842	-36.11872	1.7591
2	2; 2.2573142	-40.24508	1.881611
3	2; 2.554267; 3.418303	-40.92898	1.873954
4	2; 2.537702; 3.372022; 4.353988	-41.657	1.864682
2	2.25; 2.754878	-47.96589	1.990550
3	2.25; 2.737052; 3.524075	-48.28685	1.98942
4	2.25; 2.72918; 3.50134; 4.42942	-48.7074	1.984466
2	2.5; 3.030926	-54.30191	2.095928
3	2.5; 2.930105; 3.650287	-55.86316	2.09357
4	2.5; 2.92807; 3.63957; 4.51068	-55.9594	2.092906
2	3; 3.88623	-67.81512	2.288039
3	3; 3.376487; 4.17828	-69.18546	2.294054
4	3; 3.35398; 3.97416; 4.80736	-70.2846	2.29116
2	3.5; 4.643565	-77.21836	2.41346
3	3.5; 3.826103; 5.17453	-82.7938	2.47636
4	3.5; 3.811632; 4.384485; 5.42966	-83.5472	2.47686
3	4; 4.47028; 6.3214	-95.412	2.636806
4	4; 4.27086; 4.77531; 6.67625	-97.3896	2.648014

**Table A.5** WF  $w_s(t, b_1, b_2, \dots, b_N)$ ,  $C_{ss} = 18$  dB/oct,  $N_\infty = 1$ 

Number of Parameters	Frequency $b_i$	SLL, dB	$\Delta F_6$
2	1.4; 500	-15.20208	1.64042
3	1.4; 2.378089; 500	-19.4416	1.592094
4	1.4; 2.55973; 3.418061; 500	-21.65974	1.56301
2	1.6; 500	-20.278706	1.781389
3	1.6; 2.483348; 500	-24.493452	1.731378
4	1.6; 2.376282; 3.483558; 500	-26.776783	1.700032
2	1.8; 500	-25.638713	1.89916
3	1.8; 2.5968291; 500	-29.624189	1.85343
4	1.8; 2.505462; 3.555842; 500	-31.904634	1.822282
2	2; 500	-31.4675	1.996829
3	2; 2.7171887; 500	-34.9113	1.960934
4	2; 2.642124; 3.634295; 500	-37.0854	1.932324
2	2.25; 500	-39.814995	2.095535
3	2.25; 2.875389; 500	-41.85402	2.078174
4	2.25; 2.821662; 3.74006; 500	-43.7389	2.055044
2	2.5; 500	-48.342296	2.173559
3	2.5; 3.04; 500	-49.3226	2.179454
4	2.5; 3.009041; 3.853131; 500	-50.6284	2.165708
2	3; 500	-56.9301	2.28542
3	3; 3.469736; 500	-64.18742	2.355122
4	3; 3.400932; 4.095591; 500	-65.49388	2.353546
3	3.5; 4.240822; 500	-77.85908	2.518302
4	3.5; 3.843033; 4.539741; 500	-79.70314	2.5236434
4	4; 4.305338; 5.376281; 500	-93.32656	2.684405
4	4.5; 4.9137103; 6.42218; 500	-106.38509	2.8294814

**Table A.6** WF  $w_c(t, b_1, b_2, \dots, b_N)$ ,  $C_{sc} = 24$  dB/oct,  $N_\infty = 1$ 

Number of Parameters	Frequency $b_i$	SLL, dB	$\Delta F_6$
3	1.4; 2.51857636; 1,000	-16.9138	1.629985
4	1.4; 2.349729; 3.623464; 1,000	-19.56942	1.594117
2	1.6; 1,000	-16.40066	1.84633
3	1.6; 2.620621; 1,000	-21.5749	1.77929
4	1.6; 2.46645; 3.687565; 1,000	-24.3922	1.7383038
2	1.8; 1,000	-20.99572	1.9811186
3	1.8; 2.7312594; 1,000	-26.24906	1.911007
4	1.8; 2.5922535; 3.75856; 1,000	-29.19132	1.867258
2	2; 1,000	-25.71544	2.095355
3	2; 2.849307	-31.00025	2.027671
4	2; 2.725822; 3.835922; 1,000	-34.0162	1.983531
2	2.25; 1,000	-32.12221	2.213265
3	2.25; 3.0056083; 1,000	-37.12994	2.155634
4	2.25; 2.90197; 3.94075; 1,000	-40.14062	2.1140783

(continued)

**Table A.6** WF  $w_c(t, b_1, b_2, \dots, b_N)$ ,  $C_{sc} = 24$  dB/oct,  $N_\infty = 1$  (Continued)

Number of Parameters	Frequency $b_i$	SLL, dB	$\Delta F_6$
2	2.5; 1,000	-39.29543	2.308321
3	2.5; 3.1697628; 1,000	-43.56692	2.266916
4	2.5; 3.086543; 4.05357; 1,000	-46.4269	2.23089
3	3; 3.5141762; 1,000	-57.84979	2.449435
4	3; 3.474819; 4.298605; 1,000	-59.72495	2.431274
2	3.5; 1,000	-65.83734	2.5407214
3	3.5; 3.9223575; 1,000	-73.58677	2.59654
4	3.5; 3.88054; 4.56127; 1,000	-74.4692	2.596088
3	4; 4.641538; 1,000	-87.44663	2.737481
4	4; 4.322109; 4.968644; 1,000	-89.2459	2.744135
3	4.5; 5.37128; 1,000	-98.46473	2.842198
4	4.5; 4.78899; 5.7069; 1,000	-103.2239	2.886153

**Table A.7** WF  $w_s(t, b_1, b_2, \dots, b_N)$ ,  $C_{ss} = 30$  dB/oct,  $N_\infty = 2$ 

Number of Parameters	Frequency $b_i$	SLL, dB	$\Delta F_6$
4	1.4; 2.650662; 1,000; 1,000	-14.8566	1.6612243
5	1.4; 2.439512; 3.817512; 1,000; 1,000	-17.7969	1.620938
3	1.6; 1,000; 1,000	-13.55621	1.896219
4	1.6; 2.7495447; 1,000; 1,000	-19.23075	1.819364
5	1.6; 2.55289; 3.88014; 1,000; 1,000	-22.3852	1.7716876
3	1.8; 1,000; 1,000	-17.63677	2.0452462
4	1.8; 2.857214; 1,000; 1,000	-23.57575	1.959752
5	1.8; 2.675487; 3.949685; 1,000; 1,000	-26.92525	1.906844
3	2; 1,000; 1,000	-21.80682	2.173834
4	2; 2.9726; 1,000; 1,000	-27.94963	2.084725
5	2; 2.806054; 4.02569; 1,000; 1,000	-31.46477	2.028914
3	2.25; 1,000; 1,000	-27.25528	2.308986
4	2.25; 3.1261684; 1,000; 1,000	-33.52656	2.222467
5	2.25; 2.978801; 4.129057; 1,000; 1,000	-37.19111	2.16619
3	2.5; 1,000; 1,000	-32.10006	2.41987
4	2.5; 3.28844433; 1,000; 1,000	-39.29666	2.342876
5	2.5; 3.160425; 4.240829; 1,000; 1,000	-43.02518	2.28924
3	3; 1,000; 1,000	-46.74125	2.585523
4	3; 3.632704; 1,000; 1,000	-51.723	2.542026
5	3; 3.544303; 4.485683; 1,000; 1,000	-55.20301	2.50112
4	3.5; 3.993331; 1,000; 1,000	-65.9912	2.697789
5	3.5; 3.947912; 4.752225; 1,000; 1,000	-68.3842	2.676619
3	4; 1,000; 1,000	-74.3238	2.7777544
4	4; 4.3846225; 1,000; 1,000	-82.60318	2.823123
5	4; 4.36399; 5.03168 1,000; 1,000	-83.0788	2.823103

If necessary, we can calculate numerical values of coefficients  $C_{sn}$  and  $C_{cn}$  of the optimal WF according to the formulas (A.19) and (A.20) using the above-mentioned  $b_i$ .

#### A.4 Minimization of AWF Equivalent Noise Band

All AWFs at noise absence theoretically provide obtaining zero error for the frequency estimation of a resolvable signal; therefore, for the question about a choice of AWF type and a number of variable parameters, it is necessary to consider starting from the possibility of a frequency estimation error minimization caused by the noise. It is known that at a noise presence the equivalent noise band (ENB) of the WF influences used on the frequency estimation variance. This ENB is defined as [3]:

$$F_n = \frac{\int_{-0.5}^{0.5} [w(t, b_1, b_2, \dots, b_N)]^2 dt}{\left[ \int_{-0.5}^{0.5} w(t, b_1, b_2, \dots, b_N) dt \right]^2} \quad (\text{A.24})$$

$$F_n = M_0 \sum_0^{M_0-1} [w(m, b_1, b_2, \dots, b_N)]^2 / \left[ \sum_0^{M_0-1} [w(m, b_1, b_2, \dots, b_N)] \right]^2 \quad (\text{A.25})$$

respectively, for continuous and discrete WF.

Using these definition and taking into account (A.11) and (A.12), the analytic ENB expressions for the AWF in (A.11) and (A.15) and (A.12) and (A.16), we may reduce, respectively, to the forms:

$$F_{nS} = 1 + \frac{1}{2} \sum_{n=1}^N [C_{sn}(b_1, \dots, b_N)]^2 \quad (\text{A.26})$$

$$F_{nC} = \frac{\pi^2}{8} \frac{1 + \sum_{n=1}^N [C_{cn}(b_1, \dots, b_N)]^2}{\left[ 1 + \sum_{n=1}^N \frac{\cos(n\pi)}{2n+1} C_{cn}(b_1, \dots, b_N) \right]^2} \quad (\text{A.27})$$

Figure A.9 shows the ENB functions versus the positions of the specified zeros for the AWF  $w_s(t, b_1, b_2, \dots, b_N)$  and  $w_c(t, b_1, b_2, \dots, b_N)$  for the equality of all  $b_n = b$ . In these two functions we see a clearly expressed ENB minimum and a small value  $F_{n,\min}$  in the minima at  $b = b_{n,\min}$ . The value  $F_{n,\min}$  monotonically increases when  $N$  increases. The specification  $b_{\text{spec}} < b_{n,\min}$  leads to a fast increase of the ENB owing to an increase of the first SL forming in the frequency interval  $[b_{\text{spec}}, N + 1]$ . At  $b_{\text{spec}} > b_{n,\min}$ , the slow ENB increase is mainly caused by an increase of the main lobe width. At the same number of variable parameters,  $F_{n,S} < F_{n,C}$ .

It follows from obtained equations and plots that for any frequency  $x > 1.5$  there is the value of  $N$ , at which  $F_n$  is minimal.

Let us consider the possibility of simultaneous minimization of estimation errors caused by interference and a noise. We assume that for minimization of the estimation error caused by interference, it is necessary to specify  $N - N_n$  variable AWF parameters. We also suppose that for a specified additional number  $N_n$ , there

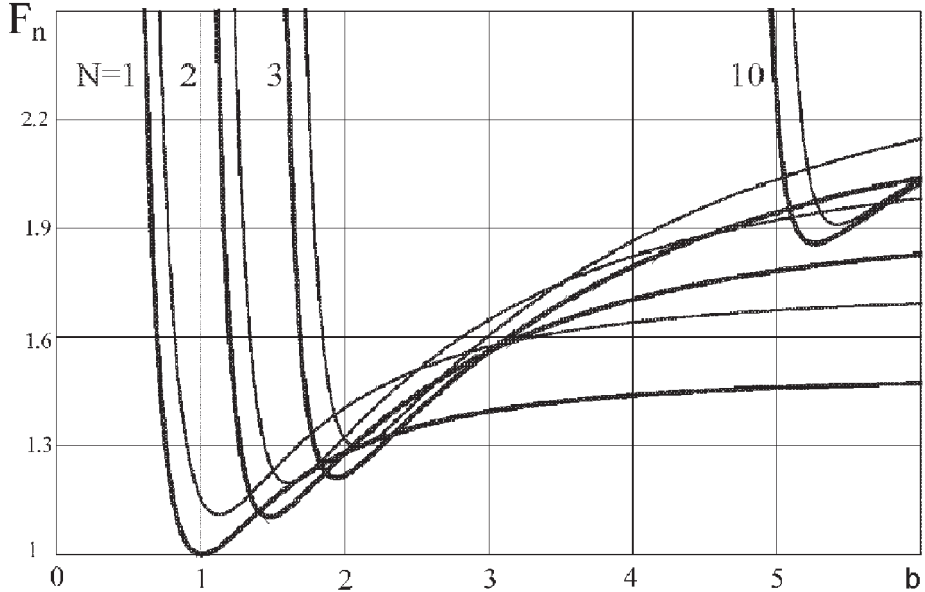


**Figure A.9** The function of the ENB of the AWF  $w_s(t, b, N)$  (bold lines) and  $w_c(t, b, N)$  (thin lines) versus the position of a specified spectrum zero.

are such values of variable parameters, at which the ENB value is  $F_n|_{N} < F_n|_{N-N_n}$ . In the specific case of the one additional variable parameter  $b_{n,\min}$ , the problem of determination of  $b$  minimizing ENB  $F_{n,\min}$  for specified number of variable parameters  $N$  has an analytical solution. For the ENB of the AWF  $w_s(t, b_{n,\min}, b_2, \dots, b_N)$ :

$$b_{n,S\min}^2 = \frac{\sum_{n=1}^N A_{sn}^2 n^4 (b_2^2 - n^2)^2 \dots (b_N^2 - n^2)^2}{\sum_{n=1}^N A_{sn}^2 n^2 (b_2^2 - n^2)^2 \dots (b_N^2 - n^2)^2} \quad (\text{A.28})$$

$$\text{where } A_{sn}(b_1, \dots, b_N) = (-1)^{n+1} \prod_{\substack{k=1 \\ k \neq n}}^N \frac{k^2}{k^2 - n^2}.$$

For the AWF  $w_c(t, b_{n,C\min}, b_2, \dots, b_N)$ , respectively:

$$b_{n,C\min}^2 = 0.25 + \frac{D_n(1+G_n) - C_n F_n}{C_n(1+G_n) - (1+H_n) F_n} \quad (\text{A.29})$$

$$\text{where } D_n = \sum_{n=1}^N B_n^2 L_n^2; \quad B_n = A_{cn} \prod_{i=2}^N \left( 1 - \frac{n^2 + n}{b_i^2 - 0.25} \right);$$

$$A_{cn}(b_1, \dots, b_N) = \frac{(-1)^{n+1}}{2n+1} \prod_{\substack{k=1 \\ k \neq n}}^N \frac{k^2 + k}{(k^2 + k) - (n^2 + n)}; \quad L_n = n_2 + n; \quad G_n = \sum_{n=1}^N B_n \frac{\cos n\pi}{2n+1};$$

$$C_n = \sum_{n=1}^N B_n^2 L_n; \quad F_n = \sum_{n=1}^N B_n \frac{\cos n\pi}{2n+1} L_n; \quad H_n = \sum_{n=1}^N B_n^2$$

In these expressions it was assumed that the AWF parameter, which earlier had the index 1 (i.e.,  $b_1$ ), is varied for the ENB minimization and the index  $n_{\min}$  is accepted for it.

At the specification of one from the variable parameters according to the ENB minimum, its value is defined by equations:

$$F_{nS\min} = 1 + \frac{1}{2} \sum_{n=1}^N A_{sn}^2 \left( 1 - \frac{n^2}{b_{nS\min}^2} \right)^2 \prod_{i=2}^N \left( 1 - \frac{n^2}{n_i^2} \right)^2 \quad (\text{A.30})$$

$$F_{nC\min} = \frac{\pi^2}{8} \frac{1 + \sum_{n=1}^N \left( 1 - \frac{n^2 + n}{b_{nC\min}^2 - 0,25} \right)^2 A_{cn}^2 \prod_{i=2}^N \left( 1 - \frac{n^2 + n}{b_i^2 - 0,25} \right)^2}{\left[ 1 + \sum_{n=1}^N \frac{\cos(n\pi)}{2n+1} \left( 1 - \frac{n^2 + n}{b_{nC\min}^2 - 0,25} \right) A_{cn} \prod_{i=2}^N \left( 1 - \frac{n^2 + n}{b_i^2 - 0,25} \right) \right]^2} \quad (\text{A.31})$$

where  $b_n$  is defined in (A.29).

Figure A.10 shows functions of minimal ENB versus  $b$ , for AWF  $w_s(t, b_{nS\min}, b_2, \dots, b_N)$  at equality of one parameter  $b_{n,\min}$  and all other parameters  $b_2 = b_3 = \dots = b_N = b$ .

Calculations show that at a simultaneous error minimization caused by interference and a noise, we may reduce more than 1.5 times of the component caused by a noise.

In some cases, it is preferable to use the WF with an increased speed of the spectrum SLL reduction. From the earlier considered AWF properties, this speed increase is performed by the specification of the necessary zero number on infinite frequency or on a half discretization frequency, respectively, at the analysis of continuous or discrete signals. Broadening the main lobe and level increase of the nearer SL of the spectrum and, hence, increase of ENB are the cost of using zeros to increase the reduction speed of SLL. The ENB minimization is possible in this case as well; however, minimal ENB levels essentially increase.

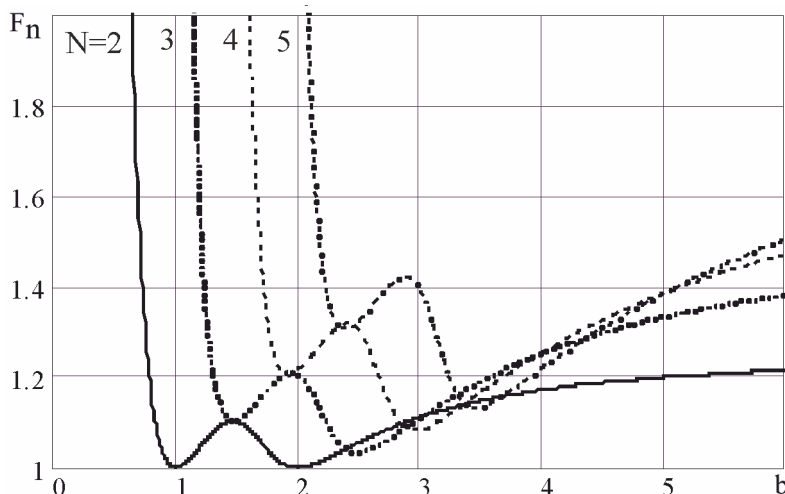


**Figure A.10** The function of the minimal ENB of AWF  $w_s(t, b, N)$  versus the position of the specified spectrum zero.

We must take into account that at specification of some roots  $b_n \rightarrow \infty$ , items including these roots become equal to 1. The above-described analytical equations can be used for the AWF with an increased speed of the SLL reduction.

## A.5 Minimization of Frequency Estimation Error

For an unbiased WF choice in the detection problems with the simultaneous estimation of the range (frequency), we connect the main lobe width and the WF SD SLL with the signal frequency estimation error on the background of a single interference. For this, we introduce two additional parameters in the known system of parameters characterizing spectral WF properties [6, 9]. The first one is the relative error of the frequency estimation  $F_{EE}$ . We define the value  $F_{EE}$  as the ratio of the envelope of the current error when using the analyzing WF  $\Delta x_{EE}(b_1, b_2, \dots, b_N)$  to the maxima value of the frequency estimation error when using the uniform WF  $\Delta x_{\max}(b_1 = 1, b_2 = 2, \dots, b_N = N)$  and  $q_{s/i} \gg 1$ :

$$F_{EE} = \left| \frac{\Delta x_{EE}(b_1, b_2, \dots, b_N)}{\Delta x_{\max}(b_1 = 1, b_2 = 2, \dots, b_N = N)} \right| \quad (\text{A.32})$$

The second parameter is the maximal relative error of the frequency estimation  $F_{EE\max}$ . We define  $F_{EE\max}$  as the ratio of the maximal envelope value of the current error of the frequency estimation when using the analyzing WF to the maximal value of the frequency estimation error when using the uniform WF and  $q_{s/i} \gg 1$ :

$$F_{EE\max} = \left| \frac{\Delta x_{\max}(b_1, b_2, \dots, b_N)}{\Delta x_{\max}(b_1 = 1, b_2 = 2, \dots, b_N = N)} \right| \quad (\text{A.33})$$

Figure A.11 shows the functions  $F_{EE}$  when using the uniform weighting function (solid bold line) and the AWF  $w_s(t) = 1 - (1 - 1/b^2)\cos(2\pi t)$  with one variable parameter  $N = 1$  for  $b = 2.2$  (dotted line) and for  $b = (\infty)$  (solid thin line).

We note some typical features of the function  $F_{EE}$  for different WFs. It has two symmetric main lobes caused by the interaction of the main lobes of the signal's SD and the interference's SD and SL sequence.

SLL  $F_{EE}$  is connected with the SLL of the used WF SD and in the frequency area, where the normalized width of the SD SL is equal to 1, and is proportional to SD

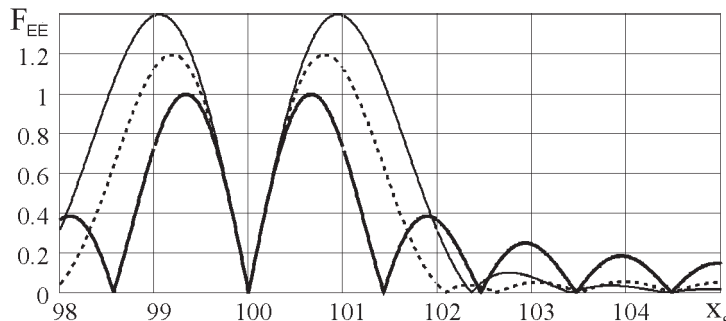


**Figure A.11** Plots of the envelope of the relative measurement error versus the current range when using the uniform WF and AWF with different values of the SD main lobe width  $2b$ .

SLL. For such WFs, the decrease speed of the SLL  $F_{EE}$  (which we designate as  $C_F$ ) is equal to the decreased speed of the SD SLL  $C_s$ . For the WF with the variable SL width (for instance, DC WF and KB WF), proportionality is disturbed but in the definitional domain of  $C_s$ , we have  $C_F \approx C_s$ .

The function  $F_{EE}$  allows the estimation of the IEZ size on a specified level. Similar to traditional definitions of spectrum parameters, it is advisable to define the main lobe width  $F_{EE}$  on a zero level and on a specified level, which, in particular, may coincide with the SL level of the function  $F_{EE}$ . The last parameter allows a real estimation of the IEZ size. For traditional WFs, the first parameter (the main lobe width  $F_{EE}$  on zero level) is defined by the frequency difference of the maxima of the main lobe and the first SL. For AWF, the main lobe width  $F_{EE}$  on the zero level can be specified by the zero position of the SD first derivative.

The maximal relative error of the frequency estimation  $F_{EEmax}$  increases with growth of the main lobe width of WF SD, but at this SLL,  $F_{EE}$  decreases.

It follows from this definition that for any WF  $F_{EE}$  is a function of the range difference between the UR and SR, and  $F_{EEmax}$  is a function of the range difference by the number characterizing a loss in the measurement error, when using any WF compared with a used uniform WF. According to this sign,  $F_{EEmax}$  is similar to the widely used parameter  $F_n$ , the ENB. We note that  $F_n$  and  $F_{EEmax}$  are unambiguously connected to each other due to their unambiguous connection with WF parameters.

The presence of the SL  $F_{EEmax}$  can be adversely affected on the measurement results if there are several SRs in the probing space.

The unambiguous connection  $F_{EE}$  with the shape of the AWF SD, the irregularity of the SL  $F_{EE}$ , and its level dependence on the frequencies of the specified zeros allow the assumption that at such a selection of specified AWF zero frequencies, the SLL  $F_{EE}$  will be minimal.

To search the necessary zero distribution, we formulate the WF optimality criteria. We assume that such a WF is optimal on the SLL  $F_{EE}$ , which has a minimal SL level of the function of the relative error of frequency estimation at a specified maximum level of the frequency estimation relative error  $F_{EEmax}$  and the specified SLL decrease the speed of the function of the frequency estimation error  $C_F = C_s$ . In other words, an equivalent criterion such as the WF is optimal, which at a specified SLL decreased speed of the relative error function for frequency estimation and at a specified SLL of this function it provides the minimal value of the maximal relative error of frequency estimation  $F_{EEmax}$ . We can formulate the following equivalent criterion: such a WF will be optimal on  $F_{EEmax}$ , which at a specified width of main spectrum lobe and a specified decreased SL speed  $C_F = C_s$  provides a minimum SLL  $F_{EE}$ .

Taking into consideration that  $C_F = C_s$  and, hence, it is defined by the view of used AWF and the number of specified zeros on infinite frequency  $N_\infty$ , the number of variable AWF zero positions when using the first and second criteria will be  $N_{var} = N - N_\infty$ , and when using the third criterion, it will be  $N_{var} = N - (1 + N_\infty)$ . Then, for SLL  $F_{EE}$  minimization when using the last criterion, the objective function can be written as:

$$\max F_{EE}(x, b_2, \dots, b_{N_{var}}) \Big|_{x \geq b_1} \Rightarrow \min \quad (A.34)$$

$$b_1 \leq b_1 \leq 10N$$

The functions of the minimal SL level  $F_{EE}$  versus  $F_{EEmax}$  for any specific AWF coincide at optimization according to all three criteria, which is caused by its equivalence. Nevertheless, at optimization according to the last criterion, the number of variable parameters is less by one according to first two criteria, which significantly reduces the time expenses of a search of the necessary zero distribution.

The values  $F_{EEmax}$ , SLL  $F_{EE}$ , and IEZ of optimal WFs obtained by us according to the offered approach for  $N = 6$  and  $C_s = 6$  dB/oct are presented in Table A.8. By obtaining these results, we did not take into account items from the frequency area  $x < 0$ . Practically, this situation is possible only for  $x \gg 1$  for a WF with  $C_s \neq 0$ . For a WF with WF c  $C_s = 0$  (DC WF) due to the nondamping SL from the frequency area  $x < 0$ , only the theoretical estimations of  $F_{EEmax}$ , SLL  $F_{EE}$ , and IEZ are possible.

Line 20 of Table A.8 corresponds to the boundary of values  $b_1, b_2, b_3$ , at which the AWF optimization is possible according to the criteria offered. To obtain the AWF with a lesser SLL  $F_{EE}$ , we need to increase  $N$ .

To compare the effectiveness of the known and offered WFs, Figure A.12 shows logarithms of functions  $F_{EE}$  versus signal frequency at a fixed interference frequency of 10 and for signal processing by three WFs.

The solid bold line corresponds to an optimal WF on  $F_{EEmax}$ , which has an IEZ on the SL level  $F_{EE} -38.773718$  dB equal to 5.2. The dotted line corresponds to the WF with  $N = 2, b_1 = 2, b_2 = 5.16353246$ , which has  $F_{EEmax}$  coinciding with the previous  $-1.35$ , and the IEZ on the same level of  $-38.773718$  dB is 8. The bold dotted line is for the Blackman WF  $b_1 = \sqrt{28}/3, b_2 = \infty$ , which has an IEZ on the level

**Table A.8 WF  $w_{sN}(t, b_1, b_2, \dots, b_N)$   $C_s = 6$  dB/oct,  $N_\infty = 3$**

$N$	Frequencies $b_1$	$F_{EE\ max}$	SLL $F_{EE}$ , dB	IEZ
1	1.10363; 1.9634756; 2.6927854	1.0	-11.113341	2.566581
2	1.15; 1.9789563; 2.7092358	1.012501	-11.882937	2.645502
3	1.25; 2.0141513; 2.74710129	1.03931	-13.594666	2.816267
4	1.4; 2.0712165; 2.8099343	1.078821	-16.284956	3.073758
5	1.6; 2.1540838; 2.9045467	1.12958	-20.075839	3.418789
6	1.8; 2.2426; 3.01056	1.177608	-24.066848	3.763904
7	2; 2.333534; 3.126187	1.2225	-28.213420	4.105807
8	2.25; 2.3242544; 3.3119933	1.262522	-31.749849	4.408618
9	2.5; 2.5; 3.54939	1.319770	-36.669657	4.853110
10	2.75; 2.75; 3.913199	1.383134	-42.280005	5.366718
11	3; 3; 4.4269384	1.443876	-48.075619	5.879149
12	3.25; 3.4371126; 5.4825578	1.521717	-56.592380	6.556808
13	3.5; 3.9609817; 6.5190642	1.587437	-64.176026	7.166845
14	3.75; 4.3739306; 7.3095371	1.632825	-69.619660	7.603479
15	4; 4.6523975; 7.916533	1.664815	-73.569385	7.918859
16	4.25; 4.6978354; 8.1266794	1.681526	-75.339694	8.103814
17	4.5; 4.5195775; 8.1535615	1.686078	-75.704378	8.165823
18	4.75; 4.75; 6.5925594	1.687513	-72.720134	8.212658
19	5; 5; 5.671635	1.687534	-71.442070	8.239690
20	5.1982811; 5.1982811; 5.1982811	1.687427	-71.202871	8.246364

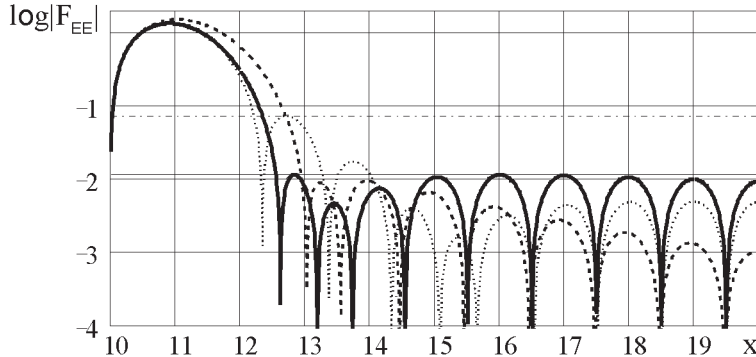


**Figure A.12** Plots of  $F_{EE}$ , logarithm modulus optimal according to  $F_{EE_{max}}$  and WF with  $b_1 = 2$ ,  $b_2 = 5.16353246$ , and the Blackman WF.

of  $-38.773718$  dB equal to 5.8 and besides  $F_{EE_{max}}$  is essentially more than  $-1.53$ . However, SLL  $F_{EE}$  here is equal to  $-40.3659333$  dB.

A comparison of plots clearly illustrates the advantages of the WF optimal in the frequency estimation error.

Among the known WFs, the DC WF (without consideration of the SL from the frequency area  $x < 0$ ) has the least SLL  $F_{EE}$  at any values of  $F_{EE_{max}}$ . The KB WF yields to the DC WF in the SLL  $F_{EE}$  from 12 dB for  $F_{EE_{max}}$  to 15.2 dB for  $F_{EE_{max}} = 1.9$ . Optimal WFs presented in Table A.8 in the SLL  $F_{EE}$  exceed all known WFs [3, 6, 7–10] by 1.5 to 18.4 dB. We should emphasize especially that the WFs optimal on a frequency estimation error have an advantage even over one SAD item for the DC WF. Already for  $N = 3$ , the advantage in the SLL  $F_{EE}$  at the admissible  $F_{EE_{max}}$  is 3 dB for the optimal WF presented in the last lines of Table A.8. Moreover, they have damping sidelobes.

From spectral AWF properties, it follows that for an increase in  $N$ , the achievable SLL minimum  $F_{EE}$  at a specified  $F_{EE_{max}}$  decreases and, hence, the advantages of the optimal (according to the offered criterion) WFs in the problems of the signal frequency estimation increase.

The presented results are evidence of the noticeable advantage of the WFs optimal on  $F_{EE_{max}}$  in the problems of the radio pulse frequency estimation and related problems, for example, such as estimating target angular coordinates for scanning antennas.

## A.6 Conclusions

AWF properties allow the minimization of the truncation error particular to the Fourier transformation during harmonic analysis of the multifrequency signal. These properties permit obtaining the WFs met to different criteria (both known and new), for instance, allowing the creation of the WFs with an extremely low SD SLL at a specified width of the main lobe and a specified decreased speed of the SD SLL or allowing the WF creation with an extremely low level of the frequency estimation error.

We can say with confidence that the advantages of the AWFs and the WFs over traditional WFs allow a significant improvement of signal processing.

## References

- [1] Davydochkin, V. M., and S. V. Davydochkina, "New Calculation Method for Effective Weighting Functions for a Spectral Analysis," *Proceedings of XII Intern. Conf. Radar Technology, Navigation and Communication*, Voronezh, Vol. 3, 2006, pp. 1662–1668. [In Russian.]
- [2] Davydochkin, V. M., and S. V. Davydochkina, "Weighting Functions for Digital Adaptive Harmonic Analysis of a Signal," *Radiotekhnika*, Vol. 9, No. 144, 2009, pp. 11–20. [In Russian.]
- [3] Harris, F. J., "On Use of Windows for Harmonic Analysis with the Discrete Fourier Transform," *IEEE Transactions on Audio Electroacoustics*, Vol. AU-25, 1978, pp. 51–83.
- [4] Voskresenskiy, D. I., et al., *Antennas and SHF Devices: Calculation and Design of Antenna Arrays and Their Radiated Elements*, Moscow, Russia: Sovetskoe Radio Publ., 1972. [In Russian.]
- [5] Dolph, C. L., "A Current Distribution for Broadside Arrays Which Optimizes the Relationship Between Beam Width and Sidelobe Level," *Proc. IRE*, No. 6, 1946, pp. 335–348.
- [6] Dvorkovich, A. V., "New Calculation Method of Effective Window Functions Used at Harmonic Analysis with the Help of DFT," *Digital Signal Processing*, No. 2, 2001, pp. 49–54. [In Russian.]
- [7] Dvorkovich, A. V., "Once More About One Method for Effective Window Function Calculation at Harmonic Analysis with the Help of DFT," *Digital Signal Processing*, No. 3, 2001, pp. 13–18. [In Russian.]
- [8] Kirillov, S. N., M. Y. Sokolov, and D. N. Stukalov, "Optimal Weighting Processing at Spectral Analysis of Signals," *Radiotekhnika*, No. 6, 1996, pp. 36–38. [In Russian.]
- [9] Kravchenko, V. F., *Lectures on Atomar Function Theory and Some Applications*, Moscow, Russia: Radiotekhnika Publ., 2003. [In Russian.]
- [10] Kharkevich, A. A., *Spectra and Analysis*, 4th ed., Moscow, Russia: Fizmatgiz Publ., 1962. [In Russian.]



# List of Acronyms

AFW	accompanying flow of waves
AWF	adaptable weighting function
AWP	antenna-waveguide path
BH	Blackman-Harris
CS	complex spectrum
CSD	complex spectral density
CW	continuous wave
DC	Dolph-Chebyshev, directional coupler
DC WF	Dolph-Chebyshev weighting function
DF	difference frequency
DFS	difference-frequency signal
DFT	discrete Fourier transformation
DP	directional pattern
DR	dielectric resonator
DS	directing system
DSP	digital signal processing
ED	error of discreteness
EE	error envelope
EMW	electromagnetic wave
EN	envelope nodes
ENB	equivalent noise bandwidth
FM	frequency modulation
FMCW RF	frequency-modulated continuous-wave range-finder
FSCW	frequency stepped continuous wave
FT	Fourier transformation
FFT	fast Fourier transformation
IEZ	increased error zone
IDFT	integral-discrete Fourier transformation
KB	Kaiser-Bessel
KB WF	Kaiser-Bessel weighting function
LF	likelihood function
LLF	logarithm of likelihood function
LLRF	logarithm of likelihood ratio function
LRF	likelihood ratio function
MC	modulation characteristic
MLM	maximal likelihood method
MQIS	methods of QI smoothing
MR	measuring room
MSD	mean square deviation
MTB	measuring test bench
PAM	parasitic amplitude modulation

PC	phase characteristic, personal computer
PFC	phase-frequency characteristic
PLL	phase-locked loop
PR	passive reflector
PSD	power spectral density
RF	range-finder
RR	radar reflector
QI	quantization interval
SAD	spectral amplitude density
SC	spectral component
SD	spectral density
SF	signal function
SIR	signal/interference ratio
SL	sidelobe
SLL	sidelobe level
SNR	signal/noise ratio
SOM	self-oscillation mixer
SPD	spectral power density
SR	spurious reflector
SRP	stationary random process
SSP	spurious spectral peaks
TRM	transmitting-receiving module
UR	useful reflector
WF	weighting function

# About the Authors



**Boris A. Atayants** was born in 1940 in Makhachkala, Russia. He graduated from the Radio Engineering Faculty of Ryazan Radio Engineering University and worked in the Radio Control and Communication department until 1984, where he taught the lecture courses Radio-Relay Communication and Radio Control of Space Apparatuses. He was the executor responsible for performing several R&D projects carried out by USSR Government Order. He worked as a member of Scientific Council of USSR Academy of Sciences on ultrahigh-band radar technology.

From 1984 he worked in the instrumentation industry. He is one of the founders of the first radar level-meters in the Soviet Union (the series LUCH).

In 1991 he helped establish the innovative scientific-industrial company Contact-1. From February 1992 he worked as the general director-chief designer of this enterprise, which was awarded “best enterprise of the industrial branch” in accordance with All-Russia and regional competitions in 2002–2012.

Boris A. Atayants has a Ph.D. in engineering. His list of scientific publications includes more than 200 published papers, one book, and more than 50 patents.

He was awarded the rank of Best Manager of Russia and was decorated with the gold medal “The Premium of Peter the Great,” and in 2012 he became the premium laureate, which was named after V.F. Utkin, in science and technology. He has been awarded diplomas at both the federal and regional levels.



**Viacheslav M. Davydochkin** was born in 1947 in the Shiringushi settlement in Russia. He graduated from secondary school in 1964 and entered Rayzan Radio Engineering University (RREU). After graduation from RREU with a concentration in radio electronic devices he worked in the Radio Electronic Devices department as an engineer, an assistant-professor, a junior researcher, and a senior researcher. In 2001 he joined the JSC Contact-1, where he works as the chief of the antenna-feeder devices’ sector.

Vacheslav M. Davydochkin combines practical industrial activity with scientific research in the field of digital radar signal processing, development of methods and algorithms for accuracy and noise-immunity increase for range measurement by short-range FM radars. In 2008 he defended his Ph.D. thesis on radio engineering including TV systems and devices and radar and radio navigation technology. He is the author of more than 100 scientific publications, including 40 patents and one book.



**Victor V. Ezerskiy** was born in 1947 in Berlin, Germany, into the family of an Soviet Army officer. In 1966 he graduated with honors from Ryazan Polytechnical College. In 1972 he graduated from Ryazan Radio Engineering University with honors in the concentration radio electronic devices. He worked as an R&D engineer in the Theoretical Fundamentals of Electrical Engineering department, and in 1975 he joined the Radio Electronic Devices department. In 1979 he began his Ph.D. and after graduation in 1983 he defended his Ph.D. thesis on radar and radio navigation technologies devoted to

the theory of polarization sign application for recognition of radar objects. From 1983 he worked as an assistant professor and associate professor in the Theoretical Fundamentals of Electrical Engineering department. From 1991 he worked as an associate-professor in the Radio Control and Communication department where he did research in the field of ultrahighband radar technology. In 1997 he combined his academic work at the university with practical and research activity at Contact-1 in the field of precision range measurement in short-range FM radar technology. In 2006 he defended his Dr. Sci. thesis in the specialty of radar and radio navigation technologies. Since 2007 he has worked as a professor in the Radio Control and Communication department of Ryazan State Radio Engineering University and as the leading researcher at Contact-1. In 2013 he was made a full professor.

Victor V. Ezerskiy performs scientific research in the fields of digital radar signal processing, development of methods and algorithms of accuracy, and noise-immunity increase for range measurement in short-range FM radar technology. He is the author of 130 publications including one book and 27 patents.

He is a member of editorial board of several scientific journals.

Victor V. Ezerskiy has the title of Honorary Worker of Higher Professional Education. In 2012 he was awarded the Ryazan Region Premium in Science and Technology, which was named after the academician V. F. Utkin.



**Valery S. Parshin** was born in 1947 in the Kaliningrad region of Russia. In 1969 he graduated from the Ryazan Polytechnical College with a concentration in radio apparatuses. For three years he worked as a technician in industry. In 1975 he graduated from the Ryazan Radio Engineering University, concentrating in radio electronic systems. He worked as an engineer and an assistant professor in the Radio Electronic Devices department. From 1980 to 1983 he studied for his Ph.D. In 1984 he defended his Ph.D. thesis in the area of radar and radio navigation technologies. The title of the Ph.D.

thesis was “Recognition of Pulse Random Interference.” He then worked as a senior researcher and assistant professor. In 1990 he was an associate professor in the Radio Control and Communication department of Ryazan State Radio Engineering University. In 2004 he combined his scientific and academic work at the university with practical and research work in industry at Contact-1 as a leading specialist. In November 2013 he defended his Dr.Sci. thesis titled “Methods and Algorithms

of Recognition and Parameter Estimation of Random Processes at Presence of Disturbing Factors."

Valery S. Parshin performs scientific research in the field of digital signal processing for radio systems in the frequency domain. The area of his scientific interests is the recognition of random signals and their parameter estimation at presence of disturbing factors and FM range measurement. He is the author of more than 130 scientific publications including one book and he holds 15 patents.



**Sergey M. Smolskiy** was born in 1946 in Moscow, Russia. In 1964 he graduated from secondary school with a medal and entered Moscow Power Engineering Institute (Technical University) (MPEI). He graduated in 1970 from the Radio Engineering Faculty of MPEI with a concentration in radio physics and electronics and was recommended to a Ph.D. course. During his Ph.D. studies at MPEI he received a scholarship named after Lenin and in 1974 defended his Ph.D. thesis on the theory of high-frequency transistor oscillators. After finishing the Ph.D. course he worked at the Radio Transmitter Department of MPEI as a senior researcher, the head of

research lab, and the head of research division. Later he moved to the position of MPEI deputy vice-rector for research and the position of MPEI vice-rector on international relations. In 1993 he defended his doctor of sciences thesis on radar and radio navigation systems. In 1994 he became a full professor and in 1995 was elected as a head of the radio receiver department. Since 2006 he has worked as a professor in this department, as well as also being the deputy director of the MPEI Institute of Radio Engineering and Electronics.

During this time he worked on a series of significant scientific and applied problems. In particular, he participated in the development of the theory of autonomous and synchronized transistor self-oscillation systems and the development of methods of mathematical modeling and effective algorithms for analysis of self-oscillating systems. He actively developed the theory and implementation of autodyne (self-oscillating mixers) systems for the short- range radar, and has done research in the field of medical electronics, radio monitoring systems, self-similar processes in telecommunications, and investigations of chaotic oscillations and signals. Professor S. M. Smolskiy is a recognized expert in these and other areas.

S. M. Smolskiy holds the academic degree of doctor of engineering sciences. He was elected as the academician of several Russian and international academies: International Academy of Electrical Sciences, International Academy of Informatization, and International Academy of Higher Educational Institutions. He is a member of IEEE and has been made honorary doctor of three foreign universities.

S. M. Smolskiy is actively and fruitfully working in the scientific areas he helped create: development of the theory and practical implementation of short-range radar systems and self-similar systems, improvement of radio monitoring and chaotic signal theory, and research in the field of medical instrumentation, electrodynamics, and quantum radiophysics.

He is the author of more than 250 scientific publications including 12 books.

Under his scientific supervision two doctor of sciences theses and 11 Ph.D. theses were prepared. He participates in conferences with reports and reviews along with lecture courses at foreign universities. Some of his pupils have become heads of departments in different Russian universities and in various companies.

Professor S. M. Smolskiy made significant contributions to the creation of All-Russia and international conferences and symposiums on the theory and implementation of oscillating and radar systems.

He is a member of Popov Scientific-Engineering Association of Radio Engineering, Electronic and Communication, and the head of the Radio Engineering Methods in Power Engineering Section. He is a scientific supervisor and a member of organizing committees for international scientific conferences.

He is the Honor Radio Engineer of Russia, and he was awarded the Gold Medal of Popov "for services in development of radio electronics and communication." He is also the Honor Worker of Russian Higher Education, and he was awarded by Polish order, the Medal of Riazansky by the Academy of Space Research.

# Index

## A

Accompanying flow of waves (AFW), 192  
Adaptable weighting functions (AWFs)  
algorithms of frequency estimation with,  
86–88  
analytical expressions for, 291–94  
application with minimal varied  
parameters, 208  
continuous, 294  
defined, 86  
function of zero frequency, 88  
irregularities, 270  
minimization of equivalent noise band,  
306–9  
minimization of truncation error, 86  
at noise absence, 87  
parameters, 212  
SAD, 200–201  
samples, 86  
SD, 295, 296  
SD logarithms, 298  
SD SLL variation, 296  
spectral properties, 291  
spectral properties in DSP problems,  
295–99  
varied parameters, 208  
Antenna aperture, reflection from  
irregularity in, 176  
Antenna-waveguide path (AWP)  
dust and moisture on elements, 200  
encapsulating insert in, 204  
encapsulation device in, 191  
family, 177  
irregularities, 168, 174, 190–91, 192  
length, 178  
reflection from elements, 199  
relative length, 175  
resonant reflections and, 168  
as signal mathematical model, 177

SR parameters in, 191  
SRs in, 174–81  
Atmosphere sensing radar, 283  
Average difference frequency, for  
modulation half-period, 141  
Average MSD  
function of logarithm of noise  
component, 62  
logarithm functions of, 59, 60  
*See also* Mean square deviation (MSD)  
Average weighted estimation  
of difference frequency, 88–91  
truncation error of, 88–91  
Average-weighted frequency estimation, 71

## B

BAR series, 290  
Bessel function, 93  
Best WFs, 300  
Bird's observation radar, 283–84  
Blackman-Harris WF, 48  
Blackman WF, 102, 128, 129, 181, 270

## C

Cancellation  
complex spectral density (CSD) for,  
226–28  
interference signal, in spectral domain,  
225  
mode activation, 224  
spectral power density (SPD) for, 228–32  
of spurious reflections, 223–32  
Chebyshev polynomial, 260  
Combined optimization  
defined, 55  
measurements, 55  
normalized error logarithm versus  
normalized range with, 56

- Combined optimization (continued)  
procedure of error minimization, 56
- Complex spectral density (CSD)  
for cancellation, 226–28  
DC WF, 74  
of DFS, 75  
measurement errors at, 227  
SC, 92
- Complex spectrum (CS), 67–68
- CONTACT-1, 264
- Continuous AWFs, 294
- Correction coefficients  
algorithm sequence, 153–54  
central frequency estimation using, 95–99  
connection with nonlinearity parameters,  
151–53  
estimation according to operating  
difference-frequency signal, 153–55  
simulation conditions, 154–55  
systematic inaccuracy of frequency  
estimation and, 91–92
- Correlation coefficients, 111
- D**
- Delay time estimation  
with MLM, 113–16  
obtaining, 116
- Delta function, 292
- Dielectric resonators (DR), 9
- Difference frequency estimation  
algorithms of, 68–71  
for algorithm with correction coefficients,  
91–92  
average weighted, 88–91  
conclusions, 103–4  
introduction to, 67–68  
maximum position of spectral density of  
difference frequency signal, 71–88  
minimization of measurement error,  
77–80  
noise influence on accuracy, 94–103  
noise interference and, 92–103  
by position of spectrum maximum,  
67–104  
stimulation of algorithms, 102–3  
systematic inaccuracy, 91–92
- truncation error at WFs, 74–77  
truncation error of range measurement,  
71–74
- Difference frequency estimation error  
reduction  
algorithm, 216–17  
answers, 217  
correcting amendment determination,  
214  
correction coefficient estimation, 215  
envelope curves and, 211  
method of, 211–15  
probability of, 213  
sequence of actions, 216  
situations, 210–11
- Difference-frequency signal (DFS)  
average, 5  
central frequency estimation, noise and,  
95–99  
CSD of, 75  
defined, 1  
error components, 12  
extreme appearance moment, 26  
extreme positions, 25  
frequency estimation error, 68  
frequency measurement, 100  
graph, 3, 4  
half-periods, 11, 17  
instantaneous, 2, 4  
number of periods, 13–14  
PAM, 8–9, 119–21  
phase estimation, 111  
phase joining, 10, 16  
phase-joining errors, 23, 28  
phase jump, 9  
phase shift, 7, 117  
phase variation, 4, 51  
preliminary analog processing, 31  
processing stages, 290  
pulling period, 13–14  
range estimation based on, 108–13  
SAD maximum, 71  
SCs of, 99, 203  
SPD, 228  
spectral density of, 92–103  
spectrum calculation, 91  
weighted sample of, 72

- zero determination, 51  
zero displacement, 173  
zero padding in, 69  
zeros, 5, 6, 29
- Digital signal processing (DSP), 67–68
- Directing system (DS)  
defined, 187  
measurement error versus relative range in, 190  
object probing in, 189  
reflector probing in, 188
- Directional coupler (DC), 188
- Directional pattern, 181
- Discrete Fourier transform (DFT), 67–68
- Discretized WFs, 292
- Displacement meters, small, 284
- Distance measurement error  
radiated power level influence on, 269  
results of experimental reduction of, 269–72  
to RR, 263
- Distribution law, 115
- Dolph-Chebyshev (DC) WF  
CSD, 74  
difference frequency estimation  
truncation error at, 74–77  
FM sweep for, 79  
measurement error at optimal values, 82  
normalized measurement error versus normalized range, 75  
normalized range, 84  
normalized range for optimal parameters, 85  
parameters, 81  
range point positions versus root number, 76  
SAD processed by, 82  
variation of SD shape, 80
- Dolph-Chebyshev method, 259
- E**
- Echo signals, error caused by, 220–21
- Edge modes, 184–86
- Eigenvector algorithm (EV)  
defined, 244  
disadvantage, 244
- in frequency range finding, 245  
MUSIC method versus, 244  
SC selection of spectrum, 245  
spectrum estimation, 244
- Electrodynamic distance, 270
- Electromagnetic waves (EMWs)  
mathematical models, 169  
reflection coefficient of, 205  
scattered, 169
- Envelope nodes (ENs)  
controlling FM sweep, 50  
defined, 40–41  
error position, 50
- Envelopes  
measurement error and, 180  
of normalized error of range estimation, 181  
of relative measurement error, 309  
shape of, 240
- Equivalent noise band (ENB)  
AWF, minimization of, 306–9  
defined, 306  
functions of, 306, 307, 308
- Error envelope (EE), 171, 172
- Experimental reduction  
of error caused by virtual interference, 266–69  
waveguide-measuring test bench, 266–67
- Extreme displacement function, 234, 235
- F**
- Fast Fourier transform (FFT), 67–68, 69, 70
- Fast oscillation, 148
- FMCW radar  
atmosphere sensing radar, 283  
bird's observation radar, 283–84  
characteristics, xix–xx  
for civil purposes, xviii  
defined, xvii  
devices, 277
- FM geo-radar, 282–83  
guarding systems, 284–85  
ice and snow blanket thickness meters, 281–82  
level-meters, 281  
navigation radar, 279

- FM geo-radar (continued)  
 practical application areas, 277–85  
 radio altimeters, 278–79  
 radio proximity fuses, 279  
 range finders for geodesic research, 283  
 robotic navigation and mapping systems,  
   285  
 small displacement meters, 284  
 theoretical analysis, xx  
 transport radar, 280–81
- FM geo-radar, 282–83
- FM nonlinearity  
 compensation of modulation  
   characteristic nonlinearity, 155–60  
 conclusions, 164–65  
 connection of correction coefficient with  
   nonlinearity parameters, 151–53  
 for counting method of frequency  
   measurement, 141–47  
 effects of, 137–65  
 estimation of correction coefficient,  
   153–55  
 introduction to, 137  
 modulation characteristic, mathematical  
   model of, 137–40  
 oscillating modulation characteristic,  
   144–47  
 quadratic modulation characteristic,  
   142–43  
 quadratic modulation characteristic with  
   oscillating component, 147  
 for weighting method of difference  
   frequency averaging, 147
- FM parameter optimization  
 combined, 55–56, 80  
 combined procedure of error  
   minimization, 56
- FM sweep, 53–55, 78–79  
 minimization of measurement error,  
   77–80  
 slow-frequency modulation, 50–53  
 truncation error minimization by, 50–56
- FM RF calibration, 265
- FM sweep  
 for DC WF, 79  
 EN control, 50  
 frequency, 146, 147
- function value, 52  
 for KB WF, 79  
 linearity of, 137  
 maximal degree of, 54  
 normalized, function of, 53  
 normalized error logarithm versus  
   normalized range, 54  
 optimization of, 53–55, 78–79  
 of SHF oscillator, 158
- Frequency estimation  
 for algorithm with correction coefficients,  
   91–92  
 approaches, 20–22  
 average-weighted, 71  
 determination, 96–97  
 first approach, 20–21  
 noise influence on accuracy, 94–103  
 noise influence with sliding half-strokes,  
   101–2  
 of SAD parameters, 205  
 second approach, 21–22, 29–30  
 shift, 97  
 stimulation of algorithms, 102–3  
 systematic inaccuracy, 91–92  
 unstable zones of, 269  
 variance calculation, 94–95  
*See also* Difference frequency  
 estimation
- Frequency estimation error  
 minimization of, 68, 309–12  
 plots, 73
- Frequency measurements  
 algorithm by eigenvector analysis in noise  
   subspace, 244–47  
 algorithm by Prony method, 247–50  
 with methods of parametric spectral  
   analysis, 244–50
- Frequency-modulated continuous wave  
 (FMCW). *See* FMCW radar
- Frequency modulation (FM)  
 parameters, 8–12  
 in range measurement, 1
- Frequency range-finder (FRF), xvii

**G**

Geodesic research, range finders for, 283

- Geo-radar, FM, 282–83  
Guarding systems, 284–85
- H**  
Harris WF, 299
- I**  
Ice and snow blanket thickness meters, 281–82  
Ideal linear FM results, 289  
Increased error zone (IEZ)  
carrier FM sweep and, 235  
defined, 170  
phase characteristic (PC) estimation error and, 239  
size reduction, 223  
in SPD for cancellation, 230–31  
UR exit from, 247  
value determination, 203  
Instantaneous error estimations, 242  
Instantaneous measurement error, 91, 227  
Instantaneous range measurement error, 231, 246, 252, 254  
Instantaneous truncation error, 103  
Integral discrete Fourier transformation (IDFT), 69  
Interference  
estimation of, 198  
property differences, 204  
pulse, 179  
SAD, 206  
simultaneous error minimization, 308  
virtual, 266–69  
Interference field  
complex amplitude, 186  
creation by toroidal wave, 186  
distribution, 186
- K**  
Kaiser-Bessel WF  
application of, 50  
approximation, 298  
defined, 42  
derivative of, 62  
difference frequency estimation
- truncation error at, 74–77  
error obtained using, 50  
FM sweep for, 79  
measurement error at optimal values, 82  
measurement error for, 62–64  
normalized measurement error versus normalized range, 77  
normalized range for optimal parameters, 85  
optimal, 49  
parameter values, 63  
profile, 43  
range of shape, 49  
range point positions versus point number, 77  
SAD processed by, 82  
SD logarithms, 298  
*See also* Weighting functions (WFs)
- L**  
Level-meters, 266, 281, 290  
Likelihood function (LF), 108  
Likelihood ratio function (LRF), 108  
Logarithm of likelihood function (LLF)  
defined, 108  
fast oscillating character, 113  
form, 108  
global maximum determination, 113, 114  
local maximums, 114  
properties in spectral domain, 112  
Logarithm of likelihood ratio function (LLRF), 108  
LUCH-2, xviii
- M**  
Maclaurin series, 142  
Mapping systems, robotic, 285  
Maximal likelihood method (MLM)  
advantages of, 108  
as asymptotically effective, 109  
benefit of accuracy, 134  
conclusions, 135–36  
defined, xviii  
delay time estimation, 113–16  
errors in application of, 116

- Maximal likelihood method (MLM)
- (continued)
  - estimates, 130
  - factors affecting range error estimation and, xxi
  - function of relative MSD for, 131
  - measurement of small ranges with, 243
  - parametrical algorithm based on, 274–75
  - for range estimation, 107–36
  - simulation of range estimation algorithm, 130–35
  - successful implementation, 117
  - total error reduction and, 133
- Mean square deviation (MSD)
- amplitude of oscillations, 59
  - average, 59, 62
  - calculation on range parts, 45
  - measurement error, 45–50
  - measurement error, virtual reflectors and, 219–20
  - of noise error component, 58
  - normalized, 41, 47
  - normalized, number versus relative range for optimal coefficients, 48
  - range estimation, 98
  - range measurement, 150
  - total error, 61, 63
- Measurement error reduction
- conclusions, 221–22
  - correcting amendment determination, 214
  - correction coefficient estimation, 215
  - of difference frequency estimation, 210–17
  - envelope curves and, 211
  - estimation of interference situation and, 198–204
  - introduction to, 197–98
  - probability of, 213
  - by virtual reflector, 217–21
  - weak signal, 204–10
- Measurement errors
- at CSD, 227
  - distance, 263
  - envelopes versus range to UR, 180
  - instantaneous, 91, 227
  - for Kaiser-Bessel WF, 62–64
- minimization on basis of FM parameter optimization, 77–80
- noise and, 57
- noisy component of, 57
- relative, functions of, 40
- SR presence and, 198
- time delay, 116–21
- for WF in form of trigonometric series, 58–62
- See also* Range measurement error
- Methods of QI smoothing (MQIS), xx, 8, 56–57
- Mixers
- combination components, in range measurement error, 192–94
  - low-frequency components, 192
- Modified Bessel function, 42
- Modulation characteristic nonlinearity
- approximation of time function of signal periods, 162–64
  - compensation of, 155–60, 165
  - counting measurement method, 164–65
  - equation system, 163–64
  - error level reduction, 165
  - estimation of extreme period parts, 161–62
  - matrix form, 163
  - nonproportional variation and, 141
  - parameters, 150, 151–53
  - at range calculation, 160–64
- Modulation characteristics (MC)
- averaged slope, 157
  - estimation of nonlinearity influence, 147
  - of industrially manufactured oscillator, 139
  - mathematical model of, 137–40
  - oscillating, 144–47
  - oscillating nonlinearity of, 151–52
  - oscillation component plot, 139
  - parameters, 138
  - performance of two stages, 140
  - quadratic, 142–43
  - quadratic, with oscillating component, 147
  - quadratic and oscillating nonlinearity of, 152–53
  - quadratic nonlinearity of, 151

- slope coefficient, 150  
spectral peak parameters, 140
- Movement speed  
nonuniform velocity, 253–55  
range prediction based on, 250–55  
uniform velocity, 250–53
- Multidimensional numerical minimization, 140
- Multiple signal classification (MUSIC)  
defined, 244  
EV method versus, 244  
as high resolution method, xviii  
spectrum estimation, 244
- N**
- Navigation radar, 279  
Navigation systems, robotic, 285
- Noise  
covariance function of, 57  
error of range measurement, 92–103  
error of weighting method, 56–64  
on filter output, 57  
influence on accuracy of central frequency estimation, 94–103  
influence on accuracy of DFS central frequency estimation, 95–99  
influence on average-weighted estimation, 99–101  
influence on DFS frequency estimation, 101–2  
measurement error caused by, 57  
in reducing accuracy of distance measurements, 289  
simultaneous error minimization, 308  
WF shape and, 62
- Noise effect  
additive, estimation of, 56–57  
time moments and, 57
- Noise error  
MSD of, 58  
variance of, 57
- Nonuniform velocity  
error accumulation, 253  
instantaneous range measurement error, 254  
range prediction based on, 253–55
- simulation conditions, 254  
of useful reflector movement, 253–55
- O**
- Observation radar, bird, 283–84  
Optimal RRs, 263, 264  
Optimal WFs  
best WFs comparison, 300  
frequencies of, 301  
KB profiles, 49  
logarithms of SD modulus of, 302  
profiles of, 47  
shapes of, 302  
variation of shape, 46
- Optimization  
combined, 55–56, 80  
of FM sweep, 53–55, 78–79  
minimization of measurement error, 77–80  
slow-frequency modulation, 50–53  
truncation error minimization by, 50–56  
of WF parameters, 80–85
- Oscillating modulation characteristic  
error value estimation, 145  
parameters, 144  
quantitative estimation, 145  
stepwise variation of measuring range, 144
- Oscillating nonlinearity  
of modulation characteristics, 151–52  
quadratic nonlinearity and, 152–53  
worst case of, 160
- Oscillation, 148
- P**
- Parametrical methods and algorithms  
cancellation of spurious reflections, 223–32  
conclusions, 255  
frequency measurement, 244–50  
introduction to, 221  
maximal likelihood method (MLM), 274–75  
parametric spectral analysis (PSA), 272–74

- “Prediction” algorithm, 275–77  
 range prediction, 250–55  
 reduction of spurious reflector influence, 232–43  
 testing of tracking distance meter, 275  
 testing results, 272–77
- Parametric spectral analysis (PSA)  
 algorithms based on methods of, 272–74  
 defined, 244  
 frequency measurement using, 244–50
- Parasitic amplitude modulation (PAM)  
 decreasing influence of, 120–212  
 defined, xx  
 DFS phase estimation error and, 135  
 elimination with WF, 121  
 frequency-dependent reflections and, 168  
 influence analysis, 119  
 influence on DFS frequency estimation, 119–21  
 influence on total error of range estimation, 120  
 presence, 119  
 range measurement and, 247
- Periodicity, 43–44
- Phase characteristic (PC), 24, 123, 124
- Phase characteristic (PC) estimation  
 ambiguity in, 123  
 at DFS reception, 124  
 displacement, 133  
 error influence, 239  
 of FMCW RF, 121–30  
 maximum likelihood, 121  
 plots, 125  
 practical determination, 122  
 procedure, 132  
 reduction of noise influence on accuracy of, 134–35  
 truncation error, 126, 129  
 variance, 126, 132
- Phase-frequency characteristic (PFC)  
 approximation error, 275  
 calculations for DFS, 274  
 defined, 24  
 estimation, 274
- Phase multiplexer, 89
- Pisarenko harmonic expansion (PHE), 244
- Power spectral density (PSD)  
 defined, 68  
 noise, 93  
 spline interpolation of, 70
- Precision measurements  
 procedure for carrying out, 266  
 synthesis of radar reflectors for, 259–64  
 test bench, 264–65
- Precision measuring system testing  
 conclusions, 286  
 distance measurement results, 272–77  
 equipment and approaches, 257–66  
 experimental reduction of distance measurement error, 269–72  
 experimental reduction of error, 266–69  
 introduction to, 257  
 practical application areas, 277–85  
 results of “Prediction” algorithm, 275–77  
 tracking distance meter, 275
- “Prediction” algorithm  
 operation, 277  
 testing results of, 275–77
- Prony method  
 defined, 223  
 frequency measurement algorithm by, 247–50  
 instantaneous error of range measurement plots, 249  
 interest in, 247  
 MSD function of range measurement, 250
- PAM deepness at application of, 250
- PSA-based algorithms and, 273  
 spectrum, 248
- Pulling period, 13–14
- Pulse interference, 179
- Q**
- Quadratic coefficient, 143
- Quadratic modulation characteristic derivative, 142  
 with oscillating component, 147  
 parameters, 142
- Quadratic nonlinearity  
 increase of degree, 148  
 of modulation characteristics, 151  
 nodal points and, 148

- normalized average error, 148  
oscillating nonlinearity and, 152–53  
worst case of, 160
- Quantization interval (QI), xx
- R**
- Radar reflectors (RRs)  
configuration illustration, 262  
creation of, 259  
defined, 257  
designing, 261  
diameter, 258  
distance measurement error to, 263  
double-lobe, 263  
electrical distance determination, 265  
geometry determination, 259  
nonsymmetric, 261  
with odd number of sectors, 260  
optimal, 260, 263, 264  
restricted size, 262  
shape definition, 261  
standard, 258  
synthesis for precision measurements,  
    259–64
- Radio altimeters, 278–79
- Radio proximity fuses, 279
- Range determination error  
algorithm of correction of range  
    calculation, 24–25  
from inaccuracy of modulation  
    adaptation, 23–25  
noise influence, 25–31  
relative MSD logarithm, 30  
*See also* Range measurement
- Range estimation  
algorithm application, 255  
algorithm at SR presence, 255  
based on difference frequency signal,  
    108–13  
introduction to, 107  
MLM for, 107–36  
normalized error of, 181  
PAM influence on total error, 120  
two-stage procedure, 135
- Range estimation simulation  
algorithm, 130–35
- results at known phase characteristic, 131  
results at unknown phase characteristic,  
    131
- Range-finder  
block diagram, 2  
FMCW, 7–8  
frequency-modulated, 2  
for geodesic research, 283  
under interference conditions, 197  
measurement error by, 183, 184
- Range measurement  
analytical estimation of truncation error  
    at, 71–74  
frequency modulation (FM) in, 1  
measurement performance and, 51  
MSD, 150  
noise interference influence on error,  
    92–103  
parasitic amplitude modulation (PAM)  
    and, 247  
at presence of SRs of small intensity,  
    242–43  
range determination error, 23–31  
on SR background, 198  
total error functions of, 134  
traditional counting method, 5–7  
truncation error, 13–23
- Range measurement error  
analysis of, 167–95  
caused by single spurious signal, 170–74  
error envelope (EE), 171, 172  
estimation at signal processing of time  
    domain, 172–74  
functions, 118  
influence of combination components in  
    mixer, 192–94  
influence of edge modes, 184–86  
influence of reflected waves, 187–91  
influence of spurious reflectors, 174–81  
influence of virtual clutter, 193–94  
instantaneous, 231, 246  
introduction to, 167–70  
minimization for weakly reflecting  
    liquids, 204–6  
plane reflector, 190  
point reflector, 190  
at presence of SR of small intensity, 243

- Range measurement error (continued)
  - by range-finder, 183, 184
  - reflector in DS, 190
  - by signal reflection from reservoir vertical wall, 181–84
  - sources, 7–8
  - wave reflected from useful reflector, 188–90
- Range prediction (movement speed)
  - nonuniform velocity, 253–55
  - overview of, 250
  - uniform velocity, 250–53
- Rayleigh’s reflection, 283
- Reflected waves
  - influence on measurement error, 187–91
  - from useful reflector on range measurement error, 188–90
- Reflector movement
  - nonuniform velocity, 253–55
  - uniform velocity, 250–53
- Reflector sizes, 185
- Robotic navigation and mapping systems, 285
- S**
- Scalar Kirchhoff approximation, 184
- Self-oscillating mixer (SOM), xix
- Sidelobe level (SLL)
  - AWF SD variation, 296
  - maximum of WF, 210
  - minimization, 299–306
- SAD, 199
- WF SD, 84
- Sidelobes (SL)
  - of AWF SD, 297
  - reduction of, 67–68
- SAD, 75
- SD, 202, 296
- Signal/interference ratio (SIR), 170, 175, 193, 238
- Signal/noise ratio (SNR), 8–9, 98
- Sliding half-strokes, 101–2
- Slope coefficient, 150
- Slow FM, 77–78
- Slow-frequency modulation, 50–53
- Slow oscillation, 148
- Small displacement meters, 284
- Smooth weighting, 35
- Spectral amplitude density (SAD)
  - adaptable weighting functions (AWFs), 200–201
  - analytical equations, 177
  - DC WF processing, 82
  - defined, 69
  - frequency estimation of parameters, 205
  - interference, 180, 206
  - KB WF processing, 82
  - minimal SLL, 199
  - modulus, 178
  - modulus maximum, 72
  - pulse interference, 179
  - pulse interference SL periodicity, 180
  - of radio pulse signal, 178
- SC, 70
  - shape variation, 74
- SLs, 75
  - spline interpolation of, 70
  - of useful signal, 205
  - WF shape, 212
- Spectral components (SCs)
  - of DFS, 99
  - with different frequencies, 167
  - distribution laws of, 68
  - edge modes, 167
  - processed, 71
- SAD, 70
  - selection of EV spectrum, 245
  - as SRs, 202
- Spectral density (SD)
  - AWF, 295, 296
  - of DFS, 74, 92–103
  - position of, xxi
  - shape distortion, 88
  - sidelobes, 202
- SL, 296
- Spectral power density (SPD)
  - DFS, 228
  - estimation, 94
  - for SR cancellation, 228, 230
- Spurious reflector reduction
  - introduction to, 232
  - phase characteristic (PC) estimation error, 239

- range measurement, 242–43  
tracking loss conditions, 240–42  
tracking modes, 237–39  
tracking procedure after local extreme, 236–37  
tracking range measuring system, 232–36  
*See also* Parametrical methods and algorithms
- Spurious reflectors (SRs)  
in accuracy of range measurement, 167  
in antenna-waveguide path, 174–81  
cancellation of, 223–32  
CSD for cancellation, 226–28  
decreasing spectrum, 198  
defined, xviii, 167  
detection characteristics, 203  
detection in FMCW RF operating zone, 201  
detection in learning mode, 199  
determined SCs as, 202  
DFS generated by, 198–99  
envelope plots, 176  
error caused by influence of, 174–81  
frequency-independent, 174  
influence on pulse character, 177–81  
in operating zone, 174–81  
parameters, 191  
range measurement on background, 198  
in reducing accuracy of distance measurements, 289  
resolution zone, 221  
of small intensity, 242–43
- SPD for cancellation, 228–32  
tracking loss and, 241  
UR and, 194–95  
virtual reflectors, 192  
waves reflected from, 190–91
- Stationary random process (SRP), 94
- Systematic inaccuracy  
of frequency estimation, 91–92  
range versus, 113
- T
- Test bench  
block diagram, 267  
CONTACT-1, 264
- illustrated, 264  
for measurement of FM RF parameters, 264–65  
waveguide-measuring, 266–67
- Time delay  
estimation with MLM, 113–16  
measurement error in, 116–21
- Total error MSD, 61, 63
- Tracking  
after local extreme, 236–37  
after useful extreme, 237  
algorithm, 232–42, 255  
algorithm application, 242  
distance meter testing, 275  
extreme displacement function and, 234, 235  
loss conditions, 240–42  
main stages of procedure, 236–37  
meter, testing results, 276  
modes, 237–39  
phase characteristic (PC) estimation error and, 239  
range measurement system, 232–36  
time delay estimation accuracy, 233
- Transmitting-receiving module (TRM), 187–88
- Transport radar, 280–81
- Truncation error  
of average weighted estimation, 88–91  
behavior, of initial phase estimations, 127  
comparison, 20  
corrected, relative variance, 21–22  
correction stages, 20  
defined, 8  
degree of reduction, 64  
extreme averaged normalized, 52  
first approach, 22  
fixed measuring of time interval, 13–16  
of FMCW RF PC determination, 129  
functions of components, 90  
of initial phase estimation, 127, 128  
instantaneous, 103  
mathematical expectation, 19, 22  
minimization at weighting average method, 45–50  
minimization by FM parameter optimization, 50–56

- Truncation error (continued)  
 minimization with adaptable weighting functions, 86  
 noise influence on, 56–64  
 PC determination, 129  
 PC estimation, 129  
 range measurement, 13–23  
 range result correction, 20–23  
 reducing, 15–16  
 relative measurement, 15  
 relative variance, 18  
 second approach, 23  
 stable component of measurement, 19  
 time interval multiple to modulation half-period, 16–20  
 value benefit, 51  
 variance versus relative range, 18  
 of weighting method, 36–45
- U**
- Uniform velocity  
 average estimation, 251  
 estimation, 253  
 formula, 250–51  
 instantaneous range measurement error, 252  
 in range prediction, 250–53  
 simulation results, 252
- Useful reflectors (URs)  
 defined, xviii  
 exit from IEZ, 247  
 nonuniform velocity of, 253–54  
 resolution zone, 221  
 SR and, 194–95  
 waves reflected from, 188–90  
 waves reflected from, simultaneous influence, 190–91
- V**
- Virtual clutter  
 defined, 193  
 influence on range estimation error, 193–94
- Virtual interference  
 distance estimation error caused by, 269  
 experimental reduction of error caused by, 266–69  
 reducing influence on, 267–69
- Virtual reflectors  
 action sequence for influence reduction, 218–20  
 error decrease caused by, 217–21  
 measures, 220–21  
 MSD of measurement error and, 219–20  
 near useful reflector, 193  
 neutralization of, 217  
 ratio of signal amplitudes from, 219  
 surrounding SR, 192
- Voltage-controlled oscillator (VCO), 137
- W**
- Waveguide-measuring test bench, 266–67
- Weak signal error minimization  
 action sequence, 206  
 interference properties and, 204  
 introduction to, 204–10  
 liquids, 204–6  
 material near antenna, 206–10  
 reservoir bottom, 210  
*See also* Measurement error reduction
- Weighting functions (WFs)  
 adaptable (AWFs), 86–88, 197–222, 291–99  
 best, 300  
 Blackman, 102, 128, 129, 181, 243, 270  
 of Blackman-Harris, 48  
 change of shape, 42  
 defined, 33  
 determination error of, 35  
 with different values, 44  
 discretized, 292  
 Dolph-Chebyshev (DC), 74–77  
 families, xxi  
 for harmonic analysis and adjacent problems, 291–312  
 Harris, 299  
 illustrated, 39  
 Kaiser-Bessel, 42, 43, 62–64, 74–77, 298  
 maximum SLL of, 210  
 measurement error in form of trigonometric series, 58–62  
 optimal, 46–47, 300

- optimal coefficients, 46  
optimization, 46  
in PAM elimination, 121  
range increasing and, 47  
relative measurement error, 40  
representation, 39  
SAD shape, 212  
shape control algorithm, 221  
shape parameter, 49  
shape versus noise influence, 62  
SLL SD, 84  
small ranges, 46  
spectral properties comparison, 300  
at spectrum calculation, 68  
use of, 291
- Weighting method  
application of, 33  
conclusions, 64
- dependence of DFS zero number, 38  
for difference frequency averaging, 33–64  
effects of FM nonlinearity for, 147–50  
envelope nodes (ENs), 40–41  
illustrated, 35  
noise influence on error, 56–64  
truncation error, 36–45  
truncation error minimization, 45–50  
truncation error minimization by optimization, 50–56
- WF parameter optimization  
error minimization and, 80–85  
simplified method of, 84

## Z

- Zero padding, 69  
Zones of inversion, 3

